Royal Academy of Medicine in Ireland (RAMI)

Section of Bioengineering

24th—26th of January 2025

Hodson Bay Hotel, Athlone

Sponsors

Gold Sponsors

Medtronic

BD

Silver Sponsors

Zwick / Roell

Engineers Ireland

I-Form Advanced Manufacturing Research Centre

Boston Scientific

Bronze Sponsors

CADFEM UK & IRELAND

shimmer DISCOVERY IN MOTION

MSC

Welcome Address

On behalf of University College Dublin and the organising committee, I am delighted to welcome you to the 30th Annual Conference of the Section of Bioengineering of the Royal Academy of Medicine in Ireland (BINI 2025). Set against the stunning backdrop of Ireland's Hidden Heartlands, this year's conference is hosted at the Hodson Bay Hotel, offering delegates the perfect setting to engage in stimulating discussions and enjoy the breathtaking surroundings.

We extend our heartfelt gratitude to all delegates who have submitted abstracts and contributed to the success of this year's conference. With over 250 registered participants from diverse research backgrounds in the field of bioengineering, BINI 2025 is a true testament to the strength and vibrancy of our bioengineering community across the island of Ireland. The conference programme will feature a wide array of topics presented across three parallel rooms, showcasing the breadth and depth of bioengineering research.

We are particularly honoured to welcome our distinguished invited speakers, Dr. Brian Johnstone from Oregon Health & Science University, Portland, Oregon, and Prof. Katja Schenke-Layland from the University of Tübingen, Germany. Both are internationally recognized leaders in their respective fields, and their contributions promise to be highlights of the event.

This year, the Royal Academy of Medicine in Ireland Bioengineering Section proudly awards the 2025 RAMI Silver Medal to Professor Bruce Murphy of Trinity College Dublin. Professor Murphy will deliver the prestigious Samuel Haughton Honorary Lecture on Saturday, an event we eagerly anticipate.

The conference also features the Engineers Ireland Biomedical Research Medal competition on Friday morning, generously sponsored by Depuy Synthes, alongside the awarding of the RAMI Bronze Medal for the best paper and several additional student prizes.

We would like to express our sincere thanks to our sponsors—Medtronic, BD, Zwick Roell, Engineers Ireland, I-Form, Boston Scientific, CADFEM, Shimmer, and MSC—whose generous support has made this event possible. We encourage you to visit their stands and engage with their representatives throughout the conference.

We hope that you find the academic presentations inspiring, the networking opportunities enriching, and the social programme enjoyable. Thank you for being a part of BINI 2025, and we look forward to an engaging and rewarding conference together!

Warm regards,

Niamh Nowlan

Conference Chair

UCD DUBLIN
University College Dublin
Ireland's Global University

ROYAL ACADEMY OF MEDICINE IN IRELAND

General Information

Organising Committee

- **Niamh Nowlan (chair)**
- **Philip Cardiff**
- **Fiona Freeman**
- **Aisling Ní Annaidh**
- **Eoin O'Cearbhaill**
- **Stephen Thorpe**
- **David MacManus**
- **Emer Doheny**
- **Mert Celikin**
- **Donal Holland**
- **Paula Bourke**
- **Connor Green**

Student/Postdoc Organising Committee

- **Dylan Armfield**
- **Jordan O'Donoghue**
- **Ashwin Mishra**
- **Ajai Kavunkara Thadayil**
- **Jan (JJ) Baguyo**
- **Cagri Yenigun**
- **Thomas Lijnse**
- **Orla Jordan**
- **Beatriz Lopez**
- **Soukaina Barroug**
- **Mauro Gisbert**
- **Jemma Falkov**
- **Hannah Kane**
- **Karin Vancikova**
- **Mariami Mtchedlishvili**

Social Programme

Social events are complementary for all delegates wearing a conference badge. On Friday night, a Buffet Dinner will take place at 8pm in The Clonmacnoise Suite, followed by awarding of the Engineers Ireland Medal and a table quiz.

On Saturday night, a drinks reception will take place at 7.00pm followed by the Gala Dinner starting at 8pm in The Clonmacnoise Suite.

Theme: Black and White Ball

Social Media

We welcome all social media posts on X or Linkedin please use the #BinI2025 to post about the conference, feel free to tag @bini_irl in any pictures.

University College Dublin
Ireland's Global University

ROYAL ACADEMY OF MEDICINE IN IRELAND

Hotel Layout

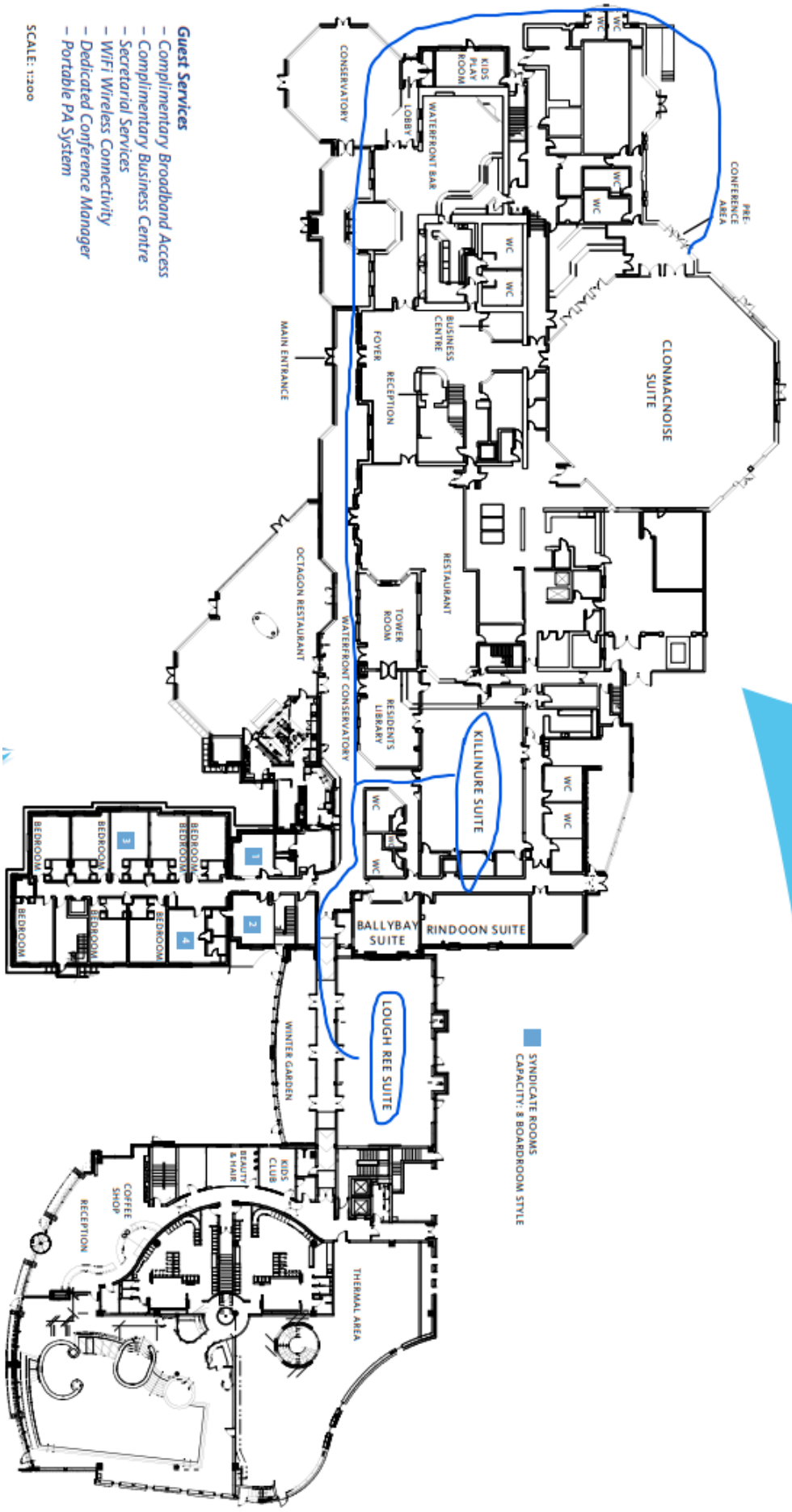

Keynote Speakers

Dr Brian Johnstone

Brian Johnstone, PhD, FIOR, FORS, is Director of Research, Department of Orthopaedics and Rehabilitation at Oregon Health & Science University, Portland, Oregon. He did his predoctoral research in England and postdoctoral studies in the USA. His main research area is skeletal tissue regeneration from which he has produced peer-reviewed manuscripts, chapters and reviews, with grants from numerous sources including NIH, Arthritis Foundation and Shriners Hospitals. He developed and patented the system for the chondrogenic induction of stem cells. Brian is a Past-President of the Orthopaedic Research Society and has served/serves on numerous grant review panels of national and international organizations and journal editorial boards. He currently chairs several scientific advisory boards for organizations in the US and Europe and is the Mercator Fellow for a German multi-center program. Brian has received numerous national and international honors including being elected into the inaugural class of Fellows of International Orthopaedic Research (FIOR), and that of the Orthopaedic Research Society Fellows (FORS). In 2017 he was awarded the Marshall R. Urist Award for his contributions to tissue regeneration research.

The title of Dr. Johnstone's talk on Friday is "***So, you've created tissue in a test-tube – now what?' Acceptable?".***

Prof Katja Schenke-Layland

Professor Katja Schenke-Layland is Professor of Medical Technologies and Regenerative Medicine at the Eberhard Karls University Tübingen

Katja received a master of science (M.Sc.) in biology, psychology and sociology in 2001; and her doctorate degree (Dr. rer. nat.) in biology in 2004 from the Friedrich Schiller University (FSU) Jena, Germany. She worked as a researcher at the Departments of Anatomy (2000-2001) and Cardiothoracic Surgery (2001-2004). She was a postdoctoral research fellow at the Saban Research Institute at the University of Southern California's Children's Hospital Los Angeles (2004-2005). Katja was a postdoctoral research fellow at the David Geffen School of Medicine at University of California Los Angeles UCLA, USA (2005-2008). In 2008 she was appointed as Assistant Research Professor in the Department of Medicine/ Cardiology at UCLA (2008-2009) and is currently an Adjunct Associate Professor. In January 2010, she became the group leader of the Fraunhofer-Attract Group at the Fraunhofer Institute for Interfacial Engineering and Biotechnology (IGB), Dept. of Cell and Tissue Engineering in Stuttgart, Germany and later accepted the position of Department Head. She was Interim Institute Director of the Fraunhofer IGB from 2016 – 2017. Katja accepted her call as Professor of Biomaterials in Regenerative Medicine at the University Hospital Tübingen UKT in 2011. She coordinates the bachelor "Vital Implants" and master "Implantology" modules in the Biomedical Technologies program. She has recently taken on the position of Deputy Student Dean of Biomedical Technologies. In 2018 she became the Director of The Natural and Medical Sciences Institute (NMI) at the University of Tübingen in Reutlingen.

The title of Prof. Schenke-Layland's talk on Saturday is ***"Developmental biology-inspired biomaterials for regenerative medicine".***

The Samuel Haughton Honorary Lecture

The **Royal Academy of Medicine in Ireland Silver Medal** is presented to a distinguished clinician or engineer who has made a significant contribution to the field of bioengineering through academic endeavour and research. The recipient delivers the distinguished Samuel Haughton Honorary Lecture at the annual Bioengineering in Ireland conference.

Professor Bruce Murphy

Dr. Bruce Murphy is a Professor in the Department of Mechanical, Manufacturing and Biomedical Engineering and Principal Investigator (PI) in the Trinity Centre for Biomedical Engineering and the Advanced Materials and Bioengineering Research (AMBER) Centre at Trinity College Dublin (TCD).

Bruce began his academic journey in 1993 at Trinity College Dublin, where he pursued a degree in mechanical engineering, graduating in 1997.

In the summer of 1997, a chance phone call led him to undertake a PhD in biomedical engineering under Prof. Patrick Prendergast, focusing on "Aspects of the Fatigue Properties of Acrylic Bone Cement." During this period, he encountered a wide range of biomedical engineering problems. It was here that he first discovered cardiovascular stents and was fascinated by their manufacturing, materials, and the elegant solution they provided for minimally invasively opening arteries. From that moment, he was hooked by medical device design, setting an unwritten goal: “to develop a minimally invasive cardiovascular device to address a clinical problem”.

In 2001, Bruce moved to University of Galway to work with Professor Peter McHugh on a PRTLI-funded cardiovascular project. During his time in Galway, he built a network of friends and colleagues in the medical device design field and established a medical device design group at NUIG. In 2009, he returned to TCD to take up a lectureship position.

Currently, Bruce is a Professor in Biomedical Engineering in the Department of Mechanical, Manufacturing, and Biomedical Engineering, and a Principal Investigator (PI) at the Trinity Centre for Biomedical Engineering and the Advanced Materials and Bioengineering Research (AMBER) Centre at Trinity College Dublin (TCD). He runs a medical device design incubator lab in Trinity’s Biomedical Sciences Institute. To date, his lab has spun out five TCD spin-outs: Croívalve, Selio Medical, Proverum, PLIO Surgical, and One Projects. These spin-outs have raised over €120 million in capital, employ over 100 full-time equivalents, and have two devices in clinical trials.

Current projects in his lab include MitrAdapt, a new percutaneous solution for treating patients with mitral regurgitation; PLIO, a new laparoscopic solution to reduce leakage rates of anastomosis in the GI tract; IndexiTap; and a breathing volume sensor. The latter two projects are collaborations with TCD's Academic Unit of Neurology and Beaumont Hospital.

ROYAL ACADEMY OF MEDICINE IN IRELAND

Programme Overview

Time	Friday 24th January		
	Clonmacnoise Suite	**Killinure Suite**	**Lough Ree Suite**
10:00 – 11:00	**Registration** *Front Conservatory*		
	Tea & Coffee		
11:00 – 11:15	**Welcome Address** *Clonmacnoise Suite , Conference Chair: Niamh Nowlan*		
11:15 – 12:15	**EI Medal Session**		
12:20 – 13:20	**Drug Delivery 1** ***Chairs: Antony Kho & Thomas Lijnse***	**Biomechanics 1** ***Sponsor: Medtronic*** ***Chairs: Claire Conway & Robert Johnson***	**Biomaterials & Clinical Translation** ***Chairs: David Hoey & Rachel Cahalane***
13:20 – 14:15	**Lunch** *Main Restaurant*		
14:15 – 15:00	**Keynote 1: Dr Brian Johnstone** Clonmacnoise Suite, *Chair: Fiona Freeman*		
15:05 – 16:05	**Drug Delivery 2** ***Chairs: Mark Ahearne & Eimear Wallace***	**Mechanobiology 1** ***Chairs: Stefaan Verbuggan & Olwyn Mahon***	**Tissue Engineering 1** ***Chairs: Andrew Daly & Ian Woods***
16:05 – 16:30	**Tea/Coffee**		
16:30 – 18:00	**Clinical & Translational** ***Chairs: Eimear Dolan & Hannah Prenderville***	**Mechanobiology 2** ***Chairs: Oran Kennedy & Syeda Masooma Naqvi***	**Immuno Engineering & Tissue Engineering** ***Chairs: Tom Hodgkinson & Meadhbh Brennan***
18:00 – 18:20			
19:30	**Buffet Dinner, EI Medal Award & Table Quiz** *Clonmacnoise Suite*		

Time	Saturday 25th January		
	Clonmacnoise Suite	**Killinure Suite**	**Lough Ree Suite**
09:00 – 10:30	**Tissue Engineering 2** ***Chairs: Annie Curtis & Avelino Ferreira***	**Biomechanics 2** ***Chairs: Kevin Moerman & Hyab Mehari Abraha***	**Medical Devices 1** ***Sponsor: BD*** ***Chairs: Brooke Tornifoglio & Giulio Brunetti***
10:30 – 11:00	**Tea/Coffee**		
11:00 – 11:45	**Keynote 2: Prof. Katja Schenke-Layland** *Clonmacnoise Suite, Chair: Eoin O'Cearbhaill*		
11:50 – 13:05	**Biomaterials 1** ***Chairs: Conor Buckley & Francisco José Calero Castro***	**Mechanobiology 3** ***Chairs: Laoise MacNamara & Mahtab Vafaeefar***	**Imaging** ***Chairs: Eoghan Cunnane & Beatriz Pinheiro Lopes***
13:05 – 14:00	**Lunch** *Main Restaurant*		
14:00 – 14:45	**Haughton Lecture: Prof. Bruce Murphy** *Clonmacnoise Suite, Chair: Caitríona Lally*		
14:50 – 16:05	**Disease Models and Biomaterials** ***Chairs: Caroline Curtin & Cansu Gorgun***	**Biomechanics 3** ***Chairs: Krishna Manda & Ryan Coleman***	**Medical Devices 2** ***Chairs: David Taylor & Soukaina Barroug***
16:05 – 16:30	**Tea/Coffee**		
16:30 – 18:05	**Biomaterials 2** ***Chairs: Joanna Ward & Juhi Chakraborty***	**Tissue Engineering 3** ***Chairs: Ciara Murphy & Nasrin Ghanamigashti***	**Medical Devices 3** ***Chairs: Bruce Murphy & Irina Khaydukova***
19:00 - 20:00	**Drinks Reception**		
20:00	**Gala Dinner** *Clonmacnoise Suite*		

Detailed Programme

Engineers Ireland Biomedical Research Medal

Awarded for outstanding contribution to biomedical engineering research in Ireland. The winner receives a commemorative EI Biomedical Research medal and €1,500 honorarium generously sponsored by DePuy Synthes.

Friday 11:15 – 12:15	**Engineers Ireland Biomedical Research Medal Session** **Sponsored By: Depuy Synthes** Venue: Clonmacnoise Suite Chairs: John Mulvihill	Page
11:15-11:30	AN AGENT-BASED ARTIFICIAL INTELLIGENCE-DRIVEN DEFORMABLE CELL FRAMEWORK TO UNCOVER THE MECHANISM UNDERLYING MECHANOSENSITIVE TUMOUR GROWTH I. Senthilkumar, B. Smeets, J. Vangheel, E. Howley, E, McEvoy E.	24
11:30-11:45	IDENTIFICATION OF GPR161 AS A NOVEL MECHANOSENSOR IN BONE AND ANTI-CATABOLIC CHRONO-THERAPEUTIC FOR OSTEOPOROSIS M. Cobban, M. Maggio, H. Hajiali, A. El Haj, A. Curtis, K. Hokamp, F.M. Roche, D. Hoey	25
11:45-12:00	A TRIP TO ANOTHER DIMENSION – 2D MATERIALS FOR TISSUE REGEN- ERATION AND ADVANCED NEURAL INTERFACES J. Maughan, J.N. Coleman, F.J. O'Brien	26
12:00-12:15	4D BIOPRINTING SHAPE-MORPHING HEART TISSUES IN GRANULAR SUPPORT HYDROGELS: SCULPTING STRUCTURE AND GUIDING MATURATION A. Pramanick, T. Hayes, V. Sergis,E. McEvoy,A. Pandit, A.C. Daly	27

Friday 12:20-13:20	**Biomechanics 1** **Sponsored By: Medtronic** Venue: Killinure Suite Chairs: Claire Conway and Robert Johnson	Page
12:20-12:24	INVESTIGATION OF THE IMPACT OF STORAGE CONDITIONS ON THE MICROSTRUCTURE AND MECHANICS OF ADIPOSE TISSUE: IMPLICATIONS FOR BREAST TISSUE Olivia Strong	28
12:24-12:33	IMPACT OF MORPHOLOGICAL DETAIL ON MITRAL VALVE MECHANICS: CONTRASTING HIGHRESOLUTION MCT-BASED MODELS WITH SIMPLIFIED PARAMETERIZED APPROACHES Hyab Mehari Abraha	29
12:33-12:42	SYNERGISTIC EFFECT OF CALCIFICATION AND STRUCTURAL DAMAGE DRAMATICALLY REDUCES LIFETIME OF PORCINE PERICARDIUM USED IN BIOPROSTHETIC HEART VALVE LEAFLETS Luke Guerin	30
12:42-12:51	A VISCOELASTIC FINITE ELEMENT MODEL OF INTERPENETRATING NETWORK HYDROGELS Prasannavenkadesan Varatharajan	31
12:51-13:00	TOWARDS A SEX-SPECIFIC UNDERSTANDING OF TRAUMATIC BRAIN INJURY BIOMECHANICS Ashwin Mishra	32
13:00-13:09	BIVENTRICULAR HEART MODEL WITH NOVEL PSEUDO-FLUID DOMAINS AND THERMODYNAMICALLY-MOTIVATED GROWTH & REMODELING Darshan Senthil	33
13:09-13:18	HEXAGONAL BORON NITRIDE NANOSHEETS ENABLE THE FORMATION OF ARTIFICIAL MEMBRANCE CHANNELS Xuliang Qian	34

Friday 12:20-13:20	**Biomaterials and Clincial and Translational** Venue: Lough Ree Suite Chairs: David Hoey and Rachel Cahalane	Page
12:20-12:24	A SYSTEMATIC REVIEW OF CORROSION STUDIES AND PROPOSED IMPROVEMENTS Arian McCallion	35
12:24-12:33	THE SCIENCE OF SPLIT ENDS: BIOMECHANICAL INVESTIGATIONS OF THE FRACTURE OF HAIR Ailsa Yale	36
12:33-12:42	MICROSTRUCTURAL EVOLUTION AND PERFORMANCE OF LPBF TI-6AL-4V LATTICE STRUCTURES UPON HOT ISOSTATIC PRESSING Ajai Sankar Kavunkara Thadayil	37
12:42-12:51	REGENERATE : A PEPTIDE NANOPARTICLE LOADED NANOGEL FOR ACCELERATED WOUND HEALING Chayanika Saha	38
12:51-13:00	DEVELOPMENT OF CARTIFIX – TISSUE SPECIFIC ECM-DERIVED SCAFFOLDS FOR OSTEOCHONDRAL DEFECT REPAIR David Browe	39
13:00-13:09	SELENIUM AND MAGNESIUM FUNCTIONALISED SCAFFOLDS FOR DUAL BONE REGENERATION AND ANTI-CANCER THERAPY Eaven Pakenham	40

Friday 12:20-13:20	**Drug Delivery 1** Venue: Clonmacnoise Suite Chairs: Mark Ahearne and Thomas Lijnse	Page

Friday 15:05-16:05	**Mechanobiology 1** Venue: Killinure Suite Chairs: Stefaan Verbuggan and Olwyn Mahon	Page

15:45-15:54	EFFECTS OF ESTROGEN DEFICIENCY ON VASCULARIZATION AND MINERALIZATION IN A NOVEL 3D HUMANIZED BONE MODEL Muhammad Munam Mustafa	54
15:54-16:03	LEVERAGING CRISPR-CAS12 TO UNCOVER THE DEPENDENCIES OF EPITHELIAL TUMOUR CELLS CULTURED IN TISSUE-SPECIFIC, MECHANICALLY RELEVANT 3D MODELS Olwyn Mahon	55

Friday 15:05-16:05	**Tissue Engineering I** Venue: Lough Ree Suite Chairs: Andrew Daly and Ian Woods	Page
15:05-15:09	BIOMIMETIC SCAFFOLDS FOR THE REPAIR AND REGENERATION OF KNEE ARTICULAR CARTILAGE Owen Wilson	56
15:09-15:18	CHARACTERISATION OF VERTEBRAL BONE MARROW MESENCHYMAL STEM CELL POPULATIONS IN PATIENTS WITH PRE-ADOLESCENT IDIOPATHIC SCOLIOSIS Avelino Ferreira	57
15:18-15:27	XENO-FREE MESENCHYMAL STEM CELLS UNDER MACROMOLECULAR CROWDING CONDITIONS AS A TISSUE-ENGINEERED SKIN SUBSTITUTE Diana Gonçalves	58
15:27-15:36	A PRO-CHODROGENIC, MULTILAYERED, REINFORCED COLLAGEN-BASED SCAFFOLD FABRICATED USING MELT-ELECTROWRITING AND ELECTROSPINNING FOR MENISCUS REGENERATION Francisco José Calero Castro	58
15:36-15:45	IN VITRO CHARACTERISATION OF 'OSSTIC': A PHOSPHOSERINE-ENHANCED ADHESIVE FOR IMPROVED BONE REGENERATION John Redmond	60
15:45-15:54	REGULATORY CUES TO MODULATE THE STRUCTURAL AND COMPOSITIONAL PROPERTIES OF 3D BIOPRINTED MENISCAL GRAFTS Kaoutar Chattahy	61
15:54-16:03	DEVELOPMENT OF A VERSATILE MUSCULOSKELETAL TISSUE BIOPRINTING PLATFORM TO DIRECT PREFERENTIAL COLLAGEN ALIGNMENT IN HIGHLY CELLULAR BIOINKS Kyle Storey	62

Friday 15:05-16:05	**Drug Delivery 2** Venue: Clonmacnoise Suite Chairs: Antony Kho and Eimear Wallace	Page
15:05-15:09	A NOVEL APPROACH FOR 3D CHARATERISATION OF DRUG RELEASE FROM DRUG DELIVERY DEVICES Joseph Tannian	63
15:09-15:18	EXPLORATION OF INDANE SCAFFOLD ANTAGONISTS FOR COMBINATION PROSTATE CANCER THERAPY WITH COLD ATMOSPHERIC PLASMA Shengxin Zhang	64

15:18-15:27	RATIONAL DESIGN AND CHARACTERISATION OF CELL PENETRATING PEPTIDE FOR NON-VIRAL GENE DELIVERY Guanjie Lin	65
15:27-15:36	COMPUTATIONAL MODELLING OF DRUG DEPOT FORMATION DURING SUBCUTANEOUS INJECTION Antony Kho	66
15:36-15:45	ULTRA-THIN COATING OF VASCULAR DEVICES Fiona O'Neill	67
15:45-15:54	JET STREAM INJECTION FOR NEEDLE-FREE GASTROINTESTINAL DIAGNOSTIC AND THERAPEUTIC FLUID DELIVERY Thomas Lijnse	68
15:54-16:03	ROBOHEAL: DEVELOPMENT OF A SOFT ROBOTIC DRUG DELIVERY SYSTEM TO IMPROVE TREATMENT OF DIABETIC FOOT ULCERS Eimear Wallace	69

Friday 16:30-18:00	**Mechanobiology 2** Venue: Killinure Suite Chairs: Oran Kennedy and Syeda Masoomanaqvi	Page
16:30-16:39	A FINITE-VOLUME SPRING-PARTICLE NETWORK MODEL FOR BLOOD FLOW Joseph Herron	70
16:39-16:48	DEVELOPING AN IN VITRO ASTROGLIOSIS MODEL BY MECHANICAL SCRATCH INJURY Alexandra karadimou	71
16:48-16:57	EXPLORING THE INFLUENCE OF SPATIAL AND SUBSTRATE CUES ON THE FORMATION OF CELLULAR BRIDGES BETWEEN TESTICULAR ORGANOIDS Stephen Rochford	72
16:57-17:06	MODULATING MACROPHAGE BEHAVIOUR IN THE FOREIGN BODY RESPONSE Parand Shokrani	73
17:06-17:15	CHARACTERIZATION OF TUMOUR CELL PHENOTYPE TRANSITIONS IN 2D AND 3D CULTURE SYSTEMS Rajakumar Vadivelu	74
17:15-17:24	A THERMODYNAMIC FRAMEWORK TO PREDICT ANEURYSM FORMATION AND DEVELOPMENT MOTIVATED BY SMOOTH MUSCLE CELL REMODELLING Ryan Coleman	75
17:24-17:33	WNT INHIBITION REDUCES TUMOR SPHEROID GROWTH IN 3D MULTICELLULAR METASTATIC MODELS Vatsal Kumar	76
17:33-17:42	MECHANICALLY ACTIVATED EXTRACELLULAR VESICLES FOR BONE REPAIR Carolina Martins	77
17:42-17:51	MECHANICAL PROPERTIES OF JUVENILE CARTILAGE Mauro Gisbert	78
17:51-18:00	EXPERIMENTAL CHARACTERIZATION OF BRAIN TISSUE MECHANICS TOWARD COMPUTATIONAL MODELLING OF CONCUSSION Conal Sheridan	79

Friday 16:30-18:20	**Immuno Engineering and Tissue Engineering** Venue: Lough Ree Suite Chairs: Tom Hodgkinson and Meadhbh Brennan	Page
16:30-16:39	3D BIOPRINTING OF ARTICULAR CARTILAGE PROGENITOR CELLS WITHIN A PHYSICALLY CONSTRAINING SUPPORT BATH TO DIRECT NEOTISSUE ORGANIZATION Aliaa Karam	80
16:39-16:48	THE DEVELOPMENT OF AN INJECTABLE HYALURONIC ACID HYDROGEL CONTAINING P2X7R SIRNA NANOPARTICLES FOR THE TREATMENT OF POST-TRAUMATIC TEMPORAL LOBE EPILEPSY Anne O'Callaghan	81
16:48-16:57	A POTENTIAL ROLE FOR OSTEOCYTE DERIVED NLRP3/IL-1ŒÍ IN POST-TRAUMATIC Antonio Franchi	82
16:57-17:06	DEVELOPMENT OF A DUAL-SYRINGE PREMIXED PHOSPHOSERINE-MODIFIED CPC ADHESIVE FOR MINIMALLY INVASIVE BONE REPAIR Antzela Tzagiollari	83
17:06-17:15	INVESTIGATING THE ANTI-TUMOUR RESPONSE OF CD27+ ΓΔT CELLS ON TRIPLE-NEGATIVE BREAST CANCER CELLS Brian Harkin	84
17:15-17:24	METABOLIC MODULATION OF HUMAN MACROPHAGE PHENOTYPE FOR THE PRODUCTION OF EXTRACELLULAR VESICLES FOR BONE REPAIR Cansu Gorgun	85
17:24-17:33	HARNESSING THE CIRCADIAN RHYTHM OF DENDRITIC CELLS TO BOOST NANOPARTICLE UPTAKE TO INCREASE SKIN VACCINE EFFICACY BY DISSOLVABLE MICRONEEDLE Christine Butler	86
17:33-17:42	MESENCHYMAL STEM CELL APOPTOTIC BODIES: WARRIORS AGAINST Fiona Buckley	87
17:42-17:51	IMMUNOMODULATORY EFFECT OF MESENCHYMAL STEM CELL-DERIVED EXTRACELLULAR VESICLES ON DENDRITIC CELLS Hannah Kimingi	88
17:51-18:00	CGAS/STING ACTIVATION AS A MODULATOR OF MACROPHAGE POLARISATION IN OSTEOSARCOMA Jordan O'Donoghue	89
18:00-18:09	A MULTI-FUNCTIONAL GENE-ACTIVATED SCAFFOLD AS AN IMMUNO-MODULATORY PLATFORMS FOR CHRONIC WOUND HEALING APPLICATIONS Juan Carlos Palomeque Chávez	90
18:09-18:18	MESENCHYMAL STEM CELL DERIVED EXTRACELLULAR VESICLES ATTENUATE B CELL ACTIVATION Pamina Ariela Contreras Kallens	91

09:18-09:27	PREDICTING THE PERFORMANCE OF TRANSCATHETER MITRAL VALVE REPLACEMENT FRAMES USING FINITE ELEMENT MODELLING Joshua Barrett	106
09:27-09:36	ADDITIVE MANUFACTURING OF ELECTRO-RESPONSIVE BIO MEDICAL ACTUATOR Cian Bregazzi-Nevin	107
09:36-09:45	IMPLEMENTATION OF LUMPED PARAMETER NETWORK BOUNDARY CONDITIONS FOR THE PATIENT-SPECIFIC CFD SIMULATIONS OF CORONARY ARTERIES IN OPENFOAM Muhmmad Ahmad Raza	108
09:45-09:54	MODELLING THE NON-LINEAR VISCOELASTIC BEHAVIOUR OF BRAIN TISSUE IN TORSION Griffen Small	109
09:54-10:03	EXPLORING THE FEASIBILITY OF EXPERIMENTAL AND COMPUTATIONAL EVALUATION OF ACTIVE DRAG TO AID SWIMMING TECHNIQUE Alexander Haskins	110
10:03-10:12	A SOFT-ROBOTIC BIOMIMETIC BENCHTOP MODEL FOR OESOPHAGEAL MOTILITY SIMULATION Sean Kilroy	111
10:12-10:21	A NEW FIBRE CONSTITUTIVE LAW FOR THE TENSILE AND COMPRESSIVE BEHAVIOUR OF FIBRIN WITH APPLICATION TO ACUTE ISCHEMIC STROKE CLOTS Kila Bein Snee	112
10:21-10:30	MULTI-SCALE MODELLING OF SURFACE GROWTH IN TISSUE Thomas Hayes	113

Saturday 09:00-10:30	**Tissue Engineering II** Venue: Clonmacnoise Suite Chairs: Annie Curtis and Avelino Ferreira	Page
09:00-09:04	GROWVALVE- A PAEDIATRIC HEART VALVE CAPABLE OF GROWTH Eleni Anna Kostopoulou	114
09:04-09:09	MAY THE FORCE SHAPE YOU: HARNESSING PHYSICAL CONSTRAINTS IN MSCS Fernanda Pena Correia	115
09:09-09:13	THE EFFECT OF MELT ELECTRO-WRITTEN SCAFFOLD PORE SIZES ON THE ENGINEERING OF ZONALLY DEFINED ARTICULAR CARTILAGE GRAFTS Max Wirth	116
09:13-09:18	DEVELOPING MECHANICALLY ENHANCED 3D-PRINTABLE BIOINKS FOR BONE REGENERATION Yuanchen Zhu	117
09:18-09:27	DECELLULARISED EXTRACELLULAR MATRICES IN CARTILAGE TISSUE ENGINEERING – A PRELIMINARY STUDY IN USING HUMAN BONE MARROW MESENCHYMAL STROMAL CELLS IN PELLET CULTURES Giovanni	118
09:27-09:36	3D BIOPRINTING PLURIPOTENT STEM CELL-DERIVED VASCULAR NETWORKS Hey Wei Wong	119

09:36-09:45	3D-PRINTING OF ELECTROCONDUCTIVE MXENE-BASED MICROSTRUCTURES IN A BIOMIMETIC TISSUE ENGINEERING SCAFFOLD DIRECTS AND ENHANCES ELECTRICAL Ian Woods	120
09:45-09:54	IN VITRO OSTEOCYTOGENESIS FROM HUMAN BONE MARROW-DERIVED MESENCHYMAL STEM CELLS: TOWARDS A BIOMIMETIC HUMAN BONE-ON-CHIP Luke Madden	121
09:54-10:03	OVX-INDUCED BONE LOSS AT DIFFERENT SKELETAL SITES IN A PRECLINICAL MODEL OF OSTEOPOROSIS Michela Uberti	122
10:03-10:12	PROTEOMIC AND TRANSCRIPTOMIC CHARACTERIZATION OF HUMAN TESTICULAR TISSUE TO INFORM THE DEVELOPMENT OF PRECLINICAL MODELS FOR RESTORING MALE FERTILITY Nasrin Ghanamigashti	123
10:12-10:21	ELUCIDATING THE EFFECT OF DIRECT AND INDIRECT HELIUM COLD ATMOSPHERIC PRESSURE PLASMA ON ADIPOSE DERIVED IMMORTALISED MESENCHYMAL STEM CELLS Sara Alsiyabi	124
10:21-10:30	ADVANCING INTERVERTEBRAL DISC REGENERATION: A COMPARATIVE STUDY OF DUAL MIRNA STIMULATED NUCLEUS PULPOSUS AND BONE MARROW-DERIVED STEM CELLS Tara Ní Néill	125

Saturday 09:00-10:30	**Medical Devices 1** **Sponsored By: BD** Venue: Lough Ree Suite Chairs: Brooke Tornifoglio and Giulio Brunetti	Page
09:00-09:04	DEVELOPMENT OF A TISSUE MODEL REPLICATING THE MICROSTRUCTURE, MECHANICAL RESPONSE, AND VASOACTIVITY OF AGED HUMAN ARTERIAL TISSUE Bhavana Pulipaka	126
09:04-09:09	SIMULATION OF GUIDEWIRE TORQUABILITY Ciaran Cummins	127
09:09-09:13	A FINITE ELEMENT MODEL FOR CRIMPING AND FREE DEPLOYMENT IN THE DESIGN OF BIOABSORBABLE METALLIC CORONARY STENTS Diego Blunda	128
09:13-09:18	COMPUTATIONAL MODELLING OF MULTIVARIABLE CONTROL OF CLOSED-LOOP DEEP BRAIN STIMULATION Seda Aksoy	129
09:18-09:27	A REPLENISHABLE THERAPEUTIC PERITONEAL IMPLANT FOR OVARIAN CANCER Aoibhin Sheedy	130
09:27-09:36	EXOSOMAL CX43 AS KEY PLAYER IN BRAF/MEK INHIBITORS EFFICACY AND DRUG RESISTANCE IN TUMOURS WITH A MUTATION IN BRAF Amanda Guitian-Caamano	131
09:36-09:45	DEVELOPMENT OF AN ACTUATABLE CELL ENCAPSULATION DEVICE Lesley Trask	132

09:45-09:54	EVALUATION OF THE CROSSING FORCES OF A VIBRATING GUIDEWIRE IN CONTACT WITH MODEL CALCIFIED MATERIALS Amir S Rezaei	133
09:54-10:03	USE OF IN-PROCESS MONITORING TO EVALUATE POROSITY GENERATED DURING THE L-PBF PRINTING OF TI-6AL-4V Andrea Villano	134
10:03-10:12	COMPARING SELECTIVE LASER SINTERING AND MULTI JET FUSION PRINT CAPABILITIES FOR DISTAL END LOAD BEARING PROSTHETIC SOCKETS WITH NYLON 12 MATERIAL Erika Dagge	135
10:12-10:21	COMPARATIVE ANALYSIS OF P300 DETECTION ACCURACY IN TRADITIONAL AND HEAD MOUNTED DISPLAY ENVIRONMENTS Muhammad Ahsan Awais	136
10:21-10:30	ESTABLISHMENT OF AN IN-SILICO FRAMEWORK FOR DESIGNING 3D-PRINTED BIOINSPIRED POLYMER HEART VALVE LEAFLETS Celia Hughes	137

Saturday 11:50-13:05	**Mechanobiology 3** Venue: Killinure Suite Chairs: Laoise MacNamara and Mahtab Vafaeefar	Page
11:50-11:54	GELATIN HYDROGEL STIFFNESS INDUCES RESISTANCE OF TRIPLE NEGATIVE BREAST CANCER CELLS TO DOXORUBICIN Charlotte Turner	138
11:54-11:59	RB DILUTION AND MECHANO-OSMOTIC FORCES DRIVE CELL DIVISION: A QUANTITATIVE MODEL Matteo Simeone	139
11:59-12:08	THE ROLE OF LEPTIN ON CARTILAGE END PLATE MATRIX SYNTHESIS AND REACTIVE OXYGEN SPECIES GENERATION Jake McDonnell	140
12:08-12:17	CONSIDERING THE EFFECTS OF DYNAMIC MECHANICAL STRESSES ON TESTICULAR CELL BEHAVIOUR TO INFORM THE DEVELOPMENT OF REPRESENTATIVE PRECLINICAL MODELS Donal O'Mahoney	141
12:17-12:26	INVESTIGATING THE ROLE OF THE BRAIN-MENINGES INTERFACE IN TRAUMATIC BRAIN INJURY Erin Reardon	142
12:26-12:35	THE EFFECT OF SUBSTRATE STIFFNESS ON ASTROCYTES AND LEPTOMENINGEAL CELLS Aisling Greaney	143
12:35-12:44	DEVELOPING HYDROGELS WITH TUNEABLE MECHANICAL AND VISCOELASTIC PROPERTIES TO EVALUATE CORNEA RESIDENT CELLS RESPONSE Matteo Mancini	144
12:44-12:53	BONE-DERIVED VESICLES AND ASSOCIATED MIRNAS: UNRAVELLING NOVEL NANOTHERAPEUTICS FOR BONE REGENERATION Mimma Maggio	145
12:53-13:02	OSTEOPOROTIC BONE CRYSTALLINITY ALTERS OSTEOGENIC DIFFERENTIATION AND MINERALIZATION UNDER ESTROGEN DEFICIENCY WHICH IS EXACERBATED UNDER MECHANICAL LOADING Mostafa Khabooshani.pdf	146

Saturday 11:50-13:05	**Biomaterials I** Venue: Clonmacnoise Suite Chairs: Conor Buckley and Francisco José Calero Castro	Page
11:50-11:54	MULTIFUNCTIONAL COMPOSITE COATINGS FOR RESORBABLE MAGNESIUM IMPLANTS. Chloe McArthur	147
11:54-11:59	DEVELOPMENT AND OPTIMISATION OF L-PBF TI64 LATTICE STRUCTURES WITH SUPERIOR MECHANOBIOLOGICAL INTERACTIONS Merve Yalcin	148
11:59-12:08	FUNDAMENTAL INVESTIGATIONS OF SINTERABILITY OF NOVEL BIORESORBABLE MG-SR-CA Ava Azadi	149
12:08-12:17	DRIVING TENDON DEVELOPMENT: A GENE THERAPY APPROACH WITH CATIONIC CELL PENETRATING PEPTIDES Elaine Gilmore	150
12:17-12:26	IMPROVING THE SUSTAINIBILITY OF MEDICAL DEVICE IMPLANTS Frederick Crowley	151
12:26-12:35	DEVELOPMENT OF ENGINEERED COMPOSITE BIOMATERIAL FOR LOAD-BEARING SUPPORT AND ZONAL REGENERATION OF ARTICULAR CARTILAGE Hadeel Abu Shaqrah	152
12:35-12:44	MULTI-ION DOPED COATINGS FOR CONTROLLED MAGNESIUM IMPLANT CORROSION AND IMPROVED BIOACTIVITY Jonathan Acheson	153
12:44-12:53	BIOPRINTING SHAPE-MORPHING TISSUES USING MAGNETIC BIOINKS Juhi Chakraborty	154
12:53-12:57	MANUFACTURING BIOINSPIRED POLYMERIC HEART VALVE LEAFLET MATERIAL Pratibha Gupta	155

Saturday 11:50-13:05	**Imaging** Venue: Lough Ree Suite Chairs: Eoghan Cunnane and Beatriz Pinheirolopes	Page
11:50-11:54	THE ROLE OF MCT-1 IN TRABECULAR AND SUBCHONDRAL BONE DYNAMICS IN A PRE-CLINICAL EXERCISE MODEL Bridget Twombly	156
11:54-12:03	PREDICTIVE MODELS FOR PROGRESSION OF THE HIP JOINT IN PATIENTS WITH PERTHES DISEASE Hannah Kane	157
12:03-12:12	3D VIRTUAL HISTOLOGY OF ARTICULAR CARTILAGE: MAPPING CHONDROCYTE CHANGES ACROSS POSTNATAL DEVELOPMENT Karin Vancikova	158
12:12-12:21	ASSESSING MOVEMENT OF PERIPHERAL INTRAVENOUS CATHETERS USING DIGITAL IMAGE CORRELATION Roland Surlis	159
12:21-12:30	CAN MRI-QSM BE USED TO CHARACTERISE THE RUPTURE RISK OF HUMAN CAROTID ATHEROSCLEROTIC PLAQUES? Francesco Digeronimo	160

12:30-12:39	EFFECTS OF TYPE 2 DIABETES ON VERTEBRAL BONE MORPHOMETRY IN ZDF RATS: A MULTISCALE CHARACTERIZATION STUDY BY X-RAY BASED NANO-CT IMAGING Wahaaj Ali	161
12:39-12:48	MAPPING GROWTH PLATE DYNAMICS IN GOATS USING MICRO-CT AND HISTOLOGY Mariami Mtchedlishvilli	162
12:48-12:57	USING SINGLE-SEQUENCE MR QUANTITATIVE SUSCEPTIBILITY MAPPING AS A SUBSTITUTE FOR MULTI-CONTRAST MRI FOR THE RISK STRATIFICATION OF CAROTID PLAQUE RUPTURE Jessica Bagnall	163

Saturday 14:50-16:05	**Biomechanics 3** Venue: Killinure Suite Chairs: Krishna Manda and Ryan Coleman	Page
14:50-14:54	MICROMECHANICAL MODELING AND EXPERIMENTAL ANALYSIS OF MAGNESIUM ALLOY WE43 Fatemeh Karamifard	164
14:54-14:59	COMPUTATIONAL DESIGN OF MICROFLUIDIC ASPIRATION DEVICES FOR HIGH-THROUGHPUT ANALYSIS OF TUMOUR CELL BIOMECHANICS Orlaith McSweeney	165
14:59-15:03	THERMODYNAMIC MODELLING TO PREDICT INTRACRANIAL ANEURYSM IN PATIENT SPECIFIC GEOMETRIES Peter McDonagh	166
15:03-15:12	FINITE ELEMENT ANALYSIS INVESTIGATION INTO THE EFFECTS OF STABILIZING AGENT STIFFNESS AND VOLUME ON THE BIOMECHANICS OF THE LUMBAR SPINE. Robert Johnston	167
15:12-15:21	FINITE ELEMENT MODELLING OF HOLLOW MICRONEEDLE INSERTION INTO SKIN Prateek Yadav	168
15:21-15:30	TOWARDS OPTIMIZING TRICUSPID VALVE REGURGITATION: 2D FLUID-STRUCTURE INTERACTION MODELING AND VALIDATION OF SIMPLIFIED HEART VALVE GEOMETRY Muhamed Badawi	169
15:30-15:39	COMPUTATIONAL EVALUATION OF GEOMETRICAL AND PHYSICAL SKULL GROWTH FOR CRANIOSYNOSTOSIS TREATMENT VIA FINITE ELEMENT ANALYSIS Mahtab Vafaeefar	170
15:39-15:48	WRINKLING INSTABILITY OF 3D AUXETIC BILAYERS IN TENSION Sairam Pamulaparthi Venkata	171

Saturday 14:50-16:05	**Disease Models and Biomaterials** Venue: Clonmacnoise Suite Chairs: Caroline Curtin and Cansu Gorgun	Page
14:50-14:54	DEVELOPMENT OF AN OSTEOSARCOMA-ON-A-CHIP DEVICE THAT MIMICS THE OSTEOSARCOMA TUMOUR MICROENVIRONMENT Erick Soloriogonzalez	172
14:54-14:59	STIFF HYDROGEL EXTRACELLULAR MATRIX MODELS MEDIATE PANCREATIC DUCTAL ADENOCARCINOMA CELL INVASION AND CHEMOSENSITIVITY Jan Baguyo	173

14:59-15:03	DEVELOPMENT OF A 3D OSTEOSARCOMA TUMOUR MODEL THAT RECAPITULATES THE BONE EXTRACELLULAR MATRIX AND NON-TUMOUR CELLS OF THE TUMOUR MICROENVIRONMENT Maire Coghlan	174
15:03-15:08	FUNCTIONALISED 3D PRINTED OPEN CELL STRUCTURES FOR TISSUE SCAFFOLD APPLICATIONS Rose Kinneen	175
15:08-15:17	USING MICROFLUIDICS TO FABRICATE HYDROGEL MICROSPHERES CONTAINING TESTICULAR CELLS AT HIGH-THROUGHPUT Jishnu Padacherri	176
15:17-15:26	COMPARATIVE ANALYSIS OF IN VIVO AND EX VIVO MODELS FOR MICROENVIRONMENTAL EFFECTS OF INTERVERTEBRAL DISC DEGENERATION Niamh Wilson	177
15:26-15:35	DEVELOPMENT OF A MICROTISSUE BASED SYNOVIAL JOINT-ON-CHIP Rosario Milazzo.	178
15:35-15:44	CANCER-ASSOCIATED OSTEOBLASTS EXHIBIT MORPHOLOGICAL ABNORMALITIES AND INHIBITED MINERAL DEPOSITION IN AN ENGINEERED BONE METASTATIC NICHE Sarah Nano	179
15:44-15:53	DEVELOPMENT OF A PHOTOCROSSLINKABLE NERVE-DERIVED EXTRACELLULAR MATRIX BIOMATERIAL FOR PERIPHERAL NERVE REPAIR Tugdual Haffner	180
15:53-16:02	IN-SITU QUALITY MONITORING DURING EMBEDDED BIOPRINTING USING INTEGRATED MICROSCOPY AND CLASSICAL COMPUTER VISION Vasileios Sergis	181

Saturday 14:50-16:05	**Medical Devices 2** Venue: Lough Ree Suite Chairs: David Taylor and Soukaina Barroug	Page
14:50-14:59	MEDICAL DEVICE MYSTERIES David Taylor	182
14:59-15:08	3D PRINTED HEART MODELS IN THE PRE-OPERATIVE PLANNING OF DOUBLE OUTLET RIGHT VENTRICLE Ross Foley	183
15:08-15:17	ADVANCING BENCH-TOP PENILE MODELS FOR IMPLANT TESTING Jaleh Amirian	184
15:17-15:26	DEVELOPING COLD PLASMA THERAPIES FOR BONE INFECTION CONTROL Orla Nic Shiurdain	185
15:26-15:35	REDEFINING TAVR MODELLING: A HIGH-FIDELITY FRAMEWORK FOR FLUID-STRUCTURE INTERACTIONS AND IN VITRO VALIDATION Dylan Armfield	186
15:35-15:44	IN-VITRO ORTHOPAEDIC SITE INFECTION MODEL DEVELOPMENT FOR COLD PLASMA ALTERNATIVE THERAPY Soukaina Barroug	187

15:44-15:53	DEVELOPMENT OF A FINITE ELEMENT MODEL TO CAPTURE MECHANICAL DAMAGE IN PENILE TISSUE AND INFORM IMPLANTABLE MEDICAL DEVICE DESIGN Majid Akbarzadeh Khorshidi	188
15:53-16:02	DEVELOPMENT OF VARIABLE DIAMETER COMPLIANCE AND FRICTION – MATCHED SYNTHETIC VESSELS FOR BENCHTOP TESTING Gang Shen	189

Saturday 16:30-18:05	**Biomaterials II** Venue: Clonmacnoise Suite Chairs: Joanna Ward and Juhi Chakraborty	Page
16:30-16:39	DEVELOPMENT OF A MICROFLUIDIC-BASED JOINT-ON-A-CHIP PLATFORM FOR BONE AND CARTILAGE Brian Collins	190
16:39-16:48	PHYSICOCHEMICAL PROPERTIES OF MACROMOLECULAR CROWDING AGENTS AFFECT THE EXTRACELLULAR MATRIX DEPOSITION IN EUKARYOTIC CELL CULTURES Lefki Chaniotaki	191
16:48-16:57	DESIGN OF BIOMIMETIC EXTRACELLULAR MATRIX-BASED BIOINKS FOR BIOPRINTING OF AN INTERVERTEBRAL DISC MODEL Maj Valerie Kersten	192
16:57-17:06	GRANULAR HYDROGEL VISCOELASTICITY PROMOTES PLURIPOTENT STEM CELL MORPHOGENESIS AND ORGANOID FORMATION Orlaith Kennedy	193
17:06-17:15	MULTISCALE PROTEOMIC ASSESSMENT OF BIOPROSTHETIC STRUCTURAL VALVE DEGENERATION AND NATIVE CALCIFIC AORTIC VALVE DISEASE Rachel Cahalane	194
17:15-17:24	EVALUATION OF THE INFLUENCE OF PEEK POLYMER PROCESSING CONDITIONS ON THE PROPERTIES OF 3D PRINTED PARTS Sadhbh Carey	195
17:24-17:33	POLYELECTROLYTE MULTILAYERS FOR BIO-SCAFFOLD APPLICATIONS- A FIRST LAYER INVESTIGATION Sarah New	196
17:33-17:42	CONTROLLED SYNTHESIS OF PLGA NANOPARTICLES IN MICROFLUIDIC CHIPS BY ANALYSING IMPACT OF MIXING PARAMETERS ON NANOPARTICLE PROPERTIES Muhammad Mubashsar Saeed	197
17:42-17:51	3D IN VITRO MODEL OF LUNG CANCER TO STUDY THE PRE METASTATIC NICHE IN LUNG CANCER Vera Almeida	198
17:51-18:00	MODULATION OF OSTEOCLASTOGENESIS BY MESENCHYMAL STROMAL CELL-DERIVED APOPTOTIC BODIES: A RANKL DEPENDENT ROLE IN MONOCYTE DIFFERENTIATION Yeyu Shen	199

Saturday 16:30-18:05	**Tissue Engineering III** Venue: Killinure Suite Chairs: Ciara Murphy and Nasrin Ghanamigashti	Page
16:30-16:34	THE ENGINEERING OF OSTEOCHONDRAL GRAFTS BY SPATIALLY PATTERNING GROWTH FACTORS INTO BATHS OF RADIALLY CONFINED MICROTISSUES Thibault Giordano	200
16:34-16:43	MACROMOLECULAR CROWDING AND HUMAN PLATELET LYSATE REGULATE IN VITRO COLLAGEN DEPOSITION FOR THE DEVELOPMENT OF TENDON TISSUE SUBSTIITUTES Andrea Rossoni	201
16:43-16:52	3D HUMAN SPHEROIDS MODELS OF ADIPOSE TISSUE FOR IMPROVING WOUND HEALING Edward Sander	202
16:52-17:01	A 4D BIOPRINTING PLATFORM TO ENGINEER ANISOTROPIC MUSCULOSKELETAL TISSUES BY SPATIALLY PATTERNING MICROTISSUES INTO TEMPORALLY ADAPTING SUPPORT BATHS Francesca Spagnuolo	203
17:01-17:10	ELUCIDATING THE IMPACT OF MACROMOLECULAR CROWDING AGENT CHEMISTRY ON MESENCHYMAL STROMAL CELL RESPONSE Giulia Giuffredi	204
17:10-17:19	EFFECT OF MECHANICAL STIMULATION ON OSTEOGENIC CAPABILITY OF PRE-OSTEOBLASTS ON A BIOMIMETIC BONE SUBSTITUTES FOR REPAIR Satish Jaiswal	205
17:19-17:28	MACROMOLECULAR CROWDING INCREASES EXTRACELLULAR MATRIX DEPOSITION BY MODULATING IN VITRO COLLAGEN BIOPROCESSING Laura Trujillo Cubillo	206
17:28-17:37	EMBEDDED BIOPRINTING OF PLURIPOTENT STEM CELLS IN GRANULAR SUPPORT HYDROGELS Laura Ventura	207
17:37-17:46	HARNESSING MICRO-X-RAY FLUORESCENCE SPECTROSCOPY AS A TOOL TO ASSESS EXTRACELLULAR VESICLE-INDUCED BIOMINERALISATION Mathieu Brunet	208
17:46-17:55	DEVELOPMENT OF MRNA VACCINES FOR BREAST CANCER IMMUNOTHERAPY USING 3D SCAFFOLDS Na Zhao	209
17:55-18:04	DNA AND MRNA VACCINES FOR NEUROBLASTOMA: DESIGN, DEVELOPMENT, AND THERAPEUTIC TESTING Olga Piskareva	210

Saturday 16:30-18:05	**Medical Devices 3** Venue: Lough Ree Suite Chairs: Bruce Murphy and Irina Khaydukova	Page
16:30–16:39	NOBOCAP: UNLOCKING MDR/IVDR REGULATIONS FOR INNOVATORS IN EUROPE Graham Gavin	211
16:39-16:48	A NOVEL EX VIVO PORCINE MODEL OF LOCALIZED OEDEMA FOR STUDYING SUB-EPIDERMAL MOISTURE Giulio Brunetti	212
16:48-16:57	FINITE ELEMENT MODELLING OF STENT EXPANSION IN THE SUPERIOR VENA CAVA Irina Khaydukova	213
16:57-17:06	BIOACTIVE COATINGS FOR ENHANCED CORROSION RESISTANCE AND BIOFUNCTIONALISATION OF MAGNESIUM MEDICAL IMPLANTS FOR SKELETAL REPAIR Tina Hashemi	214
17:06-17:15	ENHANCING CIRCULATORY LOOP SIMULATION OF RIGHT HEART HYDRODYNAMICS Nikita Belikov	215
17:15-17:24	HIGH PERFORMANCE OPEN SOURCE TOPOLOGY OPTIMISATION SOFTWARE FOR BIOMEDICAL DEVICES Chethana Rao	216
17:24-17:33	NUMERICAL AND EXPERIMENTAL INVESTIGATION OF THE DYNAMIC BEHAVIOR OF VIBRATING NITI GUIDEWIRE Mirmeysam Rafieianamagh	217
17:33-17:42	COMODO: OPEN SOURCE SOFTWARE FOR COMPUTATIONAL (BIO)MECHANICS AND DESIGN Kevin Moerman	218
17:42-17:51	TOWARDS STANDARDISED SIZING STRATEGIES FOR TRANSCATHETER AORTIC VALVE IMPLANTATION IN THE BICUSPID AORTIC VALVE: A PATIENT-SPECIFIC COMPUTATIONAL STUDY Sam Boxwell	219
17:51-18:00	SWELLING BEHAVIOR AND CHARACTERIZATION OF PH-RESPONSIVE HYDROGELS FOR BIOMEDICAL APPLICATIONS Iga Peterson	220

AN AGENT-BASED ARTIFICIAL INTELLIGENCE-DRIVEN DEFORMABLE CELL FRAMEWORK TO UNCOVER THE MECHANISM UNDERLYING MECHANOSENSITIVE TUMOUR GROWTH

Senthilkumar, I.[1, 2, 3], Smeets B.[4, 5], Vangheel J.[4, 5], Howley, E.[1, 3], McEvoy E.[2]
[1] School of Computer Science, University of Galway.
[2] Discipline of Biomedical Engineering, University of Galway.
[3] Data Science Institute, University of Galway.
[4] MeBIOS, Department of Biosystems, KU Leuven, Heverlee, Belgium.
[5] Prometheus, Division of Skeletal Tissue Engineering, KU Leuven, Heverlee, Belgium.
email: i.senthilkumar1@universityofgalway.ie

INTRODUCTION

Tumour growth is a complex mechanosensitive process guided by feedback between cells and the extracellular matrix (ECM). Sensitivity to mechanical cues can influence tumour progression and impact disease outcomes [1]. Critically, the underlying biomechanisms by which external loading impacts tumour growth remain unknown. In this study, we develop an advanced framework consisting of a novel hydromechanical cell growth model, a 3D deformable agent-based framework and a deep-neural network (DNN)-accelerated finite element (FE) solver to uncover these biomechanisms.

Materials and Methods

Hydromechanical Cell Model: Cell growth is driven by a competition between hydrostatic pressure ΔP arising from active cell stress and external loading, and osmotic pressure ΔΠ arising from biomolecule synthesis dX/dt and ion fluxes $dc(\phi)/dt$ [2] (Fig. 1A), such that the osmotic pressure across the cell membrane is given by $\Delta\Pi = RT(\Sigma\Delta c + X/V)$. Cell growth subsequently arises as $dV/dt = -L_p(\Delta P - \Delta\Pi)$.

DNN-FE Acceleration: To simulate the anisotropic hyperelastic mechanical response of a 3D matrix, a novel DNN framework was developed. Synthetic training data was generated from 20,000 Abaqus simulations and was provided to a DNN comprised of 4 layers with 8,192 neurons per layer to obtain a converged solution.

Multicellular Growth: The hydromechanical and DNN-FE models are integrated with MPacts [3], an agent-based framework for multicellular mechanics, where cells are described as fluid-filled foam membranes. Cell growth is achieved by predicting the internal pressure required to attain the target volume. Coupled with tractions from cell and matrix contact, there is feedback in turn to govern the cell growth rate. We consider that mitosis is subject to a volume checkpoint [4].

RESULTS

Cell growth is predicted to increase with biomolecule synthesis and the subsequent increase in osmotic pressure which deforms the surrounding matrix (Fig 1A). Our integrated DNN-FE framework successfully predicts 3D matrix deformation arising from growth with 99.5% accuracy (Fig. 1B, 1C), and improves computational efficiency 1.5 million-fold relative to CPU-based FE analyses (Fig. 1D). The fully coupled cell model predicts that cell proliferation is suppressed in stiff microenvironments whereby cell confinement elevates hydrostatic pressure and restricts cell growth due to fluid loss, preventing cells from reaching the critical volume checkpoint for division (Fig. 1E, F), which spheroid growth and predicted cell volumes aligning with our experimental observations (Fig. 1G, H).

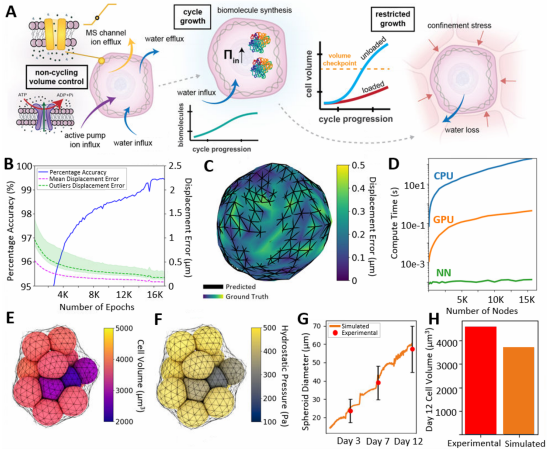

Figure 1 (A) Cell growth and proliferation is regulated by active and passive mechanisms including loading and confinement. (B) The DNN-FE framework converges over 17K epochs. (C) Contour plot of AI prediction versus the ground truth for the matrix deformation. (D) The DNN-FE framework is 1.5Mx faster than CPU-based FE analyses. (E, F) The coupled model shows that T47D cell hydrostatic pressure increases with cell volume, (G, H) aligning with experimental observations.

DISCUSSION

Our innovative model provides a fundamental new understanding into the mechanisms of stress-dependent tissue and tumour growth, which is predicted to arise from a constraint on osmotically driven growth at the cellular level. Cells are unable to attain a critical mitotic size due to mechanical loading, resulting in a reduction of cell volume. Our novel and highly efficient multicellular model gives critical insight into the evolution of tissue development at the cellular level, with broad applications to patient-specific cancer diagnosis.

REFERENCES

[1] Jain, R.K. et al. Annu. Rev. Biomed. Eng., 16 (2014)
[2] McEvoy, E et al. Nat. Commun. 11 (2020)
[3] Cuvelier, M et al. Biophys J, 122:1858-1867(2023)
[4] Varsano, G et al., Cell Reports, 20.2:397-410. (2017)

ACKNOWLEDGEMENTS

This work was supported by the Irish Research Council (GOIPG/2022/910), European Research Council (Grant number 101116234), and DSI at University of Galway.

IDENTIFICATION OF GPR161 AS A NOVEL MECHANOSENSOR IN BONE AND ANTI-CATABOLIC CHRONO-THERAPEUTIC FOR OSTEOPOROSIS

Cobban, M. [1], **Maggio, M.** [1], **Hajiali, H.** [2], **El Haj, A.** [2], **Curtis, A.** [3], **Hokamp, K.** [4], **Roche, F.M.** [4], **Hoey, D.A.** [1]

[1]Trinity Centre for Biomedical Engineering, School of Engineering, TCD [2] Healthcare Technologies Institute, Institute of Translational Medicine, School of Chemical Engineering, UoB [3]Curtis Clock Laboratory, School of Pharmacy and Biomolecular Sciences, RCSI, [4]Institute of Genetics, School of Genetics and Microbiology, TCD *email: cobbanm@tcd.ie*

INTRODUCTION

Osteocytes form a sensory network essential for coordinating bone remodelling/adaptation in response to potent environmental cues such as mechanical stimuli. Mechanosensation is known to occur at key cellular structures such as focal adhesions (FA) and at the primary cilium (PC) [1,2]. However, the molecular components involved in osteocyte mechanotransduction remain unclear. G-protein coupled receptor GPR161 is required for skeletal morphogenesis and has been linked to mechanotransduction in stromal cells [3, 4], yet whether GPR161 is expressed by osteocytes and capable of mechanosensation is currently unknown. Therefore, this study will (1) determine the expression and role of GPR161 in osteocyte physiology/mechanosensing, and (2) determine whether this GPCR may represent a novel therapeutic target to prevent bone loss. Lastly, as many aspects of bone biology display circadian rhythms, this study will (3) explore whether GPR161-mediated osteocyte physiology is regulated by the circadian clock.

MATERIALS AND METHODS

GPR161 expression was verified in osteocytes by RT-qPCR and immunocytochemistry (ICC). GPR161 knockdown (KD) was achieved via siRNA transfection. Mechanical stimulation was applied via a parallel plate flow chamber for oscillatory fluid shear (OFS) (1Pa, 1Hz, 2h), or a magnetic force bioreactor (MICA Biosystems Ltd) with magnetic nanoparticles (MNPs) targeting GPR161 (1Hz, 25-120 mT, 1h). Impact of GPR161 KD and mechanical stimulation was assessed via RNA-sequencing (Novogene). YAP activation was assessed by ICC. Osteoclastogenesis was assessed by treating CD14+ human monocytes with M-CSF and RANKL, with osteocyte-conditioned media (CM). Drug screening identified high-binding compounds (Acetylabs). Circadian synchronisation was achieved with serum starving for 12h and 100nM dexamethasone for 2h.

RESULTS

We showed for the first time osteocytes express GPR161 at an mRNA level, with ICC demonstrating protein co-localisation at the PC and FA (Fig.1A). In controls, OFS osteocytes demonstrated increases in nuclear YAP, COX2, and GPR161, yet decrease RANKL. Upon KD of GPR161, nuclear YAP is no longer mechanoregulated (Fig.1B) and RANKL:OPG expression is significantly decreased independent of OFS (Fig.1C). CM collected from mechanically stimulated osteocytes significantly inhibited osteoclastogenesis while this response was lost upon GPR161 KD (Fig.1D). RNAseq analysis grouped genes involved in 'response to shear stress'. Upon KD of GPR161, these genes are no longer mechanoregulated (in contrast to controls). Interestingly, these genes are also known to be involved in osteoclastogenesis and the circadian clock (Fig.1E).

Directly targeting GPR161 with MNP's demonstrated mechanosensitivity by significantly increasing YAP (Fig.1F) and collected CM inhibited osteoclastogenesis (Fig. 1G), demonstrating direct mechanosensitivity.

AI-based predictive drug targeting to GPR161 identified 4 molecules, among which Drug 2 elicited a upregulation of COX2 (Fig.1H), followed by a decrease in osteoclastogenesis (Fig. 1I) with intermittent dosing.

Osteocyte circadian syncing was demonstrated by cyclic expression of clock genes (Fig.1J), impacting both PC length and GPR161 co-localisation, demonstrating a circadian regulation of this novel sensor (Fig.1K).

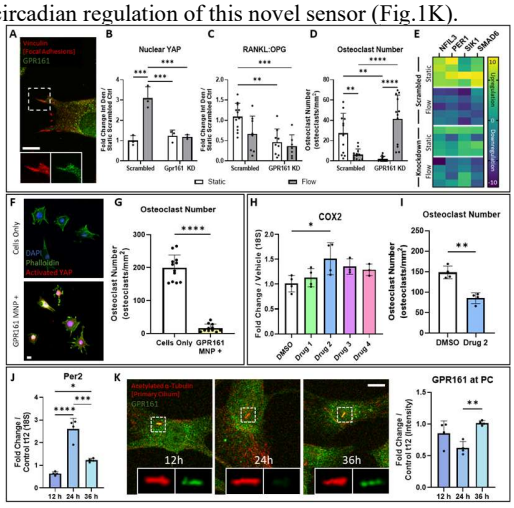

Figure 1 **(A)** ICC of GPR161/FA **(B)** Nuclear YAP expression **(C)** RANKL:OPG PCR **(D)** Quantification of osteoclastogenesis **(E)** Heatmap of RNAseq expression **(F)** ICC of activated YAP **(G)** Quantification osteoclastogenesis following MNP targeting **(H)** COX2 PCR and **(I)** Osteoclastogenesis following drug treatment **(J)** Per2 PCR and **(K)** GPR161-PC localisation following circadian syncing. Scale bars = 10μm

DISCUSSION

GPR161 was shown for the first time to be expressed by osteocytes and utilised in mechanosensing with a critical impact on physiology, downstream paracrine signalling, and the circadian clock. Taken together, these findings highlight GPR161 as a novel mechanosensor and chrono-therapeutic target to pioneer an anti-catabolic treatment for bone disorders.

REFERENCES

[1]Rubin, J. (et al.), Gene 2006 [2]Qin, Y. (et al), Biomedicine & Pharmacotherapy 2023 [3]Hwang (et al.), Development 2018 [4]Johnson, G.P. (et al.), Bone 2021

A TRIP TO ANOTHER DIMENSION – 2D MATERIALS FOR TISSUE REGENERATION AND ADVANCED NEURAL INTERFACES

Maughan, J.[1,2,3], Coleman, J. N.[1,3], O'Brien, F.J.[2,3,4]
[1] School of Physics, Trinity College Dublin
[2] Tissue Engineering Research Group, Royal College of Surgeons in Ireland
[3] Advanced Materials & BioEngineering Research (AMBER) Centre
[4] Trinity Centre for Biomedical Engineering, Trinity College Dublin
jmaughan@tcd.ie

INTRODUCTION

The pages of a book behave very strangely compared to a block of wood – two-dimensional (2D) materials are no different. 2D materials offer unique properties that differ from their bulk counterparts, and this change in dimensionality has the potential to revolutionize biomaterial design. In this work, I develop novel nanocomposite materials and demonstrate how they may be harnessed to advance nerve and bone regeneration strategies, and to create innovative neural interfacing devices. Focusing primarily on pristine graphene and 2D boron, this work showcases the wide-reaching impact of these versatile materials.

RESULTS & DISCUSSION

In the first study, graphene was applied to the challenge of neural medical device development, with a focus on using electroactive graphene composites to enhance the regenerative properties of electrical stimulation of neural tissue[1]. A soft, conductive, and biocompatible collagen-graphene composite material (NeuroGraph) was developed, with diverse fabrication capabilities into scaffolds, microneedles, and bioelectronic circuits. Electrical stimulation of neurons on NeuroGraph substrates significantly enhanced neurite outgrowth, demonstrating its potential as a promising biomaterial platform for electroconductive tissue regeneration.

Building on this, the graphene formulation was further refined for biocompatibility and conductivity, and a flexible, biocompatible polymer-graphene composite system was developed by combining the optimised graphene formulation with polycaprolactone (PolyGraph)[2]. The electrochemical properties of this material were then enhanced by surface roughening with NaOH, and coating with conductive AuPd. This enabled the creation of flexible, high-performance microelectrode neural interfaces with significant potential for applications in both electrical stimulation therapies and bidirectional neural interfacing.

Finally, building on the experience gained in developing 2D nanocomposite biomaterials, boron nanoplatelets exfoliated from a non-layered precursor using liquid-phase exfoliation were combined with collagen to form collagen-boron (BColl) scaffolds[3]. By leveraging the 2D morphology of the nanoplatelets, alongside the intrinsic bioactivity of boron and support of a collagen matrix with biophysical characteristics tailored for bone repair, these scaffolds were shown to enhance osteogenesis, angiogenesis, and neurogenesis, while also providing immunomodulatory, antimicrobial and reinforcing properties. Taken together, these results showcase the potential of 2D boron nanoplatelets to offer multifunctional benefits to clinically relevant aspects of next-generation bone biomaterial development.

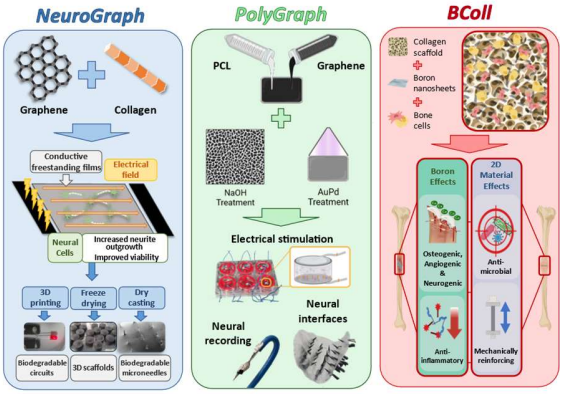

Figure 1 – 2D nanocomposites for tissue engineering and neural interfacing devices. This works demonstrates the groundbreaking therapeutic potential of 2D nanocomposites by producing collagen-graphene neural stimulation substrates (NeuroGraph), PCL-graphene microneedle neural interfaces (PolyGraph) and 2D boron-collagen bone tissue engineering scaffolds (BColl).

CONCLUSIONS

2D materials and their composites present unique opportunities for the fabrication of novel biomedical devices, thanks to the diverse properties enabled by their dimensionality. This work demonstrates the development of biomaterial platforms with enhanced electroconductive, immunomodulatory and osteogenic properties, highlighting the future promise of these materials in regenerative and augmentative medicine.

REFERENCES

1) Maughan et al., *Collagen/Pristine Graphene as an Electroconductive Interface Material for Neuronal Medical Device Applications*, Applied Materials Today 29 101629, 2022.
2) Maughan et al., *Biocompatible and Electrically Optimised Polymer-Graphene Composites for Neural Interfacing Devices*, manuscript under preparation.
3) Maughan et al., *Boron Nanoplatelets as an Osteogenic, Anti-Microbial, Mechanically Reinforcing Additive for Biomaterial Scaffolds for Bone Repair*, submitted to Advanced Functional Materials, 2024

4D BIOPRINTING SHAPE-MORPHING HEART TISSUES IN GRANULAR SUPPORT HYDROGELS: SCULPTING STRUCTURE AND GUIDING MATURATION

Pramanick, A [1,2], Hayes,T [2], Sergis,V [2], McEvoy,E [2], Pandit,A [1], Daly A.C [1,2]
[1] CÚRAM – Research Ireland Centre for Medical Devices
[2] Biomedical Engineering, University of Galway, Ireland
email: andrew.daly@universityofgalway.ie

INTRODUCTION

During embryogenesis, organs undergo dynamic shape transformations that sculpt their final shape and function [1,2]. Despite this, current organ bioprinting approaches typically employ bioinks that restrict cell-generated morphogenetic behaviours, resulting in structurally static tissues. This restricts embedded cells from initiating and engaging in self-organising behaviours that are essential for evolution into functional tissues [3]. To address this limitation, we developed a novel platform that enables the bioprinting of tissues that undergo programmable and predictable 4D shape-morphing driven by cell-generated forces. To do this, we employed embedded bioprinting to deposit ECM-based bioinks in yield-stress support hydrogels that can locally fluidise to accommodate tissue shape-morphing. We systematically investigated how cell-generated forces influence shape evolution across multiple tissue geometries and explored how these shape-morphing behaviours could impact the maturation of bioprinted iPSC-derived heart tissues.

METHODS

Embedded bioprinting was used to deposit bioinks (collagen & hyaluronic acid) into granular agarose support hydrogels. To investigate their impact on tissue shape-morphing, we varied the bioink cell density, cell type, collagen concentration, and support hydrogel viscoelasticity. Finite element modelling (FEM) was used to predict tissue shape-morphing and to evaluate internal stress. Cell and ECM organisation in the shape-morphing tissues was analysed through confocal imaging and immunofluorescence staining using the FIJI OrientationJ plugin. Induced pluripotent stem cell (iPSC) -derived heart tissues were bioprinted using co-cultures of iPSC-cardiomyocytes & cardiac fibroblasts (7:3 ratio, 20 million/ml cell density). Tissue maturation was analysed through immunofluorescence staining, PCR arrays, & contractility analysis.

RESULTS & DISCUSSION

Following deposition into the support hydrogels, bioprinted constructs (closed and open geometries) underwent significant shape change during culture (Fig.1a). Importantly, the extent of tissue shape-morphing behaviour was tunable through bioink composition, with increased tissue shape-morphing observed for higher cell densities, lower collagen concentrations (Fig 1b) and in softer support gels. Interestingly, we also observed that shape-morphing influenced internal cell-ECM organisation, with alignment emerging along the principal tissue axis (Fig 1c). FEM revealed that significant active stresses developed within the shape-morphing tissues during culture, and cell-ECM alignment mirrored the model-predicted principal strain directions within the morphing tissue (Fig.1c). Next, we observed that shape-morphing enhanced the maturation of bioprinted iPSC-derived heart tissues compared to static controls, with improved structural alignment of iPSC-cardiomyocytes, higher expression of cardiomyocyte maturation markers (SCN5A, GJA5, GJA1), & elevated contraction amplitudes (Fig.1d). Finally, we demonstrated the platform's versatility by bioprinting anatomically accurate double ventricle heart constructs (Fig.1e).

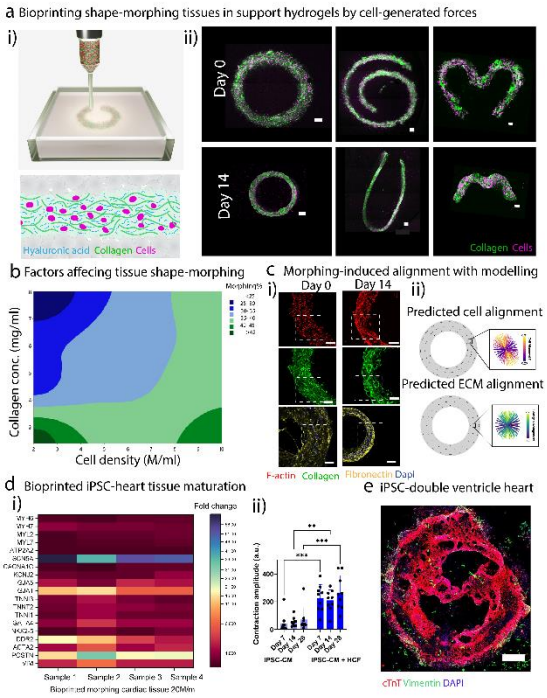

Figure 1 a (i) Schematic representation of embedded bioprinting to fabricate shape-morphing tissue, and (ii) confocal imaging of bioprinted tissue at day 0 and day 14 as it undergoes shape-morphing. **b** Contour plot demonstrating the factors affecting the extent of morphing. **c** Emergence of morphing-induced cell and ECM alignment through (i) confocal imaging, and (ii) modelling prediction. **d** (i) Transcriptomics profile, and (ii) contraction amplitude analysis of bioprinted morphing iPSC-heart tissue compared to static control. **e** Confocal imaging of bioprinted iPSC-double ventricle heart tissue on day 14.

CONCLUSION

Our 4D bioprinting platform facilitates the fabrication of tissues capable of programmable and predictable shape-morphing driven by cell-generated forces. Importantly, we demonstrate that this cell-mediated shape-morphing can sculpt internal cell and ECM alignment, offering a novel approach for programming anisotropy and maturation in bioprinted organ rudiments.

REFERENCES

[1] F. Xiong, et al., *Cell* **2014**, *159*, 415.
[2] G. A. Stooke-Vaughan, O. Campàs, *Current Opinion in Genetics & Development* **2018**, *51*, 111.
[3] A. C. Daly, et al., *Cell* **2021**, *184*, 18.

INVESTIGATION OF THE IMPACT OF STORAGE CONDITIONS ON THE MICROSTRUCTURE AND MECHANICS OF ADIPOSE TISSUE: IMPLICATIONS FOR BREAST TISSUE

Strong, O.[1, 2], Tornifoglio, B.[1, 2]
[1] Trinity Centre for Biomedical Engineering, Trinity Biomedical Sciences Institute, Trinity College Dublin [2] Department of Mechanical, Manufacturing and Biomedical Engineering, Trinity College Dublin
email: strongo@tcd.ie

INTRODUCTION

The choice of preservation method can influence the microstructure and mechanical integrity of biological tissues. Crude freezing (-20°C) can result in the formation of large ice crystals causing damage to cellular structures. Snap freezing, which employs liquid nitrogen (-196°C), minimises ice crystal formation by rapidly cooling the tissue [1]. Cryopreservation utilises cryoprotectants and extremely low temperatures to preserve the microstructure and mechanical properties of the tissue by preventing ice crystal formation and cellular damage [2]. Refrigeration (4°C) is suited primarily for short-term storage, as it decelerates cellular degradation without fully inhibiting it.

Mechanical testing is beneficial for assessing the structural integrity of biological tissues, including adipose tissue. By evaluating parameters such as stiffness, elasticity and strength, mechanical testing can provide an insight into the extent to which tissues maintain their mechanical and microstructural integrity under various storage conditions. Identifying a storage method that best preserves the mechanical and microstructural properties ensures the tissue's viability for research applications where maintaining native tissue functionality is crucial. Particularly, when human tissue is being collected to investigate novel biomarkers of disease, these considerations are of the utmost importance. However, in order to evaluate and identify such a biomarker, tissue handling and storage needs to be optimised.

The current study aims to determine the optimal storage protocol to retain microstructural and mechanical integrity of adipose tissue, which has direct implications for the collection and investigation of novel biomarkers in breast tissue.

MATERIALS AND METHODS

Fresh and crude frozen (-20°C) samples (n=5 per group) of porcine abdominal adipose tissue were used for mechanical testing. Each sample was approximately 5 mm in thickness, measured using the Mitutoyo Litematic VL-50. Indentation tests, with an indenter diameter of 2.5 mm, were carried out using a Zwick testing machine equipped with a 10 N load cell. A preload of 0.005 N was applied to the tissue, five preconditioning cycles from 0% to 10% strain, and then 50% compression at 1 mm/min. The stress (σ) was determined using the formula:

$$\sigma[kPa] = \frac{F\ [N]}{a\ [mm^2]} * 1000$$

where, F is the force and a is the cross-sectional area of the indenter. The modulus of each sample was calculated from the slope of the stress-strain curve (initial range: 5%-10% strain; final range: 40%-50% strain). Significance was tested using a parametric t-test, where $p<0.05$ is considered significant.

RESULTS

Figure 1 illustrates stress versus strain for both groups. The average initial moduli were found to be 7.66 ± 1.93 kPa and 8.38 ± 2.09 kPa for the fresh and crude frozen samples, respectively. The average final moduli were found to be 46.09 ± 28.88 kPa and 42.58 ± 17.4 kPa for the fresh and crude frozen samples, respectively. No statistical significance was found between either moduli for the two groups.

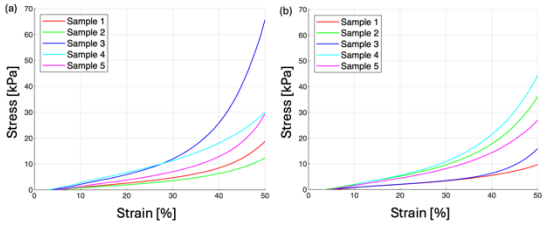

Figure 1 Stress versus strain graphs for (a) fresh and (b) crude frozen samples.

DISCUSSION

Initial mechanical testing results of porcine adipose aligns with prior indentation studies on human breast tissue [3]. The results suggest there is no significant impact from crude freezing on the mechanical properties of the adipose tissue.

Future work will investigate alternative storage methods, including cryopreservation and snap freezing, with histological analysis to assess microstructural changes. The current study will identify the optimal storage protocol for adipose tissue, which will facilitate the preservation of human breast tissue. This tissue will then be examined using non-invasive imaging to investigate the microstructure of dense breast tissue, and ultimately, the potential for novel breast cancer biomarkers.

REFERENCES

[1] van der Wijngaart *et al*., Cancer Medicine, 12: 10979-10989, 2023
[2] Jungare *et al*., Materials Today, 136: 897-910, 2022
[3] Umemoto *et al*., Ultrasound in Med. & Biol., 40(8): 1755-1768, 2014.

IMPACT OF MORPHOLOGICAL DETAIL ON MITRAL VALVE MECHANICS: CONTRASTING HIGH-RESOLUTION μCT-BASED MODELS WITH SIMPLIFIED PARAMETERIZED APPROACHES

Mehari Abraha, H[1], Javadpour S[1], O'Brien FJ[1,2,3], Conway, C[1,2]

[1]Department of Anatomy & Regenerative Medicine, Royal College of Surgeons in Ireland (RCSI), Dublin, Ireland

[2]Trinity Centre for Biomedical Engineering (TCBE), RCSI & Trinity College Dublin, Dublin, Ireland

[3]Advanced Materials and Bioengineering Research Centre (AMBER), RCSI & Trinity College Dublin, Dublin, Ireland

Corresponding author email: hyabmehariabraha@rcsi.com

Introduction

Mitral valve (MV) pathology represents a significant cardiac health challenge, with mitral regurgitation alone impairing physical function, quality of life, and longevity for over 24.5 million patients globally[1]. However, due to limitations in in-vivo imaging resolution, achieving high-resolution 3D reconstructions of the MV remains challenging. Consequently, computational simulations of MV mechanics often fall short in accurately capturing the valve's morphological variations[2]. This study introduces a comparative methodology that integrates high-resolution μCT-based models (obtained ex-vivo) with simplified, parameterized MV models to assess how each approach represents the influence of morphological variation on valvular mechanics. By employing finite element analysis (FEA), we investigate how model resolution affects predictions of leaflet stress and deformation. This approach highlights the impact of anatomical simplification on accurately capturing the complex mechanics of the MV.

Materials and Methods

This study uses ex-vivo iodine-enhanced μCT to capture the gross morphology of MVs in geriatric cadaveric hearts (n=5, ages 89-100). After embalming with a solution of methylated spirits, glycerol, formaldehyde, and phenol, samples were stained by immersion in potassium triiodide[3]. The MVs resected from the left heart, mounted with suture on a custom 3D-printed holder, and immersed in olive oil[4]. Scanning was conducted on a Nikon CT scanner with 39-46 μm resolution (190 kV, 130 μA, 1 fps). The resulting μCT data was processed in 3D Slicer (v5.03) for 3D reconstruction through semi-automatic and manual segmentation. To create parameterized simplified models, measurements were taken from the scanned MVs and used as input data for a published toolbox for creating simplified mitral geometries[5], with a uniform leaflet thickness of 1 mm. For all models. The ANSA pre-processor (v23.1.2, BETA Simulation Solutions, USA) and Abaqus (v2023 Dassault Systèmes, USA) were used for meshing (solid tetrahedral elements, 0.6 mm edge length) and model solving. Models incorporated unbranched chordae as truss elements, isotropic hyperelastic leaflets[6], and applied diastolic (8 mmHg) to systolic (120 mmHg) pressure loading, with fixed annulus and papillary posts. Analysis focused on comparing principal stress maps.

Results

High-resolution models displayed detailed stress variations, especially around thicker regions, while simplified models produced smoother stress maps **(Figure 1)**. Maximum reported von Mises stresses ranged between 0.76MPa and 5MPa for all models, which is within range of previously reported values (0.75-5.36 MPa[7]). However, simplified models showed higher maximum principal stress concentrations than their to anatomically detailed counterpart **(Figure 1)**.

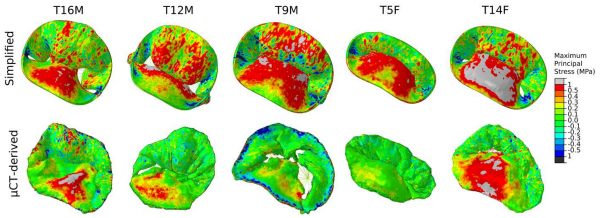

Figure 1: Maximum principal stresses found in simplified parameterized (first row) vs high resolution μCT derived (second row) finite element models of geriatric male (M) and female (F) mitral valves (n=5) at mid-systole.

Discussion

These MV models provide anatomically detailed reconstructions, capturing complex chordal attachments and variable leaflet thicknesses consistent with healthy adult measurements (annular area: 70-120 mm²)[8]. Initial FE models achieved partial coaptation, validating their physiological relevance. However, simplified models with uniform 1 mm leaflet thickness showed higher stress concentrations compared to anatomically detailed models, suggesting that simplified models may overestimate stresses. Future work will incorporate μCT-informed branched chordae and anisotropic leaflet properties, aiming to enhance model accuracy and support developments in MV prosthesis design.

References

1. Coffey et al., Nature Reviews Cardiol, 18 (12):p.853–864, 2021.
2. Baillargeon, et al., Eur J Mech A Solids, 48:p. 38–47, 2014.
3. Stephenson et al., Sci Rep, 7(1): p. 7188, 2017.
4. Stephens et al., Exp Mech, 61(1): p. 253–261, 2021.
5. deOliveira et al., Comput Biol Med, Epub, 2021
6. Prot et al., J Mech Behav Biomed Mater, 3(1): p. 167–177, 2010.
7. Gaidulis et al., Ann. of Biomed Eng, 50(7), 847–859, 2022
8. Dal-Bianco et al.,*Cardiol Clin*, 31 (2), p. 151–164, 2013

Acknowledgements

Funding: Science Foundation Ireland 20/FFP-P/8588

SYNERGISTIC EFFECT OF CALCIFICATION AND STRUCTURAL DAMAGE DRAMATICALLY REDUCES LIFETIME OF PORCINE PERICARDIUM USED IN BIOPROSTHETIC HEART VALVE LEAFLETS

Guerin, L.[1], Hughes, C. [1,2,3], Burke, R. [3], Campbell, E. [3], Growney, E. [3], Lally, C. [1,2,4]
[1] Trinity Centre for Biomedical Engineering, Trinity Biomedical Sciences Institute, Trinity College Dublin
[2] Department of Mechanical, Manufacturing and Biomedical Engineering, School of Engineering, Trinity College Dublin, Dublin 2, Ireland
[3] Structural Heart Division, Boston Scientific Corporation, Galway, Ireland,
[4] Advanced Materials and Bioengineering Research Center (AMBER), Trinity College Dublin, Dublin 2, Ireland
email: lguerin@tcd.ie

INTRODUCTION

Aortic stenosis (AS) is characterised by the narrowing and stiffening of the aortic valve, and restricts blood flow from the heart to the rest of the body. Severe AS is a common and life-threatening condition, affecting 1.48% of individuals aged 55 and older, with a four-year mortality rate of 44.9% if left untreated [1,2]. Minimally invasive treatment for AS involves the implantation of a bioprosthetic valve with porcine or bovine pericardium leaflets. These leaflets eventually succumb to failure due to regurgitation or stenosis, caused by calcification and structural damage [3]. The relationship between these two durability-limiting processes is debated. Current commercial anti-calcification treatments utilise protective chemistry alone, ignoring leaflet mechanics and treating calcification as independent from structural damage. The aim of this work is to investigate and establish the relationship between calcification and structural damage of porcine pericardium (PP), and to identify screenable tissue features which minimise both factors.

MATERIALS AND METHODS

Commercial grade PP was screened for its collagen fibre architecture using small angle light scattering (SALS) and separated into highly aligned (HA) and highly dispersed (HD) groups based on average fibre alignment across each sample. Tissue was loaded in the presence of calcification solution using a bi-directional bulge inflation rig for 30 million cycles, see *Figure 1(A)*. Structural damage and calcification were quantified at 0, 5, 10, 20, and 30 million cycles using digital image correlation and μCT imaging, respectively. Calcified and damaged samples were compared to uncalcified PP loaded under the same conditions.

RESULTS

By 30 million cycles, 16 samples ruptured in PP exposed to simultaneous calcification and structural damage. Fibre architecture of the tissue influenced its durability, with HA PP rupturing at a faster rate than HD PP when exposed to calcification and structural damage, see *Figure 1(B)*. No ruptures were observed in PP with the same loading conditions which were not exposed to calcification, nor were differences between HA and HD tissue observed. Rupture did not always occur at the most calcified region of the samples, but instead appeared to be co-located in areas with radially oriented collagen fibres, see *Figure 1(C)*.

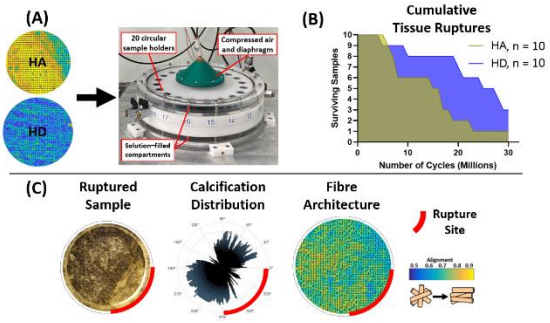

Figure 1 (A) Tissue loaded for 30 million cycles using bi-directional cyclic bulge rig [4], (B) Samples with HA fibre architecture fail sooner than those with HD fibre architecture, (C) ruptures occur in as little as 5 million cycles when calcification is present during loading, with the location influenced by collagen fibre orientation and not calcification distribution alone.

DISCUSSION

The results of this study suggest that calcification and structural damage are synergistic factors dramatically affecting bioprosthetic valve leaflet durability. This is evidenced by the high number of ruptures when PP is simultaneously calcified and loaded and none when only cyclic loading is present. While the overall presence of calcification leads to rupture, calcification and failure site are not always co-located. Instead, collagen fibre orientation appears to determine the failure site. Overall collagen fibre architecture of PP influences the likelihood of failure when exposed to damage and calcification, with HA samples failing at a faster rate during the study. The findings suggest that high collagen fibre alignment in PP bioprosthetic valve leaflets could lead to premature device failure if not aligned to support the dominant loading direction. Future work will investigate the influence of spatially varying collagen fibre architecture and calcification distribution on PP stresses and strains using finite element analysis.

REFERENCES

[1] Strange, G.A. et al., Open Heart, 2022
[2] Généreux, P. et al., 2023. J. Am. Coll. Cardiol., 2023
[3] Blackman, D.J. et al., J. Am. Coll. Cardiol., 2019
[4] Whelan, A. et al., J Mech. Behav. Bio. Mater., 2021

A VISCOELASTIC FINITE ELEMENT MODEL OF INTERPENETRATING NETWORK HYDROGELS

Varatharajan, P[1,2], Kelly, D.J.[1], Manda, K.[2]
[1]Trinity Centre for Biomedical Engineering, Trinity College Dublin, Dublin 2, Ireland
[2]School of Mechanical and Aerospace Engineering, Queen's University Belfast, Belfast BT9 5AG, Northern Ireland, United Kingdom
email: (varathap@tcd.ie)

INTRODUCTION

While single network hydrogels are widely used in the field of tissue engineering, their application is often limited by poor mechanical properties. To overcome this, interpenetrating network (IPN) hydrogels have been proposed [1], potentially enabling the development of constructs with mechanical properties comparable to load-bearing tissues such as articular cartilage. Realising this goal can be enabled by the development of computational tools capable of modelling the complex viscoelastic behaviour of these biomaterials, this study assesses a time-dependent material model through inverse finite element analysis (i-FEA) to describe the mechanical behaviour of IPN hydrogels. Later, these models will be used in designing fibre reinforced IPNs that mimic the mechanical properties of natural cartilage.

MATERIALS AND METHODS

The unconfined stress relaxation experiment data of IPN hydrogel (3.5% w/v alginate – 5% w/v GelMA) reported in the study by Schipani et al. [2] was utilised for i-FEA. Initially, a 10% strain was applied for 500 seconds, followed by constant loading for 2500 seconds. The compressive force was employed as the objective function, and the least squares approach was followed to fit the experimental force with the simulation. FEBio, an open-source finite element solver, was used to simulate the unconfined stress relaxation tests.

RESULTS

In the viscoelastic (VE) model, the Prony series was used to describe the time-dependent behaviour of the hydrogel, especially for representing the relaxation modulus. The i-FEA procedure was performed in FEBio with a four-parameter VE model. Initial estimates for transient stiffness coefficients (G_1, G_2, G_3, G_4), relaxation times (τ_1, τ_2, τ_3, τ_4), equilibrium modulus (E), and Poisson ratio (ν) were provided. The initial run with the provided input parameters took around 82 hours (on a quad-core computer with 24 GB of RAM) to complete, resulting in an R^2 value of 92%. The second run took 45 hours based on the updated parameters from the first run and achieved an improved R^2 value of 96%. Finally, with further refinement of the parameters, an R^2 value of 98.9% was attained in the third run (27 hours). The considered four parameter VE model showed a good fit (R^2=0.96) with the experimental data for the 10% compression. The fitted experimental relaxation force-time data with the 4-parameter viscoelastic model is shown in Figure 1.

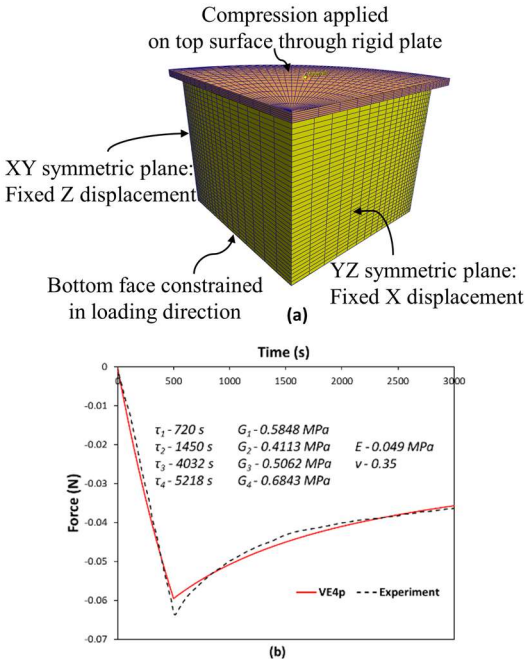

Figure 1 Stress relaxation (a) simulation performed in FEBio (b) IPN hydrogel data fitted with the four-parameter VE model.

DISCUSSION

The proposed VE model predicted the stress-relaxation behaviour of IPN hydrogels very accurately up to 30% strain with a step of 10% strain per cycle. However, at higher strain levels, the model's prediction becomes less accurate. This may be due to the limitation of the VE model that it does not account for poroelastic effects like the strain-dependent fluid flow in the hydrogel. The VE model primarily accounts for the intrinsic time-dependent behaviour of the hydrogel's solid phase only. To overcome this, future work will investigate other time-dependent material models like poro-viscoelastic and poro-hyper viscoelastic models, which can better describe the mechanical behaviour of hydrogel even under higher strain conditions.

REFERENCES & ACKNOWLEDGEMENT

[1] Du *(et al.)*, International Journal of Biological Macromolecules 266:131259, 2024. [2] Schipani *(et al.)*, Biofabrication 12:035011, 2020.

Funding: North-South Research Programme (NSRP) CARTREGEN (Strand I: Researcher to Researcher)

Towards a sex-specific understanding of traumatic brain injury biomechanics

Mishra, A., MacManus, D.B.
University College Dublin

INTRODUCTION

Traumatic brain injury (TBI) is a multi-anatomical-scale mechanical injury affecting 30 million women globally each year[1,2]. This work focuses on the sex specific biomechanics of TBI in the young adult population (18-25 years old) motivated by the highest reported incidence of TBI in people under the age of 25 years old. However, women remain underrepresented in TBI research, despite reporting worse symptoms, and having longer recovery periods with prolonged symptom durations compared to men[3].

Finite element brain models (FEBMs) have revolutionised our understanding of TBI biomechanics. However, the majority of FEBMs have been developed using single subject male-only data, limiting our understanding of TBI biomechanics to the adult male demographic. This is a major gap in TBI knowledge as there are statistically significant differences in total grey[6] and white[4,5] matter across male and female brains even after correcting for brain size. There are also region-specific volumetric differences showing increased grey matter volume in women ranging between 12.8-23.2% increase depending on cortical region[6]. It is hypothesized these region-specific differences in grey matter and white matter thickness along with volumetric differences of subcortical regions could explain the significant alterations in the biomechanics, location, and severity of TBI between male and female brains. Therefore, adult male FEBMs alone cannot describe the sex and age specific biomechanics of TBI in the female population.

Here, the progress towards the development of sex specific FEBMs is detailed. A pipeline for the construction of morphologically averaged, age and sex specific brain model templates is introduced. Preliminary results of the sex specific morphology and model development are then presented.

MATERIALS AND METHODS

Sex specific morphologically averaged brain templates were constructed using the Queensland Twin IMaging (QTIM) dataset[7] of over 1000 young adults aged 18-30 years. The dataset features fMRI/MRI images taken on a high resolution 4T scanner[7]. MRI scans of 50 individual female and 50 individual male participants in the age range of 18-22 years old were selected for this study. The pipeline begins by pre-processing the MRI images using FreeSurfer[8], an open-source software suite for analyzing and segmenting brain tissue. FreeSurfer performs operations including artefact cleanup and motion correction and produces a skull stripped intermediate 'brainmask' file that is used to construct the template. Statistical Parametric Mapping 12 (SPM12)[9] is then used to obtain a measure of intracranial volume inclusive of the CSF and meninges. The 'brainmask' files for 50 subjects of one sex and age-range are then used to construct a non-biased template brain using Advanced Normalization Tools (ANTs)[10], a neuroimage processing software. The output from this is then fed back to FreeSurfer to construct final fully segmented sex specific three-dimensional brain models. Using the volumetric information from the morphologically averaged brain templates, the normalised volumes of 19 subcortical regions were compared between the male and female templates using Student's t-test.

RESULTS

19 subcortical regions of the brain from 50 male and female subjects were normalized against brain volume. Paired t-tests showed significant statistical differences in 8 regions including thalamus and white matter with results being consistent with existing literature. These results highlight the importance of developing sex specific MRI templates and FEBMs to advance our understanding of brain mechanics and disease.

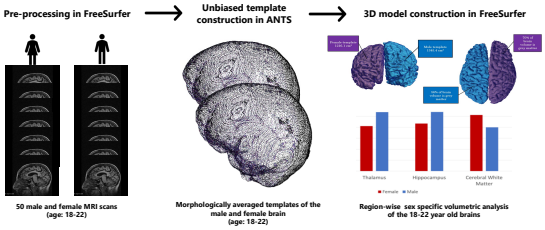

Figure 1 Pipeline for construction of sex specific MRI and 3D brain model generation.

REFERENCES

1. Biegon, *Front Neurol*. 12:576366, 2021.
2. Mollayeva (*et al.*), *Concussion Lond Engl,* 3(1):CNC51, 2018
3. Gupte (*et al.*), *Journal of Neurotrauma*, 36(22):3063–3091, 2019.
4. Passe (*et al.*), *Prog Neuropsychopharmacol Biol Psychiatry*. 21(8):1231-1237, 1997.
5. Cosgrove (*et al.*), *Biol Psychiatry*. 62(8):847-855, 2007.
6. Luders (*et al.*), *J Neurosci*. 29(45):14265-14270. 2009.
7. Strike LT (*et al.*), *Cerebral Cortex,* 29(3):952-962, 2019.
8. Fischl, *Neuroimage*, 62(2):774-81, 2012
9. Frackowiak (*et al.*), *Human Brain Function*. Academic Press USA, 1997.
10. Avants (*et al.*), *Penn Image Computing and Science Laboratory*. 1-35, 2009.

BIVENTRICULAR HEART MODEL WITH NOVEL PSEUDO-FLUID DOMAINS AND THERMODYNAMICALLY-MOTIVATED GROWTH & REMODELING

Senthil, D.[1], Concannon, J.[1], Coleman, R. J. [1], McGarry, P.[1]
[1] Discipline of Biomedical Engineering, University of Galway
email: d.senthil1@universityofgalway.ie

INTRODUCTION

A common flaw in existing finite element (FE) models of the heart is the unphysical specification of pressure or volume boundary conditions on the myocardium wall to represent the effect of the ventricle. Ventricular pressure and deformation result from active contractility of the myocardium, and should be predicted model outputs, rather than prescribed boundary conditions. To overcome this deficiency without resorting to computationally expensive fluid-structure interaction (FSI) approaches, we propose a novel FE-based approach to modelling a biventricular heart. We utilize custom user-defined materials (UMATs) to model the active contractile myocardium and we develop novel "pseudo-fluid domains" to represent blood in the right (RV) and left (LV) ventricles. To predict short and long-term cardiac Growth and Remodelling (G&R), we develop a thermodynamically-motivated growth model to predict changes in cardiac myocyte morphology to simulate tissue growth. This novel approach ensures ventricle volume and pressure are predicted model outputs.

MATERIALS AND METHODS

MRI images of healthy human hearts are processed using a custom workflow to automatically create a 3D patient-specific biventricular mesh (Fig 1A). Our myocardium material model incorporates the hyperelastic matrix as well as the anisotropic collagen and myofibres, and actively contracting cardiac myocytes [1]. A custom "pseudo-fluid" UMAT is developed to determine ventricle volume and pressure changes in response to the actively contracting myocardium. During systole, pressure and volume changes in each ventricle are governed by a Windkessel formulation that incorporates aortic (LV) or pulmonary (RV) compliance and the peripheral resistance. We integrate a novel thermodynamically-motivated G&R formulation to predict cardiac remodelling. Equation 1 shows the construction of the growth deformation gradient, $\boldsymbol{F_g}$.

$$\frac{d\boldsymbol{F_g}}{dt} = \omega_g \left\{ \exp\left(\beta_g\left(\hat{G}_H - \hat{G}_{tot}\right)\right) - 1 \right\} (\boldsymbol{f} \otimes \boldsymbol{f}) \quad (1)$$

Where $\hat{G}_H$ is homeostatic Gibbs' Free Energy, ω_g is growth rate, β_g is thermodynamic temperature representing growth based on energy differences and $\boldsymbol{f}$ is a given direction. We use the rate of entropy change given by the Clausius-Duhem inequality to predict changes in cardiac myocyte aspect ratio as well as stress fibre and sarcomere formation.

RESULTS

Contour plots of our model demonstrating the apicobasal shortening & twist observed in clinical literature are shown in Fig. 1B. To demonstrate the predictive capabilities of our model, a simulation of Inferior Vena Cava Occlusion (IVCO) over 7 cardiac cycles was conducted. The computed pressure-volume (PV) loops are shown in Fig. 1C. The model correctly predicts reductions in stroke volume (SV), end-systole pressure, and end-diastole pressure in both ventricles over a series of cardiac cycles.

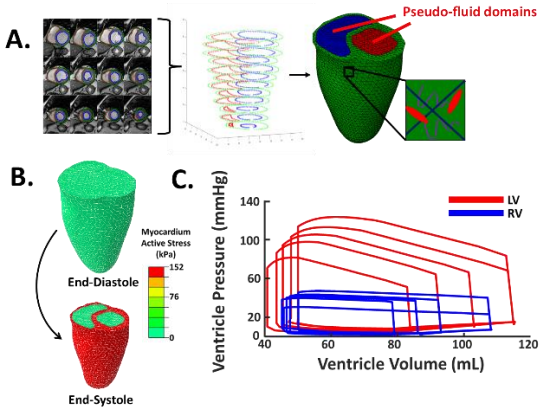

Figure 1 **(A)** Construction of 3D patient-specific meshes from MRI stacks; **(B)** Contour plots showing the model shape and computed myocardium active stress during end-diastole and end-systole; **(C)** Computed PV loops for the LV (red) and RV (blue) over a 7-cycle simulation of IVCO.

DISCUSSION

The authors are unaware of a previous FE framework that has captured the complex PV patterns present during IVCO for both ventricles simultaneously. It is also worth noting that conducting this 7-cycle simulation required only 3.5 hours on a standard desktop using our novel "pseudo-fluid" approach, which is several orders of magnitude faster than conventional FSI methods [2]. This highlights the diagnostic potential of our model in predicting real-time patient health.

REFERENCES

1. Concannon *et al*., Acta Biomater,125: p. 154-171, 2021
2. Seemann *et al*., J Cardiovas Magn Reson,. 25(1): p. 1., 2023
3. Gao, H., et al., Med Engr & Physics, 47: p. 128-136, 2017

Hexagonal Boron Nitride Nanosheets Enable the Formation of Artificial Membrane Channels

Qian, X.[1]
[1] Biomedical Engineering, University of Galway, Galway, Ireland
email: xuliang.qian@universityofgalway.ie

Introduction

Understanding the interactions between nanomaterials and biological systems, e.g., cellular membranes, is fundamental for addressing important challenges to the development of nanomedicines and safe application of nanotechnology. Nanomaterials may interact with plasma membranes prior to cellular uptake and with intracellular vesicle membranes following uptake, accompanied by multiple interaction mechanisms. In this context, systematic investigations on the pathological responses and molecular mechanisms are of key importance to the safe design, application, and regulation of novel engineered nanomaterials, in particular, two-dimensional (2D) nanomaterials. To date, most of the available data have been accumulated from studies on graphene-based materials - size and shape influence the materials' interaction with cell membranes. However, little is known about the biological interaction of other emerging 2D materials, for example, hexagonal boron nitride (hBN). In this abstract, we aim to answer some most immediate questions: How do hBN nanosheets with different shapes interact with lipid membranes? What is the driving force for such interactions? Could we harness such interactions for practical applications?

Results

Through simulations and experiments, we demonstrated that hBN nanosheets can induce artificial water channels across the lipid membrane. Two different shapes of hBN flakes - a round hBN (r-hBN) and a cornered hBN (c-hBN) with similar sizes - were simulated. Orders of magnitude difference were seen in the energy barrier for round and sharp hBN flakes to penetrate a lipid bilayer. We revealed that c-hBN nanosheets with sharp corners can penetrate lipid membranes spontaneously, whereas r-hBN cannot exhibit such behavior. In all sharp c-hBN simulations, artificial membrane channels are formed spontaneously along the pierce polar edges and remain stable once formed. The driving force of artificial membrane channel formation is that water molecules aggregate around a polar edge of a c-hBN to reduce the total free energy—validated via the free energy perturbation (FEP) method. Our in vitro experiments have provided comprehensive confirmation of these findings.

Discussion

Beyond a pure scientific discovery, our findings may have general implications and similar hydrophilic channels may exist in all binary or multi-element 2D materials if they have polar edges. Fast transportation of water molecules across the lipid bilayer is expected. Such artificial membrane channels can also be designed to be "smart" and tunable. For example, by functionalizing the material's polar edge and controlling its shape and thickness, the resulting channel can be controllably opened or closed, or designed to open to a certain degree, thus achieving tunable permeability of the target membrane. Our discovery suggests a range of opportunities for further study, for instance, strategies to achieve molecular transportation along the channel, such as drug delivery, and 2D-material-based anticancer therapy.

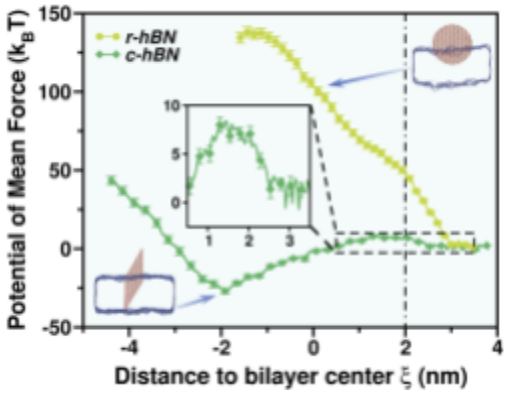

Figure 1 Potential of Mean Force (PMF) profiles of hBN piercing the lipid bilayer versus the distance between the lower tip of hBN and bilayer center. **Insets:** zoom-in view of the PMF for c-hBN within the dashed-line box; configurations of r-hBN (top right) & c-hBN (bottom left) piercing the bilayer.

References

Lucherelli *et al.*, Adv. Mater., 33: 2103137, 2021
Hu *et al.*, J. Cell Biol. 221: e202109133, 2022
Visani de Luna *et al.*, ACS Nano,17:24919-24935, 2023

A SYSTEMATIC REVIEW OF CORROSION STUDIES AND PROPOSED IMPROVEMENTS

McCallion, A.[1], Brown, A.[1], Acheson, J.[1], Ward, J.[1]
[1] School of Engineering, Ulster University, Belfast, UK
email: mccallion-a22@ulster.ac.uk

INTRODUCTION

As the average age of the population continues to increase, so too does the number of age-related conditions requiring intervention using a form of implant. The UN reports that by 2080, the number of persons aged 65+ will outnumber those under 18[1], which will further exacerbate the burden on healthcare systems.

Resorbable implants have gained interest within the orthopaedic field as temporary fixation devices, to reduce the need for secondary surgeries[2]. Magnesium (Mg) alloys are a popular material choice for these implants, due to advantages including a similar elastic modulus (~45 GPa) and yield strength (modulus 5-23 GPa) to cortical bone [3], leading to a reduction of stress shielding[4], as well as its biocompatibility[5]. However, Mg has a low corrosion resistance within electrolytic and aqueous environments, accelerating its corrosion rate *in vivo*. Therefore, it is of high importance to tailor the surface characteristics of Mg and measure the corrosion rate through corrosion studies.

Immersion, hydrogen evolution and electrochemical potential studies[6] are methods commonly utilised to measure the corrosion rate of Mg. Although, variations in these studies are present from author to author[7]. This leads to ambiguity in the results as *in vivo* conditions are not always accurately represented. Thus, there is a need to standardise corrosion studies to allow *in vivo* conditions to be replicated as best as possible, so that degradation profiling and corrosion rate calculations are accurate.

MATERIALS AND METHODS

The systematic literature review focused on the identification of variables found in corrosion studies, common differences in setups were highlighted. To streamline the search, parameters including 'magnesium implants' and 'corrosion rates' were used to gain relevant information. Search databases used to obtain sources included Scopus, EBSCO and Google Scholar.

Once differences have been recognised and relevant *in vivo* parameters identified, methods for improving corrosion analysis, to move towards a more standardized approach can be generated.

RESULTS

Important factors that are similar across corrosion studies include temperature and pH of immersion media. Current corrosion studies tend to set these to be as close to *in vivo* conditions as possible i.e. temperature is set to 37°C and pH around 7.4 to represent that of blood.

Variables that differ between corrosion studies include the type of immersion media used, surface area to volume ratio, dynamic vs static conditions of media, ion concentration and inclusion of protein/organic components. Many corrosion studies often lack dynamic aspects such as fluid flow, gas exchange or agitation within their analysis[7].

DISCUSSION

Choice of media and surface area to volume ratio differ significantly across studies leading to varying corrosion rates and outcomes.

To further improve corrosion studies, dynamic setups should be designed to allow fluid flow, gas exchange and agitation to occur as this will better represent *in vivo* conditions. Agitation is an important variable due to the multitude of mechanical stresses that occurs within hard and soft tissue. These include torsion from daily movements or increased compressive forces from surrounding capillaries and cells[8], which can lead to accelerated corrosion of the implant. The proposed setup for dynamic corrosion be seen in Figure 1.

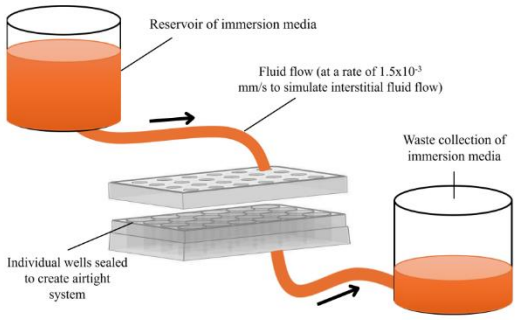

Figure 1 Dynamic corrosion setup for the replication of interstitial fluid flow.

REFERENCES

1. United Nations, World Population Prospects 2024: Summary of Results, 2024.
2. Tsakiris (*et al*), Journal of Magnesium and Alloys, 9 (6): 1884–1905, 2021.
3. Bairagi (*et al*), Journal of Magnesium and Alloys, 10 (3): 627–669, 2022.
4. Bandyopadhyay (*et al*), Progress in Materials Science, 133:101053, 2023.
5. Khorashadizade (*et al*), Journal of Materials Research and Technology, 15:6034–6066, 2021.
6. Mei (*et al*), Corrosion Science, 171:108722, 2020.
7. Esmaily (*et al*), Progress in Materials Science, 89:92–193, 2017.
8. Liu (*et al*), Frontiers in Bioengineering and Biotechnology, 10, 2022.

THE SCIENCE OF SPLIT ENDS: BIOMECHANICAL INVESTIGATIONS OF THE FRACTURE OF HAIR

Yale, A.[1], Barton, E.[1], Marty, G.[2], Santoprete, R.[3], Taylor, D.[1]
[1] Trinity College Dublin, Ireland
[2] L'Oreal, Paris, France
email:yalea@tcd.ie

INTRODUCTION

Split ends is a common hair defect, prevalent in people with long hair and those who frequently use treatments (bleaching, colouring, straightening etc). The science behind split ends is poorly understand and, until now, no method had been developed to create splitting in a laboratory experiment.

Swift (1997) proposed that splits occur as a result of the shear stresses generated when hair containing knots and tangles is brushed, causing high-stress regions to propagate along the hair strand. Hair is made from keratin fibres and is highly anisotropic. We hypothesised that age and treatments work to increase this anisotropy, making failure by longitudinal cracking more likely that transverse fracture. We aimed to develop a test machine to split hairs in a controlled manner and to compare the performance of different hair types, treatments, etc.

MATERIALS AND METHODS

Figure 1 shows the principle of our test, which we call the Moving Loop Fatigue Test. Two hairs are looped together (similar to a link in a chain). A weight is suspended from the ends of the lower hair whilst the ends of the upper hair are moved backwards and forwards, thus propagating the loop repeatedly along the full length of the upper hair.

Different hair types were tested, of different ethnicities (straight Caucasian hair and curly African hair), including a person suffering from spit ends.

RESULTS

We successfully created splits in all hair types tested. Crucially, hair from the split-ends sufferer formed splits which initiated in the middle of the hair strand and propagated long distances (fig.2a). By contrast control samples formed splits which began from the surface and propagated at a shallow angle (fig.2b).

The number of cycles to failure was significantly affected by the applied weight, varying from 1 to over 1000 cycles as the weight was reduced from 26g to 5g. As fig.1 shows, hair from the split-ends sufferer failed in relatively few cycles compared to the control. Significant differences were also found between ethnicities (curly hair was weaker than straight hair) and also following wetting, bleaching and heating with tongs.

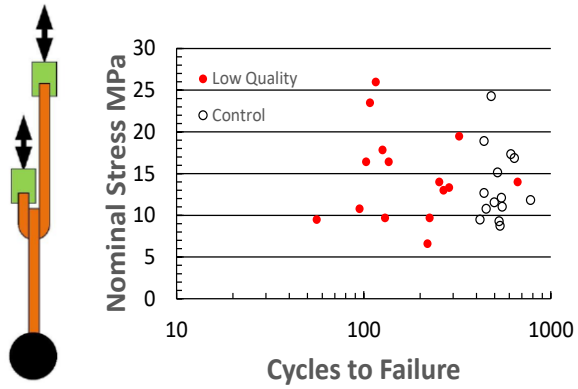

Figure 1: The Moving Loop Fatigue Test: results comparing Low Quality (splitting) hair with Control (both being straight, Caucasian hair types): cycles to failure for an applied force of 14g.

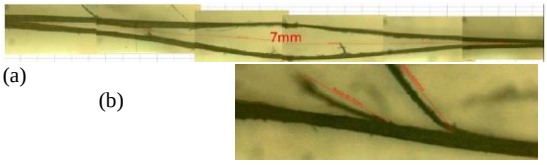

Figure 2: Examples of splitting (a) long, central split, (b) short side splits.

DISCUSSION

Interestingly, the differences between the Low Quality (splitting) and Control hair seen in fig.1 were not reflected in their tensile strengths, which were the same. This proves our hypothesis that splitting is caused not by a general reduction in strength but by an increase in anisotropy, likely caused by weaking of the bonds that join fibrous units together. For those interested in more details, some of the work described here has recently been published (Taylor et al 2024)

REFERENCES

Swift, J.Cosmetic Science 48 123-126 1997.
Conference Proceedings:
Taylor *et al*, J.Roy.Soc.Interface Focus 14(3) 2024

MICROSTRUCTURAL EVOLUTION AND PERFORMANCE OF LPBF TI-6AL-4V LATTICE STRUCTURES UPON HOT ISOSTATIC PRESSING

Thadayil, A[1]. Farhadi, A[2]. Keaveney, S[2]. Dowling ,D.P [1]. Celikin, M[1]
[1] SFI, I-Form Advanced Manufacturing Research Centre, School of Mechanical and Materials Engineering, UCD, Belfield, Dublin 4
[2]Croom Medical, Co. Limerick, Ireland, V35 YD39[2] Institution of second author
email: ajai.kavunkarathadayil@ucdconnect.ie

INTRODUCTION

Laser Powder Bed Fusion (LPBF) has emerged as a transformative technique for producing complex Ti-6Al-4V lattice structures with significant applications in aerospace and biomedical fields. Enhancing the fatigue performance of components, especially in load-bearing biomedical implants subjected to cyclic loading, requires refined microstructures and effective porosity control.

Integrating LPBF with Hot Isostatic Pressing (HIP) offers a solution to these challenges by reducing detrimental porosity, optimizing microstructural properties, and improving mechanical performance[1]. It aids in promoting bimodal microstructure (α + β), which offers superior fatigue performance compared to the α' martensitic phase typically observed in as-printed Ti-6Al-4V [2].

This study investigates the combined effects of LPBF and HIP on Ti-6Al-4V components featuring shell-core lattice structures with retained powder before HIP. During the HIP process, the retained powder consolidates under intense pressure and temperature, eliminating the need for full melting during LPBF. This approach significantly reduces laser energy consumption and fabrication time, offering enhanced sustainability and reduced manufacturing costs.

MATERIALS AND METHODS

The samples were fabricated using LPBF with a Body-Centred Cubic (BCC) lattice structure, featuring a fixed strut diameter of 0.5 mm. The unit cell sizes are varied within a cylindrical core, resulting in samples with powder content ranging from 0% to 90%. This variation influenced the volume density of the lattice in the internal shell structure. Following LPBF, the as-built components underwent HIP at 820°C for 2 hours at 170 MPa, followed by uniform rapid cooling. During HIP, the retained powder consolidated, achieving a densification level of approximately 60%, with an error margin of 0.05% based on previous studies [3]. Porosity levels in the retained powder region were quantified using X-ray computed tomography (X-ray CT) and analysed in detail through scanning electron microscopy (SEM) images with ImageJ software. Microstructural/Structural characteristics were further examined using SEM, optical microscopy, and X-ray diffraction (XRD). Micro strain analysis was performed using Hall's method, based on the XRD data. Vickers microhardness testing was conducted under a 200 g load (HV 0.2) for 15 seconds in accordance with ISO 6507-1 standards.

RESULTS AND DISCUSSION

X-ray CT and SEM analysis show that the porosity in the retained powder region after Hot Isostatic Pressing (HIP) is reduced to 0.2–0.3%, which is comparable to fully additive-manufactured components but with significantly reduced production time and laser energy consumption. The HIP process effectively densifies the material, eliminating harmful random porosity while ensuring strong bonding at the powder-shell interface.

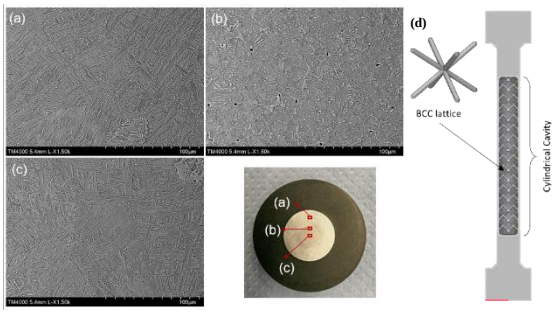

Figure 1 SEM images of HIP-ed cylindrical sample with 90% powder fraction : (a) Shell region (b) Lattice spoke (c) Powder region, (d) Sample Schematic

Microstructural analysis reveals the presence of columnar grains in the shell region and equiaxed grains in the powder region, with seamless integration between the two, ensuring mechanical integrity. XRD analysis indicates variations in crystallographic orientation and residual stresses, along with the evolution of the β-phase in the HIP-treated samples. Micro strain analysis further reveals the optimal powder volume to be 40–60%. Microhardness measurements showed that the powder region had lower hardness compared to the shell region after HIP, consistent across most samples.

This approach presents sustainable and economic advantages for biomedical applications, as it reduces manufacturing lead times while producing high-performance components with enhanced mechanical properties.

REFERENCES

[1].Simonelli, M et al. Journal of Materials Research, pp. 2028–2035, 2014.
[2]. Brika, S.E. et al. Additive Manufacturing, 2020.
[3]. Leuders, S. et al. International Journal of Fatigue, pp. 300–307, 2013.

REGENERATE : A PEPTIDE NANOPARTICLE LOADED NANOGEL FOR ACCELERATED WOUND HEALING

Saha, C.[1], Sun,Y.[1], Gilmore, E.J.[1], McErlean, E.[1], Dunne, N.[2], McCarthy, H.O.[1]
[1]School of Pharmacy, Queen's University Belfast, Belfast, Northern Ireland, United Kingdom
[2] School of Mechanical & Manufacturing Engineering, Dublin City University, Dublin, Republic of Ireland
email: c.saha@qub.ac.uk

INTRODUCTION

Wound healing is a dynamic biological process involving haemostasis, inflammation, proliferation and remodelling.[1] Disruptions in these phases, often exacerbated by comorbidities such as aging, obesity, and diabetes, can lead to delayed healing and chronic wound development, which affects over 2.2. million people in the UK alone. This presents a significant burden on the health care systems, costing the NHS approximately £5.3 million annually. Conventional chronic wound treatments primarily focus on infection control through frequent, labour intensive and expensive dressing changes. Consequently, there is a growing demand for innovative dressings, including smart dressings and targeted approach. MicroRNAs (miRs) are key post transcriptional regulators, that influence pathways critical to cell migration, cell proliferation and angiogenesis. miR-31 has been associated with upregulation of vascular endothelial growth factor-A, promoting angiogenesis and revascularisation of the wound bed. It also aids in keratinocyte migration facilitating re-epithelisation. miR-132 modulates polarisation of macrophages towards anti-inflammatory (M2) which is essential for reducing inflammation and initiating tissue repair. Both miRs contribute to reducing pro inflammatory factors via influencing the NF-κB pathway which otherwise perpetuates chronic inflammation in non-healing wounds.[2] In this study, a 15 aa linear peptide, CHAT, was utilised to encapsulate these miRs into nanoparticles. The CHAT peptide efficiently facilitates intracellular delivery of nucleic acid cargo *in vitro* and *in vivo*.[3] These peptide nanoparticles were loaded into a polyvinyl alcohol (PVA) based antimicrobial hydrogel to provide an effective self-administrable treatment for chronic wound management.

MATERIALS AND METHODS

CHAT peptide nanoparticles were formulated and characterised for size, zeta potential, and polydispersity index (PDI) using dynamic light scattering (DLS). Encapsulation efficiency was assessed via RiboGreen reagent. *In vitro* transfection efficiency was evaluated in NCTC-929 cells using flow cytometry. Optimised nanoparticles were incorporated into PVA-based hydrogel prepared using physical cross-linking through freeze-thaw cycles. The hydrogel was characterised for swellability, spreadability, viscosity, and rheological properties. Nanoparticle release from the hydrogel and subsequent functionality were evaluated fibroblast cells using flow cytometry and RT-PCR. Nanogel formulations were further tested in an *ex vivo* porcine skin graft model for antimicrobial efficacy. The therapeutic efficacy was assessed in a C57BL/6 mouse model. Wound healing outcomes, including angiogenesis, epidermal thickness, and wound closure, were evaluated through histological analysis of tissues and organs using haematoxylin and eosin (H&E) staining.

RESULTS AND DISCUSSION

Characterisation of the PVA based gels showed that gels with 10% PVA with 3h of 1-Freeze thaw cycle yielded in a gel with optimal swellability, spreadability and rheological (elasticity, viscosity) characteristics when compared with a commercial control (Fig. 1A). CHAT nanoparticles were formulated and were <100 nm in size and with a positive zeta potential (Fig. 1B i) resulting in successful transfection in NCTC-929 fibroblast cells with negligible cytotoxicity. CHAT/miR nanoparticles released from nanogels showed 75% cargo release (Fig. 1B iii) and positive functionality via *in vitro* transfection in NCTC-929 cells (Fig. 1B iv-v) and elevated the expression of target miRs such VEGF-A. CHAT nanoparticle loaded nanogels accelerated wound closure in mice model (Fig. 1C) and had positive effect on keratinocyte proliferation, migration, and angiogenesis.

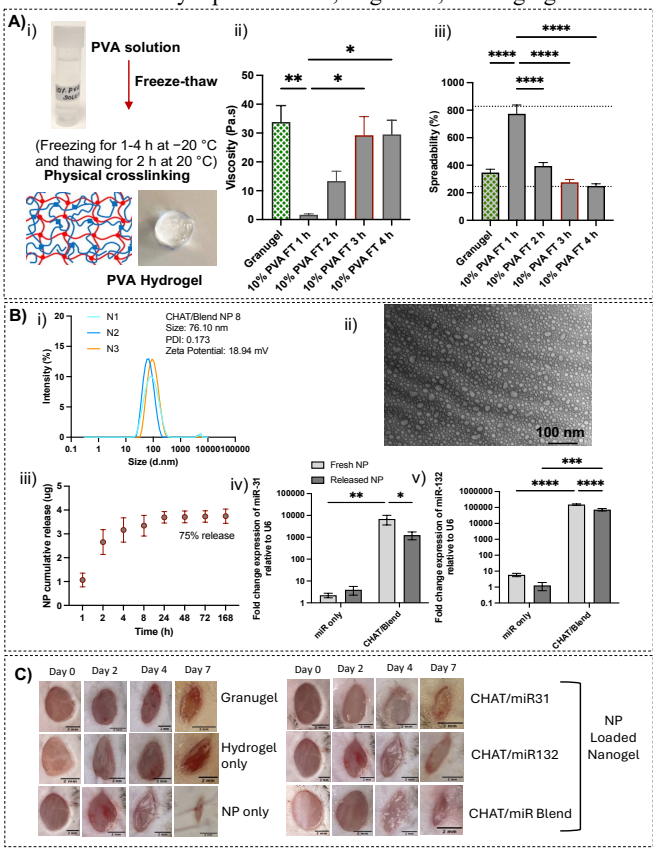

Figure 1: A) Formulation and characterisation of PVA hydrogel: i) Mechanism used for Hydrogel formulation; ii) Viscosity; iii) Spreadability; of PVA based hydrogel. B) Characterisation of CHAT/miR NP: i) Mean hydrodynamic size, PDI and zetapotential; ii) TEM image; iv) Cumulative release from nanogel; iv) and v) Elevated expression of miR-31 and miR-132 after *in vitro* transfection of released NPs in NCTC 929 cells. C) Results from the *in vivo* wound healing study.

CONCLUSION

PVA based-nanogel, thus demonstrated remarkable potential in accelerating the wound healing process. The promising results from *ex vivo* and *in vivo* models highlight its therapeutic efficacy and applicability, offering a novel approach to address the challenges of chronic wound management and improve patient outcomes.

REFERENCES

1. Xu *(et al.),* Advanced Healthcare Materials Vol. 9: e1901502, 2020.
2. Bombin *(et al.),* Acta Biomater Vol.155:304-22, 2023.
3. McErlean *(et al.),* Journal of Controlled Release Vol. 330:1288–99, 2021.

DEVELOPMENT OF CARTIFIX – TISSUE SPECIFIC ECM-DERIVED SCAFFOLDS FOR OSTEOCHONDRAL DEFECT REPAIR

Browe, DC[1,2], Buckley, CT.[1,2] , Kelly, DJ[1,2]
[1] Altach Biomedical Ltd.
[2] Trinity Centre for Biomedical Engineering, Trinity Collage Dublin
email: d.browe@altach.health

INTRODUCTION

Altach Biomedical Ltd (Altach), a Trinity College Dublin (TCD) spin-out are developing a biomimetic scaffold "CartiFix" derived from the extracellular matrix (ECM) of articular cartilage (AC- predominately type II collagen) and bone that allows for a regenerative cartilage repair in a single stage procedure. CartiFix targets the treatment of osteochondral (OC) defects that penetrate into the subchondral bone and if untreated can progress to osteoarthritis. The CartiFix scaffold is designed to be used stand alone or in conjunction with other cell-based therapies. The scaffold's unique composition creates a matrix for the patient's own cells to migrate into and regenerate cartilage and bone. CartiFix is the world's first scaffold which is manufactured using the ECM derived entirely from the joint tissues it is aiming to regenerate; specifically articular cartilage and bone. The cartilage phase of the scaffold consists primarily of type II collagen, which is the primary building block of native knee cartilage; therefore, CartiFix provides the best possible natural environment for cartilage regeneration.

MATERIALS AND METHODS

Tissue fragments (AC and Bone) are treated using a series of chemical and enzymatic washes to remove cellular components, solubilised using pepsin, purified (salting process and dialysis) and finally lyophilised for storage.

Scaffolds are fabricated by solubilising the prepared ECM in acetic acid and mixing with glyoxal (a chemical crosslinking agent). The solution is cast into moulds and subjected to a freeze-drying process to impart a porous structure designed to facilitate cellular infiltration and direct neo-tissue organization. Porous scaffolds are subjected to a secondary crosslinking step termed dehydrothermal (DHT) treatment and stored for sterilisation.

RESULTS

The key novelty of CartiFix lies in using tissue-specific bi-layered ECM-derived scaffolds (derived from cartilage and bone ECM) for the repair of damaged tissues. Key features of Altach's ECM-based scaffold technology includes:

- Only commercial scaffold derived from tissue specific ECMs
- Scaffold contains biological cues to enhance innate repair
- Single stage procedure
- Large and aligned pores for enhanced cellular infiltration and recapitulation of native tissue architecture
- Restores hyaline like cartilage
- Efficacy already proven proof-of-concept animal model

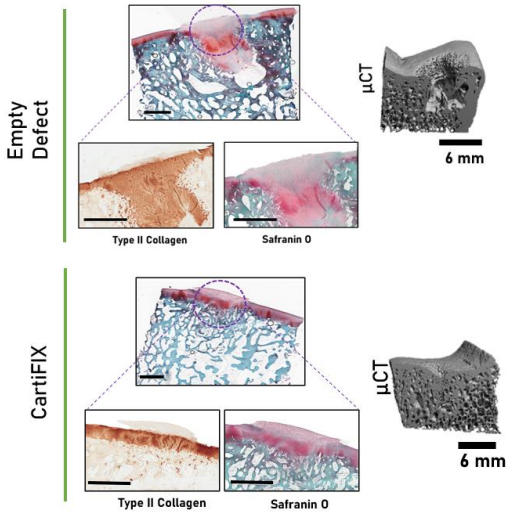

Figure 1 Evaluation of repair tissue after 6 months in a caprine pre-clinical model. CartiFIX (AC+Bone ECM) scaffolds were fabricated and implanted in a goat OC defect model (6mm x 6mm). Repair was evaluated after 6 months. Safranin-O histological staining and type II collagen immunohistochemistry was performed to evaluate the newly formed cartilage matrix in both the empty defect control group and CartiFix scaffold group. 3D µCT reconstructions of the osseous layer demonstrate improve bone regeneration.

DISCUSSION

Altach's scaffold technology represents a promising clinical option for the repair of osteochondral defects which could be used as a standalone scaffold or could be used in combination with autologous cells or growth factors to enhance repair.

REFERENCES

Browe, David C., *et al.* Acta Biomaterialia 143 (2022): 266-281.

SELENIUM AND MAGNESIUM FUNCTIONALISED SCAFFOLDS FOR DUAL BONE REGENERATION AND ANTI-CANCER THERAPY

Pakenham, E.[1], Kaur, K.[1,2], Lee, T.C.[1], Curtin, C.[1,3,4], Murphy, C.M.[1,3,4]

[1]Department of Anatomy and Regenerative Medicine, Royal College of Surgeons in Ireland (RCSI), Dublin, Ireland. [2]School of Pharmacy and Biomolecular Sciences, RCSI, Dublin, Ireland, [3]Trinity Centre for Biomedical Engineering, Trinity College Dublin, Dublin 2, Ireland [4]Advanced Material and Bioengineering Research (AMBER) Centre, Trinity College Dublin, Dublin, Ireland

email: (eavanpakenham23@rcsi.com)

INTRODUCTION

Bone related cancers defects are difficult to treat due to disrupted bone formation and bone resorption inhibiting regeneration[1], and the risk of recurrence from residual cancer cells. Incorporation of bioactive ions into biomaterials has gained remarkable attention for bone regeneration. Magnesium (Mg) is capable of modulating bone resorption and formation to promote bone repair[2]. Selenium (Se), has shown positive results as a cancer therapeutic exhibiting pro-oxidant and apoptosis-inducing effects against cancer cell lines[3]. Nano-hydroxyapatite nanoparticles (nHA) are excellent candidates for ion delivery as their crystal structure can accommodate ionic substitution. This project will utilise nHA for the dual delivery of Mg and Se to inhibit bone resorption, augment bone formation and obliterate cancer cells. Specific aims of this project include developing and characterising combined Se and Mg functionalised nHA to augment the therapeutic effects of these ions followed by Se/Mg-nHA particles being incorporated into a collagen-based scaffold to develop a multifunctional bone regenerative and anti-cancerous scaffold for the treatment of bone cancer defects.

MATERIALS AND METHODS

A range of Se, Mg and combined Se/Mg functionalised nHA particles (0 - 50 mM) were developed and characterised. Physiochemical characterisation included FTIR, ELS and DLS analysis. RAW-264.7 cells, mesenchymal stem cells (MSCs) and prostate cancer (LNCaP) cells were cultured in 2D with the concentration range of nanoparticles to determine the cytotoxic limits of the ions, using quantitative assays such as Alamar Blue™ and Pico Green™. Collagen-nHA scaffolds loaded with the functionalised nHA nanoparticles were fabricated and biocompatibility of the ion-loaded scaffolds is currently being carried out.

RESULTS

Se, Mg and Se/Mg were successfully incorporated into nHA nanoparticles (Figure 1A-C). FTIR spectra shows characteristic peaks of nHA at 560, 602 and 1019cm^{-1} with additional peaks observed with incorporation Se, Mg and Se/Mg into nHA (Figure 1A). DLS and ELS displayed optimal size and charge of the ion-functionalised nHA (Figure 1B&C). A concentration dependent effect of all three nHA groups was observed in both osteoclast and MSC activity. The highest concentration, 50mM, significantly reduced osteoclast activity in all groups. 1-10mM Mg-nHA significantly increased osteoclast proliferation. However, Se countered this effect in the Se/Mg-nHA group by Day 3, with no increase in proliferation observed between Day 3 and Day 7 (Figure 1D). MSC proliferation was inhibited at 25-50 mM in all groups (Figure 1E). Combination of Se/Mg-nHA significantly upregulated MSC proliferation at lower concentrations (1-10mM) compared to Se or Mg alone.

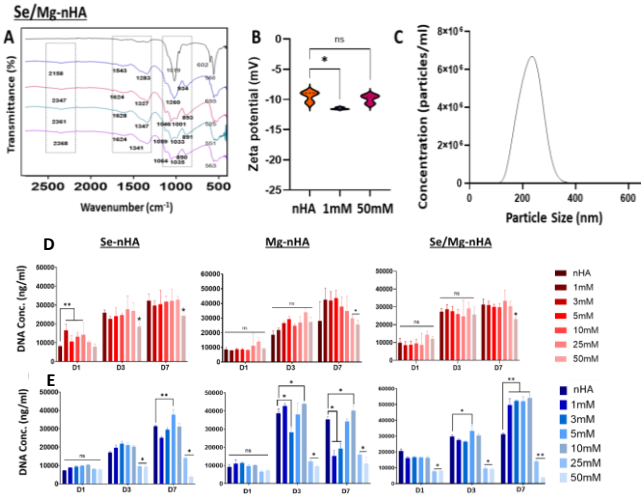

Figure 1. FTIR (A), ELS (B) and DLS (C) displayed successful incorporation and desirable size (200nm) and charge of Se and Mg nHA nanoparticles. Effect of Se, Mg, and Se/Mg-nHA concentrations on osteoclast (D) and MSC (E) proliferation. *P<0.05 vs nHA alone; **P<0.005 vs 1-10 mM concentrations.

DISCUSSION

Based on these results, there is a clear concentration dependent effect of each ion group on both osteoclast and MSC behaviour. 10mM appears to be the optimal concentration for Se, Mg and Se/Mg-nHA, with these nanoparticles displaying a synergistic effect of halting proliferation of pre-osteoclasts while enhancing MSC proliferation at this concentration.

CONCLUSIONS AND FUTURE WORK

Dual functionalised Se/Mg nHA demonstrates greatest potential as a therapeutic nanoparticle system to modulate impaired bone remodelling to promote regeneration. Current and future work involves completing biocompatibility of the ion functionalised nHA nanoparticles on LNCaP to achieve a synergistic effect of bone regeneration and cancer inhibition in 2D. Following this, biocompatibility of ion loaded scaffolds on both bone cells and LNCaP cells will be assessed to identify the optimal therapeutic concentration. Following this, differentiation and functional activity of both osteoclasts and osteoblasts will be assessed in 3D.

ACKNOWLEDGMENTS

The work is funded by the Anatomical Society.

REFERENCES

[1] D.G. Little *et al*, *J Bone Joint Surg*, 2007
[2] H. Zhou *et al*, *J. Magnes. Alloy*, 2021
[3] K. Kaur *et al*, *Adv NanoBiomed Res*, 2024.

DEVELOPMENT OF POLY(ACRYLIC ACID)-CYSTEINE-BASED HYDROGELS WITH TAILORABLE MECHANICAL PROPERTIES FOR ADVANCED CELL CULTURE APPLICATIONS

Kennedy, E.[1,2], McGourty, K.[1,2], O'Reilly, E.[1,2]
[1] Bernal Institute, University of Limerick, Ireland
[2] Chemical Sciences Department, University of Limerick, Ireland
email: ellen.kennedy@ul.ie

INTRODUCTION

Accurate mimetic in vitro cell models have become crucial in drug development, disease research, and regenerative medicine. However, traditional cell culture studies have primarily focused on 2-D environments, despite cells existing in a 3-D extracellular matrix in their natural state, surrounded by proteins and growth factors. Human tissues exhibit a stiffness of 1 to 50 kPa, while standard cell culture flasks are much stiffer at 1x107 kPa (fig. 1). This significant difference in stiffness greatly influences cell behaviour, including proliferation, differentiation, and survival. Therefore, replicating these physiological conditions is essential for obtaining accurate and reliable results in in-vitro studies.

With this objective in mind, a project was initiated to develop a hydrogel capable of bridging the gap between 2-D and 3-D cell culture for various tissues. The main focus of this study revolved around creating a customizable hydrogel with adaptable properties to enhance advanced cell culture applications.

Poly(acrylic acid) has been extensively used in hydrogel development over the years. However, its inherent biological compatibility is limited. To overcome this challenge, the study enhances the biocompatibility of poly(acrylic acid) by introducing cysteine onto the polymer. This modification creates a polymer with mucoadhesive properties, facilitating cell adhesion.

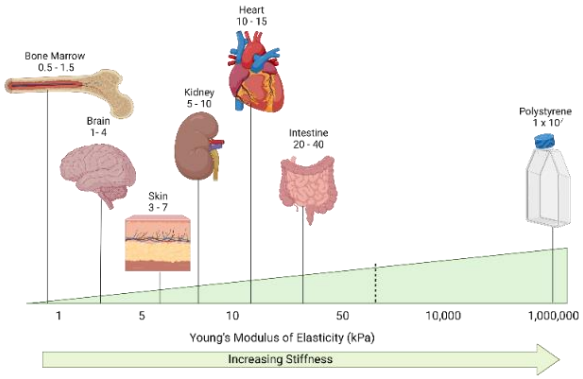

Figure 1 Demonstrating the difference in stiffness, given as Young's Modulus, between polystyrene culture flasks and in vivo organs.

MATERIALS AND METHODS

PAA was reacted with Cys to form a thiomer by activating the PAA polymer with EDC over the course of 20 minutes. L-Cysteine.HCl was added, and the reaction was run for 3 hours. The PAA-Cys product was then dialyzed using the Spectra/Por membrane over five days, under low pH conditions. The polymer solution was then freeze-dried at reduced temperature and pressure.

The freeze-dried PAA-Cys polymer was resolubilised in deionised water and crosslinked with varied concentrations of acrylic acid (0.25-7%) via a UV light induced reaction, with Irgacure 2959 as the photoinitator.

RESULTS

We set out to thiolate the PAA with a view that cysteine would be amenable to conjugation. A variety of in-house QC measures were employed to verify thiolation of the PAA polymer. The PAA-Cys polymer was structurally characterised using FTIR. Further morphological characterisation of the polymer was done using SEM. Mecmesin Compression testing was conducted on crosslinked hydrogel samples to determine the Young's Modulus of the various hydrogel samples.

DISCUSSION

We have successfully produced a biocompatible base polymer which will have broad applications in the area of tissue engineering. Our next steps will be to tailor three major properties of the hydrogel system: Biomechanics, biological factors and tissue architecture. Biomechanics will be manipulated by adjusting the crosslinking process and incorporating surface treatments to modify the material's elasticity and topography, respectively. Soluble protein factors commonly found in native tissues will be incorporated into the hydrogel by conjugating them to free thiol groups. Furthermore, tissue architecture will be addressed through the utilization of 3-D inkjet printing techniques, enabling the creation of intricate structures resembling *in vivo* architecture.

REFERENCES

Bolanta *(et al.)*, ACS Omega 7:9108-9117, 2022.

DESIGN AND DEVELOPMENT OF A NOVEL MRNA-BASED VACCINE TARGETING OSTEOSARCOMA

Kamaliasl S.[1], Saha C.[1], Dunne N.[2], McCarthy, H.O.[1]

[1] School of Pharmacy, Queen's University Belfast, Belfast, Northern Ireland, United Kingdom

[2] School of Mechanical & Manufacturing Engineering, Dublin City University, Dublin, Republic of Ireland

Email: skamaliasl01@qub.ac.uk

INTRODUCTION

Osteosarcoma (OS) is an aggressive primary bone cancer, particularly prevalent in adolescents, with limited effective treatments for metastatic and recurrent cases.[1] Immunotherapy offers a promising avenue, but the low levels of tumour-associated antigens and targeting of intracellular proteins is challenging.[2] The 5-year survival rate for localised osteosarcoma is approximately 70%, but it drops to around 20% for metastatic osteosarcoma, highlighting the urgent need for novel therapeutic strategies.[3] This study aims to design a multi-antigenic mRNA vaccine to elicit potent cytotoxic T-cell responses against OS.

MATERIALS AND METHODS

Potential OS antigens were identified through comprehensive bioinformatics analyses. To predict high-affinity epitopes with the potential to stimulate cytotoxic T-cell responses, MHC class I epitope prediction tools such as the IEDB and the NetMHCpan website were employed. A range of protein structure modelling tools, including AlphaFold, PyMOL, ProtParam, and VaxiJen, were utilised to evaluate the immunogenicity of candidate epitopes and design multi-antigenic constructs. (Fig 1A)

RESULTS

Preliminary bioinformatics analyses identified several promising MHC class I epitopes from PRAME, TP53, ATRX, DLG2, and RB1 antigens with high binding affinity and predicted immunogenicity. (Fig 1B) These epitopes were carefully selected based on criteria such as conservation across OS cell lines, and compatibility with immune system processing. Protein structure modelling confirmed that these epitopes are accessible and structurally stable, making them suitable candidates for inclusion in multi-antigenic vaccine constructs. Various vaccine designs were computationally evaluated, incorporating different combinations of epitopes to maximize antigen coverage and minimise the risk of immune escape. Future experimental work will focus on synthesizing these mRNA constructs, formulating them with peptide nanoparticles for efficient delivery, and validating them in vitro to assess their expression, stability, and capacity to generate antigen-specific cytotoxic T-cell responses.

DISCUSSION

Initial computational results indicate the potential of a rationally designed mRNA vaccine targeting OS-specific antigens. By leveraging bioinformatics tools, the study identified immunogenic epitopes with a high likelihood of inducing robust cytotoxic T-cell responses. Structural validation supports the feasibility of multi-antigenic constructs. Future in vitro studies will confirm the expression and immunogenicity of these constructs, providing critical insights into their therapeutic potential. The modular approach to vaccine design also allows flexibility in addressing antigen variability in OS, supporting its translation into clinical applications.

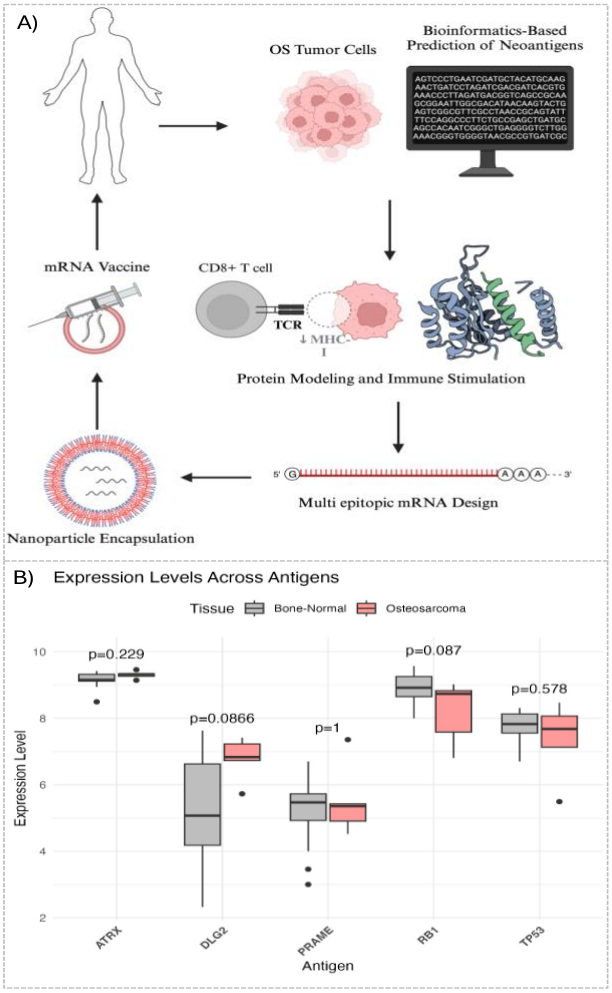

Figure. 1A) Workflow of multi-epitopic, multi-antigenic mRNA vaccine design for OS. The process involves bioinformatic analysis to identify TAAs and predict immunogenic epitopes, structural modelling of selected epitopes, mRNA construct design combining multiple epitopes, formulation of mRNA with peptide nanoparticles, and planned validation through in vitro and in vivo studies. *(Created with BioRender.com)* **1B)** Box-and-whisker plots showing the expression levels of antigens (ATRX, DLG2, PRAME, RB1, and TP53) in OS (red) and bone-normal tissues (grey). The horizontal line within each box represents the median expression level, while the box edges represent the interquartile range (IQR). Whiskers extend to 1.5× the IQR, with dots indicating outliers. P-values comparing OS and bone-normal groups are shown above each antigen.

REFERENCES

1. Kansara et al., Nature Reviews Cancer 14(11):722–735, 2014.
2. Chen et al., Cancer Letters 500:1–10, 2020.
3. Li et al., Frontiers in Immunology 12:665106, 2021.

Early Stage Researcher (PhD Year 1)		Post-Doctoral Researcher/Senior Researcher/PI	X (Postdoc)
Entry for the Engineers Ireland Biomedical Research Medal		Corresponding author has completed PhD and would like to review BinI abstract submissions	

Please place an X in any appropriate categories

BLOCKING THE INHIBITORY RECEPTOR TIGIT ENHANCES NATURAL KILLER CELL CYTOTOXICITY AGAINST OVARIAN CANCER CELL LINES

Prendeville, H.[1], O'Dwyer, M.[2], Dolan, E.B[1]

[1] Biomedical Engineering, College of Science and Engineering, University of Galway, Ireland

[2] Department of Haematology, Galway University Hospital, Ireland

email: (Hannah.prendeville@universityofgalway.ie)

INTRODUCTION

Ovarian Cancer is the most lethal gynaecological cancer with a global 5-year survival rate of 30-50%. Treatment with chemotherapy is effective initially, however most women ultimately relapse and develop chemotherapy-resistant tumours[1]. Thus, there is a pressing need to develop novel therapies and strategies to control tumour dissemination and increase patient survival.

Immunotherapies, in particular checkpoint blockade therapies, have revolutionised the treatment of many cancers, including metastatic melanoma and non-small cell lung cancers[2]. Despite these successes, immunotherapies have had limited success in Ovarian Cancer. In this study, we sought to uncover the mechanisms of immune cell dysfunction in Ovarian cancer which may uncover potential immunotherapeutic targets. Natural Killer (NK) cells are innate cytotoxic lymphocytes that are poised to kill malignant cells through the secretion of IFNγ and cytolytic granzymes. They are an attractive candidate for cancer immunotherapies as they are rapidly activated and not restricted by antigen specificity. However, suppression of NK cells within the tumour microenvironment can result in accelerated tumour growth. The inhibitory receptor TIGIT is expressed by NK cells in melanoma, breast and colorectal cancers, and contributes to immune tolerance by inhibiting NK cell cytotoxicity[3]. Using *in vitro* co-culture models, we investigated if the Ovarian cancer microenvironment causes NK cell dysfunction by increasing the expression of the inhibitory receptor TIGIT. Furthermore, we investigated if TIGIT blockade could enhance NK cell cytotoxicity against Ovarian cancer cell lines.

MATERIALS AND METHODS

NK cells were expanded (eNK cells) from murine spleens for 6 days using low dose IL-15. Flow cytometry was used to examine NK cell proportions, viability and expression of the inhibitory receptor TIGIT. We next investigated if Ovarian tumour-derived signals can influence TIGIT expression on eNK cells. To achieve this, eNK cells were cultured with 20% conditioned media from ID8 mouse Ovarian cancer cell lines + IL-15 (a known inducer of TIGIT expression) for 24hr. TIGIT expression was analysed by flow cytometry. Next, a co-culture model was used to investigate eNK cell cytotoxicity against ID8 Ovarian cancer cells. ID8 cells were pre-stained with cell trace violet (CTV) and co-cultured with eNK cells at 1:1, 2:1 and 5:1 ratios of NK:ID8 cells. Flow cytometry was used to quantify the proportion of dead CTV^+ ID8 cells, and the expression of CD107a on eNK cells – a marker of degranulation. Finally, using an anti-TIGIT monoclonal antibody (mAb), we examined the effects of TIGIT blockade on eNK cell degranulation and cytotoxicity against ID8 tumour cells *in vitro*.

RESULTS

Low dose IL-15 expands the proportion of NK cells from ~ 2 to 65% in murine splenocytes and increases TIGIT expression after 4 days (**Fig 1a**). eNK cells express high levels of TIGIT when cultured with high concentrations IL-15, and this is further increased by 20% ID8 tumour conditioned media (**Fig 1b, c**). eNK cells are highly cytotoxic against ID8 ovarian cancer cell lines *in vitro*, resulting in significant tumour cell death (**Fig 1d**). eNK cell cytotoxicity is enhanced when TIGIT is blocked, resulting in increased tumour cell death and CD107a expression (**Fig 1e, f**).

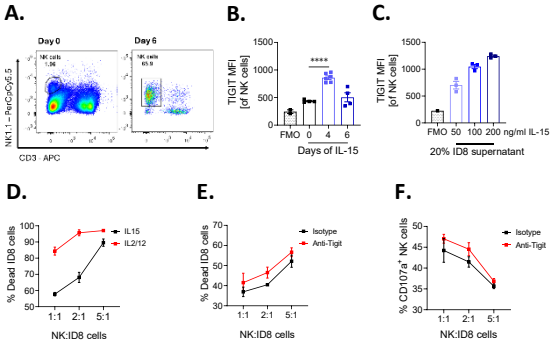

Figure 1. A. % eNK cells. **B.** eNK cells express TIGIT when cultured with IL-15. **C.** ID8 conditioned media increases TIGIT expression on eNK cells cultured with IL-15. **D.** eNK cells are highly cytotoxic against ID8 Ovarian cancer cell lines. **E.** TIGIT blockade enhances eNK cell cytotoxicity against ID8 ovarian cancer cells.

DISCUSSION

Taken together, our results suggest that TIGIT is a potential therapeutic target and may reduce Ovarian cancer burden in vivo by promoting potent NK cell cytotoxic responses. TIGIT is also expressed by cytotoxic CD8 T cells and thus is an attractive novel therapeutic target in cancer immunotherapy. We have submitted an ethical application to investigate the delivery of repeated doses of anti-TIGIT mABs to the peritoneal cavity using our mechanotherapeutic implant[4,5] in ID8 tumour bearing mice. Our strategy has the potential to be used in the clinic to treat Ovarian Cancer, as well as other abdominal cancers such as colorectal, stomach and pancreatic cancers.

REFERENCES

1. Cobrun *et al.* Int. J. Cancer (2017) **2.** Sun *et al.* Signal Transduction and Targeted Therapy (2023). 3. Zhang *et al.* Nat Immunol (2018). **4.** Dolan *et al.* Sci Robotics (2019). **5.** Whyte *et al.* Nat Comms (2022).

COLD ATMOSPHERIC PLASMA ENHANCES THE ANTICANCER PROPERTIES OF PYRAZOLOPYRIMIDINONES

Bednarz, N.[1], McEvoy, C.[2], Kinsella, G.K[1], Boehm, D.[3], Bourke, P.[3], Stephens, J.C.[2], Curtin, J.[1]
[1] Technological University Dublin
[2] Maynooth University
[3] University College Dublin
email: Natalia.Bednarz@TUDublin.ie

INTRODUCTION

Glioblastoma is an aggressive brain cancer with low survival rates. Its poor prognosis is attributed to its low response to the traditional treatment regime [1]. Cold atmospheric plasma (CAP) is a partially ionised gas, which has proven to be a promising tool for cancer therapy. CAP generates UV radiation, electrical field and reactive oxygen and nitrogen species, all of which can interact with cancer cells to promote DNA damage, induction of cell death and electroporation of cell membranes [2]. Hence, CAP has demonstrated capacity for the induction of selective cancer cell death *in vitro* and *in vivo*, and for drug sensitisation [1,3,4,5].

Pyrazolopyrimidinones are nitrogen-containing heterocyclic compounds which exhibit significant enhancement in cytotoxicity against glioblastoma cells when in combination with CAP [6]. The aim of this research was to evaluate CAP as a potential drug delivery platform for pyrazolopyrimidinones. The combinatory effect of CAP and the pyrazolopyrimidinones on the cytotoxicity of glioblastoma cells was investigated, using direct and indirect CAP treatments to evaluate the applicability of CAP as a drug delivery platform.

MATERIALS AND METHODS

The cytotoxic effect of CAP, generated via the Pin-to-Plate Leap100 system, on U-251 MG glioblastoma cells has been assessed. To investigate the effect of CAP on the cytotoxicity of the pyrazolopyrimidinone-based compounds, cells were directly exposed to the compound and 0, 10 and 30 seconds of CAP. Cells were additionally treated indirectly with CAP-conditioned compound to further assess the applicability of CAP for drug delivery.

RESULTS

CAP exhibited marginal cytotoxicity towards glioblastoma cells after a 10 seconds exposure. While a 30 seconds exposure resulted in a significant decrease in cell viability. Preliminary results indicate TUM-4-006 and TUM-4-007 alone present with relatively low cytotoxicity against glioblastoma cells. Upon exposure to CAP the cytotoxicity significantly increased for both. After 10 seconds of CAP, the cytotoxicity of TUM-4-007 increased by 8.14-fold, with a further increase of 78.04-fold after 30 seconds. Synergy was observed between TUM-4-007 and CAP, while an additive effect was observed with TUM-4-006. The results suggest the direct exposure of cells to CAP and the compound allows for a more significant enhancement in cytotoxicity at shorter CAP durations, compared to the indirect treatment with CAP-conditioned compound.

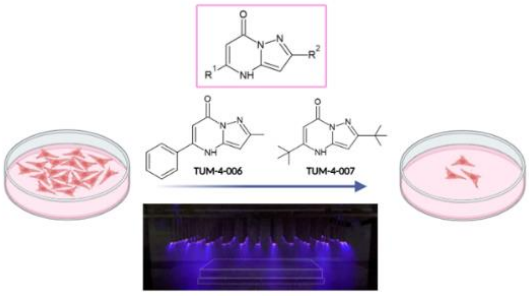

Figure 1 Pyrazolopyrimidinones present with enhanced cytotoxicity against glioblastoma cells when in combination with Cold Atmospheric Plasma generated via atmospheric air.

DISCUSSION

Cold atmospheric plasma showed to have a synergistic effect with some of the pyrazolopyrimidinones. CAP appears to sensitise glioblastoma cells to the treatment, enhancing its efficacy. The observed significant increase in cytotoxicity with the direct treatment, has promising implications in the use of CAP as a drug delivery system. Since CAP is selective in nature, can be generated via handheld devices in an accurate and precise manner, and has shown synergy with the treatment, it can be a powerful tool to drive the selective uptake of the compounds into the cancer cells, increasing treatment efficacy and reducing the rate of recurrence.

Future work will focus on the elucidation of the mechanism behind the observed synergy between CAP and the pyrazolopyrimidinones, and the selectivity of the treatment to cancer cells. The potential and the applicability of CAP as a targeted anticancer drug delivery platform will be evaluated.

REFERENCES

[1] Soni *et al.*, Cancers 14: 3116, 2022
[2] Kazemi *et al.*, Plasma 7: 233-257, 2024.
[3] Faramarzi *et al.*, Oxidative Medicine and Cellular Longevity 2021: 9916796, 2021
[4] Canady *et al.*, Cancers 15: 3688, 2023
[5] Shaw *et al.*, Cancers 13: 1780, 2021
[6] He *et al.*, European journal of medicinal chemistry 224: 113736, 2021

COLD PLASMA DEPOSITION AS A NOVEL TECHNOLOGY FOR CANCER DRUG DELIVERY

Pinheiro Lopes, B.[1,2,3], Boehm, D.[1,2], O'Neill, L.[4], Bourke, P.[3,5]
[1] School of Chemical and Bioprocess Engineering, University College Dublin
[2] Sustainability and Health Research Hub and School of Food Science and Environmental Health, Technological University Dublin
[3] Plasma Research Group, School of Biosystems and Food Engineering, University College Dublin, Dublin
[4] TheraDep Ltd., QUESTUM Innovation Centre, Limerick Institute of Technology
[5] Conway Institute, University College Dublin
email: beatriz.pinheirolopes@ucdconnect.ie

INTRODUCTION

Glioblastoma multiforme (GBM), the most aggressive brain cancer, is characterized by rapid proliferation, therapy resistance, and tissue infiltration, with a poor prognosis and average survival of 15 months despite advancements in treatment, highlighting the need for innovative approaches [1].

Cold Atmospheric Plasma (CAP) generates reactive oxygen and nitrogen species (RONS), which have been suggested to induce higher cytotoxicity in cancer cells than in healthy tissues. CAP methods, including plasma deposition, are showing promising potential to exhibit synergistic effects when combined with chemotherapeutic agents, for localized drug delivery.

Plasma deposition has been explored for biomedical applications, drug delivery systems and therapeutic coatings [2], showing promise in cancer therapy and wound healing, offering a less invasive, cost-effective alternative to systemic chemotherapy, while potentially reducing side effects [3]. Topotecan (TPT), a topoisomerase I inhibitor with potent antitumor activity, faces challenges in GBM treatment due to poor blood-brain barrier penetration and toxicity [4]. These limitations make TPT a strong candidate for drug repurposing for localized therapies.

This study aims to enhance GBM treatment by using plasma deposition to deliver topotecan (TPT) directly to cancer tissue. It evaluates the combined effects of plasma-based technologies and TPT on U-251mg cell line, proposing a novel protocol to improve therapeutic efficacy.

RESULTS

Plasma-deposited TPT significantly reduced metabolic activity and cell mass in 2D and 3D GBM models. Synergistic effects were also seen in malignant melanoma and squamous carcinoma cell lines. Notably, the deposition protocol can be used for other drugs, such as TMZ, with similar efficacy in 2D GBM cells. Spheroid models confirmed TPT's dual effect, combining short-term cytotoxicity with long-term anti-proliferation, highlighting its potential for combinatorial applications.

FUTURE PERSPECTIVES

The next phase of this work involves the 3D bioprinting of tumour spheroids through deposition of bioinks, cancer cells and relevant bacteria. This approach aims to achieve a physiologically relevant spatial assembly and organization of cells, closely resembling the native tumour structure, to further investigate cold plasma mediated drug delivery interactions within the tumour microenvironment and the tumour microbiome. Plasma deposition results plus the optimization of the tumour bioprinting models could lead to development of new combinations and strategies to provide locally activable drug delivery to tumour margins and enhanced treatment options for a variety of cancers.

METHODOLOGY

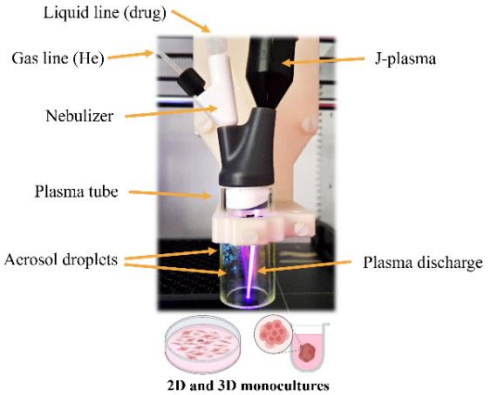

Figure 1 Schematic of the plasma deposition protocol. The J-Plasma hand piece was paired with a nebulizer, fed by a syringe pump to deliver a constant drug solution flow. The setup was inserted on a polymer block, directing the plasma discharge and aerosol spray into a confined acrylic tube for interaction before deposition onto the target substrate (2D and 3D cell models).

REFERENCES

[1] van Solinge, *et al*. Nature Reviews Neurology 18.4: 221-236, 2022.
[2] Coad, Bryan R., *et al*. Plasma Processes and Polymers 19.11: 2200121, 2022.
[3] Braný, Dušan, *et al*. International journal of molecular sciences 21.8: 2932, 2020.
[4] D'Amico, Randy S., *et al*. Journal of neurosurgery 133.3: 614-623, 2019.

EFFECT OF ACTUATED DELIVERY ON REDUCING TISSUE RESISTANCE IN SUBCUTANEOUS DRUG DELIVERY SYSTEMS

Liu, Yishu[1], Wylie, Robert [1], Brennan, Benjamin [1], O'Dwyer, Joanne [2], Duffy, Garry P.[1,3,4].
[1] Anatomy and Regenerative Medicine Institute, [2] Pharmacology and Therapeutics, College of Medicine Nursing and Health Sciences, University of Galway, [3]SFI Advanced Materials and BioEngineering Research Centre (AMBER), Trinity College Dublin & University of Galway.
[4]CÚRAM, SFI Research Centre for Medical Devices, University of Galway & RCSI, Galway, Ireland
email: joanne.odwyer@universityofgalway.ie & garry.duffy@universityofgalway.ie

INTRODUCTION

The use of continuous subcutaneous insulin infusion (CSII) in people with Type 1 Diabetes has increased by 64% over the past five years[1]. However, CSII systems often encounter rising tissue resistance over time, which can compromise both insulin delivery efficiency and patient safety. Prior studies and the pre-clinical studies in our lab indicate that the duration of cannula implantation correlates with increased tissue resistance[2]. Actuated drug delivery, which involves additional pulsed pressure to enhance drug delivery, has been shown in prior research to improve the lifetime of cannula[3]. This study examines the impact of passive versus actuated drug delivery on tissue resistance, hypothesising that actuated delivery may help mitigate tissue resistance.

MATERIALS AND METHODS

In vitro infusion resistance recording: An OB1 controller (Elveflow, France) was connected to an actuated cannula inserted into porcine subcutaneous tissue. A syringe pump (KD Scientific, USA) served as the driving source, infusing distilled water at a rate of 80 µL/min. A pressure sensor (Elveflow, France) was positioned between the cannula and syringe pump to capture pressure data. Measurements were recorded before and after both 40-second passive and actuated delivery methods. A t-test was conducted on the recorded pressure differences to evaluate the effectiveness of actuation in reducing tissue resistance during drug delivery.

RESULTS

As illustrated in Figure 1, our data indicate that tissue resistance increases during the passive infusion. In contrast, the actuated delivery method resulted in a noticeable decrease in resistance. The t-test results support the hypothesis that actuation significantly reduces tissue resistance, suggesting it as a viable strategy for maintaining efficient drug delivery over extended periods.

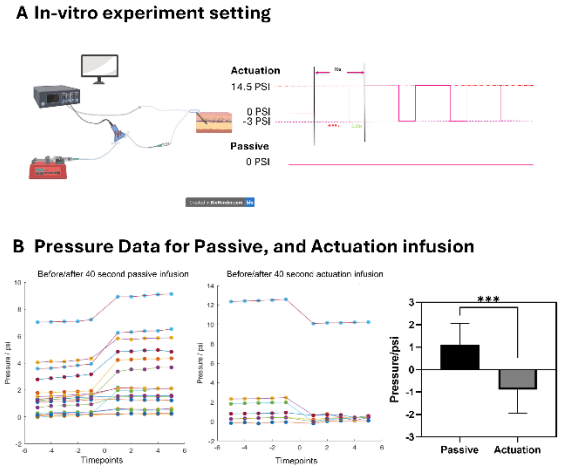

Figure 1 Infusion resistance decreased after actuation infusion. A.in vitro experimental setting; B. infusion resistance changes before and after passive/ actuation delivery. Timepoints 0 means 40seconds passive/actuation infusion. Values are shown as mean± SEM, t-test conducted, p=0.0002.

DISCUSSION

These findings suggest that actuated delivery can reduce tissue resistance, supporting the development of optimised delivery protocols for long-term subcutaneous infusion devices. Further research may refine these results and explore the mechanisms by which actuated delivery reduces infusion resistance.

REFERENCES

(1) Gandhi (et al). *Clin Diabetes*, *42* (1), 56-64, 2024.
(2) Patte (et al). *Diabetes technology & therapeutics*, *15*(4), 289-294, 2013.
(3) Beatty (et al). *Sci Robot*, *8* (81), 2023.

DESIGN OF AN EFFECTIVE PEPTIDE CARRIER FOR MRNA VACCINE DEVELOPMENT AGAINST CANCERS

Farkas, A.[1], Saha, C.[1], Dunne, N.[2], McCarthy, HO.[1]
[1]School of Pharmacy, Queen's University Belfast, Belfast, Northern Ireland, United Kingdom
[2] School of Mechanical & Manufacturing Engineering, Dublin City University, Dublin, Republic of Ireland
email: afarkas01@qub.ac.uk

INTRODUCTION

To design effective vaccine solutions against cancers, especially for mRNA vaccines, developing a carrier that delivers its cargo to the target site with high efficacy is crucial. Compared to other delivery systems such as lipid carriers and liposomes, CPPs have been highly effective in maintaining mRNA integrity at room temperature, keeping the cargo intact during transportation and avoiding toxicity. Additionally, CPPs can be structurally engineered to enhance pH sensitivity enabling conformational changes facilitating cargo release. This project focuses on designing a highly effective novel peptide carrier CPP, employing both *in-silico* and *in-vitro* investigations, to validate its efficacy and establish correlations between computational predictions and experimental data.

MATERIALS AND METHODS

Online available platforms such as CellPPD, Protparam, and Heliquest were used to predict data on the characteristics of the peptide. Peptide structure prediction and visualisation tools such as AlphaFold 3 and PyMOL aided in predicting a peptide model and presenting its native conformation. Experiments for characteristic verification included circular dichroism to observe the degree of folding, NMR to understand the influence of intermolecular interactions on the conformation, and *in-vitro* experiments for peptide functionality, including transfection and encapsulation efficiencies via RiboGreen reagent, gel electrophoresis and Ion exchange chromatography techniques.

RESULTS

Modifications were made to a well-established CPP sequence RALA (WEARLARALARALARHLARAL ARALRACEA). Alterations of a specific residue, such as from glutamic acid to aspartic acid (denoted by RALA D), significantly improved the transfection efficiency compared to RALA peptide (**Fig. 1C**) from 37.5% ± 6.0% to 67.9% ± 8.47% in NCTC-929s and marginally increased it in DC2.4s from 55.1% ± 5.33% to 66.3% ± 5.9%. Other substitutions included the replacement of cysteine with serine to remove the possibility of disulfide linkage, which resulted in high-quality nano-formulations at different N:Ps. This substitution improved the TE to 38.3% ± 1.63% in NCTCs and 65.4% ± 3.23% in DCs. The *in-silico* data suggests better folding because of Hydrogen Bonds (**Fig 1A**). The quantity and location of Histidine residues can also lead to π- π interactions, and whether this improves or hinders the peptide's performance can be observed. PyMOL helps to portray whether the aromatic rings lie in an intrinsic or extrinsic orientation and which residues they form polar interactions with. According to the plug-in RING-PyMOL, altering the Histidine locations varies the occurrence of intrinsic and inter-chain π-π stacking interactions (**Fig. 1B**).

DISCUSSION

The transfection data has demonstrated that altering glutamic acid to aspartic acid significantly improves transfection; while the serine/cysteine substitution may present suitable formulations, it does not improve transfection significantly. In conjunction, data from the circular dichroism suggests consistent folding across varying pH values. Encapsulation efficiency experiments demonstrate that the peptides keep the cargo intact, maintaining integrity even in the presence of reducing agents. The *in-silico* models indicate there are differences in the non-covalent bonds between each of the peptides and NMR was employed to determine how these bonds impact peptide dynamics. At the same time, *in-vitro* work must be conducted on the other substitution variants of the peptide to observe whether the occurrence of π-interactions improves or hinders peptide performance in each case.

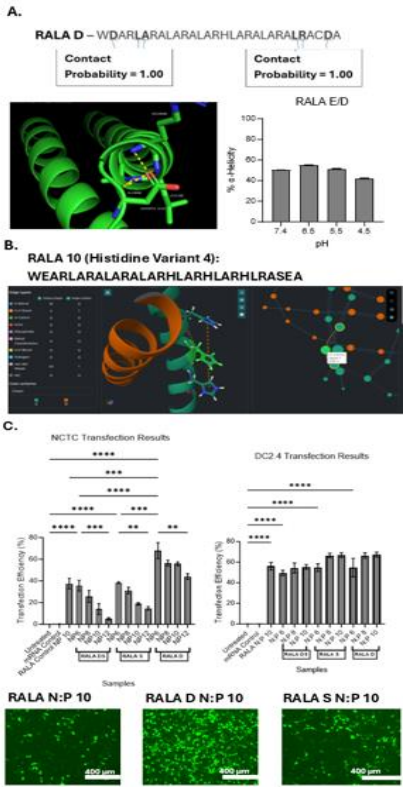

Figure 1 *A) In-Silico modelling with PyMOL and Circular Dichroism for the Aspartic Acid substitution in RALA, B) The RING-PyMOL modelling of a RALA Histidine variant resulting in more intra- and inter-chain π-stacking interactions. C) Transfection Efficiency of RALA, RALA D and RALA S peptide in C(i) NCTC 929 and C(ii) DC2.4 cells with RALA/mGFP, RALA D and RALA S at N:P 10 in NCTC-929s.*

REFERENCES

Bottens et al., Cancers, 14, 2022
David et al., Journal of Molecular Biology, 434, 167336, 2022
Piñero et al., Current Opinion in Pharmacology, 42, 111-121, 2018
Gautam et al., Journal of Translational Medicine, 11, 74, 2013
Gautier et al., Bioinformatics, 24, 2101-2102, 2008
Del Conte et al., Bioinformatics, 39, 2023
Noble et al., ACS Biomaterials Science and Engineering, 9, 2584-259
McCrudden et al., Journal of Controlled Release, 362, 536-547

DEVELOPING A TRANSPARENT CONTROLLER FOR THE HAPTIC CYCLING TRAINING REHABILITATION ROBOT

Koskas, D.[1], Holland, D.[2], Severini, G.[1]
[1] School of Electrical and Electronic Engineering, University College Dublin, Dublin, Ireland
[2] School of Mechanical and Materials Engineering, University College Dublin, Dublin, Ireland
email: daniel.koskas@ucdconnect.ie

INTRODUCTION

Robotic-assisted lower limb rehabilitation after stroke has proven effective but faces challenges associated with the mechanical limitations of the devices and with inconsistent patient responses. To address this, researchers are exploring new device designs and control.

The Haptic Cycling Training (HaCT) system integrates cycling with dynamic assistance and resistance, and can be used to design different cycling conditions up to mimicking natural gait trajectories. A key intended feature of this system is the transparent control strategy, which minimizes mechanical interference and allows the user's natural movements to guide the interaction.

This study develops and evaluates two transparent controllers for the HaCT system: a zero-torque controller and an admittance-based controller. Both aim to reduce mechanical impedance while maintaining natural movement. A comparative analysis will determine the effectiveness of each strategy.

MATERIALS AND METHODS

The HaCT hardware consists of pedals equipped with encoders and force/torque sensors and a central motor brushless direct current (BLDC) regulated by a field-oriented control (FOC) driver, all connected to a host computer through a CompactRIO platform.

The zero-torque controller minimizes mechanical interference by regulating the interaction torque, while the admittance-based controller adjusts angular velocity based on user movement intentions

In this work, we simulated the central motor and the equivalent load representing the robot are simulated through Matlab and Simulink softwares. Three velocities, corresponding to the cycling speeds required of participants for future tests, are used as setpoint for the controller. These simulations allow us to tune the gains of the three proportional-integral (PI) controllers used for FOC.

RESULTS & DISCUSSION

Based on simulations, the PI gains for both current controllers are kept at default values, i.e. 7221 mV/A for the proportional gain and 1094 µs for the integrator time respectively. However, the gains for the velocity controller are tuned to 3499 mA/Hz and 3505 µs for the proportional gain and the integrator time respectively. This allows a faster response.

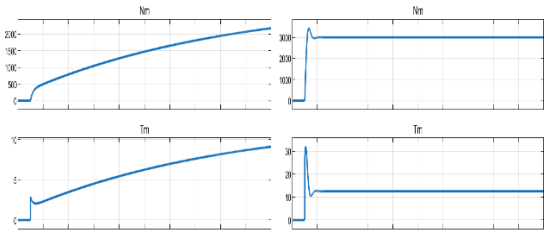

Figure 1 Output velocity (top) and torque (bottom) before (left) and after (right) tuning for a setpoint velocity of 3000 RPM

While simulations allow for partial tuning, they lack consideration of physical human-robot interaction, which is essential for evaluating the two transparent control strategies. Testing with participants cycling on the HaCT system under these different strategies and at various speeds is therefore necessary. This experiment is expected to reveal which controller—either the zero-torque or admittance-based—functions more effectively as a transparent control strategy.

REFERENCES

Journals:
Reinkensmeyer *et al.*, Journal of rehabilitation research and development, 43:657-70, 2006.
Jezernik *et al.*, Neuromodulation: journal of the International Neuromodulation Society, 6:108-15, 2003.
Ada *et al.*, Journal of physiotherapy, 56:153-61, 2010.
Hidler *et al.*, Neurorehabilitation and neural repair, 23:5-13, 2008.
Barroso *et al.*, Journal of neurophysiology, 112:1984-1998, 2014.
Barbosa *et al.*, Journal of Stroke and Cerebrovascular Diseases, 24:253-73, 2015.
Arciniegas-Mayag *et al.*, Journal of Intelligent & Robotic Systems, 104, 2021.
Erskine *et al.*, Experimental Physiology, 96:145-55, 2011.
Conference Proceedings:
Zanotto *et al.*, IEEE 13th International Conference on Rehabilitation Robotics (ICORR), Seattle, WA, USA, 2013.

AN IN VITRO MODEL TO EXPLORE NEUTROPHIL MECHANOBIOLOGY

Dillon, R.[1], Prendeville, H.[1], Duffy, G.P.[2], Dolan, E.B.[1]
[1] Biomedical Engineering, College of Engineering and Science, University of Galway
[2]Anatomy and Regenerative Medicine Institute (REMEDI), School of Medicine, College of Medicine, Nursing and Health Sciences, University of Galway
email: r.dillon13@universityofgalway.ie

INTRODUCTION

The foreign body response (FBR) is the immune system's reaction to implanted materials, characterised by a series of inflammatory processes. As a central component of the innate immune system, neutrophils are recognised as the primary drivers of the FBR, playing a crucial role as they secrete enzyme and signalling molecules. This results in the recruitment of macrophages and monocytes, accelerating the FBR, resulting in the formation of a fibrotic capsule. This is particularly detrimental for implants which rely on interactive communication with their local tissue environment, such as cell encapsulation devices, implanted sensors and controlled drug delivery devices. The formation of a hypo-permeable fibrous capsule can impede transport of molecules both to and from these implants, resulting in malfunction [1].

Our group has shown that intermittent actuation of a mechanotherapeutic implant can modulate the FBR and improve therapy delivery over time [2, 3]. We have shown that actuation of our implant results in local tissue strain and fluid flow and is associated with early clearance of neutrophils. However, this response is not fully understood. Neutrophils have been shown to be mechanosensitive cells [4], therefore gaining an in dept understanding of neutrophil mechanobiology is essential. I hypothesise that mechanostimulation will increase NCL apoptosis, increase formation of neutrophil extracellular traps (NETs) and enhance reactive oxygen species (ROS) production.

MATERIALS AND METHODS

As neutrophils are terminally differentiated cells and undergo limited expansion ex-vivo, maintaining viability presents as a challenge as neutrophils naturally undergo cell apoptosis within 24 hours. Therefore, the acute promyelocytic leukemia HL60 cell line was used as an alternative to primary neutrophils, as they can be differentiated into neutrophil-like cells (NLCs). HL60 cells were cultured in 1.3% DMSO for 7 days, and subsequently stained for myeloid marker CD11b, and neutrophil markers CD16 and CD66b to confirm a neutrophil-like cell (NLC) population. Ongoing work is evaluating the response of NLC to mechanostimulation using µ-channel slides (Ibidi). Apoptosis due to fluid flow will be assessed with Annexin V and 7-AAD. As neutrophils express Piezo1, induction of NETosis by activation of Piezo1 in NLCs via Yoda1 will also be investigated.

A computational fluid dynamics (CFD) study (Ansys Fluent) was used to predict resulting shear stress. The solution was calculated using a finite volume approach, with a steady-state laminar flow regime applied to the model. The model was meshed with significant element refinement in the channel region, a no-slip boundary was applied along the chamber walls, and a convergence criterion of 1x10-5 residuals was enforced. Fluid flow magnitudes representative of our mechanotherapeutic implant were used as inputs for our model: 2.4 mm/s - 3.04 mm/s velocity at 1 Hz [5].

RESULTS

Differentiation of HL60s: Optimisation of the differentiation protocol for HL60 to NLCs is ongoing. Preliminary results indicate that we can culture the HL60s for 14 days with viability remaining >85% and a cell doubling time of 2 days after 7 days of culture.

Computational validation of experimental set-up: The CFD model has yielded predicted fluid velocity profiles and shear stress levels. The model captures the fluid's interaction with µ-channel walls, resulting in a uniform shear stress distribution across the µ-channel. When fluid velocities within the µ-channel are representative of our mechanotherapeutic implant, cells experience shear stress levels ranging from 0.068 Pa to 0.1 Pa.

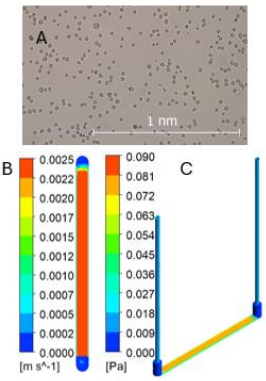

Figure 1 Microscopy image of HL60s (pre-differentiation) at passage 10 (scale bar = 1 nm) (a), CFD results of wall shear stress (b) and fluid velocity (c) in Ibidi µ-channel.

DISCUSSION

Understanding the mechanosensitivity of neutrophils is pivotal for regulating the FBR. By modulating neutrophil activity, it may be possible to minimise excessive inflammation and subsequent fibrous capsule formation, enhancing implant longevity and integration.

REFERENCES

[1] Trask et al, Biomaterials Science, 2024. [2] Whyte et al, Nature Communications, 2022. [3] Dolan et al, Science Robotics, 2019. [4] Barachati et al, Nature Communications, 2024, [5] Ward et al, Acta Biomaterialia 2024.

SPATIALLY RESOLVED DYNAMIC MICROMECHANICAL CHARACTERISATION OF HUMAN TESTIS TOWARDS THE DEVELOPMENT OF REPRESENTATIVE MODELS

Andersson, I.[1], Ghanami Gashti, N.[1], Mahon, O.[1] O'Meara, S.[2], Wittschier, J.[3], Mitchell, R.[4], Cullen, I.[2], Hess, J.[3], Stukenborg, J.B.[5], Cunnane, E.[1]

[1] Biomaterials Cluster, Bernal Institute, University of Limerick, Ireland; [2] Blackrock Clinic Dublin, Ireland; [3] Klinik und Poliklinik für Urologie, Universitätsklinikum Essen, Deutschland; [4] Royal Hospital for Children and Young People, Edinburgh, UK; [5] NORDFERTIL Research Lab Stockholm, Childhood Cancer Research Unit, Department of Women's and Children's Health, Karolinska Institutet, Sweden

email: isabel.andersson@ul.ie

INTRODUCTION

Current research and meta-analyses reveal alarming trends in male fertility whereby sperm counts are dropping at a rate that is projected to reach zero by 2045[1] for Western society. The exact mechanisms underlying this urgent trend are unclear, and the identification of effective treatment strategies requires the availability of truly representative models of the human testis and its function. The development of such models necessitates in-depth knowledge of testicular tissue mechanical properties, such as stiffness and viscoelasticity, which have a proven role in cell and tissue function[2]. However, the mechanical properties of the human testis have yet to be comprehensively characterised. We present an interdisciplinary approach to characterise the native mechanical properties of human testis samples harvested from patients at various stages of development and of varying fertility status. Furthermore, we are investigating approaches in which this knowledge can be translated to the development of biomimetic 3D cell culture systems capable of achieving in vitro spermatogenesis.

MATERIALS AND METHODS

Ethical approval has been secured to receive foetal (n=4), prepubertal (n=3), gender affirmation surgery (GAS) (n=24) and microsurgical testicular sperm extraction (mTESE) (n=6) testis tissue samples. The patient samples were sectioned using a vibratome into 200 µm thick sections. Multiple nanoindentations were performed using an Optics11Life Chiaro Nanoindenter, with a 50 µm radius probe (0.5 N/m stiffness) as a matrix scan allowing for spatial resolution. Load-indentation curves were analysed with the Hertzian contact model to generate Young's modulus. Dynamic mechanical analysis was performed as a frequency sweep with the same probe (1-16 Hz and 400 nm amplitude). An adjacent section of the tissue was taken for structural analysis, fixed for histology with formalin, and further processed for chromogenic and immunostaining.

RESULTS

Micromechanical analysis demonstrates that the testis exhibits spatially dependent, low stiffness values (0.1-2 kPa) when compared to other tissues, and viscoelastic behaviour. Interestingly, fertile adult tissue exhibits an increased stiffness as compared to tissues obtained from infertile patients with thickened basement membranes, which appears to be caused by an overexpression of ECM proteins like collagen 1 (as per immunostaining).

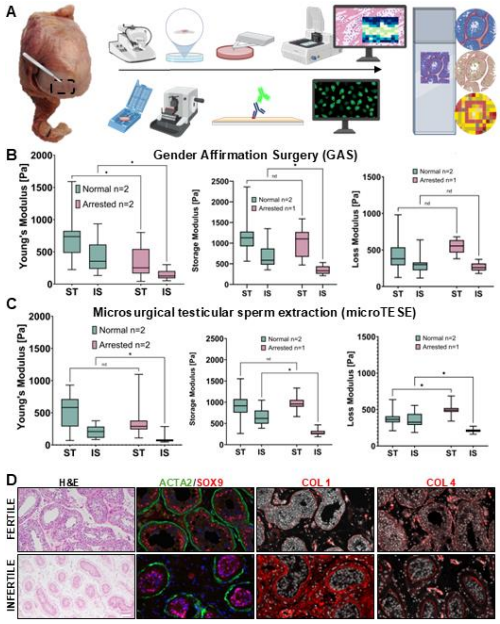

Figure 1 (A) Schematic overview of presented work, (B,C) dynamic, micromechanical analysis of human testis, (D) immunofluorescent staining of testicular ECM proteins.

DISCUSSION

This project is the first to report on human testicular micromechanical properties and to perform dynamic micromechanical analysis with spatial resolution on fresh soft tissues. Moreover, the project provides previously unreported data on testicular microstructural architecture and ECM remodelling across a large and diverse cohort of patient samples. The resulting dataset will act as a basis to increase the biomimicry of current in vitro systems and to optimise currently employed biomaterials. Furthermore, characterising the correlation between mechanical properties, ECM composition and fertility status will deepen the field's understanding of the complex role that biophysical mechanisms play in male infertility. This could advance the development of in vitro models of human testis in health and disease and aid in clinical diagnostics and the identification treatments.

REFERENCES

[1]Jørgensen *(et al.)*, Hum. Reprod. Update 23:646-659, 2017.

[2]Chaudhuri (*et al.)*, Nature 584:535–546, 2020.

MECHANOREGULATORY SKIN GROWTH MODEL IMPLEMENTING AN ANISOTROPIC SOFT TISSUE MODEL

Quinn, CQ.[1], Vaughan, TJ.[1]
[1,2] National University of Galway, Ireland
Email: conall.quinn@universityofgalway.ie, ted.vaughan@universityofgalway.ie

INTRODUCTION

Large skin defects require effective replacement to restore damaged tissue, with autologous grafts being the gold standard due to minimal rejection risk [1,2]. Skin growth models optimize tissue expansion design, but existing finite element models often oversimplify hyperelastic assumptions, failing to capture skin's non-linear, anisotropic behaviour. This study integrates an anisotropic collagen fiber model with thermodynamically consistent growth laws for improved accuracy [3].

MATERIALS AND METHODS

The Quinn-Vaughan (QV) model represents skin using an anisotropic collagen fiber distribution defined by a Fibonacci sequence and a modified von Mises-Fisher distribution (Fig.1A). Constitutive behaviour, modelled at the fiber level, captures tension and compression responses through piecewise functions (Fig.1B).

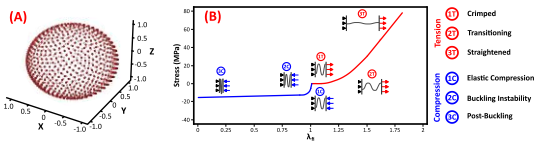

***Figure 1** – **(A)** Visualization of the Fibonacci sequence used to define the orientation of 1000 fibers. **(B)** Material response of individual collagen fibers under tension, showing (i) uncoiling, (ii) transition to straightened alignment, and (iii) fully straightened fibers, and under compression, depicting (i) initial elastic deformation, (ii) buckling, and (iii) post-buckling behaviour.*

A sigmoid function scaled the material bulk modulus as a function of the Jacobian (see Fig.2A), implicitly modeling the collapse and densification of porous, soft tissue.

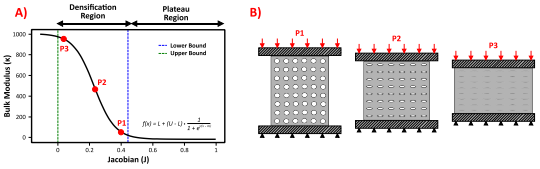

***Figure 2** – **(A)** Sigmoid function scaling bulk modulus (κ) as a function of Jacobian (J). (B) Visualisation of porous collapse and densification at points P1, P2 and P3.*

A thermodynamically consistent growth law (Eq. 5) optimizes tissue growth by minimizing strain energy (Eq. 3), ensuring growth aligns with the principle of energy dissipation. Stress-free growth is achieved through the decomposition of the total deformation gradient into elastic and growth components, allowing the model to accurately simulate anisotropic tissue expansion under mechanical stimuli [3].

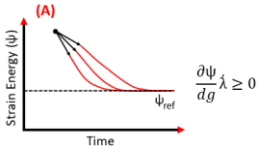

(B)

$$\boldsymbol{F} = \boldsymbol{F}_g \cdot \boldsymbol{F}_e \quad (2)$$

$$\boldsymbol{g}_{dir} = -\frac{\nabla W}{\|\nabla W\|}, \nabla W = \frac{\partial W}{\partial \boldsymbol{F}_g} \quad (3)$$

$$\Delta \boldsymbol{F}_g = \boldsymbol{g}_{dir} \cdot g_f \cdot \Delta t \quad (4)$$

$$\Delta \Psi = \Delta W_{elastic} - \Delta W_{growth} \geq 0 \quad (5)$$

***Figure 3** – **(A)** Optimal growth path taken to minimise strain energy towards reference stimulus. **(B)** Key equations governing the thermodynamically consistent growth law, including energy minimisation and growth constrains.*

RESULTS

The QV-model was fit to experimental anisotropic skin material properties in parallel and perpendicular directions obtained by Ni Annaidh et al. [4] with an excellent fit ($R^2 = 0.981$).

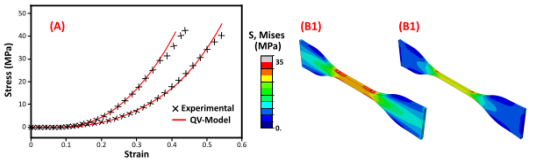

***Figure 3** – **(A)** Anisotropic computational fitting of QV-model to experimental tensile tests of human skin biopsies, see Ni Annaidh et al. [4]. **(B)** Contour plots of Von Misses stress in parallel **(B1)** and perpendicular **(B2)** directions.*

QV-model utilised thermodynamically driven growth law simulating temporal stress relaxation and growth of skin tissue due to multi-step balloon inflation.

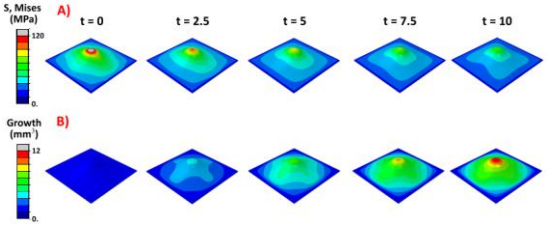

***Figure 4** –Temporal **(A)** stress relaxation and **(B)** tissue growth $(\boldsymbol{F}_g)$ of skin tissue due to balloon inflation.*

DISCUSSION

Previous skin growth studies used Gasser-Ogden-Holzapfel (GOH) models, which assume two fiber families, incompressibility, and include exponential terms prone to issues under large deformations. The QV-model aimed to develop a more physically derived soft tissue framework, accurately capturing the stretch-stress relationship of skin. This coupled with thermodynamically driven growth framework enables more realistic simulation of anisotropic tissue growth.

REFERENCES

[1]R. Serra et al., *Int Wound J*, 14(1):149–157, 2017.
[2]S. Kianian et al., *Plast Reconstr Surg Glob Open*, 11(6):e5100, 2023.
[3] E. K. Rodriguez et al., *J Biomech*, 27(4):455–467, 1994.
[4] N. A. A et al., *Ann Biomed Eng*, 40(8):1666–1678, 2012.

DEVELOPMENT AND VALIDATION OF AN ADVANCED 3D MODEL OF POSTMENOPAUSAL OSTEOPOROTIC BONE TISSUE AS A SURROGATE FOR DRUG TESTING

Naqvi, S.M.[1], Bukhari, M.M.M.[1], O'Brien, T.[1], Acharya, P.[1], Holdsworth, G.[2], McNamara, L.M.[1]
[1] Mechanobiology and Medical Device Research Group (MMDRG), University of Galway, Ireland
[2] UCB Pharma, Slough, United Kingdom
email: syeda.masoomanaqvi@universityofgalway.ie

INTRODUCTION

In postmenopausal osteoporosis, estrogen deficiency leads to increased bone resorption and primary bone loss, followed by fundamental changes in bone tissue composition [1]. One promising therapeutic approach is the use of sclerostin antibodies, which inhibit sclerostin, a negative regulator of bone formation, to restore bone density and reduce fracture risk. Developing effective osteoporosis treatments is challenging, as traditional preclinical models often fail to replicate the complex human bone environment. Indeed, only approximately 50% of therapies with promising results in animal models progress to human trials, though only about 5-10% ultimately receive regulatory approval [2]. Thus, there is a distinct need for advanced models for predictive drug-testing surrogates. We recently developed postmenopausal models, which represented the estrogen-deficient and mechanical environment of bone cells in vitro and could induce osteoclast differentiation [3-5]. However, these models lacked the cellular complexity required to act as effective surrogates for in vivo conditions. The objective of this study was to develop an advanced 3D drug-testing surrogate for postmenopausal osteoporosis, specifically designed to: (1) create a multicellular construct (osteocytes, osteoblasts, and osteoclasts), (2) apply exogenous mechanical loading, (3) investigate osteoclastogenesis under estrogen withdrawal, and (4) validate the model by evaluating the efficacy of sclerostin antibody (Scl-Ab) therapy.

MATERIALS AND METHODS

We pre-treated MC3T3 and OCY454 cells with 17β-estradiol before encapsulating them in gelatin-nHA-mtgase hydrogels. These constructs were cultured for 21 days in osteogenic media under two conditions: (1) continued estrogen (E Control) and (2) estrogen withdrawal (EW). After 21 days in culture, 17β-estradiol pre-treated osteoclast precursors encapsulated in hydrogels were layered on top of these mineralized constructs and cultured for 14 days in standard growth media. EW groups were untreated (Control), or received low (300 ng/mL EW Low) or high (3500 ng/mL EW High) doses of Scl-Ab (UCB Pharma, Amgen Inc.). Mechanical loading (compression and perfusion) was applied (~0.5% strain, ~1.2 mL/min, 1 Hz for 1 hour per day for the 14 days), with static groups serving as controls. Constructs were analysed on days 3, 7, and 14 post-osteoclast addition.

RESULTS

Osteogenic Differentiation and Mineralization: Estrogen deficiency and mechanical stimulation significantly reduced mineralization (ALP activity, calcium content) by day 7 compared to continued estrogen supplementation (Fig. 1A). Osteoblast differentiation (BSP2 gene expression) was reduced by day 14 under estrogen deficiency and mechanical stimulation compared to continued estrogen supplementation (Fig. 1B). Osteocyte differentiation was enhanced (DMP1 staining, DMP1 and SOST gene expression) at days 3 and 7 under estrogen deficiency and mechanical stimulation relative to continued estrogen-supplemented groups (Fig. 1B). ***Osteoclast Differentiation:*** Osteoclast differentiation was confirmed through active tartrate-resistant acid phosphatase (TRAP) activity and the presence of TRAP-positive multinucleated osteoclasts in all groups. Osteoclast differentiation was enhanced (OSCAR and CTSK gene expression) in the estrogen-withdrawal condition at day 14 relative to the continued estrogen-supplemented groups (Fig. 1C). ***Proof of Principle Drug testing:*** Scl-Ab treatment in estrogen-deficient constructs enhanced mineralization (ALP, calcium) at day 7 relative to untreated controls, under static and stimulated conditions (Fig. 1A). Treatment reduced osteoclast numbers at day 7 and 14 compared to untreated controls in static conditions (Fig. 1D).

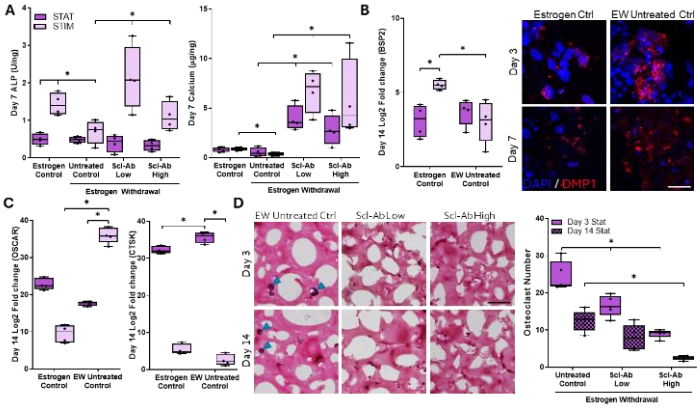

Figure 1: *(A) Day 7 ALP and calcium, (B) Day 14 BSP2 expression and Days 3 and 7 DMP1 staining; scale bar = 20 µm, (C) Day 14 OSCAR and CTSK expression, (D) Days 3 and 7 H&E staining and associated semi-quantitative data; blue arrows indicate multinucleated osteoclasts; scale bar = 200 µm. p < 0.05 (*).*

DISCUSSION

We developed an advanced 3D model of postmenopausal osteoporosis, significantly improving upon traditional 2D and 3D culture methods by incorporating multiple cell types (osteoclasts, osteoblasts, and osteocytes) and dynamic stimulation within a bioreactor to replicate the in vivo mechanical environment of bone tissue. Our model demonstrated the capacity to induce osteogenic differentiation and mineralization, as well as promote osteoclast differentiation. In an estrogen-deficient, mechanically loaded environment, mineralization was reduced, likely driven by increased activity of bone-resorbing osteoclasts. When this osteoporotic model was applied to study Scl-Ab, we observed an increase in osteoblast activity and bone formation alongside a decrease in osteoclast activity, consistent with the clinical effects of such treatments. This advanced 3D model of postmenopausal osteoporosis holds promise as a drug-testing surrogate, potentially reducing reliance on traditional in vitro cell culture and costly animal models.

REFERENCES

[1] O'Sullivan et al, Osteoporos Int, 2019. [2] Ineichen et al, PLOS Bio, 2024. [3] Simfia et al, Exp Cell Res, 2020. [4] Allison et al, Am J Physiol Cell Physiol, 2019. [5] Naqvi et al, Front Bioeng Biotechnol, 2020.

VALIDATION OF A BIOREACTOR TO MIMIC FLUID FLOW ON CORNEAL EPITHELIAL CELLS AND KERATOCYTES CO-CULTURED IN A 3D HYDROGEL MODEL

Bonizzi, M.[1,2], Ahearne, M.[1,2]
[1]Trinity Centre for Biomedical Engineering, Trinity Biomedical Sciences Institute, Trinity College Dublin
[2]Department of Mechanical, Manufacturing and Biomedical Engineering, Trinity College Dublin
email: bonizzim@tcd.ie

INTRODUCTION

Worldwide around 4 million of people suffer from corneal blindness. The current treatment is corneal transplantation, however there is a shortage of donors with only one cornea available for every 70 patients needing a transplant. To find new treatments and solutions tissue engineering has emerged as possible solution, both to find new methods to replace the cornea and to study the biology of cornea to produce accurate models as tests for new pharmacological treatments. In this field many models have been built, studying epithelium and endothelium but neglecting the response of the stroma, which is the bulk layer of the cornea and play an important structural role under mechanical stresses, to a mechanical environment[1]. The purpose of this work is to build a bioreactor system to mimic the shear stress due to tear movement during the eyeblink. The system is then used to stimulate epithelial cells and keratocytes, to analyze cells response to this mechanical environment.

MATERIALS AND METHODS

The shape of a PDMS chamber has been optimised through an iterative process. It contains 4 wells to host 4 10µl-hydrogels loaded with keratocytes, above each of which a 20µm-membrane seeded with epithelial cells is placed. The hydrogel is made of collagen type I (3.5ml/ml) and 10mM PEG-SG (polyethylene-glycol-succinimidyl glutarate). The membrane is made of electrospun PCL (polycaprolactone) coated with PDA (polydopamine). After the seeding the chamber is connected to a pumping system to provide a fluid flow over the cells co-culture at different rates.
The bioreactor was validated through YAP (Yes-Associated-Protein), which is known to be a mechanosensitive protein, on epithelial cells and Live and Dead staining on keratocytes [2]. Cells were stimulated for 24h at 1 Pa with bidirectional fluid flow.

RESULTS

The bioreactor was successfully assembled and tested for hydraulic sealing and sterility maintenance. The shear stress applied to the surface of the hydrogels was calculated using a simple fluid mechanics model and validated using computational fluid dynamics software.
Preliminary studies using collagen hydrogels showed a high degree of contraction, so PEG was introduced to the hydrogels to assist in stabilizing their dimensions.
A protocol for the set-up of the co-culture of keratocytes and epithelial cells has been optimized (Fig 1.A).
Epithelial cells showed a higher nuclear YAP expression after a dynamic stimulation, confirming that the stimulation occurred (Fig 1.B). Moreover L&D was performed on keratocytes. High viability was found at 1(Fig 1C). These results validated the bioreactor function.

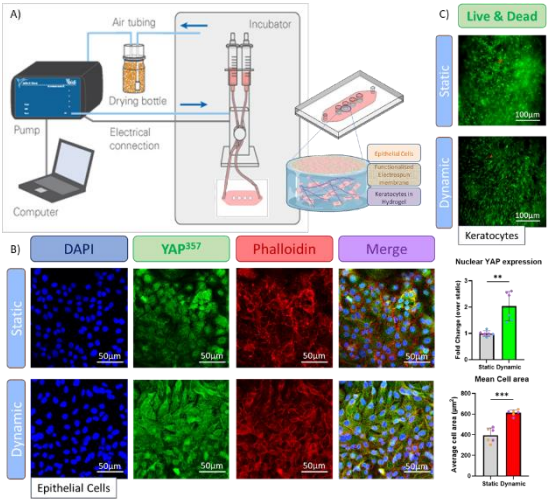

Figure 1 A) schematic view of the bioreactor and co-culture set up. B) Nuclear YAP expression in static and dynamic conditions. C) Live and Dead staining on keratocytes after 24h stimulation.

DISCUSSION

The bioreactor has been developed and successfully validated to apply shear stress to corneal hydrogel models. Short term studies, at day 1 and 3, provides a first result on the behaviour of cornea cells in response to different magnitudes of shear stress. Further implementations, such as microfluidic system, will allow long term studies at day 7 and 14 to understand possible changes in ECM (extracellular matrix) composition and arrangement.

REFERENCES

1. Li, Q., et al., *Current microfluidic platforms for reverse engineering of cornea*. Mater Today Bio, 2023. **20**: p. 100634.
2. Li, B., et al., *c-Abl regulates YAPY357 phosphorylation to activate endothelial atherogenic responses to disturbed flow*. J Clin Invest, 2019. **129**(3): p. 1167-1179.

Early Stage Researcher (PhD Year 1)	☐	Post-Doctoral Researcher/Senior Researcher/PI	☐
Entry for the Engineers Ireland Biomedical Research Medal	☐	Corresponding author has completed PhD and would like to review BinI abstract submissions	☐

Effects of Estrogen Deficiency on Vascularization and Mineralization in a Novel 3D Humanized Bone Model

Bukhari, MMM[1], **Naqvi, SM and McNamara, LM**[1]

[1]Mechanobiology and Medical Device Research Group, Biomedical Engineering, University of Galway, Ireland.

email: m.bukhari1@universityofgalway.ie

INTRODUCTION

Although osteoporosis is widely understood to be associated with bone loss, our previous research has revealed that the osteoporosis also leads to fundamental changes in the composition of the remaining bone tissue and also that bone cellular responses to mechanical loads are altered [1-3,6]. Recently, we reported that estrogen deficiency increases osteogenesis and mineralization by murine osteoblasts in a 3D model and expression of pro-osteoclastogenesis signalling in osteocyte-like cells [2, 3]. Vascularization is critical to bone formation and mineralization via the endochondral ossification process [4, 5]. Collagen X, released by hypertrophic chondrocytes, plays a pivotal role in the endochondral ossification process [8, 9]. Estrogen regulates the lipid use of bone endothelial cells, whereas vascular aging and adipocyte accumulation occurs within bone in low estrogen [7]. However, the interaction between vascular and bone cells during estrogen deficiency is not fully understood, and how estrogen deficiency influences mineralization and vascularization in bone is unknown. Thus, here we develop an advanced 3D vascularized and humanized bone model to provide a mechanistic understanding of changes in bone vascularization and mineralization in estrogen deficiency.

MATERIALS AND METHODS

Mesenchymal stem cells (HBMSCs) were isolated from bone marrow (42-year-old female) under ethical approval and informed consent (Research Ethics Committee, University of Galway). HBMSCs (P5) were encapsulated in gelatin-mtgase (3% W/W) at 2 × 10^6 cells/ml and cultured in media for 21 days to develop a chondrogenic template (Fig 1A). At day 22, vascularization of the template was initiated by culturing the constructs within a hydrogel in which human umbilical vein endothelial cells (HUVECs) and HBMSCs (1:1) were encapsulated. For non-vascular constructs, only HBMSCs were added within the hydrogel. Both vascularized and non-vascularized groups were cultured for a further 21 days (until D42) in osteogenic differentiation media with 10 nM 17β-Estradiol. At day 43 the constructs were cultured either with, or without, estrogen supplementation and under static or mechanically stimulated conditions. At day 63 constructs were analysed to quantify vascularisation and osteogenesis by histology (Von Kossa), immunofluorescence (CD31, DMP-1), immunohistochemistry (Collagen I) and biochemical assay (calcium).

RESULTS

Osteogenesis: Immunostaining confirmed the synthesis of extracellular proteins (collagen I, DMP-1, sclerostin) in the vascularized and estrogen supplemented models (Fig. 1 a, b, c). Mineral staining and calcium assay showed that, under estrogen withdrawal, there was a significant increase in the mineral content of the vascular models compared to non-vascular by day 21 (day 63 in culture). *Hypertrophy and apoptosis:* At day 21, there was intense collagen X staining in vascular and non-vascular models, under estrogen withdrawal (Fig. 1 g, h). There was a significant increase in caspase 3 gene expression in the vascularized estrogen withdrawal group at day 21 (Fig. 1i). *Vascularization:* Immunofluorescence (CD31) confirmed vessel-like structure formation in vascularized estrogen deficient groups at day 21 (Fig. 1 j, k, l).

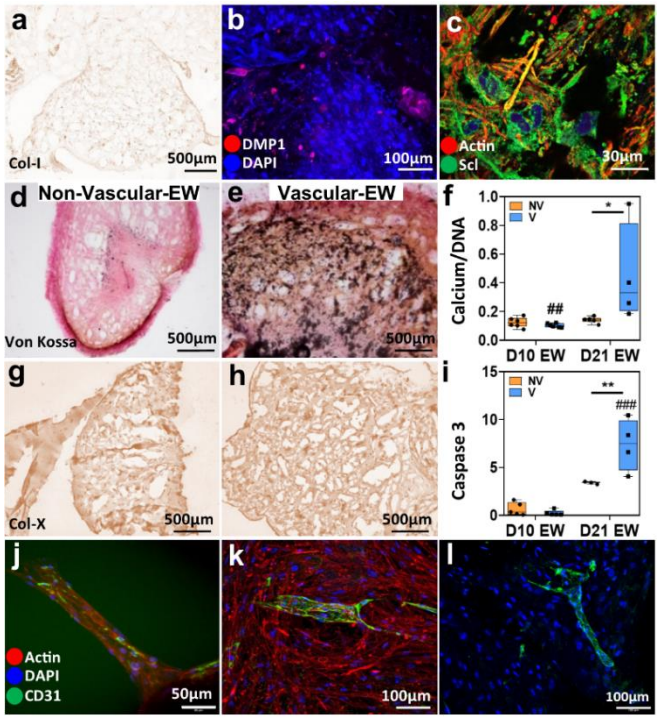

Figure 1: ***In vitro 3D vascularized and humanized bone model representative of the osteoporotic phenotype:*** *(a) IHC for Col-I, (e, f) IFC for DMP-1,Sclerostin. (d, e) mineral staining at day 21 (day 63 in culture), (f) calcium assay, (g, h) IHC for hypertrophic marker Col-X, (i) apoptosis gene expression - caspase 3. (j, k, l) Multicellular 3D vessels in estrogen withdrawal. $p < 0.05$ relative to E (*) and NV (#).*

DISCUSSION

This research provides an *in vitro* 3D vascularized and humanized bone model, which represents bone extracellular matrix protein and mineral composition, andrecapitulates estrogen deficiency representative of the osteoporotic phenotype. Under estrogen withdrawal, vascularised bone models had 3D multicellular vessel-like structures and were highly mineralised, which did not occur in non-vascular groups. An *in vivo* study reported that estrogen deficiency decreased blood vessels, increased adipocyte numbers and decreased bone mineral in ovariectomized mouse model [7]. These contrasting results might be explained by differential responses of human and mouse bone cells or differences between *in vivo* and *in vitro* studies. The significant increase in hypoxia, hypertrophy and apoptosis markers in the vascularised estrogen withdrawal conditions might explain increased mineral production. Ongoing studies are exploring molecular interactions between osteoclasts, vascular cells and osteoblasts during estrogen deficiency in the presence of mechanical stimulation.

REFERENCES: [1] Geoghegan et al. *Sci Rep* 9, 4654 (2019). [2] Geoghegan et al. *Sci Rep* 11, 9272 (2021). [3] Naqvi et al, Front Bioeng Biotechnol, 8:601, (2020). [4] Freeman et al. Tissue Eng Part A, 23(23- 24):1466-1478, (2017). [5] Freeman et al. Tissue Eng Part A, 22(19-20):1176-1190, (2016). [6] Allison et. al. BMC Mol Cell Biol 21, no. 1 (2020): 1-15. [7] Rodrigues et al. Nat Cardiovasc Res 1.10 (2022): 918-932.[8] Chen, Ning, et al. Bone Reports 19 (2023): 101698. [9] Kamakura, Takeshi, et al. JBMR plus (2023): e10737.

LEVERAGING CRISPR-CAS12 TO UNCOVER THE DEPENDENCIES OF EPITHELIAL TUMOUR CELLS CULTURED IN TISSUE-SPECIFIC, MECHANICALLY RELEVANT 3D MODELS

Mahon, O.R.[1,2,3,4], Obuseh,F.O.[5,6,7], De Matos, R.S.[2,3,4], McCarron, J.P.[8], Mooney, D.J.[5,6], Mitsiades, C.S.[2,3,4], Cunnane, E.M.[1]

[1] School of Engineering, Bernal Institute, University of Limerick, Ireland. [2] Department of Medical Oncology Dana Farber Cancer Institute, Boston, MA, USA. [4] Harvard Medical School, Boston, MA, USA. [5] Broad Institute of Massachusetts Institute of Technology (MIT) and Harvard, Cambridge, MA, USA. [6] Harvard-MIT Division of Health Science and Technology, [7] Harvard School of Engineering and Applied Science, [8] Wyss Institute, MA, USA. [9] Weill Medical College of Cornell University, NY, USA.

email: (olwyn.mahon@ul.ie)

INTRODUCTION

Solid epithelial tumours are inherently complex, characterized by heterogeneous cell populations, diverse microenvironments, and **altered tissue mechanical properties** that drive tumour progression and influence treatment response. Recent studies have highlighted the importance of considering the **viscoelastic behaviour of the tumour microenvironment** as it regulates cancer cell behaviours, such as migration, proliferation, and resistance to therapy [(1)]. However, we do not yet possess a comprehensive molecular understanding of how 3D models of solid tumours, with tissue-accurate mechanical properties, influence treatment resistance mechanisms and influence invasive cell behaviours and persistence. CRISPR-based gene editing allows for large-scale, unbiased interrogation of gene function across thousands of genes, offering insight into the genetic drivers of cancer cell dependencies and survival [(2)]. However, there are limited studies utilising CRISPR technology in 3D systems. 3D CRISPR would therefore allow us to investigate the genetic mechanisms underlying epithelial tumour cell behaviours in **mechanically mimetic 3D systems** to better understand gene functionality within the context of the tumour's mechanical environment. This study, for the first time, combines CRISPR-Cas12a gene editing, a novel Cas nuclease, with advanced 3D tissue models that exhibit tuneable viscoelastic properties [(3)].

MATERIALS AND METHODS

Cas12 cells (prostate; LNCaP, bladder; HT-1197 and breast; MCF7) were generated by transduction of EnAsCas12a plasmids (2). Cas12a expression was validated using immunocytochemistry, flow cytometry, and immunoblotting and Cas12a activity was assessed using sgRNA reporter plasmids. As a pilot study, Cas12a cells were transduced with the whole genome knock-out library, *Humagne C+D (*40,700 sgRNAs), to ensure effective nuclease activity over 2, 3, 4 & 5 weeks. gDNA was purified and sgRNA barcodes were PCR amplified and sequenced (data under analysis).

For 3D studies, norbornene modified collagen (nCol1) was fabricated as previously described [(3)]. Cells were encapsulated in fast or slow relaxing gels ($0.5x10^6$ cells/gel for RNAseq or $1.5x10^6$ for CRISPR seq); **Fig 1A**. After 2 weeks, gels were digested using collagenase and cells were isolated for RNA sequencing or gDNA purification. Data is under analysis as described in results section.

RESULTS

Stable Cas12a expression in generated lines was confirmed using immunoblotting and flow cytometry and Cas12 activity by reporter plasmids and flow cytometry; **Fig 1 B**. Data from the 2D pilot study for CRISPR screens is currently under analysis. The data analysis and algorithm will be utilised to assess 3D Cas12a CRISPR screens. Briefly, CERES scores, a metric of relative essentiality of an individual gene, will be calculated to correct for gene-independent DNA copy number effects of CRISPR gene-editing. CERES ranks and the MaGeCK algorithm will be used to identify essential and non-essential genes in 2D vs 3D. Preliminary data from 3D studies demonstrate that Cas12a MCF7 and LNCaP cells encapsulated in nCol1 gels were viable at 2 weeks post culture and were capable of proliferating; **Fig 1 C.** RNA transcriptomics for 2D vs 3D fast and slow relaxing gels is currently under analysis. *Humagne* whole genome knock-out library-transduced cells were encapsulated in nCol1 gels for 2 weeks and data will be used to identify gene essentiality in 2D vs appropriate 3D environments.

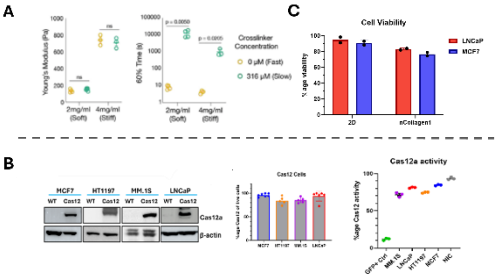

Figure 1 **(A)** Fast and slow relaxing norbornene Collagen gels from Adu-Berchie et al [(3)]. **(B)** Cas1a2 cell validation by immunoblotting and flow cytometry **(C)** Cell viability in 3D encapsulation.

DISCUSSION

This novel research will allow for the use of appropriate 3D systems to evaluate the mechanism of cancer behaviours and to uncover new insights into how genetic dependencies are shaped by mechanical cues. This approach holds promise for identifying the molecular and genetic basis for tumour progression and treatment resistance in patients with solid tumours.

REFERENCES

[1]Xin *et al. Oncogene*. **42**; 3457–3490, ***2023***
[2]DeWeirdt *et al. Nat Biotechnol.* **39;** 94-104, ***2021***
[3]Adu-Berchie *et al. Nat Biomed Eng.***7 ;**1374–1391, ***2023***

Biomimetic scaffolds for the repair and regeneration of knee articular cartilage

Wilson O.[1], Larraneta.E.L[2], Manda K[1]
[1]School of Mechanical and Aerospace Engineering, Queen's University Belfast, Belfast, UK
[2]School of Pharmacy, Queen's University Belfast, Belfast, UK
Email: owilson08@qub.ac.uk

INTRODUCTION

With the increasing prevalence of osteoarthritis (OA) linked to longer life expectancy (Wallace et al., 2017), the need for innovative and alternative OA is also on the rise. There is a growing interest in developing biomimetic scaffolds for articular cartilage that can offer required biomechanical and structural properties and provide suitable environment for functional tissue regeneration *in vivo*. Melt electrowriting (MEW) is an emerging additive manufacturing technique that enables the fabrication of highly organised, micro-scale fibrous scaffolds with tuneable mechanical properties. The aim of this work is to develop functional micro fibrous biomimetic scaffolds mimicking zonal architecture of native tissue for the repair and regeneration of knee articular cartilage. This will be done using (1) designing and developing biomimetic biomechanically suitable structures through computational homogenisation, (2) fabrication and mechanical characterisation of the developed scaffolds through MEW, (3) investigating the regenerative capabilities of the developed structures through computational modelling.

METHODS AND APPROACH

Using 3D modelling software, a series of biomimetic scaffolds will be developed and then the micro-macro relationships will be established by using homogenisation techniques and finite element analysis (FEA). The scaffold architecture will be optimised to mimic zonal apparent properties of native tissue. Using the MEW printing method, the optimised scaffolds will be fabricated on a GeSIM Bioscaffolder 3.1 (GeSiM, Germany). The use of MEW allows for higher accuracy prints using small diameters with some fibres being printed to 500nm (Javadzadeh, del Barrio and Sánchez-Somolinos, 2023). The Bioscaffolder also allows for multiple materials to be used when printing to allow for a variation in mechanical and physical properties. Once fabricated, mechanical characterisation of scaffolds will be carried out to allow for comparison with the simulated structures for improving future designs. Then, a regenerative capability of the scaffolds will be investigated by developing a computational model including the scaffold degradation and neo tissue formation over time. The model will investigate the intrinsic interplay between the swelling pressures and growth of collagen network in the growing cartilage tissue in the scaffolds.

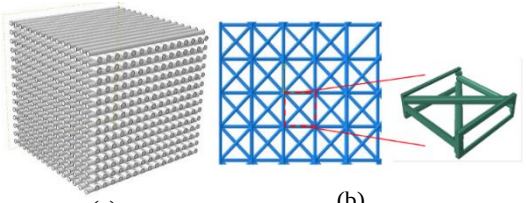

(a) (b)

Fig. 1. Scaffold structures, a) Lattice structure with strands deposited at 0-90 degrees and b) the strands deposited at 0-45-135 degrees.

RESULTS AND DISCUSSION

The results for this research will determine the suitability of allowing MEW to successfully print biomimetic scaffolds using lattice structures like the model seen in Fig.1. Similar studies have been conducted using fibre-reinforced hydrogels to improve the modelled cartilage zones (Castilho *et al.*, 2019), however they haven't investigated the regenerative potential of those scaffolds. The approach to this project aims to design, optimise and develop a computational framework to investigate regeneration of native cartilage in the scaffolds, therefore providing improved mechanical properties mimicking cartilage zones. The utilisation of an algorithm to generate a relationship between the scaffold degradation and cartilage regrowth, while monitoring the mechanical properties, will allow for the scaffold designs to be adapted to provide different properties as needed.

REFERENCES

Castilho, M. *et al.* (2019) 'Bi-layered micro-fibre reinforced hydrogels for articular cartilage regeneration', *Acta Biomaterialia*, 95, pp. 297–306. Available at: https://doi.org/10.1016/j.actbio.2019.06.030.

Javadzadeh, M., del Barrio, J. and Sánchez-Somolinos, C. (2023) 'Melt Electrowriting of Liquid Crystal Elastomer Scaffolds with Programmed Mechanical Response', *Advanced Materials*, 35(14). Available at: https://doi.org/10.1002/adma.202209244.

Wallace, I.J. *et al.* (2017) 'Knee osteoarthritis has doubled in prevalence since the mid-20th century', *Proceedings of the National Academy of Sciences*, 114(35), pp. 9332–9336. Available at: https://doi.org/10.1073/pnas.1703856114.

CHARACTERISATION OF VERTEBRAL BONE MARROW MESENCHYMAL STEM CELL POPULATIONS IN PATIENTS WITH PRE-ADOLESCENT IDIOPATHIC SCOLIOSIS

Ferreira, A.[1], Kiely, P.[2], Murphy, C.[1,3,4]

[1]Department of Anatomy and Regenerative Medicine, Royal College of Surgeons in Ireland, Dublin, Ireland. [2]Department of Orthopaedics, Children's Health Ireland (CHI) at Crumlin, Crumlin, Dublin, Ireland. [3]Trinity Centre for Biomedical Engineering, Trinity College Dublin, Dublin 2, Ireland. [4]Advanced Material and Bioengineering Research (AMBER) Centre, Trinity College Dublin, Dublin, Ireland

avelinoferreira@rcsi.ie

INTRODUCTION

Adolescent idiopathic scoliosis (AIS) patients undergo spinal fusion, with screws placed through the vertebrae pedicles and attached to rods, straightening the spine. During this procedure, a large amount of bone marrow is aspirated, but its characteristics in paediatric patients remain unstudied. This work aims to characterize the local bone marrow cell biology, which we hypothesize is a rich source of osteoprogenitor mesenchymal stem cells (MSCs) and could be utilized during surgery to improve fusion and fixation of the pedicle screws. Moreover, the impact of patient's age and sex, as well as harvest site (thoracic/lumbar, convex/concave part of the curve) in MSCs biology will also be studied.

MATERIALS AND METHODS

MSCs from bone marrow aspirates were isolated following very well-established density gradient centrifugation protocols[1]. Bone marrow aspirates were taken from lumbar and thoracic vertebrae from both convex and concave sides of the curve, and iliac crest as a control group. Expression of MSCs markers CD73, CD90 and CD105 was analyzed via flow cytometry, and osteogenic potential was assessed through calcium deposition – both staining and quantification – and gene (RUNX2, osteocalcin and osteopontin) expression.

RESULTS

MSCs were successfully isolated and expanded *in vitro*. Cells isolated from the iliac crest (IC) expressed lower MSC markers – namely CD105 – compared to both thoracic and lumbar MSCs. Moreover, IC cells express more negative markers (40%) than other cell populations (around 20%) (Figure 1A). Calcium deposition and mineralisation of lumbar MSCs was observed from 2 weeks of osteogenic differentiation in 5 out of 6 patients. Conversely, IC MSCs failed to deposit any detectable amount of calcium until week 3. In fact, even after 4 weeks, only 1 out of 3 IC MSCs showed signs of successful differentiation, suggesting lower osteogenic potential. Thoracic MSCs were generally able to differentiate and produce calcium, even if much later and in lower quantities than lumbar MSCs. Curiously, osteogenesis appears to be more easily obtained in MSCs obtained from convexity than the concavity of the curve. Staining results were confirmed by calcium quantification in independent samples. Interestingly, for IC MSCs, overexpression of master-regulator and early differentiation marker RUNX2 mirrors that of late osteogenesis marker osteocalcin, with a slight overexpression at all time points. Conversely, osteocalcin, was strongly overexpressed only at day 21 (Figure 1B). Representative images for calcium deposits staining from four MSCs populations from the same patient can be observed in Figure 1C. Lumbar MSCs deposited much more calcium than thoracic MSCs, while cells obtained from iliac crest failed to deposit any.

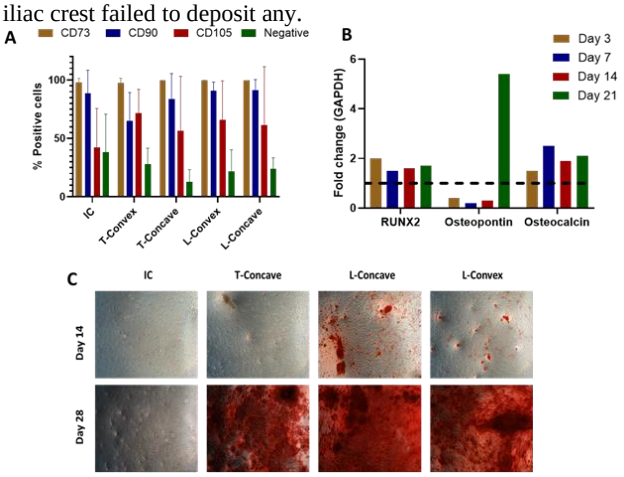

Figure 1. (A) Overall stemness markers expression, (B) Gene expression of IC MSCs, (C) Alizarin Red staining of MSCs after 14 and 28 days of osteogenesis.

DISCUSSION

MSCs were successfully isolated from IC and lumbar and thoracic vertebrae. Overall, lumbar MSCs display a stronger osteogenic potential when compared with thoracic and, IC MSCs, as they show greater calcium deposition. This can in part be explained by a general lower expression of stemness markers, namely CD105, by IC compared to MSCs originated from vertebral bone marrow. However, within each individual patient, although calcium deposition and mineralisation potential of MSCs varies between the different regions of isolation, stemness markers expression does not vary. These findings underscore patient-to-patient variability, but also how the expression of stemness markers alone is not sufficient to predict osteogenic potential of MSCs. Thus, further investigation into the correlation between these markers and osteogenic potential, as well as the effects of sex and age, is warranted to better understand MSC pathology in these patient cohorts. Finally, validation of these findings in a 3D environment, through the use of well-established osteogenic collagen-based scaffolds will be conducted.

REFERENCES

1. Pittenger et.al., Science. 1999

ACKNOWLEDGMENTS

Funded by RCSI Translational Seed Award programme

XENO-FREE MESENCHYMAL STEM CELLS UNDER MACROMOLECULAR CROWDING CONDITIONS AS A TISSUE-ENGINEERED SKIN SUBSTITUTE

Gonçalves, D.[1], Zeugolis, D.[1]
[1] Conway Institute of Biomolecular and Biomedical Research, School of Mechanical and Materials Engineering, University College Dublin, Dublin 4, Ireland
email: dimitrios.zevgolis@ucd.ie

INTRODUCTION

Skin substitutes aim to promote wound healing and closure. Currently clinically available tissue engineered skin substitutes utilise foetal bovine serum that is associated with immune response; use skin fibroblasts that are of lower therapeutic capacity than mesenchymal stromal cells; and require prolonged *in vitro* cultures that are associated with high manufacturing costs. To address these limitations, herein we describe the development of a tissue engineered skin substitute using xeno-free mesenchymal stromal cells under macromolecular crowding (MMC) conditions.

MATERIALS AND METHODS

Xeno-free human umbilical cord mesenchymal stromal cells (hUC-MSCs) from 3 donors were seeded at a density of 25,000 cells per cm^2 on tissue culture polystyrene (TCP) and cultured without and with macromolecular crowding (MMC) [10 µg/ml λ carrageenan (CR); 37.5 mg/ml 70 kDa + 25 mg/ml 400 kDa polysucrose cocktail (PSC1); 37.5 mg/ml 70 kDa + 25 mg/ml 400 kDa + 2.25 mg/ml 1000 kDa polysucrose cocktail (PSC2); 11.34 mg/ml 360 kDa polyvinylpyrrolidone (PVP); 50 µg/ml 75 kDa polystyrene sulfonic acid (PSSA); and 0.5 mg/ml 4000 kDa polyacrylic acid (PAA) for 4, 6 and 8 days. Cell morphology and ECM deposition was assessed via brightfield microscopy and electrophoresis and immunocytochemistry, respectively.

RESULTS

Among all MMC agents assessed, the PSSA induced aggregated cell morphology; CR and PAA induced the highest ECM deposition, as judged by electrophoresis and immunocytochemistry analyses. These data were confirmed among all three donors.

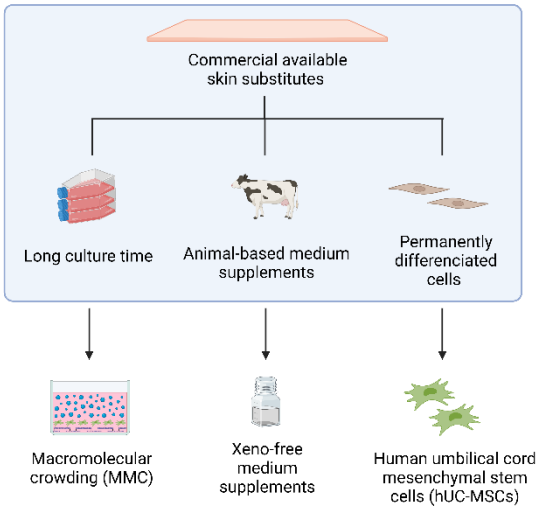

Figure 1 Progress beyond the state of the art for skin substitutes.

DISCUSSION

A promising approach to promote wound healing is the development of MSC-based advanced therapies, which offer a platform where ECM-embeded MSCs and, in particular, their secreted molecules significantly influence wound outcomes. Commercially available products are fabricated using animal-derived products, requires prolonged culture time and have lower therapeutic capacity comparing with MSCs. In this study, we assessed the culture of xeno-free hUC-MSCs under MMC conditions. CR and PAA were associated with higher ECM deposition, verified by electrophoresis and immunocytochemistry among the 3 donors.

REFERENCES

Kondej *(et al.)*, International Journal of Molecular Sciences 25:3702, 2024.
Toohey-Kurth *(et al.)*, Biologicals 47:64-68, 2017.
Zhang *(et al)*, Materials Today Bio 24:100918, 2024.
Vecin *(et al.)*, Frontiers in Medicine 10:1154567, 2023.

A pro-chodrogenic, multilayered, reinforced collagen-based scaffold fabricated using melt-electrowriting and electrospinning for meniscus regeneration

Calero-Castro, FJ.[1], Salimbeigi, G.[1], Hodgkinson T[1], Cryan, SA.[2], O'Brien FJ.[1,3]

[1]Tissue Engineering Research Group, Department of Anatomy & Regenerative Medicine, Royal College of Surgeons in Ireland, Dublin, Ireland; [2]School of Pharmacy & Biomolecular Sciences, RCSI, Ireland; [3]Advanced Materials and Bioengineering Research (AMBER) Centre, RCSI & Trinity College Dublin (TCD), Dublin, Ireland; Email: franciscocalero@rcsi.com

INTRODUCTION

Meniscal injuries, affecting 12% to 14% of the population, are the leading cause of functional impairment in the knee joint and can lead to osteoarthrisis.[1] Developing a successful engineered biomaterial with meniscus like mechanical and biological functionality is challenging.[2] Our group has extensive experience in cutting-edge scaffold fabrication processes such as electrospinning (EP) and melt-electrowritting (MEW) that have the potential to meet meniscus mechanical loading requirements.[3,4] Thus, the aim of this study is to develop an innovative biomimetic load-bearing scaffold mimicking the meniscus heterogenous extracellular matrix (ECM) combining a MEW-EP framework in combination with a collagen-glycosaminglycan (CG) matrix to enhance biological functionality thus offering fibro/chondrogenic properties to boost repair and restore the tissue.

MATERIALS AND METHODS

EP layers were fabricated using PCL, PLA and PVA on a 1000 rpm collector for aligned fibres. MEW constructs consisted in 15 layers of aligned PCL fibres topped with 15 layers of random PCL fibres. MEW-EP constructs were assembled in a thermal chamber with EP layers placed between MEW layers as previous described[3,5], forming four scaffold groups: (1) MEW-EP PCL, (2) MEW-EP PCL-PVA, (3) MEW-EP PLA, and (4) MEW-EP PLA-PCL-PVA. These frameworks were immersed in a Col I (0.5% w/v)/CS (0.05% w/v) slurry and freeze-dried to form the final composite scaffolds as previously described.[6] Fibre diameters were analysed via SEM. Tensile, compressive and shear moduli were measured. Scaffolds were cultured with human-derived bone marrow MSCs under chondrogenic conditions for 28 days for sGAG deposition as a marker of chondrogenic differentiation.

RESULTS

The scaffolds demonstrated structural and mechanical properties of different meniscal zones. EP PCL and PLA layers, mimicking the central meniscus, had compact aligned fibres with diameters of 7.74±0.93μm and 1.12±0.19μm, respectively (P<0.0001). MEW constructs, representing the middle and superficial meniscus, showed larger fibres averaging 20.82±1.30μm. PLA layers demonstrated superior tensile properties, with thermal crosslinking further enhancing tensile strength (Fig. 1 a). Compressive moduli (Fig. 1 b) ranged from 189.90 to 723.21kPa, PCL/PVA and PLA scaffold showed a compressive modulus similar to the meniscus tissue (200kPa). MEW-EP framework enhanced the CG matrix shear modulus (Fig. 1 c), while PVA improved collagen infiltration. The structural and mechanical improvements aligned with enhanced chondrogenic outcomes. MEW-EP PLA scaffolds, with the thinnest fibres and superior mechanical performance, supported the highest sGAG deposition 138.30±14.42µg/µg (Fig. 1 d), indicating their potential to mimic the native meniscal environment and promote tissue regeneration effectively.

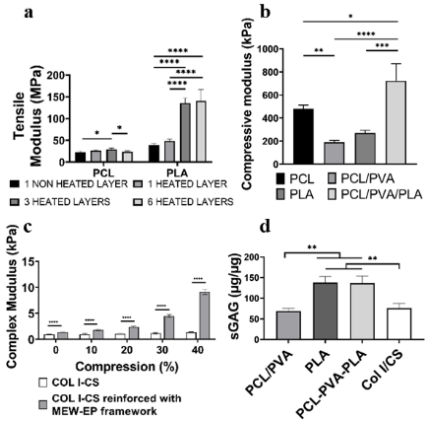

Figure 1: a. Tensile Modulus. b. Compressive modulus. c. Complex modulus. d. sGAG deposition.

DISCUSSION

The results of this study describe an innovative scaffold that overcomes the problems with existing biomaterials designed for meniscal repair. The MEW-EP framework successfully mimicked the meniscus ECM architecture and enhanced the mechanical properties of the scaffolds. Our novel composite design demonstrated a positive effect on the chondrogenic response of the MSCs at 28 day of culture.

REFERENCES

1. Krych, A. J., et al. *J. Am. Acad. Orthop. Surg.* **28**, 491–499, 2020. 2. Peng, Y. *et al. Front. Bioeng. Biotechnol.* **10**, 1–19, 2022. 3. Gouveia, P. J. *et al. Mater. Sci. Eng. C* **120**, 111657, 2021.4. Barceló, X., et al. *Acta Biomater.* **158**, 216–227, 2023. 5. Baek, J., et al. *Nanomedicine Nanotechnology, Biol. Med.* **23**, 102090, 2020.6. Intini, C. *et al. Biomater. Sci.* **10**, 970–983, 2022.

FUNDING ACKNOWLEDGEMENTS

The European Research Council (ERC) Advanced Grant n°788753 (ReCaP) support this project.

IN VITRO CHARACTERISATION OF 'OSSTIC': A PHOSPHOSERINE-ENHANCED ADHESIVE FOR IMPROVED BONE REGENERATION

Redmond, J.[1], Jaiswal, S.[1] Agarwal, S.[1], Tzagiollari, A.[2], Insley, G.[3] Levingstone, T.[1], Dunne, N.[1]
[1] Dublin City University, Dublin, Ireland. [2]Biomimetic Innovations Ltd (affiliate of PBC Biomed), Limerick, Clare, Ireland. [3]PBC Biomed, Accelerating Medical Innovation, Limerick, Clare, Ireland
email: john.redmond@dcu.ie

INTRODUCTION

Bone fractures are a global healthcare burden, notably complex bone fractures that occur in osteoporotic patients [1]. Fixation of fractured bone using metal implants via surgery is a current gold standard, though their use has limitations, where poor osteoporotic bone quality can lead to inadequate fixation. This can lead to implant failure, the need for re-operation, and long rehabilitation times.

To overcome these issues, a phosphoserine and calcium phosphate-based adhesive ('OsStic') has been developed [2]. The OsStic adhesive offers a promising solution that will adhere broken bone tissue together following fracture and facilitate rapid healing and repair of the bone. Calcium phosphate cements are frequently used in bone repair applications, due to their osteoconductivity and similarity to native bone tissue. The addition of phosphoserine not only augments the handling and mechanical properties of calcium phosphate-based cement but also provides additional functionalisation by promoting cell proliferation and differentiation [3]. This research project aims to assess the *in vitro* performance of the OsStic adhesive.

MATERIALS AND METHODS

OsStic samples (12×1.5 mm, diameter × height) were fabricated to a previously optimised composition containing phosphoserine, alpha tricalcium phosphate (αTCP) and calcium silicate [2]. Additional samples (αTCP-only and the industry standard, HydroSet™) were fabricated for comparative purposes. Before the *in vitro* studies, all samples were pre-conditioned in Ringer's solution for 72 h, followed by additional conditioning in alpha-MEM medium (aMEM) for 48 h. MC3T3-E1 cells were used for all *in vitro* studies.

Post-conditioning, cells were seeded at a density of $5x10^4$ per sample. Cell attachment, viability and proliferation assessments were performed in standard aMEM, using cell assays, SEM and fluorescence microscopy. For differentiation and osteogenesis assessments, differentiation was induced through supplementation of aMEM with ascorbic acid, β-glycerophosphate and dexamethasone. Proteins and genes associated with osteogenesis and differentiation were quantified using qPCR and ELISA.

RESULTS

Cytotoxicity testing following the ISO 10993-5 demonstrated no material-related cytotoxicity by the OsStic adhesive. Cells readily adhered and became confluent on the OsStic adhesive, visually confirmed through SEM (Fig. 1a) and LIVE/DEAD™ viability staining (Fig. 1b). Sustained proliferation and continuously increasing cell numbers were confirmed via the alamarBlue assay over 4 weeks (Fig. 1d). Alizarin red staining (qualitative and quantitative) demonstrated significant biomineralisation occurring (Fig. 1c & 1e). Alkaline phosphatase (ALP) activity was also observed through an enzymatic assay, further corroborated by positive ALP detection using BCIP/NBT staining solutions. Secretion (ELISA) and expression (qPCR) of osteogenic and differentiation markers including osteopontin, osteocalcin, collagen type 1, BMP-2 and RUNX2 were observed.

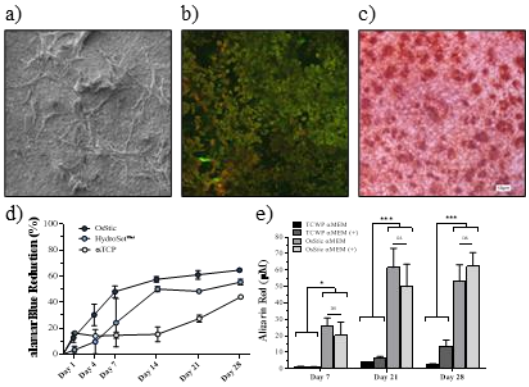

Figure 1 a) SEM image of MC3T3-E1 cells on OsStic. b) LIVE/DEAD fluorescence microscopy. c) Alizarin Red staining. d) Cell proliferation. e) Mineralisation quantification assay.

DISCUSSION

The OsStic adhesive demonstrated strong biocompatibility, as shown through the ability of cells to adhere and proliferate on its surface. Biomineralisation was observed on the OsStic surface, an essential process for bone repair. Cells cultured on OsStic also secreted and expressed osteogenic and differentiation-related factors, highlighting its potential to actively support bone regeneration and healing processes, in addition to its benefits in stabilising osteoporotic bone fractures. Results to date demonstrate OsStic's potential to enhance bone stabilisation and accelerate fracture repair when compared to proprietary technologies used in orthopaedics.

REFERENCES

[1] Wu *(et al.)*, Lancet Healthy Longev. 2(9). 580-592, 2021. [2] Tzagiollari *(et al.)*, Acta Biomater, 174, 447-462, 2024. [3] Ying *(et al.)*, Cell Biol Int. 38(3),309-317, 2014.

REGULATORY CUES TO MODULATE THE STRUCTURAL AND COMPOSITIONAL PROPERTIES OF 3D BIOPRINTED MENISCAL GRAFTS

Chattahy, K.[1] Kronemberger, GS.[1] Karam, A.[1] Kelly, DJ.[1]
[1] Department of Mechanical, Manufacturing and Biomedical Engineering, Trinity College Dublin, Dublin, Ireland
email: chattahk@tcd.ie

INTRODUCTION

Meniscal injuries affect over 1.5 million individuals annually across Europe and the USA[1]. Meniscus regeneration remains a great challenge due to their poor intrinsic healing potential, particularly in avascular lesions[2]. Common meniscal injury repair interventions alter joint biomechanics and increase the risk of developing osteoarthritis[3]. This drives the need for effective meniscal tissue engineering solutions to reconstruct the structural inhomogeneity and anisotropy of meniscus tissue, including its zonal composition, structure and biomechanics, particularly the circumferentially aligned collagen fibers that provide tensile strength and stiffness[4]. In this study, we aim to 3D bioprint biomimetic scaffold-free meniscal grafts by leveraging the capacity of meniscal progenitor cell-derived microtissues to self-organize into complex anisotropic meniscal fibrocartilage tissue. Additionally, we evaluated the effect of temporal presentations of regulatory cues, specifically transforming growth factor-beta 3 (TGF-β3) and connective tissue growth factor (CTGF), on inner and outer caprine meniscus progenitor cells (iMPC and oMPC) to engineer anatomically defined meniscal grafts with regional structure and composition. Furthermore, we cultured MPCs in different oxygen tensions (5% and 20%) to evaluate how hypoxic and normoxic conditions impact their region-specific fibrocartilaginous differentiation and extracellular matrix deposition.

MATERIALS AND METHODS

Various patterns and densities of MPC-derived microtissues (20,000, 30,000, and 40,000 microtissues per ml of bioink, with 2,000 cells per microtissue) were combined with 1% gelatin to prepare the bioink, which was then 3D bioprinted into a methacrylated xanthan gum support bath using the syringe pump printhead of the Cellink BioX6. The bioprinted constructs were cultured in chondrogenic media for 4 weeks. Simultaneously, 3D pellets of inner (iMPC) and outer (oMPC) MPCs were treated with different growth factor protocols, including sequential treatment with TGF-β3 and CTGF or continuous treatment with either TGF-β3 or CTGF for 4 weeks. Both iMPC and oMPC pellets were also cultured in hypoxic (5% O_2) and normoxic (20% O_2) conditions for 4 weeks in the presence of TGF-β3.

RESULTS

Optimal resolution and print fidelity were achieved using a 22G needle in a 1% XG-MA support bath. The bioink with 45,000 MPC-derived microtissues/ml produced the most continuous and robust filaments (Fig 1.A), with enhanced collagen and sGAG deposition, particularly type I collagen. Organised collagen fibers were observed using both the 30,000 and 45,000 microtissues/ml bioinks (Fig 1.A), demonstrating that the spatial confinement provided by the support bath direct collagen development.

CTGF alone caused shrinkage, while TGF-β3 or sequential TGF-β3/CTGF treatments (T→C/C→T) maintained size and promoted sGAG and collagen deposition. The sequential treatments created a collagen gradient, with type I at the edges and type II in the core of the construct (Fig 1). iMPCS secreted more sGAGs under 5% O_2, while oMPCs secreted more collagen at 20% O_2 (Fig 1.B).

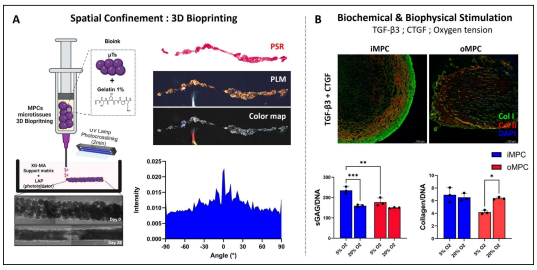

Figure 1 Effects of regulatory cues on iMPCs and oMPCs. (A) Microscopic images of 45,000 microtissues 3D bioprinted in a straight line at day 0 and 28, with PSR staining and a collagen directionality map. (B) Immunofluorescence for collagen I/II in iMPC and oMPC pellets treated with TGF-β3 and CTGF. sGAGs and collagen quantification for cultures at 5% and 20% oxygen levels.

DISCUSSION

High microtissue density bioinks (45,000 MPC-derived microtissues/ml) support strong fusion and organised ECM deposition, critical for developing meniscal grafts with enhanced structural integrity. Sequential GFs treatments yielded distinct collagen patterns, while different oxygen levels promoted either enhanced collagen or sGAG synthesis depending on the progenitor cell source, providing insight into the engineering of meniscal constructs with native-like tissue properties.

REFERENCES

[1] Bansal *et al.*, J Orthop Res 39(7):1368–1382, 2021.
[2] Yan W *et al.*, Front. Cell Dev. Biol. 9:758217. 2021.
[3] Trivedi *et al.*, Front Bioeng Biotechnol. 9:787330. 2021. [4] Vignes et al., Organoids 1, 116–134. 2022.

DEVELOPMENT OF A VERSATILE MUSCULOSKELETAL TISSUE BIOPRINTING PLATFORM TO DIRECT PREFERENTIAL COLLAGEN ALIGNMENT IN HIGHLY CELLULAR BIOINKS

Storey[1, 2, 3], KJ, Kronemberger[1, 2, 3], GS, Kelly[1, 2, 3], DJ,
[1] Trinity Centre for Biomedical Engineering, Trinity Biomedical Sciences Institute, Trinity College Dublin
[2] Department of Mechanical, Manufacturing & Biomedical Engineering,
[3]Advanced Materials & Bioengineering Research Centre (AMBER)
email: storeyk@tcd.ie

INTRODUCTION

Functional regeneration of musculoskeletal tissues requires engineered grafts that mimic the heterogenous and anisotropic structure and mechanics of the native tissue. Existing strategies fail to produce tissues that mimic this structural complexity, often leading to deficits in mechanical properties and repair failure *in vivo*. 3D bioprinting allows for the freeform patterning of cells and biomaterials at the microscale, potentially enabling the engineering of constructs that mimic the structural complexity of biological tissues. High cell density 3D embedded bioprinting has recently emerged as a versatile biofabrication tool for the generation of spatially organised tissues using high cell density hydrogel composite bioinks [1]. This technique enables the production of complex, free-form constructs using mechanically weak hydrogels. Here we hypothesise that the support bath used in such embedded bioprinting strategies can also be leveraged to direct the growth and spatial organisation of the secreted extracellular matrix (ECM). Our goal is to develop a versatile muscoskeletal bioprinting platform capable of fabricating anisotropic, mechanically functional tissues with preferential collagen alignment, leveraging the spatial cues and confinement forces from the embedded support bath.

MATERIALS AND METHODS

Goat bone marrow mesenchymal stem/stromal cells (gBMMSCs) were encapsulated within a pre-crosslinked (60mM $CaCl_2$-5min) oxidised alginate (OA) bioink at a high cell density (60e^6 cells/ml). These bioinks were subsequently bioprinted within an oxidised-methacrylated alginate (OMA) support bath using a mechanically driven syringe pump printhead, and ionically and UV crosslinked post-print and maintained in chondrogenic culture for 6 weeks. Various printing parameters such as needle size, print speed, extrusion rate, and construct spatial configuration were systematically varied to produce tissue constructs with defined resolution and preferential alignment of developing collagen fibres, whilst maintaining a robust chondrogenic phenotype. Assessment was undertaken using brightfield microscopy, biochemical and histological evaluation, and polarised light microscopy.

RESULTS

High cell density bioinks (60e^6 cells/ml-gBMMSCs-OA) were bioprinted within an OMA support bath to a high degree of resolution (200-400 μm), whilst maintaining bioprint fidelity. Print parameters could be tuned to control bioprint resolution (~200 μm) and importantly, enhance the preferential alignment of developing collagen fibres (Fig. 1c) whilst maintaining cellular viability (97% viable) (Fib. 1b). MSCs were found to undergo chondrogenic differentiation, as confirmed using an assessment of sulphated-glycosaminoglycans (sGAGs) and collagen production both biochemically and histologically (Fig. 1c).

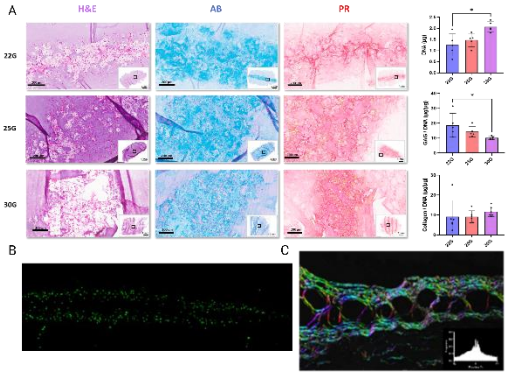

Figure 1 A) Chondrogenic evaluation of bioprinted filaments into an OMA support bath, varying needle size**. B)** Tile-scan, Z-stack image of live-dead staining of a bioprinted filament at D7. **C)** Polarised-light microscopy analysis of a picrosirius red stained bioprinted filament, demonstrating a high degree of alignment. Scale bars are equal to 200 μm in the microscopic images, and 1-2mm in the macroscopic images. * indicates significance $\rho < 0.05$.

DISCUSSION

This body of work has showcased the ability to preferentially control the alignment of developing collagen fibres within constructs generated using embedded bioprinting, whilst maintaining a high resolution and supporting a chondrogenic phenotype. Future work will focus on modulating the mechanical profile of the supporting bath to further drive alignment and modulate the chondrogenic phenotype from hyaline to fibrochondrogenic.

REFERENCES

1. Jeon, O., *et al*. Materials Horizons. 6:8:1625-1631, 2019.
2. Barceló, *et al*. Biomedicines. 10:7:1621, 2022

A NOVEL APPROACH FOR 3D CHARATERISATION OF DRUG RELEASE FROM DRUG DELIVERY DEVICES

Tannian, J[1]., Duffy, G.P.[1, 2, 3], Levey, R.E.[1].

[1] Anatomy and Regenerative Medicine Institute, Nursing and Health Sciences, University of Galway, [2] SFI Advanced Materials and Bioengineering Research Centre (AMBER), Trinity College Dublin & University of Galway. CÚRAM, [3] SFI Research Centre for Medical Devices, University of Galway & RCSI, Galway, Ireland
email: garry.duffy@universityofgalway.ie & ruth.levey@universityofgalway.ie

INTRODUCTION

Drug delivery devices represent an innovative approach towards advancing biomedical and pharmaceutical technology, addressing challenges like the foreign body response (FBR) (1). Despite various mitigation strategies, the FBR remains a significant challenge to implantable medical devices (1). To evaluate device performance against this complex response, extensive benchtop testing is essential prior to in-vivo experimentation. Agarose gels of varying concentrations have been employed to model the impedance and permeability changes associated with the progressive nature of the FBR (2). While previous in-vitro studies have been limited to 2D analysis, we have developed a novel 3D methodology for drug diffusion characterisation, providing deeper insights into diffusion dynamics and device performance.

MATERIALS AND METHODS

Requirements for a 3D image:

- Multiple 2D views – X-plane cameras
- Depth information – Y-plane camera
- Depth (voxel)
- Area Measurements
- Proper scale

Autodesk Fusion 360 was used to design camera-holding moulds to ensure accuracy and reproducibility (Figure 1). 0.6% agarose was centrally placed within the mould. A syringe pump was used for infusion. 0.04% methylene blue was used a delivery analogue for quantification. A python script was used to automatically acquire images from the X-plane at 15 second intervals for 16 minutes with Dinolite cameras. The X-plane images were analysed with an ImageJ macro to quantify the release area. At the end of the experimental run, a third Dinolite camera was used to acquire an image from the Y-plane image. The Y-plane image was used to obtain the depth of the sample, and the voxel dimensions were obtained through dividing the depth of the sample by the total number of acquired images.

RESULTS

The developed methodology enabled the creation of a 3D model suitable for analysing drug diffusion dynamics. X-plane images, captured at 15 second intervals during 16-minute infusion, provided data on diffusion areas, while a Y-plane image captured the samples depth. Voxel dimensions were calculated by dividing the depth by the number of X-plane images, enabling a 3D reconstruction. This approach offers a robust method for evaluating drug delivery systems, providing detailed insights into diffusion dynamics in a 3D context.

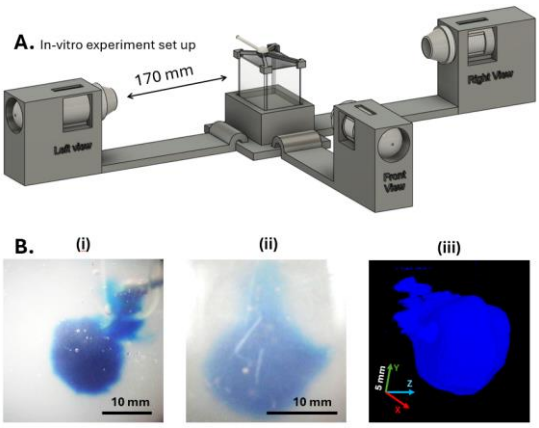

Figure 1 **A:** in-vitro experimental set up. Figure shows the centrally placed container at equal distances from the Dinolite cameras with a drug delivery device held within the center of a transparent container. **B**: 3D imaging methodology. (i) X-plane image, (ii) Y-plane image, (iii) 3D reconstruction of the sample.

DISCUSSION

The development of a 3D methodology for drug diffusion characterisation represents a significant advancement for the in-vitro evaluation of for drug delivery systems. By integrating X-plane imaging for area analysis with Y-plane depth measurements, this approach moves beyond the limitations of 2D analysis, offering a more comprehensive understanding of diffusion dynamics.

REFERENCES

(1) Dolen (et al). Sci Robots, 4, 2019
(2) Beatty (et al). Sci Robots, 8 (81), 2023

Exploration of Indane Scaffold Antagonists for Combination Prostate Cancer Therapy with Cold Atmospheric Plasma

Shengxin, Zhang.[1,2], Gemma K. Kinsella.[1,2], Tao Zhang.[1,2], James F. Curtin.[2,3]
[1]School of Food Science and Environmental Health, Faculty of Sciences and Health, Grangegorman, TU Dublin
[2]Faculty of Engineering & Built Environment, Bolton Street, TU Dublin
[3]Sustainability and Health Research Hub, Grangegorman, TU Dublin
email: james.curtin@tudublin.ie

INTRODUCTION

Cold atmospheric plasma (CAP) is a tunable source of reactive oxygen and nitrogen species (RONS) - ie. O, $^1O_2$, O_3, OH, O_2H, O^{2-}, O^{3-}, NO, NO_2 that has been successfully tested in clinical trials as an innovative cancer therapy. CAP enhances drug delivery efficiency and therapeutic outcomes by generating RONS and inducing transient cell membrane permeability, which facilitates increased penetration and transport of therapeutic agents into tissues or cells, thereby improving drug targeting and bioavailability.[1] Furthermore, CAP eliminates cancer cells but spares healthy tissues, unlike traditional chemotherapy and radiotherapy, which significantly reducing the adverse side effects. [2]

Prostate cancer (PCa), the second leading cause of cancer-related death in men, remains a significant therapeutic challenge, with limited progress in extending survival through current treatments. [3] And, several compounds of Indane derivatives have been reported to exhibit significant anti - PCa capabilities.[4]

In this study, we investigated the cytotoxic effects of nine indane derivatives in combination with a pin-to-plate device (Figure 1) for direct treatment of PCa cell lines PC3 and LNCaP. This research aims to evaluate their potential as a synergistic therapeutic strategy.

MATERIALS AND METHODS

Cell viability was analysed using Alamar Blue™ cell viability reagent. PC3 and LNCaP cells were seeded on flat - bottom 96 - well plates in 100 µl DMEM and left to adhere overnight at 37 °C in a humidified atmosphere at a density of 4.5×10^3 or 1×10^4 cells / well for 72 h incubation time post - treatment and 144 h post - treatment, respectively. DMEM media without sodium pyruvate and RPMI media which supplemented with 10% FBS and 1% penicillin/streptomycin for PC3 and LNCaP cells, respectively.

For CAP treatment, previous media was removed and 25 µl of fresh media or diluted drug in dimethyl sulfoxide (DMSO) stock solution was added for treatment in each well, unless otherwise specified. Cells were then treated using different doses of CAP. After treatment, fresh media or diluted drug in DMSO stock solution was added and cells were incubated at 37 °C using 5 % CO_2 for 72 h or 144 h.

After incubation cells were washed with sterile phosphate - buffered saline (PBS) and incubated for 3 h at 37 °C with a 10% Alamar Blue ™ solution in DMEM/RPMI media without FBS. Fluorescence was measured using an excitation wavelength of 530 nm and an emission wavelength of 595 nm with a Varioskan Lux multiplate reader (Thermo Scientific). DMSO (20%) was used as a positive control.

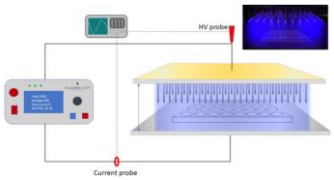

Figure 1 Pin-to-plate device.[5]

RESULTS AND DISCUSSION

One indane derivative was identified that acted as a prodrug and demonstrated significant cytotoxic synergy when combined with 10 s and 20 s CAP treatments, which alone demonstrated minimal or no toxicity toward PC3 and LNCaP cells. The IC_{50} values of the indane derivative alone and in combination with 10 s and 20 s CAP treatments for PC3 cells were 430.9 µM (373.2 µM ± 497.6 µM), 130.9 µM (104.2 µM ± 164.5 µM), and 39.11 µM (26.89 µM ± 56.88 µM), respectively. This represents a significantly enhanced in cytotoxicity due to the reactive species generated by CAP in the combination treatment.

Our findings highlight the potential of combining CAP with indane derivatives as a programmable cytotoxic therapy and a drug delivery approach. Moreover, this study provides a foundational framework for further screening and development of indane prodrug derivatives as effective cancer therapeutics.

REFERENCES

[1] Graves, *(et al.)*, Plasma Processes and Polymers, Volume: 11, no. 12, pp. 1120–1127, 2014.
[2] Semmler, *(et al.)*, Cancers, Volume: 12, 2022.
[3] Wang, *(et al.)*, Frontiers in Public Health, Volume: 10, 2022.
[4] Schreurs, *(et al.)*, Toxicology Letters Volume:156, 261–275, 2005.
[5] Aguiar, *(et al.)*, Plasma Processes and Polymers, Volume:8, 2022.

RATIONAL DESIGN AND CHARACTERISATION OF CELL PENETRATING PEPTIDE FOR NON-VIRAL GENE DELIVERY

Lin GJ.[1], Saha C.[1], Coulter J.[1], Dunne N.[2], McCarthy HO[1]
[1] School of Pharmacy, Queen's University Belfast, Belfast, Northern Ireland, United Kingdom
[2] School of Mechanical & Manufacturing Engineering, Dublin City University, Dublin, Republic of Ireland
email: (glin01@qub.ac.uk)

INTRODUCTION

Messenger RNA (mRNA) therapeutics face significant challenges due to the inherent instability and vulnerability of mRNA to enzymatic degradation, which can severely limit its effectiveness in reaching target cells.[1] Cell-penetrating peptides (CPPs) are short peptides capable of traversing cellular membranes, thereby facilitating the intracellular transport of mRNA.[2, 3] By forming stable complexes with mRNA, CPPs protect it from rapid degradation while significantly improving cellular uptake. In this study, we designed and invented a new 24-amino-acid CPP, termed HAWC, from consensus sequences found in human, viral and bacterial proteins involved in cellular transport. We complexed the HAWC peptide with mRNA and measured a range of physiochemical and *in vitro* characteristics. Additionally, the delivery mechanism of HAWC was preliminarily investigated, providing insights into its potential application as a delivery vehicle for mRNA-based therapeutics.

MATERIALS AND METHODS

Nanoparticles (NPs) were formulated through the electrostatic interaction between the negatively charged nucleic acids and the positively charged HAWC peptides, resulting in stable complexes. The physical characteristics of the NPs, including particle size and surface charge, were assessed using a Nano ZS Zetasizer equipped with DTS software (Malvern Instruments). To evaluate the encapsulation efficiency of the formulated NPs, ion-exchange chromatography (IEC) was used. For transfection studies, NCTC-929s fibroblasts were first cultured to 70-80% confluence before addition of HAWC/mRNA NPs. Transfection efficiency was analysed using flow cytometry after 24 h while cytotoxicity was assessed with propidium iodide (PI).

RESULTS

NPs with an average size of about 100 nm, a zeta potential of about +20 mV, and a polydispersity index (PDI) below 0.1 were successfully formed across a range of NP ratios (Fig. 1A). These NPs exhibited high encapsulation efficiency, exceeding 95% as determined by IEC (Fig. 1B). The transfection efficiency of these HAWC/mRNA NPs was found to range between 73.7% and 81.4% in NCTC-929 fibroblasts between different NP ratio (Fig. 1C). Notably, no cytotoxic effects were observed in this cell line.

Mechanistic studies involving the inhibition of cellular uptake pathways with various chemical inhibitors demonstrated that the HAWC NPs entered cells via clathrin-dependent endocytosis and micropinocytosis (Fig 1D).

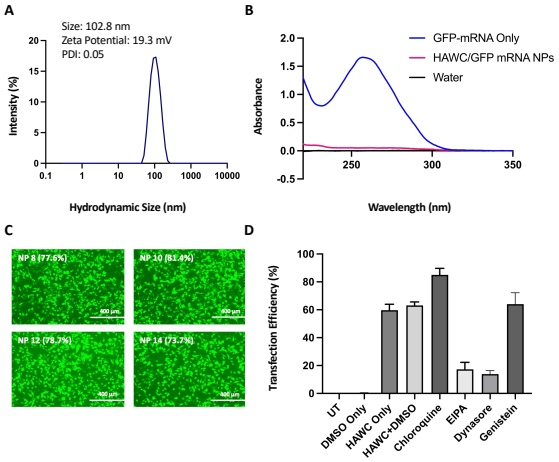

Figure 1. (A) Representative DLS spectrum of HAWC NPs. (B) The results of encapsulation efficiency of NPs were measured by IEC. (C) Images of different NP Ratio in NCTC-929s. (D) Exploring cellular uptake pathways by different chemical inhibitors.

DISCUSSION

We successfully formulated HAWC/eGFP-mRNA NPs and achieved efficient transfection into NCTC-929 cells, while confirming the non-toxic of the delivery system. Additionally, we investigated the cellular uptake mechanism of HAWC, which involves clathrin-dependent endocytosis and macropinocytosis. These findings demonstrate the potential of HAWC as a versatile carrier for the delivery of nucleic acid cargo, paving the way for further applications in gene therapy and mRNA-based therapeutics.

REFERENCES

Journals:
1. Blenke, Erik Oude, *et al*. Journal of pharmaceutical sciences: 386-403, 2023
2. Yokoo, H., *et al*. Pharmaceutics: p.78, 2021
3. Hasannejad-Asl, Behnam, *et al*. Frontiers in Pharmacology: 1072685, 2022

COMPUTATIONAL MODELLING OF DRUG DEPOT FORMATION DURING SUBCUTANEOUS INJECTION

Kho, A.S.K.[1,2], McGrath, S.[3], Wencel, D.[3], O'Cearbhaill, E.D.[4], Ní Annaidh, A.[4]
[1] School of Mechanical and Manufacturing Engineering, Dublin City University, Dublin 9, Ireland
[2] DCU Life Sciences Institute, Dublin City University, Dublin, Ireland
[3] BD Research Centre Ireland Ltd, Carysfort Avenue, Blackrock, Ireland
[4] UCD Centre for Biomedical Engineering, University College Dublin, Belfield Dublin 4, Ireland
email: antony.kho@dcu.ie

INTRODUCTION

Subcutaneous (SC) injection has been widely used to deliver drugs that require slow and sustained absorption. A key feature of SC injection is the formation of a depot at the injection site, where the drug is gradually absorbed by the circulation (Peppin *et al.* 2023). The shape and volume of depot formation during SC injection plays a crucial role in achieving the desired therapeutic effect. However, the mechanism behind depot formation and its interaction with drug release kinetics during SC injection remains poorly understood. This process involves dynamic tissue deformation during injection, i.e. separation of tissue from the cannula or needle wall. Experimental studies to capture the dynamics of SC depot formation are often constrained by technical limitations, such as monitoring tissue deformation during depot formation. Computational models offer a promising solution as they provide a means to simulate and predict dynamic tissue deformation during depot formation. To the authors' best knowledge, no study has been able to model dynamic tissue deformation during SC injection due to its complexity. Hence, this study seeks to bridge this gap by developing a computational model of SC injection that can describe dynamic tissue deformation during SC injection with the aim to provide a deeper understanding on the mechanism behind SC depot formation.

MATERIALS AND METHODS

A multiphysics model of SC injection was developed in COMSOL Multiphysics 6.2 that included solving the bulk fluid in the needle given as:

$$\rho_f \nabla \cdot \boldsymbol{u_f} = 0,$$

and dynamic tissue deformation as given below:

$$\nabla \cdot \sigma + \boldsymbol{f_b} = \rho_s \frac{\partial^2 \boldsymbol{u_s}}{\partial t^2}.$$

where ρ_f is fluid density, $\boldsymbol{u_f}$ is fluid velocity, σ denotes the total stress tensor, $\boldsymbol{f_b}$ is the body force per unit volume, ρ_s is the density of the SC tissue, $\boldsymbol{u_s}$ is the displacement of SC tissue and t is time. To model the separation of tissue from the cannula wall, an interface damage mechanics based cohesive zone model was used. The model was developed as 2D axisymmetric, which consisted of SC tissue and a 25G cannula.

RESULTS

Figure 1a shows the bulk fluid flowing through the cannula and forming the depot at the end of injection. Figure 1b depicts the corresponding pressure distribution inside the cannula and SC tissue, while Figure 1c depicts the corresponding tissue displacement.

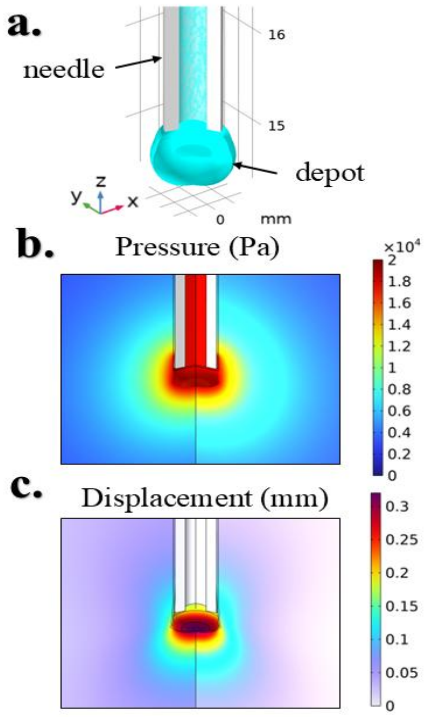

Figure 1 (a) Illustration of bulk fluid flowing through needle and forming the depot, (b) pressure distribution inside needle and SC tissue, and (c) tissue displacement at the end of injection.

DISCUSSION

To the author's best knowledge, this is the first study that has developed a computational model of SC that can account for dynamic tissue deformation during injection, which involves the separation of tissue from the cannula wall. By including the effects of dynamic tissue deformation, the model can provide a pivotal insight into the mechanisms that influence the geometry of depot formation during SC injection.

REFERENCES

Pepin *(et al.)*, Pharmaceutical Research, 40(9): pp.2195-2214, 2023.

ULTRA-THIN COATING OF VASCULAR DEVICES

O'Neill, F.[1, 2], Frewen, C.[2], O'Neill, L.[2], Bourke, P.[1]
[1] School of Biosystems and Food Engineering, UCD
[2] TheraDep Ltd., Questum, Clonmel, Co. Tipperary, Ireland.
email: (fiona.m.oneill@ucdconnect.ie)

INTRODUCTION

Traditional coatings of vascular devices are performed using dipping or spraying processes, with coating thicknesses typically within the range of 10 – 100 microns. In order to reduce this, a new coating process has been developed based on a cold plasma deposition method. This opens the door to create nano-scale coatings that can reduce thrombogenicity, enhance biocompatibility and deliver functional coatings. This study investigated cold plasma deposition as an alternative to wet spray methods for Everolimus coatings on nitinol stents as a model vascular device.

MATERIALS AND METHODS

Coatings were applied using a custom built BioDep plasma system provided by TheraDep Ltd., Ireland [1,2] Everolimus was sourced from Kemprotec Ltd. UK and ethanol was purchased from Sigma Aldrich. Lipidure was sourced from NOF, Japan. Titanium substrates were provided by Lisnabrin Engineering, Cork. Nitinol stents were provided by Admedes, Germany.

RESULTS

Everolimus Deposition:
The active pharmaceutical ingredient (API) was deposited using either a traditional wet spray method or via a plasma deposition method and the coatings were subjected to detailed chemical and physical characterisation.
The coating was deposited as a uniform and continuous nano-scale layer on the surface of the metal, as shown by AFM and microscopic examination. No significant alterations in roughness or thickness could be detected.
The chemistry of the coating was examined using infra-red spectroscopy and high-performance liquid chromatography (HPLC). This analysis produced no indication of degradation of the API due to the plasma process.
As the coating was found to be mechanically robust and chemically intact, a functional assay was carried out using cell culture techniques to determine if the API could be eluted from the surface and if it retained its anti-proliferative effect on cells in an in vitro setting. The results showed significant drug efficacy in all cases.

Polymer Coating:
Lipidure coatings were produced by spraying an ethanol solution through the same BioDep plasma process used for the Everolimus deposition. The resultant coating was deposited as a dry, smooth, conformal layer with no subsequent processing.
Electron microscopy and ellipsometry analysis suggested that the thickness could be varied from 1 – 100 nm by altering the deposition time and flow rates.

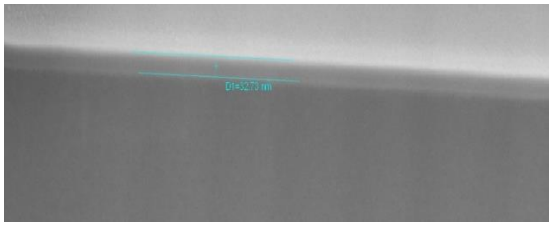

Figure 1. Scanning electron microscopy image showing deposition of a conformal coating layer of 33 nm on a silicon wafer.

The coating remained intact on the stent surface during crimping and deployment studies. Thrombus formation studies showed significant reduction in thrombus formation when compared to bare metal stents.

DISCUSSION

This work has shown that a representative vascular API (Everolimus) can be effectively deposited onto a metal surface and subsequently eluted back off using the plasma process.
Separate studies have shown that this plasma coating technique is also capable of depositing nanoscale layers of functional polymers onto vascular stents and balloons and these coating have been shown to significantly reduce thrombogenicity.
The next stage is to combine that drug layer with a nano-scale polymeric coating that can help to modulate the drug elution. When combined, these layers can give rise to a drug eluting coating with a total thickness of less than 100 nm.
This study opens the door to create nano-scale coatings to reduce thrombogenicity, enhance biocompatibility and deliver functional coatings on vascular devices.

REFERENCES

[1] Los et al,, Frontiers in Cellular and Infection Microbiology, 19, 1-9, 2019.
[2] Helms et al., Materialia, 17, 101122, 2021

JET STREAM INJECTION FOR NEEDLE-FREE GASTROINTESTINAL DIAGNOSTIC AND THERAPEUTIC FLUID DELIVERY

Lijnse, T.[1,2], O'Cearbhaill, E.[1,2]
[1] School of Mechanical and Materials Engineering, University College Dublin
[2] CÚRAM, Research Ireland Centre for Medical Devices
email: thomas.lijnse@ucd.ie

INTRODUCTION

With a rising incidence rate of gastrointestinal (GI) and specifically bowel and intestinal disorders [1], there is an increased need to be able to deliver diagnostic and therapeutic agents to the wall of the GI tract. While there are direct endoscopic procedures, such as endoscopic tattooing wherein a marking fluid is delivered to the lower GI tissue to mark polyps or lesions, these procedures are highly complex and rely on advanced operator precision to avoid perforating the GI tract while still delivering appropriate volumes of fluid to the sub-mucosal layers.

The development of a simple and effective tool for endoscopic fluid delivery to GI tissues will greatly improve diagnostic and treatment options for a wide array of GI disorders. To ensure accurate function, any tool which aims to deliver submucosal boluses must appropriately control the tissue boundary conditions and deliver fluid without risk of tract perforation, while also minimising misdirected intraluminal delivery. To accomplish this, we propose the use of a needle-free jet velocity liquid stream injection for submucosal delivery that is capable of deforming and penetrating the outer mucosal layers of tissue without damaging the underlying serosal layers.

MATERIALS AND METHODS

Fluidic and vacuum adaptors were custom designed using Autodesk Fusion and printed using FormLabs clear resin in a Form 4 printer. Fresh-frozen porcine colorectal tissues were brought to ambient temperature in a saline bath and used in testing. The jet nozzle used in this work was a commercial 0.2 mm dispensing tip (Adhesive Dispensing Ltd.).

Custom mounts hold the pressurized nozzle system in place above the tissue and a Festo pressure solenoid with custom control software is used to deliver pulses of air pressure between 20 and 50 kPa to expel fluid (marker dye modelling therapeutic agent) out of the jetting nozzle. Tissue is constrained using a low compressive force and custom printed adapter to hold down a 6.25 cm^2 square segment as shown in Figure 1. Tissue injection was monitored using a high-speed camera (Phantom VEO 1310) and qualitatively post-injection for presence of sub-mucosal fluid buildup. Histological and μCT can be employed for quantitative analysis of bleb formation.

RESULTS

Preliminary results show good fluid penetration of the mucosal layers of the tissue at a variety of pressures. As can be seen in Figure 1, there is a significant fluid sac formed within the sub-mucosal space, however there is significant fluid waste and leakage around the delivery site. This is likely due to the low force constraints applied to the tissue in this injection setup. Fluid delivery was observed in all pressures ranging from 20 – 50 kPa, however the pressure with the largest and most reliable delivery success was 40 kPa.

From analysis of the high speed footage, it appears that the initial fluid burst deforms the tissue, the mid-stream successfully punctures the outer mucosa and begins to form a fluid sac, then finally as the sac fills to its natural limit, due to tissue mechanics, the end-stream is generally deflected away and pools on the surface.

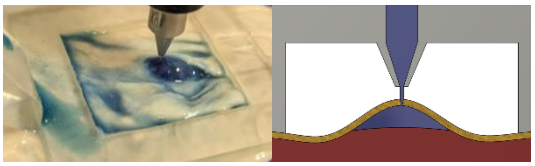

Figure 1 Left: image of a fluid sac within the submucosal layer of porcine colorectal tissue. Right: representative diagram showing a constrained jet stream injection into the sub-mucosal space between mucosa and serosa layers.

DISCUSSION

Initial results show that this needle free jet injection is a mostly reliable method of injecting fluid into the sub-mucosal space without risk of puncture. Work is ongoing to finalise a comprehensive endoscopic end-piece that is capable of tissue fixation using vacuum pressure and an integrated jet delivery nozzle. This work shows promise for a miniaturized fluid delivery system for GI tract diagnostics, interventions, and treatments that is safe, reliable, and increases treatment accessibility.

REFERENCES

[1] F. Wang *et al.*, "Global, regional, and national burden of digestive diseases: findings from the global burden of disease study 2019," *Frontiers in Public Health*, vol. 11, p. 1202980, Aug. 2023, doi: 10.3389/fpubh.2023.1202980.

Early Stage Researcher (PhD Year 1)		Post-Doctoral Researcher/Senior Researcher/PI	X (Postdoc)
Entry for the Engineers Ireland Biomedical Research Medal		Corresponding author has completed PhD and would like to review BinI abstract submissions	X

Please place an X in any appropriate categories

ROBOHEAL: DEVELOPMENT OF A SOFT ROBOTIC DRUG DELIVERY SYSTEM TO IMPROVE TREATMENT OF DIABETIC FOOT ULCERS

Wallace, E.W.[1,2,3], O'Dwyer, J.[4], Duffy, G.P.[3,5], Cameron, A.[2], Dolan, E.B.[1,3]

[1] Biomedical Engineering, School of Engineering, University of Galway;[2]FeelTect, Galway; [3]CÚRAM, SFI Research Centre for Medical Devices, University of Galway; [4]Pharmacology, School of Medicine, University of Galway; [5]Anatomy and Regenerative Medicine Institute (REMEDI), School of Medicine, University of Galway

email: eimear.wallace@universityofgalway.ie

INTRODUCTION

Diabetic foot ulcers (DFU) are a complication of diabetes mellitus with a worldwide incidence between 9.1 to 26.1 million[1]. The estimated cost of treating DFU is $1.38 billion per year with current treatment options including wound debridement, wound dressings, topical antibiotics or antiseptics, compression therapy, offloading techniques, and surgical interventions[1,2,3]. Despite these treatments, ~20% of individuals with a DFU will undergo lower-extremity amputations and 10% of individuals with DFU will die within 1 year of diagnosis[1]. **The management of DFU requires a multidisciplinary approach** and so this research aims to combine soft robotics with a drug delivery device to achieve spatiotemporal release of angiogenic growth factors, vascular endothelial growth factor (VEGF) and platelet derived growth factor (PDGF), on the wound surface and then apply compression to promote granulation to encourage healing of DFU (**Fig. 1A**).

MATERIALS AND METHODS

We are developing wearable soft robotic devices that integrates an actuation reservoir to facilitate mechanotherapy and a therapeutic reservoir to enable controlled delivery of VEGF and PDGF, to the wound surface. We are conducting in vitro wound healing assays on HUVECs to determine optimal dosing and timing of VEGF and PDGF to stimulate endothelial migration an indicator of angiogenesis. HUVECs were seeded at a density of 3 x 10^4 cells/well and at confluency a scratch was created using a P200 tip, a range of VEGF (10-50 ng/mL) and PDGF (5-25 ng/mL) concentrations were applied to the scratches to determine effective pro-angiogenic doses. We will perform in vitro drug release studies using a fluorescently labelled growth factor analogue, fluorescein isothiocyanate-Dextran, to model growth factor diffusion and release from the therapeutic reservoir to select the optimal actuation parameters for controlled delivery of VEGF and PDGF. The optimised device configuration and actuation regime will be implemented in future rodent wound healing models of DFU to evaluate the synergistic efficacy of mechanotherapy and growth factor therapy in vivo.

RESULTS

The efficacy of the VEGF and PDGF concentrations were investigated using a scratch assay (**Fig. 1D**). Six hours following gap formation and treatment addition, 10 ng/mL VEGF had produced the greatest reduction in gap width of any of the groups and was significantly ($p<0.05$) more reduced compared to the control untreated cells. At 12 h, the gap width was significantly ($p<0.01$) reduced to less than 10% of the original width in the 10-50 ng/mL VEGF and 10-25 ng/mL PDGF treated groups compared to the untreated cells (**Fig. 1E**). VEGF- and PDGF-treated groups achieved 100% wound closure by 24 hours, compared the control which achieved 90% wound closure by 24 hours.

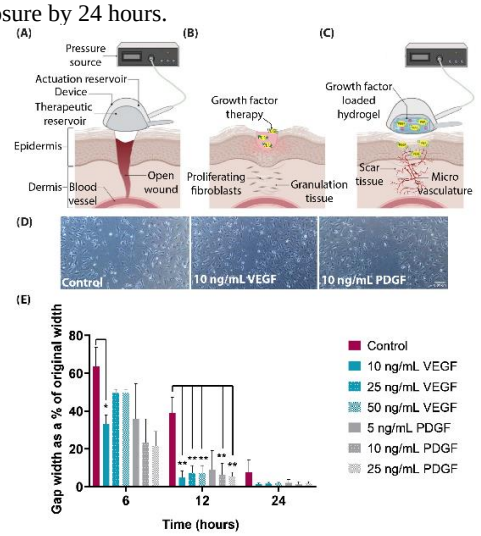

Figure 1 Schematic of RoboHeal to encourage healing of DFUs with **(A)** intermittent actuation of soft robotic device to apply compression to wound surface, **(B)** topical application of angiogenic growth factors to wound surface, **(C)** combination therapy to encourage wound healing. **(D)** 10X microscopy images of the gap area 12 h following addition of treatments in a scratch assay, scale bar = 100 µm. **(E)** Quantification of gap closure over 24 hours, n=3; *p<0.05, **p<0.01.

DISCUSSION

The observed efficacy of VEGF and PDGF in enhancing cellular migration highlights their suitability for use in regenerative therapies targeting angiogenesis. Future studies will combine mechanotherapy and growth factor therapy to investigate potential synergistic effects in wound assays to improve clinical outcomes in diabetic foot ulcers.

REFERENCES

[1] Armstrong, D. G., et al. New England Journal of Medicine. 376(24), 2367–2375, 2017; [2] Nam, S., et al. Nature Materials. 22, pages249–259, 2023; [3] Park, J., et al. Molecules, 22(8), 1259, 2017.

A FINITE-VOLUME SPRING-PARTICLE NETWORK MODEL FOR BLOOD FLOW

Herron, J.M.[1,2] **Chen, M.**[1] **& Boyle, F.J.**[1]
[1] Technological University Dublin
[2] Atlantic Technological University Galway
email: (joseph.herron@atu.ie)

INTRODUCTION

Acting as the body's transport system, blood delivers essential substances such as oxygen, nutrients and hormones, supporting cellular functions and overall health. However, experimental studies of blood flow at the cellular level can often be impractical due to the complexity of replicating physiological conditions within the human body and ethical concerns. Computational models overcome these challenges and provide a platform for analysing cellular interactions with precision and flexibility. The current state-of-the-art methods simulate blood as a suspension of deformable red blood cells (RBCs) within blood plasma. They typically adopt the same mathematical description for both phases, i.e., a continuum or particle-based approach. This work aims to combine both approaches, specifically, a finite-volume (FV) plasma with the spring-particle-network (SPN) RBC model of Chen [1]. As noted in the review by Li et. al. [2], this hybrid approach would balance biophysical fidelity and computational efficiency.

METHODOLODY

Simulating blood flow as a suspension of RBCs necessitates careful consideration of three fundamental components: the fluid phase, representing blood plasma; the solid phase, representing RBCs; and the fluid-structure interaction (FSI) method governing the coupling of both phases. In this work, the FV method implemented in foam-extend 4.0 was utilized to model the dynamics of blood plasma. The solid phase, representing the mechanical and rheological behaviour of RBCs, was simulated using the SPN model developed by Chen [1]. For the FSI coupling, the immersed boundary method (IBM) was chosen for its computational advantages, including simplified mesh generation, elimination of re-meshing, and robust handling of large deformations.

RESULTS

To ensure the FV-SPN model accurately captures known RBC behaviours in various flow environments a series of validation cases are planned. The first of these cases is the simulation of RBC stretching via optical tweezers, a method well-established in experimental biomechanics. Figure 1 shows the axial and transverse RBC diameters with increasing force compared to the experimental results of Mills et. al. [3]. Each line represents a variation in RBC parameters with the dashed line having a bending modulus $k_B = 2.5 \times 10^{-19}$ N m and shearing modulus k_S = 4.0 μN/m. The solid line represents $k_B = 2.5 \times 10^{-20}$ N m and k_S = 4.0 μN/m and the dash dot dot line represents $k_B = 2.5 \times 10^{-19}$ N m and k_S = 6.1 μN/m. The remaining RBC parameters were kept constant across all three simulations with a volume modulus k_v = 1000 N/m^2, global area modulus k_a = 1000 μN/m and local area modulus k_{al} = 100 μN/m.

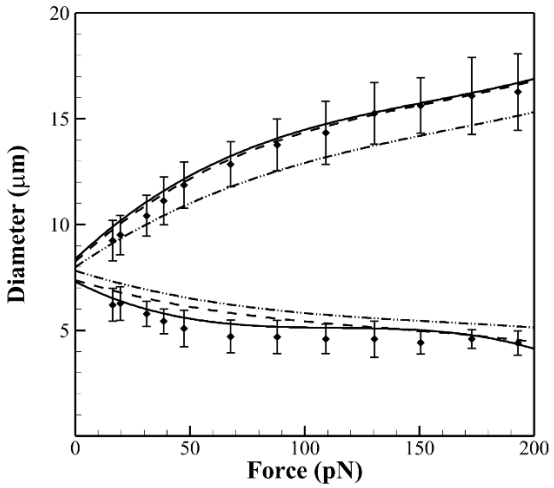

Figure 1 Axial (upper) and transverse (lower) RBC diameters with increasing force compared with Mills [3].

DISCUSSION

The results shown highlight the FV-SPN model's ability to accurately simulate deformation of RBCs via optical tweezers. These findings affirm the model's robustness in simulating the mechanical behaviour of RBCs under controlled stretching conditions, paving the way for further validation in complex flow environments such as RBC dynamics in shear and tube flows.

REFERENCES

[1] Chen *(et al.)*, J Biomech Eng, 139:121009-1-121009-11, 2017.

[2] Li *(et al.)*, J Biomech Eng, 139(2):0210081-02100813, 2017.

[3] Mills *(et al.)*, Mech Chem Biosyst, 1(3):169-180, 2004.

DEVELOPING AN IN VITRO ASTROGLIOSIS MODEL BY MECHANICAL SCRATCH INJURY

Karadimou, A[1], Abubaker, M[2], Grabrucker, A[1] Mulvihill, J[1]
[1] Bernal institute, University of Limerick
[2] Cummings School of Medicine, University of Calgary, Canada
email: alexandra.karadimou@ul.ie

INTRODUCTION

The *in vitro* scratch assay can be used to study and measure cell migration in vitro. It is a well-developed and established method with low cost(1). The *in vitro* scratch-wound model was developed to study primary astrocytes and their migration mode(2). Cell migration is a fundamental process that underlies several cell processes, such as immune response, morphogenesis, and wound healing. Regarding astrocytes, migration is linked to astrogliosis, and the scratch assay can be used to create a model of astrogliosis. Astrogliosis can play a beneficial or detrimental role, but this remains controversial(3). Reactive astrogliosis and scar formation are astrocytic reactions, which might delay or hinder regenerative responses. This reaction may contribute to the manifestation and progression of neuropathological conditions(4). This study aims to develop an *in vitro* astrogliosis model induced by mechanical injury. This will be done by performing multiple scratches under static and oscillatory culture conditions. Evaluating the pre and post injury astrocyte responses, corresponding to different astrocyte profiles (naïve, reactive, scar forming).

MATERIALS AND METHODS

Under both static and oscillatory culture conditions will be examined the astrogliosis model induced by mechanical injury. This will be done by performing pre and post injury measurements corresponding to astrocytes viability, morphology and reactive oxygen species generation assays. The alamar Blue assay will be used as a quantitatively measure of cell viability. Astrocytes changes in their morphology to adapt to the mechanical injury, migration as well as to healing will be studied by Phalloidin staining. The reactive oxygen species generation contribute to health and disease balance. For our study the astrocyte's role in oxidative stress under the frame of astrogliosis will be investigated by CellROX assay.

RESULTS

We found that 32h post 1st mechanical injury there is an increase in astrocyte viability, proliferation & metabolic activity. It is remarkable that there is a plateau among the 48h post 1st mechanical injury, 8h post 2nd mechanical injury and 24h post 2nd mechanical injury. While 32h post 2nd mechanical injury the astrocytes viability, proliferation & metabolic activity is reduced.

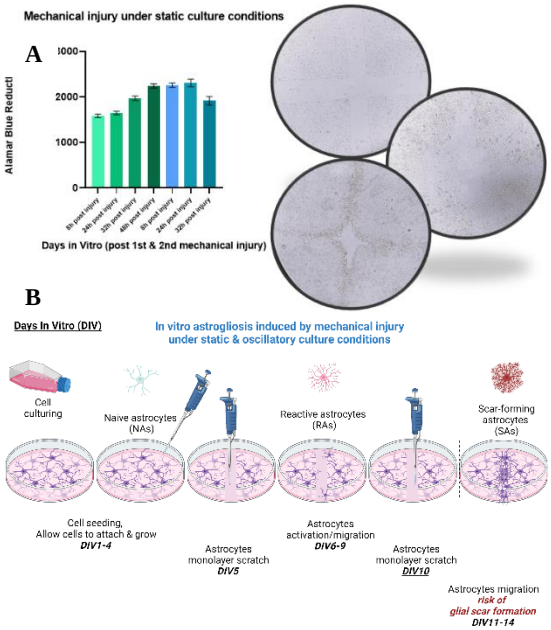

Figure 1 A: Astrocytes seeded on 96-well plate (5,000 cells/cm^2) and allowed to grow for 4 days. Afterwards, 1st mechanical injury was performed and allowed to migrate and heal. The 2nd mechanical injury was performed at the 9th day and astrocytes were allowed to migrate and heal. Astrocytes passage 7 was used and obtained 6 technical replicates. * $p < 0.05$, ($n=6$, mean ± SD). **B**: The figure represents the astrogliosis model under static culture conditions. Astrocytes (DITNC1) seeded and allowed to grow for four days. On day five the astrocytes are induced by mechanical injury. Activated astrocytes migrate to heal the wound. After four days astrocytes are induced for a second time and expected a scar-forming astrocytes response.

DISCUSSION

Overall, astrogliosis response remains a controversial topic. More research should be done to establish the astrocyte profiles (naïve, reactive and scar-forming) through the course of injury-migration-healing process. Finally, it is vital to be evaluated the astrogliosis response and its role in neurodegenerative diseases. This is why it is crucial to be developed a reliable *in vitro* astrogliosis model which we have achieved in this study.

REFERENCES

1. Liang, (et al.), Nature *Protocols*, *2*(2), 329–333. (2007)
2. Yu, (et al.), *Journal of Neuroscience Research*, *34*(3), 295–303. (1993)
3. Zhan, (et al.), *Neurochemical Research*, *42*(1), 272–282. (2016)
4. Zhang, (et al.), *Neurobiology of Disease*, *40*(1), 251–264. (2010)

EXPLORING THE INFLUENCE OF SPATIAL AND SUBSTRATE CUES ON THE FORMATION OF CELLULAR BRIDGES BETWEEN TESTICULAR ORGANOIDS

Rochford, S.[1], Ghanami Gashti, N.[1], Cunnane, E.M.[1]
[1] Bernal Institute, Health Research Institute, and School of Engineering, University of Limerick, Ireland
email: 20261837@studentmail.ul.ie

INTRODUCTION

Infertility is a growing societal concern that affects 15 – 20% of couples trying to conceive worldwide, with male factors being responsible in approximately half of cases[1]. Furthermore, male reproductive health is in rapid decline, indicated by increased rates of testicular cancer, hormone imbalances, and congenital malformation of the male genitals[2]. Research focused on understanding the causes of male infertility and the optimization of effective treatments is therefore required. Preclinical models are the most appropriate tools for achieving these research endeavors. However, current preclinical models of the male reproductive tissues do not appropriately represent primary testis functions, spermatogenesis and hormone production. Testicular organoids (TOs) have emerged as more appropriate models compared to established organ culture and 2D cell culture methods, due to the ability of organoids to represent organ functionalities. However, they do not represent the tube-like structures of the seminiferous tubules, where spermatogenesis occurs.

The discovery of intra-organoid connections (Fig. 1A) has the potential to advance the gold-standard for preclinical models of the male reproductive system by more appropriately representing the tubules compared to existing organoid models. This project aims to design, fabricate, and optimize material systems that allow for the culture and analysis of these inter-organoid connections.

MATERIALS AND METHODS

In order to analyse the morphology and composition of inter-organoid connections, a system must be designed to allow for the controlled culture of these connected structures. We have hypothesised that these connections have formed previously due to chemotaxis, where organoids seeded in close proximity send out chemical signals to migrate towards each other and aggregate. The substrate then inhibits organoid migration, resulting in the organoid processes combining to form the inter-organoid connections (Fig. 1A).

To perform controlled culture of inter-organoid structures, a negative mould was designed (Fig. 1B). Selected hydrogels such as polydimethylsiloxane (PDMS) and gelatin methacyloyl (GelMa) will be drop casted into the moulds, creating the inverse of the mould topography. The mould in Fig. 1B is scaled 10 times compared to the optimal dimensions for visualisation.

Cultured organoids will be seeded into the wells and the channels will allow for the controlled culture of intra-organoid connections. Spatial cues such as the curvature, tortuosity, and distance between wells will be analysed by varying the mould dimensions and design.

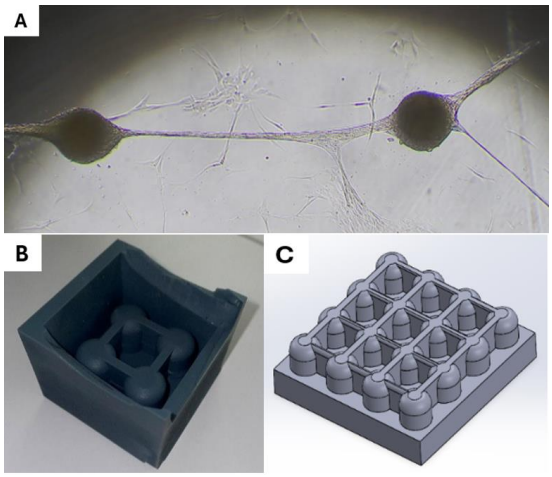

Figure 1 A) Inter-organoid connections observed between testicular organoids in close proximity. B) Initial negative mould design to facilitate the formation of inter-organoid connections during culture. C) A concept negative mould to allow for analysis of varied spatial cues on intra-organoid connection growth.

DISCUSSION

The design, fabrication and optimisation of a system for the analysis of inter-organoid connections has the potential to improve the representativeness of preclinical models of the male reproductive system. Dedicated analysis of these connections has yet to be completed, with this project aiming to bridge this gap in knowledge using TOs.

REFERENCES

1. Vollset (et al.), The Lancet, Volume 396, Issue 10258 p1285-1306, October 17, 2020
2. De Jonge (et al.), Oxford Academic, Volume 2024, Issue 2, 12 April 2024

MODULATING MACROPHAGE BEHAVIOUR IN THE FOREIGN BODY RESPONSE

Shokrani, P.[1], Prendeville, H.[1], Dillon, R.[1], Dolan, E.B.[1]

[1] Biomedical Engineering, Alice Perry Engineering Institute, University of Galway, Ireland

INTRODUCTION

Macrophages play a pivotal role in initiating and modulating the foreign body response (FBR)[1]. Macrophages exhibit a high flexibility in polarisation states in response to environmental cues such as mechanical stimuli[2], functioning as pro-inflammatory (M1) or pro-healing (M2) phenotypes. The proportion of these subsets is an important determinant in the ultimate fate of the wound healing response[3]. Our group has shown that intermittent actuation (IA) of a mechanotherapeutic implant can modulate the FBR and improve therapy delivery over time. We have shown that actuation of our implant results in local tissue strain and fluid flow [4,5]. In this study, we aim to apply a fluid flow regimen to macrophages using a parallel plate and study the resulting macrophage behaviour. We hypothesise that the applied shear stress will promote the pro-healing (M2) phenotype polarisation of the macrophages.

MATERIALS AND METHODS

Human leukemia monocytic cells (THP-1) were differentiated into naïve macrophages using 50 ng/mL Phorbol-12-myristate-13-acetate (PMA) for 48 h, followed by a 24 h rest. These M0-macrophage-like cells were polarised into M1-like cells by optimisation of Lipopolysaccharide (LPS) and interferon-gamma (IFN-γ) concentrations (LPS: IFN-γ: 10:20 ng/mL). Flow cytometry was used to analyse M0 markers (CD11b, CD14), M1 markers (CD86, HLA-DR) and M2 markers (CD163, CD206). Tumor necrosis factor (TNF) ELISA was performed to investigate TNF produced by polarised M1 macrophages. Next, THP-1 monocytes will be seeded on a chambered slide (Thermo Scientific™ Nunc™ Lab-Tek™ II). After differentiation and polarisation, the slide will be placed in the flow chamber of the parallel plate. Cells will be subjected to fluid flow profiles previously shown to be representative of our mechanotherapeutic implant: 2.4 mm/s and 3.04 mm/s velocity at 1 Hz. After 6 days, cells will be trypsinised for analysis by flow cytometry.

Ansys Fluent was used to conduct a computational fluid dynamics (CFD) study to predict fluid velocity and shear stress applied to adhered cells in the parallel plate system. A steady-state, laminar flow profile was applied to the model, using a finite volume approach. Significant mesh refinement was applied to the channel region, with a no-slip boundary condition applied to the chamber walls.

RESULTS

Flow cytometry results indicated that 50 ng/mL PMA treatment successfully differentiated the THP-1 monocytes into M0 macrophage-like cells. The expression of both M0 markers CD14 (p=0.0096) and CD11b (p=0.0161) was higher in 50 ng/mL PMA compared to 100 ng/mL (Fig.1a). The results also indicated that both M1 markers were upregulated compared to the control (M0 cells) in all three ratios of LPS: IFN-γ and the TNF production was significantly higher in ratio of 10:20 compared to other groups (Fig.1b, and c). Therefore, a concentration of 50 ng/mL PMA was chosen to be used for differentiation and consequent stimulation with 10 ng/mL LPS and 20 ng/mL IFN-γ for polarisation. CFD models provide predicted shear stress levels experienced by cells during intermittent actuation. Results show that cells exposed to fluid velocities representative of our mechanotherapeutic implants experience max shear stress levels ranging from 0.0379 Pa and 0.0589 Pa.

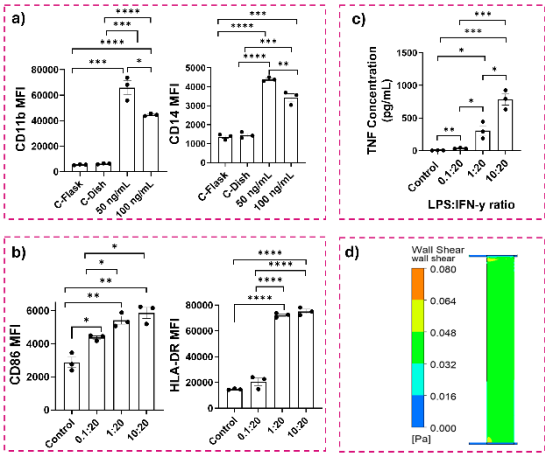

Figure 1: Flow cytometry results of a) M0 (CD11b, CD14), and b) M1 (CD86, HLA-DR) markers, indicating differentiation and polarisation, respectively. c) TNF production of different LPS: IFN- γ ratios, measured by ELISA, and d) predicted shear stress levels based on the CFD.

DISCUSSION

This study is investigating the effect of fluid flow on macrophage behaviour, enhancing our understanding of the role of shear stress in macrophage polarisation and function during the FBR. It has been shown that interstitial flow (3 µm/s) polarises macrophages into an M2-like phenotype[6]. While oscillatory shear stress (0 ± 4 dyn/cm² at 1 Hz) was shown to promote M1 macrophage polarisation and increase Plexin D1 expression[7,8]. We hypothesise that the fluid flow profile we are using which induces a shear stress of 0.0379 Pa and 0.0589 Pa, will promote a pro-healing M2 phenotype. However, we will also investigate whether the initial polarisation state of the macrophages will affect a phenotype switch.

REFERENCES

1. Sridharan, R. *et al., Mat Today* **1,** 2015. **2.** Xue, J.D.*et al., Heliyon*, 2024. **3.** Kharbikar, B. N., *et al., Adv Drug Del Rev***,** 2021. **4.** Dolan, E. B. *et al. Sci Rob*, 2019. **5.** Whyte, W. *et al., Nat Comm*, 2022. **6.** Li, R. *et al., Mol bio of the cell***,** 2018. **7.** Seneviratne, A. N. *et al., Eur Heart J***,** 2013. **8.** Zhang, S. *et al., Heliyon*, 2023.

Characterization of Tumour Cell Phenotype Transitions in 2D and 3D Culture Systems

Vadivelu, R.[1] Turner, C [1] and McEvoy, E.[1]
[1] School of Science and Engineering, Department of Biomedical Engineering
University of Galway, Ireland
email: (*rajakumar.vadivelu@universityofgalway.ie*)

INTRODUCTION

Triple-negative breast cancer (TNBC) remains the most aggressive metastatic behaviour and exerts resistance to cancer therapies[1]. The predominant requisite of metastasis is determined by the ability of cancer cells to adapt to distant mechanical microenvironments. Hence, the mechanical diversity of the environment contributes to phenotypic alternation, ensuring an increase in motility, invasiveness and survival. The process of dissemination begins as cells lose their adherence from the adjacent extracellular matrix. Subsequently, cells gain avoidance of anoikis and become freely floating viable motile cells[2]. Specifically, these cells undergo acquisition of mesenchymal phenotype through the initiation of epithelial-mesenchymal-transition (EMT). To the extent of sustaining fast migration strategy, the cells acquire ameboid features via mesenchymal-to-amoeboid transition (MAT)[3]. These events boost metastatic behaviour through collective migration and heightened chemoresistance[4].

MATERIALS AND METHODS

The murine breast cancer 4T1 cell line was cultured using RPMI. Floating cancer cells (FCCs) were collected from supernatant and seeded at the density of 1×10^5cells/75cm^2 using a culture flask for reattachment growth up to 3 days (denoted flask F_{i+1}). The propagation of FCCs was achieved by continuous collection of FCCs and subsequent reattachment. Tumour spheroids were generated by seeding 1×10^5cells onto 96 wells layered with 1% agarose cryogel. Cryogelation was carried by freezing (-80ºC) and thawing (37ºC) of the solidified agarose gel.

RESULTS

This study aims to simplify the recapitulation of malignant plasticity *in vitro* by reattaching isolated floating cancer cells (FCCs) from the supernatant of the adherent 4T1 cell lines. Noticeably, rounded patches of compact cell colonies gradually loosened their adhesion and dissociated to freely floating rounded cells with blebbing membranes defined as ameboid morphology (Fig.1A). Ameboid morphologies were obtained in reattached cultures ranging from FCCs-3 to 6. It was found that interconversion between MAT to EMT was prominent during the crowding growth phase in FCCs-6. Additionally, we observed that progression of FCCs-1 to 6 corresponded with an increase in adhesive abilities, forming compact multicellular aggregates (Fig.1B & C). Taken together, the trend in cancer cell spheroid growth may indicate existence of proliferative gradients.

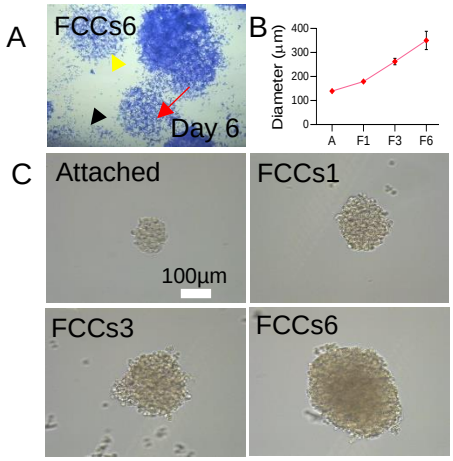

Figure 1 Behaviour of floating cancer cells in 2D and 3D culture. [A] Transition of EMT-MAT (red arrow), ameboid features (black arrowhead) and transition of MAT-EMT (yellow). [B&C] Spheroid growth at day 3. (n=21)

DISCUSSION

Amoeboid cancer cells endowed stem cell-like properties and could propose tumour heterogenicity[5]. Despite the mechanical relevance of the amoeboid cell state is unknown, its bleb organization might go beyond migration plasticity and could provide new insights on chemoresistance. The reciprocal transitioning of EMT-MAT intrinsically may be linked to the modulation of integrin and cadherin. Collectively, we hypothesize that heterotypic 3D tumour spheroids could increase secretion of their own extracellular matrix (ECM) and enhance integrin signalling. Hence, enabling recapitulation of the stiffness alternation which takes place during cancer progression in the native tumour microenvironment. Consequently, this method can be useful to characterise chemoresistance emerging from tumour heterogeneity.

REFERENCES

1. Charissa, (*et al*), Cell 879-893, 2018
2. Graziani, (*et al*), Trend in Cell Bio, 228-242, 2022
3. Pagès., (*et al*) Science Advances, 8416, 2022
4. Goutham, (*et al*) bioRxiv, 2024-10, 2024
5. Behrooz, (et al) Biochim Biophy Acta,167332, 2024

ACKNOWLEDGEMENTS

This work was supported by the European Research Council (Grant number 101116234).

A THERMODYNAMIC FRAMEWORK TO PREDICT ANEURYSM FORMATION AND DEVELOPMENT MOTIVATED BY SMOOTH MUSCLE CELL REMODELLING

Coleman, R.J.[1], **McGarry, P.**[1]
[1]University of Galway
email: ryan.coleman@universityofgalway.ie

INTRODUCTION

Analysis of cerebral arterial aneurysm tissue post-rupture show decreased presence of elastin in the artery wall, relative to healthy aortic vessels [1], highlighting aneurysmal tissue is pathologically weakened relative to healthy arterial tissue [2]. Smooth muscle cells (SMCs) differentiate into synthetic matrix-remodelling and proliferate phenotypes in cerebral aneurysm genesis [3].
We propose a novel thermodynamic framework to predict SMC remodelling and tissue growth, with an aim of describing aneurysm formation. We predict cellular remodelling of SMCs in cerebral arterial tissue to describe SMC evolution, differentiation, and resultant arterial growth, motivated towards cellular homeostasis of the system free energy.

METHODS

We propose an energetic stimulus causes free energy of the artery wall to diverge from homeostasis, motivating cellular remodelling, resulting in a competition between cell-stretch returning the system to a homeostatic state, with passive energetic requirements of the tissue.
A mathematical law is proposed for SMC remodelling predicting the concentration of stress fibres (SFs), found through thermodynamic equilibrium between chemical potentials of SFs, and unbound cytoskeletal actin-myosin proteins [4]. This thermodynamic equilibrium also effects the free energy density of the cell, calculated as an energetic competition between SF formation and passive stretch of the cell cytoplasm, shown as a function of cellular aspect ratio in Fig.1A. This is complimented by a constitutive law for arterial components of collagen, elastin, and the passive arterial matrix [5].
Cellular remodelling is predicted such that it will elongate or shorten cell aspect ratio such that Gibbs free energy of the artery wall approaches the homeostatic free energy. Further remodelling of SMCs into a synthetic state is also predicted, whereby a portion of SMCs may be differentiated into a synthetic state, generated by a Boltzmann distribution between total free energy relative to homeostatic free energy. These synthetic cells act to both decrease free energy of the system by replication of additional contractile SMCs, or causing passive tissue growth by deposition of arterial tissue, expanding vessel circumference, where this mechanism acts to increase free energy in order to maintain homeostasis.
We utilise the proposed framework to predict the cell-motivated evolution of arterial tissue in response to elastin digestion.

RESULTS

Elastin digestion causes an instantaneous increase in free energy density (Fig.1B). In cases of 30% elastin digestion, this increase in free energy is reconciled solely by increasing SMC aspect ratio (Fig.1C), returning the system to homeostasis. Increased elastin digestion to 60% and 100% maximises cellular aspect ratio with respect to minimising SMC free energy (Fig.1A,C), but does not decrease free energy to a homeostatic level. This necessitates remodelling of SMCs into a synthetic state (Fig.1D), which go on to increase SMC density in arterial tissue (Fig.1E). This increase in SMC density reduces free energy below a homeostatic level (Fig.1B), necessitating circumferential tissue growth, describing pathogenesis of fusiform aneurysm formation (Fig.1F).

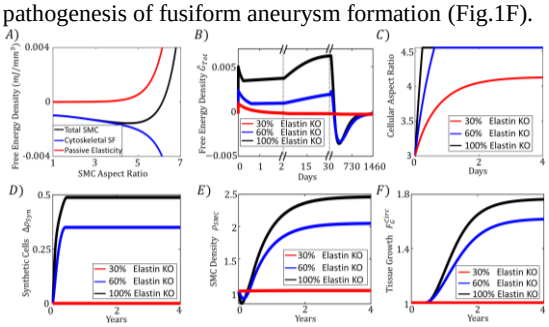

Figure 1. A) Free energy of SMC component minimises when aspect ratio is at 4.5:1. Following elastin digestion; B) Free energy response to return artery to homeostasis, C) Remodelling of cell aspect ratio, D) Transformation of SMCs into a synthetic state to potentiate mitosis and tissue growth, E) Contractile SMC density increasing, F) Circumferential tissue growth.

DISCUSSION

We have presented a novel thermodynamically motivated framework to predict the evolution of aneurysm formation, fundamentally motivated by cell mechanics. This model describes a mechanism whereby remodelling of arterial tissue is motivated solely by SMCs maintaining homeostasis with their environment, modelling the effects of: (i) SMC elongation (ii) SMC differentiation into a proliferative synthetic state, (iii) replication of additional SMCs, and (iv) circumferential arterial growth via deposition of arterial tissue.
This framework will be used within patient specific finite element models to describe evolution of sacular and fusiform aneurysm growth in arterial tissue following arterial damage and elastin digestion.

REFERENCES & ACKNOWLEDGEMENTS

[1] Robertson et al., ABME, 43:1502-1515, 2015. [2] Nakagawa et al., JAHA, 7(17) 2018. [3] Starke et al., Transl. Stroke Res., 5:338-346, 2013. [4] Shishvan et al., BMMB, 17:1631-1662, 2018. [5] Concannon et al., Acta. Biomater., 125: 154-171, 2021.
GEMINI Horizon Europe research (grant 101136438).

Early Stage Researcher (PhD Year 1) ☐ Post-Doctoral Researcher/Senior Researcher/PI ☑

Entry for the Engineers Ireland Biomedical Research Medal ☐ Corresponding author has completed PhD and would like to review BinI abstract submissions ☐

Wnt Inhibition Reduces Tumor Spheroid Growth in 3D Multicellular Metastatic Models

Vatsal Kumar, Sarah Nano, Glen L. Niebur, Laoise M. McNamara

[1]Mechanobiology and Medical Device Research Group, Biomedical Engineering, University of Galway, Ireland.

email: vatsal.kumar@universityofgalway.ie

INTRODUCTION

In metastatic bone disease, interactions between breast cancer cells and bone cells drive tumor growth and bone destruction [1,2]. Mechanical loading activates Wnt signaling in bone cells [3], which helps protect against tumor-induced osteolysis [4, 5]. Bone marrow derived cytokine IL1β activates Wnt signalling in cancer cells promoting their colonisation of the bone [6]. Inhibition of sclerostin, a Wnt antagonist, reduces tumor growth and bone destruction [7, 8]. The underlying mechanisms by which Wnt signaling governs the osteolytic-metastatic response are not fully understood. Thus, there is a need for a comprehensive analysis of the transcriptional response of bone cells and tumor cells in a multicellular environment. The objective of this research is to investigate how Wnt signalling governs the osteolytic-metastatic response in a 3D multicellular in vitro culture model

MATERIALS AND METHODS

Murine OCY454 osteocytic cells and MC3T3-E1 osteoblastic cells were encapsulated in separate gelatin hydrogel solutions and layered one on top of the other and cultured in osteogenic media for 14 days (Bone Control). A layer of hydrogel encapsulating either 4T1 tumor cells (Cancer cell mineralized model- 'CM') or a layer encapsulating 4T1 cells and RAW264.7 osteoclast precursors in 1:1 ratio was deposited onto these mineralized hydrogels (Multicellular metastatic model- 'MM'). The media was changed to standard growth media, supplemented with a Wnt inhibitor (XAV939 Tankyrase1/2 small molecule inhibitor) and sclerostin neutralizing antibody (clone AbD09097_h/mIgG2a, Bio-Rad) alone (+Sclerostin antibody) or in combination with the Wnt inhibitor (Wnt + Sclerostin inhibitor) to the culture media of the constructs at day 14. The constructs were cultured for further 7 days (Day 21). Hydrogels with 4T1 cells alone also served as control ('4T1 only'). Through qRT-PCR, osteogenic (RUNX2) and metastatic activities (PTHrP), osteoclastogenesis (RANKL:OPG) and SOST expressions were quantified at day 21. Tumor spheroid size (Actin, DAPI), pro-tumor activity (IL6 and OPN) and proliferation (KI67) were also assessed. Samples were analysed by RNA-Sequencing to identify differentially expressed genes.

RESULTS

Metastatic activity: Our results confirm a reduction in osteogenic response (RUNX2 and SOST) (Figure 1A, B) and an increase in osteoclast related signalling (RANKL:OPG) (Figure 1D) in tumor cell models (CM and MM) compared to the bone control group.

Wnt-Inhibition: In the presence of the Wnt inhibitor, tumor spheroid diameters were reduced in the 4T1 only groups (Figure 1E, F). IL-6 and OPN staining intensities were significantly reduced in CM group in the presence of Wnt Inhibitor, when compared to the untreated control group (Figure 1G-I).

Wnt and Sclerostin inhibition: In the Wnt+Sclerostin inhibitor group, some of the downregulated genes included wnt signalling target genes (Lgr6, Tcf7, Lrp5, Fzd1 and Ccnd1), genes associated with inflammatory responses and tumor growth (IL-6, IL-24 and TGF-β3), and matrix metalloproteinases (MMP8 and MMP13) (Figure 1J).

DISCUSSION

The current study provides a 3D multicellular mineralized model of bone metastasis, where we demonstrate that tumor cells and osteoclast precursor cells reduce osteogenic potential and increase osteolytic behaviour. Our results demonstrate that treatment with the Wnt-inhibitor reduces tumor spheroid size when tumour cells are cultured alone. In the metastatic models the Wnt inhibitor reduced inflammatory and tumourigenesis signaling (IL6, OPN). This could be explained by the regulation of the β-catenin pathway by the Wnt-inhibitor XAV939 [9].

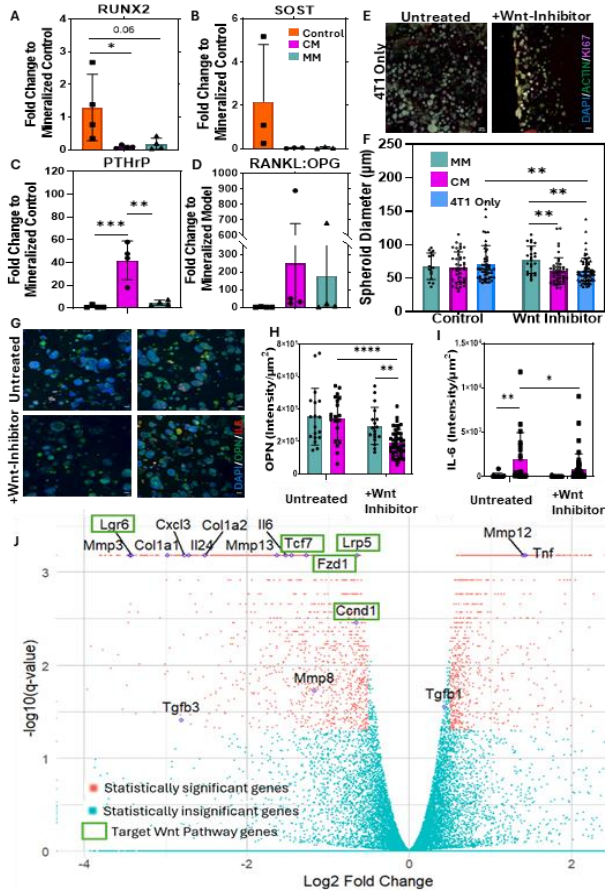

Figure 1: (A-D): Gene expression for RUNX2, SOST, PTHrP and RANKL:OPG in MM and CM models normalized to the bone control at day 21. **(E,F)**: Tumor spheroid (Actin: Green, DAPI: Blue) formation and quantification for 4T1 only groups at day 21 (untreated and wnt-inhibitor treated conditions). Scale Bar= 100 µm. **(G-I)**: Tumorigenic markers IL-6 (Red) and OPN (Green) in the untreated and treated MM and CM groups and their intensity quantification. Scale Bar= 20µm. **(J)**: Differentially expressed genes between untreated and Wnt-inhibitor and Sclerostin antibody treated samples after 7 days of culture.

Bulk RNA sequencing identified that a combination of sclerostin neutralizing antibody and Wnt-inhibition may inhibit tumor growth and matrix degradation in our multicellular mineralized model. We are conducting further pathway analysis for these treatment groups. The studies were conducted under static conditions, whereas osteocyte sclerostin expression is inhibited by biophysical stimulation. Future studies will study how Wnt signalling governs osteolysis under mechanical loading.

REFERENCES [1] T. A. Guise et al., Cancer. 88:2892-2898, 2000. [2] D.L.Waning et al., Clin Cancer Res. 20(12); 3071–7,(2014). [3] Robinson et al. J Biol Chem 281, 31720-31728 (2006). [4] Fan et al. Bone Res 8, 9 (2020). [5] Lynch et al. J Bone Miner Res 28, 2357-2367 (2013). [6] Eyre et al. Nat Commun. 2019; 10:5016. [7] Hesse et al. JCI Insight. 2019; 4(9): e125543. [8] Koide et al. Sci Rep 10, 13751 (2020). [9] Jang et al. Immunopharmacol. Immunotoxicol. 2018 41 (3), 394-402.

MECHANICALLY ACTIVATED EXTRACELLULAR VESICLES FOR BONE REPAIR

Martins, C.S.[1], Brunet, M.Y. [1], Maggio, M. [1], Madden, L. [1], Gorgun, C. [1,2], Dobricic, M.[3], Almasri, R.[4], O'Driscoll, L.[4], O'Brien, F. J.[3,5], Hoey, D. A.[1,5,6]

[1]Trinity Centre for Biomedical Engineering, Trinity Biomedical Sciences Institute, TCD [2]School of Pharmacy and Biomolecular Sciences, RCSI [3]Tissue Engineering Research Group, Department of Anatomy and Regenerative Medicine, RCSI [4]School of Pharmacy and Pharmaceutical Sciences, TBSI and Trinity St. James's Cancer Institute, TCD. [5]Advanced Materials and Bioengineering Research Centre, TCD & RCSI [6]Dept. MMBE, TCD. email: *martinsc@tcd.ie*

INTRODUCTION

The repair of bone defects remains a challenge due to the insufficient supply of grafts and the possibility of an inflammatory response. Extracellular vesicles (EVs), which are particles that can deliver biomolecular cargo and participate in cell-cell communication, have been shown to have therapeutic effects in several pathologies [1]. Additionally, exercise is known to play an important role in bone formation and repair. The effect of mechanical stimulation on EVs of different bone parent cells, such as mesenchymal stem/stromal cells (MSCs), osteoblasts, and osteocytes (OCY) is poorly understood, specifically their effect on angiogenesis (the formation of new blood vessels) and osteogenesis (formation of new bone).

The local delivery of EVs remains a challenge, due to limited loading efficiency and lack of osteoinduction from current delivery methods [2]. Melt electrowriting has emerged in recent years as an additive manufacturing technique that allows for the fabrication of precise architectures at a micron scale. Furthermore, square pore designs of these scaffolds have been shown to enhance the osteogenic capacity of MSCs[3]. However, the effect of different architectures such as offset designs that could allow for better vessel infiltration is currently unknown.

Therefore, this study aimed to determine the role of EVs derived from OCY in regulating angiogenesis, as well as the role of scaffold architectures on osteogenesis, whilst harnessing the combined effect of the two.

MATERIALS AND METHODS

MLO-Y4 OCY cells were stimulated in a custom-made parallel plate flow chamber bioreactor, where fluid shear was applied to the cells at 1 Pa and 1Hz for 2 hours. Following 24h in culture, the conditioned media was collected to obtain EVs via ultracentrifugation (110000xg, 75min). Following 18h incubation on Geltrex, GFP-tagged human umbilical vein endothelial cells (HUVECs) were imaged to assess tube formation or fixed for immunofluorescent imaging. To assess the EV effect from both static (EV^S)and mechanically stimulated (EV^{MA}) cells on angiogenesis, a tube formation assay was performed, as well as immunocytochemistry staining of CD31+. EVs were also added to the chorioallantoic membrane (CAM) of chick embryos at day 7 of culture and vascularisation was assessed at day 14. MEW scaffolds were designed and fabricated using a custom-built MEW 3D printer, with a pressure of 0.6Pa and initial voltage of 6.5 kV. 600µm square pores were designed with an offset of 200 µm every 3 layers for optimum vessel integration and imaged using SEM. Scaffolds were coated in nnHA and functionalised with DiD-labelled EVs mediated by a collagen I coating prior to EV-release assessment via flow cytometry.

RESULTS

Treatment with OCY derived EV^{MA} lead to a significant increase in tube formation with thicker vessels present, comparable to the +VEGF control (data not shown), as well as a substantial increase in CD31+ expression (Fig. 1A). Further assessment using a CAM chick embryo model showed an increase in maximum branch length when treated with EV^{MA} (Fig. 1B).

Square pore offset scaffolds were fabricated with precise architecture, which was sustained up to 48 layers (Fig. 1C). Successful EV functionalisation was confirmed with confocal fluorescent microscopy imaging of the functionalised scaffold. Comprehensive 2-week EV-release studies were then performed to determine the influence of scaffold microarchitecture on EV release profiles (flow cytometry). A sustained released was observed for both EV concentrations and architectures with total EV-release remaining below 25% at day 14. Both high EV concentration and offset-design led to a significantly greater release from day 14 compared to low EV concentration and standard box scaffold (Fig. 1D).

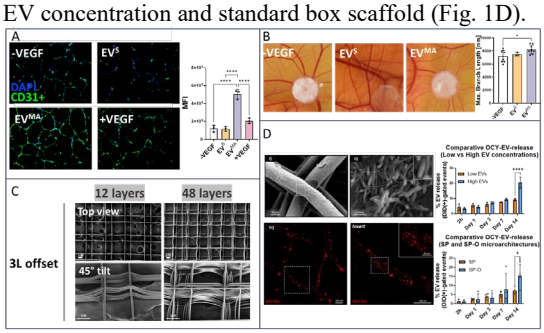

Figure 1 (A) CD31+ and DAPI staining of HUVECs treated with EV^S and EV^{MA}(B) CAM membrane of chick embryos treated with EV^S and EV^{MA}(C) SEM images of 3-layered offset scaffolds (D) SEM and confocal images of MEW scaffolds functionalized with DiD-labelled EVs and cumulative release from the scaffold over 14 days. Data presented as Mean ± SD, n≥3. *p≤ 0.05.

DISCUSSION

Herein, we demonstrate the importance of mechanical stimulation of bone cells, whilst identifying EVs as a possible angiogenic therapy. Furthermore, we successfully functionalised offset MEW scaffolds with angiogenic EVs with controlled release over 14 days. Altogether, these EV-functionalised scaffolds provide a possible therapy for bone repair.

REFERENCES: [1] Kuma (*et al.),* Sig Transduct Target Ther 9, 27(2024). [2] Deng (*et al.*), Stem Cell Res. Ther (2024). [3] Eichholz (*et al.*), Acta Biomater. (2018).

MECHANICAL PROPERTIES OF JUVENILE CARTILAGE

Gisbert M.[1], Kondiboyina V.[4,5], Griffin G.[1], Byrne T.[1], Moore S.[2], Brama P.A.J.[2], Shefelbine SJ.[4,5], Nowlan N.C.[1]

[1]UCD Conway Institute of Biomolecular & Biomedical Research, University College Dublin, Dublin, Ireland. [2]School of Veterinary Medicine, University College Dublin, Dublin. [3]Department of Bioengineering, Northeastern University Boston, MA, USA. [4]Department of Mechanical and Industrial Engineering, Northeastern University, Boston, MA, USA. mauro.gisbert@ucd.ie

INTRODUCTION

Articular cartilage (AC) is essential for joint function, providing a lubricated surface for movement and distributing mechanical loads [1]. Its limited capacity for self-repair means degeneration or injury often leads to conditions like osteoarthritis, with significant global impacts [2]. While the properties of mature AC are well-studied, the processes by which it develops from a homogeneous neonatal structure to a specialized tissue remain poorly understood [3]. This study addresses this gap by examining the structural and functional evolution of femoral condyle cartilage in goats, analysing thickness, instantaneous modulus structural stiffness, across developmental seven timepoints.

MATERIALS AND METHODS

Femoral condyle samples were collected from goats at seven developmental stages: neonates (n = 6), 6-week (n = 6), 3-month (n = 5), 6-month (n = 6), 9-month (n = 6), 12-month (n = 6), and 8-year-old (n = 6). These samples underwent comprehensive biomechanical and biochemical analyses to assess structural and compositional changes in articular cartilage during development. Biomechanical properties were evaluated using a Biomomentum Mach-1 Mechanical Tester. Thickness, Instantaneous Modulus and Structural Stiffness parameters assessed were to evaluate the load-bearing and elastic properties of the tissue. Equilibrium modulus, viscoelastic loss, and deformation time were calculated using the Hertz contact model to provide a detailed understanding of the cartilage's mechanical response to loading (). These analyses together provided an integrated understanding of the biomechanical changes properties of AC as it develops [1, 2, 3].

RESULTS

Biomechanical characterization (Figure 1) revealed that significant biomechanical changes occur early in development. Neonatal cartilage exhibited the higher thickness (3.0 mm) but showed the lower stiffness and modulus values (4.2 MPa and 0.8 N/mm). In contrast, the highest stiffness and modulus were observed in the 6-week group (18.0 MPa and 7.1 N/mm). Average biomechanical properties remained consistent during the early stages of development until 12-months-old, however all values showed a drop off in the 8-year-old group.

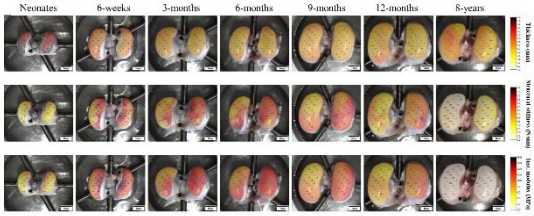

Figure 1 Biomechanical characterization maps (thickness, and instantaneous modulus) and lateral vs. medial comparison graphs (thickness, viscoelastic loss, instantaneous modulus and equilibrium modulus) of seven age groups of goats (neonates, 6-week, 3-month, 6-month, 9-month, 12-month and 8-years.

DISCUSSION

Changes in thickness, instantaneous modulus, and structural stiffness values occurring around 6-weeks-old samples suggested that the most substantial mechanical changes occur early in development. These findings enhance our understanding of AC maturation and provide a foundation for targeted therapeutic strategies in cartilage repair and regeneration. While the direct implications for preventing degenerative conditions such as osteoarthritis remain uncertain, these specific biomechanical properties could be crucial for developing targeted therapeutic strategies for cartilage repair and regeneration, allowing scientists to gain more insight into tissue functionality, personalized treatments, material selection, the design of interventions and therapies, predicting outcomes, and especially the prevention of further damage such as osteoarthritis.

REFERENCES

[1] Brown WE, et al., (2019) Acta Biomaterialia 87, 235-244.
[2] Bielajew BJ, et al., (2022). Acta Biomaterialia 143, 52-62
[3] Niasar EHA, et al., (2024) JMBBM 154, 106534.

EXPERIMENTAL CHARACTERIZATION OF BRAIN TISSUE MECHANICS TOWARD COMPUTATIONAL MODELLING OF CONCUSSION

Sheridan, C., Concannon , J.
Discipline of Biomedical Engineering, College of Science and Engineering, University of Galway
email: c.sheridan21@universityofgalway.ie

INTRODUCTION

The damage mechanism for concussion in unknown, and diagnosis hinges upon the lack of evidence of damage on MRI/CT scanning [1]. The clinical hypothesis for the mechanism of damage of concussion, being the delamination of the grey/white matter boundary [2], [3] has not been validated, while it has been seen that repeated concussion contributes to neurodegenerative conditions such as Parkinson's, CTE and Dementia [4]. Many publications refer to "brain tissue" as a homogenous material, neglecting regional and grey/white matter variance [5], [6]. As a first step in understanding the response of brain tissue to impact, this study performs regional mechanical testing on the grey and white matter of ovine brain tissue, investigating variance in behaviour between tissue types and regions.

METHODS

Fresh ovine brain tissue obtained from a local abattoir was dissected to isolate samples of each tissue type from each lobe. Unconfined compression, unconfined tension, stress relaxation (tension and compression), and shear tests were then carried out for grey and white matter, across the frontal, parietal, temporal and occipital lobes for both, and for the corpus callosum for white, and the deep brain (thalamus & basal ganglia) for grey. Baseline tests were performed to 50% strain, at a quasi-static load rate of 25%/s. Additionally, regional viscoelastic behaviour was investigated by varying the strain rate (100 and 500 %/s) and by performing stress-relaxation tests in tension and compression. Mode I fracture tests were carried out to characterize and test the clinical hypothesis for damage outlined above, also at 25%/s. A subgroup analysis was performed, investigating fresh vs frozen samples in tension and compression to assess feasibility of frozen tissue in mechanical characterization. Ogden (n=3) parameters were then fit to the fresh tissue behaviour for in silico modelling.

RESULTS

It was found that white matter is significantly stiffer than grey in compression up to 50% strain ($p<0.05$ throughout), with both showing compression/tension asymmetry, with their tensile loading paths being distinct. As shown in Figure 1 (A), white matter displays a linear loading path ($R^2 = 0.9905$) to 50% strain, while grey matter shows strain softening, its stress response plateauing after 15% strain. In-silico analysis demonstrates that a single Ogden constitutive law ($\mu_1 = -0.296\ MPa,\ \mu_2 = 0.158\ MPa,\ \mu_3 = 0.139\ MPa,\ \alpha_1 = -0.148,\ \alpha_2 = 0.181,\ \alpha_3 = -0.468,\ d_{1-3} = 0\ \ MPa^{-1}$) cannot capture key features of both grey and white matter. Loading rate was observed to have an impact on the tangent moduli of the tissues more so than the peak stress, with increased load rates causing the brain tissues to undergo higher stresses at lower,

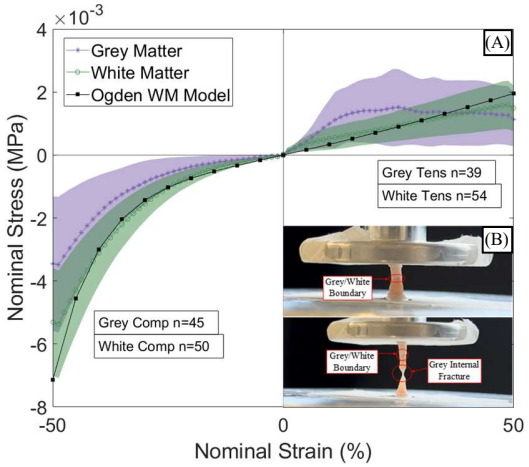

Figure 1 (A) Mode I fracture test, tear visible in bulk grey matter. (B) Stress-strain curves for grey and white matter, with an Ogden material model fit to white matter, showing positive alignment with white matter throughout, while overpredicting stress for grey matter in compression, and underpredicting in 10-25% tensile.

clinically relevant strains [7], with all tissues relaxing by ~73-86% at 50% strain, across tension and compression.

In mode I fracture testing, tears were seen to occur not only at the grey/white matter boundary, but also within the bulk grey and white matter, as in Figure 1 (B).

DISCUSSION

Variation in mechanical behaviour as observed in the above results, between both grey and white matter, and between regions of the brain, indicates that brain tissues cannot be treated homogenously in computational modelling. This is evident in the divergence of the Ogden model fit to white matter from the grey matter behaviour at various points in the strain range shown in Figure 1 (A). The stress relaxation and rate-dependent loading behaviour indicates the need for viscoelastic components to model the material behaviour, while fractures in bulk grey & white matter indicate that predefined paths for separation of grey from white matter, such as in cohesive zone modelling, cannot be relied upon. Further investigation in required regarding the clinical hypothesis of boundary delamination, and the temporal variance in mechanical properties throughout healing long-term damage phases.

REFERENCES

[1] Parizel et al.; Diseases of the Brain, Head and Neck, Spine 2020-2023: Diagnostic Imaging, Springer Intl., (2020).
[2] Alisafaei et al; Biophys. J., 119 (7), (2020).
[3] Pankatz et al.; J. Clin. Med., 12 (16), (2023)
[4] Ledreux et al.; Front. Neurosci., 14, (2020)
[5] Wu et al., Ann. Biomed. Eng.: 47, 1908-1922, (2019).
[6] Budday et al., Arch. Comput. Methods Eng.: 27(4), (2020).
[7] Meaney et al. J. Biomech. Eng: 136(2), (2014)

3D BIOPRINTING OF ARTICULAR CARTILAGE PROGENITOR CELLS WITHIN A PHYSICALLY CONSTRAINING SUPPORT BATH TO DIRECT NEOTISSUE ORGANIZATION

Karam, AS.[1], Kronemberger, GS.[1], Chattahy, K.[1], Kelly, DJ.[1]
[1] Trinity Centre for Biomedical Engineering, Trinity Biomedical Sciences Institute, Trinity College Dublin, Dublin, Ireland.
email: karama@tcd.ie

INTRODUCTION

Engineering functional articular cartilage (AC) remains a challenge in tissue engineering. Recapitulating the arcade-like collagen structure of native AC, crucial for its strength and stiffness, is key to developing functional grafts [1]. This motivates the need for innovative strategies that can direct collagen alignment and, hence, generate functional AC grafts. The overall goal of this study was to use embedded bioprinting strategies to provide spatially defined boundary conditions to AC progenitor cells (ACPs) to help direct neotissue organization. Towards this goal, here we sought to 1) investigate how the physical constraint provided by external hydrogel boundaries of different widths (Fig. 1B) influences collagen organization and 2) determine if a support bath can function as an external boundary to guide neotissue growth of bioprinted ACPs (Fig. 1D).

MATERIALS AND METHODS

ACPs were isolated from goat AC through differential adhesion to fibronectin. Positive moulds with 12mm long, 1mm high, and 250, 500 or 750µm wide cuboidal channels were printed using a stereolithography printer (Formlabs, United States) and were used to cast channels in agarose (4% w/v). Cells (80e6 ACPs/mL 4% oxidised alginate) were cast into the agarose channels (Fig. 1C). Methacrylated xanthan gum (XGMA) was prepared by dissolving xanthan gum (0.5% w/v) in deionized water then adding glycidyl methacrylate (7.41% v/v, overnight at 60°C). The solution was dialyzed (MWCO 6-8kDa) and freeze dried. ACPs were extrusion bioprinted in XGMA (0.5% w/v) using a 27G needle (CELLINK BIOX6, Sweden). A print speed of 5 and 10mm/s were used to bioprint filaments with 160 and 900µm widths, respectively. For all experiments constructs were cultured in chondrogenic media for 3 weeks. Chondrogenesis was assessed through histology, immunohistochemistry, and biochemical assays.

RESULTS AND DISCUSSION

All channel spacings supported chondrogenesis, as evident by the positive glycosaminoglycans and collagen staining. The thinner 250µm channel had a significantly higher collagen/DNA level compared to the other widths. Polarised light microscopy revealed collagen fibres aligning parallel to the edges of the agarose boundary in the 500 and 750µm channels. A thicker level of organisation was seen throughout the tissue in the 250µm channel with fibres preferentially aligned parallel to the long axis of the channel (Fig. 1C). Likewise, in the bioprinted tissues, the 160µm filament had a greater collagen alignment than the 900µm filament (Fig. 1D).

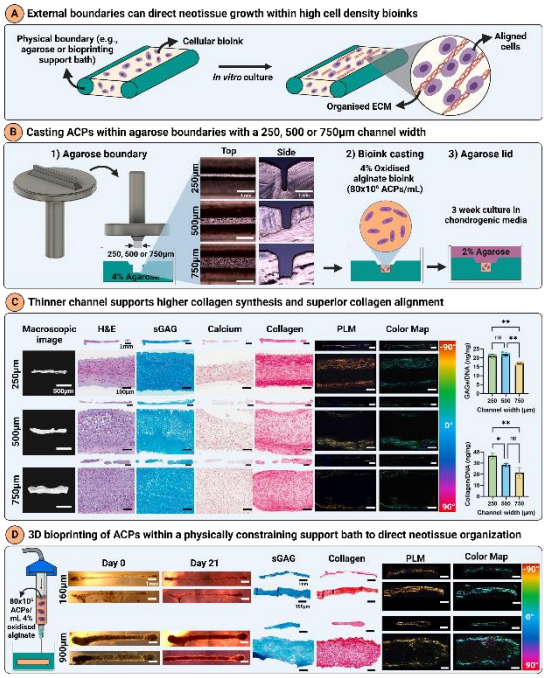

Figure 1 A) Physical boundaries guiding neotissue growth. B) Fabrication of agarose channels. C) Histological staining with hematoxylin and eosin, alcian blue (sGAG), alizarin red (calcium), and picrosirius red (collagen). Polarized light microscopy imaging. Biochemical quantification of sGAG/DNA and collagen/DNA. D) Through bioprinting, filaments with a 160 and 900µm width were achieved with a greater collagen alignment in the thinner filaments. A ordinary one-way ANOVA with Tukey's post-hoc test was used for statistical analysis (ns = not significant, * ($p<0.05$), ** ($p<0.005$), *** ($p<0.001$), **** ($p<0.0001$)). Created with BioRender.

CONCLUSIONS

These findings reveal that external hydrogel boundaries can control neotissue collagen alignment within high cell density bioinks. Increased collagen alignment was observed in the thinner (250µm) casted and (160µm) bioprinted filaments. Future work on bioprinting functional AC will incorporate guiding structures with a 160µm spacing with a view towards achieving grafts with an arcade-like collagen architecture.

REFERENCES

[1] Khoshgoftar *(et al.)*, Biomechanics and modeling in mechanobiology 12:901–913, 2013.

THE DEVELOPMENT OF AN INJECTABLE HYALURONIC ACID HYDROGEL CONTAINING P2X7R SIRNA NANOPARTICLES FOR THE TREATMENT OF POST-TRAUMATIC TEMPORAL LOBE EPILEPSY

O'Callaghan, AM.[1,2,3], Douglas, C.[4], Loane, D.[4], Dixon, J.[5], Dervan, A.[1,2], Woods, I.[1,2], Engel, T.[3,6], O'Brien, FJ.[1,2]

[1]Tissue Engineering Research Group, Dept. of Anatomy & Regenerative Medicine, Royal College of Surgeons in Ireland (RCSI), 123 St. Stephen's Green, Dublin, Ireland
[2]Advanced Materials & Bioengineering Research (AMBER) Centre, RCSI, 123 St. Stephen's Green, Dublin, Ireland
[3]FutureNeuro, RCSI, 123 St. Stephen's Green, Dublin, Ireland
[4]Neurotrauma and Neuroimmunology, Trinity College Dublin, Dublin, Ireland
[5]School of Pharmacy, University of Nottingham Biodiscovery Institute, Nottingham, UK
[6]Department of Physiology and Medical Physics, RCSI, 123 St. Stephen's Green, Dublin, Ireland
anneocallaghan23@rcsi.com

INTRODUCTION

Temporal lobe epilepsy (TLE) is the most prevalent acquired seizure disorder, often caused by brain injury. Anti-seizure drugs are ineffective in 33% of patients, who are classed as having drug-refractory TLE [1]. These systemic treatments have additional short-comings such as cognitive side effects and a failure to tackle the underlying disease pathophysiology. The purinergic receptor P2X7R, highly expressed on microglia within injured brain regions, contributes to chronic inflammation in TLE by driving microglial activation. Systemic P2X7R inhibition produces disease-modifying effects in murine TLE models [1] and similar results were found using silencing RNA (siRNA) which is associated with minimal off-target binding [2]. However, as P2X7R is widely expressed throughout the body, focal delivery is crucial to developing future P2X7R-targeting therapies. Therefore, the key aim of this study was to develop a brain-compatible injectable hydrogel carrying encapsulated siRNA targeting P2X7R for non-viral focal delivery to the brain for the treatment of TLE.

MATERIALS AND METHODS

Fabrication of a photo-crosslinkable biomimetic hydrogel. Hyaluronic acid was methacrylated by reacting with methacrylic anhydride and degree of methacrylation was measured by NMR spectroscopy. Gel properties were characterised by uniaxial compressive testing, and swelling and degradation assays. *Non-viral delivery of siRNA targeting microglial P2X7R.* By complexing P2X7R-targeting siRNA (siP2X7R) with the non-viral GET (GAG-binding Enhanced Transduction) peptides [3], peptide-siRNA nanoparticles (NP) were formed. The NP were then incubated with murine microglial cells and knockdown of P2X7R mRNA expression was validated by rt-PCR. The effect of knockdown on cytokine release was quantified by ELISA.

RESULTS

Methacrylated hyaluronic acid (MeHA) was observed to crosslink in response to blue light in the presence of a photo-initiator (Fig 1.A). The crosslinked hydrogels had a stiffness of 543 Pa (Fig 1.B) which is compatible with cells of the central nervous system (CNS) [4], and a mesh size of 297.3nm, which is suitable for NP retention. The hydrogels degraded rapidly in hyaluronidase, an endogenously produced enzyme. Using reporter siRNA, an optimal NP concentration of 50nM was found to achieve high cellular internalisation with minimal signs of cytotoxicity. P2X7R knockdown was achieved in reactive microglial cells (Fig 1.C) and this was shown to reduce IL-1β, TNFα, and IL-18 release (Fig 1.D).

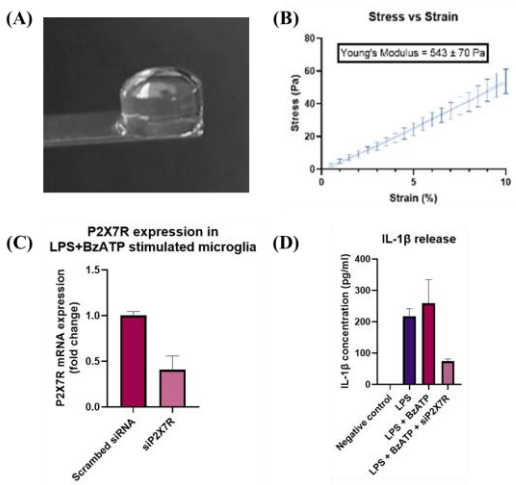

Figure 1 Gene-activated Injectable Hydrogel for Epilepsy Applications. (A) Methacrylation of hyaluronic acid produces a photo-crosslinkable hydrogel with (B) biophysical properties similar to native CNS tissue. (C) Non-viral delivery of siRNA targeting P2X7R reduces release of (D) pro-inflammatory cytokine Il-1β from reactive microglia.

DISCUSSION

Injectable hydrogels can act as tuneable drug delivery vehicles for CNS applications that overcome several limitations associated with systemic drugs including difficulty crossing the blood-brain barrier [4]. Here we tuned the physicochemical properties of a MeHA hydrogel to mimic the native CNS tissue to optimise it for use as an injectable therapeutic delivery platform for P2X7R-targeting siRNA. The results of our study indicate that siRNA transfection promotes knockdown of P2X7R mRNA expression which reduces the production of neurotoxic cytokines from microglia *in vitro*, and future work will involve confirming the disease-modifying effects of this system *in vivo* using a well-established murine injury model of TLE In summary, this gene-activated hydrogel demonstrates potential to act as a novel disease-modifying treatment strategy for drug-refractory TLE patients, with future applications within the wider field of neurotrauma.

REFERENCES

[1] Jimenez-Pacheco *et al.*, J. Neurosci, 36:5920-32, (2016)
[2] Amorim *et al.*, Purinergic Signalling, 13:467-78, (2017)
[3] Dixon *et al.*, PNAS, 113:E291-99, (2016)
[4] Aurand *et al.*, Neuroscience Research, 72:199-213, (2012)

This project is funded by a Government of Ireland Postgraduate Scholarship provided by Research Ireland.

A POTENTIAL ROLE FOR OSTEOCYTE DERIVED NLRP3/IL-1B IN POST-TRAUMATIC OSTEOARTHRITIS (PTOA)

Franchi, A.[1], Hodgkinson, T. [1,2], Kennedy, O.D.[1,2]
[1] Tissue Engineering Research Group, Department of Anatomy and Regenerative Medicine, Royal College of Surgeons in Ireland (RCSI),
[2] Trinity Centre for Biomedical Engineering, Trinity College Dublin (TCD)
email: antoniofranchi23@rcsi.com

INTRODUCTION

Osteoarthritis (OA) is the most common type of arthritis and a primary cause of mobility-related disabilities, affecting approximately 528 million people worldwide [1]. There are no treatments to stop or delay the progression of OA or that can provide symptomatic relief [2]. Post-traumatic osteoarthritis (PTOA), a sub-type of OA, develops after acute joint trauma and has a defined starting point, enabling earlier intervention [3].
It is imperative to define which tissues initiate the inflammatory cascade resulting from injury/trauma, and can drive PTOA. It is estimated that 80% of ACL injuries promote the formation of bone marrow lesions (BMLs) in the subchondral bone [4]. Within BMLs, osteocytes are thought to undergo cell death, inducing nearby osteocytes to orchestrate the resolution of bone injury, by regulating osteoclasts activity [5].
Due to their acute nature, we hypothesize that BMLs induce an inflammatory response in osteocytes to promote bone remodelling, and that this inflammation can affect chondrocytes metabolism, providing a novel source of inflammation in PTOA. We also aim to define if osteocytes-derived inflammation is mediated by the NLRP3 inflammasome, with the release of IL-1β.

MATERIALS AND METHODS

Primary murine osteocytes (OCY) derived from calvaria bones and the MLO-Y4 cell line were studied. Both cell types were seeded on different 2D ECM matrices to create a microenvironment similar to that found in vivo. The resulting groups were control (plastic), collagen I and collagen I-hydroxyapatite (Coll/HA). Cells were analysed in terms of metabolic activity, proliferation and cell morphology. To determine whether cells can mount an inflammatory response, they were exposed to LPS for 24 hours and ATP. In addition, one group was treated (before ATP exposure) with MCC950, a selective NLRP3 inflammasome inhibitor, to determine the specificity of the inflammation. Here, cytotoxicity was measured with LDH assay, while IL-1β release was measured with ELISA assay.

RESULTS

Cells seeded on ECM matrices showed increased metabolic activity, higher DNA content and a phenotype more similar to that found in vivo compared to the controls. LPS exposure significantly increased cytotoxicity and cell death in both MLO-Y4 and OCY. The further addition of MCC950 was in most cases effective to reverse this effect. Additionally, LPS-treated OCY were found to release IL-1β in the cell media and, again, this behaviour was inhibited by MCC950.

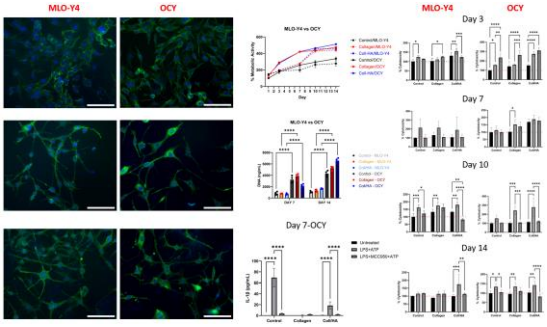

Figure 1: Fluorescence images of DAPI (blue) and Phalloidin (green) stained MLO-Y4 and OCY seeded on control, collagen and coll/HA; metabolic activity and DNA content of MLO-Y4 and OCY; cytotoxicity and IL-1β release following LPS and MCC950 exposure in MLO-Y4 and OCY.

DISCUSSION

This study highlighted the novel role of osteocytes as source of inflammatory factors and the use of different ECM coatings to promote cell proliferation and phenotype differentiation.
Metabolic activity and DNA content were found to be increased on collagen and coll/HA coatings compared to the control, as well as their phenotype, characterized by the dendritic shape found in vivo. This confirms a beneficial role of ECM matrices for cell attachment and proliferation. The inflammatory study suggests that osteocytes respond to LPS exposure by undergoing pyroptosis, with the subsequent release of IL-1β. The simultaneous use of MCC950 tends to reverse this effect, implying a possible involvement of NLRP3 inflammasome activation.
Together these results provide a novel study on endogenous inflammation of bone cells and suggest a possible therapeutic target for the treatment of PTOA.

REFERENCES

[1] Langworthy et al., *SAGE Publications Ltd*., 2024.
[2] Grässel et al., *F1000 Research Ltd*., 2020.
[3] Wang et al., *BioMed Central Ltd.*, 2020.
[4] Muratovic et al., *Bone*, vol. 108, pp. 193–201, 2018.
[5] Ru et al., *Springer Nature*, 2020.

DEVELOPMENT OF A DUAL-SYRINGE PREMIXED PHOSPHOSERINE-MODIFIED CPC ADHESIVE FOR MINIMALLY INVASIVE BONE REPAIR

Tzagiollari, A.[1,2,3], Levingstone, T.J.[2,3], Insley, G.[4], Dunne, N.[2,3]
[1]Biomimetic Innovations, Limerick, Clare, Ireland, [2]School of Mechanical and Manufacturing Engineering, Dublin City University, Dublin 9, Ireland, [3]Centre for Medical Engineering Research, Dublin City University, Dublin 9, Ireland, [4]PBC Biomed, Accelerating Medical Innovation, Limerick, Clare, Ireland
email: (antzela@biomimeticinnovations.com)

INTRODUCTION

Despite their promising properties, calcium phosphate cements (CPCs) face challenges in clinical applications, particularly in achieving consistent mixing and injectability during minimally invasive procedures like vertebroplasty and bone defect repair. Traditional CPCs often suffer from phase separation during injection, leading to compromised mechanical properties and limited applicability [1]. Premixed CPC formulations have been investigated to address these challenges; however, issues such as prolonged setting times, uneven mixing, and phase instability persist [2].

This study focuses on developing a two-component premixed paste-based phosphoserine-modified CPC (PM-CPC) adhesive for minimally invasive delivery via a dual-syringe system. The proposed formulation addresses challenges related to phase separation, rapid setting, and mechanical strength, ensuring enhanced handling, stability, and adhesion. Shifting from manual to mechanised on-demand mixing, this innovation seeks to provide a ready-to-use, consistent adhesive that meets clinical requirements for bone defect repair and implant stabilisation [3].

MATERIALS AND METHODS

A dual-syringe injectable adhesive was developed (Fig. 1a), comprising of two paste components, an accelerator paste with phosphoserine (25 wt.%) and calcium silicate (1 wt.%), and an α-TCP paste containing α-TCP powder (74 wt.%). Both were mixed using Kolliphor EL at oil-to-powder ratios of 0.3–0.6 mL/g, homogenised using planetary ball milling and stored in syringes. The two components were combined through a dual-syringe system with a mixing nozzle for on-demand delivery.

Analytical evaluations, including phase separation, injectability, and 48-week viscosity monitoring, confirmed the stability of the adhesive. Cytotoxicity and cell proliferation studies were conducted with MSC and MC3T3-E1 cell lines to demonstrate cell viability and metabolic activity.

RESULTS

The two-component PM-CPC adhesive showed excellent performance, with an optimal oil/powder ratio (0.4 mL/g) ensuring uniform, stable pastes without phase separation. Injectability was enhanced, with extrusion forces reduced to 22.2 N (accelerator paste) and 15.9 N (α-TCP paste), achieving 71.2% and 67.6% injectability, respectively. Stability tests confirmed sustained viscosity and injectability over 48 weeks. Clinical benchmarks for setting time (3.1–3.8 minutes), compressive strength (20 MPa), and adhesive strength (3.5 MPa) were exceeded.

In vitro washout resistance showed minimal mass loss (<5.2%) after 5 min, highlighting excellent stability in wet environments. Biological activity assays showed excellent cytocompatibility, with >95% cell viability and significant cell proliferation after 21 days with SEM confirming apatite crystal formation, indicative of bioactivity.

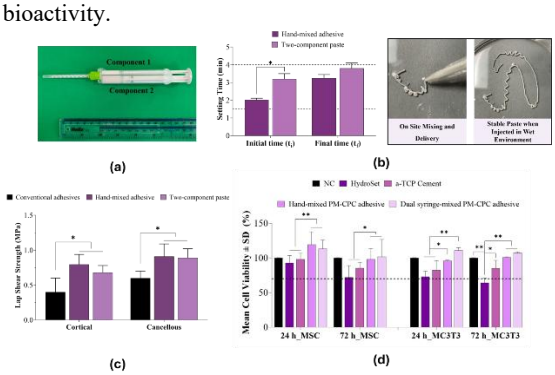

Fig. 1: (a) Syringe system for on-demand mixing. (b) Handling, (c) mechanical properties, and stability in wet conditions. (d) Biological performance of the adhesive.

DISCUSSION

The dual-syringe on-demand mixing PM-CPC adhesive is a breakthrough in bone adhesive technology, enabling precise mixing during injection for uniformity and eliminating variability of hand-mixed CPCs. Optimised at a 0.4 mL/g oil-to-powder ratio, it meets critical clinical benchmarks for handling, strength, and injectability. This innovative system simplifies application, ensuring stability and reproducibility during minimally invasive procedures. Demonstrating long-term stability, cohesion, and bioactivity in wet environments, it is ideal for vertebroplasty and bone defect repair. By enhancing the ease of use and promoting bone regeneration, this system is poised to become a standard in orthopaedic bone repair applications.

REFERENCES

[1] Carey (et al.), Biomaterials 26:5002–5014, 2005., [2] Xu (et al.), Dental Materials 23:43–52, 2007., [3] O'Neill (et al.), Acta Biomaterialia 64:367–377, 2017.

INVESTIGATING THE ANTI-TUMOUR RESPONSE OF CD27$^+$ γδT CELLS ON TRIPLE-NEGATIVE BREAST CANCER CELLS

Harkin, B.[1,2], Wiesheu, R.[3], Coffelt, S.[4], McNamara, L.[1,2,5], McEvoy, E.[1,2]
[1] Discipline of Biomedical Engineering, University of Galway
[2]SFI Research Centre for Medical Devices, University of Galway
[3]Dana-Farber Cancer Institute, Boston, Massachusetts, United States
[4]Immune Cells and Metastasis Group, Cancer Research UK Scotland Institute
[5]Mechanobiology and Medical Device Research Group, Biomedical Engineering, University of Galway
email: b.harkin6@universityofgalway.ie

INTRODUCTION

Understanding tumour cell cytotoxic interactions is crucial in advancing cancer therapies and guiding treatment frameworks. This study aims to isolate, purify, and expand CD27+ expressing γδT cells. Phenotyping will characterise isolated cells and assess purity. Isolated cells will be used in co-culture to investigate cytotoxic effects. Effector:target (E:T) ratios will determine an optimal gamma delta to cancer cell ratio.

MATERIALS AND METHODS

γδT Cell Isolation
Axillary, brachial and inguinal lymph nodes were harvested from C57BL/6 male mice and pooled in a single-cell suspension. Cells were cultured in 96 U-well plates at 37°C and propagated at a density of 2×10^5 cells/well. Cells were isolated using a γδ TCR+ T cell Isolation Kit (Miltenyi Biotec). Cells were cultured in RPMI 1640 medium supplemented with FBS, penicillin/streptomycin, Sodium Pyruvate, β-ME, and murine IL-2, -7 and -15. Expanded cells were stained with anti-CD3, CD4, CD8, CD27 and TCRγδ and analysed on a Northern Lights 3000 cytometer to confirm purity.
Co-Culture
EO771 mammary carcinoma cells were plated at a density of 10^4 cells in a flat bottom 96-well plate. After 6 hrs, 10^5 γδT cells were added to wells in E:T ratios of 1:1, 5:1, and 10:1. Co-cultures were incubated for 24 hours at 37 °C. Cells were collected and blocked with FcX TruStain and stained with anti-CD3. Zombie Green™ was added as a live/dead marker to measure cancer cell death (n=4).

RESULTS

Statistical analysis was performed using GraphPad Prism software with unpaired t-tests or one-way or two-way ANOVA used to quantify the statistical significance of differences ($P \leq 0.05$) between groups.
Purity
We used flow cytometry plots generated by FlowJo software to express proteins. Fluorescence minus one (FMO) controls were used to set gating. We found that the post-sort positive fraction expressed 89% of CD3+ cells. 52.6% of these cells expressed the TCRγδ receptor indicating pure γδT cells. We also confirmed >1% contamination from CD4+ and CD8+ receptors.
Cytotoxicity
After 24-hour co-culture, the stained CD3+ cells were gated to separate cancer and γδT cells. Dead-stained cells were then gated. The 1:10 E:T ratio indicated 56% of cells stained positive for zombie green showing the greatest killing ability. 1:5 and 1:1 E:T ratios indicated 21% and 1% cell death respectively.

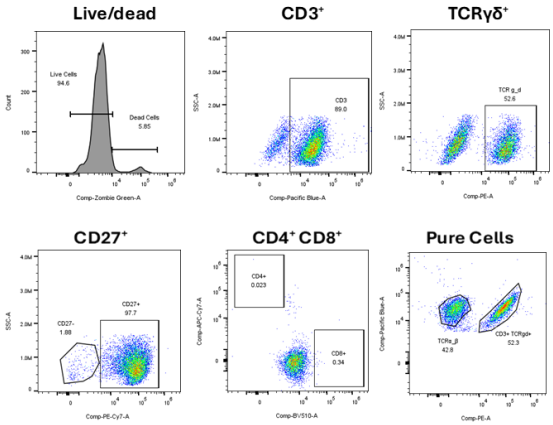

Figure 1 Flow cytometry plots expressing surface markers for γδT cells. Our cells express high levels of CD3 (89%) with 52.6% expressing the TCRγδ+ antigen. We also confirm minimal contamination by the lack of CD4+ and CD8+ markers.

DISCUSSION

This subset is more effective in immune responses than conventional T-cells due to its cytotoxic molecules and increased cytokine production [1]. Our work shows this cytotoxicity where killing efficacy increases with greater E:T ratios. A ratio of 10:1 is most effective which is concurrent with literature in this cell line.
As a next step, it will be critical to understand the key factors that govern this response, including the influence of the tumour microenvironment and intracellular communications and exchange, which are known to play an essential role in cancer development in addition to regulating immune cell activation and response [2, 3].

REFERENCES

1. Wiesheu et al., The EMBO Journal Vol. 43:2878-2907, 2024.
2. Bonacquisti and Nguyen, Cancer Letters Vol. 442:439-444, 2019.
3. McEvoy et al., Nature Communications Vol. 11:6148, 2020.

METABOLIC MODULATION OF HUMAN MACROPHAGE PHENOTYPE FOR THE PRODUCTION OF EXTRACELLULAR VESICLES FOR BONE REPAIR

Gorgun C.[1,2], Klavina P.[1], Martins C.[2], Payet C.[1], Cavanagh B.[3], Curtis A. [1,4,5*], Hoey D. [2,4,5*]
[1] School of Pharmacy and Biomolecular Sciences, RCSI. [2] Trinity Centre for Biomedical Engineering, School of Engineering, TCD.[3] Cellular and Molecular Imaging Core, RCSI.[4] Tissue Engineering Research Group, RCSI.[5] Advanced Materials& Bioengineering Research Centre.
* Authors contributed equally.
email: cansugorgun@rcsi.ie

INTRODUCTION

Macrophages play a pivotal role in bone repair, transitioning from a pro-inflammatory M1 phenotype in the early stages of healing to an anti-inflammatory M2 phenotype during later stages. While M1 macrophages aid initial repair processes, prolonged activation can lead to chronic inflammation, and an excessive M2 response may promote fibrosis. Both the M1 phenotype and the transition to M2 are crucial for successful bone repair, with intracellular metabolic reprogramming driving these phenotypic shifts. As secretory cells, macrophages influence other cells involved in repair through the release of extracellular vesicles (EVs). While the regenerative roles of M1- and M2-derived EVs are well-documented in murine models[1-2], significant differences in metabolism and inflammatory responses between human and murine macrophages[3] suggest species-specific EV functions. Therefore, this study investigates the regenerative properties of human M1- and M2-derived EVs and examines the potential of the Pyruvate Kinase M2 (PKM2) activator, DASA-58, to promote the metabolic reprogramming of M1 macrophages. By facilitating the critical shift toward an anti-inflammatory phenotype, this approach aims to enhance the release of regenerative EVs, offering a novel strategy to optimize macrophage-mediated bone repair.

MATERIALS AND METHODS

Primary human monocytes were isolated from buffy coats and polarized to macrophages: M0 (untreated), M1 (100 ng/mL LPS and 20 ng/mL IFN-gamma), and M2a (20 ng/mL IL-4 and 10 ng/mL IL-13). Macrophages were treated with the PKM2 activator DASA-58 for 2 hours prior to M1-polarization. Metabolic profiling was performed with a Seahorse XF-analyzer, and qPCR and ELISA were used to assess polarization. EVs were separated through ultracentrifugation and characterized per MISEV standards. Size and concentration were evaluated using NTA and surface markers were analyzed via flow cytometry with a bead-based multiplex assay. The angiogenic and osteogenic potency of EVs was evaluated *in vitro* on HUVEC cells for migration, proliferation, and tube formation, and on human MSCs for migration, proliferation, and osteogenesis respectively.

RESULTS

Our findings demonstrate that human M1 macrophages are metabolically distinct from M2 macrophages, exhibiting greater oxygen consumption and heightened glycolytic activity, marked by increased expression of PKM2, Hexokinase 2, and HIF1α. While macrophage polarization does not alter the core properties of EVs—such as count or protein content—it significantly affects EV yield depending on the donor variability (Fig.1A). Additionally, MACSplex analysis identified polarization-dependent markers, including CD9, CD63, CD44, CD49E, CD146, and HLA-ABC. Functionally, M1-derived EVs suppressed HUVEC migration and angiogenesis (Fig.1B-C) but enhanced MSC migration, proliferation (Fig.1D-F), and ALP activity by day 7. Conversely, M2-derived EVs promoted angiogenesis and vascular activity while having minimal impact on MSC functions. Metabolic reprogramming of macrophages through PKM2 activation reduced glycolytic enzymes and M1 markers (CXCL10, CD38) while increasing the M2 marker IL-10. EVs from metabolically modulated macrophages enhanced HUVEC proliferation, migration, and tube formation, promoting angiogenesis without affecting osteogenesis.

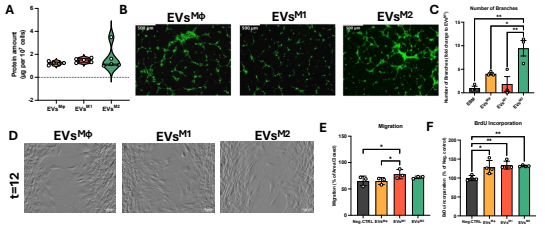

Figure 1: Quantitative analysis of EV yield (A). Representative images of GFP-HUVECs which were treated with 1 µg/mL EVs for 9 hours on GelTrex **(B)**. Quantitative analysis of total tube length number of branches **(C).** Representative images of scratch assay with MSCs which were treated with 1 µg/mL EVs **(D)**. Quantitative analysis of MSCS migration at 12th hour **(E).** BrdU incorporation for MSC proliferation **(F).** Error bars in the graphs represent mean ± SD. **p < 0.01, *p < 0.05.

DISCUSSION

This study unveiled that M1-EVs promoted early MSC activity, while M2-EVs enhanced angiogenesis. Strikingly, DASA-58 reprogramed M1-macrophages to produce angiogenic EVs without compromising osteogenic support, spotlighting macrophage metabolism as a powerful target for tissue regeneration.

FUNDING

This project is funded by the European Union under the Marie Skłodowska-Curie Postdoctoral Fellowship No. 101106209, "METABOLATE."

REFERENCES

[1]Daneshvar A. et al. Archives of oral biology, 166: 1662024,2024. [2]Kang M. et al. Bone, 141:115627, 2020. [3] Verberk, S. et all. Cell reports methods, 2(4), 100192, 2022.

HARNESSING THE CIRCADIAN RHYTHM OF DENDRITIC CELLS TO BOOST NANOPARTICLE UPTAKE TO INCREASE SKIN VACCINE EFFICACY BY DISSOLVABLE MICRONEEDLE

Butler, Christine, T.[1], Payet, Cloé.[1], Cavanagh, Brenton.[1], Kennedy, Oran, D.[1], Donnelly, Ryan, F.[2], Curtis, Annie, M.[1]

[1] Royal College of Surgeons in Ireland, Dublin

[2] Queens University, Belfast

email: (christinebutler22@rcsi.ie)

INTRODUCTION

The body's central clock coordinates peripheral clocks in our tissues and cells, aligning the circadian rhythm—a 24-hour cycle—with external cues like light and food [1]. Research has illustrated that our immune system is strongly controlled by our 24-hour circadian clock, and growing evidence shows that time-of-day vaccination leads to higher efficacy of antibody production [2].

Dendritic cells (DCs), key vaccine targets, process and present antigens to naïve T cells, driving adaptive immunity. Our lab has shown that the DC clock regulates antigen processing via mitochondrial morphology and metabolism, impacting T cell activation [3]. The skin has a rich network of dendritic cells, which can be efficiently targeted with microneedles (MNs) for intradermal vaccine delivery to the skin DCs.

We propose dissolvable microneedles (MNs) for time-specific intradermal vaccination, leveraging the circadian properties of skin dendritic cells to enhance vaccine delivery and efficacy.

MATERIALS AND METHODS

Bone marrow-derived DCs (BMDCs), bone marrow-derived macrophages, and murine fibroblasts were isolated, and the serum shock method was used to synchronise them according to the time of day. The specific cell type was isolated and plated in a 24-well plate at $1.25x10^5$ cells per well in complete DMEM. After 24 hours, cells were shocked with 50% Horse Serum and 50% DMEM for 2 hours. Fresh, complete DMEM was then replaced. Cells were then treated with Cy5-tagged PLA/ PLGA nanoparticles NPs (100ug/ml) at 12, 24 and 36 hours post-serum shock. Unsynchronised cells were also treated. The cells were then placed in the CellDiscoverer7 imaged for cellular uptake of NP every 15 minutes over 5 hours.

RESULTS

BMDCs were serum shocked and the expression of core clock genes was analysed by PCR. Expression of clock genes such as *Bmal1*, *Per2*, *Rev-erba* and *Cry2* were all shown to oscillate, confirming that our BMDCs were synchronised. Using the CellDiscoverer7, the fold change in mean intensity fluorescence of our Cy5 tagged NP within the cell over 4 hours was calculated for each 15-minute visualisation. Two points were visualised in each well, and the mean intensity was calculated from these two images, Figure 1 (A). The area under the curve was calculated in Figure 1 (B). We see a significant increase in NP uptake when NPs were added at 12hrs or 36hrs post serum shock compared to unsynchronised cells, Figure 1(A) and (B). This increase in uptake at 12 hours and 36 hours represents subjective dawn. We performed this on bone marrow-derived macrophages and murine fibroblasts; however, we did not see the same effect.

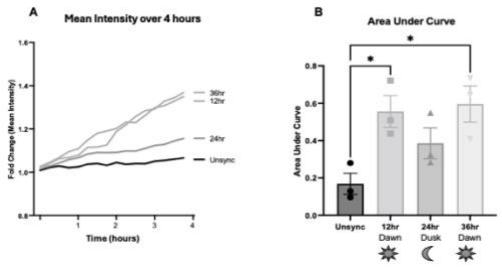

Figure 1. Nanoparticle uptake is under the influence of the clock, (A) Mean fold change in intensity over 8 hours in unsynchronised, 12hr, 24hr, and 36hrs post serum shock BMDCs. (B) The area under the curve, mean ± SEM (n = 3). ANOVA statistical testing was performed with significance denoted as *$p<0.05$.

DISCUSSION

These experiments suggest a role for the clock in NP uptake by immune cells. Specifically, we demonstrate that NP uptake is time-of-day dependent in immune cells but not fibroblasts, with BMDCs showing increased uptake at subjective dawn. This circadian effect appears unique to immune cells, reinforcing the relevance of circadian rhythms in vaccination outcomes. Future work will explore this across various cell types and elucidate the underlying mechanisms. Further, these findings will help to inform our chrono-tailored MN patch containing our NPs to enhance vaccine uptake and efficacy at the optimal time of day.

REFERENCES

1. Roenneberg, T. & Foster, R. G. et al. Photochemistry and Photobiology 66, 549–561 (1997).
2. Otasowie et al, Frontiers in Immunology 13, (2022).
3. Cervantes-Silva et al. Nat Commun 13, 7217 (2022).

MESENCHYMAL STEM CELL APOPTOTIC BODIES: WARRIORS AGAINST INFLAMMATION

Buckley, F.[1, 2], Contreras-Kallens, P.[1, 2], Brennan, M Á[1, 2].
[1] Regenerative Medicine Institute (REMEDI), School of Medicine, University of Galway.
[2] Biomedical Engineering, School of Engineering, University of Galway.
email: meadhbh.brennan@universityofgalway.ie

INTRODUCTION

Mesenchymal stem cells (MSCs) are multipotent stem cells with regenerative potential. The concept of mediating tissue regeneration using transplanted MSCs was primarily based on the early hypothesis that MSCs would engraft and differentiate, to replace damaged tssue[1]. However, analysis of engraftment rates provided evidence that transplanted MSCs are transient and are subjected to apoptosis post-transplantation[2]. Despite the low survival rates, MSCs retain their potent immunomodulatory and tissue repair capabilities. These observations gave rise to the "dying stem cell hypothesis", whereby the beneficial effects of transplanted MSCs are attributed to the immunomodulatory effects of apoptosis. The process of apoptosis results in the formation of apoptotic bodies (ABs), a subset of extracellular vesicles, which can be cleared by phagocytosing immune cells. It is hypothesized here that UV irradiation of MSCs in vitro produces ABs with the potential to reduce the inflammatory profiles of efferocytosing immune cells.

MATERIALS AND METHODS

Apoptosis was induced in the D1 ORL UVA MSC cell line using UV irradiation in serum-free conditions, to avoid contaminating the sample with serum extracellular vesicles. To isolate the ABs from the conditioned media of the apoptotic MSCs, differential centrifugation was used. First, the conditioned media was centrifuged at 500 x g for 10 minutes to pellet dead cells. The supernatant was collected and further centrifuged at 3,000 x g for 30 minutes. ABs were washed once. ABs were characterised by TEM, DLS, BCA protein quantification, and flow cytometry for extracellular vesicular markers CD9, CD63 and CD81, and MSC markers CD73, CD90 and CD105. The immunomodulatory potential of MSC-ABs was tested using allogenic murine phagocytes in vitro.

RESULTS

UV irradiation induces apoptosis in the D1 ORL UVA MSC cell line. MSC-ABs isolated at 3,000 x g are approximately 1 µm in diameter and express extracellular vesicle markers CD9, CD63 and CD81, and MSC markers CD73, CD90 and CD105. MSC-ABs are efferocytosed by phagocytes, and show potential to reduce the inflammatory profiles in vitro including surface markers, migratory properties and inflammatory cytokine secretion.

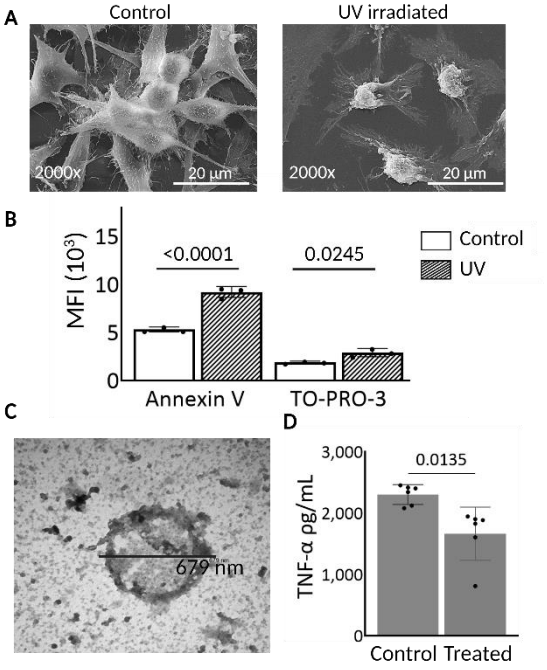

Figure 1 Mesenchymal stem cell apoptosis and the anti-inflammatory effects of apoptotic bodies. (A) Morphology and (B) Annexin V-FITC and TO-PRO-3 staining of control and UV irradiated MSCs. (C) Morphology of MSC apoptotic bodies. (D) TNF-α secretion of phagocytes post-apoptotic body efferocytosis.

DISCUSSION

This work demonstrates a rapid and chemical-free method of generating MSC-ABs with immunomodulatory potential, providing a promising insight into novel therapies against inflammation.

REFERENCES

[1] Kholodenko, I.V. et al. (2013) Journal of Regenerative Medicine and Tissue Engineering, 2(1), p. 2. doi:10.7243/2050-1218-2-4.
[2] Preda, M.B. et al. (2021a) Cell Death & Disease, 12(6). doi:10.1038/s41419-021-03839-w.

IMMUNOMODULATORY EFFECT OF MESENCHYMAL STEM CELL-DERIVED EXTRACELLULAR VESICLES ON DENDRITIC CELLS

Kimingi, HW.[1], Buckley, F.[2], Contereras, PK.[2], Aris, HM.[1], Brennan, MÁ.[1,2,3]

[1.] Biomedical Engineering, School of Engineering, College of Science and Engineering, University of Galway, Galway, Ireland

[2.] Regenerative Medicine Institute (REMEDI), School of Medicine, College of Medicine, Nursing and Health Sciences, University of Galway, Galway, Ireland

[3.] CÚRAM, SFI Research Centre for Medical Devices, University of Galway, Ireland

Email: H.Kimingi1@universityofgalway.ie or meadhbh.brennan@universityofgalway.ie

INTRODUCTION

Dendritic cells (DCs) are professional antigen-presenting cells (APCs) that link the innate and adaptive immune systems. Integration of different signals by DCs like the cytokine milieu at the inflammation site may determine the activation of DCs to either tolerance (tolerogenic DCs) or immunogenic DCs (1). Overactive DCs are implicated in inflammation-related bone loss by activating T-cells as reported in rheumatoid arthritis (RA) (2) and chronic periodontitis (3). Therefore, there is a need for therapies that can modulate DCs towards tissue-repair effectors. It has been shown that mesenchymal stromal cells (MSCs), and more recently their secreted extracellular vesicles (EVs), can influence the immune system (4). This study investigates the influence of MSC-EVs' potential to modulate dendritic cell differentiation and activation.

MATERIALS AND METHODS

Murine MSCs were cultured on tissue culture plastic in EV-depleted media for 48 hours. EVs released by the MSCs were isolated by using differential centrifugation, ultrafiltration, and size exclusion chromatography (SEC). EVs were characterized by particle size and concentration using nanoparticle tracking analysis (NTA) and by protein content using bicinchoninic acid (BCA), for morphology, as well as surface marker expression. MSC-EVs were treated on monocyte-derived dendritic cells isolated from C57BL/6 mice. EVs were treated at increasing dosages (0, 3.8e+009, 7.59e+009, 8.165e+009 and 2.25e+010 EV particles per mL) on days 0, 3, and 6 for differentiation assay and one day after activation for activation assay. The uptake of the EVs by DCs was monitored by tracking palmitoylated-tandem dimer Tomato (PalmtdTomato) EVs using confocal microscopy. DC surface markers analysed by using flow cytometry, and cytokine secretion, were employed to assess the effect of MSC-EVs on differentiation, activation, and intracellular cytokine release by dendritic cells.

RESULTS

The size of the isolated MSC-EVs ranged between 30 and 380 nm with the majority of EVs having the size of 130 ± 40 nm. MSC-derived EVs caused a significant dose-dependent reduction in the expression of MHC-II, CD11c, CD40, and CD86 surface markers and increased expression of CD11b surface marker and PD-L1 immune checkpoint marker.

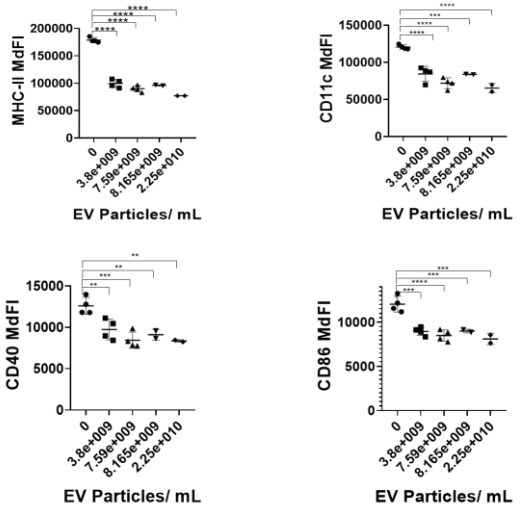

Figure 1 Expression of different dendritic cell surface markers presented as MdFI (Median fluorescent intensity). The mean of the MdFI for each treatment was compared to the mean of MdFI for control (0 EV treatment) using one-way ANOVA and Dunnett's multiple comparisons test. * p< 0.05, ** p<0.01, *** p<0.001, **** p<0.0001

DISCUSSION

MSC-EVs inhibited the differentiation and activation of monocyte-derived dendritic cells. To understand the underlying mechanisms behind these findings we are currently investigating the role of EV-treated dendritic cells on the activation and proliferation of T-cells. Further, we will investigate the transcriptome, miRNA, and protein cargo profiles of the murine MSC-EVs.

REFERENCES

1. Fucikova *et al.,* Induction of Tolerance and Immunity by Dendritic Cells: Mechanisms and Clinical Applications. Front Immunol. 2019 Oct 29;10:2393.

2. Page *et al.,* RANK and RANKL expression in RA synovium and lymph nodes as markers of dendritic cell-T cell interactions. Arthritis Res Ther. 2004;6(Suppl 3):62.

3. Cirrincione *et al.,* Lamina Propria Dendritic Cells Express Activation Markers and Contact Lymphocytes in Chronic Periodontitis. Journal of Periodontology. 2002 Jan;73(1):45–52.

4. Jiang *et al.,* Immune modulation by mesenchymal stem cells. Cell Prolif. 2019 Nov 15;53(1):e12712.

CGAS/STING ACTIVATION AS A MODULATOR OF MACROPHAGE POLARISATION IN OSTEOSARCOMA

O'Donoghue, J.C[1,2], Freeman, F.E[1-3]

[1] School of Mechanical and Material Engineering and Materials Science Centre, University College Dublin, Ireland
[2] Conway Institute of Biomolecular and Biomedical Research, University College Dublin, Ireland
[3] Trinity Centre for Biomedical Engineering, Trinity Biomedical Sciences Institute, Trinity College Dublin, Ireland
email: Jordan.odonoghue@ucdconnect.ie

INTRODUCTION

Osteosarcoma is an aggressive paediatric bone cancer with a highly immunosuppressive tumour microenvironment that limits immunotherapeutic efficacy. The cGAS/STING pathway, known for detecting intracellular DNA and inducing inflammation, has immunomodulatory functions that influence tumour immunity [3]. Although STING agonists are being tested in preclinical trials for various cancers, their impact in osteosarcoma remains unexplored. Tumour associated macrophages (TAMs) which can constitute up to 50% of the tumour volume, promote metastasis and suppress anti-tumour immunity, making them a key target for immunotherapy [1,2].

Herein, we aimed to investigate the potential of the STING agonist (CL656) to repolarize TAMs to a more tumoricidal M1-like phenotype and evaluate whether this would enhance chemotherapy's therapeutic potential. Additionally, we examined the timing of CL656 delivery relative to chemotherapy and whether prolonged STING activation could reduce macrophage responsiveness, seeking an optimal balance in boosting chemotherapy without causing chronic activation.

MATERIALS AND METHODS

2.1 Temporal STING modulation: Human osteosarcoma cells (Saos-2) and monocytes (THP-1) were seeded (250,000 cells/well, *n*=6). Monocytes were polarized to M0 macrophages with 10 nM PMA for 24 hours, then treated with LPS/IFN-γ (M1), IL-4/IL-13 (M2) or left untreated (M0) for another 24 hours. Macrophages received CL656 (10µM) either before (*pre*) or after (*post*) exposure to doxorubicin-treated osteosarcoma-conditioned medium (+DOX). Conditioned medium was prepared by exposing osteosarcoma cells to ±IC^{50} doxorubicin (1.7µM) for 24 hours, followed by fresh medium collection after 24 hours. STING activation was assessed via Western blot (*STING, pIRF3, IRF3*) and cytokine release (IL-6, IL-10). ***2.2 STING Activation Time Response:*** M0-polarized monocytes were treated with CL656 for various durations (untreated, 2, 4, 8, 24 hours). Optimal treatment time for inducing a pro-inflammatory response without chronic activation was determined via ELISAs and Western blots. ***2.3 Optimum STING Activation balance:*** M0- or M1-polarized monocytes were treated with CL656 for 6 hours (from 2.2) pre-exposure to doxorubicin-treated osteosarcoma-conditioned medium (from 2.1). Immune responses were measured post-STING activation and post-conditioned medium using ELISAs and Western blots.

RESULTS

IL-6 expression in M0 and M2 macrophages was unaffected by agonist timing, while IL-10 expression decreased regardless of timing. In M1 macrophages, IL-6 increased with pre-treatment but not post-treatment (**Fig. 1A,B**). CL656 treatment for 24 hours led to STING degradation across all macrophage phenotypes (data not shown), while 4–8 hours induced a pro-inflammatory response (increased IL-6) without chronic STING activation (**Fig. 1C**). A 6-hour pre-treatment suppressed IL-10 in M0 macrophages without affecting IL-6, and enhanced IL-6 in M1 macrophages without altering IL-10 (**Fig. 1D,E**).

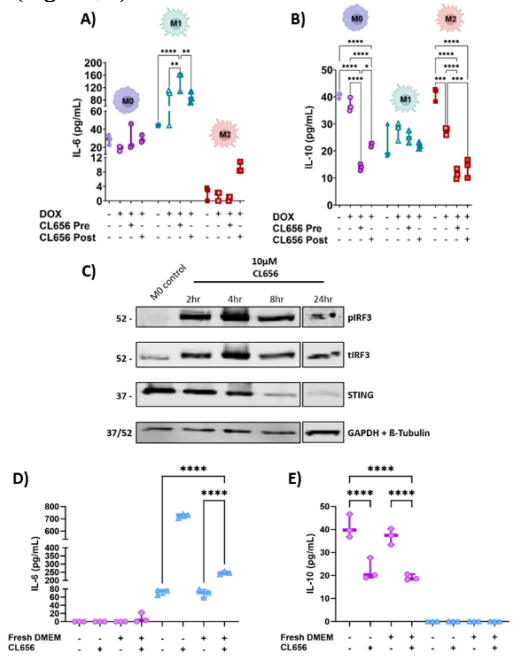

Figure 1: (A,B) IL-6 and IL-10 expression in macrophages ± CL656 treatment 24 hours before or after osteosarcoma-conditioned medium. **(C)** Western blot of macrophage lysates post-CL656 treatment. **(D,E)** IL-6 and IL-10 expression in macrophages pre-treated with CL656 before osteosarcoma-conditioned medium. Error bars indicate standard deviation.

DISCUSSION

This study introduces a combinational approach for osteosarcoma treatment, using STING agonists to reprogram M0 and M2 macrophages in the tumour microenvironment (TME) towards a pro-inflammatory phenotype. Pre-chemotherapy STING agonist treatment was most effective, polarizing all macrophage phenotypes and creating a "hot" tumour more susceptible to chemotherapy. However, excessive STING activation caused chronic activation and degradation, risking loss of immune responses and memory. Optimizing agonist concentration and regimen is crucial to avoid chronic macrophage activation.

REFERENCES

[1] Luo *et al.*, Frontiers in Oncology, Volume 10, 2020. [2] Cersosimo *et al.*, International Journal of Molecular Sciences, Volume 21, 2020. [3] Gan *et al.*, Frontiers in Immunology, Volume 12, 2022

A MULTI-FUNCTIONAL GENE-ACTIVATED SCAFFOLD AS AN IMMUNO-MODULATORY PLATFORMS FOR CHRONIC WOUND HEALING APPLICATIONS

Palomeque-Chávez, J. C.[1, 2], McGrath, M.[1,2], Dobricic, M.[1], O'Connor, C.[1,2],Kearney, C.[1, 3], Browne, S.[1,4], O'Brien, F. J.[1, 2].

[1]Tissue Engineering Research Group, Department of Anatomy and Regenerative Medicine, RCSI, Dublin, Ireland. [2]Advanced Materials and Bioengineering Research Centre, RCSI and TCD, Dublin, Ireland; [3]Kearney Lab, Department of Biomedical Engineering, University of Massachusetts Armhest, Armhest, USA. [4]Centre for Research in Medical Devices (CURAM), University of Galway, Galway, Ireland. Email: juancarlospalom21@rcsi.com

INTRODUCTION

Macrophage polarisation play an essential role in wound healing. The initial inflammatory response is facilitated by M1-type macrophages, whereas the subsequent resolution of inflammation and promotion of vascularisation are mediated by M2-type macrophages. However, this balance is dysregulated at a genetic level in chronic wounds, increasing the M1-type macrophage presence, enhancing inflammation, and reducing vascularisation. While collagen-based (CG) scaffolds show some promise for tissue repair and remodeling in skin wounds, additional functionalisation is required to overcome this gene dysregulation and elicit healing of chronic wounds.[1] miRNAs are non-coding RNAs that regulate gene expression in many biological processes, including inflammation and angiogenesis in wound healing.[2] miRNA-155 inhibition, in particular, has shown anti-inflammatory outcomes in vivo, while increasing the expression of pro-angiogenic markers.[3] Thus, we propose that targeted delivery of a miRNA-155 inhibitor from CG scaffolds to macrophages will promote M2 polarisation, effectively attenuating inflammation. Additionally, we assessed the interaction between miRNA-155-treated macrophages and endothelial cells, and their ability to enhance angiogenic processes necessary for chronic wound healing.

METHODS

Nanoparticles were synthesised by complexation of negatively charged miRNA and positively charged non-viral vector GAG-binding enhanced transduction (GET) peptide.[3] miRNA-activated scaffolds were formed by soak-loading miRNA nanoparticles onto lyophilised CG scaffolds. The effect of miRNA-155 delivery on macrophage polarisation towards non-polarised (M0) and pro-inflammatory (M1) phenotypes was assessed using THP-1 monocytic cells. Cell phenotype and polarisation state was assessed by confocal microscopy through staining and quantification of pro-inflammatory (CD80) and anti-inflammatory (CD206) markers. The effect of macrophage polarisation on angiogenesis was also evaluated by examining THP-1 cells interactions with endothelial cells via paracrine signalling in migration and tube formation assays. Analysis of the expression of key inflammatory and angiogenic markers was carried out by PCR and ELISA.

RESULTS

miRNA-activated CG scaffolds supported increased expression of anti-inflammatory and pro-angiogenic markers, such as IL-10 and VEGF, from M0 and M1 macrophages over 7 days. An increased number of CD206+ macrophages were observed from M0-seeded scaffolds, while reduced CD80+ macrophages were observed in M1-seeded scaffolds after 3 and 7 days post-transfection, indicating M2 macrophage polarisation in both scenarios. Endothelial cell migration and organisation into vascular-like structures was also enhanced when exposed to the conditioned media from miRNA-activated scaffolds. (**Figure 1**)

DISCUSSION & CONCLUSIONS

In this work, we show that miRNA-activated CG scaffolds enhance an anti-inflammatory M2 macrophage phenotype confirmed through gene expression and the staining, imaging, and quantification of CD206+ and CD80+ expression. We show that the secretome from these macrophage-seeded miRNA-activated scaffolds enhance pro-angiogenic processes in endothelial cells, essential for the vascularisation of the wound. Taken together, this data indicates that miRNA-activated scaffolds enable M2 macrophage polarisation; key for the reduction of inflammation, promotion of angiogenesis, and the resolution of chronic wounds.

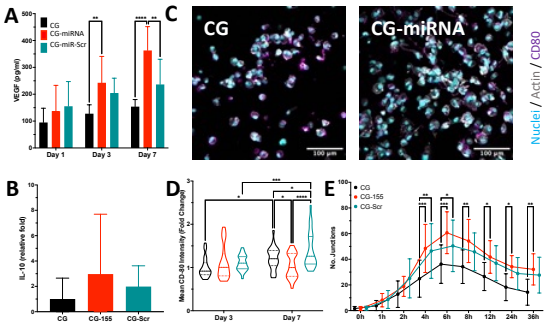

Figure 1. Quantification of VEGF and IL-10 expression on M1-seeded scaffolds (A-B).Confocal images of CG and CG-miRNA scaffolds seeded with M1 macrophages, and quantification of CD80 expression (C-D). Quantification of junctions from endothelial cell vascular networks exposed to M1 macrophage secretome (E).

REFERENCES

1 McGrath et al., ACS Appl. Mat. Inter., vol.15, 2023
2 Banerjee et al., Adv. Exp. Med. Biol., vol. 888., 2015
3 Ye et al., IJLEW, vol. 16., 2017
4 Raftery et al., Biomaterials, vol. 216., 2019

ACKNOWLEDGMENTS

Research Ireland Advanced Materials and BioEngineering Research Centre (SFI/12/RC/2278_P2)

MESENCHYMAL STEM CELL DERIVED EXTRACELLULAR VESICLES ATTENUATE B CELL ACTIVATION

Contreras Kallens, P.[1, 2], Williams, M.[3], Kimingi H.[1, 2.] Shen, Y.[1, 2] , Aris, H.[1, 2], Malinova D.[3], Brennan M.[1, 2]

[1] College of Medicine, Nursing, & Health Sciences, University of Galway, Ireland
[2] College of Science and Engineering, University of Galway, Ireland
[3]Wellcome Wolfson Institute for Experimental Medicine, Queen's University Belfast, Northern Ireland
email: Meadhbh.brennan@universityofgalway.ie

INTRODUCTION

Autoimmune diseases (ADs) are characterized by B cell function dysregulation. Novel therapies such as antibody-mediated B cell depletion have significant side effects[1]. Mesenchymal stem cells (MSCs) have been proposed as an alternative therapy for ADs, as these cells bear potent immunomodulatory capacities, particularly when exposed to inflammatory conditions known as 'licensing' [2]. MSC-derived extracellular vesicles (EVs) have been proposed as an acellular alternative to MSCs. The aim of this study was to evaluate the effect of EVs derived from licensed and unlicensed MSCs on B cell function and activation

MATERIALS AND METHODS

Bone marrow murine MSCs (BM-MSCs) were cultured on tissue culture plastic in EV-depleted media with IFN-γ and TNF-α to 'license' them, or in standard conditions for 48 hours. The conditioned media was then collected, and the MSC~~s~~-EVs were isolated by size exclusion chromatography. EVs samples' particle concentrations and protein concentrations were measured by NTA and BCA, respectively.
For assessing the effect of EVs on B cells, primary B cells were isolated from an allogenic strain mouse and activated both in a T-cell independent and T-cell dependent way. The effect of licensed and unlicensed EVs on the expression of activation surface markers and proliferation of B cells was measured by spectral flow cytometry.

RESULTS

The presence of pro-inflammatory cytokines in the media caused an increase in the expression of both constitutive markers, such as CD73, and inducible markers, like MHCII, on the BM-MSCs. These cells were also capable of secreting more EVs per cell, and these EVs contained a higher content of protein per particle compared to unlicensed EVs. BM-MSCs derived EVs could modulate the expression of early activation markers on allogeneic murine B cells. The EVs capacity of modulating B cells proliferation was also studied and was found to be modulated by both unlicensed and licensed BM-MSCs EVs.

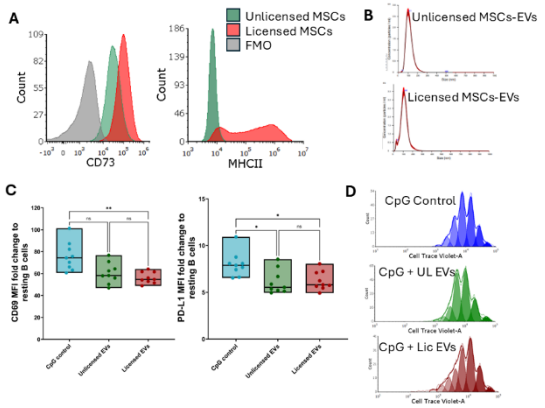

Figure 1. Licensed murine BM-MSCs characterization and modulation of activated B cells through extracellular vesicles. A. Representative histogram of CD73 and MHCII of unlicensed and licensed BM-MSCs. B. Representative histogram of unlicensed (top) and licensed (bottom) BM-MSCs derived EVs. C. Modulation of CD69 and PD-L1 early activation markers on CpG activated B cells by unlicensed and licensed BM-MSCs derived EVs. D. Representative histograms of proliferation modulation of CpG activated B cells by unlicensed and licensed BM-MSCs derived EVs. Krustal-Wallis test; ns: non-significant; *, p< 0.05; **, p<0.005. *UL, unlicensed; Lic, licensed.*

DISCUSSION

Our findings demonstrate that BM-MSCs-derived EVs can modulate B cell activation and function *in vitro*. Moreover, our study highlights the influence of MSCs' culture conditions on EV effects, suggesting potential therapeutic versatility in diseases characterized by immune dysregulation, such as ADs. Further elucidation of the underlying mechanisms is crucial to fully harness the clinical potential of MSCs-derived EVs as immune therapies.

REFERENCES

[1]Hofmann *(et al.),* Frontiers in Immunology 9: 835, 2018.
[2]Prockop, Molecular Therapy 17: 939-946, 2009.

BANFA: BIOMECHANICALLY ADJUSTED NEUROVASCULAR FUNCTION ASSESSMENT — PROTOCOL DEVELOPMENT AND INITIAL RESULTS

O'Connor, J.D.[1], Newman, L.[2], Knight, S.P. [2]
[1] School of Engineering, Ulster University, Belfast, Northern Ireland, UK
[2] The Irish Longitudinal Study on Ageing (TILDA), School of Medicine, Trinity College, University of Dublin, Ireland
email: j.oconnor1@ulster.ac.uk

INTRODUCTION

A fifth of all the energy used in the body is used by the brain. The biological systems involved in supplying the brain with blood are constantly working to ensure optimal brain blood flow in the face of many daily challenges including exercise, posture change, digestion and the external environment. Impairment of our protection systems for brain blood flow can lead to loss of consciousness (and falls) in the short term and changes in brain function and structure over longer periods. Measurement of flow during simple movements such as standing from a seated or lying position can give an indication of how quickly an individual can adjust to their optimal level of blood flow (Mol *et al.* 2020). However, these tests do not currently account for how quickly a person performs the activity (O'Connor *et al.* 2020). This means that two individuals may be evaluated as equal (in their ability to rebound after a challenge) despite the exertion being different (e.g., one person took 2 seconds to stand up while the other took 10 seconds). The aim of the BANFA project is to use data from a device that measures movement (i.e., an accelerometer) to develop a standardised method for evaluating the brain's response to challenge. These methods may be used in multiple applications including to assess the risk of falls and brain health decline in the older adult population as well as measuring response to exercise.

MATERIALS AND METHODS

Recruitment (target sample size: n=30) for this study was through university-wide emails and posters. Testing lasted approximately one hour. Participants had their height, weight, blood pressure and heart rate measured while seated. Participants were then asked to rest in a supine position (lying on their back) for 10 minutes before standing (repeated for a slow and fast stand). Several parameters were continuously monitored: cerebral oxygenation, electrocardiogram (ECG), accelerometery, and video recording of the movements. Cerebral oxygenation was be tracked using a Near-Infrared Spectroscopy (NIRS) device, affixed to the forehead, which gauges the absorption of near-infrared light by haemoglobin in the brain's frontal lobe. A chest strap was used to record ECG and heart rate data. Video recording of the participants' movements was collected to assess their standing speed. Video based standing speed was compared against accelerometer-based adjustment of cerebral oxygenation.

RESULTS

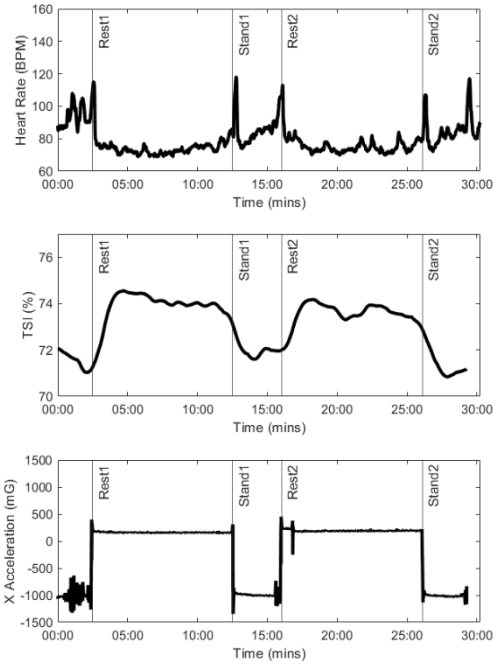

Figure 1. Heart rate, tissue saturation index and acceleration measured over the course of two stands (the first faster and the second slower) for one participant.

Representative data from a single participant shows expected peaks in heart rate after standing as well as a nadir in TSI for both fast and slow stands. Accelerometry data showed a clear transition between supine and standing positions.

DISCUSSION

A workflow for collecting synchronised heart rate, TSI and accelerometer data during standing was successfully implemented and trends in the data show promise for developing an automated method for adjusting tests for movement speeds. Future work will increase sample size to 30 and focus on the biomechanical adjustment method.

REFERENCES

O'Connor *et al.*, Hypertension, Vol. 75, Issue 2, Pages 524–531, 2020; Mol *et al.*, Frontiers in Physiology, Vol. 11, 2020

PERFORMANCE ASSESSMENT OF NOVEL TRACKING METHODS USING HIGH-DENSITY SURFACE ELECTROMYOGRAPHY

Liegey J.[1], McManus M.[2], Lowery M.[1]
[1] University College Dublin
[2] Trinity College Dublin
email: Jeremy.liegey1@ucdconnect.ie

INTRODUCTION

Surface electromyography (sEMG) involves the recording and analysis of electrical signals generated by muscles during their contraction. High-density sEMG utilizes arrays of electrodes to record this muscle activity. This multi-dimensional recording of the activity allows, in turn, to decompose the sEMG signal into its constituent motor units, allowing the peripheral study of more central motor control. Another advantage offered by HD-sEMG over classical sEMG is the potential to track individual motor units from one trial to another. Current methods for motor unit tracking rely on cross-correlation or individual waveforms or informed decomposition of secondary trials [1]. Both these methods struggle with changes in action potentials shapes from one trial to another as well as changes in action potential distributions across the array. In this study, we propose a novel method for tracking motor units across trials using the high-dimension representations of their action potentials.

MATERIALS AND METHODS

Simulated data were generated using an anatomically correct model of the first dorsal interosseus (FDI) [2] muscle and experimental data recorded from young healthy control participants (Study was approved by University College Dublin Ethics Committee and informed consent was collected prior to recording). Two hundred datasets containing between 10 and 30 motor units with overlap between datasets ranging from 20% to 100% were constructed using the simulated data and 30 sets containing between 11 and 27 motor units with overlap ranging from 30% to 70% were generated from the experimental data. The simulated data were used to perform forward selection of the most robust sets of features among 11 features computed using multi-dimensional representations of the motor unit action potentials. Once the set of most robust features was identified, both experimental and simulated data were used to verify the performance of the algorithm against cross-correlation (CC) based algorithms at different threshold values. The 2 thresholds selected for comparison were 0.8 and 0.9 based on values used in the literature [3].

RESULTS

The set of most robust features was identified across a wide range of motor unit numbers and overlap amounts. Using these features, the proposed method outperformed both low (0.8) and high (0.9) threshold CC based algorithms. The F1 score was used as the performance metric, the comparison of the 3 algorithms is presented on Fig1.

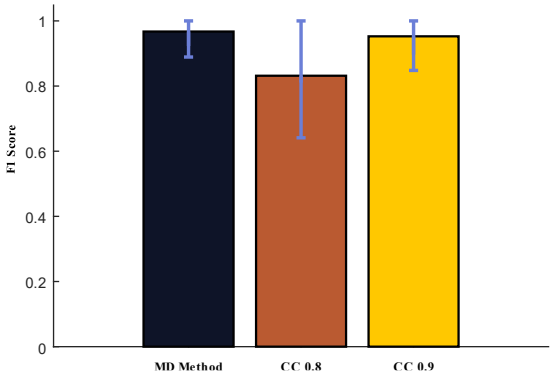

Figure 1 F1 scores for the 3 algorithms. The error bars were computed as the standard deviation.

DISCUSSION

The results demonstrate the performance of the proposed method against cross-correlation based algorithms that are widely used for tracking. The performance of the algorithm was not affected by the number of motor units in the set but it increased with the amount of overlap between the two sets used. This increase in performance can be attributed to the clustering aspect of the method where a denser cluster is easier to identify. The data used to test the algorithm were all generated or recorded from the hand. The FDI being a lean muscle, the action potential shapes are more unique than if they originated, for example, from a lower body muscle with more subcutaneous fat. The higher amount of fat would lead to the action potentials being spatially filtered, possibly requiring another set of features being extracted to capture the more subtle differences between the signals.

REFERENCES

[1] A. Frančič *(et al)*, *IEEE Access*, vol. 9, pp. 115227–115236, 2021.
[2] D. P. Botelho *(et al)*, *PLOS Computational Biology*, vol. 15, no. 8, p. e1007267, 2019.
[3] E. Martinez-Valdes *(et al)*, "*The Journal of Physiology*, vol. 595, no. 5, pp. 1479–1496, 2017.

DEVELOPMENT OF A GENE-ACTIVATED IPSC-NEURON SEEDED SCAFFOLD FOR SPINAL CORD INJURY REPAIR

Mullally, R.[1,4], O'Connor, C.[1,4], Woods, I.[1,4], Stewart, R.[2], Dervan, A.[1,4], Caldwell, M.[3], O'Brien, F.J.[1,4,5]

[1] Tissue Engineering Research Group, Dept. of Anatomy and Regenerative Medicine, Royal College of Surgeons in Ireland, Dublin, Ireland
[2] Dept. of Physiology & Medical Physics Dublin, Royal College of Surgeons in Ireland, Dublin, Ireland
[3] Dept. of Physiology & Trinity Inst. of Neurosciences (TCIN), Trinity College Dublin, Dublin, Ireland
[4] Advanced Materials and Bioengineering Research Centre, Dublin, Ireland
[5] Trinity Centre for Biomedical Engineering, Trinity College Dublin, Dublin, Ireland
email: renamullally23@rcsi.com

INTRODUCTION

Spinal Cord Injury (SCI) is a traumatic life-changing injury that induces permanent loss of function and paralysis in affected individuals. In the injured cord, repair is limited by the formation of a growth-inhibiting lesion cavity, coupled with the loss of neurons and the poor ability of damaged axons to regrow through the lesion site [1]. Recent advances in biomaterial-mediated cell transplantation offer the potential to drive recovery after SCI. However, few implants are optimally designed to actively support axonal regrowth and support the viability of transplanted human induced pluripotent stem cell (iPSC)-derived neurons, which have emerged as a promising cell source for the treatment of SCI [2]. Therefore, this study aimed to develop a hyaluronic acid-based biomimetic scaffold carrying axon growth-inducing nucleic acid cargoes, encapsulated in nanoparticles that are capable of transfecting implanted iPSC-neurons.

MATERIALS AND METHODS

Optimisation of non-viral nanoparticle (NP) delivery to iPSC-neurons in 2D. Non-viral NPs were generated by complexing the GAG-binding enhanced transduction peptide with reporter plasmid DNA and thereafter added to growing iPSC-neurons to determine the optimal NP concentration for achieving safe and effective transgene expression in neurons. *Fabrication and characterisation of the gene-activated scaffold.* iPSC-neurons were first cultured on a range of native cord matrix proteins (collagen-IV, fibronectin, laminin-1, laminin-2, or laminin-10) to identify the optimal substrate for neuronal viability, and outgrowth. Hyaluronic acid slurries were then prepared using a modified carbodiimide chemistry process [3], functionalised with the optimised neurotrophic mix collagen-IV and fibronectin (0.1 mg/mL each), and freeze-dried as previously described [4]. Scaffolds were soak-loaded with non-viral NPs encapsulating plasmid DNA for assessment of scaffold incorporation, loading efficiency, and NP release dynamics. Thereafter, scaffolds were seeded with iPSC-neurons to validate effective scaffold-mediated transfection and assess growth-induced changes in neuronal axon outgrowth.

RESULTS

We first demonstrated successful and sustained non-viral transfection of iPSC-neurons without inducing changes in cell viability, cytotoxicity or morphology, indicating biocompatibility of the NPs (Fig. 1A, B). Next, we showed that the dual formulation of collagen-IV and fibronectin enhanced iPSC-neuronal survival and neurite outgrowth, and subsequently when incorporated into the hyaluronic acid-based scaffold. Scanning electron microscopy then demonstrated the successful loading and distribution of NPs throughout the scaffold architecture (Fig. 1C). NP loading efficiency was greater than 96%, and further evaluation of the NP release profile demonstrated a high retention rate (Fig. 1D), with scaffolds retaining the total loaded genetic cargo for the 7-day period. Finally, ongoing analysis validates scaffold-mediated transfection, demonstrating enhanced infiltration, survival and outgrowth of iPSC-neurons on the developed neurotrophic gene-activated scaffold.

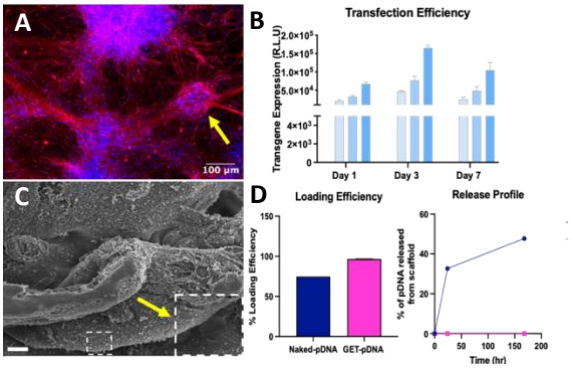

Figure 1 A) ECM proteins collagen-IV and fibronectin trophically support iPSC-derived neuron clusters (arrow). B) Effective non-viral transfection in human iPSC-neurons over 7 days. C) Successful nanoparticle incorporation in scaffolds (arrow). D) NPs demonstrated a high loading efficiency and retention in the scaffolds.

DISCUSSION

Here we show the optimisation of non-viral nanoparticle-encapsulated plasmid DNA for iPSC-neuronal delivery and demonstrate efficient nanoparticle-loading, yielding a gene-activated biomimetic scaffold platform conducive to sustained delivery of neurotrophic genes, iPSC-neuronal uptake, survival and growth. Overall, this work demonstrates the potential of gene-activated biomaterial scaffolds to enhance cell transplantation therapies and support axonal regrowth through the injured cord.

ACKNOWLEDGMENTS & REFERENCES

This work was supported by a joint funding initiative of the Irish Rugby Football Union (IRFU) Charitable Trust and the Research Ireland Advanced Materials and Bioengineering Research Centre (AMBER).

1.Bonner (et al.), *Brain research*,1619,115-123, 2015.
2.Lu (et al.), N*euron*, *83*(4), 789-796, 2014.
3.O'Connor (et al.), *Current Protocols* 3(2), e688, 2023.
4.Woods (et al.), *Advanced Healthcare Materials*, 11(3), 2101663, 2022.

REPETITIVE SALIVA SWALLOW TEST: A SURFACE ELECTROMYOGRAPHY-BASED APPROACH

Appiah, A. B., Doheny, E. P.
School of Electrical and Electronic Engineering, University College Dublin
email: afua.appiah@ucdconnect.ie

INTRODUCTION

The Repetitive Saliva Swallow Test (RSST) is an established clinical method to monitor oropharyngeal dysphagia [1], a prevalent symptom of Parkinson's disease [2]. During the RSST, patients swallow their saliva as many times as possible in 30 seconds, with clinicians traditionally counting swallows by palpating the larynx [3]. Surface electromyography (EMG) is a reliable method to assess muscle activity during swallowing [4]. A limited number of previous studies have used EMG to investigate suprahyoid and infrahyoid muscle activity during saliva swallowing tests [4,5]. These studies highlight the potential of EMG to assess muscle activity during the RSST. This study investigates the potential of augmenting the RSST with EMG, enabling comprehensive assessment of swallowing muscle function.

MATERIALS AND METHODS

Surface EMG data (Delsys Trigno Mini; 1926 Hz) were recorded from the suprahyoid and infrahyoid (IH) muscles in 12 healthy adults (29.0 ± 5.7 years; 9 female) during two repetitions of the RSST. Participants were instructed to swallow their saliva as many times as possible in 30 s, while counting their swallows to provide a reference (S_{ref}). Ethical approval was obtained from the UCD Human Research Ethics Committee.

EMG data were bandpass filtered 20-450 Hz and notch filtered at 50 Hz. To obtain the signal envelope, data were rectified and lowpass filtered at 1 Hz using a zero-phase 8^{th} order Butterworth filter. Peaks corresponding to muscle contractions were detected using an adaptive threshold based on the signal envelope amplitude (Figure 1A).

For each recording, the mean and coefficient of variation (CV) were calculated for the time between peaks and the amplitude of the peaks.

The agreement between the number of detected contractions (S_{det}) and S_{ref} was assessed using Bland Altman and intraclass correlation (ICC (2,1)) analysis. Pearson's correlation coefficient was also calculated to assess the linear correlation between the two variables.

RESULTS

Across all participants, the mean ± standard deviation (SD) of the time between peaks was 2.09 ± 0.49 s, and the CV was 32.18 ± 14.45 %. The mean ± SD of the amplitude of the peaks was 0.02 ± 0.01 mV, and the CV was 19.83 ± 7.43 %. The ICC and the linear correlation coefficient between S_{ref} and S_{det} were estimated to be 0.7 and 0.74 ($p<0.01$) respectively.

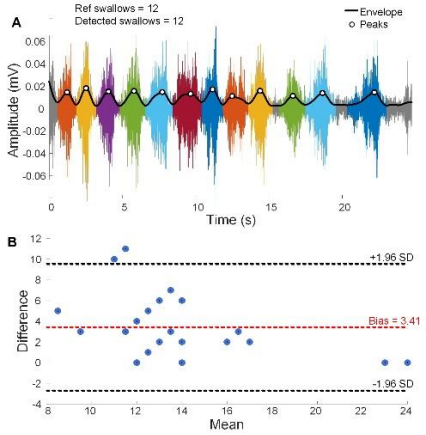

Figure 1 A: Sample data showing filtered IH EMG, the signal envelope and peaks corresponding to swallowing-related contractions, with individual contractions in different colours. B: Bland-Altman plot showing the agreement between S_{ref} and S_{det}, across all repetitions for all participants.

DISCUSSION

Bland Altman analysis (Figure 1B) revealed that the swallow count, S_{ref}, was 3.41 less than the number of detected contractions on average, as multiple infrahyoid muscle contractions corresponded to a single swallow in some cases. This difference is also reflected in the ICC of 0.7, indicating moderate agreement between S_{det} and S_{ref} [7]. These results suggest that the addition of surface EMG could provide additional information not captured by the traditional RSST. EMG opens the possibility to assess muscle activity and timing of individual swallows, and each swallow phase. In future work, we will examine frequency domain and non-linear EMG features and compare swallowing in healthy participants with participants with Parkinson's disease.

REFERENCES

[1] Ben-Hayoun *(et al.)*, Dysphagia, 2024.
[2] Hirschwald J (et al.), BMJ Evidence-Based Medicine 28:93–100, 2023.
[3] Persson *(et al.)*, Dysphagia 34: 271–278, 2019.
[4] Monaco, A. *(et al.)*, BMC Oral Health 8, 6, 2008.
[5] Ikeno *(et al.)*, The Japanese Journal of Dysphagia Rehabilitation 16: 148-154, 2012.
[6] Ohashi *(et al.)*, Medical Engineering & Physics 115: 103980, 2023.
[7] Portney & Watkins, Foundations of clinical research: applications to practice, Vol. 892, pp. 11-15, 2009

The Impact of Arm Variations on the Accuracy of Dehydration Monitoring

Liu, X.[1,2], O'Loughlin, D.[1,2]
[1] Electronic and Electrical Engineering, Trinity College Dublin, D02PN40, Ireland.
[2] Trinity Centre for Biomedical Engineering, Trinity College Dublin, D02PN40, Ireland.
email: xliu2@tcd.ie

INTRODUCTION

Dehydration can lead to a range of clinical impacts, such as reduced physical performance [1] and hospital-associated Disability (HAD) [2], and the treatments required vary depending on the severity of dehydration and other clinical factors. Mild dehydration may require only increased fluid intake, while severe dehydration may require intravenous fluids or medical intervention.

Although important, there are few clinically validated, techniques for hydration monitoring. Bioimpedance and microwave technology are emerging technologies for hydration status assessment due to the non-ionising and non-invasive nature of the devices. The electrical properties of biological tissues vary due to the hydration status and water content and microwaves are sensitive to these changes. By measuring the electrical properties, hydration status can be inferred.

Volunteer studies with microwave transmission measurements through the body have been promising, with studies with 8 healthy athletes in Garrett et al. suggesting a change in average properties of 2% for each 1% loss of mass due to dehydration. However, the findings are highly variable and subject to a lot of confounding factors.

This study aims to investigate confounding factors that may affect the accuracy and efficacy of microwave hydration status asssessment such as healthy variations in skin and anatomy and other changes in the electrical properties due to environmental conditions and others.

MATERIALS AND METHODS

Typically, these systems estimate the average electrical properties of the forearm by transmitting low-power microwaves through the arm. In this work, we use an analytical model to understand and model potential experimental variabilities arising from changes in the anatomy due to compression and other healthy variations in the tissue properties not caused by dehydration. By quantifying the sensitivity of the transmitted signals to these variabilities, it is possible to evaluate whether these may impair the potential accuracy and efficacy of this technique.

In this work, a layered-planar model of the arm with skin, fat and muscle tissues was used with representative electrical properties data for each layer. Experimental variations are modelled by adjusting the layers as would happen from inconsistent contact with the sensors, changes in the skin due to sweating and other factors.

RESULTS

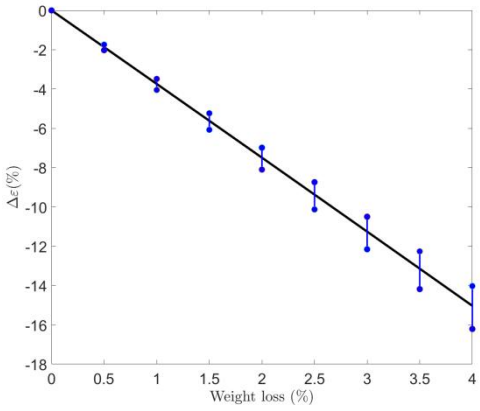

Figure 1 Estimated average permittivity vs water loss.

Fig. 1 shows the estimated average electrical properties from the analytical model with respect to the modelled dehydration for a 5 cm arm. The error bars show the range of possible estimates from the model if realistic variations in the electrical properties, anatomy and acquisition hardware are modelled. Although a clear trend in decreasing properties is evident and on a similar order of magnitude to the volunteer studies in the literature, the resolution of the measurements is limited by the uncertainties from these experimental errors.

DISCUSSION

These results suggest that microwave measurements can estimate hydration status, however, these measurements are sensitive to other changes in the body, such as variations in skin compression, contact, and other experimental uncertainties.

REFERENCES

1. Pichan *et al.*, Int.J. Biomet., 32, 176-180, 1988.
2. Nagae et al., Eur. Ger. Med., 14(1), 113–121, 2023.
3. Garrett, *et al.*, IEEE J. Elec., RF and Microwaves in Medicine and Biology 3(4), 292-299, 2019.

A COMPUTATIONAL AND EXPERIMENTAL ANALYSIS OF DRUG-COATED MICRONEEDLE INSERTION INTO SKIN: THE MODE OF ADMINISTRATION MATTERS

Shu W.T.[1], Kilroy S.[1], Lijnse T.[1], Ní Annaidh A.[1], O'Cearbhaill E.[1]
[1] UCD Centre for Biomedical Engineering, School of Mechanical and Materials
email: *aisling.niannaidh@ucd.ie, eoin.ocearbhaill@ucd.ie*

INTRODUCTION

Due to an incomplete understanding of the biomechanics of microneedle (MN) skin insertion and subsequent therapeutic delivery, MN device performance often falls short, hindering their clinical translation. Here, the application pressure and duration of that pressure are hypothesised to greatly influence drug delivery efficiency. This study develops state-of-the-art MN-skin-insertion-and-drug-delivery computational and experimental models with adjustable boundary conditions that accurately capture strain-dependent drug diffusion in skin. Previously described drug-coated 3D printed stainless steel MNs are used in both computational and experimental model systems [1].

MATERIALS AND METHODS

Skin tissue is a hyperelastic, anisotropic heterogeneous porous media. To reflect skin drug diffusion complexities, a multiphysics approach was employed using ABAQUS 2018. This consisted of a two-step approach whereby MN insertion mechanics were first accurately established (Holzapfel-Gasser-Ogden model) for skin [1]. Skin deformation and subsequent induced strains resulting from MN insertion were then coupled with the aqueous pore pathway hypothesis [2] to determine drug coated MN strain-dependent diffusion.
In vitro transdermal drug delivery by drug-coated MNs was tested in bespoke Franz diffusion cells (FDCs). Custom 3D-printed MN-specific FDC donor chambers that incorporate a compression spring to simulate application were fitted with FDC receptors (Phoenix DB-8, Teledyne Hanson Research Inc). Drug-coated metallic MN patches (6X6 arrays) were 3D-printed using Direct Metal Laser Sintering (Mlab Cusing G02, Concept Laser) (tip radius=16±2µm; MN height=871±10 µm; coating= 7.2±0.2 µL per MN of 1% CMC with 1% FD4).
Three scenarios were considered here to investigate the influence of time-dependent skin strain and skin deformation in silico and in vitro: (i) Drug-coated MNs were held in place for 5 min to allow for full dissolution of the loaded drug, then removed from the tissue, (ii). MNs were removed after 6h, (iii). MNPs were kept in situ for 10h during the permeation assays.

RESULTS AND DISCUSSION

The optimised 3D hyperelastic, anisotropic pre-stressed multi-layered skin material model can determine how skin pretension affects both the MN penetration force and insertion efficiency, and quantified how adjacent MNs impact the overall performance of the MN patch. Secondly, the strain dependent transdermal drug delivery model, coupling skin deformation and strain due to MN insertion and retention, indicates that once the mechanical strain is removed i.e. through removal or dissolution of the array, the permeation through the skin will recover. The delivery of high molecular weight (MW) compounds may be most susceptible to strain-induced changes in drug permeation, which significantly implies the importance of microneedle administration modes when targeting, for example, intradermal or transdermal delivery. Thirdly, histological fluorescent imaging indicates the MNs physically succeed in delivering high MW compounds (>500 Daltons), however MN removal or dissolution is necessary to mitigate strain-induced resistance to drug permeation. Finally, the in vitro skin absorption assays, conducted using bespoke FDCs, experimentally validate the computational model results.

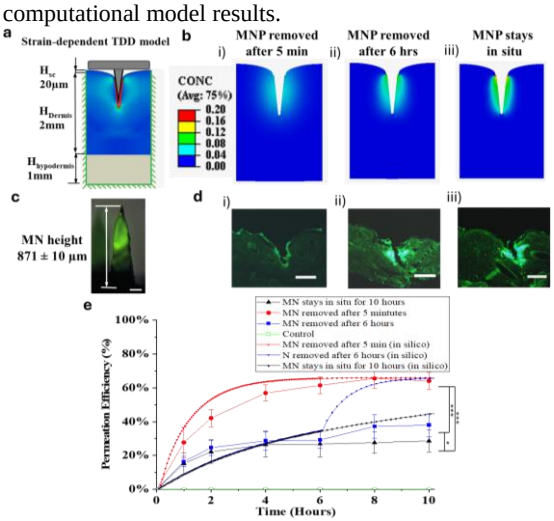

Figure 1 a) TDD modelling configuration, b) the visualisation of FD4 distribution across dermis, c) The fluorescent image of a side view of FD4-loaded MN (Scale bar: 200µm), d) histological sections of skin puncture sites for each scenarios (Scale bar: 500µm), e) the predicted (computational) and experimentally-measured permeation efficiency for each described delivery mode.

Importantly, we show that the time at which you remove a drug-coated MN patch after administration has a significant impact on MN drug delivery efficacy, something that has not been previously reported in MN research. These finding has major implications for the design of applicator systems, the modes of delivery and the clinical translation of MN technology.

REFERENCES

[1] Shu *(et al.)*, Acta Biomater., 135: p. 403-413, 2021.
[2] Shu *(et al.)*, Available at SSRN: http://dx.doi.org/10.2139/ssrn.4880237

DEVELOPMENT OF A NEXT GENERATION ELECTROCONDUCTIVE BIOMATERIAL FOR PERIPHERAL NERVE REGENERATION

Burke, J.[1,2], Brunetti, G.[1,2], Maughan, J.[1,2,3,4], Coleman, J.N.[2,3,4], Hibbitts, A.[1,2,5,6], O'Brien, F.J.[1,2,5]

[1] Tissue Engineering Research Group (TERG), Dept. of Anatomy and Regenerative Medicine, Royal College of Surgeons in Ireland (RCSI), Dublin, Ireland

[2] Advanced Materials and Bioengineering Research Centre (AMBER), RCSI and TCD, Dublin, Ireland

[3] School of Physics, University of Dublin, TCD, Ireland

[4] Centre for Research on Adaptive Nanostructures and Nanodevices (CRANN)

[5] Trinity Centre for Biomedical Engineering, Trinity College Dublin (TCD), Dublin, Ireland

[6] LEP Biomedical Ltd. Kildare, Ireland

email: (juliaburke23@rcsi.com)

INTRODUCTION

Peripheral nerve injury affects 5 million people worldwide annually. Current biomaterial-based repair options are insufficient for injuries over 3 cm long [1]. To address this poor regenerative capacity, conductive pristine graphene has been successfully used in neural tissue applications within RCSI due to its high conductivity and stability [2]. This study aims to translate those results into a clinically meaningful biomaterial by enhancing a collagen-based nerve guidance conduit (NGC) with an electroconductive phase in the form of pristine graphene. The specific aims were to 1) determine the optimal concentration of graphene to integrate in the collagen biomaterial, 2) select the most suitable method of graphene incorporation for the NGC, and 3) evaluate the NGC biocompatibility *in vitro*.

METHODS

10-50 vol%, 2D collagen/pristine graphene films were investigated for optimal conductivity and charge transfer resistance measurements, as well as initial biocompatibility evaluation using S42 Schwann cells.

The best performing graphene concentration was then incorporated into the lumen of the NGC using a variety of methods (Fig. 1D). Each design was compared based on ease of reproduction for manufacturing and enzymatic degradation.

3D *in vitro* biocompatibility of the optimised collagen/graphene NGC was assessed using S42 Schwann cells.

RESULTS

The collagen film with 30 vol% graphene exhibited optimal 2D conductivity, low charge transfer resistance, and high charge storage capacity (Fig. 1B, C). S42 Schwann cells showed no significant differences in metabolic activity or cytotoxicity when seeded on 2D collagen/graphene films over seven days.

An NGC containing homogenously distributed graphene throughout the internal lumen was selected for future experiments due its high reproducibility (Fig. 1D). Over nine days in an enzyme solution, this electroconductive NGC also effectively retained the graphene flakes in the stricture more effectively than the other leading designs.

S42 culture on 3D collagen/graphene luminal fillers exhibited excellent biocompatibility compared with the collagen control (Fig. 1E).

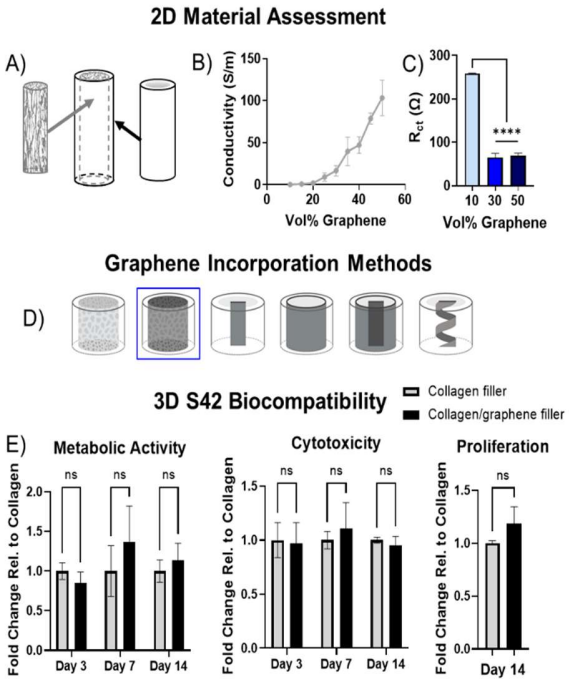

Figure 1. (A) Collagen NGC with a porous inner luminal filler and stiff outer layer. 2D assessment of (B) conductivity and (C) charge transfer resistance measurements of collagen/graphene films. (D) Various methods of graphene incorporation into the NGC with the optimal method outlined in blue. (E) *In vitro* 3D biocompatibility of S42 cells on inner luminal fillers.

DISCUSSION

These results demonstrated an NGCs with 30 vol% graphene integrated throughout the inner filler have been selected for in-depth examination. The future focus will be on electrical stimulation of *ex vivo* Schwann cell and neuron-seeded samples prior to *in vivo* assessment. On achieving these goals, we hope that nerve repair can be accelerated to reach functional recovery.

REFERENCES & ACKNOWLEDGEMENTS

[1] Hibbitts *(et al.),* Matrix Biology 106: 34-57, 2022.
[2] Maughan *(et al.),* App. Mat. Today 29:101629, 2022.

Funding is provided by the Fulbright Commission, RCSI, and Irish Research Council (Government of Ireland).

COMPUTATIONAL MODELLING OF THE INFLUENCE OF IMPLANTABLE ELECTRODE PROPERTIES ON INTRACORTICAL NEURAL SIGNALS

Saikia, Prarthana.[12], Kennedy, Philip.[3], Andreasen, Dinal.[4], Sridhar, Karthik.[5], Lowery, Madeleine[12]
[1] School of Electrical and Electronic Engineering, University College Dublin, Ireland.
[2] Insight SFI Research Centre for Data Analytics,
[3] Neural Signals Inc., Duluth, GA,
[4] Georgia Tech Research Institute, Cobb County, GA,
[5] Institute of General Electrical Engineering, University of Rostock, Germany
email: prarthana.saikia@ucdconnect.ie

INTRODUCTION

Intracortical microelectrodes that record neural activity are among the most promising solutions for enabling communication through brain-computer interfaces (BCIs). However, the effectiveness of chronically implanted BCIs declines over time due to factors such as the influence of electrode-tissue interface properties [1]. The most widely used intracortical microelectrode array, the Utah array, significantly loses its ability to detect signals after three years of implantation [2]. Neurotrophic electrodes aim to provide more stable, long-term recordings of neural activity[3]. The NeuroNexus neurotrophic electrode (NXNE, NeuroNexus Technologies, Michigan, USA) consists of platinum wires inside a glass cone filled with a neurotrophic growth factor that facilitates the growth of neurites from neighbouring neurons, with limited gliosis around the electrode contacts. As these new technologies emerge, understanding the relationship between recorded intracortical neural signals and the relative location of axons, the influence of the electrode properties and the electrode materials becomes critical for designing electrodes that are optimized for long-term recording of neural activity for BCIs. Computational modelling can provide insights into such factors to better understand how electrode configuration and material properties influence the recorded signal. In this study, we developed a computational model of the NXNE to investigate how the electrode-tissue interface and electrical double layer (EDL) affects the electric field distribution for an intracortical microelectrode.

METHODS

A finite element (FE) model of an NXNE and surrounding brain tissue in the rat cortex was developed. The electrode was comprised of 16 recording contacts of diameter 70 µm embedded within an insulating polyimide and glass conical structure. The electrode was 1956 µm long, with a diameter of 126 µm and 494 µm at the narrower and wider end, respectively, as shown in Fig. 1. A thin-layer approximation representing the EDL at the electrode-tissue interface was also implemented [4]. Using the FE model the effects of the EDL on the distribution of the electric field, the current density at the electrode surface, and the amplitude of the detected action potentials was examined.

RESULTS

Incorporating the EDL at the electrode interface altered the distribution of the electric field in the tissue surrounding the electrode resulting in a more uniform distribution of the field on the surface of the electrodes. We also computed the average value of the voltage on the surface of the electrodes. Although there is a change in the field distribution due to the presence of the electrical double layer, the change in the detected voltage was relatively small, less than 1% of the amplitude of the detected extracellular action potentials.

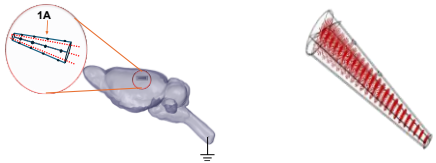

Figure 1 3D FE model of rat brain with NXNE placed in the cortex. Points shown in red represent nodes along single nerve fiber. 1500 internal fibers of length 4 mm passing through the volume of the electrode were simulated.

DISCUSSION

To improve the long-term stability and performance of BCIs, it is critical to understand and address the challenges of intracortical signal recording. In simulation of both recording and stimulation electrodes, the electrical double layer at the electrode interface is commonly neglected. The results presented provide insight into the effect of the electrical double layer on the electric field and the relationship between electrode properties and detected signals. Though the effect of the double layer on the amplitude of the detected action potentials is relatively small, the presence of the double layer alters the distribution of the electric field in the surrounding tissue and the distribution of the current density across the electrode. This is a particular concern for the design of stimulation electrodes where higher current densities with the potential for Faradaic charge transfer arise [5]. The use of computational models in this way facilitates the optimization of electrode designs for intracortical BCIs.

REFERENCES

[1] Vomero *(et al.)*, Biomaterials, 281, p.121372, 2022
[2] Ganesh *(et al.)*, Frontiers in Human Neuroscience, 16:874199, 2022.
[3] Kennedy *(et al.)*, Neuroreport, 3(7):605–608, 1992.
[4] Cantrell *(et al.)*, Journal of neural engineering, 5(1), 54, 2007.
[5] Sridhar *(et al.)*, Journal of Neural Engineering. 2024 Feb 14;21(1):016024.

CONTROLLING BLOOD PRESSURE AND FLOW INCREASES THE LIKELIHOOD OF SUCCESSFUL

Glynn, A.[1,2], McCarthy, R.[2], Murphy, B.[1,3], Lally, C.[1,3]
[1] Trinity Centre for Biomedical Engineering & School of Engineering, Trinity College Dublin, Dublin 2, Ireland.
[2] Cerenovus, Galway, Ireland.
[3] Advanced Materials and Bioengineering Research Centre (AMBER), RCSI & TCD, Dublin, Ireland. *email: aoglynn@tcd.ie*

INTRODUCTION

Aspiration thrombectomy is an established method of clot removal in acute ischemic stroke [1]. Advancements in catheter technology have resulted in the advent of newer generation 8Fr, balloon guide catheters (BGCs) and superbore catheters (SBCs), that can be used to deliver 6Fr large bore catheters (LBCs) to perform clot retrieval. In comparison to conventional 8Fr guide catheters (CGCs), placed in the internal carotid artery (ICA), BGCs achieve proximal flow control via inflation of a balloon in the ICA [2]. SBCs, designed for intracranial use, offer local flow and pressure control, as they can be navigated to distal vascular regions [1,2] (Fig.1 (b)). Little research has been completed to-date comparing these systems, their impact on pressure and flow, and likelihood of clot retrieval success. Thus, the aim of this work was to assess these technologies in vitro. We hypothesize that control of blood pressure and flow during clot retrieval will increase the likelihood of retrieval success. This study will provide critical insights into the clinical use of these emerging technologies.

MATERIALS AND METHODS

To evaluate the systems in clinically challenging environments, two distinct in vitro anatomical models were used (Fig.1 (a)). Five (n=5) aspiration devices were investigated. Devices were placed in the models as per Fig.1 (a) and used as per manufacturer's instructions by two interventional neuroradiologists. Two groups of thrombus analogues: cohesive and friable, were prepared with ovine blood [3]. Analogues were used to create an occlusion in the M1 Middle Cerebral Artery (MCA) (Fig.1(a)). To simulate the clinical use of the devices, tracking to the target location and clot retrieval performance were evaluated (n=5 replicates per device). Physiological blood pressure and flow were simulated and monitored throughout the experiment at defined time points: prior to device introduction, following device placement and during and after device use. Aspiration was applied through the LBCs via a 60cc syringe.

RESULTS

The SBC system significantly reduced the pressure in the MCA during device tracking in both in vitro models ($p<0.001$), see Fig.1(d)). The impact of inflation of the BGC was not significant in Model 1 due to collateral flow supplied via the Circle of Willis. The BGC and SBC systems had the highest rates of clot retrieval success for the friable clot in Model 1 (Fig. 1(c)).

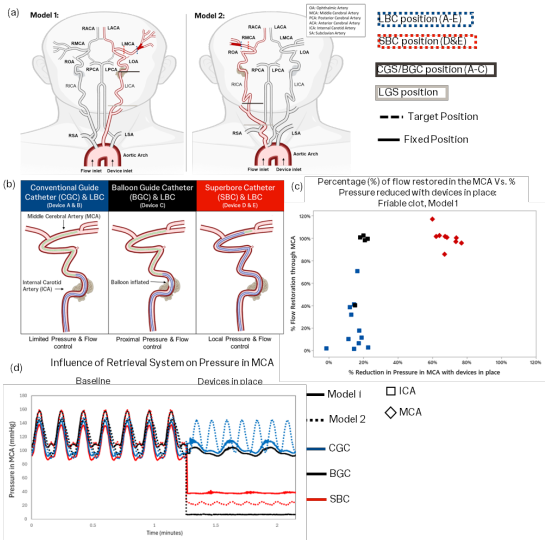

Figure 1 (a) In vitro models 1 & 2 with occlusion location and device positions, (b) Illustration of aspiration systems, CGC and BGC systems placed in ICA, and SBC system placed in MCA (c) Successful clot retrieval indicated by higher % flow restored through the MCA after first pass aspiration. Location reached by each system specified by shape, system indicated by colour, (d) Representative pressure measurements in MCA at baseline and with each aspiration system in the target position.

DISCUSSION

The CGC system had limited flow control in the M1 (Fig 1(d)), resulting in reduced flow restoration for the friable clot. In contrast, through proximal and local flow control, the BGC and SBC systems had significantly higher rates of flow restoration (Fig 1(c)). The greatest challenge with SBCs is their ability to track to distal vascular locations. In one case, the SBC could not be tracked to the MCA to complete clot retrieval. Interestingly, this study suggests that using proximal flow control with a BGC may provide equivalent results in such cases. These ground-breaking results illustrate the importance of pressure and flow control during aspiration to maximize the likelihood of clot retrieval. These critical insights can now support clinical device selection and the design of next generation aspiration devices.

REFERENCES

[1] Patki *et al.* Cardiovasc Eng Tech 15:481–502, 2024.
[2] Nogueira, *et al.* JNIS 14:184-188, 2022.
[3] Johnson *et al.* JNIS 12(9):853-857, 2020.

SPEED-ACCURACY TRADEOFF IN RESPONSES TO ELECTROTACTILE STIMULATION

Jarto, F.[1], Dupan, S.[2]
[1] School of Electrical and Electronic Engineering, University College Dublin
[2] School of Public Health, Physiotherapy and Sports Science, University College Dublin
email: felix.jarto@ucdconnect.ie

INTRODUCTION

Prosthetic users mainly rely on their vision for feedback during control of the device in absence of the tactile and proprioceptive modalities[1]. The overreliance on vision increases cognitive load during prosthesis use, resulting in reduced control performance[2]. Thus, the provision of additional feedback through other modalities is necessary to improve closed-loop prosthetic control. Fast and accurate recognition of feedback is particularly important when we consider that both delays and inaccuracies can destabilize closed-loop control environments[3]. Among the many available forms of feedback, transcutaneous electrotactile stimulation is a promising technology with advantages including non-invasiveness and simplicity[4]. It is not yet clear, however, which variables influence the speed and accuracy of response to electrotactile stimuli. In this study, we set out to investigate how we can influence response parameters to an instantaneous change in stimulation intensity by manipulating both stimulus-related and environmental variables.

MATERIALS AND METHODS

The study included two experiments with 20 participants each. Participants provided written informed consent , and the study was approved by the UCD Human Research Ethics Committee – Sciences (LS-22-46-Dupan). Experiment 1 aimed to compare the reaction times (RTs) between visual and electrotactile stimuli. Experiment 2 consisted of an intensity discrimination task, where participants were asked to indicate the direction of change during an instantaneous shift in stimulus intensity in a short amount of time, while prioritising either speed or accuracy. The amplitude of the shifts in intensity were modulated, ranging from 1 time the Just Noticeable Difference (JND) to 4xJND. The JND was measured through a staircase procedure[5]. Additionally, in half of the experimental blocks participants were instructed to listen to an excerpt from an audiobook and answer multiple choice questions afterwards in order to increase the cognitive load during the task.

RESULTS

The results of the reaction time task confirmed lower average response times for electrotactile stimuli compared to visual stimuli by a median of ~50ms ($p = 0.008$), which is in line with the existing literature[6]. Figure 1a and 1b show that increased shift intensities led to a decrease in missed responses and an increase in average response accuracies ($p<0.001$). Post-hoc analysis found that the only non-significant comparison was between shifts of 3xJND and 4xJND. In terms of speed, each increase in shift level led to a significant decrease in average response times (Fig. 1c), lowering the median reaction times from 1.44s to 0.69s. The presence of cognitive load increased average response times ($p < 0.001$), but did not affect response accuracies ($p = 0.42$). An interaction effect was perceived between direction and intensity of shift for response accuracies. This was noticeable in significantly different average correct responses at the lowest intensity of shift ($p = 0.005$), which did not appear in subsequent intensities of shift.

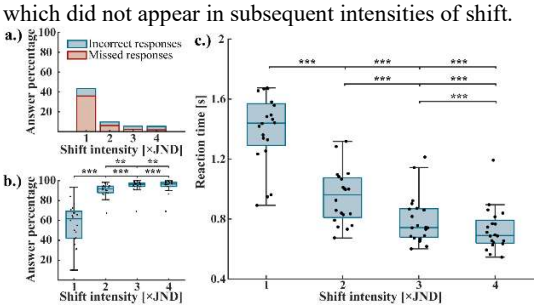

Figure 1 *Response accuracies and reaction times as a function of shift intensity; a: The number of incorrect and missed responses decrease as shift intensity gets larger. b: Average response accuracy per participant increases with shift intensity; red dots denote averages of individual participants. c:Average reaction times per participant decrease with shift intensity ; only correct responses were considered in this case.*

DISCUSSION

The results of the intensity discrimination task imply that the magnitude of intensity shift needs to be well beyond the just noticeable difference to ensure fast and accurate responses to electrotactile stimulation. We argue that providing electrotactile stimulation using bigger shifts in perceived intensity could result in the supplementary feedback making closed-loop control of prosthetic devices more reliable.

REFERENCES

[1]Wilke *(et al.)*. Journal of NeuroEngineering and Rehabilitation, 16(1), 155. 2019.

[2]Gillespie *(et al.)*. Annual International Conference of the IEEE Engineering in Medicine and Biology, 5077–5080. 2010.

[3]Molnar *(et al.)*. Stability, Control and Application of Time-delay Systems (pp. 209–226). 2019.

[4]Li *(et al.)*. IEEE Sensors Journal, 17(9), 2625–2635. 2017.

[5]Wetherill and Levitt. The British journal of mathematical and statistical psychology, 18, 1–10. 1965.

[6]Akamatsu *(et al.)*. Ergonomics, 38(4), 816–827. 1995.

PATIENT-SPECIFIC FINITE ELEMENT ANALYSIS FRAMEWORK FOR VERTEBRAL REFRACTURE RISK ASSESSMENT IN OSTEOPOROTIC PATIENTS

Koh, C. R.[1], Purcell, P.[1], Tiernan, S.[1], Morris, S.[2]
[1] School of Mechanical Engineering, TU Dublin, Ireland
[2] Mater Misericordiae University Hospital (MMUH)
email: D21125318@mytudublin.ie

INTRODUCTION

Osteoporosis is a global health problem and the most common bone disease affecting the elderly. Reports have estimated 209,000 osteoporosis patients in Ireland and 32,000 new fragility fractures in 2019, which are projected to grow to 51,000 by 2034[1]. In clinical practice, the management of fragility fractures are challenging especially in older adults due to comorbidities and frailty, and many patients will not require hospital admission but may develop complications[2]. To improve the post-discharge care for these patients, the MMUH developed the Silver Trauma Review Clinic (STRC), providing multidisciplinary specialist assessment[2].

They performed an evaluation to assess the compliance of the clinic with the protocol to manage vertebral compression fracture (VCF) by reviewing the patient cohort attending the STRC over the first two years. Of the 534 patients that attended, 19% of them had VCF, where 31% of the patients with VCF were referred for vertebroplasty[2]. The high proportion of patients referred for surgical intervention demonstrates the importance of early identification of conservative management failure.

Studies have identified risk factors for refractures in VCF patients[3]. However, a biomechanical analysis could provide more specific fracture risk assessment for individual patients. Finite element analysis (FEA) has been used extensively to study the biomechanical behaviour of bone, and numerous patient-specific approaches to FEA have proven their efficacy for the assessment of vertebrae under different conditions. Therefore, a CT-based individualised FEA could help identify patients with a higher fracture risk who may benefit from early surgical intervention.

The primary aim of this ongoing research is to predict the risk of vertebra refracture for VCF patients managed conservatively. To achieve this, the main objectives of this paper were to develop a computational framework to generate patient-specific finite element model (FEM) and to determine the mesh sensitivity of the model.

FRAMEWORK DESIGN

A CT-scan of a L3 vertebra was obtained from an open source database[4]. The images were imported into 3D Slicer[5] to be manually segmented into a 3D solid model, which was then meshed in ANSYS Workbench to generate a FEM. A mesh sensitivity study was conducted to determine optimum mesh size by observing the Von Mises stress within a region of interest (ROI) in the vertebral body that is distal to the boundary conditions. The Young's modulus of each element for the model with optimum mesh size were assigned based on bone density calculated from the CT data in Bonemat[6]. The inferior endplate and facet joints of the vertebra were fixed in all directions, and a uniformly distributed compressive force of 600N[7] was applied to the superior endplate. The stress and strain distribution in the vertebra were analysed.

RESULTS

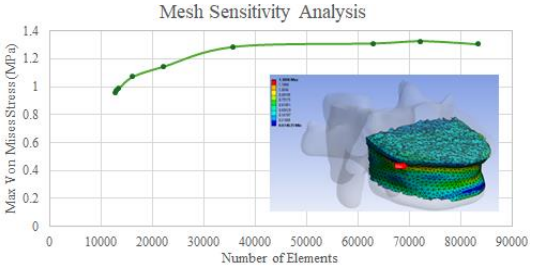

Figure 1 Mesh Sensitivity Analysis and Illustration of ROI.

DISCUSSION

Mesh sensitivity analysis found that mesh body sizing smaller than 2.5mm achieved a converging max stress. Therefore, an individualised FEM of a L3 vertebra with mesh body sizing of 2.0mm and Young's modulus assigned to each element was generated and analysed from the developed methodology. Future work will apply the FEA framework to the patient cohort of the STRC review study to enable early identification of patients at high risk of secondary fracture.

REFERENCES

1. Willers (et al.), Archives of Osteoporosis, Volume 17: Article 23, 2022.
2. Hannah (et al.), Emergency Medicine Journal, Volume 40(10): 721-725, 2023.
3. Alexandru (et al.), The Permanente Journal, Volume 16(4): 46-51, 2012.
4. Deng (et al.), CTSpine1K, Version 4, 2024.
5. Fedorov (et al.), Magnetic Resonance Imaging, Volume 30(9): 1323-1341, 2012.
6. Taddei (et al.), Medical Engineering and Physics, Volume 29(9): 973-979, 2007.
7. Dreischarf (et al.), Journal of Biomechanics, Volume 49(6): 833-845, 2016.

A NOVEL METHOD FOR MEASURING THE TOUGHNESS OF BONE AND OTHER MATERIALS

Allahdiniyan, A.[1,2], Hoey, D.A[1,2], Taylor, D.[1,2]
[1] Trinity Centre for Biomedical Engineering, Trinity College Dublin (TCD)
[2] Department of Mechanical, Manufacturing, & Biomedical Engineering, School of Engineering, TCD.
email: allahdia@tcd.ie

INTRODUCTION

The accurate assessment of fracture toughness in bone and other biological materials is essential for predicting fracture risk; however, conventional approaches encounter major challenges due to complex experimental setups and imaging limitations[1]. At the microscopic level, crack opening displacement is relevant for both mechanical behavior and biological response[2]. Accurately measuring these displacements in bone is particularly challenging due to the complexity at the microstructural level and the inadequate resolution of available imaging techniques[3]. Although high-resolution imaging and nano-CT capture complex details (Figure 1a), their efficacy in precisely locating crack tips is inadequate[3].

Finite element models (FE models) offer essential insights into the correlation between damage propagation and structural architecture across various length scales, aiding in the identification of regions susceptible to fracture[4]. Conventional techniques for assessing fracture toughness by crack opening displacement (COD) often focus on near-tip measures[5]; however, we present an innovative method that utilizes the entire crack profile, which can be validated via finite element analysis.

MATERIALS AND METHODS

We propose a modified version of the Westergaard infinite-plate model for COD as follows:

$$\mathbf{K} = \mathbf{C}.\boldsymbol{E}\,\frac{\mathbf{COD}\sqrt{\mathbf{a}}}{\sqrt{a^2 - x^2}} \qquad (1)$$

Where, a is crack length, x is the distance from centre of the crack and E is a Young's modulus. C is a constant which depends on geometry, allowing for extension of the approach to different cases. The method was developed with FE models of 2D plates with various geometries of cracks. K was obtained from the FEA using a contour integral approach with quadratic quadrilateral elements (CPS8R): COD and K were compared with equation (1) to find C.

RESULTS

In the case of a finite plate with width *W* and crack length *a*, C was found to be a function of *a/W*

$$\mathbf{C}=(\mathbf{0.4959} + \mathbf{0.0266}\left(\frac{\boldsymbol{a}}{\boldsymbol{W}}\right) + \mathbf{0.1131}\left(\frac{\boldsymbol{a}}{\boldsymbol{W}}\right)^{\mathbf{2}}) \qquad (2)$$

The method showed excellent agreement for centre-cracked plates, with errors less than 2%. When properly normalized, the relationship was valid for various crack lengths and widths (Figure 1b). Analysis of angled cracks demonstrated the method's capability to assess both opening (Mode I) and sliding (Mode II) displacements, with normalized results showing consistent behaviour across different angles (Figure 1c). The derived correction factor C(a/W) captured the geometric effects, as validated by comparison with FE results.

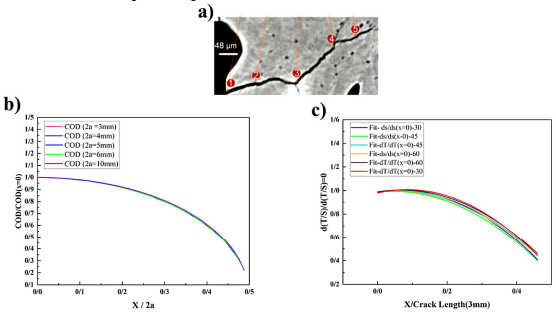

Figure 1 a) synchrotron images of bone under load, showing crack opening[3], b), c) COD along the crack face for different crack lengths (b) and angles (c).

DISCUSSION

FE analyses here demonstrate that this new approach utilizing the full crack profile, as opposed to near-tip measurements alone, yields accuracy in predictions of the stress intensity factors in elastic materials. These capabilities dealing with centre-cracked and angled-crack geometries provide a background for analyses of more complicated crack configurations in different materials, where geometric features impact fracture behaviour. The method will have wide applicability for determination of toughness in bone and in other biological materials and for risk assessment in civil and mechanical engineering structures.

ACKNOWLEDGMENTS

This research was conducted as part of the GAP Project and was supported by the Marie Curie Scholarship. The authors are grateful for the financial support and resources that have enabled the progress of this research.

REFERENCES

[1] Yan, L. *et al.* Journal of the Mechanical Behavior of Biomedical Materials. *J. Mech. Behav. Biomed. Mater.* **109**, 103838, 2020.
[2] Taylor, D., Hazenberg, J. G. & Lee, T. C.. *J. Theor. Biol.* **225**, 65–75, 2003.
[3] Buccino, F. *et al*. *Eng. Fract. Mech.* **270**, 108582 ,2022.
[4] Buccino, F. & Vergani, L. M, 2021.
[5] Nowell, D. & Kartal, M. E. 42–49, 2011.

BIOMECHANICAL ANALYSIS OF PATIENT-SPECIFIC 3D-PRINTED SPINAL CAGES

Yenigun, C.[1], O'Cearbhaill, E. [1], Ní Annaidh, A.[1]
[1] University College Dublin, School of Mechanical and Materials Engineering
email: (cagri.yenigun@ucd.ie)

INTRODUCTION

Interbody fusion is a surgical procedure that fuses two or more vertebrae in the spine by removing the intervertebral disk and placing an implant, or device, in its place. The goal of this procedure is to create a stable fusion that can support normal body weight and movement, while preserving the disk height and ensuring proper spinal alignment; and cage-like implants, or spinal cages, are developed specifically to meet these objectives [1]. Typically, spinal cages are developed to hold bone grafts, and they can be used alongside plates, rods, or screws. Cage subsidence, a common complication following lumbar intervertebral fusion (LIF), is the migration or settling of an interbody fusion cage into the vertebral bodies, potentially leading to a loss of disc height, instability, and spinal misalignment [2]. Subsidence is a prevalent complication in LIF techniques, with rates of 26.9% for lateral LIF without pedicle screws and 21.4% for transforaminal LIF, though comparisons are hindered by the lack of a standard definition. [2][3]. Factors associated with subsidence can be broadly grouped into three categories: Patient, Device, and Surgery. Patient factors include bone density, paravertebral muscle strength, age, body mass index, activity level, and post-operative conditions. Device factors cover the material, size, shape, and manufacturing methods of the implant. Surgical factors, on the other hand, include inadequate restoration of disk height, selected technique, and alignment [4]. Previous biomechanical studies have found that the most influential device factors affecting the subsidence risks are the size, cage stiffness, curvature similarity with vertebral endplates, and placement [5]. Interbody fusion cages can be customized to control device factors thus enhancing the surgical outcome. With 3D models of the patient's vertebral endplates generated with CT or MRI scans, patient-specific cages can be manufactured using industrial additive manufacturing (AM). Specifically, AM titanium implants can provide tailored cage stiffness, increased contact surface area, enhanced osseointegration through pores, and surface features such as ridges, teeth, or pins; all of which can lower the subsidence risk associated with the device factors.

Our target is to assess the biomechanical performance of additively manufactured, patient-specific spinal cages. Particularly, via finite element models (FEMs), we will assess peak stress regions and deformation on the vertebral endplates under various loading conditions. We will analyse the effects of various lattices, wall thicknesses, struts on the stiffnesses in compression and shear.

MATERIALS AND METHODS

In this project, a comprehensive review of literature will be conducted to identify subsidence risk factors associated with LIF and biomechanical evaluations of AM titanium spinal cages. Next, factors contributing to subsidence risk that can be addressed using AM titanium cages will be identified. The material properties of the prototyped titanium cages, including mechanical strength, porosity, and lattice structures, will be clearly characterized. After, FEMs will be performed to identify potential failure points, such as stress concentrations and areas of plastic deformation. By exploring and iterating design parameters like lattice structure, porosity, and contact area, we aim to balance stiffness differences, improve osseointegration, and hence reduce subsidence risks. Mechanical tests, including compression, torsion, combined compression and shear, and fatigue tests based on ASTM F2077 and ASTM F2267, will be conducted to assess the prototypes **(**see **Figure 1)**. Finally, FEM results and experimental data will be validated, and the effectiveness of the designs will be discussed.

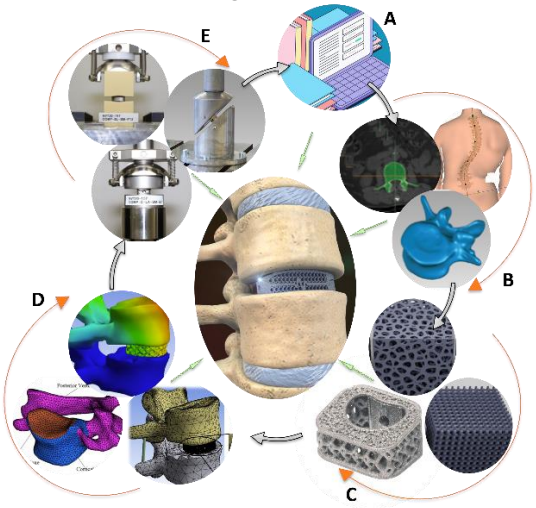

Figure 1 Proposed iterative and circular methodological approach: A: Literature review B: Patient imaging data and solid models C: AM titanium cages D: FEMs E: Mechanical testing.

REFERENCES

[1] McEntee *(et al.)*, Handbook of Spine Technology, Springer International Publishing, 961-995, 2021.
[2] Parisien *(et al.)*, International Journal of Spine Surgery 2022, 16 (6):1103-1118, 2022.
[3] Aguirre *(et al.)*, Neurosurg Rev 47: 332, 2024.
[4] Liu *(et al.)*, J Orthop Surg Res 19 Article No. 7, 2024.
[5] Calvo-Echenique *(et al.)*, Comp Meth and Prog in Biomedicine, 162:211-219, 2018.

MECHANISMS UNDERLYING THE MECHANOREGULATION OF IMMATURE CARTILAGE

Falkov, J.L.[1], Brama, P.A.J.[2], Nowlan, N.C.[1]
[1] School of Mechanical and Materials Engineering, University College Dublin, Dublin, Ireland;
[2] School of Veterinary Medicine, University College Dublin, Dublin, Ireland
email: iemma.falkov@ucdconnect.ie

INTRODUCTION

Osteoarthritis (OA) is a degenerative joint disease which leads to pain and disability. Between 1995 and 2021 there was a 112% increase in the prevalence of OA worldwide (Vos et al., 2020). Focal cartilage defects have been linked to a higher risk of OA development (Kwon et al., 2019). Although surgical techniques exist to treat focal cartilage defects, these techniques cannot regenerate the complex zonal structure of articular cartilage (AC) (Matsiko et al., 2013). This zonal structure involves layers of differing structural and biochemical properties which are not present in neonatal AC. The zones observed in mature AC are known to emerge between birth and sexual maturity and are essential for AC function (Decker et al., 2015).

Mechanical loading plays a significant role in the development of AC (Brommer et al., 2005; Julkunen et al., 2010; Hoogen et al., 1999). This study aims to modulate zonal emergence through mechanical loading and to investigate differential gene expression under various loading conditions. We will look at the proximal regions of phalange 1 and 2 (P1 and P2) of two- to six-week-old neonatal goats. We are interested in how altered loading will influence articular cartilage, bone and physis development. Single-cell RNA sequencing (scRNAseq) will allow us to evaluate which genes could be responsible for the changes to biochemical and structural composition observed in these tissues over development. We will also observe which cell populations are present and active within these tissues and how their expression profiles are modulated by changing loading conditions.

MATERIALS AND METHODS

Removal of a claw from one of the digits on the forelimb of a neonate goat will produce a model with under- and over-loaded P1 and P2 (Figure 1). The counter-lateral limb will provide an internal control, with normal loading conditions. Approximately four weeks post-removal, P1 and P2 will be dissected, cores taken from the proximal P1 and P2 condyles, and scRNAseq will be performed on the bone, cartilage, and physis from these cores.

The position of osteocytes within a bone-mineralised matrix makes them difficult to extract and study (Prideaux et al., 2016). We have developed a protocol to extract osteocytes and osteoblasts from bone tissue, and chondrocytes from cartilaginous tissue, adapted from the protocol outlined by Prideaux et al. (2016). This requires the separation of the bone and the cartilage so that the two protocols can be executed in the separate tissues to retrieve the different cell types (Figure 2).

To distinguish between cells from the articular cartilage, and cells from the physis, the core from proximal P1 will be bisected at the secondary ossification centre. Cells from the AC sample and the proximal half of the secondary ossification centre will be pooled for sequencing, whilst cells from the physis and primary ossification centre will be pooled for sequencing. This will allow us to assess variability in cell populations and gene expression between these two locations within the epiphysis under varying loading conditions.

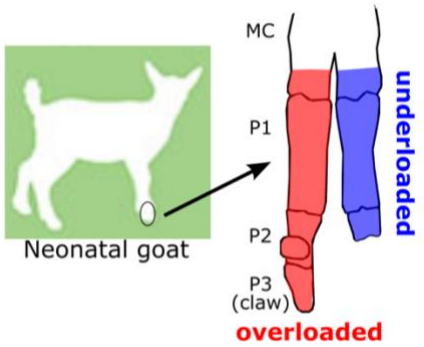

Figure 1 The claw removal model has been designed to create altered loading conditions and involves the dissection of P3 from one of the digits within a neonatal goat, creating an underloaded and overloaded digit.

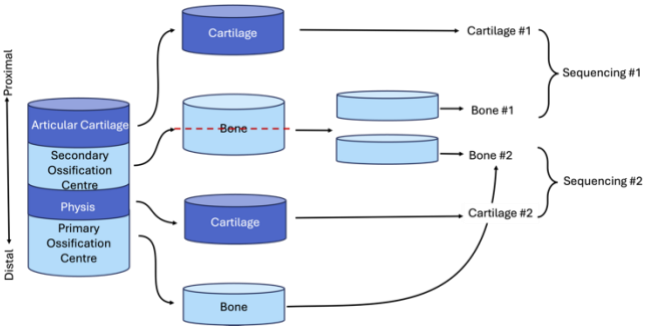

Figure 2 Schematic diagram indicating the isolation of bone and cartilage tissue from a core taken from proximal P1. This process will result in two samples which proceed with sequencing.

REFERENCES

Vos *et al.*, The Lancet 396: 1204–1222., 2020.
Decker *et al.*, Curr Osteoporos Rep 13: 407–414., 2015.
Kwon *et al.*, Nat Rev Rheumatol 15: 550–570., 2019.
Matsiko *et al.*, Materials 6: 637., 2013.
Prideaux *et al.*, Bone 88: 64–72., 2016.

PREDICTING THE PERFORMANCE OF TRANSCATHETER MITRAL VALVE REPLACEMENT FRAMES USING FINITE ELEMENT MODELLING

Barrett, J.[1], O'Brien F.J.[1,2,3] , Conway, C.[1,2]

[1]Tissue Engineering Research Group, Royal College of Surgeons in Ireland (RCSI)
[2]Trinity Centre for BioEngineering (TCBE), Trinity College Dublin & RCSI
[3]Advanced Materials and Bioengineering Research Centre (AMBER), TCD & RCSI
email: (joshuabarrett21@rcsi.com)

INTRODUCTION

Mitral regurgitation (MR), backflow of blood from the left ventricle to the left atrium during ventricular systolic ejection, affects 24 million worldwide[1]. Treatments for MR include – mitral repair and mitral replacements – both surgically and via minimally invasive transcatheter approaches. Due the complex anatomical features of the mitral valve (MV), transcatheter treatment techniques have had limited success. With no large animal model of MR pathology existing for emerging transcatheter mitral valve replacement (TMVR) device assessments, finite element analysis (FEA) models have the ability to advance our understanding of pathological biomechanics.

The goal of this work is to computationally evaluate emerging TMVR frame apposition under both healthy and pathological conditions. Specific frame sizes (diameters, Ø: 35, 40, 50, 55, 60 mm) were analysed in terms of paravalvular leakage (PVL) to gain insight in frame sizing effect on apposition.

MATERIALS AND METHODS

The crimp-release process for a TMVR frame was conducted in Abaqus/Explicit (v2023, Dassault Systèmes). Three generic frames (Ø: 35, 40, 50 mm) were deployed in a baseline healthy MV (anteroposterior Ø, AP, 30 mm; intercommissural distance, IC, 43 mm). 60,000 to 80,000 linear hexahedral elements with reduced integration were applied to the TMVR frames and MV. The crimping tool, modelled as a cylindrical surface, was meshed with 1,500-2000 linear quadrilateral reduced integration elements.

Larger frames (Ø 50, 55, 60 mm) were required to assess the impact of varying the IC/AP Ø ratio. AP dimension was increased, reflecting its tendency toward dilation in the more compliant posterior aspect[2]. Material properties were assigned as follows: super-elastic nitinol characteristics for the TMVR frames[3], and an isotropic hyper-elastic 5th-order polynomial model to the MV leaflets[4], based on healthy human MV radial experimental testing. TMVR frames crimped via a tool and subsequently released, allowing it to expand freely within the fixed MV annulus (radially unconstrained). Frictionless contact was implemented between components, except for a penalty friction model ($\mu = 0.1$) applied to TMVR frame self-contact. PVL via the gap area between the frame and annulus was quantified via ImageJ (NIH, USA).

RESULTS

MR reduction through the complete apposition of the frame to the mitral annulus was quantified via gap area calculations. As frame Ø increased (35, 40, 50 mm), the predicted gap area decreased (3330, 3225, 3000 mm², respectively), suggesting effective mitigation of potential PVL in our baseline MV for increasing degrees of oversizing.

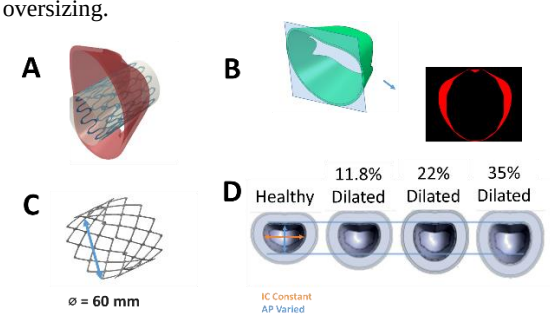

Figure 1 A) Crimp-Release Process; Crimptool (grey); MV Red; TMVR Frame (blue) B) PVL calculation method, C) Ø60mm TMVR frame for pathological models D) Severities of dilation of IC/AP diameter ratio

DISCUSSION

The proposed workflow provides an efficient and effective method for comparing the structural performance of generic cylindrical TMVR frames under healthy and pathological conditions. With the FEA workflow presented here, we can generate valuable recommendations that enhance pathological assessments for new and emerging TMVR devices. Understanding the impact of cylindrical frame oversizing on the apposition of prosthetic frames to the native D-shaped mitral annulus could offer crucial insights into the viability of similarly designed frames. However, using larger diameters also introduces possible stress-related issues for the surrounding environment[5].

ACKNOWLEDGEMENTS

SFI Funding (20/FFP-P/8588)

REFERENCES

1. Aluru *et al*, Med. Sci., 10, 32, 2022. .. **2.** Gunning *et al*, Determination of the tensile mechanical properties of the segmented mitral valve annulus, J Biomech, 47(2):334–340, 2014 **3.** McGrath *et al*, *J Mech Behav Biomed Mat*, 40:252–263, 2014. **4.** Prot *et al*, J Mech Behav Biomed Mat, 3(1):167–177, **5.** Fan *et al*, *Mech Behav Mater Prosthetic Heart Valves*: Dev Crit Rev, 2024.

ADDITIVE MANUFACTURING OF ELECTRO-RESPONSIVE BIO MEDICAL ACTUATOR

Mr. Bregazzi-Nevin, C.[1], Dr. Nugent, M. [1], Dr. Mooney, J. [1]
[1] Technological University of the Shannon, Midlands Campus, Athlone.
email: cian.bregazzinevin@tus.ie

INTRODUCTION

Understanding the complex interplay of muscle structure, mechanics, and motion drives ongoing bioengineering research. Engineered muscle mimicking actuators can take many forms and are subdivided into six categories, separated by their excitation method [1]. The focus of this study is electrical activation.

This study explores the integration of fused deposition modelling (FDM) with conductive hydrogels to develop an electro-responsive, customisable mechanical unit (CMU). The proposed CMU consists of conductive hydrogel discs that are attached to a flexible polymer scaffold which deforms on application of electrical stimuli. Inspired by Keplinger et al., the CMU demonstrates potential for customised geometry and advanced applications, such as inclusion of medicinal compounds within the scaffold [2].

MATERIALS AND METHODS

The scaffold structure of the CMU was designed in Solidworks and printed using an Ultimaker S7Pro, Figure1. Polyurethane (TPU) served as the primary material, printed at 210ºC with a 0.2mm layer height. The support structure was laid down using a Polyvinyl Alcohol (PVA) filament. Removal of the supports was achieved through 15min ultrasonic cycles at 65ºC in diH_2O. Cycles were repeated until all PVA was dissolved. An average of six cycles were required. The resulting cleaned scaffold had all geometry and features preserved.

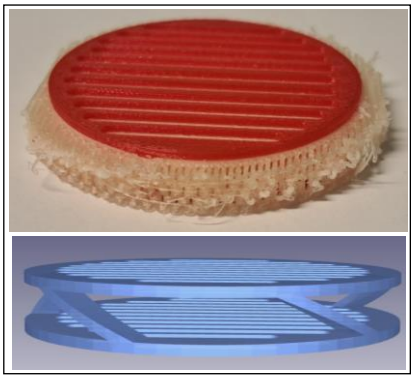

Figure 1 Top - ⌀40mm circular TPU scaffold (Red) with PVA support structure. Bottom – Solidworks Model with spring elements visible.

The hydrogel was synthesised using an accelerated freeze thaw method [3]. 10g of PVA 145x10^3MW was dissolved in 100ml of diH_2O. This solution was stirred and heated at 65ºC for two hours. Following full dissolution 5g of powered Graphite <20µm was added and mixed until fully incorporated to add conductivity. The hydrogel liquid was then cast into a 200x100x4mm mould and placed in an insulated liquid Nitrogen filled chamber for 60mins, then allowed to heat to 20^{O}C.

Once thawed the hydrogel sheet was removed from the mould, mounted on 125µm Polyethylene terephthalate (PET) film and cut into ⌀35mm discs using a Mantech 80W CO_2 Laser Cutter. The discs were then placed film side down on opposing sides of the scaffold structures. Adhesive copper electrodes were attached either side and connected to an UltraVolt 20HVA24-BP1 high voltage amplifier.

Voltage was applied to the CMU in 250V increments from 0V in a step wave form. Voltage was unipolar and the CMU was discharged to ground after each excitation.

Following testing, the CMUs were refrigerated with diH_2O soaked pads in sealed containers to preserve moisture content.

RESULTS

Excitation below 5.5kV yielded no displacement. Between 5.5–13kV, full clamping of the CMU platens was observed. Applied voltages above 13kV caused dielectric breakdown and arcing between hydrogels. During this occurrence the platens remained clamped until excitation was removed.

DISCUSSION

Improved scaffold geometry and material exploration are recommended to address flexing in the CMU top platen under excitation. Hybrid designs incorporating PLA platens and TPU internal springs may enhance stability.

The electro-responsive CMU shows promise for applications in muscle simulation and drug delivery systems, with ongoing refinement needed to optimise its structural and functional capabilities.

REFERENCES

[1] Hines *(et al.)*, Advance. Materials., vol. 29, no. 13, p. 1603483, 2017.
[2] Mitchell *et al.*, Advanced Science, vol. 6, no. 14, p. 1900178, 2019,
[3] Louis *(et al.)*, Journal of Drug Delivery. Sci. Technol., vol. 101, p. 106209, Nov. 2024.

IMPLEMENTATION OF LUMPED PARAMETER NETWORK BOUNDARY CONDITIONS FOR THE PATIENT-SPECIFIC CFD SIMULATIONS OF CORONARY ARTERIES IN OPENFOAM

Raza, M. A.[1], Ivankovic, A.[1], Tuković, Ž.[2], Jaeger, P. D.[3], O'Rourke, M. J.[1]
[1] School of Mechanical and Materials Engineering, University College Dublin, Ireland.
[2] Faculty of Mechanical Engineering and Naval Architecture, University of Zagreb, Croatia.
[3] RADar Learning and Innovation Center, AZ Delta General Hospital, Belgium.
email: muhammad.a.raza@ucdconnect.ie

INTRODUCTION

Computational simulations, though useful for analysing hemodynamics[1], are rarely used to predict pulsatile flow and pressure fields in 3D coronary artery (CA) networks, largely due to the complex interplay between the heart and arterial system. Unlike other arterial systems, coronary blood flow decreases during ventricular contraction (high intramyocardial pressure) and increases during relaxation (low intramyocardial pressure)[2], necessitating integrated models that account for for the heart, arterial system and their dynamic interactions. However, most 3D studies have neglected such interactions, prescribing coronary flow as boundary conditions (BC) instead of predicting it, leading to unrealistic pressure modelling. To solve this problem, Kim *et al.*[3] introduced a robust and stable approach capable of handling complex flow dynamics and coupling across various scales to provide physiologically accurate predictions of flow rates and pressures within patient-specific CA trees introduced. A 0D lumped parameter network (LPN) model representing coronary vascular bed, derived from a simplified version of the model developed by Mantero *et al.*[4], was employed to represent downstream impedance for CA while a 3-element windkessel model[5] was applied at non-coronary boundaries to define impedance. The aim of this study is to implement and validate the windkessel and coronary LPN model BCs in OpenFOAM─ an open-source CFD software.

MATERIALS AND METHODS

Customized outlet pressure BCs were developed in OpenFOAM using ODEs representing LPNs, discretized with backward differencing. Various 0D windkessel models─1-element (R), 2-element (RC), 3-element (RCR), and 4-element (RCRL) series and parallel─were implemented for larger vessels like the aorta, while coronary vascular beds were modelled using ODEs representing coronary LPN for coronary outlets, as shown in Figure 1(c). A simple 3D cylindrical domain representing the aorta (D = 30 mm) and LCA (D = 3 mm) was meshed with hexahedral elements, as shown in Figure 1(b). Patient-specific flow profiles, shown in Figure 1(a), were applied as inlet BCs, and custom LPN models were coupled with the 3D domain at outlet. Blood was modelled as a Newtonian fluid ($\rho = 1060$ kg/m³, $\nu = 3.77\times10^{-6}$ m²/s). Laminar simulations were run for 8 cardiac cycles (1 s period) using the pimpleFluid solver in solids4Foam with specified corrector settings. Total flow rate and area-weighted pressure at inlets and outlets were recorded. LPN ODEs were also solved in MATLAB using Runge-Kutta solvers for validation against OpenFOAM results, as shown in Figure 1(d).

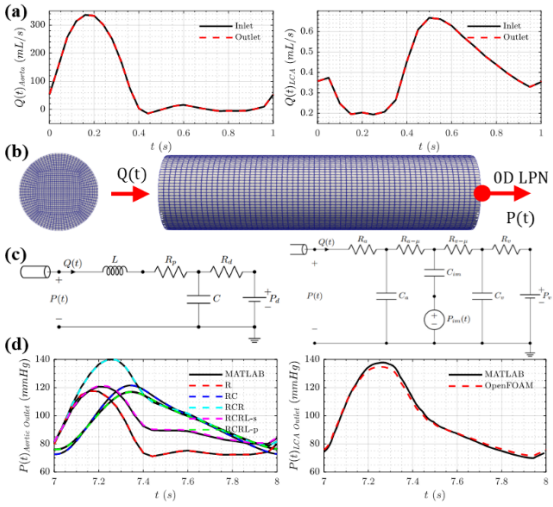

Figure 1 (a) Flow rate prescribed at the inlet of 3D domain; **(b)** 3D computational domain; **(c)** 0D LPN model coupled at the outlet of 3D domain; **(d)** Pressure at the outlet of 3D domain obtained by OpenFOAM simulation.

DISCUSSION

The numerical implementation, validated against MATLAB solutions of LPN ODEs, demonstrates high accuracy and consistency. The robust backward finite differencing schemes ensure stability in solving the ODEs, while the integration of flow and pressure histories enhances computational reliability. Results confirm the suitability of the developed models for capturing hemodynamic phenomena in both large and small vessels, especially the "out-of-phase" relationship between flow and pressure for CA. Both of these LPN BCs, with 3- or 4-element windkessel model at the aortic outlet and coronary model at coronary outlets can be used to analyse the complete patient-specific CA trees with physiological accuracy. The most important application of these BCs is in the fluid-structure interaction (FSI) modelling of vessels where usually used zero pressure outlet BC causes reflection of pressure wave at the outlet due to impedance mismatch. The modular framework supports future extensions to boundary condition models.

REFERENCES

[1] Taylor *et al.*, Annual Review of Biomedical Engineering, 11: 109-34, 2009.
[2] Opie *et al.*, Heart Physiology: From Cell to Circulation, Williams and Wilkins, 2003.
[3] Kim *et al.*, Annals of Biomedical Engineering, 38(10): 3195–3209, 2010.
[4] Mantero *et al.*, Journal of Biomedical Engineering, 14(2): 109–116, 1992.
[5] Westerhof *et al.*, Medical & Biological Engineering & Computing, 47(2): 131–141, 2009.

MODELLING THE NON-LINEAR VISCOELASTIC BEHAVIOUR OF BRAIN TISSUE IN TORSION

Small, G.[1], Ballatore, F.[2], Giverso, C.[2], Balbi, V.[1]
[1] School of Mathematical and Statistical Sciences, University of Galway, Ireland
[2] Department of Mathematical Sciences "G. L. Lagrange", Politecnico di Torino, Italy
email: *g.small1@universityofgalway.ie*

INTRODUCTION

Brain tissue accommodates non-linear deformations and exhibits markedly viscoelastic behaviour such as stress relaxation. While the literature is replete with non-linear viscoelastic models, they are generally cumbersome and computationally expensive, particularly regarding fitting and material parameter estimation. The relative simplicity of the modified quasi-linear viscoelastic (MQLV) model—recently reappraised in [1] and largely unexploited—offers an attractive framework for modelling the viscoelastic behaviour of brain tissue.

Torsion is one of the most robust testing protocols for measuring brain tissue's mechanical behaviour. It can be readily implemented using a rotational rheometer, which measures the torque and normal force required to twist a cylindrical sample [2]. Although stress relaxation in torsion has been explored in brain tissue [3], previous studies have focused on measuring only the torque, neglecting the normal force.

In this work, we exploit the latent potentials of the torsion protocol and the MQLV model to determine the viscoelastic properties of brain tissue.

MATERIALS AND METHODS

All experiments were performed using brains from freshly slaughtered, 6–9 month-old, mixed-sex sheep obtained from a local European Union-approved slaughterhouse (Athenry Quality Meats Ltd, Galway, Ireland). We performed ramp-and-hold relaxation tests in torsion on cylindrical samples of diameter 25 mm and height 10 mm. The tests were conducted using a rotational rheometer at varying twist rates of 40, 240 and 400 rad m^{-1} s^{-1}, with the twist remaining fixed at 88 rad m^{-1}, which generated two independent datasets for the torque τ and normal force N_z (Figure 1a).

The complete set of viscoelastic material parameters was estimated via a simultaneous fit to the analytical expressions for the torque and normal force predicted by the MQLV model. The model's predictions were further validated through finite element simulations in FEniCS.

RESULTS AND DISCUSSION

Our results show that the MQLV model accurately fits the experimental data (Figure 1b). Moreover, the estimated material parameters align with those obtained in previous studies on brain samples under torsion [2]. When coupled with bespoke finite element models, these parameters could enhance our understanding of the forces and deformations involved in traumatic brain injury and contribute to the design of improved headgear for sports such as boxing and motorsports. On the other hand, our novel testing protocol offers new insights into the mechanical behaviour of soft tissues other than the brain.

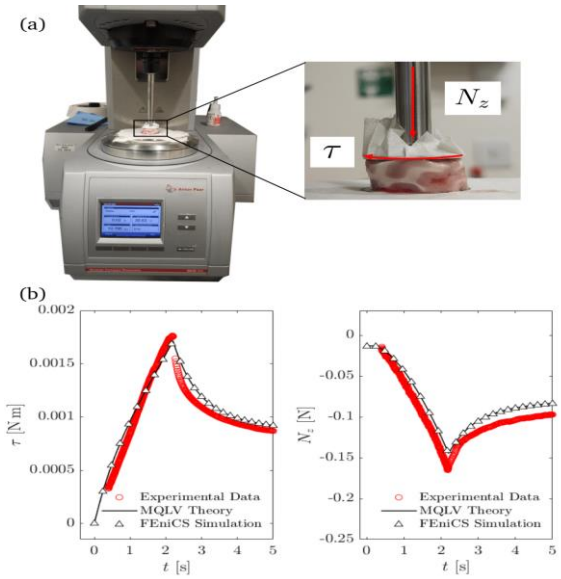

Figure 1 (a) Rotational rheometer used to perform the torsion tests and (b) results of the numerical simulations in FEniCS (triangles), analytical predictions with the MQLV model (solid lines) and experimental data (circles) for a twist rate of 40 rad m^{-1} s^{-1}.

ACKNOWLEDGEMENTS

This research was jointly funded by the Irish Research Council under grant number GOIPG/2024/3552 (Griffen Small), and by the College of Science and Engineering at the University of Galway under the Millenium Fund scheme for the project "Modelling Brain Mechanics" (Valentina Balbi).

REFERENCES

[1] De Pascalis *et al.*, Proc. R. Soc. A: Math., 470: 20140058, 2014.
[2] Balbi *et al.*, Soft Matter, 15:5147–5153, 2019.
[3] Chatelin *et al.*, Biorheology, 47:255–276, 2010.

EXPLORING THE FEASIBILITY OF EXPERIMENTAL AND COMPUTATIONAL EVALUATION OF ACTIVE DRAG TO AID SWIMMING TECHNIQUE

Haskins, A.[1], McCabe, C.[2], Keating, R.[2], Kennedy, R.[2], Lennon, A.[1], Chandar, D.[1]
[1] Queen's University Belfast, [2] Ulster University
email: (ahaskins02@qub.ac.uk)

INTRODUCTION

In elite level swimming, margins are fine, with the 2008 Olympic 100 m Butterfly decided by 0.01 s. To maximise athlete performance, it is important to understand the biomechanics of swimming technique, which affects the drag forces slowing a swimmer during the complex motion of a stroke (*active* drag). Active drag constantly changes across a stroke cycle and is relatively understudied, highly variable, and difficult to predict. This work aimed to use experimental and computational methods to analyse active drag profiles during freestyle swimming, with focus on predicting how technique changes impact active drag. This was completed in two phases: first, foundational and innovative experiments were undertaken to quantify active drag profile alongside development of a novel computational model of freestyle swimming. Second, the computational model was used to predict active drag, aiming to investigate differences due to technique changes.

MATERIALS AND METHODS

Experiments: A new methodology was developed, useable by coaches[1], to measure how active drag changes across a stroke cycle, without towing requirements that can inflate drag forces (**Fig. 1A**). Using a load cell (Fully Tethered) and 1080 Sprint (Semi-Tethered), assuming a constant power output between trials, and ensuring the measured data using each piece of equipment is synchronised across a stroke cycle, drag was calculated across a stroke cycle using equation (1).

$$\boldsymbol{D = T_{FT} - T_{ST}} \quad \textbf{(1)}$$

A suite of experiments was then conducted to measure both active and passive (streamlined pose) drag for elite swimmers.

Computational Model: A novel immersed boundary surface method (IBSM) approach, allowing for stop-motion solving of moving body problems based on sequential positions of a surface mesh, was developed using the foam-extend-5.0 fork of OpenFOAM. This can allow quicker and more precise approximations of drag profile, with much greater control of key technique parameters compared to experimental methods.

Computational Validation: Initial validation was performed using existing literature. Simulations of an athlete in a streamlined position and animated positions of a freestyle stroke were then compared against existing literature and the acquired experimental data (**Fig. 1B**).

Impact of Technique Changes: Different technique changes, e.g. kick frequency, were captured by modifying the animations, with drag profiles compared and impact quantified and presented.

RESULTS AND DISCUSSION

Experimental and simulated *passive* drag (72 and 116 N) results were similar to literature (**Fig. 1C, 1D**), although passive drag pose differences did have an impact on computational results, as well as tow/simulation velocity. **Fig. 1C** shows expected dependence of passive drag tow velocity with an additional effect from athlete sex at higher velocities[2].

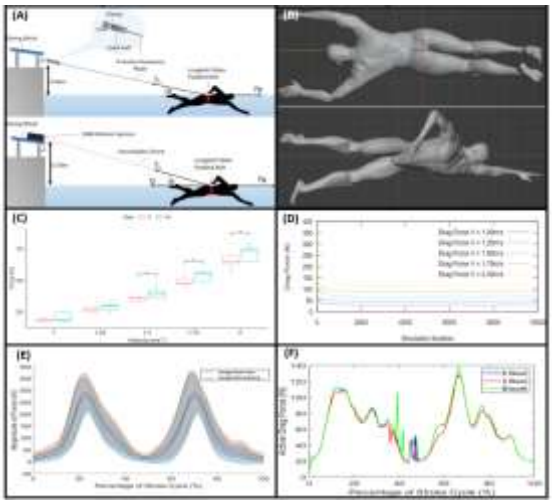

Figure 1*: (A) Experimental set-up and (B) computational geometries. (C) and (D) display passive drag experimental and computational results at different velocities. (E) and (F) display experimental and computational active drag results*

Experimental values of mean *active* drag agreed with literature, varying between 76 – 140 N. The drag profile (**Fig. 1E**) also displays high inter cycle variability (± 100 N for the athlete shown, with the average across all trials also large, at ± 80.7 N). The high variability implies technique repeatability is an area that can be improved. As stroke rate increased, so did full width half-max values, implying a relationship between stroke rate and time spent at higher drag values. Average quasi-steady *simulated* active drag profiles were prone to some noise (**Fig. 1F**). Relative to experimental results, predictions were lower but reasonable (45 N); this may be due to the lack of inertial forces in quasi-steady simulations. Technique changes had little impact on overall profile.

This work demonstrates the feasibility of estimating active drag profiles using CFD and experimental methods, including the impact of technique changes. Future refinement, e.g. multiphase simulations and use of 3D scanning and motion capture systems, should improve predictive ability and ultimately enable CFD-informed training tools.

ACKNOWLEDGEMENTS

The authors would like to thank the DfE, Swim Ireland and Lisburn City Swimming Club.

REFERENCES

[1] Haskins et al., Scientific Reports, Jul 2023, [2] Haskins et al, EJCM Jul 2024.

A SOFT-ROBOTIC BIOMIMETIC BENCHTOP MODEL FOR OESOPHAGEAL MOTILITY SIMULATION

Kilroy, S.[1,2], Patankar, N.A.[3], Traverso, C.G.[2,4,5], O'Cearbhaill, E.[1]
[1]School of Mechanical & Materials Engineering, University College Dublin; Dublin, Ireland.
[2]Division of Gastroenterology, Brigham and Women's Hospital, Harvard Medical School; Boston, USA.
[3]Department of Mechanical Engineering, McCormick School of Engineering; Northwestern University, Evanston, Illinois, USA.
[4]Department of Mechanical Engineering, Massachusetts Institute of Technology; Boston, USA
[5]Department of Chemical Engineering and Koch Institute for Integrative Cancer Research, Massachusetts Institute of Technology; Boston, USA
email: sean.kilroy@ucdconnect.ie

INTRODUCTION

Dysphagia, or difficulty swallowing, can be due to malignancy, such as cancerous tumours, or diseases such as achalasia. The most common palliative treatment for malignant dysphagia is stenting, despite 13-37% migration occurrence rates [1]. Conversely, treatment of achalasia has excellent results, if diagnosed correctly which, unfortunately, is often not the case. Furthermore, there is a lack of evidence-based dietary recommendations for patients with the disease. Current methods for evaluating these issues remains limited to expensive and time-consuming pre-clinical and clinical studies that lack multiple timepoints and repeatability. To address this, benchtop models have been developed [2], however, they do not simulate key motility aspects such as tissue interaction and longitudinal muscle contraction. Here, we propose a soft-robotic biomimetic benchtop model of the oesophagus, that can address these limitations. We demonstrate the versatility of the model by evaluating stent migration, simulating the effects that bolus properties have on achalasia diagnosis, and providing evidence to support clinical dietary recommendation for achalasia.

MATERIALS AND METHODS

The soft-robotic oesophageal model design was optimised computationally using Abaqus. A hexagon shape was selected to replicate oesophageal mucosal folding. Computational results dictates that a dual material (EcoFlex 00-30 and DragonSkin 20) model was necessary to achieve independence between circumferential and longitudinal muscle movement, and thus required a complex lost-wax casting procedure to be moulded. Once built, the physical model was used to carry out three studies. Swallowing conditions were defined by values given in the Chicago Classification 4.0 [3] and validated using high resolution manometry (Sierra Systems, ManoScan). Where indicated, porcine oesophageal tissue was fixed on either end of the model, running through its inner lumen.

Firstly, a study on the migration of 6 different types of stents under normal swallowing conditions with a 5mL bolus of water (n=5) was performed (with and without tissue). Secondly, a study on the effect of bolus viscosity on the diagnosis of swallowing under achalasia conditions was conducted with tissue (n=3). The boluses used were water, glycerol mixed with water (50%wt, 75%wt, and 100%wt) and ThickenUp mixed with water (0.6%wt, 2.1%wt, and 3.6%wt). The swallows were recorded and analysed using ManoScan Acquisition and ESO Analysis. Lastly, the model (with tissue) was used to study the swallowing efficiency of mixed and unmixed Greek yoghurt under achalasia type II and type I conditions.

RESULTS

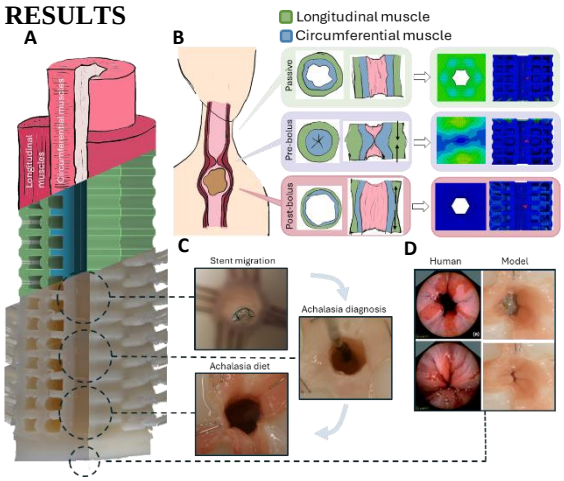

Figure 1 (A) Design approach of computational and physical models of soft robotic oesophagus. **(B)** Model replicates the three main stages of a swallowing wave. **(C)** Studies investigate (1) stent migration, (2) manometry diagnosis, and (3) bolus viscosity. **(D)** Comparison of oesophagus passive and contracted states in a human (left) and the fabricated model (right).

DISCUSSION

In the stent migration studies without tissue, the stent type had the largest influence on migration. However, with tissue, uncovered stents and larger diameter showed significantly lower migration rates. Detection of achalasia type III, through a 20.8% decrease in distal latency, significantly increased with the 3.6%wt non-Newtonian bolus, unlike with the Newtonian bolus. A significant difference in swallowing efficiency was seen between stirred and unstirred yoghurt for achalasia type I ($p=0.0317$) but not type II ($p=0.0984$). This versatile model provides valuable insights related to dysphagia not achievable through current *in vivo* methods.

REFERENCES

[1] J. H. Lee *et al.*, *Gastrointest. Endosc.*, vol. 78, no. 2, pp. 312–324, 2013.
[2] D. Bhattacharya *et al.*, *Soft Robot.*, vol. 8, no. 4, pp. 397–415, 2021.
[3] R. Yadlapati *et al.*, *Neurogastroenterol. Motil.*, vol. 33, no. 1, p. e14058, 2021.

A NEW FIBRE CONSTITUTIVE LAW FOR THE TENSILE AND COMPRESSIVE BEHAVIOUR OF FIBRIN WITH APPLICATION TO ACUTE ISCHEMIC STROKE CLOTS

Bein Snee, K.[1], McCarthy, R.[2], McGarry, P.[1]
[1] Biomedical Engineering, University of Galway, Ireland
[2] Johnson & Johnson MedTech, Ireland
email: k.beinsnee1@universityofgalway.ie

INTRODUCTION

Traditional models for fibre-reinforced soft tissues such as the Holzapfel–Gasser–Ogden (HGO) model assume that fibres are only active in tension [1-4]. In such models it is assumed that wavy fibres, such as collagen, will buckle when shortened and therefore cannot support compressive stress. However, compression-tension experiments of pure fibrin blood clots, such as retrieved from acute ischemic stroke (AIS) patients, suggest that fibre networks can support both tensile and compressive stress [5, 6]. Therefore, a fibre model in which shortening results in the development of compressive stress is required for the modelling of fibrin networks and clots.

In the current study we propose a constitutive formulation for the tensile and compressive behaviour of fibrin. Firstly, we demonstrate that the simple extension of existing fibre formulations to the shortening/compressive regime results in unphysical behaviour of fibres in compression. We then develop a novel constitutive law for fibres (compression-tension fibre (CTF) model) which allows us to model pure fibre networks without isotropic matrix contributions. We further demonstrate the CTF model's application by calibrating it to experimental data of pure fibrin clots and simulating aspiration thrombectomy.

METHODS & RESULTS

Published constitutive laws for fibres in fibre-reinforced soft tissues include exponential formulations such as the HGO model [1,2], the Modified Anisotropic (MA) model [3] and bilinear models [4]. The mathematical framework of such models results in the computation of softening during high levels of fibre compression, as shown in Figure 1A. Therefore, we propose a novel fibre constitutive law which prevents such softening in compression (see Figure 1A,B). The newly proposed compression-tension fibre (CTF) model can be used in linear, bilinear or trilinear formulations.

In order to simulate a fibrin clot, we construct a network of discrete fibres, whereby the mechanical behaviour of each fibre is described by our novel constitutive law. The fibre model is implemented in Abaqus/Standard using a user defined subroutine (UMAT). Converged results were achieved with 1741 fibre segments. The bilinear CTF formulation can replicate asymmetric experimental compression and tension data for pure fibrin platelet contracted human blood clot analogues [5] (see Figure 1C).

Finally, we use this novel material model to simulate the aspiration of a fibrin clot using a thrombectomy catheter, whereby a suction pressure of 80 kPa is applied (see Figure 1D). This simulation correctly predicts the corking of the clot at the tip of the catheter and reveals areas of shortened fibres where the clot is pressed against the catheter wall and areas of fibres in tension within the catheter where the aspiration pressure is applied.

The proposed CTF model will be extended to include 1D fibre plasticity and viscoelasticity in order to model the viscoplastic behaviour observed in AIS clots.

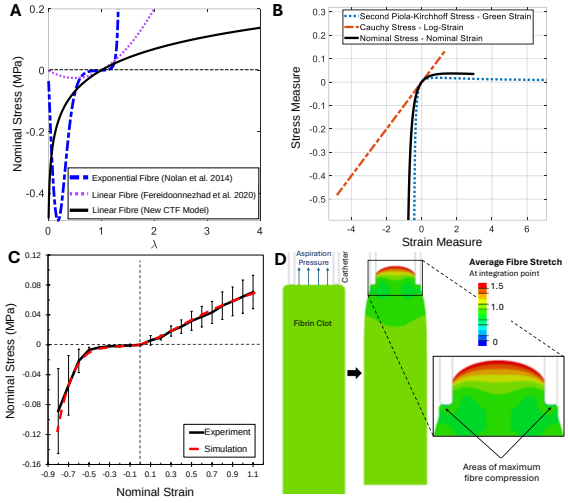

Figure 1 Results for a single 1D fibre (A)-(B): (A) Comparison of the CTF model to existing fibre laws (B) Various stress-strain measures of the CTF model; Results for a fully dispersed fibre material model (C)-(D): (C) Calibration of the CTF model to experimental data of pure fibrin clots [5]; (D) Simulation of the partial aspiration of a fibrin clot using previously calibrated material parameters.

REFERENCES & ACKNOWLEDGEMENTS

Funding: Irish Research Council (EPSPG/2022/379) and Enterprise Partner Johnson & Johnson MedTech (Neuravi Ltd.).

1. Gasser et al., J. R. Soc. Interface., 3:15-35, 2006
2. Holzapfel et al., J. Elast., 61:1-48, 2000
3. Nolan et al., J. Mech. Behav. Biomed. Mater., 39:48-60, 2014
4. Fereidoonnezhad et al., J. Biomech., 111:110006, 2020
5. Cahalane et al., Ann. Biomed. Eng., 51:1759-1768
6. Johnson et al., Ann. Biomed. Eng., 49:420-431

MULTI-SCALE MODELLING OF SURFACE GROWTH IN TISSUE

Hayes, T.[1,2], McEvoy, E.[2], Zurlo, G.[1]
[1] Discipline of Biomedical Engineering, University of Galway
[2] School of Mathematical and Statistical Sciences, University of Galway
email: t.hayes5@nuigalway.ie

INTRODUCTION

Surface growth is essential for the development, adaptation, and regeneration of biological tissues. Tissue-specific characteristics, such as microstructure and mechanical properties, critically influence how growth patterns are biologically mediated in response to environmental stimuli. Active contraction in tissue is a key player in how tissues optimize this growth. Notably, out-of-plane surface growth has been observed in active tissues such as skeletal muscle [1], yet the mechanisms underlying this phenomenon are not well understood. In this study, we elucidate a thermodynamically consistent method of surface growth in active contractile tissues occurring out of plane to the direction of active contraction and loading.

METHODS

The temporal evolution of growth is governed by the principle of positive dissipation, expressed in terms of active power P_a, mechanical power P_m and internal energy U:

$$P_a + P_m - U \geq 0. \quad (1)$$

Rearranging this inequality, it is possible to derive an equation for the rate of growth of a surface

$$\dot{\Lambda} = \Lambda(t)\mathbf{E}. \quad (2)$$

Where $\Lambda(t)$ is the surface as a function of time, and $\mathbf{E}$ represents Eshelby stress defined in the context of surface growth as:

$$\mathbf{E} = \int P_a|_{\Lambda(t)} - U|_{\Lambda(t)}, \quad (3)$$

where $\int P_a|_{r(t)}dt$ is the work done and $U|_{r(t)}$ is the energy of newly deposited material. For an actively contracting tissue (3) takes the form:

$$\mathbf{E} = \boldsymbol{\sigma}_\mathbf{a}(\mathbf{F}_e)(\mathbf{F}_e - \mathbf{I})|_{\Lambda(t)} - W(\mathbf{F}_e)|_{\Lambda(t)} + f(\Delta S). \quad (4)$$

$\boldsymbol{\sigma}_\mathbf{a}$ is the active stress tensor, W the energy density in the and $\mathbf{F}_e$ the elastic deformation gradient evaluated at the surface. ΔS is the change in entropy of the process. Isotropic Neo-Hookean material properties were assigned. A symmetric, strain-sensitive active stress was defined to approximate the behaviour of actomyosin functional units [2]. Specifically, the active stress is expressed as

$$\boldsymbol{\sigma}_\mathbf{a}(\mathbf{F}_e) = \sigma_{max}\mathrm{Cauchy}(\mathbf{F}_e). \quad (5)$$

Where σ_{max} is the maximum stress, the tissue can actively generate.

RESULTS

Active Tissue subject to a longitudinal tensile force T in the configuration shown in (Fig. 1A) laterally grows over time (Fig. 1B). The relationship between σ_{max} and T has a significant impact on the extent and whether growth occurs. Higher active stress leads to higher growth σ_{max} provided greater than tensile force factor T.

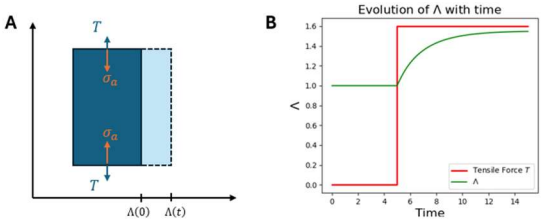

Figure 1 Reference configuration with Tensile force T and active stress (A), Surface growth in response to tensile load (B)

DISCUSSION

This framework has shown that active contraction and mechanical loading can significantly influence out of plane surface growth, aligning with observations in skeletal muscle [3]. This model can offer insights into the subcellular mechanism of skeletal muscle hypertrophy and atrophy. Understanding this mechanism has tremendous potential for developing treatments for muscle-wasting diseases such as sarcopenia and ALS, where controlling muscle growth and preventing atrophy is critical.

REFERENCES

1. Morkin, *Science,* 1970
2. McEvoy *et al., BmMb,* 2019.
3. Green *et al., Regulatory and Integrative Physiology,* 1999.

Early Stage Researcher (PhD Year 1)	X	Post-Doctoral Researcher/Senior Researcher/PI	
Entry for the Engineers Ireland Biomedical Research Medal		Corresponding author has completed PhD and would like to review BinI abstract submissions	X

GROWVALVE- A PAEDIATRIC HEART VALVE CAPABLE OF GROWTH

Kostopoulou, E.A.[1,2,*], O'Brien, F.J.,[2] Brougham, C.M.[1,2]
[1] Towards People Oriented Technology (tPOT) Research Centre, School of Mechanical Engineering, Technological University Dublin, Ireland
[2] Tissue Engineering Research Group, Dept. of Anatomy & Regenerative Medicine, RCSI University of Medicine and Health Sciences, Dublin, Ireland
[*]*email: D24126842@myTUDublin.ie*

INTRODUCTION

With 8 out of 1000 live-born full-term children being affected by congenital heart disease, pulmonary heart valve replacements have been commonly employed as a treatment option for severe cases of this condition. However, the currently available treatments lack remodelling capability resulting in multiple reoperations as the child's heart grows. Our research aims to eliminate the need for additional surgeries, by developing a tissue engineered pulmonary heart valve for paediatric patients with the ability to remodel and grow in tandem with the patient. This requires development of a prosthesis which will withstand the challenging hemodynamic conditions of the heart from the moment of implantation. This prosthesis must also fully integrate with the native heart tissue to enable somatic growth.
In previous work, our group successfully developed a novel polymer scaffold for soft tissue applications. This fibrin-collagen based scaffold has viscoelastic properties similar to those of native valves and provides an excellent biological environment for cells. This novel natural biomaterial scaffold will enhance the viscoelastic properties of the neotissue formed within its matrix, ensuring development of an effective replacement valve [2][3].

PROJECT AIMS

This PhD project aims to further develop this technology and is part of a larger project. The specific aims of this PhD project are:

- Develop a functioning coculture of primary cells within the HV scaffold
- Dynamically condition this TEHV with previously identified parameters and measure the functional and performance characteristics of the TEHV as per ISO 5840. Characterise the biological attributes of the TEHV including in vitro immune response.
- Ascertain non-destructive monitoring indicators for TEHVs
- Create an appropriately sized valve for a pilot preclinical trial with a young animal model.

IMPACT

The expected outcome of this project is the development of a tissue engineered heart valve. The development of such technology will also create an in vitro model of a human heart valve for research into heart valve diseases.

REFERENCES

[1] Bouma and Mulder, Circulation Research, vol 120:908–922, 2017
[2] Almeida-González (et al.), Materials Science & Engineering: C, vol. 120, 2021.
[3] Brougham (et al.), Advanced Healthcare Materials, vol. 6, 2017.

FUNDING

Taighde Eireann- Research Ireland (Frontiers of the future) 22/FFP-P/11399

MAY THE FORCE SHAPE YOU: HARNESSING PHYSICAL CONSTRAINTS IN MSCS MICROTISSUES CONSTRUCTS

Correia, C.[1], Kronemberger, G.S.[1], Wirth, M.[1], Giordano T.[1], Kelly, D.J.[1,2]
[1] TCBE, Trinity Centre for Biomedical Engineering, Trinity College Dublin
[2] AMBER Centre, SFI Centre for Advanced Materials and Bioengineering Research
email: penacorf@tcd.ie

INTRODUCTION

Articular cartilage (AC) is a non-vascular, aneural tissue that is integral to synovial joint function. Organized into three zones, AC has unique structural and functional properties. The surface zone is characterised by tightly packed collagen fibers aligned parallel to the articular surface, which provides a smooth surface and resists shear forces. The collagen fibers are more randomly oriented in the middle zone, which is rich in proteoglycans, providing resistance to compressive forces. The deep zone is characterised by radially oriented collagen fibers that anchor the tissue to the subchondral bone. This zonal collagen organization is critical to the biomechanical properties of AC.

Mesenchymal stem/stromal cells (MSCs) are commonly used for engineering AC grafts. MSC derived microtissues (µTs) can be used as biological building blocks to engineer scaled-up tissues, but without physical boundaries, these constructs tend to compact into spherical shapes with unorganized collagen, compromising their functionality.

The aim of this study is to explore how physical boundaries influence the structural development of tissues generated by the fusion of multiple MSC-derived µTs. Ultrapure agarose was used as a physical boundary to shape µTs into rings or cylinders, then their morphology and collagen organization were analyzed in physioxic and normoxic conditions. We compared constructs shaped as spheres (no agarose constriction), cylinders (agarose on top), and rings (agarose on top and center of mold) as shown in fig 1.

MATERIALS AND METHODS

Microtissue fabrication was performed as described previously (1). MSC-derived microtissues were fabricated using an in-house high-throughput nonadherent agarose hydrogel microwell system (2). For microtissue formation, MSCs at passage 3 were seeded on top of each mold at a final density of 1×10^3 or 2×10^3 cells/microtissue in chondrogenic media. The microtissues were then harvested and casted into new agarose molds with a cylindrical shape (6mm diameter by 1.5mm deep). After 6 weeks of culture in physioxic and normoxic conditions, the constructs were accessed histologically and biochemically. Histological and biochemical analyses provided insights into tissue structure, collagen distribution, and extracellular matrix composition. Polarized light microscopy enabled the visualization of collagen fibre alignment and orientation.

Figure 1: Visual Representation of using the agarose as a constricting agent throughout cell culture.

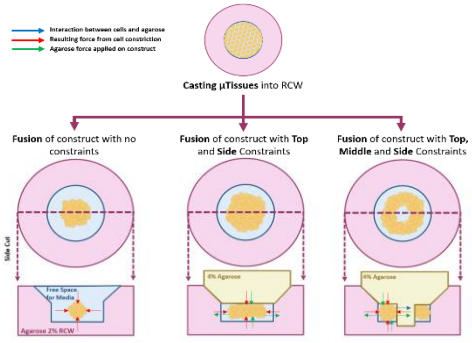

RESULTS

Robust chondrogenesis of the MSC derived µTs was observed in all applied boundary conditions. When not confined from the top, the µTs generated spherical constructs with circumferentially aligned collagen fibers around the periphery of the construct. When confined by agarose on the top, the µTs generated more cylindrically shaped constructs. When confined from the top and in the centre, the µTs generated rings of cartilage. In the body of these ring, collagen fibers were aligned radially, whereas around the periphery of the construct, the collagen was aligned in a circumferential direction.

DISCUSSION

These results support a continuous use of microtissues as biological building blocks that can be matured in culture using physical boundaries that can engineer oriented AC grafts.
Future work will focus on comparing how MSC derived µTs and AC progenitor cell derived µTs respond to different oxygen tensions and physical boundaries throughout culture, with a view to engineering AC grafts that mimic the zonal structure and composition of the native tissue.

REFERENCES

(1) Burdis R, Kelly DJ. Acta Biomater. 2021 May;126:1-14.
(2) Burdis R, Kelly DJ. Biomaterials. 2022 October;289: 121750

THE EFFECT OF MELT ELECTRO-WRITTEN SCAFFOLD PORE SIZES ON THE ENGINEERING OF ZONALLY DEFINED ARTICULAR CARTILAGE GRAFTS

Wirth, MD.[1], Kronemberger, GS.[1], Correia, C.[1], Giordano, T.[1], Kelly, DJ.[1],
[1] Trinity Centre for Biomedical Engineering, Trinity Biomedical Sciences Institute, Trinity College Dublin, Dublin, Ireland.
email: wirthm@tcd.ie

INTRODUCTION

Articular cartilage (AC) is a zonally-defined connective tissue that translates mechanical loads and provides nearly frictionless motion in synovial joints. The properties of this tissue are dependent on the organization of articular chondrocytes and type II collagen into arcade-like structures. However, due to its avascular and aneural nature, there is a limited healing capacity in this tissue. Therefore, damage to AC typically progresses, leading to the development of osteoarthritis [1], a joint disease that has a significant impact on the quality of life of millions of people worldwide [2]. Current clinical treatments for damaged articular cartilage are limited in their ability to fully recapitulate the key morphological composition, collagen organization and function of this tissue. Treatment options such as mosaicplasty and autologous chondrocyte implantation often trend towards the formation of fibrocartilage-like tissues that ultimately do not mimic the arcade-like structures of native AC and thus fail to provide long-term regeneration solutions [3]. This motivates the increased interest in cartilage tissue engineering approaches to address this challenge. Emerging additive manufacturing techniques such as 3D (bio)printing have shown potential as approaches to enabling the engineering of such complex musculoskeletal tissues [4,5]. Previous work performed by our lab (Dufour et al., 2022) has explored the integration of melt-electro written (MEW) scaffolds with inkjet bioprinting to engineer structurally organized AC grafts [6]. Although this work showed promising results *in vitro*, the MEW scaffold architecture needs to be further optimized to engineer a more homogenous and biomimetic cartilage graft. Therefore, this study aims to assess how pore size in MEW scaffolds affects the overall organization and mechanical properties of the engineered cartilage tissue.

MATERIALS AND METHODS

Bone marrow-derived mesenchymal stromal cells (bmMSCs) were isolated from skeletally mature female goats as previously described [7]. Next, melt electro-written scaffolds were fabricated using an in-house custom-made MEW printer. Scaffolds with 0.2, 0.4, and 0.8 mm, square pores were printed with polycaprolactone (PCL) at previously optimized parameters. A final concentration of 30 million cells/mL was seeded into each scaffold. Constructs were then cultured in chondrogenic induced medium for up to 6 weeks. Following the culture period, the constructs will be assessed histologically, biochemically and mechanically.

RESULTS AND DISCUSSION

Preliminary images of the constructs at 4 hours and 24 hours post seeding show differences in cell alignment and tissue formation across the three pore sizes with larger cellular aggregates forming in the scaffolds with larger pores (Fig 1A arrows – for example). These preliminary results indicate that MEW scaffold pore sizes may have an impact on morphology and organization.

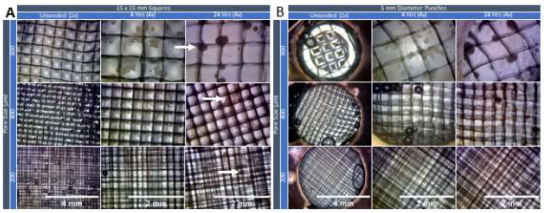

Figure 1: Pore ratios of MEW scaffolds influence bmMSCs morphology and organization. Phase contrast microscopy images of square (A) and punched (B) MEW scaffolds and constructs at 4 and 24 hours after seeding of bmMSCs

CONCLUSION

Additional analyses will be undertaken to investigate the morpho-functional properties of the bmMSCs. Future work will explore using inkjet bioprinting to deposit cells into MEW scaffolds with the pore ratio that shows the most promising cartilage tissue formation. In conclusion, this work has the potential in the field to address challenges of engineering articular cartilage grafts.

REFERENCES

[1] Tew *(et al.),* Arthritis Rheum., vol. 43, no. 1, pp. 215–225, 2000
[2] Helmick *(et al.),* Arthritis Rheum., vol. 58, no. 1, pp. 15–25, 2008
[3] Solheim *(et al.),* J. Orthop. Rep., vol. 1, no. 4, pp. 100097, 2022
[4] Liu *(et al.),* Frontiers in Bioeng. and Biotech., vol. 12, pp. 1339916, 2024
[5] Park *(et al.),* Annals of Biomed. Eng., vol. 52, no. 7, pp. 1883-1893, 2024
[6] Dufour *(et al.),* Biomaterials, vol. 283, pp. 121405, 2022
[7] Burdis *(et al.),* Biomaterials, vol. 289, pp. 121750

Early Stage Researcher (PhD Year 1)	X	Post-Doctoral Researcher/Senior Researcher/PI	
Entry for the Engineers Ireland Biomedical Research Medal		Corresponding author has completed PhD and would like to review BinI abstract submissions	

DEVELOPING MECHANICALLY ENHANCED 3D-PRINTABLE BIOINKS FOR BONE REGENERATION

Zhu, Y[1], Johnston, R[1] , Pepper, J[1] , Kaur, K[1,2] , Murphy, C.M[1,3,4]

[1]Tissue Engineering Research Group (TERG), Dept of Anatomy and Regenerative Medicine, Royal College of Surgeons in Ireland (RCSI), Dublin, Ireland. [2] School of Pharmacy and Biomolecular Sciences, RCSI, Dublin, Ireland. [3]Trinity Centre for Biomedical Engineering, Trinity College Dublin (TCD), Dublin, Ireland. [4] Advanced Materials and Bioengineering Research Centre (AMBER), RCSI and TCD, Dublin, Ireland

Email: (yuanchenzhu24@rcsi.com)

INTRODUCTION

Gelatin methacryloyl (GelMA) and methacrylated collagen (ColMA) are known for their excellent biocompatibility, injectability, and biodegradability, as well as their ability to mimic the extracellular matrix. However, the optimal formulation of these hydrogels for 3D-printing bioinks in bone tissue engineering remains uncertain. This study seeks to address this by conducting a comparative analysis of GelMA and ColMA, both individually and in combination, to determine the most effective formulation for 3D-printing bioinks aimed at bone regeneration.

Bone regeneration is a complex process that requires scaffold materials to offer not only biological compatibility but also mechanical strength to support tissue repair and withstand physiological loads. In bone defect repair, particularly through 3D-printed hydrogels, a major challenge is achieving sufficient mechanical strength and ensuring controlled release of bioactive factors to support effective healing. Previous studies indicate that nano-hydroxyapatite (nHA) and graphene oxide (GO) can enhance both osteogenic differentiation and mechanical properties, making them promising additives. Incorporating nHA and GO into natural polymer-based hydrogels has been shown to improve their mechanical stability, allowing them to resist deformation under compressive, tensile, and bending forces. This enhancement is especially relevant for spinal fusion applications, where the scaffold must facilitate bone regeneration and maintain sufficient mechanical resilience to prevent subsidence.

This study will further functionalize nHA and GO with strontium (Sr) to enhance the osteogenic properties of the hydrogels, aiming to develop mechanically robust, regenerative bioinks optimised for spinal fusion. By combining GelMA, ColMA, and functionalized nHA and GO, this study aims to develop a printable hydrogel with the structural and regenerative characteristics required for effective spinal fusion and bone defect repair

MATERIALS AND METHODS

GelMA, ColMA and GelMA/ColMA composite hydrogels were prepared and compared for their mechanical properties and 3D printability. A range of GelMa and ColMa concentrations and GelMA/ColMa ratios were investigated to determine the optimal hydrogel formulations. Sr functionalised nHA and GO was incorporated at different concentrations into the hydrogels. Mechanical tests, including compressive and tensile tests, were conducted to compare the mechanical properties of the hydrogels before and after the addition of the therapeutic nanostructures. Degradation and swelling behaviour were assessed by immersing samples in phosphate buffered saline (PBS) at 37°C for specific time intervals. Biocompatibility of the hydrogels was assessed using Alamar Blue to determine cell viability and identify the cytotoxic limitations of nHA and GO. The functionalised hydrogels capacity to support mesenchymal stem cell (MSC) proliferation was evaluated using Pico Green assay.

RESULTS AND DISCUSSION

The aim this research aims to develop mechanically enhanced 3D-printable bioinks using GelMA, ColMA, Sr functionalised nHA, and GO. The focus will be on optimizing the concentrations and formulations of these hydrogels to achieve favourable biocompatibility, osteogenic properties, and printability.

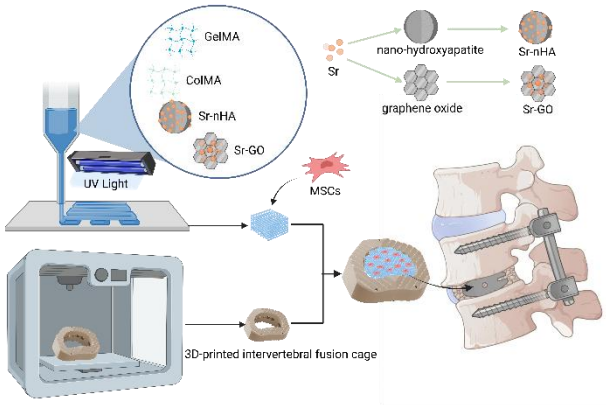

Figure 1. *Schematic of the 3D-printed mechanically enhanced hydrogel scaffold and intervertebral fusion cage, along with a diagram illustrating the combination of the stem cell-loaded hydrogel scaffold with the fusion cage for spinal fusion.*

A key-targeted application of these bioinks will be their integration with 3D-printed biodegradable polymeric intervertebral fusion devices. These hydrogels will not only facilitate spinal fusion but also simulate the biomechanical properties of the intervertebral disc, ensuring proper load distribution. This approach is particularly critical for osteoporotic patients, where the risk of implant subsidence is high. By combining advanced bioink formulations with biodegradable fusion devices, this research seeks to overcome challenges in spinal fusion surgery, improving long-term outcomes and the success of the procedure. Future studies may focus on refining these bioinks, investigating their performance in vitro and vivo, and confirming their clinical potential for treating bone defects and supporting spinal fusion.

REFERENCES

1. Guo et al., *Materials Today Bio. Vol*, 24, 100939, 2024.
2. Pien et al., *Mater Sci Eng C Mater Biol Appl. Vol*, 130, 112460, 2021.
3. Alexa et al., *Int. J. Mol. Sci.* 23, 1841-1865, 2022.

ACKNOWLEDGEMENTS

The work being conducted for this project is funded by RCSI.

DECELLULARISED EXTRACELLULAR MATRICES IN CARTILAGE TISSUE ENGINEERING – A PRELIMINARY STUDY IN USING HUMAN BONE MARROW MESENCHYMAL STROMAL CELLS IN PELLET CULTURES

Lauretta, Giovanni.[1] **Zevgolis, Dimitrios.**[1]
[1] Regenerative, Modular & Developmental Engineering Laboratory (REMODEL), Charles Institute of Dermatology, Conway Institute of Biomolecular & Biomedical
Research and School of Mechanical & Materials Engineering, University College Dublin (UCD), Dublin, Ireland
email: giovanni.lauretta@ucd.ie

INTRODUCTION

Osteoarthritis and trauma-induced articular cartilage defects are among the most prominent musculoskeletal disorders, mostly due to the poor self-healing capacities of the articular cartilage, and as such they pose a heavy burden on the quality of patients' life. Current therapies fall short of fully restoring the native function and structure of articular cartilage and patients often resort to invasive procedures like arthroplasty. In this context, tissue engineering holds great promise for cartilage repair and regeneration using engineered scaffolds and progenitor cells. However, current approaches struggle to replicate the complex native cartilage extracellular matrix (ECM), limiting their regenerative capacity. Decellularised ECMs (dECM) have gained clinical interest due to their superior regenerative potential and biomimicry, compared to synthetic or other natural biomaterials.
This study explores the use of dECMs to promote chondrogenesis using human bone marrow mesenchymal stromal cells (hBM-MSCs) in pellet cultures.

MATERIALS AND METHODS

dECMs were produced using standard protocols. Decellularisation efficiency was assess by DNA quantification and histology analyses. dECMs were then pellet-cultured with hBM-MSCs for 21, 28 and 35 days. The chondrogenic potential of dECMs was evaluated by histological and gene expression analyses and correlated to commercially and clinically available products.

RESULTS

DNA quantification revealed a drastic reduction in nucleic acid content in the dECMs, compared to the non-dECMs. The amount of DNA after decellularisation was in line with the FDA-approved products included in this study (**Figure 1)**. Histological evaluation confirmed no cellular residues and showed that the dECMs maintained the ECM composition of the original tissue. Histological analysis of the pellets revealed that the hBM-MSCs were successfully incorporated the dECMs by day 21 without affecting cell survival and proliferation. Moreover, the dECMs demonstrated superior chondrogenic potential compared to both pellet cultures alone and the commercially available products. Gene expression work is ongoing.

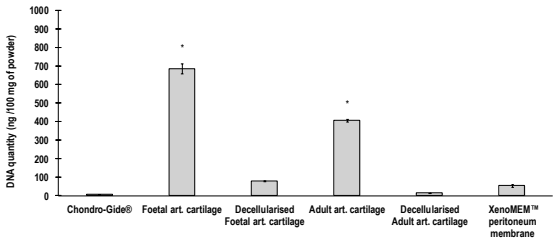

Figure 1 DNA quantification by PicoGreen™ assay of non-decellularised and decellularised matrices.

CONCLUSION

This work highlights the remarkable chondrogenic properties of dECMs in cartilage engineering. The decellularisation protocol employed reduced the amount of DNA to regulatory approved standards; did not reduce the bioactivity of the dECMs and induced the highest chondrogenesis (in comparison to pellet alone cultures and commercially available devices) in pellet culture.

REFERENCES

Zhai *et al.*, Regenerative medicine*, 14*(7), 663–680, 2019.
Capella-Monsonís *et al.*, Xenotransplantation, 28(4), e12683, 2021.
Shologu *et al.*, Biomaterials, *287*, 121642, 2022.
Chen et *al.*, Bioactive *materials*, *44*, 220–235, 2024.

3D BIOPRINTING PLURIPOTENT STEM CELL-DERIVED VASCULAR NETWORKS

Wong HW.[1,2], **Daly, A**[1,2]
[1] Biomedical Engineering, University of Galway, Galway, Ireland
[2] CÚRAM, SFI Research Centre for Medical Devices University of Galway, Galway, Ireland
email: (andrew.daly@universityofgalway.ie)

INTRODUCTION

3D bioprinting is a biofabrication method to introduce vascular networks into cardiac organoids and has extensive research on vascular network bioprinting.[1] Nevertheless, these printed vasculatures have a low level of maturity and physiological significance and have hindered the perfusing of oxygen and nutrients within the cardiac tissue.[2] Forskolin, a cAMP signalling activator, has played a key role in endothelial differentiation by activating the PKA/cAMP pathway, increasing the expression of VEGF receptors, and directing iPSCs toward endothelial lineage specification.[3] While numerous studies have been performed using HUVECs, these cells cannot produce organ-specific vasculature. There is limited understanding of bioprinting functional vasculature in cardiac organoids using iPSCs-derived endothelial cells. Future work will explore how morphogenetic processes influence the maturation of the iPSC-derived vascular network.

MATERIALS AND METHODS

The iPSCs were differentiated into endothelial cells following a protocol outlined by Pavlova et al. To determine the effect of the concentration of VEGF -165 during the endothelial lineage specification, 0ng/ml, 50ng/mL, 100ng/mL and 200ng/mL were added to the cells after the mesodermal-induced iPSCs for 48h. To determine the effect of Forskolin with the combination of VEGF-165 in endothelial lineage specification, 2µM of Forskolin was added together with the 50ng/mL VEGF-165 for 48h. The media were replaced with RPMI/B27-media supplemented with 50ng/mL VEGF-165 until day 6. To determine the vascular tube formation, 2M cells/mL HUVEC and cardiac fibroblast cells with different ratios (100% HUVECS, 2:1, 1:1) were encapsulated in collagen hydrogel with the presence of angiogenic factor. The hydrogel with the cells was then physically crosslinked in a 37°C incubator for 1 hour.

RESULTS

During endothelial lineage specification, 200 ng/mL VEGF-165 yielded the highest differentiation efficiency compared to other concentrations (Fig 1A). The addition of Forskolin with VEGF also enhanced iPSC-endothelial specification (Fig 1B). The modified protocol with Forskolin resulted in a differentiation efficiency of 29%. We also observed positive CD31 staining in VEGF-free controls, indicating spontaneous iPSC-endothelial specification in the cultures.

In the 100% HUVEC encapsulation in the collagen hydrogel, vascular network formations found in the hydrogel but the co-culture of both HUVEC and cardiac fibroblast with a 2:1 ratio demonstrated more vascular network formation and more vascular sprouting. However, no vascular network formation or sprouting of the vascular network found 1:1 ratio co-culture.

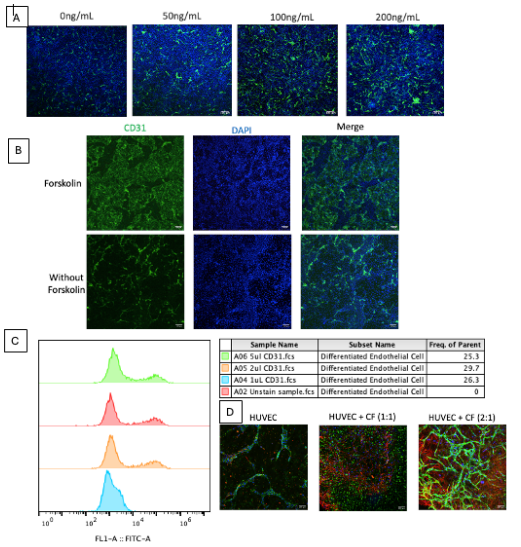

Figure 1. A. Immunofluorescence images of comparison of different concentration of VEGF in endothelial differentiation. B. Immunofluorescence images of the effect of Forskolin in endothelial differentiation. C. Flow analysis of the differentiation efficiency with the presence of Forskolin. D. The encapsulation of both HUVEC and cardiac fibroblast cell in different ratio. (Blue-DAPI, Green-CD31, Red-Vimentin) (Scale Bar- 200µm)

DISCUSSION

The combination of Forskolin and VEGF, demonstrate improved differentiation of iPSCs towards the endothelial lineage specification.[3] Cardiac fibroblast cells secrete ECM components such as collagen type I and fibronectin, which is one of the main ECM contents that play an important role in the capillary stimulator and elongation of vessels. Other than that, the co-culture of cardiac fibroblast also provides support for the capillary-like and helps in the maturation of vasculature.[4]

REFERENCES

1. Song*(et al.)*, *Advance Function Material*, 28:1801331, 2018
2. Devillard & Marquette, *Frontier in Bioengineering and Biotechnology* 9:1-21, 2021.
3. Namkoong*(et al.)*, Cell Signaling 21:906-915, 2009.
4. Costa-Almeida*(et al.)*, *Tissue Engineering* 21:1055-1065, 2015.
5. Pavlova*(et al.)*, Methods in Molecular Biology 2549:169-186, 2022.

3D-PRINTING OF ELECTROCONDUCTIVE MXENE-BASED MICROSTRUCTURES IN A BIOMIMETIC TISSUE ENGINEERING SCAFFOLD DIRECTS AND ENHANCES ELECTRICAL

Ian Woods[1,2], Dahnan Spurling[3], Sandra Sunil[1], Jack Maughan [1,2,4], Javier Guttierez-Gonzales [1,2,3], Tara McGuire[1,2], Liam Leahy[1,2], Adrian Dervan [1,2], Valeria Nicolosi[3], Fergal J O'Brien[1,2,5*]

[1]Tissue Engineering Research Group, Royal College of Surgeons in Ireland (RCSI)
[2]Advanced Materials and Bioengineering Research (AMBER) Centre, RCSI/TCD
[3]School of Chemistry, Centre for Research on Adaptive Nanostructures and Nanodevices (CRANN)
[4]School of Physics, University of Dublin, Trinity College Dublin (TCD), Ireland
[5]Trinity Centre for Biomedical Engineering, Trinity College Dublin (TCD), Ireland
*** E-mail: fjobrien@rcsi.ie**

INTRODUCTION

Neurotrauma leads to the disruption of neuronal connections, inflammation and repair-inhibitive scarring and no effective treatment currently exists. The multifaceted therapeutic benefits of electrical stimulation of neural tissues present opportunities to develop multifunctional electroactive tissue engineering scaffolds for neurotrauma repair. We hypothesized that the microstructure an electroconductive scaffold could be designed to enhance delivery of electroactive signalling to drive neural repair. Our aim was to 3D-print tunable conductive microstructures capable of enhanced delivery of electrical stimulation, by functionalizing melt-electrowritten polycaprolactone (PCL) microfibre structures with highly conductive 2D MXene (Ti3C2TX) nanosheets. These electroconductive microstructures were then incorporated into a previously developed macroporous scaffold consisting of hyaluronic acid (HA) functionalized with neurotrophic proteins [1]. The capacity of these novel composite scaffolds to enhance the delivery of electrical stimulation to neurons and neurospheres was then examined.

MATERIALS AND METHODS

Multilayer Ti3C2Tx MXenes were etched from Al-rich Ti3AlC2 MAX phase and dispersed into delaminated sheets and centrifuged to form a concentrated MXene ink (Fig.1(A)). To 3D-print conductive microstructures, a microfibrous PCL mesh was melt-electrowritten (MEW) with a rectilinear pattern containing fibre spacings of 500, 750 and 1000 μm (corresponding to High, Medium and Low fibre densities, respectively) and then functionalized with the MXene ink to form a conductive composite MXene/PCL structure (B). These 3D-printed microstructures of varying fibre density were then embedded within the neurotrophic HA-based matrix (ECM), containing collagen type-IV and fibronectin, to produce soft, biomimetic (0.6 - 3.25 kPA) composite MXene-ECM scaffolds (C). The MXene-ECM scaffolds were then seeded with human neuronal cells or murine stem cell-derived neurospheres and electrically stimulated in for up to 7 days.

RESULTS

The electroconductive properties of the MEW MXene/PCL microstructures were highly tunable through changing fiber density and MXene content (0.081±0.053 - 18.87±2.94 S/m) and exhibited electrochemical properties equivalent to metallic electrodes. Neurons exhibited significantly increased neurite length (a 1.47 ± 0.14-fold increase) following electrical stimulation (200 mV/mm) within the MXene-ECM scaffolds. Stem cell-derived neurospheres, electrically stimulated on MXene-ECM composite scaffolds with higher microfibre densities, exhibited a >2-fold ($p<0.05$) increase in maximum axonal length compared to lower density scaffolds (Fig.1(D)) and increased expression of βIII-tubulin, a marker of neuronal differentiation.

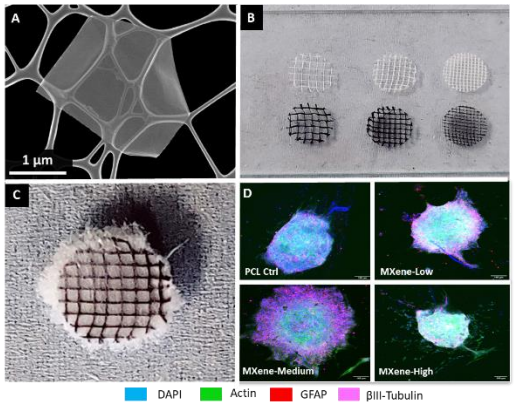

Figure 1 Electroactive MXene-HA Composite Scaffolds. (A) 2D MXene nanosheets. (B) PCL & MXene/PCL MEW microstructures (C) MXene-HA Scaffold. (D) Neurospheres electrically stimulated on MXene-HA scaffolds.

DISCUSSION

This study describes the incorporation of a highly conductive nanocomposite microstructure within a neurotrophic and immunomodulatory biomimetic scaffold, producing a novel multifunctional tissue engineering implant capable of driving key repair-relevant behaviours in neurons and neuronal stem cells by enhancing the therapeutic characteristics of exogenous electrical stimulation. Furthermore, these findings indicate that the spatial organization of conductive materials plays an essential role in regulating repair-critical cellular responses to electrical stimulation and demonstrates the broad therapeutic potential of 3D-printable electroconductive scaffolds

REFERENCES

[1] Woods *et al.* Adv Healthcare Mats 11, 2101663, 2022.

IN VITRO OSTEOCYTOGENESIS FROM HUMAN BONE MARROW-DERIVED MESENCHYMAL STEM CELLS: TOWARDS A BIOMIMETIC HUMAN BONE-ON-CHIP

Madden, L.[1,2], **Milazzo, R.**[1], **Kelly, D.J.**[1,2], **Hoey, D.A.**[1,2]
[1] Trinity Centre for Biomedical Engineering, School of Engineering, TCD
[2] Advanced Materials and Bioengineering Research Centre (AMBER), Ireland.
email: maddenlu@tcd.ie

INTRODUCTION

Bone is a dynamic, multifaceted tissue with an array of unique cell types which play significant roles in maintaining homeostasis and facilitating the adaptation of bone tissue to mechanical stress. Of these cell types, the osteocyte represents 90% of total cells and is considered the "master signaller" of the tissue, signalling other bone cells to control the deposition and resorption of the mineralised extracellular matrix (ECM), thereby maintaining a delicate balance [1]. Disruption of this balance is known to be a leading mechanism in life-changing diseases such as osteoporosis and osteoarthritis. The search for effective cures for these diseases has proven challenging, largely due to the lack of effective models of bone tissue [2]. Animal models do not fully recapitulate the human bone environment, while current *in vitro* models do not incorporate human osteocytes due to the difficulty of isolating or differentiating these cells, limiting their ability to mimic the bone environment. Organ-on-chip and microtissues offer two possible improvements on current models, both more accurately mimicking the 3D environment of bone tissue, but both face similar issues of available cell type. Therefore, a method for the differentiation of osteocytes from human mesenchymal stem cells (hMSCs) would allow for the development of a more biomimetic *in vitro* model of human bone tissue for testing of therapeutics for bone diseases. We aim to investigate the use of collagen type I and nanoneedle hydroxyapatite (nnHA) to create a biomimetic scaffold for osteocytogenesis from hMSCs, to develop an osteocytic bone-on-chip model, as well as microtissues of human osteocytic bone tissue.

MATERIALS AND METHODS

Briefly, a collagen type I gel working solution (8 mg/mL) was made according to the manufacturer's protocol, and nnHA (0.27 mg/mL) and human MSCs ($2x10^6$ cells/mL) were incorporated. Gel suspension was then pipetted into cylindrical silicone moulds (⌀ = 6.25 mm, h = 2mm) and crosslinked at 37 °C for 60 minutes. Constructs were then cultured in osteogenically-supplemented culture media (100 nM dexamethasone, 10 mM β-glycerol phosphate, 0.05 mM ascorbic acid) for 1, 21, or 42 days. Constructs were cryoembedded, sliced at 10 µm thickness, and stained for alizarin red or immunofluorescence. Constructs were also lysed and reverse transcribed for analysis by RT-qPCR.

RESULTS

Mineralisation was observed in samples at D21 by alizarin red staining (Figure 1A). As ECM mineralised, dendrite formation marker E11 was expressed at D21 and was limited at D42 (Figure 1B). These results were corroborated by RT-qPCR, which showed upregulation of osteocyte markers DKK1, SOST, and MEPE at D42 (Figure 1C). Upregulation of mature osteocyte markers SOST and MEPE indicate the presence of a mature osteocytic phenotype at D42 and the capacity of the osteocytes to regulate bone homeostasis.

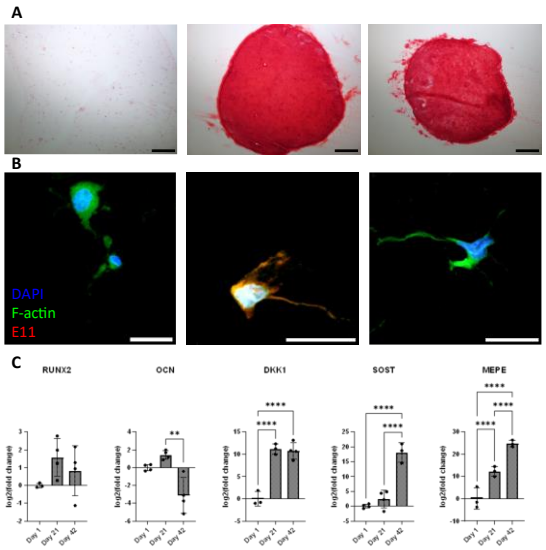

Figure 1 Mineralisation and osteocytogenesis of constructs were assessed at days 1, 21, and 42. (A) Alizarin red staining of constructs at timepoints. Scale bar = 500 µm. (B) Immunofluorescence staining of constructs. Scale bar = 20 µm. (C) Log_2 of relative gene expression of constructs. * $p \leq 0.05$, ** $p \leq 0.01$, *** $p \leq 0.001$, **** $p \leq 0.0001$.

DISCUSSION

A collagen-nnHA scaffold has been demonstrated to give rise to an early and mature osteocytic phenotype after 21 and 42 days, respectively. These findings represent the capacity for this scaffold system to be used to create *in vitro* models of bone tissue including human osteocytes in a scalable fashion. As a hydrogel, the scaffold may be used in a microfluidic chip or used to create microgels, which may then mature into bone microtissues, which is the focus of current work. This scaffold will potentially allow for the creation of healthy and diseased models of human bone in a variety of forms.

REFERENCES

1. Schaffler et al., Cacified Tissue International, Volume 94, pg. 5-24, 2013
2. Cope et al., Osteoarthritis Cartilage, p. 230-239. 2019.

OVX-INDUCED BONE LOSS AT DIFFERENT SKELETAL SITES IN A PRECLINICAL MODEL OF OSTEOPOROSIS

Uberti, M.[1,2,3], **Intini, C.**[1,2,3], **Matheson, A.**[1,2,3], **Brunetti, G.**[1,2,3], **Hodgkinson, T.**[1,2,3], **Kennedy, O.D.**[1,2,3]
[1] Tissue Engineering Research Group, Department of Anatomy and Regenerative Medicine, Royal College of Surgeons in Ireland (RCSI), [2]Trinity Centre for Biomedical Engineering, Trinity College Dublin (TCD); [3]Advanced Materials and Bioengineering Research Centre (AMBER), RCSI and TCD.
Email: **michelauberti23@rcsi.com**

INTRODUCTION

Osteoporosis is a disease that affects more than 200 million women worldwide. It is characterised by a systemic impairment of bone mass and quality that can result in fragility fractures (1). The ovariectomized (OVX) rodent model, is a well established experimental model for investigation of postmenopausal osteoporosis due to estrogen deficiency in women. The OVX mouse is an ideal candidate for studying of pathogenesis of postmenopausal osteoporosis, while the OVX rat model is largely used for the evaluation and development of new drug compounds for postmenopausal osteoporosis treatments (2). However, it remains unknown whether bone loss occurs in the same way at different skeletal sites in these models. Therefore, the aim of this study was to assess bone changes, in particular trabecular microarchitecture by microCT and histology at tibial, vertebral and patellar site in a rodent model of osteoporosis.

MATERIALS AND METHODS

Female Sprague Dawley rats 26 weeks old were divded into control (n=8) and OVX (n=8) groups, where OVX surgery was carried out at 11-12 weeks. After sacrifice, samples from different skeletal sites were harvested, fixed and then scanned using a standard benchtop microCT. Imaging software CTAn version 1.16 was used to measure the bone microstructural parameters OVX. Samples were then decalcified, embedded in paraffin and sectioned to 10µm thickness, deparaffinised and then stained using Haematoxylin & Eosin (H&E), Masson Goldner's Trichome and Tartrate-resistant acid phosphatase (TRAP) for qualitative analysis.

RESULTS

Overall, the results demonstrated that all OVX samples exhibited significantly lower mineralized bone content compared to controls. OVX tibia, vertebra, patella showed decreased BV/TV [%], Tb.N [1/mm], and Tb.sp [um] in comparison to their respective healthy counterparts (Figure 1). Furthermore, histological assessment confirmed the trends observed in BV/TV analysis.

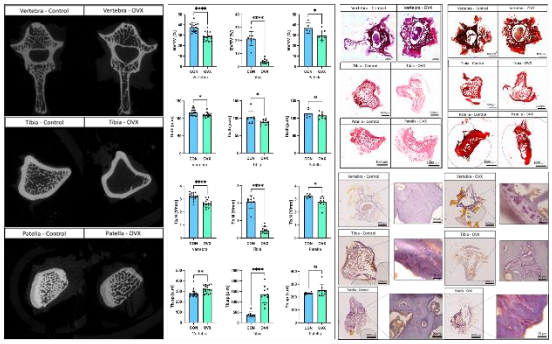

Figure 1 Images collected by using µCT; measuring of BV/TV [%], Tb.Th [um], Tb.N [1/mm], Tb.sp [um] of control and OVX tibia, vertebra, patella; histological confirmation.

DISCUSSION

This study underscores the unique impact of osteoporosis on bone specimens isolated from vertebra, tibia and patella. The findings from our analysis, which were validated by histological evaluation, showed that bone loss is most pronounced in proximal tibia while patella is comparatively less affected. Specifically, it is similar to that of the vertebral body. This discovery is significant as patellae are relatively less complex than long bones and vertebrae, making it easier to isolate for experimental studies. Furthermore, this study suggests that the patella could serve as a new model for studying osteoporosis-related bone loss, especially in terms of mechanotransduction and potentially other processes like bone-cartilage crosstalk. These results underline how osteoporosis afflicts in different intensities various bone locations, suggesting that clinical pretreatments might need to consider tibia bone more than others.

REFERENCES

(1) Tilman DR et al., Osteoporosis: now and the future, The Lancet, (2011) (2) Inada M et al., Animal models for bone and joint disease. Ovariectomized and orchidectomized animals, Clinical Calcium, (2011)

Proteomic and transcriptomic characterization of human testicular tissue to inform the development of preclinical models for restoring male fertility

Gashti, Nasrin[1,2], Andersson, Isabel[1,2], Padacherri, Jishnu[1,2], Henry, Michael[3], Meleady, Paula[3], O'Meara, Sorcha[4], Wittschier, Jacqueline[5], Cullen, Ivor[4], Hess, Jochen[5], Cunnane, Eoghan[1,2]

(1) Biomaterials Cluster, Bernal Institute, University of Limerick, Limerick, Ireland; (2) School of Engineering, University of Limerick, Limerick Ireland; (3) National Institute for Cellular Biotechnology, Dublin City University; (4) Department of Urology, Beaumont Hospital, Dublin, Ireland; (5) Department of Urology, University Hospital Essen, University Duisburg-Essen, Essen, Germany.

Email: Nasrin.GhanamiGashti@ul.ie

Introduction

Preclinical models of the human testes are the most appropriate tools for addressing the growing burden of male fertility. However, current models fail to accurately represent testicular tissue and do not mimic natural testicular functions. Methods that combine ECM-mimicking hydrogels and primary cells can generate models that better represent the native tissue[1] compared to existing models. However, the cell and ECM composition of testis tissue must be comprehensively characterized in order to provide an accurate baseline for representative models. This study therefore characterizes human testicular tissue using liquid chromatography with tandem mass spectrometry (LC-MS/MS) and bulk RNA barcoding and sequencing (BRB-seq) to inform the development of models aimed at restoring male fertility.

Materials and Methods

Human testicular samples were obtained from gender affirmation patients (Essen, Germany) and surgical sperm retrieval patients (Dublin, Ireland). Histopathological analysis was performed using H&E staining, assigning a Johnson's score for spermatogenesis status, and ECM specific stains including Picrosirius Red, Masson's trichrome, and Movat's Pentachrome to access connective tissue components such as collagen, elastin, mucin, fibrin and muscle. Testicular samples were prepared using PreOmics® iST sample preparation kit and QIAGEN RNeasy Plus Mini Kit for LC-MS/MS and BRB-seq, respectively. LC-MS/MS was performed by Dionex Ultimate 3000 RSLC and Orbitrap Tribrid Fusion MS (Dublin City University). BRB-seq has been performed by SciLicium, Rennes, France.

Results

Based on the histopathological analysis, testicular samples were categorized into 6 subtypes: 1) Normal spermatogenesis, 2) Arrested spermatogenesis without thickening of seminiferous tubule basement membrane, 3) Arrested, slightly thickened, 4) Arrested, thickened, 5) Complete hyalinization of seminiferous tubules, 6) Sertoli cell only syndrome. This diverse cohort of testicular samples presents different histological morphology after staining (Fig 1A, B, C, D). LC-MS/MS and BRB-seq analysis provides a detailed understanding of cell and ECM differences in these pathological subtypes. Results show a significant difference in proteomic and transcriptomic profile of testicular samples with different pathological status (Fig 1E).

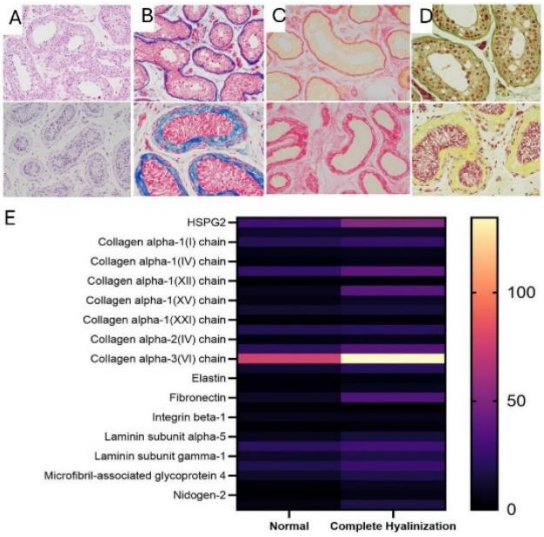

Figure 1 Histopathological analysis of testicular tissue: A) H&E, B) Masson's trichrome, C) Picrosirius Red, D) Pentachrome. E) LC-MS/MS data showing ECM proteins profile based on spectral counts that represent relative protein concentrations in normal and complete hyalinization groups.

Discussion: Representative models of the human testis should mimic the testicular microenvironment and simulate physiological conditions to effectively maintain testicular cells in culture. The development of such models can utilise primary testicular cells and ECM-mimicking hydrogels, both of which can be derived from human testis tissue. Healthy human testes are difficult to obtain for research purposes, while testicular samples from gender affirming cases represent a source of whole testis that is otherwise considered surgical waste. These patients are treated with anti-androgens and oestrogens prior to surgery that can cause spermatogenic impairment in testes. The histopathological findings of this study show that some samples still exhibit normal spermatogenesis. However, most samples exhibit impaired spermatogenesis. LC-MS/MS and BRB-seq analysis demonstrates that testicular samples with different pathological status have significantly different proteomic and transcriptomic profiles. Therefore, samples with normal and arrested spermatogenesis (without thickening) are recommended for use in model development.

References: Horvath-Pereira BO, et al. Front Endocrinol (Lausanne). 14:1085872. Mar 2023.

ELUCIDATING THE EFFECT OF DIRECT AND INDIRECT HELIUM COLD ATMOSPHERIC PRESSURE PLASMA ON ADIPOSE DERIVED IMMORTALISED MESENCHYMAL STEM CELLS

Alsiyabi, Sara.[1], Boehm, Daniela.[2]
[1] University College Dublin, School of Chemical and Bioprocess Engineering
[2] University College Dublin, School of Chemical and Bioprocess Engineering
email: sara.a.alsiyabi@ucdconnect.ie

INTRODUCTION

Mesenchymal Stem Cells (MSCs) are multipotent cells that have the ability to self-renew and to differentiate into multiple lineages. Due to their capabilities, MSCs have been intensely researched as a potential regenerative therapeutic agent [1]. Cold Atmospheric Plasma (CAP), a partially ionized gas that contains electrons, electromagnetic fields, UV and Reactive Oxygen and Nitrogen Species (RONS) has wide applications in medicine, which include wound healing, bactericidal effects as well as its ability to promote cell proliferation [2]. This study aims to investigate the effect of CAP, and plasma-activated media (PAM) on Human Adipose-Derived Immortalised Mesenchymal Stem Cell (AD-MSC) proliferation.

MATERIALS AND METHODS

Experiments were conducted using ASC52telo-hTERT MSCs (ATCC). Plasma treatment was performed using a helium-based Atmospheric Pressure Plasma Jet (APPJ) device (J-Plasma, Apyx Medical). Reactive species generated by the plasma system were characterized through quantification of total oxidative species, H2O2, and nitrites generated in water at different exposure times. For direct CAP experiments, cells were exposed directly to plasma at different parameters or indirectly through treatment with PAM. The effect of medium conditioned by plasma-treated cells on untreated cells was also assessed. Cell responses were quantified as metabolic activity and cell mass using resazurin and crystal violet, respectively. Long-term repopulation capacity was measured using clonogenic analysis.

RESULTS

Cells showed a treatment-time dependent response to plasma exposure. At higher exposure times, cells exhibited a loss of metabolic activity and eventual cell death, compared to shorter exposure times (<30s), which showed low cytotoxic effects on MSCs. This finding determined that treatment durations of less than 30 seconds represent a safe window for plasma application (Fig.1). Treatments with both PAM and conditioned media illustrated less cytotoxicity towards the cells, indicating that the long-lived reactive species play a lesser role in the cellular response. Exposure to conditioned medium provided indication on cell signaling factors which may be secreted by cells in response to plasma treatment.

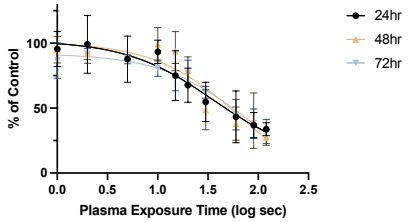

Figure 1 Dose-response curve showing plasma treatment time-dependent decrease in hTERT-MSCs metabolic activity with increasing exposure time. Metabolic activity was determined 24, 48 and 72h after plasma treatment using the resazurin assay and is presented in comparison to untreated cells.

DISCUSSION

Plasma exerts its effect on cells through a combination of its physical and chemical attributes. Eliminating direct contact with plasma enhances cell survival and reduces CAP's cytotoxic effects. The findings presented here may help to optimize treatment parameters for non-toxic treatments that may be used to stimulate growth or modulate MSC behaviour.

REFERENCES

PITTENGER (ET AL.), REGENERATIVE MEDICINE, 4: 1-15, 2019.

BRANÝ (ET AL.), INTERNATIONAL JOURNAL OF MOLECULAR MEDICINE, 21, 29-30, 2020.

ADVANCING INTERVERTEBRAL DISC REGENERATION: A COMPARATIVE STUDY OF DUAL MIRNA STIMULATED NUCLEUS PULPOSUS AND BONE MARROW-DERIVED STEM CELLS

Ní Néill, T[1,2], Wilson, N[1,2], McDonnell, J[1,2], Brama, P.A.J. [1,3], O'Brien, F.J.[1,2,4,5], Dixon, J.E.[6,7], Curtin, C.M.[1,4,5], Buckley, C.T.[1,2,4,5]

email: nnillt@tcd.ie

[1]Trinity Centre for Biomedical Engineering, TBSI, Trinity College Dublin (TCD), Ireland [2]MMBE, School of Engineering, TCD, Ireland, [3]School of Veterinary Medicine, University College Dublin, Ireland, [4]AMBER Centre, Royal College of Surgeons (RCSI) & TCD, Ireland, [5]Tissue Engineering Research Group, Department of Anatomy and Regenerative Medicine, RCSI, Ireland, [6]Regenerative Medicine and Cellular Therapies, The University of Nottingham Biodiscovery Institute (BDI), University of Nottingham, UK, [7]NIHR Nottingham Biomedical Research Centre, University of Nottingham, UK

INTRODUCTION

Introducing nucleic acids, such as microRNAs (miRNAs), into degenerated intervertebral discs may enhance the regenerative potential of cells by regulating catabolic and inflammatory signals in the native microenvironment. Both nucleus pulposus (NP) and bone marrow-derived stem cells (BMSCs) offer unique benefits and limitations for cell-based treatments. Here we employed pro-discogenic miRNA-149-5p mimic and miRNA-221-3p inhibitor, complexed with the cell penetrating peptide GET-FLR [1] for successful delivery, in monolayer and microtissue cultures, to evaluate the response of anabolic and catabolic markers.

MATERIALS AND METHODS

Goat NP and BMSCs were isolated as previously described [2]. For all experiments, cells were seeded, allowed to attach overnight, followed by serum starvation and TNF-α (50 ng/µl) and IL-1β (10 ng/µl) treatment, both for 24 hours. miRNA dosage in 2D was determined by delivery of a fluorescently tagged miRNA, with internalisation assessed using flow cytometry and confocal microscopy. All monolayer experiments evaluated protein expression 3 days post-transfection. For microtissue cultures, cells were prepared for transfection as before, with microtissues of 50,000 cells formed and assessed histologically, biochemically, and with immunofluorescence at day 3 and 14 of culture. Protein expression of 2 and 3D cultures incorporating anabolic and catabolic markers was assessed. Differences between groups were assessed by one and two-way ANOVA with Tukey's multiple comparisons test using GraphPad Prism 10.2.3, with *p* values <0.05 considered to be significant.

RESULTS

Fluorescent miRNA internalisation was significantly upregulated for both cell types at doses above 5 ng/µl ($p < 0.001$). Modest differences in 2D were evident in matrix markers, however expression of ADAMTS5 was significantly higher in transfected BMSCs compared to miRNA-pair NP cells ($p = 0.016$). MMP13 expression was increased in miRNA stimulated cells. Trends of increased collagen deposition in transfected BMSCs were also detected ($p = 0.075$, Fig. 1A).Sulphated glycosaminoglycans (sGAGs) were upregulated across all conditions at culture cessation ($p < 0.05$, Fig. 1B), and evidence of a trend in SOX9 expression in miRNA-BMSCs was identified ($p=0.057$). Regarding catabolic enzymes, ADAMTS5 was again significantly elevated in miRNA-BMSCs compared to miRNA-NP ($p = 0.017$, Fig. 1C), with a trend towards elevation compared to the NT group ($p = 0.064$). Likewise, IL-1β expression was significantly upregulated in miRNA-BMSCs compared to all other groups ($p < 0.05$, Fid. 1D).

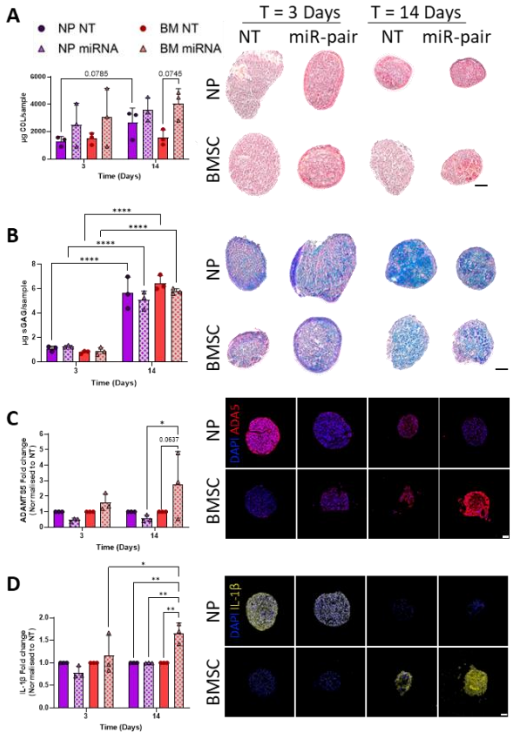

Figure 1. A. Microtissue culture collagen deposition. **B.** 3D sGAGs production**. C.** ADAMTS5 protein expression. **D.** IL-1β protein expression. Scale bars 50 µm. N = 3 independent biological replicated. Data displayed as mean ± SD.

DISCUSSION

This study established a foundation for identifying the most appropriate cell source to facilitate regeneration following miRNA stimulation. There are indications of increased anti-catabolic protein expression in NP cells after transfection compared to their BMSC counterparts. Future research will explore goat ex vivo organ culture models to examine differences within a more physiologically relevant system.

REFERENCES

[1] Blockpoel Ferraras et al. ACS Applied. Nano Materials 4, 2021. [2] McDonnell et al, JOR Spine 6(3), e1279 2023. [3] Barcellona et al., Advanced NanoBiomed Research, 4(7), 2024.

ACKNOWLEDGEMENTS

This work was supported by the European Research Council (ERC-2019-CoG-864104: INTEGRATE).

Development of a Tissue Model Replicating the Microstructure, Mechanical Response, and Vasoactivity of Aged Human Arterial Tissue

Pulipaka, B.[1,2,5], Lally, C.[1,2,3], McCulloch, A. [4], Walkingshaw, J.[5], Tornifoglio, B.[1,2]

1. Trinity Centre for Bioengineering, Trinity Biomedical Sciences Institute, Trinity College Dublin
2. Department of Mechanical and Manufacturing Engineering, School of Engineering, Trinity College Dublin
3. Advanced Materials and Bioengineering Research (AMBER) Centre, Royal College of Surgeons in Ireland & Trinity College Dublin
4. Stryker Neurovascular, Research and Development, Fremont, CA, 94538, USA
5. Stryker Neurovascular, Cork

email: pulipakb@tcd.ie; bhavana.pulipaka@stryker.com

INTRODUCTION

Stroke is the second leading cause of death in Europe, causing over one million deaths annually and leading to long-term disability [1]. Its incidence increases sharply with age, rising by a factor of 100 between 40 and 80 years. Ischemic stroke, caused by clots in cerebral vessels, accounts for 55 to 90% of cases [2]. Current treatment options for ischemic strokes include thrombolysis and thrombectomy. However, the effects of these procedures on cerebral vessel function remain unclear [3].

Cerebral arteries and arterioles are structured in three layers: the tunica intima, which contains endothelial cells and the internal elastic lamina (IEL); the tunica media, composed of smooth muscle cells (SMCs), elastin, and collagen; and the tunica adventitia, primarily made of collagen fibres, fibroblasts, and perivascular nerves. Unlike systemic arteries, cerebral arteries lack an external elastic lamina and have fewer elastic fibres, resulting in a thinner adventitia [4]. Aging impacts these structures significantly, particularly in the intima, where the IEL thickens, and the luminal surface becomes irregular. The tunica media may experience fragmentation and degeneration of elastic fibres, along with decreased SMCs and increased collagen and acid mucopolysaccharides [5][6].

Currently, no tissue model exists which captures the complexities of cerebrovascular structure and function for studying device-tissue interactions [7]. As ischemic strokes predominantly affect older individuals, developing an aged arterial model is essential to better investigate the interactions between devices and arterial tissue, ultimately facilitating improved device design. The primary objective of this study is to characterise the differences between healthy and aged arterial tissue to develop an accurate model of aged tissue.

MATERIALS AND METHODS

In order to develop methods which will be used on harvested cerebral arteries, cryopreserved porcine carotid arteries were thawed and fixed in 4% paraformaldehyde to preserve tissue structure. After fixation, the arteries were sectioned into 5 mm segments, processed, and embedded in paraffin wax. The tissue was then sliced into 8 µm sections using a microtome. These sections were mounted on glass slides and stained with haematoxylin and eosin (H&E), allowing for the visualisation of the cellular and structural components of the different layers of the arterial tissue.

RESULTS

Figure 1 presents an H&E-stained axial section of the native porcine carotid artery, which reveals the distinct structural organisation of the arterial wall. The three layers—the tunica intima, tunica media, and tunica adventitia—can be identified.

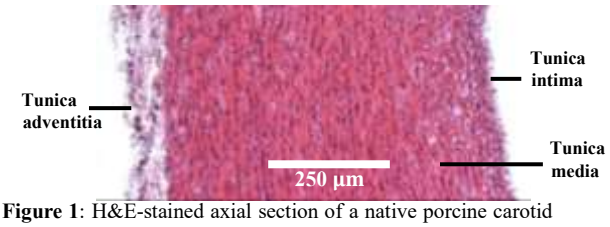

Figure 1: H&E-stained axial section of a native porcine carotid artery.

DISCUSSION

Future work will aim to characterise cell density in porcine cerebral arteries and examine how it correlates with vasoactivity. This will involve mechanical testing, where the responses of the arterial tissue to vasoconstrictors and vasodilators will be compared against cell density measurements. These findings will contribute to the development of an arterial model that replicates the mechanical and vasoactive properties of aged human cerebral tissue.

REFERENCES

[1] Aguiar de Sousa, D. et al., Eur Stroke J, 8:618-628, 2023.
[2] Béjot, Y. et al., La Presse Méd, 45: e391-e398, 2016.
[3] Hurd, M. D. et al., Regenerative Ther, 18: 408-417, 2021.
[4] Cipolla, M. J., Colloquium Series on Integrated Systems Physiology, 1: 1-59, 2009.
[5] Klassen, A. C. et al., J Neuropathol Exp Neurol, 27: 621-642, 1968.
[6] Nanda, B. S. & Getty, R., Exp Gerontol, 6: 453-460, 1971.
[7] Liu, Y. et al., J NeuroInterv Surg, 13: 816-822, 2021.

ACKNOWLEDGEMENTS

This project has received funding from the Irish Research Council (IRC) under the Employment-based Postgraduate Programme 2024.

SIMULATION OF GUIDEWIRE TORQUABILITY

Cummins, C.[1], Clancy M.[2] Dickenson, R.C.[3], Ronan, W.[1]
[1] School of Engineering, University of Galway
[2] Integer Holdings Corporation, Parkmore, Galway
[3] Integer Holdings Corporation, Salem VA, USA
email: william.ronan@universityofgawlay.ie

INTRODUCTION

Guidewires are long, slender, flexible devices with a metal core that are used to navigate through complex networks of blood vessels to enable the placement of medical devices. In some instances, the guidewire can exhibit undesirable phenomena such as "lag" and "whip", where the movement input by the surgeon proximally is not transferred to the distal end of the device during a procedure. This severely impedes the correct use of the guidewire and can lead to damage of the surrounding tissues, especially in critical areas, where blood vessels could be torn or burst [1]. The relationship between the inherent material properties, the geometry of the pathway and these wire phenomena are poorly understood. Previous studies have shown the influence of material phenomena such as plasticity in steels and phase transformation in Nitinol [2,3,4]

In this study, the influence of material properties and guidewire microstructure on guidewire performance in complex tortuous paths is explored. Computational modelling, supported by experimental testing is carried out to analyse these devices and uncover key material mechanisms that cause the unwanted behaviours.

MATERIALS AND METHODS

FEA modelling using Abaqus/Standard (2023) is carried out to simulate the wire in an anatomically relevant path (Fig. 1A). Elastic-plastic (with linear strain hardening Fig 1C) and superelastic materials are used which are representative of steel and Nitinol cored guidewires, respectively. R3D4 and C3D8 elements are used with direct, frictionless contact with a rigid path. Boundary conditions guide the wire and, once the wire has traversed the path, a rotation is applied to the proximal end of the wire. The output rotation at the distal end is recorded. A benchtop experiment will validate the results of the computational model. The influence of material and geometric parameters is then explored: the length of the curved section is controlled by varying the angle ϕ (as shown in Fig. 1A) from $\pi/2 \rightarrow 4\pi$ and the radius of curvature R is varied relative to the wire diameter r with different lengths for the straight section L

RESULTS

The model successfully captures the lag and whip phenomena. When comparing perfectly elastic to perfectly plastic materials, lag builds up as the wire rotates due to plastic dissipation. In a linear hardening plasticity model (Fig. 1B), the whip response occurs as plastic dissipation reduces due to hardening, after which, the rotational response matches the input rotation. Similarly, dissipation during austenite to martensite transformations in Nitinol cause lag and whip (Fig. 1D)

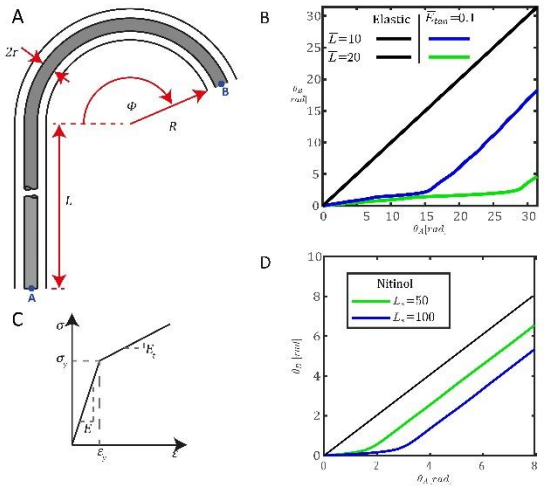

Figure 1 A. Diagram of computational model. B. Effect of wire length on lag and whip phenomena. C. Linear hardening material model. D. Graph of output angle vs input angle for Nitinol materials

DISCUSSION

The lag and whip phenomena can be seen in the computational models, showing their value for better understanding these devices. By changing variables such as curve angle and radius, and wire length and diameter a better understanding of these material properties can be gained leading to improved manoeuvrability and control of the guidewires. Comparing these simulations to benchtop testing can validate the models. By experimenting with different path geometries and recording the rotational response throughout the wire, in both experimental and computational models, a greater understanding of the causes of these phenomena is possible.

ACKNOWLEDGEMENTS

This project received funding from the IRC Enterprise Postgraduate Scheme 2024 (EPSPG/2024/2136)

REFERENCES

1. Tóth (et al.) *Heart* 101, no. 8 (2015): 645-652.
2. Ronan (et al.), Eur. J. of Mechanics, 102:105101, 2023
3. Shirazi (et al.), JMPS, 151:104405, 2021
4. Sutou (et al.), Minimally Invasive Therapy & Allied Technologies 15: 204–208, 2006.

A FINITE ELEMENT MODEL FOR CRIMPING AND FREE DEPLOYMENT IN THE DESIGN OF BIOABSORBABLE METALLIC CORONARY STENTS

Blunda, D.[1], Vaughan, T.J.[1]
[1]Biomedical Engineering, School of Engineering, College of Science and Engineering, University of Galway
email: diego.blunda@universityofgalway.ie

INTRODUCTION

Cardiovascular diseases (CVDs) are the leading global cause of death[1], with myocardial infarction, due to coronary artery occlusion, being a common manifestation[1]. Percutaneous Transluminal Coronary Angioplasty (PTCA) with drug-eluting stents (DES) is the current standard treatment to prevent infarction. While effective, DESs pose risks such as chronic inflammation, late thrombosis and restenosis due to their permanent presence in the body[2,3]. Bioresorbable stents, which degrade over time, offer a promising alternative by providing temporary support until the vessel heals and re-endothelializes[3]. Magnesium is a promising material for bioabsorbable stents, but its lower mechanical strength compared to DESs and manufacturing challenges necessitate innovative design solutions. This study focuses on the design and optimization of a thin-strut Mg/Zn bioresorbable coronary stent, with the first phase developing a crimping and free deployment finite element model (FEM) to analyze the impact of geometric parameters on stent performance.

MATERIALS AND METHODS

To develop the crimping and free deployment FEM, the Abaqus finite element solver was used. Figure 1 illustrates the process, involving several components: an internal rigid shaft (simulating the catheter), a folded balloon, the stent, and crimping tools. The shaft was modelled as a hollow 3D cylinder with a stiff linear elastic material behaviour (E = 1000 GPa, ν = 0.3). The balloon's geometry, based on previous simulations similar to the one described by Geith et al.[4] was modelled using a hyperelastic (1st order Ogden) material, with parameters fitted from nylon testing.
The stent geometry, derived from an open-source model, featured a close-cell design and was assigned an elasto-plastic material model to simulate magnesium WE43 (E = 44.7 GPa, ν = 0.3)[5]. The crimping tools (n = 12) were modelled as rectangular rigid bodies.
The simulation consisted of four steps: in the first step, the crimping tools crimp the stent onto the folded balloon; in the second step, the crimping tools were removed; in the third step, the stent was deployed by inflating the balloon (applying positive pressure to the internal surface); and in the fourth step, the balloon was deflated, allowing for the observation of stent recoil. The simulation was performed using the SIMULIA Abaqus FEA explicit solver.

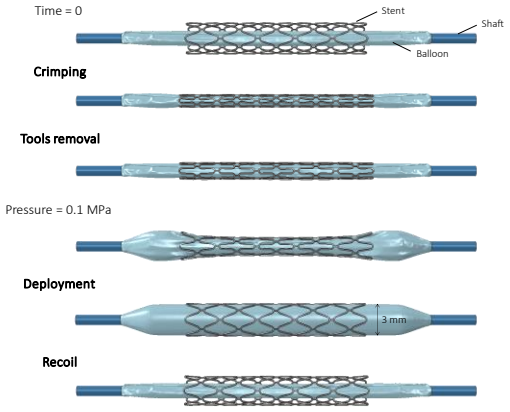

Figure 1 Assembly components, key steps (in bold), and important time points in the crimping and free deployment simulation.

RESULTS

The simulation results showed that the stent was effectively crimped onto the balloon, undergoing plastic deformation. In the second step, the stent recovered its elastic deformation. The stent was expanded to a maximum internal diameter of approximately 3 mm, which resulted in a peak Von Mises stress of 357 MPa. Finally, during the last step, the overall stent recoil was approximately 10%.

DISCUSSION

This study demonstrated an efficient and rigorous FEM for crimping and deployment, which will be further refined and utilized to design and optimize a biodegradable coronary stent design. As observed, the stent recoil value of 10% is higher than the typical 5% threshold for most DESs, indicating that design optimization will be essential to improve the mechanical performance.

REFERENCES

[1] WHO, Cardiovascular diseases (CVDs) Fact Sheet, 2021.
[2] Kapoor *et al.*, Materials and Design, 2023.
[3] Udriste *et al.*, Materials, 2021.
[4] Geith *et al.*, International Journal for Numerical Methods in Biomedical Engineering, 2019.
[5] Van Gaalen, Degree of Doctor of Philosophy, University of Galway, 2023.

COMPUTATIONAL MODELLING OF MULTIVARIABLE CONTROL OF CLOSED-LOOP DEEP BRAIN STIMULATION

Seda, Aksoy.[1], **Jakub, Orłowski.**[1], **Madeleine, Lowery.**[1]
[1] University College Dublin
seda.aksoy@ucdconnect.ie

INTRODUCTION

Deep brain stimulation (DBS) delivers continuous electrical stimulation to specific brain targets to manage motor symptoms of neurological disorders, including Parkinson's disease [1]. Currently, stimulation is delivered in a continuous manner, with stimulus parameters remaining fixed overtime. Conventional DBS systems, therefore, can not adapt to fluctuating symptoms, leading to periods of under- or over-stimulation, which can exacerbate bradykinesia or dyskinesia. They also struggle to modify parameters in response to disease progression. Adaptive DBS systems offer the potential to address these limitations by using real-time biomarkers to adjust the stimulus parameters automatically. Adaptive or closed-loop DBS uses measurable neural signals, or biomarkers, to indicate the patient's current symptom state, allowing the system to evaluate and adjust stimulation parameters automatically. This dynamic adjustment aims to better align the therapy with patients' needs by optimizing stimulation parameters such as amplitude and frequency [2]. Adaptive DBS systems investigated to-date have focused on single-variable control, which is insufficient to handle Parkinson's dynamic profile [3–5].

Emerging evidence underscores the promise of multivariable adaptive control systems that integrate multiple biomarkers for personalized and responsive DBS [2]. Such systems could improve symptom management, enhance battery efficiency, and better adapt to disease progression in real-life settings. To achieve this, our study proposes the design of a multiple-input-multiple-output (MIMO) system for closed-loop DBS.

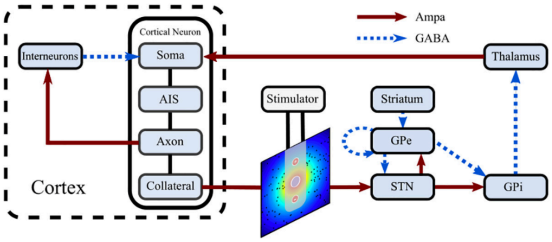

Figure 1 Corticobasal Ganglia Network Model [2]

METHODS AND MATERIALS

The corticobasal ganglia network model [2], illustrated in Figure 1, serves as the foundation for incorporating new biomarkers and developing a multivariable control system for DBS. This model captures the key pathways and interactions between regions involved in motor control, including the cortex, striatum, globus pallidus externus (GPe), globus pallidus internus (GPi), subthalamic nucleus (STN), and thalamus. Within the cortex, interneurons provide inhibitory inputs to modulate cortical neuron activity, which then projects excitatory signals to the basal ganglia network. The striatum receives these inputs and relays inhibitory signals to the GPe and GPi. The GPe, in turn, inhibits both the STN and GPi. The STN, an excitatory nucleus, projects excitatory signals to the GPi, which subsequently inhibits the thalamus. Acting as a relay center, the thalamus transmits excitatory feedback to the cortex, thereby completing the neural communication loop essential for motor control. The model is implemented using Python and the NEURON simulation environment, enabling precise computational analysis of neural dynamics and interactions.

DISCUSSION

Using this model, a multivariable control approach for closed-loop DBS will be developed and tested. This system will incorporate additional biomarkers to refine DBS strategies and optimize stimulation parameters for a broader range of Parkinson's disease symptoms. By utilizing multiple inputs and outputs, the proposed system aims to dynamically adjust stimulation in real time, ensuring that the parameters remain optimal for managing the complex and fluctuating nature of Parkinson's symptoms. Furthermore, advanced computational modelling and rigorous experimental validation will strengthen the system's adaptability and reliability, paving the way for its successful translation into clinical applications.

REFERENCES

[1] Kogan et al.,Neurosurgery Clinics 30:137–146, 2019.
[2] Fleming et al., Frontiers in Neuroscience. 14:166, 2020.
[3] Evers et al., Neuromodulation 27:476–488, 2024
[4] Schmidt et al., *Brain* 147:911–922, 2024.
[5]Oehrn et al., *Nat. Med.* 30:3345–3356, 2024.

A REPLENISHABLE THERAPEUTIC PERITONEAL IMPLANT FOR OVARIAN CANCER

Sheedy, A[1,2,3,4], Shetty, M[3,4], Weis, A[3,4], Bendzick, L[3,4], Geller, M[3,4], Felices, M[3,4]*, Dolan, E[1,2]*

[1]Biomedical Engineering, SoE, CSE, University of Galway. [2] CÚRAM, University of Galway. [3] Masonic Cancer Centre, University of Minnesota, [4]Department of Medicine, University of Minnesota.

email: a.sheedy2@universityofgalway.ie

INTRODUCTION

In a 2006 clinical trial (GOG172[1]) for intraperitoneal (IP) delivery of chemotherapy for ovarian cancer, increased median overall survival compared to intravenous (IV) delivery. Yet, only 42% of patients completed the prescribed six rounds of treatment due to catheter related complications[2]. The widespread clinical adoption of IP therapy is limited by complications with repurposed catheters, including blockages, leaks, port and infections. We present a purpose-build, implantable therapeutic platform for the repeated delivery of cellular and biological therapies directly to the peritoneal cavity. Additionally, the implant can sample the peritoneal fluid for minimally invasive monitoring of the IP space.

MATERIALS AND METHODS

A mono-material (thermoplastic polyurethane) implant, featuring a transcutaneous port connected to a catheter and reservoir with 100 µM pores was developed. NSG mice received our peritoneal implant on day-14. On day-3 $1x10^5$ human ovarian cancer cells (DlucOVCAR8) were administered by IP injection. Mice were irradiated (200cGy) on day-1 and tumour burden was monitored weekly with bioluminescence imaging (BLI) using IVIS (PerkinElmer). First, targeted IP delivery through implant was validated using Fluorescent Probe (Genhance) over 21 days. Next, our therapeutic regimen of expanded Natural Killer cells ($5x10^6$ 1/week) + IL-15 (3/week) was delivered via our implant and compared to delivery though a 32G needle (gold standard for IP injection in mice) over 42 days. Finally, peritoneal fluid was collected via the implant and analysed by flow cytometry.

RESULTS

Tumour burden, (BLI, blue line, **Fig. 1A**), increased significantly from day 0 ($1.26 \pm 0.36 \times 10^9$) to 21 ($15.26 \pm 7.34 \times 10^{10}$p/s), while delivery of therapy analogue, Genhance (red line, **Fig. 1A**), remained consistent from day –7 ($2.06 \pm 0.17 \times 10^{11}$) to day 21 ($2.77 \pm 0.80 \times 10^{11}$). This shows that even with increasing tumour burden, therapy can be consistently delivered to the IP space. To directly compare therapeutic regimen (eNK cells + IL-15) delivery modalities, we normalised each BLI reading to its day 0 value and the area under the curve (AUC) was quantified. At day 35 ($p<0.05$) and 42 ($p<0.01$) tumour burden was controlled significantly better when our therapeutic regimen was delivered through our implant compared to IP injection (**Fig. 1B**). BLI on day 7 showed saline control had significantly higher tumour burden than eNK + IL-15 ($p<0.0001$, **Fig. 1C**) and when this was compared to sampled peritoneal fluid, the same trend was observed. Saline control had significantly more DLucOVCAR8 cells compared with eNK + IL-15 (11155±1196 vs 733±119, $p<0.05$ **Fig. 1D**). As expected, $CD56^+$ cells were identified in the eNK + IL-15 group but not saline control group (231±75 and 0, **Fig. 1E).** This shows cancer and immune cells can be detected and quantified from the peritoneal fluid.

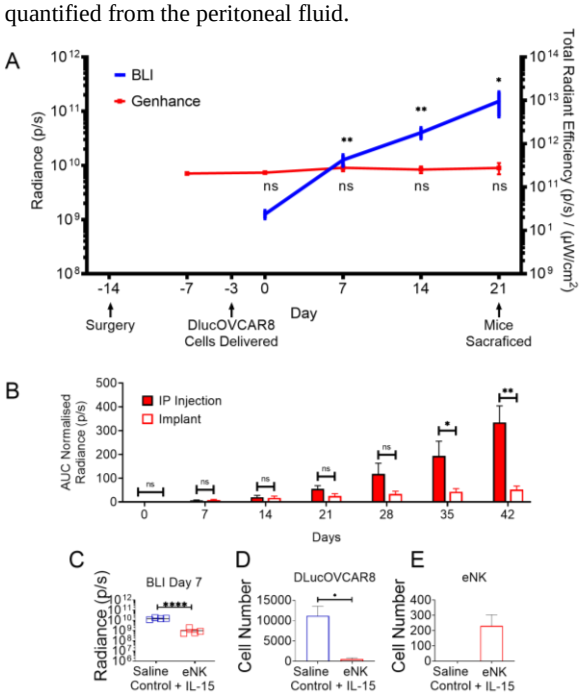

Figure 1: **A**: BLI (blue line), quantified tumour burden and Genhance, (therapy analogue, red line), quntified diffusion in peritoneal cavity in mouse, over five weeks. **B** AUC for Normalised Radiance (p/s) comparing delivery of our therapeutic regimen through our implant to IP injection up to 42 days. **C**: Tumour burden was quantified for both groups on day 7. Fluid as minimally invasively sampled from the implant on day 7 **D:** D-luc+OVCAR-8 and **E:** hCD56 cells were quantified.

DISCUSSION

IP treatment in ovarian cancer provides an increase of 16 months in overall survival, despite catheter related complications encountered by many patients. Previous efforts to enhance IP delivery showed tumour control but encountered challenges with in vivo release profiles[3] and was not designed to replenish drug, nor sample peritoneal fluid[3]. We present a promising platform for personalised cancer treatments through repeated, localised therapeutic administration and real-time monitoring, potentially improving outcomes.

REFERENCES

1. Armstrong, D. K. et al. N. Engl. J. Med. (2006), **2.** Walker, J. L. et al. Gynecol. Oncol. (2006) **3.** Tanenbaum, L. M. MIT Thesis (2016).

EXOSOMAL CX43 AS KEY PLAYER IN BRAF/MEK INHIBITORS EFFICACY AND DRUG RESISTANCE IN TUMOURS WITH A MUTATION IN BRAF

Guitián-Caamaño, A.[1,2], Varela-Vázquez, A.[3], Carpintero-Fernández, P.[4], Varela-Eirín, M.[5], Carneiro-Figueira A.[4], Bravo S.B.[6], Calleja-Chuclá T.[7], Varela-Quindós M.[8], Fonseca E.[9], Mayán M.D[4].

[1]School of Mechanical and Materials Engineering, Engineering and Materials Science Centre, UCD, Dublin, Ireland
[2]Conway Institute of Biomolecular and Biomedical Research, UCD, Dublin, Ireland
[3]Barst Cancer Institute, Centre for Tumour Microenvironment, Queen Mary University of London, Charterhouse Square Campus, London, UK
[4]CELLCOM Research Group. Biomedical Research Center (CINBIO) and Institute of Biomedical Research of Ourense-Pontevedra-Vigo (IBI), University of Vigo. 36310, Pontevedra, Spain
[5]Instituto de Investigación Biomédica de A Coruña (INIBIC), Servizo Galego de Saúde (SERGAS), A Coruña, Spain
[6]Instituto de Investigación Sanitaria de Santiago de Compostela IDIS, Santiago de Compostela, Spain.
[7]Hospital Pharmacy Service. CH-Universitario A Coruña (XXIAC). SERGAS, A Coruña, Spain.
[8]Translational Cancer Research Group, Instituto de Investigación Biomédica de A Coruña (INIBIC). CH-Universitario A Coruña (XXIAC). Servizo Galego de Saúde (SERGAS). A Coruña, Spain.
[9]Dermatology Department, University Hospital of A Coruña, A Coruña, Spain.

email: amanda.guitiancaamano@ucd.ie

INTRODUCTION

Mutations in the oncogenic protein kinase BRAF play a crucial role in the development of various tumors, with a mutation frequency exceeding 50% in melanoma[1]. Currently, BRAF/MEK inhibitors (BRAF/MEKi), administered either as monotherapy or in combination with immunotherapy, are the standard of care for BRAF-mutated melanoma[2]. However, resistance to these therapies remains a significant challenge[3]. Our research identifies connexin43 (Cx43), a regulator of cell growth[4] and differentiation found in extracellular vesicles (EVs)[5], as a key enhancer of BRAF/MEKi efficacy in BRAF-mutated tumors, although the underlying mechanisms are not fully understood.

MATERIALS AND METHODS

In this study, we investigate the therapeutic potential of Cx43-enriched EVs in targeting BRAF-mutated human cell lines. EVs were isolated via ultracentrifugation, characterized using nanoparticle tracking analysis (NTA), electron microscopy, and Western blotting, and further analyzed through liquid chromatography-tandem mass spectrometry (LC-MS/MS) and RNA sequencing.

RESULTS

Cx43 has been revealed as a key regulator of EV function and the recruitment of proteins into EVs. Our results demonstrate that Cx43 significantly enriches proteins involved in various cellular processes, including cell senescence (PPP1CC, TGFB1), mitochondria-mediated apoptosis (APAF1, AIFM1), cell cycle regulation (PSME2, CDK1), DNA repair (H2AFX, RAD50), pol-II transcription regulation (POLR2, NELFA) and immune response (HLA-DPB1, PPP6C), among others. Notably, CSTB, a pro-apoptotic and cell cycle regulator protein, is not only enriched in EVs-Cx43 but also directly interacts with Cx43 within these vesicle (Fig.1).

We further explored the potential of EVs as a drug/protein delivery system to restore Cx43 in BRAF-mutant tumour cells. Our findings indicate that exosomal Cx43 enhances the efficacy of BRAF/MEKi and prevents drug resistant by promoting cellular senescence, increasing ROS production and DNA damage, and inducing apoptosis through Caspase-3 activation.

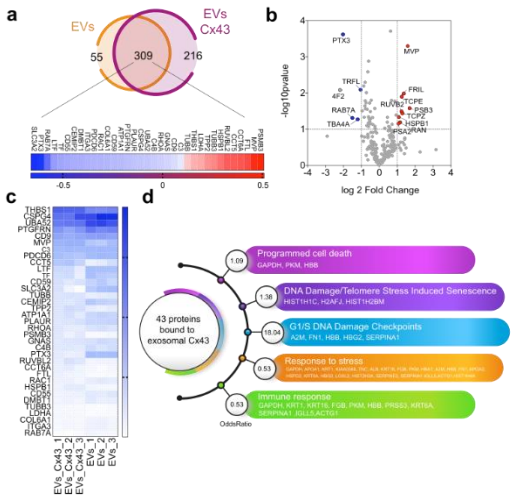

Figure 1. Cx43-enriched EVs as active drug targeting drug delivery vehicles.

DISCUSSION

Our findings demonstrate that Cx43 overexpression reduces proliferation while increasing senescence and apoptosis in BRAF-mutated cells, both with or without BRAF/MEKi treatment. Cx43-enriched EVs exhibit altered functional capabilities and distinct protein and RNA content, underscoring Cx43's role in recruiting specific molecules. Restoring Cx43 via EVs in BRAF-mutated tumors significantly enhances the efficacy of BRAF/MEKi and prevents resistance by promoting senescence and inducing cell death.

This study highlights the potential of EVs as delivery vehicles for transmembrane proteins like Cx43, offering a promising therapeutic approach for managing metastatic tumors and advanced disease.

REFERENCES

[1]Davies, H.; et al. *Nature* 2002, 417 (6892), 949-954. [2] Pasquali, S: et al. S. *Cochrane Database Syst Rev* 2018, 2 (2). [3] Haist, M.; et al. *Cancer Metastasis Rev* 2023, 42 (2), 481- 505. [4] Su, Y. A.; et al.. *Mol Carcinog* 2000, 28 (2), 119- 127. [5] Soares, A. R: et al. *Sci Rep* 2015, 5, 13243

DEVELOPMENT OF AN ACTUATABLE CELL ENCAPSULATION DEVICE

Trask, L.[1], Ward, N.[1], Prendeville, H.[1], Dillon, R.[1], Fallon, U.[1], O'Dwyer, J.[2], Roche, E.T.[3], Duffy, G.D.[2], Dolan, E.B.[1]

[1] Biomedical Engineering, College of Science and Engineering, University of Galway.
[2] Anatomy and Regenerative Medicine Institute (REMEDI), University of Galway.
[3] Institute for Medical Engineering and Science, Massachusetts Institute of Technology.
email: l.trask1@universityofgalway.ie

INTRODUCTION

Medical implants are being developed to encapsulate therapeutic cells to treat chronic conditions such as diabetes[1]. Despite having some success, many have limited long-term performance due to the foreign body response (FBR) and resulting fibrous capsule (FC) impeding vital transport[2]. Our group previously designed an actuatable drug delivery device which is cyclically pneumatically inflated and deflated to drive local mechanical changes and overcome the FBR. This enabled sustained insulin delivery over an 8 week period in mice[3]. However, the original design was not suitable for cell cargo as the deflecting membrane was superimposed on the therapy reservoir, leading therapy to be compressed or expelled by actuation. Here, we describe the design and development of an actuatable cell encapsulation (ACE) device (**Fig 1A**). We evaluated the performance *in vitro* and performed a preliminary *in vivo* study to monitor cell viability and FC progression.

MATERIALS AND METHODS

The device was manufactured using variations of procedures previously described in Whyte[3]. Device deflection was modelled in Abaqus and validated experimentally (DinoCapture camera) to determine the input pressure. Cell viability of mouse mesenchymal stem cells transfected with firefly luciferase (F-cells, $1.67x10^5$ seeded) was measured *in vitro* (IVIS®) with and without actuation (10 mins/day, 1Hz). As a further test, pseudo-islets (PIs) were generated with the INS1E rat β-cell line and added to a Spongostan™ carrier (SF). Distribution of PIs on SF was verified by DAPI staining (Olympus FV300). PI function in media and on SF was measured by GSIS index (ratio of insulin production) as a baseline for later testing in devices. The device was then implanted subcutaneously in C57BL6 mice for 13 days. F-cells ($0.5x10^6$) were delivered via transcutaneous port after 72 hours and viability was measured over time (IVIS®). Post-euthanasia, the device and tissue were prepared for nanoCT (Xradia 620Versa) as in Whyte[3].

RESULTS

The ACE device achieved similar deflections to those in previous studies[3] at the pressure of 27.5 kPa (**Fig 1B**). Actuation of the device at the selected pressure did not impact cell viability at any time point with signal increasing ~2.5 fold by day 13 (**Fig 1C**). Additionally, proper distribution and function of the PIs on SF was achieved, matching baseline free values (**Fig 1D**).

In our preliminary *in vivo* study, we demonstrated progressive cell death in the non-actuating group, as expected (signal decrease >99%) (**Fig. 1E**). Interestingly, there was no significant difference in FC thickness between devices with (+) and without (-) cells delivered (**Fig 1F**). This work is ongoing.

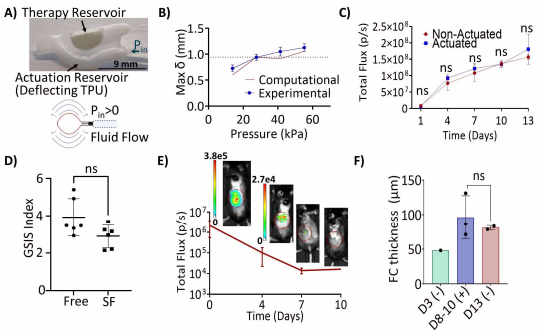

Fig 1 A) Schematic of the device. B) Max deflections at various pressures. C) *In vitro* bioluminescent signal (n=1 repeat). D) GSIS index in media and SF to mark function. E) IVIS® signal *in vivo* with sample images. F) FC thickness with (+) and without (-) cells.

DISCUSSION

We are completing *in vitro* testing of the new design, demonstrating that actuation regimes previously used *in vivo* to modulate the FBR (drug delivery devices)[3] do not impact encapsulated cell viability. We are also determining the suitability of the ACE device to support demanding cell types such as insulin producing cells for the treatment of Type 1 diabetes[1]. Our ongoing preliminary *in vivo* study followed expectations for progressive failure in the non-actuating group[3] and showed no evidently enhanced FBR with encapsulated cells. Though results are preliminary, they show promise for the ACE device to successfully modulate the FBR[3] without negatively impacting encapsulated cell viability. Additionally, past *in vivo* results and computational modelling of pulsatile fluid flow in such devices[4] support these promising results towards future implementation of the ACE device.

REFERENCES

[1] Keymeulen B et al., *Nat Biotech*, 47:1507-1514, 2024. [2] Veiseh O et al., *Adv Drug Deliv Rev*. 144:148–161, 2019. [3] Whyte W et al., *Nat Comm*. 13:4496, 2022 [4] Trask, L. et al,.*Biomat Sci.,* 12, 2899-2913, 2024.

EVALUATION OF THE CROSSING FORCES OF A VIBRATING GUIDEWIRE IN CONTACT WITH MODEL CALCIFIED MATERIALS

Rezaei, A., Raut, S. and Gavin, G.
School of Mechanical Engineering, Technological University Dublin
email: graham.gavin@tudublin.ie

INTRODUCTION

Peripheral arterial disease (PAD) affects millions globally, with over 21 million cases reported in the U.S. in 2020 [1]. It occurs when leg arteries become narrowed or blocked, leading to complications like critical limb ischemia, where blood flow is severely restricted. Standard treatments, such as bypass surgery and endovascular procedures, aim to restore blood flow [2]. However, advanced chronic total occlusions with calcified plaques, often prevent flexible guidewires crossing into the true lumen of the distal vessel, accounting for approximately 80% of procedural failure [3]. The use of high-frequency (20- 50 kHz) mechanical vibrations (0-50 µm) delivered to the distal tip of specialist guidewires has been shown to ablate calcified plaques, as shown in Figure 1 [4].

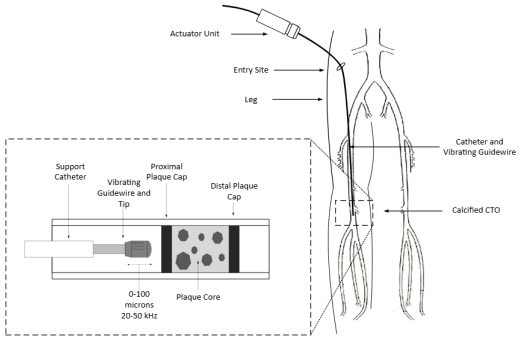

Figure 1 Vibrating guidewire in peripheral artery

This study evaluates the ability of a vibrating guidewire to ablate centrally though model calcified materials of known composition and measure the crossing forces under controlled feed- rates. The results aim to inform the optimal design parameters for vibrating guidewires, enhancing their ability to cross calcified lesions and improve PAD patient outcomes.

MATERIALS AND METHODS

An experimental setup was developed to control the feed-rate of a vibrating guidewire for precise measurement of forces during ablation of calcified samples. The NiTi guidewire (distal-tip diameter ~ 18 tau) was coupled to an actuator unit and vibrates with an amplitude of approximately 10-20µm in the 35- 45 kHz range. The guidewire, enclosed in a catheter, was submerged in a fluid-filled tank at 37°C, with calcified samples mounted on a load cell. The setup was controlled via LabVIEW software, which interfaced with a data acquisition system. BegoStone samples, prepared at three concentrations, were tested by advancing the vibrating guidewire through them and capturing the force data. Force profiles for all crossings (10 per concentration) and at three feed-rates were recorded and statistical metrics, including mean crossing force and maximum force and were extracted and compared across batches.

RESULTS

The plot of mean crossing force vs feed-rate in shown in Figure 2 As material concentration increased, the force required to ablate also increases, with a median of mean forces ranging from 0.2 to 3 cN. Higher feed-rates consistently led to increased mean forces across all concentrations. For the current test setup the active guidewire failed to penetrate the densest BegoStone batch at the highest feed-rate (40 mm/min). This issue resulted in the exclusion of this batch from the analysis.

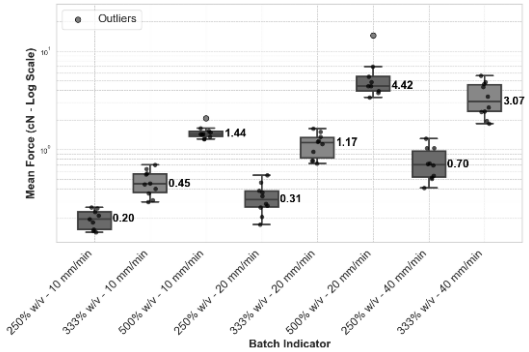

Figure 2 Box plot of mean forces for BegoStone batches.

DISCUSSION

The vibrating wire ablated centrally through all samples of Begostone concentration at feed-rates of 10 and 20 mm/min. At the highest concentration of Begostone and feed-rate of 40 mm/min the crossing force exceeded the buckling load of the wire.

REFERENCES

[1] The Current U.S. Prevalence of Peripheral Arterial Disease, HMP Global Learning Network website (accessed August 13, 2024).
[2] Hiramoto *(et al.)*, Nat Rev Cardiol 15:332–50, 2018.
[3] Sakes *(et al.)*, Cardio. Eng Technol 15:103-117, 2016.
[4] Gavin, Exp. and Num. Invest. of Therap. Ultrasound Angioplasty, PhD, DCU, 2005.

ACKNOWLEDGEMENT

This work is funded under a DTIF award managed by the Department of Enterprise, Trade and Employment and administered by Enterprise Ireland.

USE OF IN-PROCESS MONITORING TO EVALUATE POROSITY GENERATED DURING THE L-PBF PRINTING OF TI-6AL-4V

Villano, A.[1], Hoare, C.[1], Golpayegani, F.[2], Dowling, D. P.[1]
[1] I-Form Centre, School of Mechanical and Materials Engineering, UCD, Belfield, Dublin 4, Ireland
[2] School of Computer Science, UCD, Belfield, Dublin 4, Ireland
email: andrea.villano@ucdconnect.ie

INTRODUCTION

The additive manufacturing of Ti-6Al-4V medical implants is widely applied due to the alloy's biocompatibility, as well as its superior mechanical properties close to that of human bone. During the printing of the alloy by laser powder bed fusion, part defects such as porosity, can be generated. In this study the objective is to identify if the formation of these print processing defects can be identified, as they are being generated.

MATERIALS AND METHODS

An optical emission in-process monitoring sensor system called InfiniAM, was used to monitor radiation emission intensity at the point where the laser interacts with the powder (called the meltpool). The study was carried out during the printing of 20 x 18 x 7 mm Ti-6Al-4V spinal cage devices. The in-process data was correlated with the properties of the printed parts, the latter evaluated to characterise the printed alloy's morphology (SEM, microscopy, profilometry), crystal structure (XRD), mechanical strength (microhardness) and porosity (µCT scans).

RESULTS

The study demonstrated that the print geometry of the spinal cage can have a significant influence on the presence of porosity, as well as grain microstructure variations. In particular where ridges and print edges, are subject to higher thermal conditions during processing, a significant higher level of porosity can be obtained, compared with that observed within the bulk alloy.

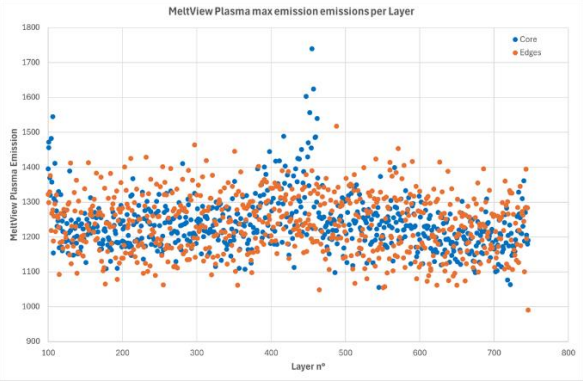

Figure 1 Comparison of the maximum emission recorded by the MeltView Plasma system between the sharp edge and the bulk alloy across the print layers.

DISCUSSION

The study details as to how the variations in the microstructure and in the mechanical properties, such as the porosity, can be corelated with the in-process monitoring data, opening the possibility for further studies aimed to develop a real-time in-process monitoring system.

REFERENCES

Wang *et al.*, Progress in Natural Science: Materials International: 671-677, 2016.

Beyl *et al.*, IOP Conference Series: Materials Science and Engineering, Riverside Sun, Vanderbijlpark, South Africa, 2019.

Xu *et al.*, Vacuum: 364-373, 2019.

COMPARING SELECTIVE LASER SINTERING AND MULTI JET FUSION PRINT CAPABILITIES FOR DISTAL END LOAD BEARING PROSTHETIC SOCKETS WITH NYLON 12 MATERIAL

Dagge, E.[1,2], Clancy, B.[3], Casey, B.[4], Keane, G.[1], Devine, D.[1,2]
[1] Technological University of the Shannon, Midlands, Athlone
[2] Cúram Medical Devices, Science Foundation Ireland, Galway
[3] Atlantic Prosthetic & Orthotic Services Ltd, Galway
[4] South East Technological University, Carlow
email: A00314291@student.tus.ie

INTRODUCTION

Additive manufacturing (AM) of prosthetic and orthotic medical devices has been noted for its ability to reduce material waste, manufacturing times and clinical resource requirements compared to their traditional manufacturing methods [1]. When using AM technologies for the manufacture of prosthetic load bearing lower limb prosthetic sockets, high strength and durability are necessary properties for the device [2]. Selective laser sintering (SLS) and Multijet Fusion (MJF) AM solutions are commonly used to achieve these desired properties in socket production.

Understanding the difference in both solutions regarding the weight, finish, dimensional accuracy and internal print defects can give potential investors an idea of the difference in both SLS and MJF solutions for the printing of prosthetic sockets before committing to investment.

MATERIALS AND METHODS

The design of the sample incorporates componentry commonly used in transtibial socket production and assembly; the male 4-hole adapter system (used for joining the remainder of the prosthetic assembly, including pylon and foot), and the pin locking system (used to ensure a secure connection between limb and prosthesis). This setup was approved by an Irish P&O company based in Galway, and follows their current 3D printed devices tested and commercialised for use. The samples were designed using Autodesk Fusion 360 and can be seen in Figure 1.

Three samples were then manufactured with AM technologies. Sample A was manufactured through an external supplier, using EOS P3 SLS technology and PA2200 material with a 50/50 refresh ratio. Samples B and C were printed in-house with HP 5200 MJF technology and HP High Reusability PA12 material using an 80/20 refresh ratio (80% recycled, 20% fresh powder material).

Sample A was naturally cooled for 48 hours. Sample B was allowed cooling of 39 hours according to HP natural cooling requirements. Sample C was fast cooled in 5 hours. Sample A was tumbled in post processing where samples B and C were sand blasted.

All samples were printed with 100% density parameters (no hollowing was used for any samples).

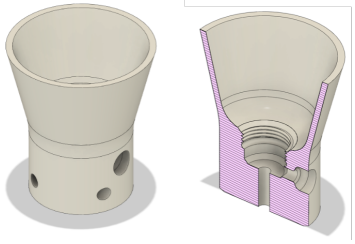

Figure 1 3D model and cross-sectional analysis of the distal end samples designed using Autodesk Fusion 360.

RESULTS

Sample B (MJF Natural Cooling) resulted in the lightest print with an 11.5% reduction in weight compared to Sample A (SLS). Sample C (MJF fast cooling) was 10.7% lighter than SLS Sample A.

For dimensional accuracy, all samples were within 0.5mm of tolerance to the original 3D model specifications. For overall height, body and top diameter, sample B was most accurate to original dimensions. Sample A dimensions were generally smaller than the intended values. Sample B was most accurate aside from Z axis holes printed, where they were 0.5mm smaller. Sample C varied in dimensional accuracy across axes, showing signs of distortion after sandblasting. Only sample A had the ability to be dyed to another colour given its white material nature. Samples B and C were grey and dark grey respectively due to UV light curing requirements.

DISCUSSION

Overall, MJF natural cooling proved to be the lightest and most dimensionally accurate option for transtibial distal end manufacturing. SLS prints have smaller dimensional results after tumbling, by up to 0.5mm.

Testing these samples according to ISO 10328: Structural Testing of Lower Limb Prostheses is recommended to follow suit to this research. It is also advised to add lattice structure infills to this sample design to reduce weight while maintaining mechanical strength and durability properties.

REFERENCES

[1] Dagge *et al.*, JEAST, Volume 6(4): 1-5, 2024
[2] Campbell *et al.*, Canadian Prosthetics & Orthotics Journal, Volume 1(2): 1-8, 2018

Funded by SFI & APOS Ltd - Grant no. 13/RC/2073_P2

COMPARATIVE ANALYSIS OF P300 DETECTION ACCURACY IN TRADITIONAL AND HEAD MOUNTED DISPLAY ENVIRONMENTS

Awais, Muhammad Ahsan.[1], Healy, Graham.[1], Ward, Tomas.[1]

[1] Insight Research Ireland Centre for Data Analytics, School of Computing, Dublin City University, Dublin, Ireland

email: (muhammad.awais2@mail.dcu.ie)

INTRODUCTION

The Rapid Serial Visual Presentation (RSVP) is an approach for Brain Computer Interfacing in which a series of images are displayed at high speed [1]. Participants are asked to differentiate between a set of target images and a set of standard images, where the P300 event-related potential (ERP) is evoked by a target image but not by non-target images [2].

Despite the extensive use of RSVP paradigms for P300 elicitation, most studies rely on traditional computer monitor displays. This experimental setup offers a consistent and familiar visual environment, reducing distractions and delivering accurate data for P300 detection. However, real-world applications of BCIs frequently go beyond the boundaries of a standard laboratory setting, necessitating systems that work in dynamic and engaging environments. For example, BCIs designed for immersive gaming or other settings that mimic real-world situations.

This study seeks to close this gap by comparing the effects of two display modalities—traditional monitor vs. head-mounted display (HMD)—on P300 prediction accuracy. We aim to know if an immersive, HMD-based environment influences the reliability of ERP detection and if it can deliver equivalent or better performance than regular settings. This study will assist those designing future BCIs for real-world applications, where they will be deployed in dynamic, engaging, and interactive environments.

MATERIALS AND METHODS

This study uses the two datasets of 'AMBER: Advancing Multimodal BCIs for Enhanced Robustness—A Dataset for Naturalistic Settings' [3], collected at Dublin City University, Ireland. An Ethical approval (DCUREC/ 2021/175) was obtained to record Data-1 (with monitor screen) and Data-2 (with head-mounted display) with ten healthy participants aged 20–35 in each variant. A 32 channel ANT-Neuro eego sports system, with CPz as the reference was used to record EEG data at 1000 Hz. Each participant completed four 90-second RSVP blocks, containing 360 images (324 non-targets, 36 targets) per block.

A Bayesian Ridge Regressor [4] was used for single-trial P300 detection [5, 6].

RESULTS

Considering the class imbalance of the data, ROC-AUC was used to assess model performance and the results for both datasets are given in the Figure 1.

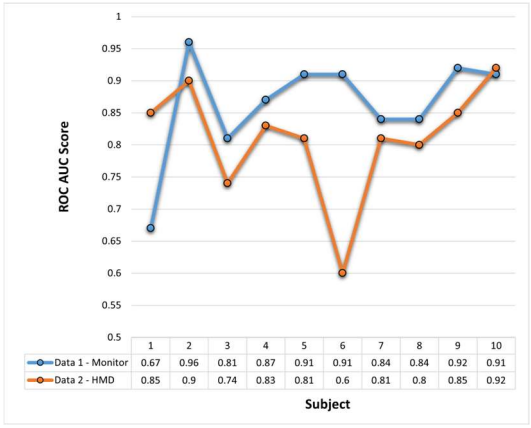

Figure 1 Comparison of ROC AUC scores for each subject for monitor vs HMD RSVP display.

DISCUSSION

The ROC AUC results obtained in monitor-based setting are high, with an average of 0.864 across 10 subjects. This indicates that P300 prediction using a monitor setup is more performant.

The head-mounted display, while slightly less effective in terms of AUC scores (average of 0.811), demonstrates that the HMD environments can still provide valuable data for P300-based studies. However, the lower scores suggest increased mental fatigue or a greater cognitive load impacting the subjects' responses.

CONCLUSION

Results show that a traditional monitor remains a reliable choice for P300 detection. Although the head-mounted display's performance is slightly lower, it indicates the feasibility of using immersive environments for P300 studies, possibly targeting applications that benefit from realistic and engaging scenarios.

Researchers designing future experiments should take these performance differences into account when designing their experiments.s

REFERENCES

1.Wang *(et al.),* Brain Computer Interfaces, 5, 132–145.
2. Luck, MIT press, 2014.
3. Awais *(et al.)*, Front. in Neuroergonomics, 4, 1216440.
4. MacKay *(et al.)*, Neural computation, 4(3), 415-447.
5. Rahman *(et al.)*, IEEE EMBC, Glasgow, 2022.
6. Awais *(et al.)*, J. Neural Engg., 21(4), 046011.

ESTABLISHMENT OF AN IN-SILICO FRAMEWORK FOR DESIGNING 3D-PRINTED BIOINSPIRED POLYMER HEART VALVE LEAFLETS

Hughes, C.[1,2,3], Johnston, R.D[1,2,4] , Campbell, E.[3], Lally, C.[1,2,4]
[1] Trinity Centre for Biomedical Engineering, Trinity Biomedical Sciences Institute, TCD, Ireland
[2] Dept of Mechanical, Manufacturing, and Biomedical Engineering, School of Engineering, TCD, Ireland
[3] Structural Heart Division, Boston Scientific Corporation, Galway, Ireland
[4] Advanced Material and Bioengineering Research (AMBER) Centre, RCSI & TCD, Ireland

INTRODUCTION

Aortic stenosis (AS) affects 4% of people over 70 and has a 50% chance of mortality within 2 years when untreated [1,2]. Prosthetic heart valves used to treat AS have significant drawbacks such as the need for lifelong anticoagulant therapy or premature failure within 25 years [3]. Bioinspired polymer valves have the potential to remove these drawbacks; however, to fully embrace these into future treatment we need a directed approach to design and assess these valves. In this research, we present a novel framework for the development and optimisation of 3D-printed, bioinspired polymer leaflets using finite element (FE) modelling. Informed by imaging and mechanical characterisation of native porcine aortic leaflets in our previous work [4], this provides a novel preclinical design tool to inform material selection and optimise leaflet structure for different valve leaflet shapes and varying clinical cases.

MATERIALS AND METHODS

A FE-based valve model inspired by the ACURATE neo2™ Aortic Valve (Boston Scientific, Massachusetts, USA) was developed to represent silicone-based polymer leaflets with a polycaprolactone (PCL) bioinspired fibre reinforcement structure made using melt electrowriting (MEW), as described previously [5], see Figure 1 (a-c). A design of experiments (DOE) approach was taken to determine the optimal combination of key structural features: fibre spacing (0.5-2 mm), fibre layers (2-10), and overall leaflet thickness (0.2-0.5 mm). Using the determined optimum combination, a fibre reorientation algorithm adapted from Creane, et al. [6] was applied to further improve the leaflets' mechanical response. This reorients the fibres along the max and mid principal strain directions to maximise load bearing capacity.

RESULTS

Development of the FE model allowed for extensive assessment and improvement of the bioinspired, fibre-reinforced polymer leaflet. The DOE enabled us to identify the optimum combination of leaflet structural features based on material response and valve opening behaviour: fibre spacing of 0.5 mm, 2 MEW layers, and 0.3 mm thick, see Figure 1(d). Using the fibre reorientation algorithm further improved the leaflet's material response, reducing the average principal strain across the leaflet from 17.4 to 14.3%, potentially extending leaflet lifetimes, see Figure 1(e).

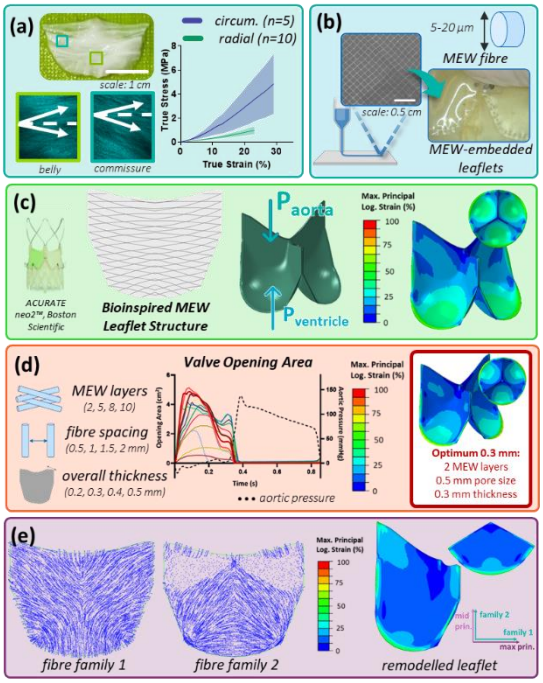

Figure 1 (a) Mechanical testing and SHG imaging of native porcine leaflets, (b) MEW printing and MEW-embedded silicone leaflets, (c) bioinspired leaflet FE model informed by a and b, (d) DOE to inform optimum structural combination, (e) using fibre remodelling to optimise fibre orientations.

DISCUSSION

This study established a novel FE-based framework to design, develop, and optimise 3D-printed, fibre-reinforced polymer leaflets based on native aortic leaflets. This methodology can now be utilised to design and manufacture heart valves for patient-specific anatomies with varying disease states. Overall, this tool will enable effective development of bioinspired polymer heart valves that can outperform current commercial devices and improve patient outcomes.

REFERENCES

1. Ambrosy, *et al.*, *Int. J. Cardiol*, 384 :107-111, 2023
2. Généreaux, *et al.*, *JACC*, 82(22): 2101–2109, 2023
3. Otto, *et al.*, *Circulation*, 143(5): 72-227, 2021
4. Hughes, *et al.*, *SSRN*, 2024
5. Hughes, *et al.*, SB3C, Vail, Colorado, 2023
6. Creane, *et al.*, *Biomech. Model. Mechanobiol*, 10: 831–43,2011

GELATIN HYDROGEL STIFFNESS INDUCES RESISTANCE OF TRIPLE NEGATIVE BREAST CANCER CELLS TO DOXORUBICIN

Turner, C.[1], Vadivelu, R.[1], Harkin, B.[1], McEvoy, E.[1]
[1] Biomedical Engineering, College of Science and Engineering, University of Galway, Galway, Ireland
email: c.turner11@universityofgalway.ie

INTRODUCTION

Breast cancer (BC) is the leading cause of cancer death in women globally. Triple negative BC forms aggressive tumours, with increased rates of metastasis and chemoresistance. An increase in hydrogel stiffness can restrict the growth, proliferation [1,2] and potentially impact the diffusion of biochemicals through the encapsulated tumour spheroids, causing inherent chemoresistance. The aim of this study is to explore and compare the response and resistance of BC spheroids to chemotherapies in soft and stiff hydrogel models.

MATERIALS AND METHODS

Murine mammary carcinoma 4T1 cells were cultured in Roswell Park Memorial Institute (RPMI) growth media supplemented with 10% FBS, 100 U/mL penicillin and 100 µg/mL streptomycin. Cells were incubated at 37°C in a humidified 5% C02 environment.

25,000 cells/well were seeded into 96-well plates and incubated for 24 hours. The wells were treated with 0.01-200µM of Doxorubicin and incubated for an additional 24, 48, and 72 hours. An MTT assay was used to determine doxorubicin cytotoxicity and IC_{50}.

$1x10^6$ 4T1 cells/mL were added to liquified 9% gelatin and either 0.3% w/w or 1.0% w/w microbial transglutaminase in a 1:1:1 ratio. 150µL of the solution was pipetted into moulds and set at 5°C for 15 minutes. The gels were transferred into a 32-well plate with 2mL of RPMI growth media and incubated, with media changes every 3 days. The gels were periodically photographed using light microscopy and spheroid diameter was measured using ImageJ processing software. Following 7 days of growth, the gels were treated with 1µM of doxorubicin in media and incubated for a further 3 days. Spheroid diameter was measured at 24-, 48-, and 72-hour timepoints.

RESULTS

Doxorubicin IC_{50} in the 2D was calculated as 10µM. Spheroid diameter in all gels increased over the 7-day incubation period to an average size of 64.1 and 56.5 µm in the 0.58 and 1.1 kPa gels respectively. The 1.1 kPa gels produced significantly smaller spheroids than the 0.58 kPa gels ($p < 0.001$). Following treatment with doxorubicin, the sizes of the spheroids significantly decreased in the 0.58 kPa gels ($p < 0.001$) following 24 hours of treatment. In comparison, the spheroids in the 1.1 kPa gels continued to steadily increase in size.

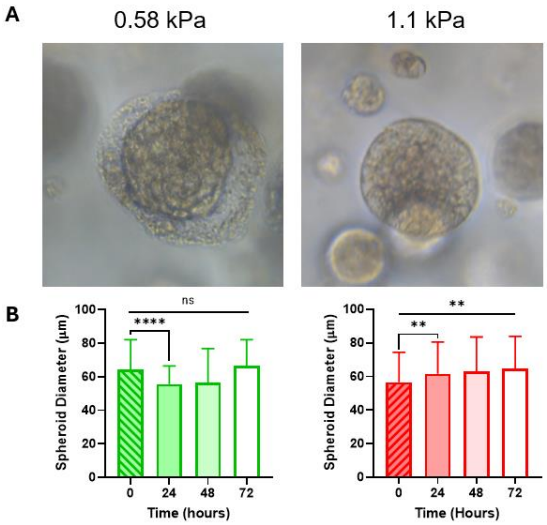

Figure 1 Spheroids embedded in 0.58 (green) and 1.1 (red) kPa gelatin mTG hydrogels were treated with 1µM Doxorubicin A) Spheroids following doxorubicin treatment. B) Spheroid diameters across 24-hour timepoints following single treatment.

DISCUSSION

BC tumour environments are stiffer than the surrounding breast tissue [3]. This study illustrates how 4T1 cells cultured in soft gels generate larger spheroids than those in stiff gels, suggesting downregulated proliferation or increased cell compaction. A reduction in spheroid size following treatment with doxorubicin was only observed in the soft, 0.58 kPa gels. Interestingly, some of the spheroids in the soft gels left a cavity of dead cells, outlining where the spheroids had shrunk (**Figure 1A**). The stiff gel spheroids exhibited an increase in spheroid size, which implies greater chemoresistance. Overall, these results suggest that the stiffness of the tumour environment is influencing mechanobiological pathways, which have downstream effects on cellular behaviours such as proliferation and could be constricting movement of the drugs through the spheroids.

REFERENCES

[1] Lovitt *(et al.), BMC Cancer* vol 18: 41, 2018.
[2] Rizzuti *(et al.), Phys Rev Lett*, vol 125: 128103, 2020.
[3] Barbazan *(et al.), Current Opinion in Cell Biology* vol 56: p. 71-79, 2018.

ACKNOWLEDGEMENTS
This work was supported by the European Research Council (Grant number 101116234).

Rb Dilution and Mechano-Osmotic Forces Drive Cell Division: A Quantitative Model

Simeone, M.[1], **Senthilkumar, I.** [1,2,3], **McEvoy, E.**[1]
[1] Discipline of Biomedical Engineering, University of Galway
[2] Data science institute, University of Galway
[3] School of computer science, University of Galway
email: m.simeone2@universityofgalway.ie

INTRODUCTION

Emerging evidence suggests that the Retinoblastoma protein (Rb) plays a crucial role in regulating the cell cycle by serving as a size sensor during the G1 phase [1]. Cells initiate the G1 phase with a specific number of moles of Rb, which remains the same during the growth. As the cell grows, the concentration of Rb reduces due to dilution, until a threshold controlling the G1/S transition is reached. This mechanism ensures that cells divide only when they reach a sufficient size. In this study, we develop a novel growth model to investigate the interactions between cell growth, Rb concentration, and mitosis.

MATERIALS AND METHODS

We propose a mechano-osmotic single-cell model to simulate the evolution of G1-phase cell growth. The regulation of cell volume arises from a balance between hydrostatic pressure ΔP, generated by active cellular stress and external mechanical loading, and osmotic pressure ΔΠ, which is driven by ion fluxes [2] and biomolecule synthesis such that:

$$\frac{dV}{dt} = -L_{p,m}(\Delta P - \Delta\Pi) \quad (1)$$

where $L_{p,m}$ is the membrane water permeability. Osmotic pressure is governed by a competition between permeable ion concentrations Δc and impermeable biomolecules X which are synthesised to drive fluid intake and subsequent growth, whereby $\Delta\Pi = RT(\Sigma\Delta c + X/V)$. The number of Rb proteins n_{Rb} remains constant during G1 [1], and thus the concentration c_{Rb} becomes diluted with growth:

$$c_{Rb} = n_{Rb}/V \quad (2)$$

In our model, as the Rb concentration approaches a critical threshold, the probability of cell division P(c_{Rb}) increases (Fig 1A).

RESULTS

Cell volume was predicted to increase over time in response to biomolecule synthesis, while a constant number of Rb proteins was maintained. Our model suggests that a cell entering the G1 phase with a high initial volume will divide after a shorter time period (Fig 1B), as the concentration of Rb is more dilute, bringing it closer to the critical Rb-threshold concentration required to trigger mitosis. This aligns with the experimental observations of Zatulovskiy et al (2020) [1]. In further agreement, the resulting curve of initial volume versus time to mitosis exhibits a positive concavity in the intermediate nuclear volume range, consistent with experimental findings.

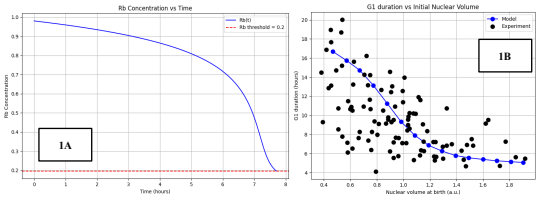

Figure 1 1A: Rb concentration decreases in time until an Rb threshold concentration is reached, when cell division can occur. **1B**: Experimental data points of nuclear volume at birth vs G1 duration are correctly described by our model. Due to the Rb dilution, the time to mitosis is reduced when a cell starts growing from an initial higher volume, following a form consistent with the experimental observations [1].

DISCUSSION

The regulation of cell size is essential for maintaining cellular function, as it influences the scale of organelles, intracellular transport, and biosynthetic processes. The mechanisms by which cell growth directly regulates cell division have long been unclear, motivating development of the proposed model. Our model provides a rationale for the experimental evidence regarding the role of the Rb protein in the cell cycle, within the context of the complex cell-cell and cell-environment interactions underlying cell growth, paving the way for new studies on cell proliferation and cancer progression.

ACKNOWLEDGEMENTS

This work was supported by the European Research Council (Grant number 101116234).

REFERENCES

1. Zatulovskiy (et al.), Science 369, 466-471, 2020.
2. McEvoy (et al.), *Nat Commun* **11**, 6148 (2020).

THE ROLE OF LEPTIN ON CARTILAGE END PLATE MATRIX SYNTHESIS AND REACTIVE OXYGEN SPECIES GENERATION

McDonnell, J. [1,2], Wilson, N.[1], Ní Néill, T.[1]Brama, P.A.J. [3], Butler, J.S.[2,4], Buckley C.T. [1, 5, 6]

[1] Trinity Centre for Biomedical Engineering, Trinity Biomedical Sciences Institute, Trinity College Dublin. [2] National Spinal Injuries Unit, Mater Misericordiae University Hospital. [3]School of Veterinary Medicine, University College Dublin. [4] School of Medicine, University College Dublin. [5]AMBER Centre, Royal College of Surgeons in Ireland; Trinity College Dublin. [6]Tissue Engineering Research Group, Department of Anatomy and Regenerative Medicine, Royal College of Surgeons in Ireland.

email: (jmcdonn6@tcd.ie)

INTRODUCTION

Degenerative disc disease (DDD) is commonly attributed to repetitive biomechanical overloading leading to degenerative processes within the intervertebral disc over time [1]. However, a notable proportion of patients with DDD are younger non-obese patients, suggesting other potential mechanisms of degeneration. This work aimed to investigate the role of metabolic dysregulation of cartilaginous end plate (CEP) cells in relation to DDD. Specifically, it evaluated how leptin, an adipokine, can influence the function of CEP cells, in terms of matrix synthesis and ectopic mineralisation. Furthermore, the relationship between leptin and reactive oxygen species (ROS) generation in CEP cells was evaluated.

MATERIALS AND METHODS

CEP cells were isolated from skeletally mature Saanen goats and treated with physiological relevant levels (0.9nM, 3.6nM) of leptin for a period of 3 weeks in both monolayer and 3D microtissue (+2 weeks priming) cultures. Cells were cultured in XPAN, comprised of low glucose Dulbecco's Modified Eagle Medium (low glucose DMEM, Sigma), 2% penicillin/streptomycin (Pen/Strep, Gibco) and 10% Foetal Bovine Serum, in 5% O_2 conditions in a humidified atmosphere at 37°C and used at passage 3. Cell viability, matrix synthesis (GAG, collagen) and ectopic mineralization were assessed using histological and biochemical analysis. ROS generation was assessed using the 2',7' –dichlorofluorescin diacetate (DCFDA) assay. Statistical analysis was performed using one- and two-way ANOVA with p values below 0.05 considered to be significant.

RESULTS

In monolayer, leptin exhibited notable increases in mineralisation compared to controls, with less prominent alcian blue staining for GAGs (Figure 1A). In microtissues, no difference was evident between control and leptin (0.9nM and 3.6nM) for DNA, GAG and collagen production (Figure 1B-D). Similar to monolayer culture, Le1 (65.62µmol/L; $p<0.05$) and Le2 (74.79 µmol/L; $p<0.01$) showed a significant dose-dependent increase in mean mineralisation compared to control (58.24 µmol/L) (Figure 1E). With respect to ROS generation (Figure 1F, 3.6nM of leptin resulted in significantly higher levels of ROS compared to controls and 0.9nM leptin demonstrating a dose-dependent increase in ROS levels when exposed to leptin (data not shown).

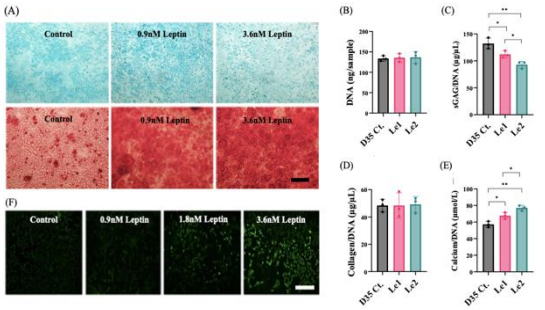

Figure 1 Figure 1: A) Alcian blue and alizarin red histological staining of CEP cells with no leptin (control), 0.9nM and 3.6nM leptin. B) DNA C) GAG/DNA D) collagen/DNA and E) calcium/DNA of CEP microtissues cultured for 5 weeks (2 weeks priming, 3 weeks insult) with no leptin (D35 Ct.), 0.9nM (Le1) and 3.6nM (Le2) leptin. F). ROS generation in CEP cells with no leptin (control), 0.9nM and 3.6nM leptin, as highlighted using DCFDA fluorescent assay. Scale bar = 100µM.

DISCUSSION

Metabolic dysregulation can lead to increased levels of circulatory adipokines, particularly leptin. While leptin is known to play a role in normal physiological processes, upregulation of leptin may influence pathological processes such as DDD. Our work is the first to assess the relationship between leptin-induced ROS generation in CEP cells and matrix synthesis rates. Our results to date highlight that leptin can induce ectopic mineralisation in CEP cells, while generating ROS in tandem. Our future work aims to further evaluate this relationship, and identify available formulations which can be employed to specifically interfere with pathophysiologic pathways, potentially mitigating against leptin-induced degenerative processes within the CEP.

ACKNOWLEDGEMENTS

This work was supported by the Research Ireland (Irish Research Council: GOIPG/2022/0159.

REFERENCES

[1] Wilder (et al.), Jour Spinal Disorders, 1(1), 16-32 (1988).

CONSIDERING THE EFFECTS OF DYNAMIC MECHANICAL STRESSES ON TESTICULAR CELL BEHAVIOUR TO INFORM THE DEVELOPMENT OF REPRESENTATIVE PRECLINICAL MODELS

O Mahoney, D.[1], Cunnane, E.M.[1]
[1] Bernal Institute, Health Research Institute, and School of Engineering, University of Limerick, Ireland
email: (omahoney.donal@ul.ie)

INTRODUCTION

Given that infertility affects approximately one in six couples, research into male reproductive health is of paramount importance[1]. Pre-clinical models lie at the forefront of male reproductive health research as they seek to represent the physiological processes that testicular cells exhibit in vivo. Pertinently, the cells within the testes are subjected to dynamic mechanical stresses due to the presence of pressurised fluid, pulsatile contractions and fluid flow. Despite the proven role of such stresses in key cellular processes, the role of shear stress, tensile stress and pressure in the context of testis modelling remains relatively unexplored[2]. This study characterises how the shear stress, tensile stress, and pressure present within the testes affects the growth and maturation of testicular cells.

MATERIALS AND METHODS

A cone & plate will be utilized to test the effect of shear stress on cells. Vacuum will be applied to a centrally supported substrate to analyse the effects of tensile stress on cells. However, this project is currently focused on charcterising the effects of pressure on testicular cells. A co-culture cell-material system will be placed in a sealed pressure chamber and pressure will be applied to the apical aspect of the co-culture system. The response of somatic and germ cells to different pressure profiles will be characterised. A flow device is attached to the top of the 'pressure chamber' and regulated flow is provided. The outcome will be a system that can support testicular cells in co-culture while applying varying pressure profiles.

RESULTS

Multiple models of the pressure chamber have been developed and printed. The most promising models have been attached to the flow device and pressure has been applied to a PDMS substrate to ensure that the system is water-tight. An internal locking system was deemed the most appropriate design as it demonstrated complete liquid retention and avoided damage to the PDMS substrate.

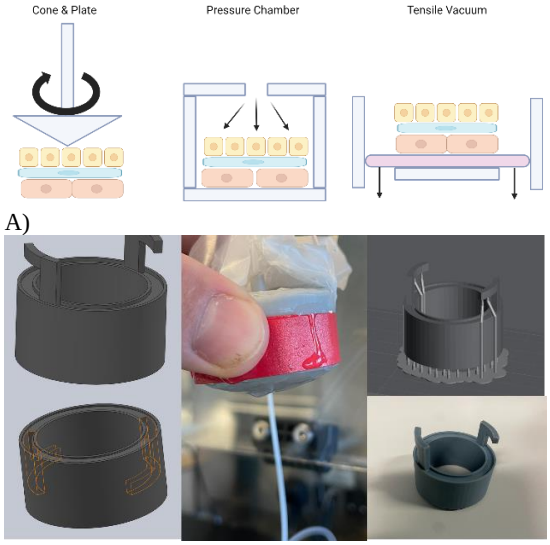

Figure 1 A) – Graphical depiction of how each dynamic mechanical stress will be applied to testicular cells. B) – CAD design, printing and testing of a pressure chamber model.

DISCUSSION

Little research has been performed to date regarding the role of dynamic mechanical stimuli on the growth and development of testicular cells. Such insights stand to advance the refinement of preclinical models, thereby facilitating the development of more comprehensive tools for studying male reproductive health.

REFERENCES

1. Njagi *(et al.)*, Human Reproduction Open, Volume 2023, Issue 2, 2023
2. Michael Delaine-Smith *(et al.)*, Bonekey Rep, 4: 728, 2015

INVESTIGATING THE ROLE OF THE BRAIN-MENINGES INTERFACE IN TRAUMATIC BRAIN INJURY

Reardon, E[1], Greaney, A[1], Abubaker, M[1], Cunnane, E[1], Mulvihill, J J.E.[1]
[1] School of Engineering, Bernal Institute, University of Limerick
email: reardon.erin@ul.ie

INTRODUCTION

Someone in the world receives a Traumatic Brain Injury (TBI) every 2 seconds[(1)]. TBI is a result of direct and subsequential damage to cells resident in the brain and surrounding tissues[(2)]. These resident cells are nourished and sustained through the movement of fluid in and out of the brain, and this movement is facilitated by cell barriers [(3)]. One significant issue with cell barriers in the brain is the prevention of drug delivery to the site of injury. This is a major reason why there are no effective therapeutic treatments for TBI[(4)]. Therefore, alternative paths and barriers should be considered to assess drug access to the brain such as the brain-meninges barrier which comprises primarily of leptomeningeal and astrocyte cells.

This research aims to develop an *in vitro* model of the brain-meninges interface using primary human astrocytes (ASCs) and leptomeningeal cells (LMCs). This will be done by examining direct co-culture, cell culture inserts, and Transwell co-culture (Fig1A).

MATERIALS AND METHODS

Firstly, using direct co-culture, the optimal growth conditions will be examined through testing cell viability, metabolic activity, and morphology. This will be done using the MTT assay, AlamarBlue assay, xCelligence system, and immunostaining. More advanced co-culturing methods will be examined such as Transwell inserts and cell culture inserts. Furthermore, the direct co-culture and Transwell co-culture will be further studied through use of bulk RNA sequencing. This aims to find more specific markers of the meningeal cells and understand the communication between the meningeal cells and astrocytes.

RESULTS

The direct co-culture method showed high cell viability (Fig.1B) and similar metabolic activity (Fig.1C) when compared to a monoculture control across various media compositions and cell ratios. Following this, significant change in cell morphology was found when the two cell types were cultured together when stained with DAPI and phalloidin (Fig.1D).

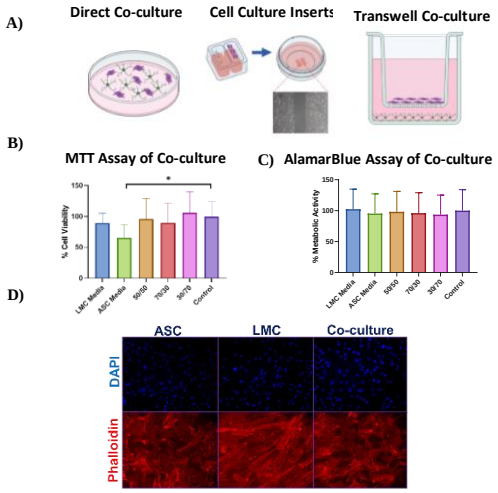

Figure 1: A) Methods of co-culture I will be examining. B) MTT assay showing the cell viability of the direct co-culture in 1:1 cell ratio in different media compositions compared to monoculture control. C) AlamarBlue assay showing the metabolic activity of the co-culture in 1:1 cell ratio in different media compositions compared to monoculture control. 6-8 technical replicates per condition, with two experimental replicates. D) Immunostaining of astrocytes, leptomeningeal cells, and co-culture using DAPI and phalloidin.

DISCUSSION

Overall, the direct co-culture has shown promising cell viability and altered cell morphology. Current work is ongoing in the examination of direct, and in-direct, and Transwell co-culture, which will include bulk RNA sequencing, transepithelial electrical resistance (TEER) testing, and protein analysis.

Overall, the brain-meninges interface is an understudied barrier in the brain. This *in vitro* co-culture model may have important implications in drug screening applications and the understanding of both homeostatic and pathophysiological conditions of the brain.

REFERENCES

1. Dewan et.al, J Neurosurg. 2018 Apr 27;130(4):1080-97. Epub 2018/04/28
2. Scheltens et al, The Lancet.2021 2021/04/24/;397(10284):1577-90.
3. Ray et al. Fluids. 2019;4(4):196.
4. Ross et al. Journal of Controlled Release. 2019 2019/02/28/;296:202-24.

THE EFFECT OF SUBSTRATE STIFFNESS ON ASTROCYTES AND LEPTOMENINGEAL CELLS

Greaney, A.[1], Abubaker, M.[1], McCarthy, C.[1], Cunnane, E.[1], Mulvihill, J.J.E[1]
[1] School of Engineering, Bernal Institute, University of Limerick, Limerick, Ireland.
email: aisling.greaney@ul.ie

INTRODUCTION

Multiple studies have proven that the tissues change in composition and stiffness as we age [1, 2]. As the structure and stiffness of our tissue's extracellular matrix (ECM) regulates cellular function, changes in its stiffness with ageing can alter the mechanosensitivity of the cells resident to the tissue. Consequently, to accurately study cellular responses, it is essential to replicate the mechanical environment of the native tissue. Research shows that as we age our cerebral ECM softens [2], with healthy adult brain tissue having a mean Young's Modulus value of ~1kPa. Concurrently, the meninges (~8MPa [3]), a protective tissue surrounding the brain, similarly alters in stiffness as we age. Therefore, the leptomeningeal cells (LMC) adjacent to the brain and the brain cells adjacent to the meninges (astrocytes) undergo different alterations as we age. This difference in stiffness between these two tissues in contact needs to be studied further to aid in understanding the neurological environment more in-depth to be able to diagnose disease and offer better treatments. Therefore, the aim of this research is to determine how astrocytes and LMCs respond to substrate stiffnesses mimicking native tissues under healthy and aged conditions, providing insights into the cellular interplay between the brain and its protective meninges.

MATERIALS AND METHODS

PDMS substrates were prepared using Sylgard 527 and Sylgard 184 to mimic the mechanical properties of brain tissue and leptomeninges, respectively. Primary human astrocytes and LMC's were cultured on these substrates to model the *in vivo* environments. Cell mechanics were assessed using the Optics11 Chiaro indenter (0.025 N/m stiffness, 3 µm radius probe) for single-cell indentation, with data processed in DataViewer V2. For protein analysis, cells were cultured on PDMS substrates and prepared for western blotting and immunofluorescence staining. For western blot analysis, cells were grown for 5 days, then pelleted, lysed, and subjected to electrophoresis. For immunofluorescence, cells were fixed on days 3 and 5 and stained with DAPI, phalloidin, vimentin, vinculin, and YAP, followed by imaging with the IMX confocal microscope. Cellular morphology and protein intensity was analysed using Cell Profiler.

RESULTS

Figure 1 illustrates the effects of substrate modifications on the biophysical and biochemical properties of LMCs and astrocytes, specifically examining changes in cellular stiffness (A), vinculin expression levels (B, C), and morphological characteristics (D).

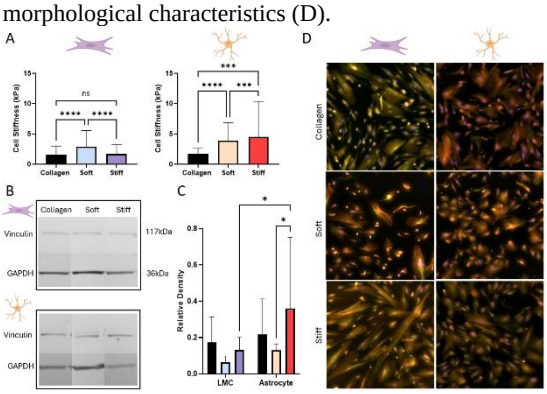

Figure 1 (A) Bar charts illustrating the effective Young's modulus (kPa) of leptomeningeal cells (LMCs, left) and astrocytes (right) cultured on substrates with stiffness levels mimicking in vivo conditions, with collagen serving as the control substrate. (B) Western blot analysis showing the mean vinculin expression in LMC's (top) and astrocytes (bottom), with (C) accompanying bar charts quantifying the expression levels. (D) Morphological images illustrating cellular structure under each experimental condition.

DISCUSSION

LMCs and astrocytes exhibit distinct mechanical responses to substrate stiffness. LMCs become stiffer on brain-like substrates (3 vs 1.5 kPa), suggesting a compensatory mechanism to maintain structural integrity in less favourable conditions. In contrast, astrocytes show a slight increase in stiffness on meningeal-like substrates (4 vs 4.5 kPa), indicating their ability to adapt to higher mechanical demands. Morphological and protein analyses reveal that astrocytes can remodel their cytoskeleton and adjust biochemical properties to function across a range of stiffnesses. LMCs, however, show limited adaptability to softer, brain-like substrates, impacting their structural and functional response. This difference may affect their ability to maintain cellular function in brain-like environments. Future research will explore whether astrocyte-derived exosomes offer neuroprotection to LMCs under healthy conditions in comparison to neurological diseases like Alzheimer's and meningitis.

REFERENCES

1. Hall *(et al.)*, Eu. J. of Neurosci 53; 3851-3878, 2020
2. Takamura *(et al.)*, J. of Mag. Reso. Imag. 51; 727-733, 2019
3. Walsh *et al.*, J. Neurotrauma Vol. 38; Pages 1748-1761, 2021

DEVELOPING HYDROGELS WITH TUNEABLE MECHANICAL AND VISCOELASTIC PROPERTIES TO EVALUATE CORNEA RESIDENT CELLS RESPONSE

Mancini, M[1], Ahearne, M.[2]
1 Trinity Centre for Biomedical Engineering, Trinity Biomedical Sciences Institute, Trinity College Dublin
2 Department of Mechanical, Manufacturing and Biomedical Engineering, Trinity College Dublin
mancinim@tcd.ie

INTRODUCTION

Cornea blindness can be caused by several factors, including damages induced by several types of injuries and diseases.[1,2]

Cornea transplantation represent the gold standard treatment, but unfortunately the number of patients that can be treated is severely affected by the lack of donors.[3]

Artificial scaffolds are a promising alternative, but even though many types of materials and techniques have been investigated, most scaffolds still fail to replicate important features of the native cornea.

Time-dependent mechanical properties are a fundamental aspect of the extracellular matrix (ECM) and although their role is less clear compared to other material properties (i.e. stiffness, substrate morphology) it has been demonstrated that they also play an important part in regulating cell behaviour.[4]

Therefore, it is crucial to better understand how these types of mechanical properties can affect corneal cells and how by modulating these properties we can achieve better results in engineering scaffolds in corneal tissue engineering.

To this end the aim of this project is to develop hydrogels that possess variable viscoelastic properties and assess how changes in these properties affect cornea stromal and epithelial cells.

MATERIALS AND METHODS

Alginate with variable molecular weight (MW), which was modulated by autoclaving, was used as the base material for the hydrogels. The different alginates were then mixed with Collagen type I and PEG Succinimidyl Glutarate to produce 3 types of scaffolds. Gels mechanical properties were tested through compression and rheology, moreover cytocompatibility was also evaluated. The effects on cells were assessed through histology, RT-qPCR and immunofluorescence.

RESULTS AND DISCUSSION

Gels showed very close values of elastic modulus, but large differences in viscoelastic properties (i.e. stress-relaxation). We demonstrated that these properties can be modulated by varying the concentration of the $CaCl_2$, which was used to crosslink the gels and which also visibly affected the transparency of the constructs.

Hydrogels proved to sustain cell viability for cornea stromal cells, furthermore, remodelling of the gels was observed over the course of 2 weeks this led to an increase in transparency.

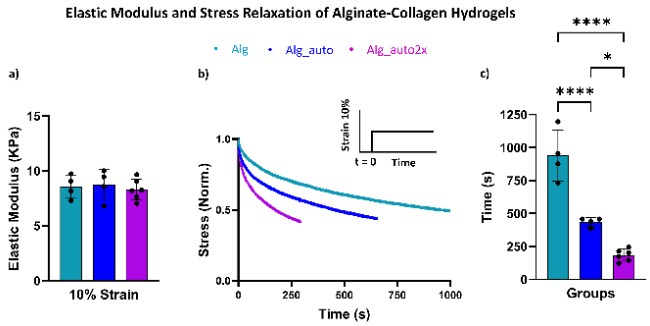

Figure 1. (a) Gels show constant elastic modulus. **(b)** Representative stress relaxation profiles for hydrogels. **(c)** Stress Relaxation time is largely different among gels and decreases with each autoclaving cycle. * Indicates statistically significant difference between groups ($p < 0.05$).

ACKNOWLEDGEMENTS

This project is supported by the Irish Research Council Laureate Award (IRCLA/2022/3731).

REFERENCES

1 Li, C. *et al. EClinicalMedicine* **62**, 102-134 (2023).
2 WHO, G. World Report on Vision. (2019).
3 Gain, P. *et al. JAMA Ophthalmol* **134**, 167-173 (2016).
4 Lee, H. P. *et al. Nat Mater* **16**, 1243-1251 (2017).

BONE-DERIVED VESICLES AND ASSOCIATED MIRNAS: UNRAVELLING NOVEL NANOTHERAPEUTICS FOR BONE REGENERATION

Maggio, M.[1], Martins, C.[1], Petrousek, S.[1], Gorgun, C.[1], Almasri, R.[2], Brunet, M.Y.[1], Ní Néill, T.[1], Buckley, C.T.[1], Hokamp, K.[3], Roche, F.M.[3], O'Driscoll, L.[2], Hoey, D.A.[1]

[1] Trinity Centre for Biomedical Engineering, School of Engineering, TCD. [2]School of Pharmacy and Pharmaceutical Sciences, Trinity Biomedical Sciences Institute, and Trinity St. James's Cancer Institute, TCD. [3]Smurfit Institute of Genetics, School of Genetics and Microbiology, TCD

email: maggiom@tcd.ie

INTRODUCTION

Osteoporosis arises in part from an imbalance in bone remodelling leading to increased resorption mediated by osteoclasts. Bone cells regulate osteoclastogenesis via the secretion of paracrine factors in a manner strongly dependent on local mechanics [1,2], yet the extent and mechanisms by which this occurs is poorly understood. Extracellular Vesicles (EVs) are nanoparticles released by cells facilitating cell-cell communication. However, it is unclear whether EVs are involved in regulating bone remodelling. Moreover, despite their multitargeted pro-regenerative properties, clinical translation of EVs suffers from variability and scalability issues. Matrix Vesicles (MVs) are a class of EVs which are embedded within tissues and may represent an alternative abundant source [3], although their regenerative properties are largely unknown. Therefore, this study aimed to i) investigate the role of bone cell-derived EVs on osteoclastogenesis and determine how this is affected by lineage commitment and by the mechanical environment, ii) identify the regenerative components within EVs, and iii) explore MVs as alternative source of vesicles for bone repair.

MATERIALS AND METHODS

Human marrow-stromal/stem cells (MSC), osteoblasts (OB) and MLO-Y4 osteocytic cells (OCY) were exposed to oscillatory fluid shear (1 Hz, 1 Pa, 2h) in parallel flow chambers. EVs from both static (EV^S) and mechanically activated (EV^F) cells were obtained via conditioned media ultracentrifugation (70Ti-fixed-angle rotor, 110000g, 75min) and characterised via NTA, TEM and flow cytometry. Human $CD14^+$ monocytes (hMφ) were treated with EVs under osteoclastogenic conditions, followed by TRAP/DAPI staining to assess differentiation. EV-compositional analysis was performed by miRNA sequencing, followed by the transfection of selected miRNA into hMφ to evaluate its effect on osteoclastogenesis. MVs were isolated from 5-month-old mice long bones through tissue digestion and ultracentrifugation (TH660 swinging rotor,10000g, 90min). MVs anti-catabolic and anabolic potential was assessed by adding MVs to hMφ and hOBs under osteoclastogenic or osteogenic (OM) conditions.

RESULTS

MSC-EV^S and EV^F significantly inhibited osteoclast formation comparably. OB-EVs were a shown to possess anti-catabolic potential, with stronger inhibition demonstrated with EV^F. OCY-EVs strongly inhibited osteoclastogenesis, evidenced to a greater extent following mechanical stimulation (Fig.1A). miRNA-seq of OCY-EVs identified miR-150-5p as a highly expressed mechanoregulated miRNA. Transfection of miR-150-5p into hMφ significantly inhibited osteoclastogenesis, highlighting its possible therapeutic application (Fig.1B, C). MVs were successfully isolated from murine bone in high quantity, overcoming the challenge of extracting vesicles from highly mineralised adult tissues. In addition, MVs expressed functional ALP, suggestive of a pro-mineralising potential. Moreover, they demonstrated both anti-catabolic and anabolic properties, inhibiting osteoclastogenesis (Fig.1D) and enhancing mineralisation (Fig.1E) in a dose dependent manner, showcasing for the first time their multi-targeted regenerative potential.

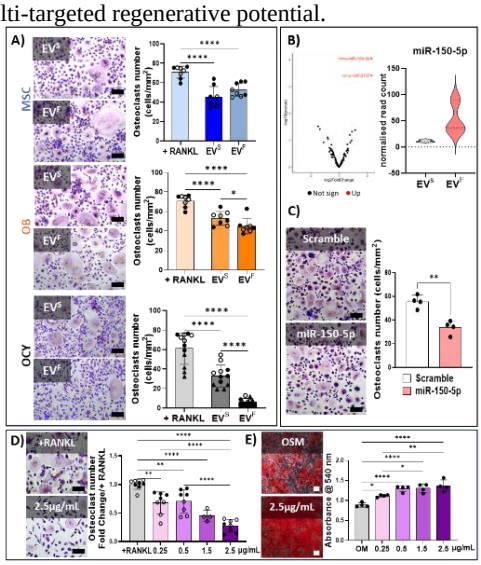

Figure 1. (A) TRAP/DAPI stain/osteoclast quantification following treatment with MSC, OB, and OCY EV-S and -F. (B) OCY EV-miR sequencing. (C) TRAP/DAPI stain/osteoclast quantification following miR-150-5p-transfection (D) and MVs treatment. (E) Alizarin Red following MVs treatment.

DISCUSSION

These results highlight the role of osteocytes as mechanosensors and regulators of osteoclastogenesis via a novel EV-mediated mechanism, in which miR-150-5p is upregulated and packaged for delivery. Moreover, we have developed a method to abundantly isolate MVs, and demonstrated their multitargeted regenerative properties beyond mineralisation. Together, these studies highlight the OCY-EV^F, miR-150-5p, and MVs as novel nanotherapeutics for bone regeneration.

REFERENCES

[1] Eichholz (et al.), Stem Cells Transl. Med. 9: 1431-1447,2020 [2] Shen (et al.), J. Tissue Eng. 14, 2023. [3] Bonucci (et al.), J. Ultrastruct. Res. 20 :33-50, 1967.

Early Stage Researcher (PhD Year 1) ☐

Entry for the Engineers Ireland Biomedical Research Medal ☐

Post-Doctoral Researcher/Senior Researcher/PI ☐

Corresponding author has completed PhD and would like to review BinI abstract submissions ☐

Osteoporotic bone crystallinity alters osteogenic differentiation and mineralization under estrogen deficiency Which is exacerbated under mechanical loading

Khabooshani, M.[1], Naqvi, S.M. [1], Von Euw, S. [2], McNamara, L.M. [1]

[1] Mechanobiology and Medical Devices Research Group (MMDRG), University of Galway, Ireland

[2]School of Biological and Chemical Sciences, University of Galway, Ireland.

email: M.khabooshani1@universityofgalway.ie

INTRODUCTION

Postmenopausal osteoporosis (PO) is characterized by changes in bone mass, microstructure, composition, and mechanobiology associated with altered estrogen levels [1,2]. Osteoblasts and osteocytes exhibit changes in differentiation and mineralization when subjected to mechanical stimulation under estrogen deficiency [3]. A major component of bone mineral is nanohydroxyapatite (nHA), which is characterised by a crystalline core and a hydrophilic amorphous surface (HASL) [3] and plays a critical role in bone strength [4-7]. Changes in the proportion of the hydrophilic amorphous layer and its crystallinity have been reported in osteoporotic bone [8]. Osteogenesis by bone cells can be influenced by the hydrophilic amorphous layer. However, the effect of changes in mineral phase of bone nanostructure on bone cell function during osteoporosis are not fully understood fully. Objectives of this study are to (1) develop a 3D in vitro bone model representative of healthy and osteoporotic bone mineral structure, and (2) investigate how changes in nHA crystallinity independently contribute to altered bone cell activity during osteoporosis.

MATERIALS AND METHODS

Novel synthetic bone-like proxies were prepared using platelet-shaped carbonated hydroxyapatite nanoparticles coated with different proportions of HASL, representing healthy (HE: 35%) and osteoporotic (OS: 20%) bone mineral crystallinity. These healthy and osteoporotic nHA proxies were then incorporated into gelatin hydrogels at different relative concentrations (50%, 25% or 12.5% w/w). Osteoblasts (MC3T3-E1) were pre-treated with 17β-Estradiol for 7 days and then encapsulated within these gelatin-nHA hydrogels (10^6 cells/ml) and cross-linked with 1% wt mtgase and cultured for 21 days. Subsequently, these constructs were cultured for a further 21 days in media supplemented with or without estrogen as follows: (1) continued estrogen and healthy mineral proxy (E, HE), (2) estrogen withdrawal and healthy proxy (EW, HE), (3) continued estrogen and osteoporotic mineral proxy (E, OS), and (4) estrogen withdrawal and osteoporotic proxy (EW, OS) in static (STAT) or mechanically stimulated (STIM, compression and perfusion) conditions within a bioreactor. To quantify the extent of osteogenic differentiation and mineralization TEM, XRD, SSNMR, biochemical assays (DNA, ALP, and calcium content), histological staining (DMP1/actin, Von-Kossa), mechanical testing and micro-CT scanning were conducted

RESULTS

Nano HA characterization: TEM, XRD and SSNMR results confirmed the formation of platelet shaped nanosized calcium phosphate particles, with a HASL and a crystalline HA core, for both healthy and osteoporotic bone mineral proxies. Crystallinity in HE and OS proxies were 65 % and 80 % respectively. ***Cell proliferation and differentiation:*** By day 21 and 42, MC3T3-E1 cells developed dendritic processes, signifying cellular differentiation. DNA analysis showed a decrease in cell number in the 12.5% nHA group on day 21 and 42, likely due to osteoblasts differentiation progress (Fig. 1B). DMP1 staining confirmed osteocyte differentiation, with lower intensity in OS relative to HE in 25% nHA (Fig. 1G). ***Osteogenesis and mineralization:*** There was a significant increase in ALP activity under E for OS compared to HE by day 42 for 12.5% and 25% nHA-gelatin hydrogels (Fig. 1C). Normalized calcium content was lower in OS than HE under both E and EW conditions in the 12.5% nHA groups by day 42 (Fig. 1D). Mineral density was significantly lower in OS compared to HE when cultured in estrogen € under mechanical loading. A similar trend, though not statistically significant, was observed under EW, for both static and stimulated conditions, and under E conditions in the static group (Fig. 1E). Compression stiffness was higher in OS than HE under EW, particularly for 12.5% nHA (Fig. 1F). Von Kossa staining and nanoCT analyses indicate that mineral deposition and bone volume fraction (BV/TV) were lower in OS than HE under E and mechanical loading, whereas BV/TV was higher in OS than HE in EW in both 12.5% and 25% nHA under mechanical loading.

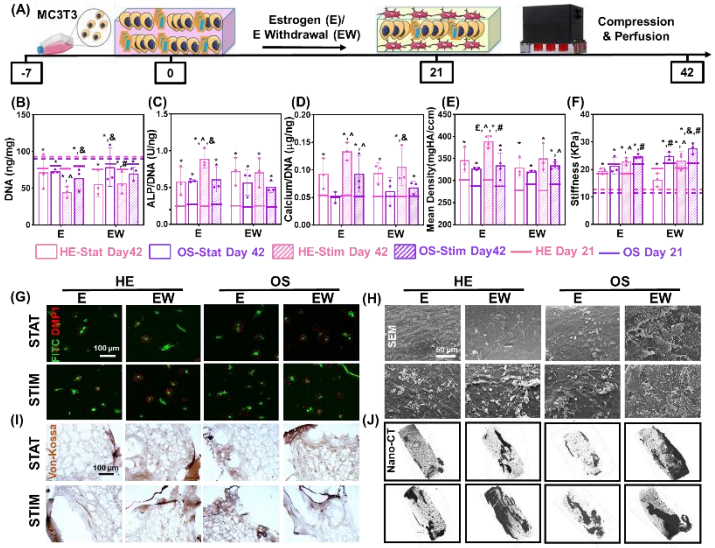

Figure 1: Osteocyte differentiation and osteogenesis are altered when bone cells are cultured on a mineral proxy with a hydrophilic amorphous surface layer representing osteoporotic bone. (A) Experimental Design, and analysis at Day 42 (B) DNA content, (C) ALP activity, (D) Calcium content, (E) mean density, (F) Compression stiffness, (G) Actin (green), DMP1 (red), DAPI (blue) staining, (H) SEM, (I) Von Kossa staining, (J) Nano-CT analyses of nHA-gelatin hydrogels. Significant differences ($p < 0.05$) indicated relative to early time point (*), continuous estrogen (#), Healthy (&), Static (^). Hash line: day 0, solid line: day 21.

DISCUSSION

In this study, we successfully synthesized bone-like carbonated hydroxyapatite nanoparticles with varying proportion of hydrophilic surface layer to model bone mineral crystallinity in healthy bone and following postmenopausal osteoporosis. Our findings demonstrate that osteoporotic conditions significantly inhibit osteocyte differentiation and reduce mineral density under mechanical loading, relative to healthy conditions. Specifically, these effects are associated with increased crystallinity of hydroxyapatite and changes in estrogen hormonal levels during osteoporosis. The reduction in the hydrated amorphous surface layer (HASL) and water content on the HA surface can influence new mineral deposition, as the thermodynamic instability of the HASL phase, compared to the stable crystalline HA core, releases more Ca^{2+} and PO_4^{3-} ions, allowing osteoblasts to ossify the surrounding environment more densely in HE [9]. These results provide an insight into the crucial role of mineral crystallinity and estrogen level in osteoporosis.

REFERENCES: [1] Brennan et al, J Mech Behav Biomed Mater, 29:161, 2014. [2] Simfia et al, Exp Cell Res, 392(1):112005, 2020. [3] Naqvi et al, Front Bioeng Biotechnol, 8:601, 2020. [4] S.Von Euw al, Geosciences, 8:12, 2018. [5] Zeng et al, ACS Biomat Sci and Eng, 7.3: 1159-1168, 2021. [6] S.Von Euw, Scientific Reports,9.1:1-11, 2019. [7] Gamsjaeger, Acta Biomaterialia, 124, 2021, [8] Zeng et al, ACS Biomat Sci and Eng, 7.3: 1159-1168, 2021.

Multifunctional Composite Coatings for Resorbable Magnesium Implants.

McArthur, C.[1], Burke, G.[1], McFadden, R.[1], Ward, J.[1]

[1]School of Engineering, Ulster University, Belfast BT15 1AP, UK

email: mcarthur-c3@ulster.ac.uk

INTRODUCTION

Bone disease along with bone fractures has contributed to an increasing health concern with an increasing population and an increasingly ageing population, cases of bone fractures are also increasing. Since in 2019 there were 178 million new fracture cases reported worldwide. (1)

In cases where external fixation and alinement devices are unsuitable it is common for bone grafting to be used to align and attach segments of bone. The current 'gold standard' for bone grafting is to use autologous bone, this method isn't used widely in clinical applications due to the limitation in the shape of bone, the amount available and the high morbidity at the extraction site. (2)

Hence, research into resorbable implants is so prevalent due to the need for fixation devices and implants that can be used to both replace and stabilise bone fragments while also promoting osteogenesis. The aim being to greatly reduce the need for after removal surgery and/or post-surgical revisions caused by factors such as periprosthetic infection, caused by bacterial infection at the implantation site. (3)

The most prevalent resorbable material with mechanical properties that are similar to bone is Magnesium (Mg). However, the corrosion rate of the metal needs to be altered as pure Mg resorbs into the body at a faster rate than bone healing. (4) This can be done by applying different materials in the form of coatings, such as hydroxyapatite (HA) and calcium phosphate (CaP) to promote osteointegration and biocompatibility or chitosan which allows for drug delivery and has antibacterial properties. (5)

MATERIALS AND METHODS

A systematic review was completed to identify the research trends surrounding composite coatings on Mg substrates for enhanced *in vivo* interaction.

The primary search strategy was completed through the use of the Scopus database, wherein search terms such as 'magnesium', ' implants', 'multifunctional', 'multilayer', 'bone', 'osteointegration' and 'coating' were used to find research papers.

RESULTS

Of the various coating techniques used to form thin films, there are a number that are more commonly used for Mg. Adonisation provides good adhesion and a porous surface finish, whereas spin and dip coating provide a facile method for forming ultra-thin coatings (7) and electrospinning for its high surface to volume ratio. (8)

Consequently, there are other thin film techniques that have been identified as less suited for this process, such as plasma spraying due to poor surface adhesion (9) and physical vapor deposition for the stress it induces on the substrate. (10)

DISCUSSION

Investigations into chitosan and CaP thin films on anodised Mg substrates will take place ("**Figure 1**"). Subsequent mechanical, physical and chemical characterisation will be completed to ascertain the interlayer adhesion and surface morphology. Building on this, in vitro studies will be completed to assess bioactivity and antibacterial effects.

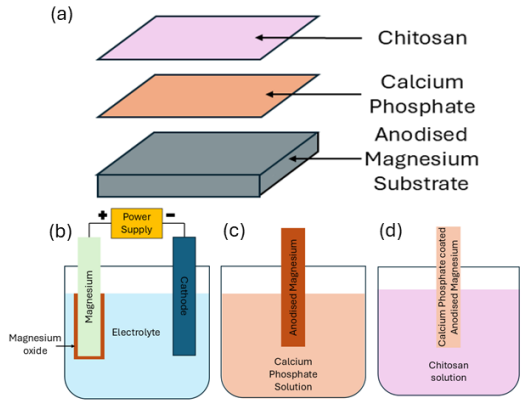

Figure 1 - Proposed coating process. (a)Layer order, (b)Adonisation process, (c)Calcium phosphate coating process, (d)Chitosan coating process.

REFERNCECES

(1) Wu *(et al.)*, Lancet Healthy Longev 2: 580–92, 2021
(2) Ribeiro *(et al.)*, Journal of Cranio-Maxillofacial Surgery 46 1: 142-147, 2018.
(3) Schwarz *(et al.)*, *J Clin Periodontol* 45(Suppl 20): S246–S266, 2018.
(4) Witte (et al.) Acta Biomaterialia 6,5: 1680-1692 2010
(5) Rahayu *(et al.)*, Carbohydrate Polymers Volume 289: 119385, 2022.
(6) Cipriano *(et al.)*, Acta Biomaterialia 62: 397–417, 2017.
(7) Mustafa *(et al.)*, JASTT 02: 119 –123, 2021.
(8) Bhardwaj *(et al)*, Biotechnology Advances 28: 325–347, 2010.
(9) Maximov *(et al.),* MDPI Coatings 11(11):1386, 2021.
(10) Khlyustova *(et al.)*, Journal of Materials B 31, 6588-6609, 2020.

DEVELOPMENT AND OPTIMISATION OF L-PBF TI64 LATTICE STRUCTURES WITH SUPERIOR MECHANOBIOLOGICAL INTERACTIONS

Yalcin, M.Y.[1,2*], Brabazon, D.[2,3], Celikin, M.[1,2]
[1] University College Dublin, Dublin, Ireland.
[2] I-Form Advanced Manufacturing Research Centre, University College Dublin, Dublin, Ireland.
[3] Dublin City University, Dublin, Ireland.
**email: merve.yalcin@ucdconnect.ie*

INTRODUCTION

Ti6Al4V (Ti64) is a widely used alloy in biomedical applications due to its excellent biocompatibility and corrosion resistance. However, its moderately high elastic modulus leads to stress shielding, a phenomenon where the implant bears the load, reducing mechanical stimulus to the surrounding bone. This results in bone resorption and impaired tissue growth (Reed, 2022). Enhancing tissue growth also requires an increased surface area to promote cell adhesion. To address these issues, porous lattice structures have been proposed as a solution to improve elastic modulus compatibility between the implant and bone while supporting tissue regeneration (Koju, 2022). Additive Manufacturing (AM) methods are employed for the production of porous lattice structures due to their feasibility in manufacturing complex-shaped structures that cannot be produced by Powder Metallurgy (PM). However, the increase in porosity levels makes the lattices susceptible to fracture due to the lack of deformability of matrix phase and stress concentration roles of defects and coarse-acicular shaped particles distributed in the matrix (Rani, 2024; Zhang, 2023). In addition, it has been stated that the coexistence of the high-temperature phase, β, which has lower elastic modulus and higher toughness than α, improved the crack growth resistance of the alloy (Naab, 2024). Moreover, Noronha (2023) stated that the toughness of the Ti64 lattices can be improved by refining the microstructure. On the other hand, dispersoids are known for their roles in microstructure refinement and stabilisation. When the amounts of dispersoids are designed accordingly, they act as heterogeneous nucleation points in the matrix phase; once the cell/grain boundaries are formed, dispersoids stabilise the boundaries and inhibit grain growth (Yo, 2022).

In this study, Ti64 alloy will be modified by dispersoid formation in the microstructure; the effects of different types of dispersoids on microstructural refinement and toughness improvement will be investigated with the aim of improving the mechanobiological performance of Ti64 alloy while decreasing elastic modulus to the level of bone's elastic modulus.

MATERIALS AND METHODS

Three different modified Ti64 alloys will be developed and produced by L-PBF method. The microstructural evolution of Ti64 in equilibrium conditions is simulated using Thermo-Calc software to develop heat treatment routes. Resulting microstructural properties and phase compositions will be analysed via optical microscopy, SEM, EDS, EBSD, and TEM analyses, where mechanical properties will be investigated by microhardness and compression tests. Cytotoxicity tests will be performed using MG63 osteoblast-like cells to investigate the biocompatibility of the alloys.

RESULTS

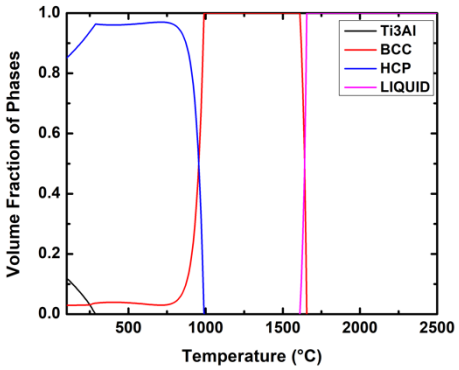

Figure 1 Equilibrium phase diagram of Ti64 alloy obtained from Thermo-Calc software.

REFERENCES

Reed *(et al.)*, Acta Materialia 229:117749, 2022.
Koju *(et al.)*, Metals 12:687, 2022.
Rani *(et al.)*, Materials Science and Engineering: A 900:146400, 2024.
Zhang *(et al.)*, Materialia 30:101838, 2023.
Naab *(et al.)*, Materials Science and Engineering: A 903:146658, 2024.
Noronha *(et al.)*, Additive Manufacturing 72:103637 2023.
Yo *(et al.)*, Materials Science and Engineering: A 854:143811, 2022.

Fundamental Investigations of Sinterability of Novel Bioresorbable Mg-Sr-Ca Implants

Azadi, A., O'Cearbhaill, E.D., Celikin, M.
School of Mechanical and Materials Engineering, University College Dublin, Ireland
email: (ava.azadichegeni@ucdconnect.ie)

INTRODUCTION

Magnesium (Mg) alloys with trace additions of Strontium (Sr) and Calcium (Ca) are promising candidates as potential temporary implants for orthopaedic and cardiovascular applications due to their excellent biocompatibility and bioresorbability [1]. Additionally, having a low elastic modulus (45 GPa) close to the human bone decreases the stress shielding effect [2]. The customisation of biomedical Mg-based alloys via additive manufacturing (AM) technologies has remarkably enabled patient-specific designs over a short period of time. However, the low sinterability of Mg-based alloys is a key issue limiting the efficiency of post-processing required for the low temperature AM techniques (i.e., extrusion-based techniques). Liquid phase sinetring (LPS) offers significant advantages over the solid-state sintering by providing capillary forces and a transport medium to promote diffusion during sintering process. Hence, the aim of this research is to evaluate the sinterability of the Mg-Sr-Ca-based alloys processed by powder metallurgical routes in terms of porosity level, and fundamentally investigate the effects of liquid phase sintering (LPS) on the sinterability of the Mg-based alloys.

MATERIALS AND METHODS

Starting material in the form of powder was fabricated via an in-house developed process. Thermodynamic calculations and differential scanning calorimetry (DSC) were used to select the sintering parameters. Wettability analyses were employed to investigate the high temperature interactions and mutual solubility of liquid-solid phases during sintering. Sinterability (i.e., porosity level) of Mg-Sr-Ca alloys was investigated based on Archimedes principle, Scanning Electron Microscopy (SEM) Image Analysis, and X-ray Computed Tomography (X-ray CT) techniques.

RESULTS

Figure 1 shows the X-ray CT analysis of the sintered parts. The pore distributions can be observed across the sample thickness for ternary compositions. In the composition notation, the digits indicate the Sr / Ca ratio in the alloy (e.g., Mg-12 represents a Sr / Ca ratio of 1:2). CT scans revealed that the porosity levels are higher in Mg-21 compared to Mg-11 and Mg-12 compositions, and Mg-12 composition is less porous after sintering. In addition, the quantitative porosity measurements based on the Archimedes analysis show that the porosity levels of Mg-12, Mg-11 and Mg-21 are 1.85 %, 5.36 %, and 11.47 %, respectively, consistent with the X-ray CT analysis.

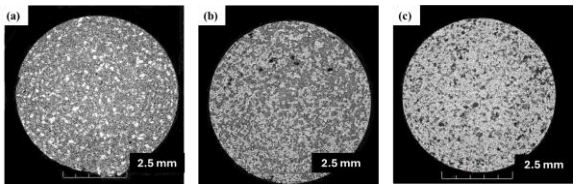

Figure 1 X-ray CT cross sections of (a) Mg-12, (b) Mg-11, (c) Mg-21 sintered compositions showing the pore distributions.

Table 1 porosity % per composition measured based on Archimedes principle.

Composition Designation	Porosity (%)
Mg-12	1.85
Mg-11	5.36
Mg-21	11.46

DISCUSSION

The higher Ca content in the overall alloy (i.e., lower Sr / Ca ratio) lowers the phase transformation temperature of the $Mg_{17}Sr_2$ intermetallic phase to liquid phase. Since $Mg_{17}Sr_2$ is the major liquid formation phase during sintering, the lower transformation temperature in the Mg-12 alloy, which has the highest Ca content, facilitates liquid phase formation, which justifies the higher densification obtained for this composition. Moreover, the ease of liquid formation in the Mg-12 alloy is further supported by its high Ca content. The Ca forms a lamellar eutectic phase, specifically the Mg_2Ca intermetallic, alongside α-Mg. The α-Mg phase adjacent to this eutectic region, enriched with Ca (since Ca has a solubility limit of 0.65 wt.% in solid Mg), may melt at a lower temperature compared to the α-Mg phase adjacent to the $Mg_{17}Sr_2$ intermetallic, which consists of nearly pure Mg (as Sr solubility in solid Mg is very low, at around 0.11 wt.%). This localised melting behaviour contributes to the increased liquid content and enhanced densification in Mg-12.

REFERENCES

[1] Amukarimi *(et al.)*, MedComm, 2:123-144, 2021.
[2] Jamel *(et al.)*, Metals, 12:85, 2022.

DRIVING TENDON DEVELOPMENT: A GENE THERAPY APPROACH WITH CATIONIC CELL PENETRATING PEPTIDES

Gilmore, E.J.[1], Elkashif, A. [1], Saha, C. [1], Buckley, N.E.[1], Dunne, N.[2], McCarthy, H.O.[1]
[1] School of Pharmacy, Queen's University Belfast, Belfast, Northern Ireland, United Kingdom
[2] School of Mechanical and Manufacturing Engineering, Dublin City University, Dublin, Ireland
email: e.gilmore@qub.ac.uk

INTRODUCTION

Tendons are a type of soft tissue that play an integral role in mobility and exist in a state of high tension making them susceptible to injury. The hypocellular and hypovascular nature of tendons limits repair capacity meaning surgical intervention is often required. The biological mechanisms underpinning tendon development/healing processes are complex and can be summarised into three overlapping stages including inflammation, proliferation and remodeling. Key regulators involved in embryonic tendon development and therefore repair processes are FAK and YAP as they drive mechanotransduction. FAK promotes extracellular matrix organisation while YAP acts as a coactivator for both differentiation and proliferation of tenocytes, contributing to tenocyte maturation. Currently there is an unmet need to develop a biomaterial that can replicate the mechanical and biological function of such tissues as no engineered material has been able to match the performance of simplest tensile load-bearing soft tissue including tendons and ligaments.[1,2] A critical barrier to the development and implementation of tendon constructs is the lack of knowledge regarding key structural features that must be replicated in order to match mature tendon function and the biological mechanisms/switch in signaling pathways, which are required to complete the construct maturation.[3]
Therefore, the aim of this study is to identify both structural changes and biological mechanisms driving normal tendon development and to use this knowledge to enhance maturation of engineered tendon constructs using targeted nanoparticle gene delivery. This will be achieved using the cell penetrating peptide RALA which has been shown to encapsulate anionic cargo and overcome the limitations associated with naked DNA delivery, allowing successful cellular delivery and uptake.

MATERIALS AND METHODS

RALA peptide nanoparticles were formulated and characterised for size, zeta potential, and polydispersity index (PDI) using dynamic light scattering (DLS).
In vitro transfection efficiency was evaluated in HEK293T cells, Rat MSCs and chicken tenocytes using flow cytometry. Following transfection with RALA-FAK and RALA-YAP nanoparticles, protein and mRNA expression levels of FAK, YAP and other target genes (such as CTGF, ANKRD1 and AXL) was assessed by Western Blot and RT-PCR.

RESULTS AND DISCUSSION

RALA/FAK and RALA/YAP nanoparticles were formulated successfully and were <150 nm in size with positive zeta potential and polydispersity index (PDI) <0.3 observed across the N:P ratios (Fig.1 i and ii). For both formulations, transfection efficiencies (Fig.1 iii and iv) in HEK293T cells was >60%. Elevated expression of FAK and YAP was confirmed at both mRNA (Fig.1 v and vi) and protein (Fig.1 vii and viii) level following transfections in cell lines such as HEK293Ts and chicken tenocytes at various N:P ratios. PCR analysis shows elevated expression suggesting RALA/FAK and RALA/YAP particles are capable of delivering cargo into cells, inducing transcription/translation of target genes.

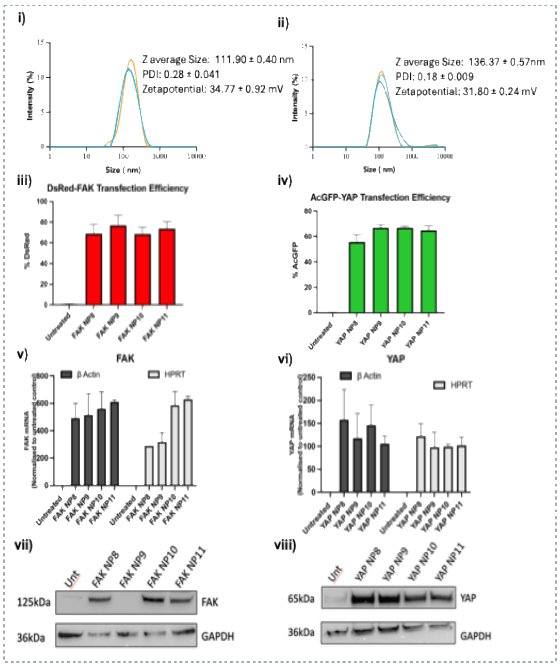

Figure 1: Characterisation of RALA nanoparticles using DLS (i and ii). Transfection of HEK293Ts using reporter plasmids (iii and iv). PCR expression (v and vi) and protein expression (vii and viii) of FAK and YAP target genes.

CONCLUSION

The non-viral vector delivery system RALA has been shown to successfully form_ulate FAK and YAP plasmid DNA nanoparticles and deliver these into cells. These nanoparticles will be incorporated into a hydrogel to facilitate delivery into tenocytes grown in 3D using a fibrin gel. In this way, tendon constructs will be created which mimic normal development of tendons and possess mechanical characteristics of human tendons.

REFERENCES

1. Kalson (et al.), Matrix Biol. 29(8):678–689, 2010.
2. Calve (et al.), Tissue Eng. 10(5–6):755–761, 2004.
3. Huang (et al.), J Orthop Res. 33(6):800–812, 2015.

IMPROVING THE SUSTAINIBILITY OF MEDICAL DEVICE IMPLANTS

Crowley, F.[1], Darwish, S.[1,2], Morales, L.[2], Mulvihill, J.J.E.[1]
[1] School of Engineering, Bernal Institute, University of Limerick
[2] Boston Scientific, Clonmel
email: crowley.frederick@ul.ie

INTRODUCTION

Medical device-associated infections are notoriously difficult to treat, despite of best practices followed infection rates of up to 18% have been reported[1]. Every year, more than 1.5 million people receive cardiovascular implantable electronic devices (CIED)[2]. In the medical implant field there is a push to reduce the size and increase the lifetime of medical implants – dubbed 'smart implants'. However, smart implants are susceptible to bacterial infection, where the infection creates a biofilm consisting of a polysaccharide matrix surrounding the microorganisms that prevents antibiotics from reaching the infection-site[3] (**Figure 1A**). The main solution is dosing the patient with high levels of antibiotics, leading to antibiotic resistance[4]. This project will examine a unique material interface for medical implants that fights infections. Various materials will be coated with specialised coatings where the composition and adhesion properties will be examined through analytical methods and its effects on cells, bacteria and tissue will be studied by in vitro and ex vivo tests. The identification of an optimal material interface will increase the lifetime of smart implants of any size and allow miniaturisation to save on material usage, improving their sustainability.

MATERIALS AND METHODS

The work presented will examine a unique material interface for medical implants that combats infections reducing the need for antibiotics or additional device components. Various materials will be coated with specialised substrates via dip coating. The composition and adhesion properties of this coating will be examined through mechanical (scratch test) and surface characterisation (SEM/EDX) techniques as well as its biocompatibility and antimicrobial properties *in vitro* and *ex vivo*. The identification of an optimal material interface through altering the dip coating solution, immersion speed, dwell time and immersion time will increase the lifetime of smart implants of any size and allow miniaturisation to save on material usage, improving their sustainability.

RESULTS

After the dip coating and antimicrobial testing is carried out a ramp load scratch test is applied to the coupons. The coating adhesion test is performed to ensure that the selected coupons exhibit maximum interfacial adhesion between the coating and the surface. Coatings with promising antimicrobial and adhesion properties are subjected to further surface and mechanical characterisation. With the results gathered from testing an optimal coating technique will be established which will have the potential be used on a range of medical devices, minimising the risk of infection.

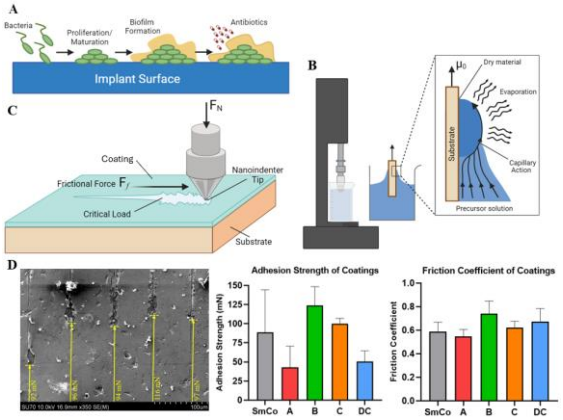

Figure 1 (A) Formation of biofilm protecting microorganisms from antibiotics. (B) Dip coating testing set-up and surface chemistry. (C) Schematic of scratch test process. (D) SEM image and results of scratch test.

DISCUSSION

Implantable medical devices with a stable interface can potentially eliminate or reduce the microorganism burden on the surface of an indwelling medical devices. However, to the best of our knowledge, there is no commercially viable technology available utilising this approach. There is therefore a requirement to develop an antibiotic-free route to fight implant infections before the implant becomes infected. The identification of an optimal material interface through altering the precursor solution, immersion speed, dwell time and immersion time will increase the lifetime of smart implants of any size and allow miniaturisation to save on material usage, improving their sustainability.

REFERENCES

1. Hanna *et al.*, *Journal of Clinical Oncology*, 22(15), pp.3163-3171, 2004
2. Leake, *Nature Reviews Cardiology*, 16(6): pp.320-321, 2019.
3. Almqvist *et al.*, *Infective Endocarditis*, 2018.
4. Sohail, *Infectious Disease Advisor*, 2019.

DEVELOPMENT OF ENGINEERED COMPOSITE BIOMATERIAL FOR LOAD-BEARING SUPPORT AND ZONAL REGENERATION OF ARTICULAR CARTILAGE

Abu Shaqrah, H. J. N.[1], Lobianco, F.[1]., O'Shea, D. G.[1], Woods, I.[1,2], O'Byrne, J. M.[1,3], O'Brien, F.J.[1,2,4], Hodgkinson, T.[1]

[1]Tissue Engineering Research Group, Department of Anatomy & Regenerative Medicine, RCSI, Dublin, Ireland, [2]Advanced Materials and Bioengineering Research Centre (AMBER), RCSI and TCD, Dublin, Ireland, [3]National Orthopaedic Hospital Cappagh, Dublin, Ireland [4]Trinity Centre for Biomedical Engineering, TCD, Dublin, Ireland. *email: hadeelabushaqra22@rcsi.ie*

INTRODUCTION

Articular cartilage degeneration from injury or osteoarthritis (OA) affects over 500 million people, causing pain and reducing quality of life. Current treatments cannot repair damaged cartilage or halt degeneration[1]. Advanced biomaterials have the potential to promote regeneration by creating instructive cell environments. However, engineering biomaterials recreating the zonal, load-bearing properties of cartilage while providing softer, cell regenerative environments has proven challenging. Advanced additive manufacturing, such as fused deposition modelling (FDM) and melt electrowriting (MEW), enables precise engineering of such constructs. This study combines cartilage-regenerative hydrogels with microfibrous scaffolds to mimic the zonal properties of articular cartilage, enhancing regeneration and load-bearing capacity for targeted repair.

MATERIALS AND METHODS

For load bearing, tri-layered microfibrous scaffolds were fabricated in various designs through combined FDM/MEW of polycaprolactone. The effect of scaffold design and fibre characteristics on mechanical properties was analysed (tensile/ compressive). For regenerative hydrogels, methacrylated gelatin (GelMA) and methacrylated hyaluronic acid (MeHA) blends were synthesised in-house and their mechanical, swelling, and degradation properties were analysed. Top candidate hydrogels, selected for a range of mechanical properties, were tested with human articular chondrocytes (hAC) (ethics: Capp/2019/ETH/SH-CEO-234) or mesenchymal stem cells (hMSC) to assess biocompatibility and chondrogenic potential. MEW scaffolds with cell-laden GelMA hydrogels were cultured for 42 days to assess the impact of fibre geometry on cell morphology and ECM deposition, using immunofluorescence and second harmonic generation microscopy, respectively.

RESULTS

MEW scaffold fibre properties, diameter (14-17 µm) and spacing (340-350 µm), were controlled through manufacturing parameters, enabling uniform scaffold fabrication. Fibre properties influenced scaffold mechanics, with the diamond design showing a threefold increase in compressive modulus between 400 µm and 200 µm fibre spacing. Both tensile and compressive moduli were within the reported stiffness range of the superficial layer of human articular cartilage[2,3]. GelMA/MeHA hydrogel formulations varied in compressive properties, including Young's moduli (0.81 – 95.29 kPa). All formulations showed excellent hAC and hMSC viability, with the highest metabolic activity in the soft GelMA/MeHA group (~0.81 kPa) by day 21. Hydrogel stiffness and composition influenced hAC morphology, with softer formulations promoting elongation and stiffer encouraging roundness, as shown by immunofluorescence. The softest group showed aggrecan upregulation after 7 days culture, while stiffer hydrogels (~26.3 kPa) displayed increased collagen X by 21 days. MEW scaffolds with hAC-laden GelMA hydrogels showed that diamond pattern elicit precise cellular orientation with ~50% of hAC aligning within the diamond design fibres after 42 days.

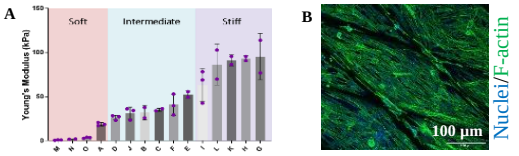

Figure 1(A)Characterisation of a range of MeHA/GelMA blends with tunable Young's modulus (B)hAC in diamond design MEW-incorporated GelMA hydrogels exhibit increased alignment, visualised through confocal microscopy.

DISCUSSION

This work demonstrates the potential of MEW/FDM/hydrogel composites to support both regenerative environments and load-bearing for zonal cartilage regeneration. By varying hydrogel formulations and scaffold designs, cell phenotypes and mechanical properties were precisely controlled, with the GelMA/MeHA stiffness and ratio influencing cell morphology, gene expression and ECM deposition. This approach shows promise for developing zonal biomaterials that replicate the cell phenotypes and mechanical properties of healthy cartilage.

REFERENCES

[1]Hodgkinson,et al.doi.org/10.1038/s41584-02100724-w.
[2]Fischenich, et al. doi.org/ 10.1016/j.joca.2020.06.007
[3]Antons, et al. doi.org/ 10.1007/s10856-018-6066-0

ACKNOWLEDGEMENTS

This work has emanated from research conducted with the financial support of Science Foundation Ireland under Grant number: 21/PATH-S/9306.

MULTI-ION DOPED COATINGS FOR CONTROLLED MAGNESIUM IMPLANT CORROSION AND IMPROVED BIOACTIVITY

Acheson, J.G.[1], McFerran, A.[1], Boyd, A.[1], Ward, J.[1], Lemoine, P.[1], McGarry, P.[2], Van Den Beucken, J.[3] Meenan, B.J.[1]

[1] School of Engineering, Ulster University
[2] College of Science and Engineering, University of Galway
[3] Radboud University Medical Centre, Netherlands
email: j.acheson@ulster.ac.uk

INTRODUCTION

Resorbable bone fixation devices present an opportunity to reduce the number of follow-up device removal surgeries and improve patient outcomes over the use of semi-permanent implants, typically made from stainless steel or titanium.

Magnesium (Mg) alloys are naturally bioresorbable and decompose into safe, excretable biocompatible compounds [1], however, their corrosion can be difficult to control in physiological environments [2] and often the implant degrades too quickly.

This work studied the creation of various ion containing calcium phosphate (CaP) coatings on a variety of Mg alloys, as a means to both tailor and control their biocorrosion [3] and offer improved bioactivity [4]. Various ion containing coatings were studied to explore their corrosion resistance, alloy adhesion and in vitro behaviour.

MATERIALS AND METHODS

Ion-containing CaP coatings were deposited via RF magnetron sputtering using a custom-built physical vapour deposition high vacuum chamber. Target materials varied from sintered hydroxyapatite to strontium-substituted apatites depending on the desired coating composition.

Coated alloys were characterised chemically using SEM-EDX (Hitachi SU 5000) and ToF-SIMS (ION-TOF). Corrosion rates of coated Mg alloys were determined via immersion testing using simulated body fluid (SBF) for a period of 14 days.

Corroded samples were characterised using gravimetric analysis, optical microscopy, SEM and Micro-CT. Coating adhesion was studied using a double lap shear tensile test. In vitro testing was conducted using U2-OS osteosarcoma cells to assess biocompatibility and potential bioactivity.

RESULTS

Deposition of uniform CaP coatings reduced the corrosion rate of Mg samples by delaying its onset as the coating underwent dissolution and acted as a protective layer. Altering the thickness of the deposited coating allowed for control over the corrosion rate with thicker coatings taking longer to undergo dissolution than thinner coatings, thereby delaying the onset of Mg alloy corrosion.

Including Strontium in the CaP coating didn't significantly improve or reduce the corrosion rate over its non-ion containing counterpart, **Figure 1**.

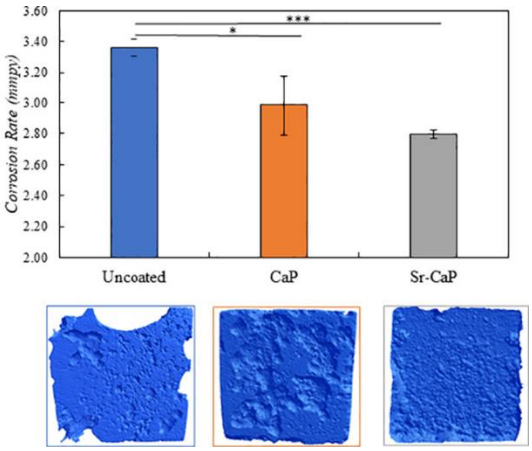

Figure 1 Corrosion rate of uncoated, CaP coated and Strontium-CaP coated Magnesium alloys after 14 days in SBF. MicroCT reconstructions or corresponding samples below. * p-value <0.05, *** p-value < 0.001

DISCUSSION

By varying the deposited coating thickness, the onset of corrosion can be controlled accurately to allow the implant volume to remain unaffected post-implantation until a specified timepoint.

It is well known that inclusion of Strontium can improve bone cell proliferation and differentiation to osteoblast lineages. Other ions which will be investigated for incorporation into the coating include Zinc, Silver and Silicon to produce multi-ion doped coatings.

REFERENCES

[1] Yoshizawa S. et al., Acta Biomater. 10: 2834-2842, 2014.
[2] Acheson J.G. et al., Surf and Coat Tech 421: 127446, 2021.
[3] Acheson J.G. et al., Materialia 6: 100291, 2019.
[4] Capuccini P. et al., Acta Biomater. 4: 1885-1893, 2008.

BIOPRINTING SHAPE-MORPHING TISSUES USING MAGNETIC BIOINKS

Chakraborty, Juhi[1,2]., Kelly, Daniel[1,2]., Daly, Andrew C[1,2]

[1]CÚRAM, SFI Research Centre for Medical Devices, University of Galway, Galway, Ireland
[2]Biomedical Engineering, University of Galway, Galway, Ireland
email: *andrew.daly@universityofgalway.ie*

INTRODUCTION

The spatial arrangement of cells in 3D-engineered cardiac structures can be controlled by a wide range of technologies.[1] To regulate cellular organization on a macroscale, the next generation of dynamic systems such as magnetic procedures can remotely alter and regulate cellular activities.[2] Shape morphing materials generated via magnetically labelled cells in the presence of an external magnetic device has been used to improve the differentiation of cells towards chondrogenic[3], osteogenic lineage and also has proven to improve the cell seeding efficiency of hydrogels.

In the present study we are developing a novel framework for creating controlled geometries in tissue morphologies to mimic the cardiac loop formation occurring at the embryonic stage. We would employ external magnetic fields to guide the patterning and assembly of human iPSC derived cardiomyocytes in collagen based bioink laden with magnetic nanoparticles (MNPs) in a suitable support bath. We speculate that the tissue shape-morphing via 4D bioprinting by cellular loading with MNPs directed by an external magnetic field would be sufficient to drive the cardiomyocytes along the field lines and pattern them to the desired controlled geometries within the collagen hydrogels.

MATERIALS AND METHODS

MNPs (Fe_3O_4) of varying concentrations (0-5 mg/ml) were mixed with 4.8 mg/ml of neutralized collagen to form the acellular bioink. Rheological analysis in terms of (i) viscosity as a function of shear rate (ii) and time sweep were carried out using the MCR 302, Anton Paar using a stainless-steel parallel plate of 25 mm diameter with a gap distance of 0.5mm at 25°C. Human iPSC derived cardiomyocytes (10^7 cells/ml) were added to the acellular bioink to form the magnetic bioink. Live dead assay was carried out on Day 1 and 7 using ethidium homodimer-1 (6 μM) and calcein-AM (4 μM) for 30 min at 37 °C, 5% CO_2 in the dark.

Different geometric patterns were printed with the acellular bioink in a support bath composed of 0.5% agarose using syringe pump printhead of BioX extrusion printer. The extrusion rate was optimized to 5µl/s and speed to 3mm/s. Thixotropic properties of the agarose support bath were assessed by applying low ($1s^{-1}$) and high ($100s^{-1}$) stress rate, periodically. Further, the conjugation of the Fe_3O_4 to collagen protein were prepared for docking using UCSF Chimera software followed by Autodock Vina docking.

RESULTS

The magnetic acellular bioinks with varying MNPs concentration exhibited shear thinning property (Figure 1A). The crosslinking time increased by around 10-15 min compared to the control bioink, i.e. it took around 45-50 min for the magnetic acellular bioink to crosslink (Figure 1B). It was possible to print specific geometric patterns such as spiral and U-shape using the BioX platform with high printing resolution (Figure 1C).

The viability percentage assessed from Live dead assay showed a viability of more than 75 % in presence of MNPs even after Day 7(Figure 1D). The support bath exhibited shear thinning property and good yield strength (Figure 1E)

Computational modelling revealed that Fe_3O_4 exhibited a strong binding affinity with an impressive C-score of -2.9 (Figure 1F). Additionally, the Ramachandran Plot (Figure 1G) demonstrated the structural stability of the collagen protein even after conjugation with Fe_3O_4.

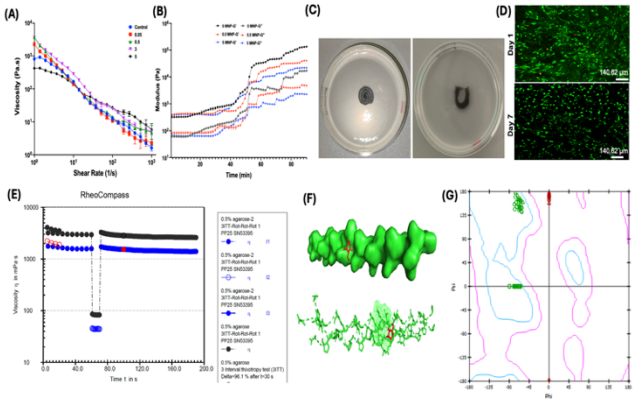

Figure 1: (A)Flow behaviour and (B)Time sweep analysis of collagen acellular bioink with varying MNP concentration; (C) Spiral and U-shaped printed pattern in support bath; (D) Live/dead assay of collagen hydrogels on day 1 and 7. Live cells are displayed in green and dead cells in red; (E) Thixotropic analysis of the agarose support bath; (F) Computational modelling prediction of conjugation of collagen with Fe_3O_4 (G) Ramachandran plot illustrated the native conformation of the amino acid residues on modification of the collagen with Fe_3O_4

DISCUSSION

We developed a shear thinning magnetic bioink with high printability and viability. The ongoing work involves magnetic actuation of iPSC derived cardiomyocytes laden bioprinted constructs in the presence of an external magnetic field. This would mimic the embryonic level cardiac loop formation.

REFERENCES

[1] Rogozinski *et al*, Current methods for fabricating 3Dcardiac engineered constructs *iScience*, 25 104330, 2022

[2] Zwi-Dantsis *et al*, Remote Magnetic Nanoparticle Manipulation Enables the Dynamic Patterning of Cardiac Tissues *Advanced Materials,* 32 1904598,2020

[3] Chakraborty *et al*, Development of 4D-bioprinted shape-morphing magnetic constructs for cartilage regeneration using a silk fibroin-gelatin bioink *CR-PHYS-SC,* 5, 2024

Manufacturing Bioinspired Polymeric Heart Valve Leaflet Material

Gupta, P.[1,2,4], Hughes, C.[1,2,3], Vahab, A.[1], Lally, C[1,2,4]
[1] Trinity Centre for Biomedical Engineering, Trinity Biomedical Sciences Institute, TCD, Dublin, Ireland
[2] Dept of Mechanical, Manufacturing, and Biomedical Engineering, School of Engineering, TCD, Dublin, Ireland
[3]Structural Heart Division, Boston Scientific Corporation, Galway, Ireland
[4]Advanced Material and Bioengineering Research (AMBER), TCD, Dublin, Ireland

INTRODUCTION

Aortic valve stenosis represents the most prevalent valvular heart disease in developed nations [1]. A dysfunctional heart valve can be replaced by either mechanical or bioprosthetic heart valves [2]. However, both pose challenges such as a life-long need for anticoagulants or a high risk of leaflet calcification and valve failure [3, 4]. Polymeric heart valves may offer a viable alternative to current biomaterials used for heart-valve manufacturing. They possess highly tuneable and controlled properties along with the possibility of anti-coagulation and anti-calcification characteristics [5, 6]. Mimicking the native aortic heart valve tissue involves replicating mechanical properties like its characteristic J-shaped curve stress-strain curve and anisotropic collagen-elastin fibre orientation [7]. Melt-electrowriting offers an advantage as it enables pre-programmed fibre deposition, controlled spatial orientation and customisation of design to achieve desired mechanical properties [8].

Ultimately, this study aims to combine the versatile properties of suitable polymers to create bioinspired leaflet materials which minimise calcification and thrombosis. Specifically, this initial work aims to establish a repeatable and reliable manufacturing methodology for such materials.

MATERIALS AND METHODS

To investigate a range of potential material combinations, polycaprolactone (PCL) MEW fibre structures were created by varying two key parameters: fibre angle and layer count. Fibres were printed at angles 45° and 80° with both two and four layers per orientation, giving a total of four different structures, see Fig.1A. A custom metallic mould was designed to embed the MEW framework in polydimethylsiloxane (PDMS). The mould system consisted of a base, a top plate, and spacer sheets (shims), see Fig.1B. Two shims of 0.1 mm and 0.05 mm each were used to achieve a precise PDMS film thickness of 0.3 mm and centre the MEW. The mould assembly involved placing the required number of shims over the base, secured by positioning the top plate and fastening it with screws to ensure a closed system, see Fig.1B.

The PDMS solution, SYLGARD-184 (Dow Chemical Company, Michigan, USA), was prepared by mixing the elastomer base with a curing agent in a 16:1 weight ratio. The mixture was injected into the assembled mould using a syringe and a funnel system, see Fig.1B. The filled moulds were placed in a vacuum chamber for 30 minutes to remove air and cured in an oven at 40°C for 60 hours to ensure complete cross-linking of the PDMS. After curing, samples were imaged to assess fibre angle, fibre diameter, and PDMS film thickness, see Fig.1C and D.

RESULTS

Successful fabrication of MEW structures was achieved with consistent fibre deposition across various orientations, resulting in high-quality samples with uniform fibre diameters. A standardised protocol was developed to produce composite materials, with PCL fibres embedded within the PDMS. Fibre alignments were maintained accurately at both 45° and 80° orientations, and uniform PDMS film thickness was evident post-embedding, see Fig. 1D.

DISCUSSION

The alignment of fibres is crucial for replicating the collagen architecture of native heart valve tissue and mimicking the anisotropic properties of valve leaflets. A low PDMS film thickness was achieved (0.3 mm), which would enable transcutaneous valves to have a low profile during delivery. This initial work focused on standardising the moulding procedure using PCL and PDMS to create consistent leaflet structures. Future research will explore and test different polymer combinations to develop a novel material optimised for aortic valve replacement applications and modify surface properties to minimise calcification and thrombosis.

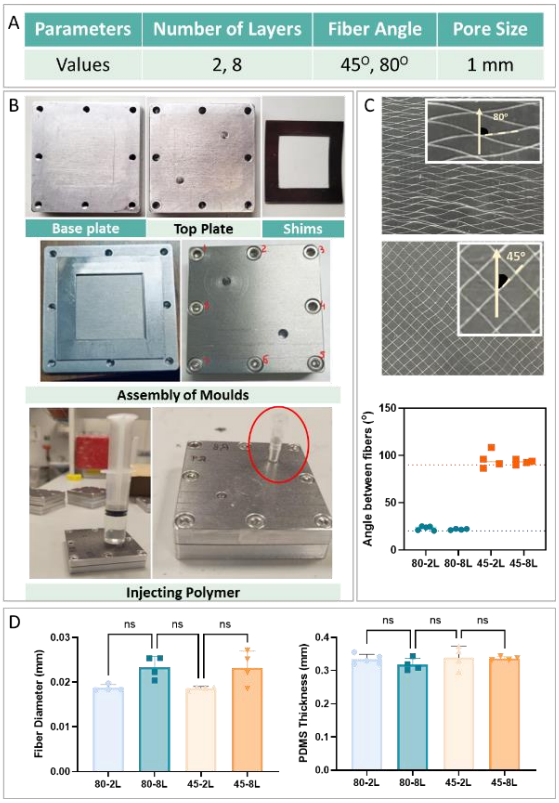

Figure 1 A) MEW printing parameters **B)** PDMS film moulding process **C)** MEW embedded PDMS film and fibre diameter analysis **D)** Fiber angle after MEW framework embedding and PDMS film thickness.

REFERENCES

1.Aluru (et al.), Médical Sciences, 10(2) : 32, 2022.
2.Kostyunin (et al.), JAHA, 9(19): e018506, 2020.
3.Rahimtoola, JACC, 55(22): 2413-2426, 2010.
4.Siddiqui (et al.), Histopathol, 55(2) : 135-144, 2009.
5.Jenney (et al.), Adv Nan Res, 1(2): 2000032, 2021.
6.Hu (et al.), Acta Biomater, In press, 2024.
7.Saidy (et al.), Small, 15(24) : 1900873, 2019.
8.Xu (et al.), J Nanobiotechnology, 22(1) :378, 2024.

PREDICTIVE MODELS FOR PROGRESSION OF THE HIP JOINT IN PATIENTS WITH PERTHES DISEASE

Kane, H[1], Hoare, SM[2], Murphy, TB[1], Green, CJ[1,2,3], Nowlan, NC[1]
[1] University College Dublin, [2] Children's Health Ireland, [3] National Orthopaedic Hospital at Cappagh
email: hannah.kane@ucdconnect.ie

INTRODUCTION

Legg-Calvé-Perthes disease (Perthes disease) is an idiopathic hip disorder which produces ischemic necrosis of the growing femoral head [1]. Perthes disease occurs when the blood flow to the femoral head is restricted resulting in bone tissue death within the epiphysis, often leading to a lasting deformity of the femoral head. The cause of this disease is unknown and arises spontaneously in children.

Predicting prognosis for Perthes patients at presentation is challenging. Prognosis can be assessed using the Lateral Pillar Classification (LPC) system [2], which enables the prediction of outcomes but can only be applied at the midpoint of the disease. Definitively identifying the midpoint is difficult and hinders outcome prediction when a patient presents early in the disease. Contrast-enhanced magnetic resonance imaging (MRI) enables earlier diagnosis and may provide an earlier insight into outcomes [3].

In this paper, we derive quantitative data on tissue types from 3D contrast-enhanced MRI scans and correlate them with their corresponding stages of disease progression. Disease progression can be determined using the Modified Waldenström Classification [4], a system that differentiates the stages of Perthes disease based on radiographic abnormalities and defines seven distinct temporal phases of the disease. We analyse this data using mixed-effects linear regression analysis to evaluate hip joint progression in patients with Perthes disease.

MATERIALS AND METHODS

Contrast-enhanced MRI scans were obtained from 21 patients with unilateral Perthes disease diagnosed at Children's Health Ireland (CHI) in 2018, under the 2020 CHI ethics guidelines. The patient cohort consisted of 8 females and 14 males, aged 3 to 11 years. Radiographs taken within six weeks of these MRI scans were classified using the Modified Waldenström staging system [4], with four stages represented in the dataset: IA,IB, IIA,IIB.

Bone (epiphyseal), cartilage (epiphyseal and physeal), and malperfused regions were segmented in three-dimensions for both hips of each patient using Synopsys Simpleware ScanIP. Further analysis revealed unlabelled regions in all hips. We identified two novel tissue types within these unlabelled regions based on different signal properties. The first is hypothesised to represent forming bone and the second hypothesised as necrotic/fibrotic tissue.

The volumes of the five tissue types, along with their sum and the malperfused region, were correlated with the Modified Waldenström stage.

Linear mixed-effects models were constructed via backward stepwise regression resulting in a final predictive model for each tissue type.

RESULTS

The predictive model of bone volume indicates an overall increase with age, though this is significantly affected by disease stage, with sharp decreases observed at Stages IA and IIA, as illustrated in Figure 1. Age acts as a moderating factor in the overall total volume, generally remaining constant compared to the corresponding contralateral hip across all stages. Epiphyseal cartilage volume is positively associated with age, while physeal cartilage volume is predominantly affected by sex, with males exhibiting larger physes. Physeal tissue volume remains relatively stable over the disease course. Necrotic tissue volumes and regions of malperfusion exhibit variability based on stage, sex, and age. The volume of malperfusion demonstrates a general decline as the disease progresses, a trend that is more pronounced in older male patients.

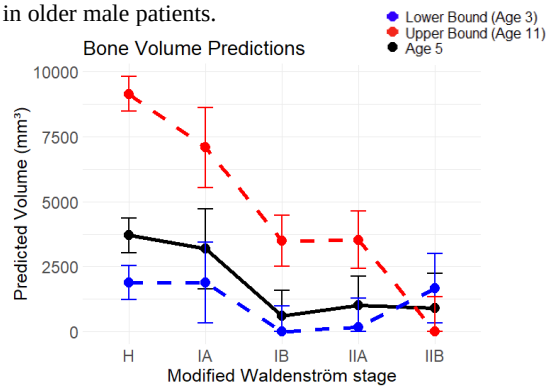

Figure 1 Graph of predicted bone volume across the stages of Perthes for a patient aged 5. (H:Healthy, IA, IB: Avascular stage, IIA, IIB: Fragmentation stage)

DISCUSSION

We have identified two novel tissue types in the Perthes hip, hypothesised to be forming bone and fibrotic/necrotic tissues. Volumetric predictive models highlight the variance between different patients at the same disease stage, indicating that the analyses of these tissues may provide valuable insights into progression and prognosis of Perthes disease.

REFERENCES

[1] Kim HKW, JAAOS 18:676–686, 2010.
[2] Herring JA *et al*, Journal of Pediatric Orthopaedics 12:143-150, 1992.
[3] Sebag G *et al*, Paediatric radiology 27:216-220, 1997.
[4] Hyman JE *et al*, JBJS 97:643-650, 2015.

3D VIRTUAL HISTOLOGY OF ARTICULAR CARTILAGE: MAPPING CHONDROCYTE CHANGES ACROSS POSTNATAL DEVELOPMENT

Vancíková, K.[1], Moore, S.[2] Khatib, N.S.[2], Pierantoni, M.[1], Isaksson, H.[2], Labberté, M.C.2, Marathe, S.[1], Brama, P.A.J.[2], Nowlan, N.C.[2]

[1]University College Dublin, Dublin, Ireland; [2]Lund University, Lund, Sweden; [3]Diamond Light Source, Oxfordshire, UK; [4]Queen Mary University of London, London, UK;

karin.vancikova@ucdconnect.ie

INTRODUCTION

Chondrocytes play a central role in building and maintaining the cartilage matrix [1]. While early postnatal cartilage has densely packed, randomly arranged chondrocytes, mature cartilage develops a specific zonal distribution of chondrocytes vital for its function [2]. However, little is known about how chondrocyte organization changes during maturation and development, a gap critical for advancing tissue engineering and cartilage repair in adults. This study seeks to fill this gap through histology and high-resolution synchrotron-based phase contrast tomography (SR-PhC-CT), providing detailed 3D imaging at the microscale [3].

MATERIALS AND METHODS

Caprine osteochondral cores were obtained from the right front leg, specifically from the proximal region of the medial and lateral sides of the second phalanx across a seven time point during postnatal development (n=5–6 per group), fixed, decalcified, and paraffin-embedded. Sections from medial phalanges were stained with hematoxylin and eosin, scanned and analysed semi-automatically with QuPath software. Samples from the lateral phalanges were imaged at the I13 Imaging Beamline of the Diamond Light Source using a polychromatic beam (~27 keV) and the Pco.edge 5.5 detector with 2x magnification (2000 projections, exposure 0.05 seconds, a pixel resolution 1.625 µm, field of view 4.2x3.5mm). Tomographic reconstruction was performed with SAVU software, with post-processing in Fiji utilizing the 3D Trainable Weka Segmentation plugin for cell detection and 3D Suite-3D Manager for segmentation and analysis. Statistical analysis was performed using one-way ANOVA ($p < 0.05$).

RESULTS

Preliminary analyses of neonatal articular cartilage showed three distinct layers in both histological and tomography images. The outer layer contains rounded chondrocytes, the middle layer flattened chondrocytes free from cartilage canal invasion, and the deepest layer near the subchondral bone has enlarged chondrocytes in circular clusters, with visible cartilage canals (Fig. 1:X). Neonatal cartilage displays a pronounced depth-wise variation in chondrocyte count and volume, with distinct layered structures (Fig. 1:Y, Z). Quantitative analysis of cell density decreased significantly across most time points in both histology and tomography data.

DISCUSSION

Neonatal cartilage exhibits the highest cell density, which decreases progressively with development. We propose the superficial layer represents permanent cartilage, evolving into the adult zonal structure (Fig. 1:X, region 1). The intermediate region of flattened chondrocytes, observed to be free from cartilage canal invasion, may act as the transition between the upper and lower layers (Fig. 1:X, region 2).

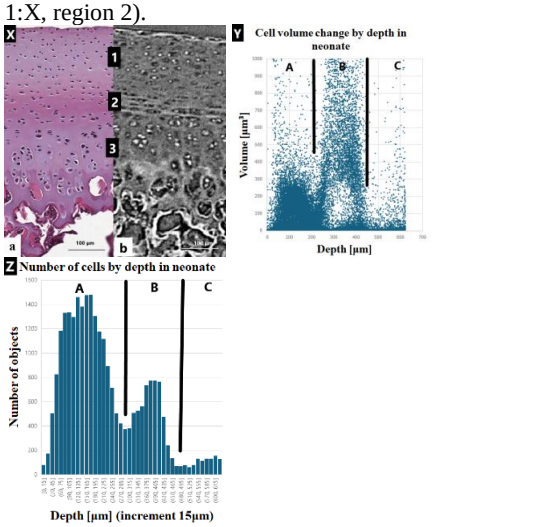

Figure 1 **X**: Sagittal slices of (a) histology and (b) tomography image from the neonate. (1) Represents hypothesised permanent cartilage, (2) border in between and (3) transient cartilage. **Y**: Cell volume change by depth in neonate sample. **Z**: Change in number of chondrocytes depthwise in the neonatal sample. A, B, and C represent distinct areas from a single neonatal sample: A is permanent cartilage, B is transient cartilage, and C is the bone.

The innermost layer consists of transient cartilage, which is expected to calcify over postnatal development (Fig. 1:X, region 3). The statistically significant decrease in cell density reflects a transition from hypercellular juvenile cartilage to hypocellular, anisotropic mature cartilage with zonal structures.

Understanding these developmental changes is essential for enhancing cartilage repair strategies leading to better therapeutic outcomes [4].

This research is supported by the Science Foundation Ireland (Grant No. 21/FFP-A/9090), and Diamond Light Source (instrument I13-2, proposal MG31326).

REFERENCES

[1] Fox et al. Sports Health 1(6):461-8, 2009, [2] Decker et al. Dev. Biol. 1:426(1):56-68, 2017, [3] Horng et al. Biomed. Sci. 28, 1–14, 2021, [4] Chen et al. Am J Physiol Cell Physiol. 305(12):C1202-8, 2013.

Assessing Movement of Peripheral Intravenous Catheters Using Digital Image Correlation

Surlis, R.[1,2], **Carr, J. P.**[3], **Moerman, K. M.**[1,2]
School of Engineering, Mechanical Engineering, University of Galway, Ireland
Lero, the SFI Research Centre for Software, Limerick, Ireland
School of Nursing and Midwifery, University of Galway, Ireland
email: r.surlis1@universityofgalway.ie

INTRODUCTION

Peripheral intravenous catheters (PIVCs) are the most common invasive medical devices used in hospitals and healthcare worldwide, with over 2 billion inserted annually[1]. Despite their prevalence, and repeated synthesis on this topic, PIVCs are associated with an unacceptably high failure rate of 35-50%[2]. Proper PIVC securement is vital, since inadequate securement can lead to catheter dislodgement, extravasation, and thrombophlebitis, which can lead to catheter-related bloodstream infections. These complications often necessitate premature catheter removal and reinsertion, causing patient discomfort, treatment delays, and increased healthcare costs[2]. Recent research has shed light on the critical role that catheter positioning and securement play in PIVC performance. In addition, the catheter insertion angle and tip position, significantly impact the hemodynamic environment within the vein[3]. Finally relative motions and deformations of the device and local tissue can compromise securement and exacerbate vessel irritation. Given the substantial impact of PIVC failure on patient outcomes and healthcare resources, there is an urgent need for an improved understanding of the biomechanics of PIVC performance. This work contributes to this understanding by proposing digital image correlation (DIC), as a novel method to assess device and tissue motion and deformation during and after securement.

MATERIALS AND METHODS

DIC is an effective and versatile non-contact optical measurement technique widely used in the field of materials testing and experimental mechanics to measure displacements on the surfaces of specimens undergoing deformations[4]. Typically DIC involves the correlation of a timelapse of photographs taken as the specimen undergoes deformation. Image correlation, between cameras, and over time, provides accurate assessment of 3D displacements and therefore the derivation of surface strain metrics. To improve correlation, contrasting speckles are applied to the surface. In this study, a volunteer was recruited and a clinician applied a PIVC device (with the needle removed) to the mid-region of the arm (Fig. 1A). Next, contrasting speckles were applied to the local skin and the PIVC surfaces, through stencil based skin-friendly paint transfer. A novel 2-camera DIC setup, featuring low-cost Raspberry Pi HQ cameras and the StereoPi system, was used for imaging (Fig. 1B). Imaging was performed without (Fig. 1C) and with a device present (Fig. 1D). During imaging local tissue and device displacements were manually induced by pulling the skin up (top Fig. 1C) and by pulling the device cable down (top Fig. 1D), both of which aimed to simulate realistic physiological motions. Finally, the open source software DuoDIC[5] was used for DIC and 3D displacement and deformation analysis. Ethical approval was obtained by the University of Galway ethical committee.

RESULTS

Figure 1C shows how the presented DIC methods were able to track local motions and deformations. The visualisations are for the first principal stretch and overlaid direction vectors are inline with the expected predominantly upward/downward tensions respectively. Average first principal stretches in the order of 1.15 were observed for the upward skin tension test (bottom Fig 1C), and 1.05 for the downward cable tension test (bottom Fig 1D), with clear directions towards the source as expected.

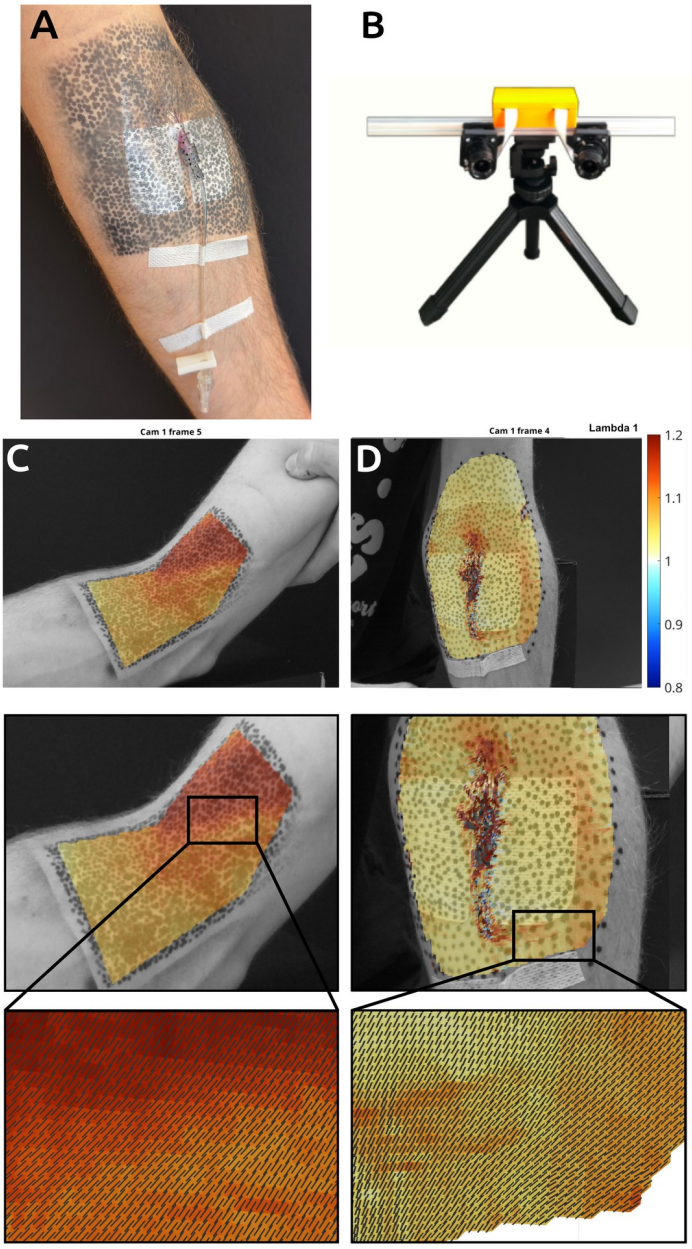

Figure 1 Overview of full experimental procedure and setup.

CONCLUSION

This study demonstrates the feasibility of using DIC to assess local tissue and PIVC device motion. Understanding such relative motions are important in terms of studying local vessel pathology as well as device dislodgement and overall performance. Future work will focus on the further deployment and refinement of the method to study PIVC performance.

REFERENCES

1. Parreira, P. et al., Int. J. Environ. Res. Public. Health 16, 3301 (2019) 10.3390/ijerph16183301.
2. Helm, R. E. et al., J. Infus. Nurs. 42, 149–150 (2019), , 10.1097/NAN.0000000000000326.
3. Piper, R. et al., Sci. Rep. 8, 3441 (2018), 10.1038/s41598-018-21617-1.
4. N. McCormick et al., Materials Today 13 (2010), 10.1016/S1369-7021(10)70235-2.
5. D. Solav et al., J. of Open Source Software 7 (2022), 10.21105/joss.04279.

CAN MRI-QSM BE USED TO CHARACTERISE THE RUPTURE RISK OF HUMAN CAROTID ATHEROSCLEROTIC PLAQUES?

Digeronimo, F.[1-3], Bagnall, J. [1,2], Tornifoglio, B.[1,2], Shmueli, K.[4], Lally, C.[1-3]
[1]Trinity Centre for Biomedical Engineering, Trinity College Dublin, Dublin, Ireland; [2]Department of Mechanical, Manufacturing and Biomedical Engineering, Trinity College Dublin, Dublin, Ireland; [3]Advanced Materials and BioEngineering Research (AMBER) Centre, Royal College of Surgeons in Ireland and Trinity College Dublin, Dublin, Ireland. [4]Department of Medical Physics and Biomedical Engineering, University College London, UK
Email: digeronf@tcd.ie

INTRODUCTION

Carotid artery disease (CAD) involves the accumulation of plaque within the carotid arteries, with plaque rupture causing 15-20% of acute ischemic strokes [1]. However, not all plaques carry the same rupture risk and current clinical assessments primarily classify plaques based on vessel blockage (% stenosis), offering limited insight into the risk of mechanical rupture [2]. Magnetic resonance imaging quantitative susceptibility mapping (MRI-QSM or QSM) can measure tissue magnetic susceptibility (χ) allowing for a more detailed and insightful visualisation of plaque morphology compared to standard clinical MRI (e.g. T1-/T2-weighted) [3]. Additionally, QSM has a high sensitivity to arterial tissue collagen content [4], a key structural component that may influence plaque stability [5-6]. This study explores the potential of QSM for CAD diagnosis using *ex vivo* MRI and mechanical testing of excised human atherosclerotic plaques.

MATERIALS AND METHODS

In a previous study [6], fresh human plaques (N=7) were collected from endarterectomy surgeries at St. James's Hospital, Dublin, and imaged *ex vivo* with a 7T Bruker BioSpec 70/30. T2*-weighted Multi-Echo Gradient Echo (ME-GRE) MRI was acquired. To derive QSM from the ME-GRE data, a two-pass masking post-processing pipeline [7] was first optimised on datasets from three plaque types (II, IV, and VI [8]). This was followed by uniaxial mechanical testing to failure of 2-mm circumferential strips. K-means clustering (k=3) on all extracted mechanical properties was used to identify mechanically relevant strip clusters. Strip χ distributions, extracted via manual masking, and morphological features, were compared across clusters.

RESULTS & DISCUSSION

A QSM pipeline was optimised for type II and IV plaques, but high noise in type VI limited reliable analysis to 4 datasets. K-means identified clusters with increasing rupture likelihood at lower stresses and strains (A to C), Figure 1 (b-c). Clusters B and C mostly contained Lipid Rich Necrotic Cores (LRNCs), a rupture-risk feature [9]. More stable strips had more homogeneous and diamagnetic susceptibility ($\chi < 0$), which suggests a higher elastin and collagen content. Groups A and B showed more diamagnetic susceptibility values than group C, with group B median χ being statistically significantly different from group C.

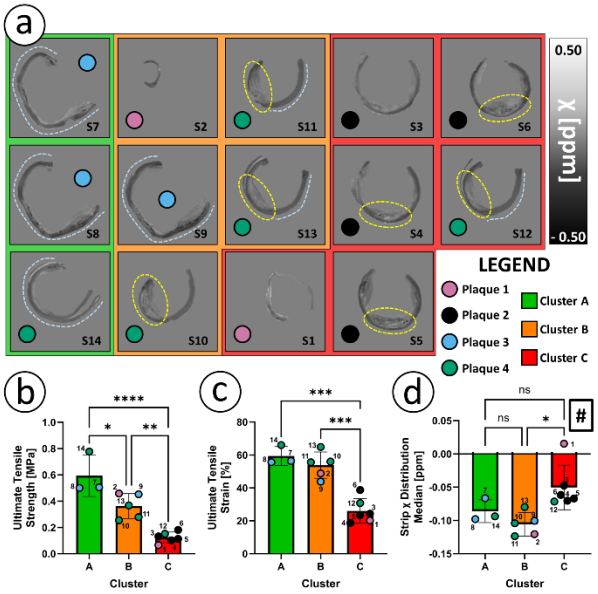

Figure 1 Comparison of plaque strip QSM and mechanical properties: (a) Axial χ map of plaque strips (n=14), with fibrous walls (light blue dashed) and LRNCs (yellow dashed). (b-d) K-means clustered ultimate tensile strength and strain, and median χ distribution (mean ± σ). Significance: ANOVA with Tukey's post hoc (ns, *p<0.05, **p<0.01, ***p<0.001, ****p<0.0001). [#]Similar trend to (d) was observed for mean-χ distributions (ns).

CONCLUSION

Insights on potential χ map-based vulnerability features were gathered, and some significant association was established between mechanics and median χ-distribution properties (i.e. Group B and C). Current work is focused on the optimisation of the QSM pipeline for heavily diseased plaques (type VI) and increasing the sample size for the QSM and mechanical dataset.

REFERENCES

[1] Dossabhoy (*et al.*), Seminar Vasc Surg, 34(1):3-9, 2021. [2] Saba (*et al.*), JVS Vasc Sci, 2:149-158, 2021. [3] Wang (*et al.*), J. Magn. Reson. Imaging, 52(2):534-541, 2020. [4] Stone (*et al.*), Magn Res Med, 86(5):2512-2527, 2021. [5] Johnston (*et al.*), Acta Biomater, 124:291-300, 2021. [6] Tornifoglio (*et al.*), Biomech Model Mechanobiol, 2023. [7] Karsa (*et al.*), ISMRM Annual Meeting, London, 2022. [8] Stary (*et al.*), Circulation, 92(5):1355-74, 1995. [9] Saba (*et al.*), JACC: Cardiovascular Imaging, 17(1):6-11, 2024.

EFFECTS OF TYPE 2 DIABETES ON VERTEBRAL BONE MORPHOMETRY IN ZDF RATS: A MULTISCALE CHARACTERIZATION STUDY BY X-RAY BASED NANO-CT IMAGING

Ali, Wahaaj[1], McNamara[2], Laoise, Vaughan, Ted[1]
[1] Biomechanics Research Centre (BioMEC), Biomedical Engineering, College of Science and Engineering, University of Galway, Galway, Ireland
[2]Mechanobiology and Medical Device Research Group (MMDRG), Biomedical Engineering, College of Science and Engineering, University of Galway, Galway, Ireland
email: (syedwahaajali.rizvi@universityofgalway.ie)

INTRODUCTION

Type 2 Diabetes (T2D) affects millions of people worldwide where T2D patients can face up to a 3-fold higher risk of bone fractures, despite high or normal bone mineral density, making it difficult to predict the risk for bone fractures during this disease [1]. Besides elevated fracture risk, patients with T2DM have increased mortality following fracture compared to patients without diabetes [2]. Clinical studies shows that T2D associated bone fragility is a multi-factorial disease which can alter the composition and structure of bone in spatial and temporal manner. However, our understanding of these mechanisms is still limited [2][3][4]. Therefore, this study aims to uncover the mechanisms for bone fragility in Type 2 Diabetes by exploring the alterations in mineral content and micro/nano structural features of vertebrae and tibial bones extracted from Zucker Diabetic Fatty (ZDF) rats through advanced high-resolution X-ray based Nano-CT imaging technique.

MATERIALS AND METHODS

A longitudinal 46-week study using male Zucker Diabetic Fatty [(ZDF: fa/fa) (T2D) and Zucker Lean (ZL: fa/+) (Control)] (Charles River, France) rats at 12-, 26- and 46-weeks of age (n = 7–9, per age, per condition) was conducted to investigate the multi-scale effects on bones, as explained in our previous study [1]. Frozen L3-L6 vertebrae and fixed tibia bones were used in this study as these bones are more prone to fractures in T2D patients [1][2]. X-ray based Nano-CT imaging system (Zeiss Xradia Versa 620) was used to scan bones at a medium resolution of ~10 µm pixel size to determine bone morphometric parameters with the help of Bone Analysis Module of DragonFly (Comet, Canada). A further scan was taken at high resolution (~1 µm pixel size) to analyse nano-scale features in bone. Hydroxyapatite (HA) phantoms (PTW dosimetry, Germany) were used for calibrating pixel intensities with respective HA densities in bone while DragonFly software was used for extensive image analysis of 3D datasets.

RESULTS AND DISCUSSION

Medium-resolution scan conditions of vertebrae (Fig. a, b) and tibia bones (Fig. d, e) were found to be suitable for determining the bone morphometric parameters such as cortical thickness and porosity, trabecular volume, thickness, separation, number, etc. High resolution scans (Fig. 1g) of bones revealed the local mineral density, lacunae and vascular canals, which were analysed in DragonFly to determine quantifiable parameters such as lacunae quantity, volume and aspect ratio, peri-lacunar mineral density variation, vascular canal volume, number of lacunae per canal, etc. Results of a trial experiment from cortical bone of lamb tibia are shown in Fig. 1h. The analysis was further extended to determine alterations with respect to age, bone type (cortical vs trabeculae), cortical locations (endosteum vs periosteum) revealing many unreported mechanisms of bone fragility in T2D for the first time.

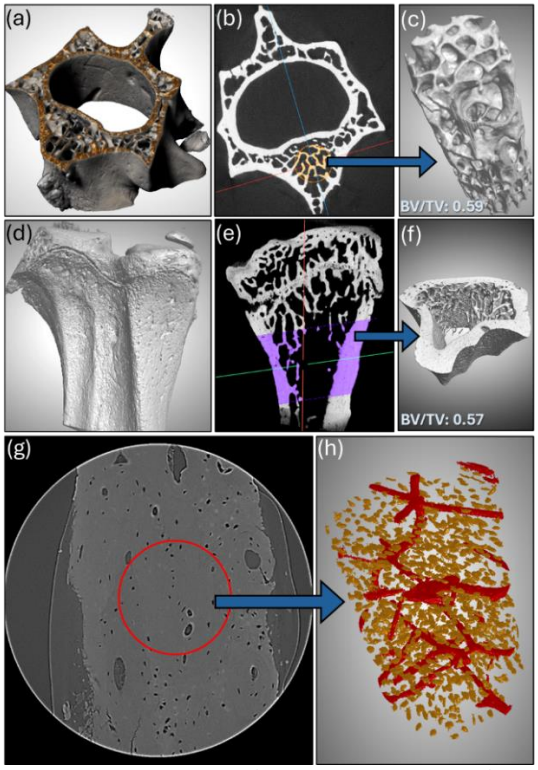

Figure 1 (a, d) 3D rendering of vertebrae and tibia bone of ZDF rats scanned by X-ray based CT imaging, (b, e) 2D projection from reconstructed 3D datasets, (c, f) Selected volume of interest for bone morphometric analysis in DragonFly, (g) High-resolution scan of cortical bone of lamb, (h) 3D rendered image of volume of interest marked by red circle in (g) showing lacunae (in yellow) and vascular canals (in red).

REFERENCES

[1] Monahan et. al, Bone 170:116672, 2023
[2] Faraj et al., The Journal of Clinical Endocrinology & Metabolism 00: 0, 2024
[3] Britton et al., Bone 187: 117190, 2024
[4] Wolfel et al., Bone 165: 116546, 2022

MAPPING GROWTH PLATE DYNAMICS IN GOATS USING MICRO-CT AND HISTOLOGY

Mtchedlishvili, M.[1], Vancíková, K.[1], Green, CJ[1,2,3], Brama, P.[1], Nowlan N.C.[1]
[1] University College Dublin, Dublin 2, Ireland;
[2] Children's Health Ireland at Temple Street, Dublin, Ireland;
[3] The National Orthopaedic Hospital at Cappagh, Dublin, Ireland
email: mariami.mtchedlishvili@ucdconnect.ie

INTRODUCTION

The growth plate is critical for bone elongation, and disruptions in its development can lead to various orthopaedic conditions[1,2,3,4]. To understand normal growth plate development, goats serve as a suitable model due to their physiological similarity to human skeletal growth[5]. This study aims to characterise the structural and cellular changes in the goat growth plate across developmental stages, providing insights that may improve our understanding of growth plate dynamics.

MATERIALS AND METHODS

We examined goat growth plates (n=40) in forelimbs' 2nd phalanx at seven developmental time points (neonates, 6 weeks, 3 months, 6 months, 9 months, 12 months, adults). For histological analysis, the samples were fixed, decalcified in EDTA solution, dehydrated and embedded in paraffin. Serial sections of 6 µm thickness were prepared using a microtome. The sections were stained with hematoxylin and eosin (H&E) to examine cellular architecture and chondrocyte organisation. Images were captured using a high-resolution digital slide scanner (Leica Biosystems) and analysed with QuPath software. For micro CT analysis, contralateral limbs of the same goats were used to look at the 3D shape of the growth plate with Phoenix Nanotom® M and The Phoenix V|tome|x M, depending on the size of the sample. The CT scans were segmented using the 3D Slicer software.

RESULTS

Histological qualitative analysis revealed significant developmental changes in the growth plate across different stages. In neonates, the growth plate exhibited numerous chondrocyte nests located near the boundary of the growth plate and the secondary ossification centre. With the presence of these cells, growth plate exhibited anisotropic cellular arrangement. By 6 weeks, the number and size of these nests decreased, and the overall growth plate architecture appeared more organized. By 12 months, the growth plate lacked distinct zones. In this age group, three distinct growth plate conditions were observed: some goats retained a fully intact growth plate, others exhibited remnants of the growth plate, and some had no growth plate remaining, indicating closure. Micro-CT imaging facilitated the 3D segmentation of the growth plate. The growth plate displayed an irregular shape that was consistent across its structure. The reconstruction confirmed a continuous growth plate in neonates, which gradually thins with age as observed in histological sections.

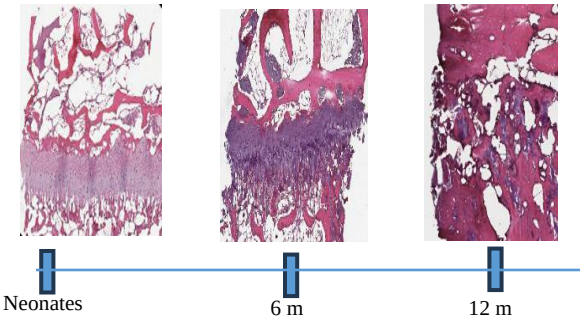

Fig. 1 Maturation of the growth plate from neonates to 12 months. H&E staining.

DISCUSSION

The study captures the structural evolution of goat growth plates during development. Neonates exhibited anisotropic architecture with chondrocyte "nests," which diminished by 6 weeks, resulting in organized growth plate zones. By 12 months, the growth plate lacked distinct zones, and chondrocyte columns were irregular, indicating closure. This age group displayed varying degrees of closure.
Micro-CT confirmed a consistently irregular growth plate shape and progressive thinning over time. These findings provide foundational insights into growth plate dynamics, with implications for understanding normal development and orthopaedic conditions.

REFERENCES

1. Hunziker E.B. et al., Microscopy Research and Technique 28:505–519, 1994
2. López J.M. et al., International Journal of Molecular Sciences 25:6767, 2024.
3. Ornitz D.M. et al., Developmental Dynamics 246:291–309, 2017.
4. Pines M. et al., Poultry Science 70:1806–1814, 1991.
5. Chu C.R., Szczodry M., Bruno S., Tissue Engineering Part B: Reviews 16:105–115, 2010.

The Role of MCT-1 in Trabecular and Subchondral Bone Dynamics in a Pre-clinical Exercise Model

Twombly, B[1,2,3], Telesford, L[1], Uberti, M[1,2,3], Barad Z[4], Maggio, M[2,3], Kelly, A[4], Hoey, D[2,3], Hodgkinson T[1,2,3], Kennedy, O.D [1,2,3]

[1]Tissue Engineering Research Group, Department of Anatomy and Regenerative Medicine, Royal College of Surgeons in Ireland (RCSI), [2]Advanced Materials and Bioengineering Research Centre (AMBER), [3]Trinity Centre for Biomedical Engineering, Trinity College Dublin (TCD), [4]Dept of Physiology, Trinity College Dublin

Email: bridgettwombly24@rcsi.ie

INTRODUCTION

Physical activity is well-established as a determinant of musculoskeletal health, with long-term exercise exerting beneficial effects on bone density and microstructure (1). The role of metabolic modifiers, such as MonoCarboxylate Transporters (MCT) are thought to be important in this process, but their role in exercise-induced skeletal adaptations remains unclear. Since these factors are prominent in hypoxic conditions, they are likely important. As part of a larger study on the physiological effect of exercise and MCT inhibition, we investigated potential parallel effects of exercise on bone microstructure at two sites in the tibia: the commonly used metaphyseal trabecular bone region, and the subchondral bone compartment, which may have relevance to bone cartilage crosstalk. Bone microarchitecture was quantitatively assessed using micro-computed tomography (microCT). While a range of outcomes have been assessed in related studies, here we solely report on the skeletal outcomes, providing insights into the interaction between exercise, metabolic regulation, and bone health.

MATERIALS AND METHODS

Equal numbers of male and female C57BL/6J mice, at 3 months old, were used for this study. Animals were divided into four male, and four female, groups (n=3/group). Exercise groups ran on a laboratory-based rodent treadmill 3x/week for 30 min. Drug-treatment groups received 50 nmol of AR-C155858 (MCT1/2 inhibitor) with each exercise session, and each group was run with the appropriate control. Animal studies were carried out under institutional ethical license and approval, mice were euthanized at 14 months. After sacrifice, knee joints, including the tibia and femur, were harvested fixed and then scanned using a benchtop Scanco/Bruker microCT system (mCT-40). The scan parameters were applied as follows: Energy/intensity: 70kVp, 114 µA, 8 W and Calibration: 7:70 kVp, BH: 1200mg HA/ccm, scaling. The analysis software CTAn version 1.16 was used to measure the bone parameters in the two sites of each sample. Metaphyseal and subchondral trabecular bone Regions of Interest (RoI) were determined by standards from the literature.

RESULTS

The microCT data showed that in the exercise group bone volume fraction (BV/TV%) and trabecular number (Tb.N) were increased following MCT inhibition in both male and female mice in the metaphyseal trabecular bone region. There was no significant difference in the subchondral bone region in male or female mice. Furthermore, there were no significant differences in Tb.Th in any experimental group in either region. Interestingly, BV/TV% and Tb.N in the subchondral region tended to increase, in all groups, in the male animals compared to females.

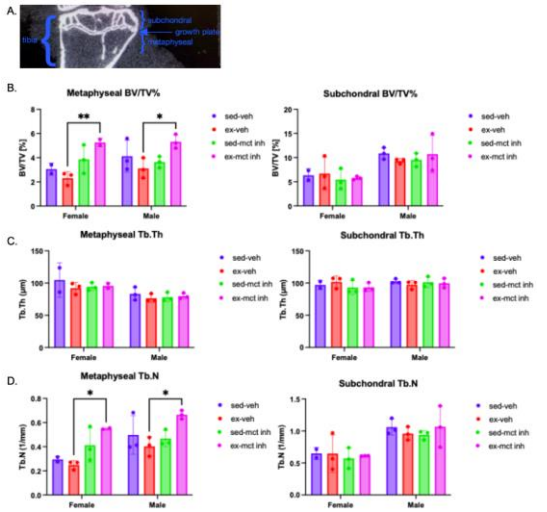

Figure 1. (A) Coronal view of tibial metaphyseal and subchondral bone compartments (B) BV/TV of metaphyseal and subchondral compartments. (C) TbTh of metaphyseal and subchondral compartments. (D) TbN of metaphyseal and subchondral bone compartments.

DISCUSSION

The study highlights the responses of metaphyseal and subchondral bone tissues to exercise and MCT inhibition. Metaphyseal BV/TV% increased in the exercise group based on MCT inhibition. No changes were found in the subchondral region suggesting an anabolic mechanism is involved. Subchondral bone tissue shares properties regarding porosity and surface area to metaphyseal bone and is subject to a larger load bearing role. It is intriguing that similar changes are not observed in this area. Tb.Th remained consistent across all groups and regions, but the metaphyseal region increased in Tb.N between the exercise-vehicle and exercise-MCT inhibitor groups. The subchondral bone did not change in Tb.Th nor Tb.N, emphasising the site-specific nature of bone remodelling and suggesting that MCT inhibition may selectively enhance exercise-induced changes in these regions.

REFERENCES

(1) Santos, L. *et al*., Biogerontology, 2017

USING SINGLE-SEQUENCE MR QUANTITATIVE SUSCEPTIBILITY MAPPING AS A SUBSTITUTE FOR MULTI-CONTRAST MRI FOR THE RISK STRATIFICATION OF CAROTID PLAQUE RUPTURE

Bagnall, J.[1,2], Digeronimo, F.[1,2], Tornifoglio, B.[1,2], Mooney, C.[3], Zhang, M.[4], Lally, C.[1,2,5]
[1]Trinity Centre for Biomedical Engineering, Trinity College Dublin, Dublin, Ireland; [2]Department of Mechanical, Manufacturing and Biomedical Engineering, Trinity College Dublin, Dublin, Ireland; [3]UCD School of Computer Science, University College Dublin, Dublin 4, Ireland; [4]School of Computer Science and Statistics, Trinity College Dublin, Ireland; [5]Advanced Materials and Bioengineering Research Centre (AMBER), Royal College of Surgeons in Ireland and Trinity College Dublin, Dublin, Ireland.
email: bagnallj@tcd.ie

INTRODUCTION

Carotid artery disease is the build-up of plaque within the carotid arteries, affecting 21% of the global adult population [1]. Carotid plaque rupture accounts for 15-20% of acute ischemic strokes [2]. Percent stenosis, or degree of vessel lumen narrowing, is the current diagnostic criterion for stroke prediction. Assessing plaque composition and morphology, however, can improve the specificity of identifying plaques vulnerable to rupture, as outlined in the stroke risk classification system: carotid plaque-RADs [3]. Optimal visualisation of carotid plaque composition and morphology typically requires multiple imaging modalities, including multi-contrast MRI and CT [4]. Quantitative susceptibility mapping (QSM) is an MRI method which can quantify the magnetic susceptibility of biological tissues and can distinguish between calcification and intraplaque haemorrhage (IPH) which have been identified as key features for evaluating carotid plaque vulnerability [3,5]. QSM has the potential to non-invasively characterise carotid plaque composition and morphology and hence serve as a single-sequence imaging technique for evaluating plaque rupture risk. In this study, QSM combined with deep learning are explored to automate the characterisation of carotid plaque composition and morphology for the risk stratification of carotid plaque rupture.

MATERIALS AND METHODS

Excised human carotid plaques (n=2) were fixed with 10% formalin and placed in PBS in a custom holder to accommodate registration between imaging modalities. *Ex vivo* multi-contrast MRI (T1W, T2W, PD, MP-RAGE) and ME-GRE data for QSM were acquired using a 7T Bruker BioSpec 70/30 USR system (Bruker, Ettlingen Germany). QSM images were generated using a two-pass masking approach optimised for *ex vivo* carotid plaque visualisation. Multi-contrast MRI was used to identify IPH, lipid and fibrous tissue and will be further validated with Movat's Pentachrome staining accompanied by brightfield microscopy. µCT was generated using an optimised acquisition sequence (12 µm isotropic resolution) using a Nikon XTH225 ST system to validate the presence of calcification. Plaque rupture risk was informed using an explainable stroke risk classification system: carotid plaque-RADs [3].

RESULTS

Calcification, validated using µCT, appears hypointense in multi-contrast MRI and diamagnetic ($\chi<0$) in the QSM image, see Fig. 1. A paramagnetic ($\chi>0$) region appears in the QSM image which is indicative of IPH. This delineation of the calcification and IPH regions is specific to the QSM sequence when compared to the other standard clinical imaging modalities, see Fig. 1.

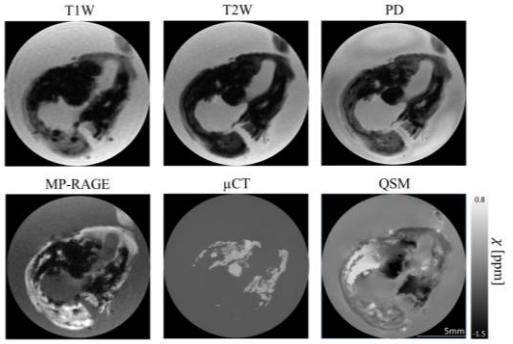

Figure 1 *Ex vivo multi-contrast MRI, µCT, and QSM of a carotid plaque. µCT identifies the calcified region.*

DISCUSSION

From the preliminary results, the calcified region appears distinctly diamagnetic in the QSM image whilst the presence of paramagnetic IPH will be further validated with histology. Future work will expand the dataset to nine carotid plaques and provide data to train and validate a self-configuring U-Net for segmentation of plaque components [6]. The U-Net model has previously been optimised for calcification and IPH segmentation in human cadaver carotid plaques [7]; however, it lacked a robust ground truth. This new dataset will ultimately have a ground truth for each plaque component using multi-contrast MRI, µCT and histology. Establishing a single-sequence QSM imaging technique, with automated feature delineation using deep learning, can provide a robust diagnostic tool for informing plaque rupture risk.

REFERENCES

[1] Song (*et al.*), Lancet Glob. Health, 8(5): p. e721-e729, 2020. [2] Dossabhoy (*et al.*), Semin. Vasc. Surg., 34(1): p. 3-9, 2021. [3] Saba (*et al.*), JACC: Cardiovasc. Imaging, **17**(1): p. 62-75, 2024. [4] Saba (*et al.*), AJNR, **39**(2): p. E9-E31, 2018. [5] Ikebe (*et al.*), MRMS, 19(2): p. 135-140, 2020. [6] Isensee (*et al.*), Nat. methods, 18(2): p. 203-211, 2021. [7] Bagnall (*et al.*), BINI, Queen's University Belfast, 2024.

MICROMECHANICAL MODELING AND EXPERIMENTAL ANALYSIS OF MAGNESIUM ALLOY WE43

Karamifard, F.[1], Vaughan, TJ. [1], McHugh, PE.[1]
[1] Biomedical Engineering department, College of Science and Engineering, University of Galway
email: F.Karamifard1@universityofgalway.ie

INTRODUCTION

Bioresorbable materials are a critically important part of the next generation of medical implants, where the implant can degrade and resorb harmlessly into the body once it has completed its function [1]. Bioresorbable metals, such as magnesium (Mg) alloys, hold great promise for cardiovascular and orthopaedic implant applications where tissue structural support of is needed while the tissue heals and recovers normal function. Mg alloys provide great structural support on implantation. However, they tend to have relatively high degradation rates in the bodily environment, resulting in the premature loss of structural support, and researchers have been actively exploring ways to retard degradation rates [2,3].

This study focuses on understanding the behavior of magnesium alloy WE43 through both micromechanical modeling and experimental analysis. The models will be enhanced to simulate the bioresorption of the material (corrosion of the Mg alloy).

MATERIALS AND METHODS

Magnesium alloys have distinct deformation behavior compared to other metals. This distinction stems from their hexagonal-close-packed (HPC) lattice structure [4]. The micromechanical modeling utilizes crystal plasticity finite element (CPFE) modeling of the HCP crystal structure. The plastic deformation of a single crystal is assumed here to arise from crystalline slip and twining. A UMAT subroutine is used to model the plastic deformation. In the first stage, a 2D Representative Elementary Volume (RVE) including 10 grains (Fig.1-a) was developed, and periodic boundary conditions were applied to this model.
The experimental analysis in this study involves the use of 3D Diffraction Contrast Tomography (DCT), available using an in-house Zeiss Versa 620 system to replicate typical grain size and shape statistics. The scanning images allow the construction of the CPFE models that will realistically represent the microstructure (representative volume elements RVEs). DCT scans have been done for 2 samples with dimensions of 0.5×0.5×2 mm. For each sample, three sections at different lengths were individually modelled. Fig.1-b shows one section with dimensions of 0.304×0.304×0.304 mm, containing 78 grains.
NEPER is an open-source software that was used to generate tessellation corresponding to the polycrystal and to mesh it for FEM simulation (Fig.1-b). In this case, each grain has its own ID and real orientation.

RESULTS

Fig1.a depicts unique crystallographic orientation and size, leading to variations in how grains deform under applied load. Consequently, the contour of strain provides valuable insights into the distribution and magnitude of strain across the entire sample.

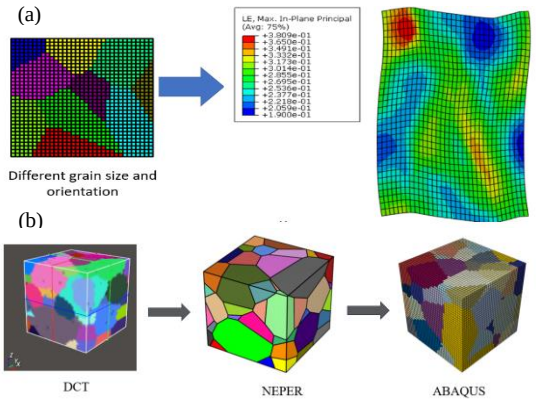

Figure 1 (a) model with 10 grains and random orientation, (b) process of polycrystalline modelling from the DCT data

Fig.1-b depicts the result from the DCT scan and the final model in Abaqus which is very similar to each other.

DISCUSSION

This study has successfully demonstrated the development of a near-to-reality model using scan data, providing valuable insights for micromechanical and corrosion modeling. By employing a near-to-reality model, it becomes possible to determine the microstructural design changes required to minimize overall degradation rates and maximize the mechanical integrity and lifetime of the implants which are next steps of this study. The main novelty in this research will be that the micromechanical and bioresorption modelling combination has not been realised before and therefore its success will represent a significant scientific achievement.

REFERENCES

[1] Hussain. (et al.), Heliyon 10, 2024.
[2] Tsakiris. (et al.), Journal of Magnesium and Alloys 9:1884–1905, 2021.
[3] Wang. (et al.), Engineering 6:1267–1275, 2020.
[4] Grogan *(et al.)*, Journal of the Mechanical Behavior of Biomedical Materials 34:93–105, 2014.

COMPUTATIONAL DESIGN OF MICROFLUIDIC ASPIRATION DEVICES FOR HIGH-THROUGHPUT ANALYSIS OF TUMOUR CELL BIOMECHANICS

McSweeney, O., McEvoy, E.
Discipline of Biomedical Engineering, University of Galway
email: o.mcsweeney2@universityofgalway.ie

INTRODUCTION

Breast cancer is the most common cancer globally. Current treatments overlook the mechanobiology of tumour growth and metastasis; relying instead on biological and clinical insights. An engineering-focused approach could enable tailored treatments by understanding the stress-dependence of cancer cell proliferation and survival [1]. This project aims to explore cancer's stress response via single cell aspiration in a microfluidic chip. By trapping single cells via a pressure gradient between main and microchannel, ΔP, their biomechanical properties can be analysed [2], aiding in the development of models for tumour growth and treatment response.

MATERIALS AND METHODS

Cells can be trapped via micropipette aspiration when a ΔP from main channel to microchannel of ~100 Pa is achieved [3]. Chip geometries were designed in Autodesk Inventor. An initial model consisted of a tapered U-bend channel (UB), connected by a microchannel. The taper from wide inlet to narrow outlet facilitated the pressure gradient. Assuming laminar flow and a no-slip wall condition, Ansys was used to analyse how varying inlet velocity, v_{in} (1–5 m/s) and inlet and outlet diameters (D_i: 2.25–3.25 mm, D_o: 1–1.5 mm, respectively), influenced pressure gradient ΔP.

A second chip design was based on previous studies that manipulated channel resistances to control flow and pressure exerted on aspirated cells, analogous to voltage and current in a Wheatstone bridge (WB) [2]. The geometry included three microchannels adjoining two main channels, where the number of "open" microchannels, N, was varied, i.e., those without trapped cells. Inlet flow rate, Q_{in}, ranged from 20-120 µL/h to investigate the effect on microchannel pressure gradients, ΔP_A, along their centrelines. Results were compared to analytical values using the equation $\Delta P_A = Q_B R_A / N$ where Q_B is the flow rate through the bridge channel, and R_A is flow resistance of the single aspiration channel.

RESULTS

The UB channel dimensions were varied until a distinct but smooth ΔP was established between the chip's main channel and the microchannel inlet, shown by the pressure contour plot of the axial cross-section of the U-bend in Figure 1(A). A low v_{in} (1 m/s) and gradual change in U-bend diameter (D_i/D_o = 1.5) allowed for a smooth pressure distribution, and the lowest ΔP_A. This is demonstrated by the phase diagram of Figure 1(B), showing the dependence of ΔP_A on both D_i/D_o and v_{in}. Specifically, it was found that increasing D_i and v_{in} resulted in a larger ΔP_A across the microchannel, but changing D_o was less impactful.

The WB geometry was assessed at N=1 and N=3. Figure 1(C) shows the pressure contour of an axial cross-section when N=3, depicting a homogenous ΔP_A across each microchannel. ΔP_A was found to be positively proportional to Q_{in} and higher with increasing N. The model closely agrees with analytical results, shown by the closely aligned plots of Figure 1(D). Low v_{in} and D_i/D_o ratios result in reduced flow acceleration and minimal pressure drop, hence ΔP_A is lowest at these conditions. At high N, flow is distributed evenly, reducing microchannel flow rate and ΔP_A.

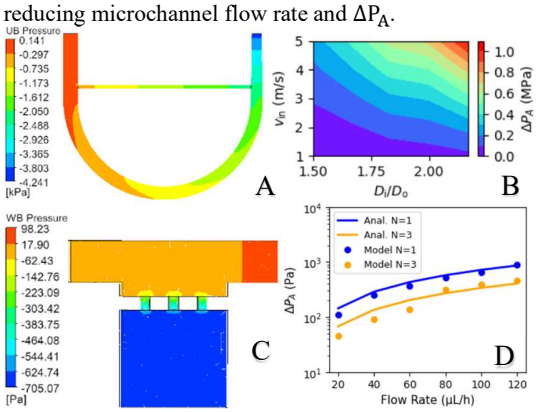

Figure 1 (A) Pressure contour of axial UB cross-section. (B) ΔP_A phase diagram varying D_o/D_i and v_{in} across UB micro-channel (C) Pressure contour of axial WB cross-section. (D) ΔP_A comparison between analytical (solid) and model (markers).

DISCUSSION

This study investigated multiple chip designs to explore the influence of channel geometries, velocity and number of open channels on aspiration pressures. Micropipette aspiration is a promising emerging technique for measuring cell deformation by application of a known pressure, for high throughput characterisation of single cell biomechanics. Future research will involve combining this with finite element simulations to understand complex non-linear cell biomechanics.

REFERENCES

[1] Cross *et al.,* Nanomechanical analysis of cells from cancer patients, 2: 780-783, 2007.
[2] Li *et al.*, A Microfluidic Micropipette Aspiration Device to Study Single-Cell Mechanics Inspired by the Principle of Wheatstone Bridge, Micromachines, 2019.
[3] Reynolds *et al.*, On the role of the actin cytoskeleton and nucleus in the biomechanical response of spread cells, 35: 4015-4025, 2014.

ACKNOWLEDGEMENTS

This work was supported by the European Research Council (Grant number 101116234).

THERMODYNAMIC MODELLING TO PREDICT INTRACRANIAL ANEURYSM IN PATIENT SPECIFIC GEOMETRIES

McDonagh, P.[1], McGarry, P.[1]
[1] University of Galway
email: p.mcdonagh23@universityofgalway.ie

INTRODUCTION

Intracranial aneurysms (IAs) are localized dilations of cerebral arteries that pose significant clinical risks, particularly when ruptured, causing subarachnoid haemorrhage (SAH). Unruptured IAs affect 2–5% of the population, with risks influenced by factors like age, gender, genetics, hypertension, and smoking [1,2].

During IA evolution, significant extracellular matrix (ECM) changes occur, including Elastin degradation, Collagen remodeling, and loss of smooth muscle cells (SMCs), leading to reduced vessel wall strength and elasticity [3]. Despite advancements in imaging techniques, rupture risk assessments largely rely on qualitative metrics and clinician judgment lacking integration of patient-specific variations in aneurysm morphology, hemodynamic, and vessel wall biology. Patient-specific models aim to address these gaps by incorporating individualized data, such as vessel geometry and tissue remodelling, to predict IA progression.

We propose a framework to predict arterial growth fundamentally motivated by cell level remodelling, to provide a diagnostic tool to predict IA growth in patients.

METHODS

A constitutive law is implemented to describe Elastin, Collagen, passive matrix components, and smooth muscle cell (SMC) contractility, using a framework developed by Concannon et al. [4], where strain energy components of these models are also calculated. Growth is modelled when free energy of the system $\hat{G}_{Tot}$ increases above the homeostatic free energy $\hat{G}_H$, caused by deformation in Collagen, Elastin, SMCs and the passive matrix component, where circumferential tissue growth is calculated as:

$$\frac{dF_G}{dt} = \omega\left(\exp\left(\beta\left(\hat{G}_{Tot} - \hat{G}_H\right)\right) - 1\right)$$

where β is a thermodynamic temperature, and ω is a rate of growth.

Idealised fusiform and saccular IA geometries are then investigated. A patient specific mesh of the internal carotid artery is created, using image segmentation with SimVascular (Fig.1A), and a mesh of the vessel is created using the GIBBON toolbox (Fig.1B).

A finite element (FE) model of an artery is developed in Abaqus, with our constitutive law for arterial components alongside our growth model, applied as a user-defined material (UMAT). Steady state conditions for artery homeostasis are predicted for a vessel at 120 mmHg. We then study the effects of growth in a vessel experiencing hypertensive 130 mmHg conditions, and circumferential growth is predicted in the vessel. An additional study investigates Elastin and SMC degradation in an identical model, to examine their effects on vessel growth, alongside a parametric study to predict resulting vessel remodelling.

RESULTS

The effect of complete Elastin and SMC digestion leads to an increase in vessel radius of 14% in the local fusiform patch (Fig.1C). Growth further amplifies radius changes, highlighting the role of growth processes in IA development. Hoop stress analysis shows distinct deformation patterns for fusiform and saccular IAs, with smaller regions in the saccular model experiencing less growth due to geometric constraints (Fig.1D).

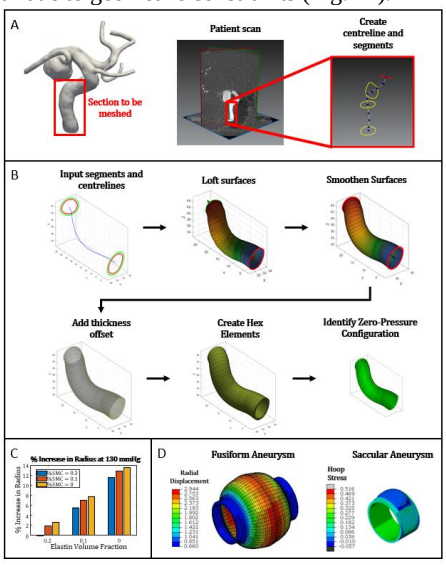

Figure 1 (A) Image segmentation using SimVascular. (B) Patient specific meshing using GIBBON. (C) Prediction of vessel remodelling due to Elastin and SMC degradation. (D) Fusiform and saccular IA geometries after induced growth.

DISCUSSION

The results from Figure 1C show that Elastin and SMC degradation significantly influence IA radius changes. Incorporating growth is essential to replicate the magnitude of radius change observed in fully developed IAs.

Future work will focus on enhancing the model by integrating subcellular-scale thermodynamically based frameworks. This includes modelling SMC transitions from contractile to synthetic phenotypes and capturing ECM remodelling processes, such as Collagen deposition and organization. These advancements will bridge cellular and tissue-level phenomena, enabling accurate predictions of IA initiation, progression, and rupture.

REFERENCES

[1] Rinkel GJ et al., *Stroke* 29:251–256, 1998, [2] Brinjikji W. et al., *AJNR Am J Neuroradiol* 37:615–620, 2016, [3] Morel S. et al., *Neurosurg Rev* 45:1233–1253, 2021, [4] Concannon J. et al., *Acta Biomaterialia* 125:154–171, 2021.

FINITE ELEMENT ANALYSIS INVESTIGATION INTO THE EFFECTS OF STABILIZING AGENT STIFFNESS AND VOLUME ON THE BIOMECHANICS OF THE LUMBAR SPINE.

Johnston, R.D[1], Murphy, C.M[1,2,3]

[1]Tissue Engineering Research group, Department of Anatomy and Regenerative Medicine, Royal College of Surgeons in Ireland, Dublin, Ireland. [2]Trinity Centre for Biomedical Engineering, Trinity College Dublin, Dublin 2, Ireland
[3]Advanced Material and Bioengineering Research (AMBER) Centre, Trinity College Dublin, Dublin, Ireland
email: (robertjohnston@rcsi.com)

INTRODUCTION

Osteoporosis is known to be the most prevalent bone disease in the world, contributing to 8.9 million fractures annually [1]. Osteoporotic vertebral fractures (OVFs) are the most common complication and often lead to secondary fractures, reducing functional capability and quality of life. Conventional procedures for restoring structural integrity of the fractured vertebrae such as vertebroplasty or balloon kyphoplasty, use polymethacrylate (PMMA) bone cement as its stabilizing agent [2]. Due to the stiffness mismatch between PMMA and native bone and the occurrence of secondary fractures, alternative treatment approaches are being developed. Hydrogels that can have tuneable mechanical properties and allow for bone regeneration have been touted as a possible solution [3]. The aim of this work is to computationally investigate through finite element analysis (FEA) the mechanics of the lumbar spine when its considered healthy, osteoporotic, and osteoporotic with PMMA or a hydrogel being used as the stabilizing agent at two different volumes.

MATERIALS AND METHODS

Finite element models were created from images of the lumbar spine, with a focus on the L2-L4 vertebrae for biomechanical assessment, as shown by Fig. 1. Constitutive models and material parameters for each component were taken from literature [4]. Six different biomechanical loading conditions were simulated to observe the stress distribution within the vertebrae in healthy, osteoporotic, osteoporotic with PMMA volume of 3mL and 6mL in the L3 vertebrae and osteoporotic with hydrogel volume of 3mL and 6mL in the L3 vertebrae respectively.

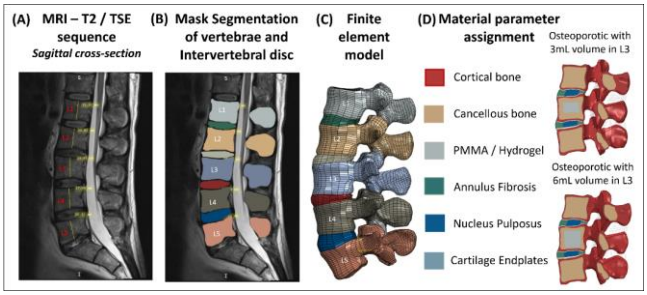

Figure 1: *(A) Initial MRI image showing sagittal cross-section of the spine (B) Mask segmentation and creation of sets (C) Finite element model created (D) Material assignment within the finite element model.*

RESULTS

Max von mises stress increases from 73.18 MPa to 80.04 MPa under compression loading when considered healthy and osteoporotic respectively, see Fig. 2A, 2B. Using higher volumes of the hydrogel increases the stress distribution observed at implant site, see Fig. 2C, whilst higher volumes of PMMA increase the stress distribution observed in adjacent vertebrae, see Fig. 2D.

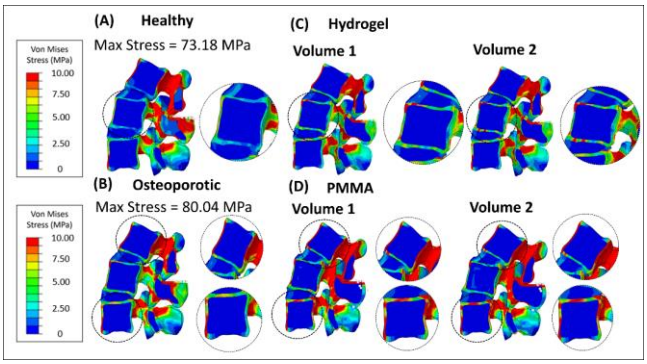

Figure 2: *Von Mises stress (MPa) distributions observed for the L2-L4 vertebrae under compression (A) Healthy (B) Osteoporotic (C) Osteoporotic with hydrogel volume of 3ml and 6ml (D) Osteoporotic with hydrogel volume of 3ml and 6ml.*

DISCUSSION

Our results show that for every loading condition simulated, the peak stresses observed within the L2-L4 segment increases when comparing osteoporotic to healthy simulations. In our PMMA simulations, there is a higher volume of elements experiencing higher stresses in the adjacent vertebrae with a lower stress observed in the implant site. This high stress would agree with clinical observations, in which secondary fractures occur proximal and distal to the implant site. The opposite trend to PMMA is observed when we consider the hydrogel, with higher stresses observed at the implant site, suggesting that a stiffness transition must occur that redistributes the stress within the vertebrae to prevent secondary fracture occurrence.

CONCLUSIONS

Overall, FEA of the lumbar spine can provide critical insights into the mechanical implications of different treatment options and aid in the development of new medical devices for the treatment of osteoporotic vertebral fractures.

ACKNOWLEDGMENTS

European Research Council Consolidator Grant under agreement GAP-101125820 (RESTORE)

REFERENCE

[1] T.J. de Villiers et al., (2022) 1–3. https://doi.org/10.1080/13697137.2021.1965408.
[2] I.H. Lieberman et al., (2005) S305–S316. https://doi.org/10.1016/j.spinee.2005.02.020.
[3] K. Kaur, R. et al., (2023) 806–814. https://doi.org/10.1007/s11914-023-00839-x.
[4] S. Mondal, et al., (2024) 1–12. https://doi.org/10.1002/jbm.b.35359

FINITE ELEMENT MODELLING OF HOLLOW MICRONEEDLE INSERTION INTO SKIN

Yadav, P.R.[1], Shu, W.T.[1], Ní Annaidh, A.[1], O'Cearbhaill, E.D.[1]
[1] School of Mechanical and Materials Engineering, University College Dublin, Belfield, Dublin 4, Ireland
email: prateek.yadav@ucd.ie

INTRODUCTION

Hollow microneedle (HMN)-based intradermal drug delivery has garnered significant attention as an alternative to subcutaneous delivery owing to its minimally invasive nature and potential to provided targetted administration into the skin.[1] HMN are typically <2mm long and pierce the *stratum corneum* (SC), the outermost layer of skin, enabling efficient drug transport of liquid based therapeutics, including drugs and vaccines. Despite its potential, challenges persist around inefficient needle insertion, which can result in drug leakage at the skin surface. Additionally, issues such as needle-tip coring or blockage and dermal tissue compression during microneedle insertion can increase backpressure, highlight the need for further optimization of HMN design and insertion mechanics to enhance performance and reliability.[2]

In this study, *an in silico* model is developed to simulate the insertion of HMN into skin. This study evaluates the effects of HMN insertion depth and angle on the mechanical behaviour of the skin and microneedle, incorporating the skin's layered structure and nonlinear material properties for realistic simulations. The model provides a robust framework for optimising microneedle designs and insertion strategies, paving the way for safer and more effective transdermal drug delivery systems.

MATERIALS AND METHODS

Numerical analysis is conducted using Finite Element Modelling (FEM) with ABAQUS/Explicit software. HMN design is based on the commercially available NanoSoft MN, with a height of 0.6 mm and lumen diameter as 70 µm. The skin is modelled as a hyperelastic Neo-Hookean material, as previously described.[3] A 5% skin pretension is applied, followed by HMN insertion at 45º angle to the skin surface, with a constant velocity of 0.6 mm/s. Element deletion based on maximum stress conditions is implemented using the VUSDFLD subroutine to simulate the puncture process and capture skin failure during HMN penetration. To save computational time, only half of the symmetric HMN and skin system is simulated. HMNs (typically silicon or stainless steel) are modelled as a rigid material and skin meshed with hexahedral elements.

RESULTS & DISCUSSION

Figure 1(a) illustrates the deformation and stress distribution in the skin during HMN insertion. The interaction between the MN and the skin shows that the von Mises stress is concentrated around the needle tip during penetration. When the von Mises stress at the HMN tip exceeds the yield stress of different skin layers (e.g., $\sigma_{y,sc}$=18 MPa), the failed elements are immediately deleted. This enables the HMN to penetrate further into the skin. As seen in Fig.1 some part of the skin enters the MN lumen, but no coring is observed initially. The needle is unable to penetrate further due to design restrictions. At the final stage, a portion of the SC enters the MN lumen. The skin pretension reduces the HMN penetration force. The reaction force versus displacement plot indicated that the force increases with MN displacement (Figure 1(b)). Upon puncture, the force drops sharply and then increases again as the HMN progresses further.

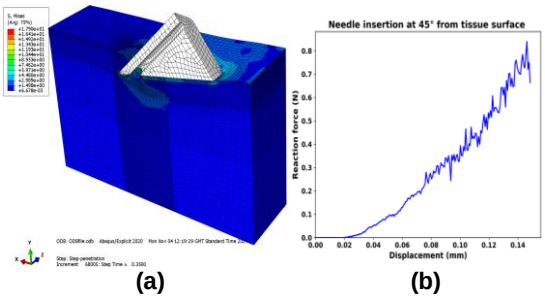

Figure 1 (a) FEA model illustrating deformation and von Mises stress (MPa) on skin during hollow MN insertion. (b) Plot of reaction force vs displacement as HMN penetrates the tissue.

The study also demonstrated how insertion angle influences stress distribution and insertion forces, while depth of penetration affects the efficacy of drug delivery. This finite element model enables detailed and quantitative analysis of the microneedle-skin interaction, which can be used to optimise HMN design. Future work will integrate fluid dynamics to simulate drug transport post-insertion.

REFERENCES

1. Cárcamo-Martínez *et al.*, Int. J. of Pharmaceutics, 599:120455-120462, 2021.
2. Gupta *et al.*, Biomaterials, *32*(28):6823-6831, 2011.
3. Shu *et al.*, Acta Biomaterialia, 135:403-413, 2021.

TOWARDS OPTIMIZING TRICUSPID VALVE REGURGITATION: 2D FLUID-STRUCTURE INTERACTION MODELING AND VALIDATION OF SIMPLIFIED HEART VALVE GEOMETRY

Albadawi, M. [1], **Belikov, N.V.**[1], **Kenny, G.** [2], **Abaei, A.R.** [2], **O'Rourke, M.J.** [1]
[1] UCD Centre for Biomedical Engineering, School of Mechanical and Materials Engineering, UniversityCollege Dublin, Ireland
[2] Croívalve, Dublin, Ireland
email: muhamed.albadawi@ucd.ie

INTRODUCTION

The tricuspid valve is one of four heart valves. Its anatomy includes three main leaflets. The dynamic structure, supported by chordae, papillary muscles, and a flexible annulus, adapts to the cardiac cycle's demands [1]. The tricuspid valve is crucial for maintaining unidirectional blood flow within the right side of the heart. It acts as a one-way valve, opening to allow blood to pass from the right atrium to the right ventricle during diastole and closing to prevent backflow into the atrium during systole. Tricuspid regurgitation (TR) is a condition characterized by the backflow of blood into the right atrium during systole, primarily due to improper closure of the tricuspid valve [2].

Computational fluid dynamics (CFD) simulations have emerged as essential tools in studying the biomechanics of the tricuspid valve and the pathological dynamics of tricuspid regurgitation (TR). These methods enable detailed analyses of flow patterns, pressure distributions, and valve leaflet mechanics under physiological and pathological conditions. In TR, CFD simulations provide insights into the hemodynamic impact of regurgitant flow. FSI models, by integrating the interaction between blood flow and the deformable valve structure offer a comprehensive understanding of leaflet behaviour under varying loading conditions[3].

Fluid-Structure Interaction (FSI) simulations play an essential role in understanding how medical devices perform under real-life physiological conditions. In this study, we developed and validated a 2D FSI model using a simplified valve geometry. This work marks an important step toward improving treatments for tricuspid regurgitation (TR), helping to bridge the gap between complex valve mechanics and better patient outcomes.

MATERIALS AND METHODS

A simplified 2D geometry of the valve was modelled in both Abaqus and ANSYS as shown in Figure 1(a), replicating the geometry for Amindari [4]. The valve leaflets were modelled as linear-elastic materials, Young modulus of the leaflets was assigned at 2 MPa, the Poisson's Ratio was set at 0.3, and the density was set at 1060 kg/m^3. While the blood flow was treated as a Newtonian fluid and set at 0.0035 $Pa.s$ and the density was assigned at 1060 kg/m^3. Pulsatile flow profile and zero pressure were applied in both platforms to simulate the physiological boundary conditions as shown in Figure 1(b). The geometry was modelled to simulate the two-way FSI interaction between blood flow and valve leaflets. the platforms handling and managing the structural deformation of the leaflets and the fluid flow dynamics.

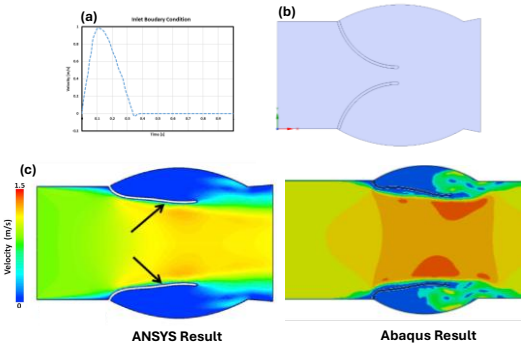

Figure 1 (a) Inlet transient velocity boundary condition**; (b)** Model geometry**; (c)** Velocity contours at systole, with a high-velocity jet indicated by arrows.

RESULTS

The simulation results for the tricuspid valve provide insights into the hemodynamic, focusing on the velocity distribution within the geometry. The comparative analysis revealed good agreement between the two software platforms in terms of leaflet motion, pressure distribution, and flow patterns. However, minor discrepancies were observed in regions of high deformation, highlighted the impact of each platform's numerical methods and settings. The velocity distribution is a key parameter in assessing the efficiency of the valve and its role in maintaining proper blood flow as depicted in Figure 1(c). These findings emphasize the importance of validating models across different tools to ensure their accuracy and reliability.

This study provides a solid foundation for understanding the simplified heart valve dynamics. The findings will offer valuable insights for computational models of more complex valves' geometries, ultimately improving the treatments for TR.

REFERENCES

[1] Dahou *et al.*, JACC Cardiovasc Imaging, vol. 12, no. 3, pp. 458–468, 2019.
[2] Sala *et al.*, Journal of the Society for Cardiovascular Angiography & Interventions, vol. 2, no. 5, p. 101041, Sep. 2023.
[3] Wang *et al.*, Comput Methods Programs Biomed, vol. 254, p. 108270, Sep. 2024.
[4] Amindari *et al.*, Inform Med Unlocked, vol. 9, pp. 191–199, 2017.

COMPUTATIONAL EVALUATION OF GEOMETRICAL AND PHYSICAL SKULL GROWTH FOR CRANIOSYNOSTOSIS TREATMENT VIA FINITE ELEMENT ANALYSIS

Vafaeefar, M.[1], Quinn, C.[1], Vaughan, T.[1]
[1] Biomedical Engineering Department, University of Galway
email: mahtab.vafaeefar@universityofgalway.ie

INTRODUCTION

Craniosynostosis, a condition where cranial sutures fuse prematurely, affects about 1 in 2,000 infants, leading to abnormal head shapes and facial features [1, 2]. Current treatments involve invasive surgeries to relieve brain pressure of the closed suture on the brain, such as removing fused sutures, reshaping bones, or spring-assisted cranioplasty. The synchronized growth of the brain and skull, the biomechanics of this process remain poorly understood, with limited studies addressing this gap through biomechanical and mechanobiological environment. This study aims to develop a finite element framework to simulate calvarial growth from 0-12 months of age, exploring how physical and geometrical constraints influence cranial development.

MATERIALS AND METHODS

The skull geometry was approximated as an ellipsoid, with a cephalic index of 78, including 6 regions of bone (frontal, parietal and occipital bones), and suture tissue. The brain tissue was modelled as a solid section, with the same index, offset from the skull geometry (**Fig. a-i, ii**). The z-direction was constrained, as well as planar constraint on the skull elements on the bottom z-face (**Fig. a-iii**). Bone and suture material behaviour were assumed to be linear elastic having Young's moduli of 3,000 MPa, and 30 MPa [3], respectively, and a Poisson's ratio of 0.3. Brain was considered as a Neo-Hookean hyperelastic material. Skull and brain are in normal and tangential frictional contact. Growth algorithms were applied on through field equations of kinematics, constitutive behaviour, mechanical equilibrium and growth kinetics, as shown in equations (1-4). Brain grows with a growth rate of GR_B. The bone undergoes a growth process consist of remodelling and mechanobiological term, driven by applied deformation from brain beyond an activation stretch ($ActSrt_b$), and suture undergoes a mechanobiological growth factor only.

$$\boldsymbol{F} = \boldsymbol{F}_e.\boldsymbol{F}_g \quad (1)$$

$$\boldsymbol{F}_{g,Brain} = GR_B.dt \quad (2)$$

$$\boldsymbol{F}_{g,bone} = [(\boldsymbol{F}_e - ActSrt_b).GR_b.dt] + [GR_b\,.dt] \quad (3)$$

$$\boldsymbol{F}_{g,suture} = (\boldsymbol{F}_e - ActSrt_s).GR_s.dt \quad (4)$$

Different growth schemes and rates are accommodated to different tissues, using UMAT subroutine into the finite element (FE) model. The algorithm is validated for a healthy case skull growth first, and further used for recreating a sagittal craniosynostosis condition.

RESULTS

According to the results (**Fig. b, c**) of the simulations, the algorithm predicted healthy skull growth, whereby the model predicted a volume increase by a factor of 2.23, which head cranial length and breadth, and height increased by a factor of 1.28 to 1.35, in time of 1 year of age.

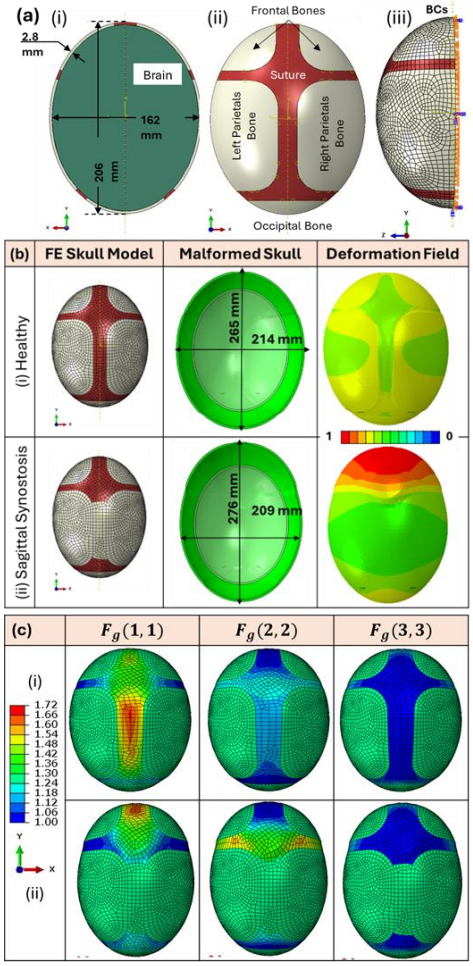

Figure (a-i) 3D idealized skull model, and (ii) dimensions, (iii) boundary conditions for FE analysis. (b) FE results for skull growth on (i) a healthy case, and (ii) a sagittal synostosis. (c) Growth deformation gradients in principal directions for (i) a healthy, and (ii) a sagittal synostosis.

DISCUSSION

This study provides an advanced calvarial growth algorithm, capturing the skull growth indices, that is regulated by biomechanical factor, like brain growth induced deformation on the skull. The model can predict the skull shape and dimensions upon growth and reveal the importance of the mechanobiological interface such as growth factors, as well as geometric role of the relative arrangement of bones and sutures. The brain soft tissue growth mechanism in this study allows to investigate its interaction with different cranial reconstructions.

REFERENCES

[1] Weickenmeier, J., *(et al.), 2017.*
[2, 3] Malde, O., *(et al), 2019, 2020.*
[4] Dekaban, A. S, *1977.*

WRINKLING INSTABILITY OF 3D AUXETIC BILAYERS IN TENSION

Pamulaparthi Venkata, S.[1], Fu, Y.[2], Balbi, V.[1], Fu, Y.[3], Danesh, H.[4], Conway, C.[5], Destrade, M.[1]
[1] School of Mathematical and Statistical Sciences, University of Galway, Ireland
[2] Department of Mechanics, Tianjin University, China
[3] School of Computer Science and Mathematics, Keele University, United Kingdom
[4] Institute of Applied Mechanics, RWTH Aachen University, Germany
[5] Department of Anatomy and Regenerative Medicine, RCSI Dublin, Ireland
email: S.PamulaparthiVenkata1@universityofgalway.ie

INTRODUCTION

Bilayers, where thin stiff films are bonded to thick soft substrates, are commonly found in nature with examples including skin tissue and organ membranes. This study examines wrinkling instabilities in auxetic bilayers (materials with negative Poisson's ratio) under tension, revealing insights that could enable precise control of surface patterns. This control is crucial for applications like skin grafts [1] and hydrogel organ patches [2], where tailored mechanical responses improve functionality and integration.

We model analytically the onset of wrinkles and validate our predictions using Finite Element (FE) simulations in ABAQUS. Numerical simulations are conducted using a user-defined subroutine for implementing constitutive behaviour and custom-written Python scripts to apply periodic boundary conditions. We derived asymptotic expressions that could be applied to buckling-based metrology under finite strain.

We also conducted a wrinkling analysis on bilayers with microstructural patterns. These patterns were designed to achieve desired effective Poisson's ratios through inverse analysis. A comparative study was then performed between bilayers with microstructures and homogenised models [3].

MATERIALS AND METHODS

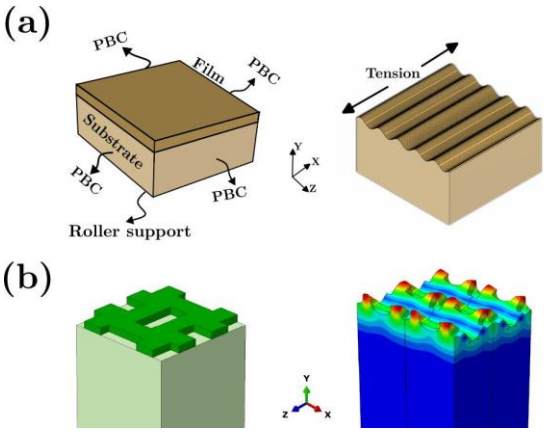

Figure 1 (a) Our model of a bilayer system with periodic boundary conditions (PBCs). The system is infinite in the X- and Z-directions and is stretched along the X-direction. (b) Comparison of undeformed and deformed configurations in bilayer with auxetic microstructures.

We model the mechanical behaviour of each layer with the Blatz–Ko strain energy function in the following form:

$$W = C_1\left(I_1 - 3 + \frac{I_3^{-\beta} - 1}{\beta}\right) + C_2\left(\frac{I_2}{I_3} - 3 + \frac{I_3^{\beta} - 1}{\beta}\right),$$

where C_1, C_2 depend on shear modulus and β depends on the Poisson's ratio of the material. We use the Blatz–Ko model to derive the critical stretch and wavenumbers for different cases: $(\nu_s, \nu_f) \in [-0.95, 0.495]$. Here ν_s and ν_f are the Poisson ratios of the film and substrate layers, respectively.

RESULTS & DISCUSSION

We demonstrate that uniaxial tension induces wrinkling in bilayers when the substrate's Poisson ratio exceeds that of the film, with wrinkles vanishing as their Poisson ratios converge. Asymptotic expressions for critical stretch ratios and wavenumbers are derived for finite strains, aiding buckling-based metrology. Additionally, through inverse analyses, we design film microstructures to achieve specific effective Poisson's ratios and further validate the effective properties using the finite element code, FEAP. The critical stretch ratio for buckling in bilayers with microstructured films shows strong agreement with predictions from homogenised models.

Future work will involve developing anisotropic constitutive models with auxetic behaviour to investigate left ventricular mechanics. These models will inform the design of auxetic cardiac patches, optimised through inverse analysis, to improve mechanical compatibility with cardiac tissues, see Figure 1.

ACKNOWLEDGEMENT

This project has received funding from the European Union's Horizon 2020 research and innovation programme under the Marie Skłodowska-Curie Grant Agreement no. 956401.

REFERENCES

[1] Gupta *et al.*, Biomechanical Modelling of Hierarchical Metamaterials for Skin Grafting, Springer Nature, Singapore, 2023.
[2] Chansoria *et al.*, Advanced Functional Materials, 32:2207590, 2022.
[3] Pamulaparthi Venkata *et al.*, arXiv: 2404.12873 (under review).

DEVELOPMENT OF AN OSTEOSARCOMA-ON-A-CHIP DEVICE THAT MIMICS THE OSTEOSARCOMA TUMOUR MICROENVIRONMENT

Solorio González, E.[1,2], Freeman, F.E[1-3]

[1] School of Mechanical and Material Engineering and Materials Science Centre, University College Dublin, Ireland
[2] Conway Institute of Biomolecular and Biomedical Research, University College Dublin, Ireland
[3] Trinity Centre for Biomedical Engineering, Trinity Biomedical Sciences Institute, Trinity College Dublin, Ireland

email: erick.soloriogonzalez@ucdconnect.ie

INTRODUCTION

In oncology research, Osteosarcoma (OS) remains a significant challenge due to its aggressive nature and high metastatic potential, most commonly affecting rapidly growing long bones such as the tibia and femur [1]. Despite significant advances in treatment seen in other cancers, no major improvements in outcomes have been achieved since the introduction of chemotherapy in 1970s. This has led to the overall 5-year survival rate for resistant forms of osteosarcoma remaining below 20% [2][3]. Studies have consistently found that results from drug testing in preclinical animal models are poor predictors of human responses [4] with estimated failure rates as high as 90% [5]. Despite this, animal models remain the main preclinical model for validating potential drug candidates. Therefore, there is clearly a critical need for more sophisticated bioinspired testing systems with the capability of predicting a patient's response to potential new therapies [4].
Organ-on-a-chip technologies represent a promising alternative as they allow for controllable cell culture within n organotypic microarchitecture environment, providing a simple yet more physiologically relevant platform for drug screening [5][6]. Herein, we aim to develop the first osteosarcoma-on-a-chip device that truly models osteosarcoma and its surrounding bone microenvironment as a predictive pre-clinical model for drug screening.

MATERIALS AND METHODS

Development and Fabrication of Microfluidics Housing: Computer-Aided Design (CAD) and fluid simulations (ANSYS) will be used to optimize the geometric conditions, focusing on factors such as channel angle (90° vs 45°), channel geometry (rectangular vs circular), pillar spacing, and the characteristics of pillars versus phase guides. Additionally, the simulations will examine the interaction and communication between multiple channels to ensure optimal performance (**Figure 1A**). Digital Light Processing (DLP)-based 3D printing will be employed to create high-resolution moulds for various geometries of the housing. Using these moulds, the microfluidic chips will be fabricated through polydimethylsiloxane (PDMS) casting (**Figure 1B**). Modelling of glucose transport within the different geometries will be performed using a diffusion-reaction mass transport model in ANSYS. The optimal geometry will be evaluated based on its fabrication feasibility and efficiency in nutrient transport.

Comparing Microfluidic Systems on DLP Bio-printed Chips and PDMS Casted Chips: CAD will be used to create STL files for various organ-on-chip geometries. Traditional methods involve printing a high-resolution mould for the organ-on-chip. Once the mould design is optimised, microfluidic chips will be fabricated using 184 polydimethylsiloxane (PDMS). For a more advanced approach, a DLP-based 3D bioprinter (CELLINK, LumenX) will be used to create the optimised organ-on-chip housing in a single step using PEGDA photo-ink. The accuracy of each biofabrication technique will be assessed by comparing the fabricated devices to the original CAD designs using microscopy. The time required to produce each device will also be measured to assess the efficiency of the biofabrication techniques.

Addition of physiological flow: Once the optimum geometry and fabrication technique is determined, CAD and fluid simulations (ANSYS) will be used to model physiological blood flow. An open-loop microfluidic system will be developed by connecting the inlet of the device to a syringe pump and the outlet to a collection reservoir. The flow rate (50-250µL/hr) will be assessed and validated using fluorescent nanobeads and ANSYS Fluent models (**Figure 1C**) to minimise excessive shear stress on the cells within system and optimise nutrient transport.

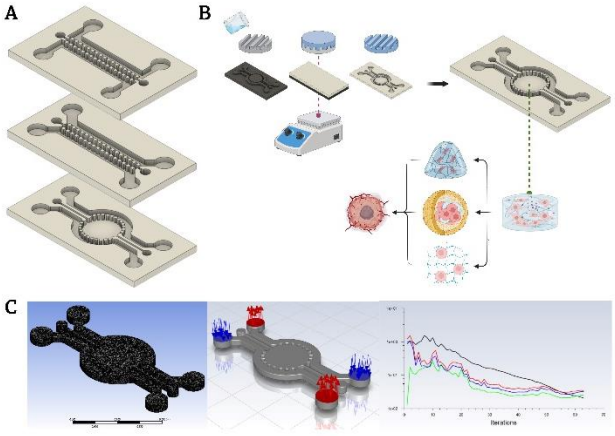

Figure 1: Design, Workflow, and Simulation of Microfluidic Platforms for Tumour Microenvironment Replication. (A) CAD design for the osteosarcoma-on-a-chip PDMS representation. (B) Workflow schematic depicting PDMS casting, hydrogel injection, and cell culture to visually represent the step-by-step process for creating the microfluidic system. (C) Computational representation using ANSYS Fluent simulations, showcasing fluid dynamics analyses and a 3D-rendered representation of the final microfluidic platform.

REFERENCES

[1] De Luca, *et al.*, Journal of Experimental - Clinical Cancer research, 37:2 (2018)
[2] Brooks, *et al.*, Cancers, 13, 388 (2021)
[3] Bassi, *et al.*, Nature Research: Scientific Research 10:22294 (2020)
[4] Chow, *et al.*, Tissue Engineering & Regenerative Medicine International Society, Part B. (2020)
[5] Van Norman, *et al.*, Basic to Translational Science. Vol. 4, No. 7 (2019)
[6] Tan, *et al.*, Biomolecules, 13(9), 1362 (2023)
[7] Sawyer, *et al.*, Journal of Tissue Science & Engineering, 7:2 (2016)
[8] Leung, *et al.*, Natures Reviews, Methods Primers 2:33 (2022)

STIFF HYDROGEL EXTRACELLULAR MATRIX MODELS MEDIATE PANCREATIC DUCTAL ADENOCARCINOMA CELL INVASION AND CHEMOSENSITIVITY

Baguyo, J.J.[1,2], Doyle, C.[1,2], Fallon, L.[1,2], Thorpe, S.D.[1,2,3]
[1] UCD School of Medicine, University College Dublin, Dublin, Ireland
[2] UCD Conway Institute of Biomedical and Biomolecular Research, University College Dublin
[3] Trinity Centre for Biomedical Engineering, Trinity College Dublin, Ireland
email: jan.baguyo@ucdconnect.ie

INTRODUCTION

Pancreatic Ductal Adenocarcinoma (PDAC) is a lethal form of cancer with a 5-year survival rate of approx. 10%.[1] PDAC is associated with an unusually dense and stiff extracellular matrix (ECM) mostly consisting of collagen type I. This stiff ECM is thought to promote cancer invasion and metastasis.[2] Additionally, the stiff ECM acts as a barrier, protecting cancer cells from chemotherapeutic treatment.[3] Syndecan-4 is a transmembrane protein which acts as a co-receptor facilitating cell adhesion and migration.[4] Syndecan-4 has also been shown to act as a mechanosensor regulating focal adhesion dynamics and cell contractility.[5] Syndecan-4 is upregulated in PDAC,[6] and we have shown that it supports cancer progression both by supporting stromal matrix remodelling and cancer cell migration and invasion. However, the role of syndecan-4 in the cancer cell response to increased substrate stiffness associated with PDAC is unknown. This study will address the hypothesis that syndecan-4 functions to support substrate stiffness mediated treatment resistance in PDAC cells in 2D and 3D culture environments.

MATERIALS AND METHODS

Hydrogel stiffness was assessed using rheometry (TA Instruments). Mouse pancreatic cancer organoids derived from a *KRAS*$^{+/LSL\text{-}G12D}$*; Trp53*$^{+/LSL\text{-}R172H}$*; Pdx-Cre* (KPC) mouse were encapsulated in basement membrane extract (BME; Geltrex, Thermo Fisher Scientific), collagen type I hydrogels (1-6 mg/mL; Telocol, Advanced BioMatrix), or a mixture of 2 mg/mL BME and 2 mg/mL collagen type I for 3 days. ATP content was measured as a proxy for viability using the Celltiter-glo 3D assay (Promega), while morphological alterations were assessed through immunofluorescent staining for vimentin and f-actin and confocal microscopy (Olympus FV3000). SUIT2-007 metastatic PDAC cells with CRISPR mediated syndecan-4 knock out, and re-expression of wild type or mutant syndecan-4 were cultured on polyacrylamide gels with stiffness mimicking normal and PDAC tissue. After 24 h of culture, gemcitabine, paclitaxel and 5FU were added for 48 h. Metabolic activity was measured as a proxy for viability using the alamarBlue assay (Thermo Fisher Scientific). Statistics were conducted using GraphPad Prism 10.

RESULTS

Storage modulus increased with collagen concentration ranging from 0.1-2 kPa. PDAC organoid viability over 3 days was not reduced with culture in collagen hydrogel as compared to BME (Geltrex) control. However, the BME-collagen combination did result in a ~40% decrease in ATP content relative to the BME control. Immunofluorescent imaging revealed notable morphological changes in collagen-cultured organoids, with organoids generating irregular elongated actin-rich protrusions, suggesting that increasing collagen concentration drives an invasive organoid phenotype. Morphological heterogeneity was increased with culture in all collagen-containing conditions.

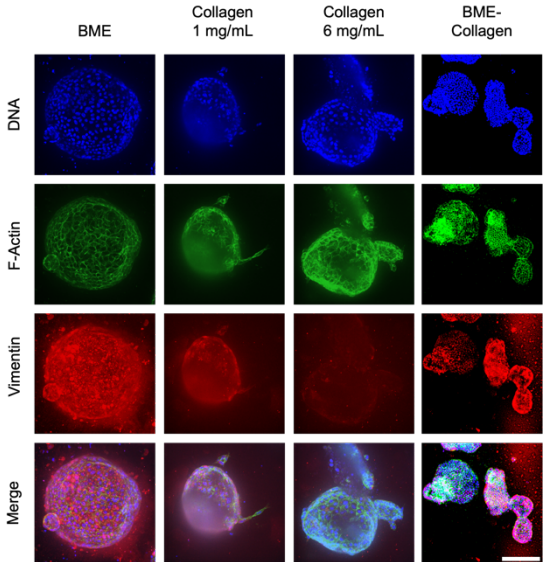

Figure 1 Representative maximum projection confocal microscopy images of immunofluorescently stained KPC mouse organoids cultured for 72 h. Scale bar 200 µm.

DISCUSSION

Mouse PDAC organoids can be successfully cultured in collagen hydrogels. The findings suggest that increasing collagen concentration supports organoid invasion. This model will provide a platform for the assessment of syndecan-4 function in the context of collagen remodelling in PDAC. Studies to assess the role of syndecan-4 in mediating PDAC cell response to substrate stiffness and chemosensitivity are ongoing.

REFERENCES

[1] Siegel *(et al.)*, CA Cancer J Clin 71:7-33, 2021. [2] MacCurtain *(et al.)*, J Clin Med 10:2711, 2021. [3] Sherman and Beatty, Annu Rev Pathol 18:123-148, 2023. [4] Afratis *(et al.)*, FEBS J 284: 27-41, 2017. [5] Chronopoulos *(et al.)*, Nat Mater 19:669–678, 2020. [6] Zhu *(et al.)*, BMC Cancer 22:1042

DEVELOPMENT OF A 3D OSTEOSARCOMA TUMOUR MODEL THAT RECAPITULATES THE BONE EXTRACELLULAR MATRIX AND NON-TUMOUR CELLS OF THE TUMOUR MICROENVIRONMENT

Coghlan, M.[1,2], Freeman, F.E.[1-3]
[1] School of Mechanical and Materials Engineering, University College Dublin, Ireland
[2] Conway Institute of Biomolecular and Biomedical Research, University College Dublin, Ireland
[3]Trinity Centre for Biomedical Engineering, Trinity Biomedical Sciences Institute, Trinity, Ireland
email: maire.coghlan@ucdconnect.ie

INTRODUCTION

Osteosarcoma (OS) is the most common primary bone malignancy in children and adolescents with a 5-year survival rate exceeding 60%, and this drops to 20% for resistant or metastatic cases[1]. Despite the urgent need for new treatments, no significant advancements have been made in OS therapy in the past 50 years.

Traditional cancer drug models, such as 2D cell cultures and animal models, fail to fully mimic the tumour microenvironment (TME). While 2D cultures are simple, they lack 3D complexity, and animal models, though widely used, are costly, time-intensive, and often untranslatable due to physiological differences, with failure rates as high as 90%[2]. Moreover, OS's rarity makes large clinical trials challenging, underscoring the need for bioinspired systems to predict patient responses to new therapies.

Recent studies have advanced 3D OS models using patient-derived cells, bone extracellular matrix (ECM), and non-tumour cells, improving our understanding of TME interactions[1,3,4]. However, a comprehensive model integrating all TME components is still required to replicate the OS microenvironment fully.

Herein, we aim to develop an OS model that recapitulates the surrounding bone ECM and incorporates the non-tumour cells of the TME. Currently, no in vitro model fully captures the interactions between the tumour, bone cells, and surrounding vasculature to study the origin, progression, and drug response of OS. Developing such a model is crucial for advancing drug discovery and therapeutic innovation.

MATERIALS AND METHODS

Investigation into the crosstalk between tumour and non-tumour cells in the OS microenvironment.

Immune Cells: Osteosarcoma cells (SaOS2) and monocytes (THP-1) were co-cultured using a transwell system. Monocytes were polarized to M0 macrophages with PMA (10 ng/mL) for 24 hours, then treated with LPS/IFN-γ (M1), IL-4/IL-13 (M2) or left untreated (M0) for another 24 hours. Co-cultures with SaOS2 cells were maintained for 48 hours, and osteosarcoma migration (DAPI) and macrophage proliferation (DNA assay) were assessed.

Neurons/Endothelial Cells: Osteosarcoma cell conditioned medium from metastatic (MG-63) and non-metastatic (SaOS2) cells was added to SH-SY5Y (neurons) and HUVECs (endothelial cells) in an indirect co-culture. Cultures were monitored for 48 hours using an Incucyte microscope. Neuronal and endothelial proliferation (DNA assays), NGF and VEGF release (ELISA), vessel lengths, and neurite outgrowth (ImageJ) were analysed.

Development and characterisation of a bone ECM scaffold. Decellularized bone (dECM) was prepared as described previously[5]. Hydrogels were created by adding dECM (0, 0.1%, 1%, 5% w/v) to collagen, mixed with cell-seeded fibrinogen, and crosslinked in a thrombin bath. Tumour and non-tumour cells will be seeded within the hydrogels to mimic the TME (**Fig. 1A**). Relatively low concentrations of dECM will be used, as OS is an osteolytic tumour[6]. IL-8 and TGF-β1 levels (ELISA) will be quantified to identify the optimal hydrogel composition for tumorigenic factor expression.

RESULTS

Osteosarcoma cell migration significantly increased when co-cultured with macrophages, regardless of macrophage phenotype (**Fig. 1B**). Notably, M0 and M2 macrophages showed increased proliferation upon co-culture, while M1 macrophages exhibited no change (**Fig. 1C**).

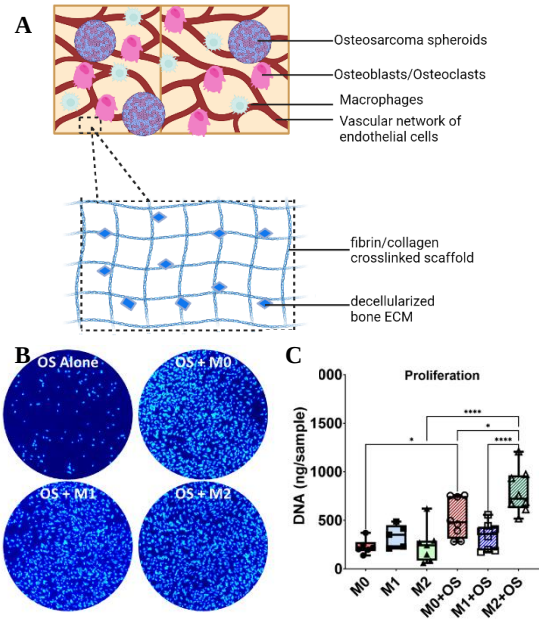

Figure 1: (A) Schematic of the OS tumour model incorporating non-tumour TME elements. **(B)** DAPI staining of osteosarcoma cells that migrated through the transwell insert after 48 hours of co-culture. **(C)** DNA content of macrophages ± co-culture with osteosarcoma cells. Data resented as mean ± SD; $n = 8$.

REFERENCES

[1] Chim *(et al.),* Biomaterials, 296: p. 122076, 2023. [2] Ingber *(et al.),* Advanced Science 7(22) : p. 2002030, 2020. [3] Pierrevelcin *(et al.)* Advanced Healthcare Materials 11(19), 2022. [4] Freeman *(et al.),* Advanced Healthcare Materials 11(7), 2022. [5] Freeman *(et al.),* European Cells and Materials 38: p. 168-187, 2019. [6] Corre *(et al.),* Cells 9(4): p. 976, 2020.

FUNCTIONALISED 3D PRINTED OPEN CELL STRUCTURES FOR TISSUE SCAFFOLD APPLICATIONS

Kinneen, R.[1], Ward, J.[1], McFadden, R.[1], Acheson, J.G.[1]
[1] School of Engineering, Ulster University, Belfast, UK
email: Kinneen-r@ulster.ac.uk

INTRODUCTION

Critical size bone defects present a significant challenge in regenerative medicine and orthopaedics, with bone being the second most commonly transplanted tissue worldwide [1]. These defects involve bone loss beyond a critical size threshold, preventing spontaneous healing within the patient's lifetime, even with stabilisation [2]. Consequently, bone grafts or substitutes are often required, yearly 2.2 million bone graft procedures are carried out globally [3]. As the current standard of care for these defects involves autologous transplantation, a procedure that is often painful and prolongs the healing process [4], it is evident that there is a need for an artificial bone replacement. However, many of these artificial structures fail to replicate the physical and mechanical properties of an implant site, and often feature simple repeating geometries that lack functionality, leading to limited osseointegration [4]. Therefore, there is a need for the development of a novel, patient-specific functionalised tissue scaffold. This research aims to explore the printing of patient cancellous bone, functionalised with a therapeutic release coating and to examine the response in 3D *in-vitro* environments. 3D printing techniques will be optimised to produce accurate cancellous morphology with required properties. Layer-by-layer assembly will be utilised to produce a functional therapeutic reagent release coating throughout the entirety of the scaffold morphology. Reagent release will improve osteointegration throughout the scaffold architecture. Comprehensive characterization of the 3D printed cancellous bone scaffold will be conducted, along with 3D tissue cell culture analysis of the structure within a bioreactor to evaluate how the scaffold supports cell growth, differentiation, and proliferation.

MATERIALS AND METHODS

After a comprehensive review of literature on various 3D printing techniques, the use of Fused Deposition Modelling (FDM) was analysed for 3D printing the cancellous bone scaffold. For this, an UltiMaker 3 extended was used to print polylactic acid/ polyhydroxyalkanoate (PLA/PHA) and Polycaprolactone (PCL) benchmarks using a 0.4 mm and 0.25 mm nozzle respectively.

RESULTS

The 3D Benchy benchmarks were used to find the optimal printing parameters for each material, to minimise errors such as stringing, uneven layers, drooping, or warping. After each print, an examination was done to identify any errors and optimise the printing parameters to better the outcome of following prints, to achieve the best results when printing the cancellous bone structure. As can be seen in **Figure 1,** a benchmark was successfully printed using PLA/PHA with minimal to no printing errors, this technique will then be replicated to print the cancellous bone structure that can be seen below it.

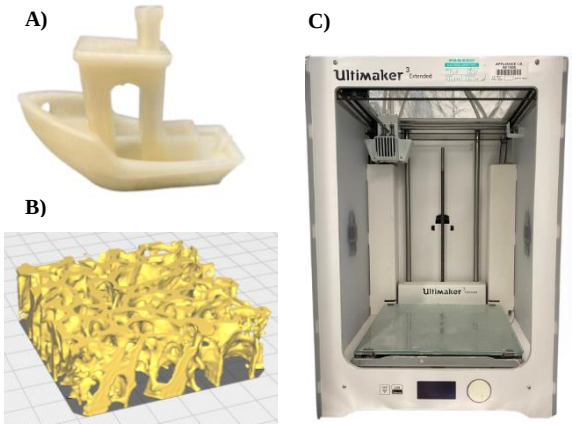

Figure 1 A) 3D Benchy printed with PLA/PHA B) Cancellous bone structure C) UltiMaker 3 Extended printer

DISCUSSION AND FUTURE WORK

From preliminary work, results suggest that the FDM printing technique shows promise for reproducible printing of complex open-celled structures with mechanical and physical properties in required ranges. Further experimentation with PCL and Poly(lactic-co-glycolic acid) (PLGA) will be conducted to assess the viability of these materials for use in cancellous bone tissue scaffolds. Once successfully printed the subsequent steps will involve developing and adding the functional coating and building a custom perfusion style bioreactor for 3D cell culture analysis.

REFERENCES

1. Lee *(et al.)*, Matter 5 :2722-2759, 2022
2. Huang *(et al.)*, Journal of Orthopaedic Translation 36:64-74, 2022
3. Ratnayake *(et al.)*, Journal of Biomedical Materials Research Part B:Applied Biomaterials 105:1285-1299, 2017.
4. Webb *(et al.)*, Asme International Mechanical Engineering Congress and Exposition, New Orleans, 2023.

USING MICROFLUIDICS TO FABRICATE HYDROGEL MICROSPHERES CONTAINING TESTICULAR CELLS AT HIGH-THROUGHPUT

Jishnu Padacherri Vethil [1], Nasrin Ghanami Gashti [1], Olwyn Mahon[1], Jacqueline Wittschier [2], Jochen Hess [2], Tara Dalton [1], Eoghan Cunnane [1]

[1] School of Engineering and Bernal Institute, University of Limerick, Ireland.

[2]Department of Urology, University Duisburg Essen, University Hospital Essen, Essen, Germany

email: (Jishnu.padacherri@ul.ie)

INTRODUCTION

The growing burden of male infertility presents a profound concern with far-reaching societal implications. Current therapeutic approaches remain empirically driven and often inadequately address this complex issue[1]. To formulate effective strategies for male infertility, it is imperative to establish preclinical testicular models that accurately represent the architecture of testicular tissue and the natural functions of the human testis. A platform that can create representative testicular models is therefore required. Microfluidic approaches can be used to fabricate cell-laden microspheres[2] with compartmentalized structures that closely mimic the cell niches of the testis, thereby providing an accurate representation of the natural human testicular environment. This research project fabricates testicular microgel models at high throughput using a microfluidic approach.

MATERIALS AND METHODS

Preparation and Characterization of Sodium Alginate Hydrogel: The hydrogel was synthesized by blending Sodium Alginate with a crosslinker, calcium-EDTA /acetic acid. The microstructure of the hydrogel was examined via scanning electron microscopy (SEM). Pore size characterization was achieved by measuring individual pore diameters. Nanoindentation was used to measure key mechanical properties of hydrogels. The biocompatibility of the hydrogel was assessed by encapsulating CHO-GFP cells and culturing for 2 weeks.

Generation of Cell-Laden Microspheres: Cell-laden monodispersed hydrogel microspheres were generated using a microfluidic T-junction. A combination of equimolar concentration of sodium alginate/Ca-EDTA containing cells and the crosslinker acetic acid.

RESULTS

Characterization of Hydrogel: The microstructure of sodium alginate/Ca-EDTA hydrogels was analysed using SEM revealing pore sizes with diameters ranging from 2.05 to 3.85 microns (Fig. 1A. The elastic modulus of the hydrogels, evaluated via nanoindentation, were found to be of the same order of magnitude as native tissue, underscoring their suitability for biomimetic applications.

Generation of Cell-Laden Microspheres: The examination of cell viability within the hydrogel microspheres during a 14-day static culture period provided substantial evidence supporting the compatibility of the cells with the hydrogel (Fig: 1 E).

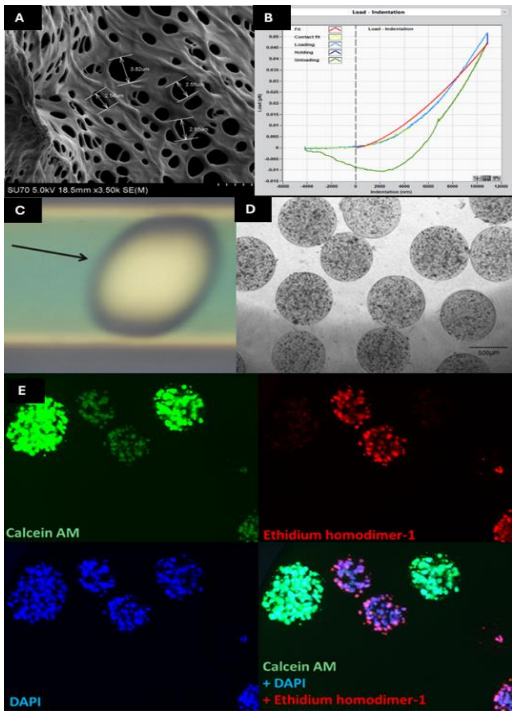

Figure 1 A) Microstructure of the Sodium Alginate hydrogel was analysed via SEM to evaluate pore diameter. B) Mecahnical properties of SA hydrogel were characterised using nanoindentation. C) Fabrication of monodispersed microspheres using a T-junction. E) Phase-contrast image of cell-laden microspheres (4X, 500µm). E) Cell viability was evaluated using calcine AM/EthD-1 staining of CHO-GFP cells.

DISCUSSION

In this study, a microfluidic system was developed for the fabrication of hydrogel microspheres containing encapsulated testicular cells. The uniform encapsulation of cells within these droplets ensures consistent distribution and interaction of cells. This advancement enhances the development of physiologically relevant human testis models, with potential applications in research and therapy.

REFERENCES

1. Vollset SE *(et al.)* The Lancet; 396:1285–1306, 2020.
2. Crafa A *(et al).* Journal of Clinical Medicine, 12(9), 3152, 2023.

COMPARATIVE ANALYSIS OF IN VIVO AND EX VIVO MODELS FOR MICROENVIRONMENTAL EFFECTS OF INTERVERTEBRAL DISC DEGENERATION

Wilson, N.[1], Ní Néill, T.[1], McDonnell, J. [1,2], Labberté, M. C.[3] Brama, P.A.J. [3], Buckley C.T. [1, 4, 5]
[1] Trinity Centre for Biomedical Engineering, Trinity Biomedical Sciences Institute, Trinity College Dublin. [2] National Spinal Injuries Unit, Mater Misericordiae University Hospital. [3]School of Veterinary Medicine, University College Dublin. [4]AMBER Centre, Royal College of Surgeons in Ireland; Trinity College Dublin. [5]Tissue Engineering Research Group, Department of Anatomy and Regenerative Medicine, Royal College of Surgeons in Ireland.
email: (wilsonni@tcd.ie)

INTRODUCTION

The intervertebral disc (IVD) microenvironment is essential for the viability and function of the intradiscal cells[1,2]. Degenerative changes within the disc can cause disruptions, posing a challenge for regenerative cell-based therapies[3]. This study aims to assess the degree of degeneration induced by varying concentrations of chondroitinase ABC (cABC), an enzyme that degrades glycosaminoglycans (GAGs). Subsequently, this work seeks to understand if these degenerative states can be recapitulated in an ex vivo culture model. Understanding the IVD microenvironment is critical to the development of physiologically relevant clinical models for a more targeted approach to degeneration therapies. Additionally, validating ex vivo organ culture models comparable to in vivo conditions will advance therapeutic development in vitro and provide a suitable replacement to animal studies.

MATERIALS AND METHODS

Studies were approved by the Health Products Regulatory Authority (HPRA) and the Animal Research Ethics Committee (AREC) at the school of veterinary medicine, University College Dublin. cABC was injected into the discs of 8 skeletally mature Saanen goats to induce degeneration in vivo. 4 levels were treated per goat, a saline sham, and 3 cABC units (1U, 2U, and 4U), with untreated discs used as controls. Ex vivo discs were cultured in custom bioreactors with two cABC doses (2U and 4U) and an untouched control. Microenvironmental profiling was performed for in vivo (post 12 weeks) and ex vivo (post 2 weeks) studies. Oxygen and pH were measured using PreSens needle-type microsensors (Presens, Germany), fluorescence-based probes that operate on a principle of proton and fluorescence quenching. Biochemical assays were developed to quantify glucose and lactate using glucose liquid (Sentinel Diagnostics 17630H) and lactate dry fast (Sentinel Diagnostics 17285). Osmolarity was measured using a vapor pressure osmometer (Vapro ELITechGroup). Statistical analysis was performed using one- and two-way ANOVA.

RESULTS

Oxygen was the microenvironmental factor that showed the most significant changes with increasing degeneration (in vivo p = 0.0244, 0.0464 and 0.0002 for 1U, 2U and 4U cABC respectively when compared to the untreated control). No significant differences were observed between in vivo and ex vivo measurements (Fig.1Av). A significant increase in in vivo DNA content was noted at 1U cABC when compared to untreated (p=0.0173) and sham groups (p = 0.044) (Fig. 1B). GAG and collagen content were not significantly altered (Fig.1C,D). All cABC groups showed a significant reduction in disc height when compared to the pre-degeneration group (p = 0.0059, 0.0006 and 0.0133 for 1U, 2U and 4U cABC respectively (Fig. 1E).

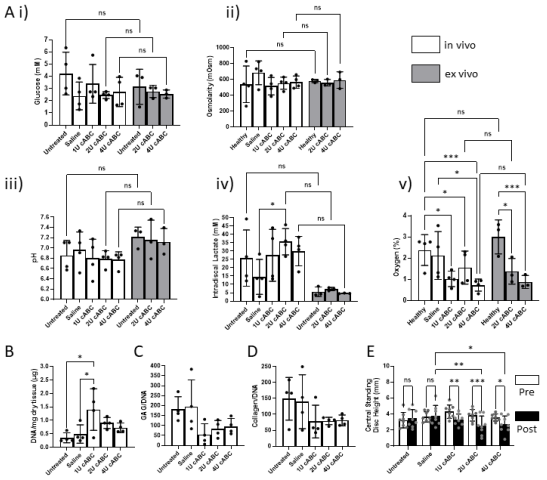

Figure 1 In vivo and ex vivo IVD degeneration model. A) IVD microenvironment profiles i) glucose, ii) osmolarity, iii) pH, iv) lactate, v) oxygen. B-E in vivo measurements. B) DNA, C) GAG/DNA, D) Collagen/DNA, E) Central disc height pre and post 12 weeks degeneration. *: p<0.05, **: p<0.01, ***: p<0.001. (in vivo: N=4, ex vivo: N=3)

DISCUSSION

Ex vivo culture is limited in duration due to culture. Despite this, degenerative changes were observed in both models as a result of cABC insult, both visually through disc height and microenvironmentally through oxygen concentration, highlighting the importance of microenvironmental factors when developing intradiscal therapies. The comparative analysis of IVD microenvironments of ex vivo culture models to that of the in vivo study demonstrated comparable results indicating it to be a suitable alternative.

ACKNOWLEDGEMENTS

This work was supported by the European Research Council (ERC-2019-CoG-864104; INTEGRATE).

REFERENCES

[1] Schol (et al.), International Orthopaedics, 43, 1011-1025 (2019) [2] Sakai (et al.), Journal of Orthopaedic Translation, 9, 8-18 (2017) [3] McDonnell (et al), JOR Spine, 6, e1279 (2023).

DEVELOPMENT OF A MICROTISSUE BASED SYNOVIAL JOINT-ON-CHIP

Milazzo, R.[1,2], Madden, L. [1,2], Gonnella, G.[1,2], Kronemberger, G. [1,2], Anton, D. [3], Veale, D.[4], Fearon, U. [3], Kelly, D.J[1,2,5]., Hoey, D.A. [1,2,5]

[1]Trinity Centre for Biomedical Engineering, TCD. [2]Department of Mechanical, Manufacturing, and Biomedical Engineering, School of Engineering, TCD. [3]Department Molecular Rheumatology, Trinity Biomedical Science Institute. [4]St. Vincent's University Hospital, Dublin, Ireland. [5]Advanced Materials and Bioengineering Research Centre (AMBER), Royal College of Surgeons in Ireland and Trinity College Dublin, Dublin, Ireland.

email: milazzor@tcd.ie

INTRODUCTION

Rheumatoid arthritis (RA) is a chronic autoimmune disease affecting millions worldwide [1]. Despite advancements in treatment, there remains substantial unmet need for effective therapies primarily due to a lack of reliable preclinical models that accurately capture the complexity of RA such as 2D culture approaches and animal models. To address this challenge, we will leverage two emerging technologies: organ-on-chip (OoC) and microtissues. OoC replicate the microenvironment of specific organs, enabling the study of complex biological processes using low volumes. Microtissues, three-dimensional cell cultures, mimic the architecture and function of tissues. By combining these approaches, we aim to first create individual cartilage and synovium models and ultimately to develop a chondro-synovial unit to recapitulate key interactions of RA. This model will enable the study of RA pathophysiology and drug response in a controlled and scalable manner, accelerating the development of effective therapies.

MATERIALS AND METHODS

Chip design and fabrication Chips are obtained by replica moulding of PDMS on 3D printed resin moulds (Elegoo), designed on Solidworks. The chip was designed to incorporate a hydrophobic barrier made of micropillars. *Cartilage model* hMSCs are seeded at a density of $400x10^3$ cells/mL on microwells with chondrogenic medium for 2 weeks to obtain 400 microtissues prior harvesting, suspension in 3% alginate and loading onto the chips for one week. Alginate is chemically crosslinked by adding a 50mM $CaCl_2$ solution into the medium channels. Similarly, an hMSCs cell suspension in alginate with equal number of cells is used as a control. *Synovial microtissues optimisation* Cell density for Fibroblast-like synoviocytes (FLS) microtissues was investigated. Two cell densities were compared, namely 1000 and 2000 cells per microtissue, cultured in DMEM plus 2% FBS and Ascorbic acid.

RESULTS

The microfluidic chips were loaded with microtissues or hMSCs suspension in alginate, which the hydrophobic barrier, made of micropillars, succeeded to contain in the culture channel (**Fig. 1A, 1B**). Chondrogenesis of the hMSCs microtissues will be compared with the cell suspension in terms of Collagen and sGAG secreted, as well as cell viability. The FLS fused into microtissues in both 1000 and 2000 cells/microtissue groups. Histological analysis on day 7 showed a homogenous cells distribution across the tissue, while after 21 days cells are distributed on the edges, indicating a reorganisation **Fig. 1C**. Immunohistochemistry showed the secretion of Lubricin, a protein typical of native synovium, lining the microtissues.

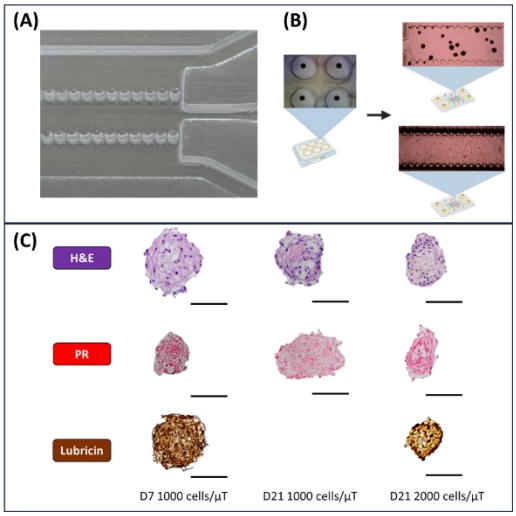

Figure 1 A) Stereoscopic image of PDMS chip. B) Schematic representation of cartilage on chip: top right, microtissues; bottom right, cell suspension. C) Histology of synovial microtissues. Scale bar 100 µm

DISCUSSION

A 3D printing-based approach was developed to fabricate OoCs. A consistent method to load cartilage microtissues on chip has been established and such model will be compared to a standard cell suspension to assess the impact of 3D culture on chondrogenesis. We developed the first scaffold-free approach to fabricate reproducible synovial microtissues presenting spatial reorganisation and mimicking native tissue architecture after the period of culture which secrete key synovial protein like lubricin. Our future aims are to establish a model of synovial microtissues on chip and finally to fabricate a chip for the coculture of cartilage and synovial microtissues to examine the signalling between the two tissues and identify novel therapeutic targets for RA.

REFERENCES

1. Smolen, J.S., D. Aletaha, and I.B. McInnes, *Rheumatoid arthritis.* Lancet, 2016. **388**(10055): p. 2023-2038.

Cancer-associated Osteoblasts Exhibit Morphological Abnormalities and Inhibited Mineral Deposition in an Engineered Bone Metastatic Niche

Sarah Nano[1,2], Laurie E. Littlepage[1,2], Laoise M. McNamara[3], Glen L. Niebur[1,2]
[1]Bioengineering, [2]Harper Cancer Research Institute, University of Notre Dame, IN, [3]Biomedical Engineering, University of Galway, Galway, Ireland
snano@nd.edu

INTRODUCTION

Bone is the most common site of breast cancer metastasis, with cancer cell dissemination to bone occurring even before primary tumor diagnosis [1]. Metastatic tumors alter normal bone physiology and can cause uncontrolled bone resorption (osteolysis) leading to fracture risk along with altered haematopoiesis and immune response [2]. Biochemical factors (IL-6, PTHrP, TNFα) produced by cancer cells trigger bone resorption by osteoclasts, releasing cytokines and chemokines that drive further metastatic progression in a vicious cycle. Mechanical stimulation has been reported to inhibit tumor progression and prevent bone destruction [3,4,5] whereas other studies have reported an increase in tumor burden under mechanical stimulation, in a dose dependent manner [6]. We previously developed metastatic bone models to show that mechanical stimulus provided protective effects against tumor-induced osteolysis and promoted osteogenic activity [7]. Cancer cells induce an osteoblast inflammatory response [8] and disrupt osteoblast arrangement when in physical contact [9], suggesting that phenotypically modified osteoblasts – *i.e.* cancer-associated osteoblasts (CAO) – may drive altered bone physiology during metastasis, but this is not fully understood. The goals of this study were to 1) measure the effects of cancer cells on osteoblast differentiation, proliferation, and mineralization, and 2) determine whether mechanical stimulation can rescue the normal osteoblast phenotype in the presence of cancer cells.

MATERIALS AND METHODS

We engineered a segregated coculture hydrogel model to isolate the paracrine effects of cancer cells on osteoblasts. MC3T3-E1 murine osteoblastic cells (MC3) were expanded in standard conditions and embedded at 2×10^6 cells/mL in 3% w/v gelatin, 5.5% v/v nano-hydroxyapatite (nHA) and cross-linked with 0.3% w/w microbial transglutaminase. Triple negative murine mammary cancer cells (4T1) were expanded and embedded in a separate hydrogel with the same formulation. MC3 hydrogels were cultured alone (CTL; N=6) or in the same well as a 4T1 hydrogel as segregated co-cultures (N=6). All culture groups were supplemented with osteogenic media for 21 days to induce mineralization. Unloaded controls remained in static culture, whereas mechanically stimulated groups were subject to 0.5% strain for 30 minutes, each for 7 days (CellScale Mechanoculture TX). Live-dead staining was performed at day 21 to quantify cell viability and apoptosis in all groups. FITC, DAPI, DMP1, and Ki67 staining were performed at days 7, 14, 21, and 28 to analyze cell morphology, differentiation, and proliferation. DNA, calcium, and ALP assays were performed at days 21 and 28 to analyze cell number and osteogenic differentiation.

RESULTS

Osteoblasts viability was lower when cultured with cancer cells (Fig. 1B). Osteoblasts were smaller and more circular in cancer coculture compared to monoculture (Fig. 1A, C). MC3 cells deposited mineral in the gelatin matrix, which was enhanced by mechanical loading in the CTL group (Fig 1D). Surprisingly, no calcium was present in any MC3 constructs in the cancer coculture, with or without mechanical loading. ALP expression increased on day 28 in both unloaded conditions, though was higher in cancer coculture and only increased over time for the cancer coculture under loaded conditions (Fig.1E). We also conducted experiments with RAW cell (osteoclast precursors) coculture and found that the cancer-cell associated changes in osteoblast morphology and mineralization were maintained (data not shown).

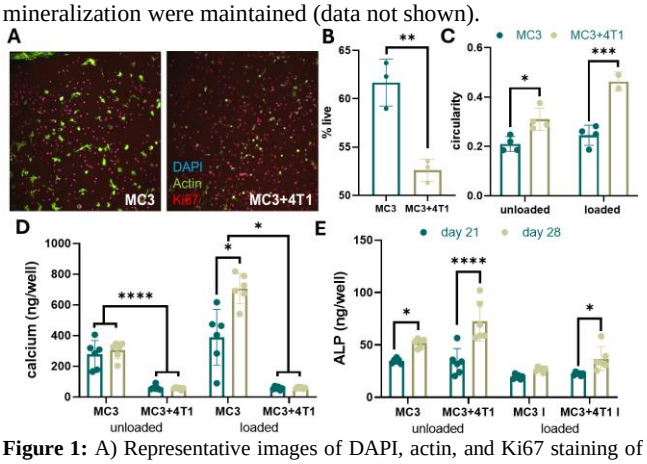

Figure 1: A) Representative images of DAPI, actin, and Ki67 staining of MC3 hydrogels on day 28. B) Percent of live cells and C) circularity quantified from immunofluorescent images. D) Quantification of calcium in MC3 hydrogels and E) ALP from media on days 21 and 28 in unloaded and loaded cultures.

DISCUSSION

In our novel model of the breast cancer metastatic niche in bone, we report that osteoblast viability, morphology and differentiation were altered by soluble factors from tumor cells. Notably, osteoblast mineral deposition was absent in the presence of cancer cells, an effect not previously demonstrated in metastatic models. This effect occurred regardless of mechanical stimulation, which otherwise increased calcium deposition in these constructs. Concurrently, osteoblasts exhibited a less spread morphology in cancer coculture compared to monoculture, but it is not clear whether this is a consequence of the inhibited mineralization or an effect of cancer secreted factors. In contrast, ALP expression increased at later timepoints, suggesting a potentially delayed mineralization effect in coculture. Overall, we have shown that triple negative mammary cancer cells inhibit mineralization in a 3-D model of metastases, even under mechanical stimulation. Thus, cancer-associated osteoblasts (CAO) may contribute to altered bone physiology in the presence of metastasis. Transcriptomic profiling of the cancer-associated osteoblasts could uncover the specific epigenetic phenotype of these CAOs.

REFERENCES

[1] Braun, S et al., N Engl J Med, 342:525-533, 2000. [2] Breuer, EK et al., Cell Death & Dise, 10:1-15, 2019. [3] Yang, S et al., The FASEB Journal, 33:10742-10752, 2019. [4] Lynch, ME et al., JBMR, 28:2357-2367, 2013. [5] Wang, S et al., Bone, 153:116100-116112, 2021. [6] Fan, Y et al., Bone Research, 8:1-11, 2020. [7] Kumar Vet al., *Cell Rep*, 43(5):114043, 2024. [8] Kinder, M et al., Experimental Cell Research, 314:173–183, 2008. [9] Kimura Y et al. Scientific Reports, 7: 1–11, 2017.

DEVELOPMENT OF A PHOTOCROSSLINKABLE NERVE-DERIVED EXTRACELLULAR MATRIX BIOMATERIAL FOR PERIPHERAL NERVE REPAIR

Haffner, T.[1,2], Buckley, CT.[1,2,3]
[1] Trinity Centre for Biomedical Engineering, Trinity College Dublin, Ireland
[2] AMBER Centre, Royal College of Surgeons in Ireland & Trinity College Dublin
[3] Tissue Engineering Research Group, Department of Anatomy and Regenerative Medicine, Royal College of Surgeons in Ireland
email: thaffner@tcd.ie

INTRODUCTION

Peripheral nerve injury affects over one million people every year worldwide [1]. Autografts are considered the gold standard for nerve repair, with nerve guidance conduits (NGCs) being the preferred alternative for small gap repairs. The development of novel biomaterials combined with 3D printing offers the potential to create multifunctional implants with spatial control and has gained significant interest in the field of nerve tissue regeneration [2]. Native extracellular matrix (ECM) derived biomaterials are among these promising new materials due to their high biocompatibility and ability to provide a biologically relevant microenvironment for cell culture [3]. However, ECMs often require exogenous crosslinking to provide adequate mechanical properties. In this work methacrylation of nerve ECM (nECM-MA) was chosen for its ease of use and control over crosslinking [4]. The overall goal of this study was to develop and characterise a new nerve-derived ECM material for NGC biofabrication.

MATERIALS AND METHODS

Nerve tissue was harvested from adult porcine joints and pepsin solubilised followed by methacrylation to obtain the final nECM-MA. Photo-crosslinking was performed after thermogelation using a 405nm blue light for 60 seconds. Biochemical analysis (hydroxyproline, DNA, sGAG), mechanical testing, swelling and degradation analysis were performed to characterise the developed materials. 2D monolayer cultures (PC12 cell line and *ex-vivo* dorsal root ganglion (DRG) model) were used to assess cell viability, neurite outgrowth and density on coatings of the developed materials for one week. DRGs were seeded on a range of 3D hydrogels (0.5-8% w/w) and cultured for one week in neurobasal media. Cells were fixed and stained for Phalloidin/Hoechst.

RESULTS

After decellularising native nerves, the resulting nECM and nECM-MA were primarily composed of collagen, with any residual DNA content effectively removed. Following solubilisation, adjusting the material concentration was shown to modulate the stiffness of the resulting hydrogels, achieving levels comparable to native tissue. When swelling was minimal, the hydrogels degraded more slowly than native nerve tissue across all tested concentrations. nECM-MA displayed better neurite outgrowth than the collagen control using PC12 cells. For 3D DRG models, 2% hydrogel substrates resulted in the maximum nerve outgrowth with significant release of MCP-1/VEGF. These factors play a role in recruiting macrophages and promoting vascularization, which are crucial for creating an environment that supports nerve repair.

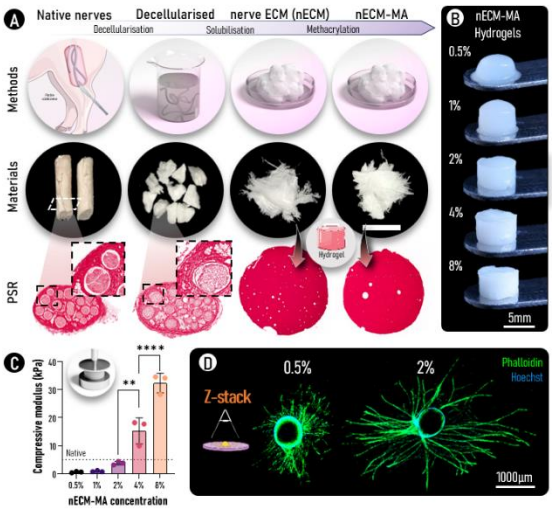

Figure 1 – Development of photocrosslinkable nerve-derived biomaterial nECM-MA. A. Material processing from native nerve to nECM-MA. B. Range of nECM-MA hydrogels after photocrosslinking (0.5-8% in w/v). C. Stiffness increases with material concentration during unconfined compression. D. *Ex-vivo* DRG model in culture for 1week on nECM-MA hydrogels.

DISCUSSION

This work highlights the potential of tissue specific ECM derived biomaterials to create next generation NGCs. This study shows that 2% nECM-MA hydrogels replicate mechanical properties closely matching the stiffness of native nerve tissue while also enhancing nerve outgrowth. Due to their ease of handling, photocrosslinkable nECM-MA hydrogels and their derived inks present new opportunities for NGC biofabrication.

ACKNOWLEDGEMENTS

Supported by Taighde Éireann- Research Ireland and AMBER (12/RC/2278_P2)

REFERENCES

[1] Daly (et al.), Journal of The Royal Society Interface 9: 202-221, 2012. [2] Yu (et al.), Polymers 12(8):1637, 2020. [3] Youhwan (et al.), International Neurourology Journal 20: S23-29, 2016. [4] Nichol (et al.), Biomaterials 31: 5536-5544, 2010.

IN-SITU QUALITY MONITORING DURING EMBEDDED BIOPRINTING USING INTEGRATED MICROSCOPY AND CLASSICAL COMPUTER VISION

Sergis, Vasileios.[1,2,4], Kelly, Daniel.[1,2,4], Pramanick, Ankita.[1,2], Britchfield, Graham.[1,2], Karl, Mason.[3], Daly, Andrew.[1,2,*]

[1] CÚRAM, SFI Research Centre for Medical Devices, University of Galway, Galway, Ireland
[2] Biomedical Engineering, University of Galway, Galway, Ireland
[3] School of Computer Science, University of Galway, University Road, Galway, Ireland
[4] Equal contribution
email: andrew.daly@universityofgalway.ie

INTRODUCTION

Bioprinted organs promise to revolutionise medicine by tackling the organ transplant shortage and providing new animal-free platforms for drug screening and discovery. Despite significant advances, 3D bioprinting technologies, such as extrusion bioprinting, suffer from reproducibility challenges that will hamper deployment in clinical or industrial settings. The reproducibility challenges with existing bioprinting technology can be attributed to its inherent open-loop nature, which lacks capabilities for monitoring extrusion outputs. Overcoming this limitation is crucial for advancing bioprinting from research to industrial and clinical applications, where producing consistent, scalable, and high-quality outputs in compliance with Good Manufacturing Practice (GMP) standards is essential.

MATERIALS AND METHODS

As a key step towards a solution, we developed a novel bioprinting platform integrating a high-resolution camera for in-situ monitoring of extrusion outcomes during embedded bioprinting. Using classical computer vision and image analysis, we created custom software to assess print quality, enabling quantitative comparison of printer outputs to input points of the CAD model 2D projection, measuring area and positional accuracy. To showcase the platform's capabilities, we investigated various inks, bioinks, dyes, and support materials, demonstrating cell viability and ink visibility in 2D and 3D path trajectories. Additionally, we studied how the rheological properties of granular support hydrogels impact print quality during embedded bioprinting, illustrating a practical application of the equipment.

RESULTS

The integration of the novel camera setup and image analysis enabled comprehensive insights into embedded bioprinting processes and the particle-particle interactions in granular support hydrogels with viscosity ranges between 10 to 1000 Pa·s. Our results demonstrated that lower viscosity, faster thixotropy recovery, and smaller particle sizes significantly enhance print fidelity. This novel bioprinting platform, equipped with integrated process monitoring, holds great potential for establishing robust, reliable, and auditable biofabrication processes for industrial applications.

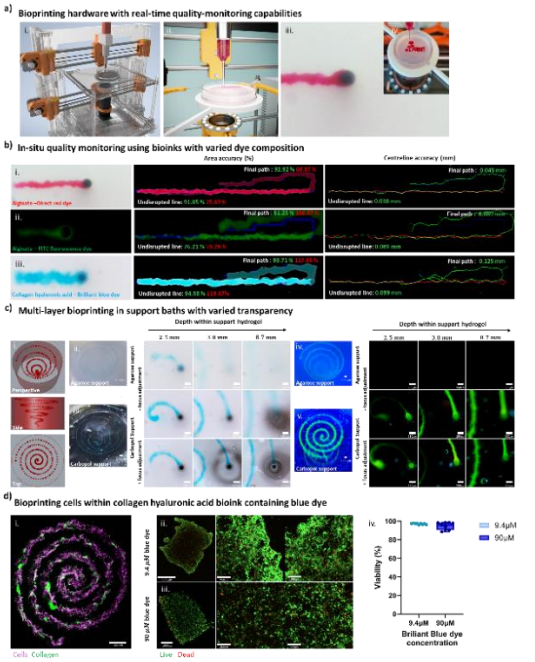

Figure 1 Developed bioprinter with integrated microscopy showcasing various inks, bioinks, dyes, and support bath materials along with the cells' viability and inks' visibility in 2D and 3D path trajectories.

DISCUSSION

Previous camera systems in bioprinting were positioned at large distances or oblique angles, preventing detailed monitoring of bioink flow, filament formation, and small features within the bioprinted construct. The techniques applied in our work have not been used before to automatically extract print quality data, generate detailed video output, or provide real-time feedback to users.

REFERENCES

Mladenovska, T. *et al*, Regen. Med., The regulatory challenge of 3D bioprinting, 18, 659–674, 2023.
Garces, D. G. *et al*, Biofabrication, On the reproducibility of extrusion-based bioprinting: round robin study on standardization in the field, 16, 015002, 2023.
Daly, A. C., Adv. Healthc. Mater., Granular Hydrogels in Biofabrication: Recent Advances and Future Perspectives, 2301388, 2023.

MEDICAL DEVICE MYSTERIES

Taylor, D.[1]
[1] Trinity Centre for Biomedical Engineering, TCD
email: dtaylor@tcd.ie

INTRODUCTION

In my forensic work I often come across defective medical devices: products which fail owing to an inherent design flaw, causing pain and distress to large numbers of patients.

In some cases (such as Depuy ASR hip implants and surgical mesh devices) the nature of the defect has already been explained, or I was able to explain it. This talk, however, is about some products whose defects have not yet been explained.

BREAST IMPLANTS

Certain types of silicone breast implant with textured surfaces have been associated with a cancer known as anaplastic large cell lymphoma[1] . Though very rare this has affected many patients who, once they hear about it, elect to have the implants removed. Particularly prevalent in one manufacturer (Allergan Biocell) the problem occurs also in other products. It is somehow caused by the texturing process but currently we don't know how.

KNEE JOINT REPLACEMENTS

The NexGen knee arthroplasty, made by Zimmer, is extremely popular and successful. But a leading Irish surgeon experienced an unusually high failure rate for these products implanted over a 2-year period[2]: asceptic loosening caused by debonding of the tibial tray. The cause is unclear but seems to be a combination of two factors: pre-coating of the metal surfaces and use of a particular type of bone cement.

CPAP MACHINES

These machines are used to aid respiration for patients suffering from sleep apnea. Recently Phillips issued a recall of over 3 million such devices owing to the presence of particles and organic gases which were being inhaled by patients, causing health problems[3]. This seems to be related to a polymer foam material which was used for sound insulation and may be subject to environmental degradation. Design questions also arise as to how particles of the material could have got into the air line and thus be inhaled.

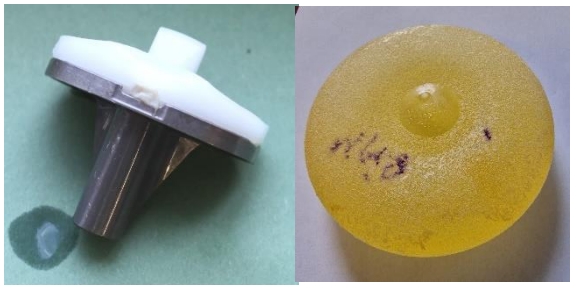

Figure 1 NexGen knee joint and Allergan textured breast implant.

DISCUSSION

Part of my work involves establishing whether a failed product is defective, in the legal sense (Liability for Defective Products Act 1991). Such failures don't occur due to problems during manufacturing or use (though they happen too) but rather are inherent in the original design. I try to find the technical reason for the failure and consider whether the designer should have known about it at the time. Plaintiffs can win their cases even if we don't know the ultimate cause, provided we can show a significant failure rate and a clear link between the product and the patients' symptoms (pain, disfunction). But of course it helps if we know why it happened.

Surgeons can be criticised for not informing themselves about defective products and for not warning their patients of risks and side effects.

Mysteries such as these can act as a stimulus for further research and the development of new, better, medical devices.

REFERENCES

[1]Keech and Creech *J Plas & Recon Surg* pg554 (1997).
[2]Keohane et al *The Knee* 27 459-468 (2020)
[3]Owens et al *Am J Respir Crit Care Med* 204 887-890 (2021).

3D PRINTED HEART MODELS IN THE PRE-OPERATIVE PLANNING OF DOUBLE OUTLET RIGHT VENTRICLE

Foley, R.[1,2], **O'Cearbhaill, E.**[1], **McMahon, C.**[1,2]
[1] University College Dublin
[2] Children's Health Ireland, Crumlin
email: foley.ross@gmail.com

INTRODUCTION

Double outlet right ventricle (DORV) is a rare form of complex congenital heart disease (CHD) in which both outflow tracts, namely the aorta and pulmonary artery (PA), arise from the right ventricle (RV) with an associated ventricular septal defect (VSD).
DORV anatomy can vary considerably between patients. Understanding the complex 3-dimensional relationship between the VSD and the outflow tracts is vital when determining what surgical repair to carry out.
Recent advancements in 3D printing technology have led to the ability to generate high fidelity 3D heart models. The use of these models has become increasingly common in the pre-surgical planning of DORV given the spacial complexity of the repair (Bhalta et al., 2017; Gareker et al., 2016; Valverde et al., 2017; Zhao et al., 2018).
The cost of 3D printed models varies widely, largely based on the type of printing technology and materials being used, with more expensive models being those generated using advanced technologies that can print with softer polymers that better simulate the characteristics of heart muscle tissue. These allow the surgeon to perform simulated surgery on the models prior to the operation but can cost over €1000 per model.
We aim to generate models using more cost-effective technologies and materials that can still simulate heart muscle tissue characteristics.

MATERIALS AND METHODS

The generation of 3D models involves three steps; data acquisition, image segmentation/processing and 3D printing.
Data acquisition involved carrying out computed tomography (CT) cardiac angiogram with contrast timed to delineate the blood pool within the heart. This generates DICOM images which are used in the segmentation process.
Image segmentation was carried out using the open-source software tool 3D slicer. This involves a semiautomatic process where the blood pool is segmented from the background using image analysis algorithms. 3D mesh file is produced that can be used to print the models. The mesh file is now processed using slicing software that uses properties of the 3D printer and material to format the file for printing.
We have generated models using two affordable printers, the Bambulab A1 mini fusion deposition modelling (FDM) printer and the Anycubic Photon M5s liquid resin printer. We have printed in a range of materials from rigid Polylactic acid (PLA) to softer Thermoplastic polyurethane (TPU). In addition, we printed 3D moulds using water soluble Polyvinyl alcohol (PVA) and injected them with silicone which is cheap and simulates heart muscle characteristics well.

RESULTS

We have generated models from eight of our DORV patients. We have found that they are accurate with less than 0.5mm difference between the models and CT on measurements of key structures. Figure 1 demonstrates some of our models in different materials.

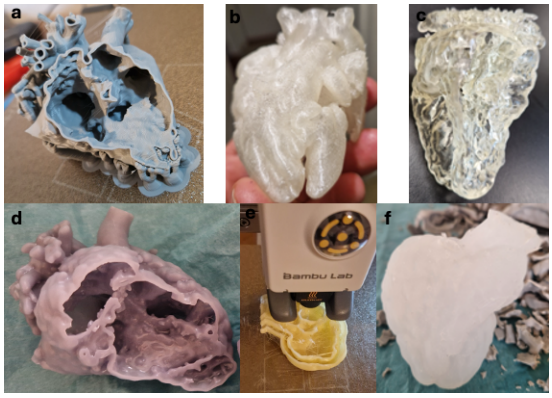

Figure 1 3D printed heart models in different materials. **a.** PLA. **b.** TPU. **c.** soft resin. **d.** hard resin. **e.** PVA mould. **f.** Silicone.

DISCUSSION/FUTURE WORK

We have achieved promising initial results in our aim to generate affordable and useful 3D heart models, particularly using 3D printed moulds to generate silicone models. We are receiving iterative feedback from our cardiothoracic surgeon and plan to optimise this process further. Ultimately, we plan for these models to be compared directly to industry standard models in the presurgical planning of DORV patients.

REFERENCES

Bhalta (et al.), Echocardiography., 34: 802– 4, 2017.
Garekar (et al.),World J Pediatr Congenit Heart Surg., 7: 344– 50, 2016.
Valverde (et al). Eur J Cardiothorac Surg., 52:1139–48, 2017
Zhao (et al), J. Card. Surg., 33:24–27, 2018

ADVANCING BENCH-TOP PENILE MODELS FOR IMPLANT TESTING

Amirian, J.[1, 2, 3], **Khorshidi M.A.** [1, 2, 3], **Watschke B.** [4], **Sinnott, T.**[5], **Mareena, E.**[5], **Lally, C.** [1, 2, 3]

[1]Trinity Centre for Biomedical Engineering, Trinity Biomedical Sciences Institute, Trinity College Dublin, Dublin, Ireland,[2]Department of Mechanical, Manufacturing & Biomedical Engineering, School of Engineering, Trinity College Dublin, Ireland;[3]Advanced Materials and Bioengineering Research Centre (AMBER), Royal College of Surgeons in Ireland and Trinity College Dublin, Dublin, Ireland; [4]Urology, Boston Scientific Corp, Inc, Minnetonka, MN, USA; [5]Urology, Boston Scientific Corp, Inc, Clonmel Co, Tipperary, Ireland.

email: (lallyca@tcd.ie)

INTRODUCTION

A bench-top model for penile implant testing requires materials that mimic the viscoelastic properties of penile tissues to achieve robust and realistic simulations [1]. This study focuses on the Tunica albuginea (TA) and Corpora cavernosa (CC), as these penile tissues most influence the success of inflatable penile prostheses (IPP) for treatment of erectile dysfunction [1-3]. An IPP consists of two cylinders in the CC, a pump in the scrotum, and a reservoir in the abdomen, designed to facilitate erection, see Fig.1(a) [4]. Developing a bench-top model for the penis with good realistic biomechanical properties would provide key insights into the impact of an IPP on penile tissues, see Fig.1(b) [4]. This study aims to create such a model using synthetic viscoelastic materials that mimic the biomechanical properties of penile tissue. To achieve this goal, we investigated various biomaterials, assessing their viscoelastic and mechanical properties to determine their suitability for a bench-top penile model that replicates penile tissue characteristics relevant for implant testing [5-9].

MATERIALS AND METHODS

Three human penises from donors aged 75-89 were obtained from the Science Care donations centre, with a post-mortem interval of 1–5 days. Tissues were stored at -20°C until evaluation. Segments were prepared for testing of the TA (5:1 length-to-width ratio) and CC (6 mm length, 4.6 mm diameter) and stored in PBS, and tested within 24 hours to characterize their stress-strain response and viscoelastic properties. To assess material suitability, we evaluated key parameters, including printability, tensile strength, burst strength, viscoelastic behavior, suturability, mouldability, adhesive qualities, and compatibility with ultrasound imaging.

RESULTS

A preliminary investigation revealed that CC tissue exhibits viscoelastic characteristics, namely hysteresis, stress softening, creep and relaxation. Further analyses will be conducted to fully evaluate the viscoelastic properties of both TA and CC tissues. Based on our estqablished criteria (above), we reviewed, compiled, and scored several promising polymers—including PVA [6], polyvinyl amine (PVA(m)), polyacrylamide (PAAm) [7], PCL [8], PU [8], silk fibrin [5, 9], alginate and PEG, see Fig.1(b). Using this scoring system, we assessed each material's effectiveness in meeting the requirements for developing a penile bench-top model for IPP testing.

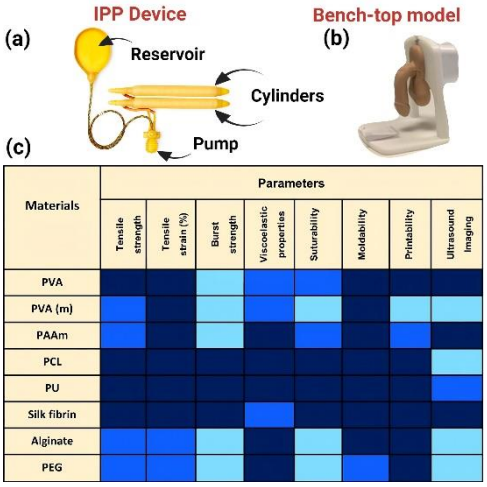

Figure 1. (a) IPP device showing components, **(**b) benchtop model of penile tissue [4], (c) assessment of biomaterials for bench-top penile model; grading: high (Dark blue), moderate (medium blue), and low (light blue)).

DISCUSSION

Based on their reported properties, PCL, PU, silk fibrin, PVA, and PAAm exhibited suitable tensile strength, flexibility, and biocompatibility, making them ideal candidates for creating a durable, adaptable bench-top penile model for IPP implant testing. These materials offer a reliable foundation for accurately replicating penile tissue properties essential for effective penile implant testing.

REFERENCES

[1] Zhang (et al.), J Mech Behav Biomed Mater.103: 103570. 2020. [2] Akbarzadeh (et al). Eur Urol Open Sci. 67. S3. [3] Khorshidi (et al.), Acta Biomater. 184: 226. 2024. [4] Madhusoodanan (et al.), JSM. 33: 652. 2021. [5] Ahmady (et al.), Int. J. Pharm. 608: 121037. 2021. [6] Zhu (et al.) RSC Advances. 8: 36999. 2018. [7] Han (et al.), NPG Asia Mater. 9: e372.2017. [8] Krol (et al.), Colloid and Polym Sci. 298:1077. 2020. [9] Alessandrio (et al.), Frontiers in Bioeng and Biotech. 7: 356. 2019.

Developing Cold Plasma Therapies for Bone Infection Control

Nic Shiurdain, O.[1], Dobbyn, P.[1], Barroug, S.[1] Boehm, D.[2], Bourke, P.[1]
[1] School of Biosystems and Food Engineering, University College Dublin
[2] School of Chemical and Bioprocess Engineering. University College Dublin
email: orla.nicshiurdain@ucdconnect.ie

INTRODUCTION

Orthopaedic implant infections cause a significant burden on healthcare systems worldwide. Current treatments include debridement of the infection site and loading the site with antibiotics. In some cases, the device must be removed via revision surgery. Treatment of these infections is further complicated by antibiotic resistant bacteria such as *Staphylococcus aureus* and their ability to form treatment resistant biofilms on the device.

There is a need for alternative treatments for orthopaedic implant infections. Cold atmospheric plasma (CAP) and plasma functionalised liquids (PFLs) could be a viable option for treating these infections. CAP and PFLs have demonstrated antimicrobial and wound healing effects (Nyguyen et al., 2018) and have the potential to be applied in sequence or combined with current therapies to treat these infections. This study assesses the efficacy of two different PFWs generated from an in-house pin discharge system known as the RSS system in a Spark discharge mode (Lu et al., 2017) and a microwave discharge system – MidiPlexc (Handorf et al., 2019), against MRSA biofilms grown for up to 72 hours.

MATERIALS AND METHODS

PFLs were generated by exposing deionised water to either MidiPlexc or Spark plasma systems for 30 minutes.
The generated Nitrates, nitrites and hydrogen peroxide concentrations were measured using colorimetric assays. *S. aureus* USA300 biofilms were grown on 96-well plates and titanium implants in tryptic soy broth for 24, 48, and 72 hours (fig. 1). Biofilms were treated with MidiPlexc and Spark PFLs for 15- and 30-minute contact times respectively. Recovery and XTT assays were performed to assess the effect of PFW treatment on bacterial load and metabolic activity respectively.

RESULTS AND DISCUSSION

The colorimetric tests showed MidiPlexc and Spark PFLs had different compositions in terms of nitrates, nitrites and hydrogen peroxide concentrations. MidiPlexc PFLs had nitrites, high concentrations of nitrates, and no detectable hydrogen peroxide. Spark PFLs had hydrogen peroxide, nitrates, and no detectable nitrites.

Biofilms that were grown on 96-well plates were more tolerant to PFL treatment compared to biofilms grown on titanium implants. PFLs generated by the Spark and MidiPlexc plasma systems were able to reduce the microbial load and metabolic activity in *S. aureus* biofilms, however the MidiPlexc PFL achieved these effects with a shorter contact time.

Although both PFLs were effective at reducing bacterial biofilm numbers, this was a function of biofilm maturity. The more mature 48- and 72-hour biofilms were more tolerant to PFL treatment than the 24-hour biofilms, highlighting a pathway for sequential PFL application for recalcitrant biofilms, compatible with Operating Room timelines. These results indicate that PFLs could be an effective treatment for orthopaedic implant infections. Further investigations should be performed to assess the efficacy of PFLs in combination with current therapies to treat orthopaedic implant infections.

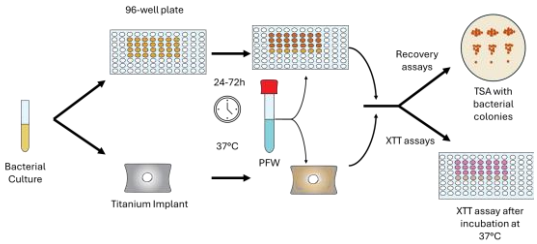

Figure 1 Experimental design for biofilm growth and treatment with PFLs.

REFERENCES

Handorf *(et al.)*, Microbial biotechnology 12:1034-1048, 2019.
Lu *(et al.)*, Plasma processes and polymers 14, 2017
Nguyen *(et al.)*, Biol Chem 400: 77-86, 2018.

REDEFINING TAVR MODELLING: A HIGH-FIDELITY FRAMEWORK FOR FLUID-STRUCTURE INTERACTIONS AND IN VITRO VALIDATION

Armfield, D.[1], Boxwell, S.[2], McNamara, L.[2], Cook, S.[3], Conway, S.[3], Celikin, M.[1], Cardiff, P.[1]
[1] School of Mechanical and Materials Engineering, University College Dublin, Dublin, Ireland
[2] College of Science and Engineering, University of Galway, Galway, Ireland
[3] Structural Heart, Boston Scientific Corporation, Galway, Ireland
email: dylan.armfield@ucdconnect.ie

INTRODUCTION

Transcatheter Aortic Valve Replacement (TAVR) represents a continually expanding treatment modality for conditions such as aortic stenosis. Originally conceived primarily for high-risk patients, this intervention has recently been deemed applicable to medium- and low-risk populations [1]. As the demographic of patients eligible for TAVR increases, so too does the array of specifications that a TAVR device must satisfy to be classified as an efficacious treatment strategy.

Traditionally, the development of new devices has relied heavily on costly and time-intensive physical prototyping. Considering this, the focal point of our research has centred on creating a high-fidelity computational framework designed to predict device performance *in vitro*. Previous computational studies often rely on simplifications, particularly in modelling leaflet mechanics or other critical aspects of the device and either modelling mechanical deployment or fluid transport through the deployed device independently [2]. In contrast, our prior work has demonstrated the significant influence of collagen fibre orientation in pericardium leaflets on overall device dynamics [3]. Building on these insights, this framework integrates both structural and fluid-structure interaction (FSI) analyses, capturing the entire device lifecycle with improved fidelity. This approach aspires to facilitate the virtual design of next-generation TAVR devices per ASME V&V40, expediting time to market, enhancing performance, and ultimately improving patient outcomes.

MATERIALS AND METHODS

Using the Boston Scientific Acurate Prime™ TAVR device as a basis, a representation of the complete device has been developed, including the self-expanding nitinol stent, treated as a superelastic material, and the PET reinforcement strip, represented by a Neo-Hookean elastic law. The porcine pericardium valve leaflets and skirts exhibit hyperelastic, anisotropic behaviour, described by a calibrated multi-fibre constitutive law based on multi-protocol biaxial tissue tests [3, 4].

The established framework incorporates an initial leaflet assembly phase, accounting for the tissue strains due to attachment to the stent frame. Following this, the complete TAVR assembly undergoes crimping to reach 90% of the catheter deployment diameter. The TAVR device is then deployed into the *in vitro* seating (circular, elliptical or patient-representative), and a directly coupled FSI simulation is performed on the deployed device under varying pulse-duplicator conditions, where the saline fluid is considered Newtonian and weakly compressible. The complete framework is built in Abaqus 2023.

RESULTS AND DISCUSSION

The established framework (see Figure 1) facilitates the virtual evaluation of the most critical aspects of TAVR device design, specifically addressing paravalvular leakage, durability, crimping damage, and thrombogenicity [1].

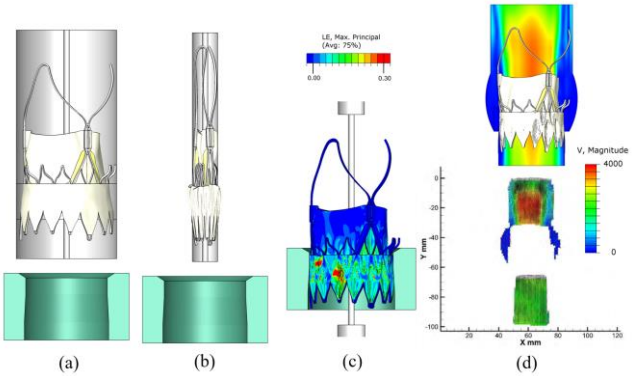

Figure 1 TAVR *in vitro* simulation framework includes (a) device assembly, (b) crimping, (c) cumulative strain post-deployment and (d) FSI simulation compared to PIV

The FSI framework was validated by comparing the *in vitro* commissural post-deflections and leaflet dynamics to high-speed images of the device functioning within the pulse duplicator. Particle Image Velocimetry (PIV), pulse duplicator pressure and flow measurements are employed to authenticate the flow dynamics. The framework's successful validation has led to its adoption as a key tool for evaluating design advancements in a commercial setting.

REFERENCES

[1] Rotman *et al.*, Expert Review of Medical Devices, Volume 15 pp. 771-791, 2018
[2] Hirschhorn *et al.*, Med Eng Phys 78 pp. 1-13, 2020
[3] Armfield *et al.*, Journal of the Mechanical Behaviour of Biomedical Materials 157, 2024
[4] Hu *et al.*, Journal of Biomechanics 40, pp. 2559–63, 2007

IN-VITRO ORTHOPAEDIC SITE INFECTION MODEL DEVELOPMENT FOR COLD PLASMA ALTERNATIVE THERAPY

Barroug, Soukaina.[1], Shiurdain, Orla Nic.[1], Bourke, Paula.[1]
[1] School of Biosystems and Food Engineering, University College Dublin
email: paula.bourke@ucd.ie

INTRODUCTION

Orthopaedic site infections pose serious issues in clinical practice during or post-surgical interventions that require hardware implantation, removal, or revision surgeries. They often prolong patient recovery, with the potential for severe complications, especially for immune-suppressed patients, and incur high medical expenses. Pathogens including *Staphylococcus aureus* and *Pseudomonas* spp are among these nosocomial infections characterized by biofilm formation and antibiotic resistance. Alternative therapies that replace or enhance current therapies are required. The present work focuses on developing a 3D in-vitro model that mimics a multipart orthopaedic site infection and facilitates biofilm growth. The purpose is to develop a model that allows realistic exploration of cold plasma technology as an innovative intervention for infection management pertinent to orthopaedic surgeries.

MATERIALS AND METHODS

1. Bio-Ink

The bioink optimized for 3D printing is comprised of sodium alginate hydrogel solution, filter sterilized liquid chicken juice, and calcium chloride ($CaCl_2$). The bioink was inoculated with a bacterial suspension of a fresh culture of *Staphylococcus aureus* ATCC 25923 to form a Tissue Infection model (TIM).

2. 3D Printing

A 3-D bio-printer (CELLINK BIOX, UK) was used to print a dispersed infection model using the bioink. The model was printed on a polished stainless-steel surface representing the orthopaedic implant used during the surgical interventions (figure 1).

3. Infection Model

A solid chicken juice model, developed in previous work [1], was used to mimic the femoral muscles. It was placed on the top of the printed dispersed infection model. The final model is named the Dispersed Tissue Infection Model (D-TIM). To promote the infection phase and biofilm growth, D-TIM was incubated at 37 °C within a humid environment from 0 to 7 days. The level of infection was assessed using a microbial recovery test.

4. Cold plasma setup and treatment

Cold plasma intervention was introduced as plasma functionalized water (PFW). A reactive species specificity (RSS), electrode-based plasma setup was used to functionalize PFW. D-TIM was treated with PFW by dip-washing for 1 to 20 min in separate and/or sequential treatments. The efficiency of treatments was assessed by microbial recovery test. The chemical profile of PFW was characterized in terms of pH, conductivity, and levels of nitrate, nitrite, peroxide, and hydrogen peroxide.

RESULTS

The dispersed Infection Model supported infection and biofilm growth for up to 7 days. The microbial load significantly increased from 1.92 $\log_{10}$CFU/g on day 0 to 18.70 $\log_{10}$CFU/g on day 7. Results also highlighted the potential of PFW for reduction of *Staphylococcus aureus* ATCC 25923 by 4.35 $\log_{10}$CFU/g post-treatment compared to the control. Re-incubation (37 °C) of D-TIM post-treatment indicated no bacterial recovery and further reduction to 10 $\log_{10}$CFU/g compared to the control. The chemical characterization of PFW showed that the spark discharge generated both reactive oxygen and nitrogen species, where the generation time and discharge configuration are key factors. NO_3^- (22.53 mM), NO_2^- (0.019 mM), H_2O_2 (0.68 mM), and peroxide (0.84 mM) were detected after 30 min. While pH dropped from 5.79 to 1.74, conductivity increased from 1.56 to 5325.56 µS.cm^{-1} after 30 min generation time.

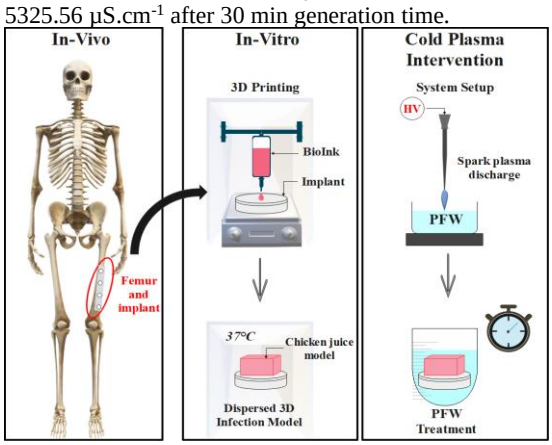

Figure 1 Experimental design for bioink development, dispersed infection model printing, and cold plasma therapy to control orthopedic surgery site infections.

DISCUSSION

The in-vitro 3D infection model developed in the present research helped mimic orthopaedic site infections, understand bacterial behavior and treatment efficacy when hosted in complex environments, and propose how PFW can be incorporated into the treatment protocol compatible with Operating Room time constraints. The outcome can reduce the amount of costly and time-consuming animal trials.

REFERENCES

[1] Barroug, Controlling *Campylobacter* spp and *Salmonella* spp in Poultry Processing using Cold Plasma and Natural Antimicrobials, PhD, UCD, 2024

DEVELOPMENT OF A FINITE ELEMENT MODEL TO CAPTURE MECHANICAL DAMAGE IN PENILE TISSUE AND INFORM IMPLANTABLE MEDICAL DEVICE DESIGN

Majid Akbarzadeh Khorshidi[1,2,3], Brian Watschke[4], Thomas Sinnott[5], Evania Mareena[5], Caitríona Lally [1,2,3*]

[1]Trinity Centre for Biomedical Engineering, Trinity Biomedical Sciences Institute, Trinity College Dublin, Dublin 2, Ireland.

[2]Department of Mechanical, Manufacturing and Biomedical Engineering, School of Engineering, Trinity College Dublin, Dublin 2, Ireland.

[3]Advanced Materials and BioEngineering Research Centre (AMBER), Royal College of Surgeons in Ireland and Trinity College Dublin, Dublin 2, Ireland.

[4]Urology, Boston Scientific Corp, Inc, Minnetonka, MN, USA.

[5]Urology, Boston Scientific Corp, Inc, Clonmel Co, Tipperary, Ireland.

INTRODUCTION

Erectile dysfunction (ED) refers to a deficiency in the sexual functioning of the penis, affecting approximately 52% of men over the age of 40, with prevalence increasing with age [1,2]. Inflatable penile prostheses (IPP) are used to treat ED, and consist of two composite rubber cylinders, a pump, and a reservoir. The performance of the IPP within the tissue can be influenced by inelastic effects such as viscoelasticity, material softening, and permanent deformation of the soft tissues. These inelastic behaviours can be assessed through specific experimental tests. Computational models can help to identify the appropriate testing platform [3] and evaluate the impact of inelasticity on IPP inflation and deflation. This study presents a finite element (FE) model that captures softening and permanent deformation during IPP operation in penile tissues, particularly the corpus cavernosum (CC) and tunica albuginea (TA).

MATERIALS AND METHODS

The geometry of the penis was reconstructed from a 2D cross-sectional image of an aged human penis using Abaqus/CAE 2022. This cross-sectional sketch was then extruded to create a 3D model of a penile segment of length 10 mm. The hyperelastic behaviour of the CC and TA layers was defined using the 2nd-order Ogden model and the HGO anisotropic model, respectively. To account for tissue softening and permanent deformation, a continuum damage model proposed by Balzani et al. [4] was applied to the TA, and a pseudo-elastic damage model proposed by Dorfmann and Ogden [5] was applied to the CC. Two custom user subroutine codes (UMATs) were developed to integrate the hyperelastic properties and inelastic effects into the FE analysis (Abaqus, 2022). A parametric study was conducted to evaluate the sensitivity of the damage parameters. Subsequently, the model was used to simulate the IPP inflation and deflation processes, similar to [3].

RESULTS

The model successfully captured both stress softening and permanent set behaviours in the CC and TA under uniaxial loading conditions, see Figs. 1a & 1b. Tissue softening observed after the first loading cycle (IPP inflation) led to a reduction in tissue resistance. Consequently, the subsequent unloading (IPP deflation) and reloading (IPP re-inflation) followed distinct pressure-diameter trajectories, see Fig. 1c. Minimal permanent strain was observed in the tissue after IPP deflation, see Fig. 1d.

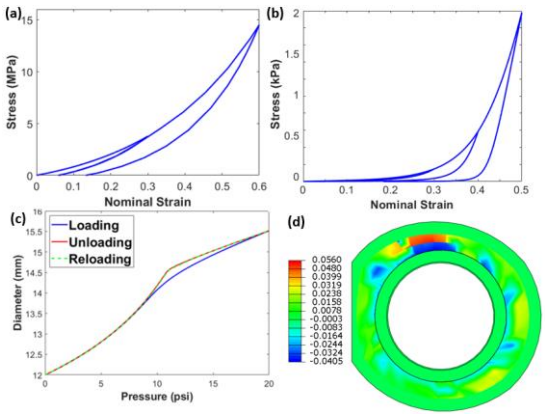

Figure 1 Stress vs strain for (a) TA and (b) CC layers. (c) Pressure-diameter curves for loading, unloading, and reloading scenarios. (d) The absolute maximum principal strain contour including TA, CC, and the IPP cylinder.

DISCUSSION

This study demonstrates the ability of the developed FE model to simulate the inelastic behaviours, specifically stress softening and permanent deformation, in penile tissues during IPP inflation and deflation. These inelastic effects could impact device performance and patient outcomes, as lower resistance may alter the pressure required for subsequent inflations. Further refinement of the model to fully include all viscoelastic properties, informed by experimental tests, will help to optimise IPP design and improve therapeutic efficacy for patients.

REFERENCES

[1] Bose, et al. Sex. Med. Rev. 11(3), (2023) 268-277.
[2] Feldman, et al., J. Urol., 151, (1994) 54–61.
[3] Fereidoonnezhad, et al., Comput. Biol. Med. 166 (2023) 107524.
[4] Balzani, et al. Comput. Methods Appl. Mech. Eng. 213–216 (2012) 139–151.
[5] Dorfmann, et al. Int. J. Solids Struct. 41 (2004) 1855–1878.

DEVELOPMENT OF VARIABLE DIAMETER COMPLIANCE AND FRICTION – MATCHED SYNTHETIC VESSELS FOR BENCHTOP TESTING

Shen, G.[1,2], Khaydukova, I.[1,2], Hulk, V.[3], Kenny, G.[3], O'Cearbhaill, E.D.[1,2]
[1] UCD Centre for Biomedical Engineering, University College Dublin, Ireland
[2] School of Mechanical & Materials Engineering, University College Dublin, Ireland
[3]Croívalve, Dublin, Ireland
email: gang.shen@ucd.ie

INTRODUCTION

Novel endovascular devices are being continuously developed for clinical indications in a broadening range of arteries and veins [1,2]. To optimise the functionality of those devices, vessel models are used throughout the entire development cycle to simulate their use. Typically, thin-walled silicone tubes are used to simulate blood vessels [3,4]. However, these models typically suffer from (1) excessive friction force, (2) limited matching of mechanical properties and (3) can lack incorporation of basic geometric features, such as vessel tapering. Consequently, there can be a poor translation in device performance measurement from benchtop to pre-clinical assessment and ultimately clinical use. Similarly, there is a lack of accurate models that simulate endovascular device deployment for physician training.
Therefore, developing compliance and friction-matched vessel models is beneficial for the medical device industry in accelerating endovascular medical device translation. We propose that rotational-axis 3D printing can be a versatile tool in enabling rapid fabrication of composite synthetic vessels, which match the variable compliance and friction of target vascular anatomies.

MATERIALS AND METHODS

In this study, a three-layer vessel model was developed (Fig 1): (1) inner layer: Ecoflex 00-10 (Smooth-on, USA), 0.85 mm thickness; (2) middle layer: Filaflex 82A, sinusoidal curves; and (3) Encapsulation layer: Ecoflex Gel (Smooth-on, USA), 0.85 mm thickness. The silicone injection was used to fabricate the inner and encapsulation layers, while the stereolithography (SLA) technique was used to fabricate the needed molds (Form4, clear resin). The middle layer was fabricated through the fused deposition modelling (FDM) with the assistance of a rotation mandrel. Grasshopper (Rhino V7) was used to generate the G-code for FDM.

Two stages of studies were carried out. The first stage involves only cylindrical vessel models. The correlation between compliance and different designs of the middle layer was obtained. In the second stage, the diameter of a representative human vena cava was measured. Then, based on the findings of the first stage, a patient-specific and compliance-matched vessel model was constructed (see Fig 1).

In addition, a custom-built friction measurement device was integrated into the universal mechanical tester (LS1, Ametek). Synthetic and natural oils were mixed with Ecoflex 00-10 to tailor its friction performance.

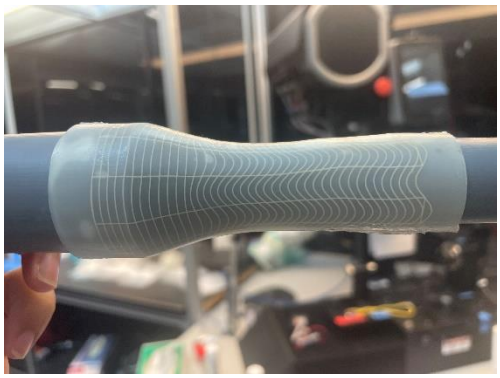

Figure 1 An example of a variable diameter and variable compliance synthetic vessel.

RESULTS AND DISCUSSION

This study confirms that the three-layer structure is an effective tool for fabricating compliance-matched vessel models. By altering the width, thickness, amplitude and gap of the middle layer, the compliance can be tailored to each specific requirement. Furthermore, it also proves that mixing silicone with natural oils can significantly reduce the frictional properties of silicone.

Future studies will focus on matching the compliance and friction properties of specific vessels (aorta, arteries, and veins).

REFERENCES

[1] Guéroult AM, et al. *Heart.* 108(21):1707-15, 2022.
[2] Pineda-Castillo SA et al. Polymers. 14(13):2526, 2022.
[3] Tie JL, et al. Journal of Hand and Microsurgery. 16(4):100133, 2024.
[4] Byrne O, et al. Biomaterials Science. 9(12):4343-55, 2021.

DEVELOPMENT OF A MICROFLUIDIC-BASED JOINT-ON-A-CHIP PLATFORM FOR BONE AND CARTILAGE TISSUE ENGINEERING APPLICATIONS

Collins, B.[1], Davoodi, P.[3], Dunne, N.J[1], Bendechache, M. [2], Levingstone, T.J.[1]
[1] Centre for Medical Engineering Research, School of Mechanical and Manufacturing Engineering, Dublin City University;[2] Adapt Centre, University of Galway, [3] Guy Hilton Labs, Keele University.
email: brian.collins29@mail.dcu.ie

INTRODUCTION

Osteoarthritis is a common joint-based pathology resulting from bone/cartilage damage that compromises mobility and quality of life [1]. Current treatments do not meet clinical requirements, and new treatment developments are hindered by the limitations associated with existing research methods [1]. Specifically, 2D/3D culture models oversimplify the biological environment and lack shear or cyclic forces [2]. Whereas mouse models of aged or damaged joint tissue are costly, time-consuming, and often translate poorly to human medicine [1]. Recent organ-on-a-chip model advances present a reliable, animal-free, safer, and lower-cost approach for therapeutic testing [2]. The overall project aim is to develop an organ-on-a-chip model capable of supporting the culture of bone and cartilage cells. Specifically, this study aimed to identify the optimal culture conditions, exploring the optimal composition and thickness of support hydrogels incorporated in the chip model.

METHODS AND MATERIALS

Microfluidic-based chips were fabricated from laser-cut poly-methyl methacrylate (PMMA) sheets (0.5-1 mm thick) with 1 cm^2 cell wells and attached by double-sided pressure-sensitive adhesive (PSA) sheets (0.15 mm thick). Support hydrogels of various GelMA (*g*) compositions (5%, 7.5%, 10% w/v), ±1% w/v hyaluronic acid (*h*) and a defined thickness (i.e., 0.75 mm) were incorporated into the cell wells and seeded with MC3T3 pre-osteoblast cells place on top at 20 $x10^3$ cells/cm^2. Cells were cultured in standard growth media (Opti-Mem I 1x 10%FBS media) at 37 ºC and 5% CO_2. Cell viability was assessed on Day 3 using trypan blue (n=3). Viable cell activity and proliferation were assessed using Alamar Blue absorbance (560 nm) and ViaFluor (488 nm) fluorescence at 7, 14, 21 and 28-day timepoints (n=3). Mineralisation in osteogenic media was assessed using alkaline phosphatase absorption (575 nm) at 14 and 21 Days (n=3) assays, and terminal Alizarin Red staining at Day 28 (n=3). Samples were imaged by a Nikon Olympus confocal microscope. This same-day test procedure was repeated to determine the optimal hydrogel thickness. The optimal hydrogel composition was assessed at thicknesses of 0.5, 0.75 and 1 mm thickness with 200 µL or 400 µL media/well in triplicate with blank media and cell-only controls.

RESULTS

Microfluidic-based chips were successfully designed and fabricated. Day 3 cell average viability was > 80%. Assessing mineralisation in the support hydrogels showed the highest level of alkaline phosphatase at Day 28 was in the 10% GelMA with 1% hyaluronic acid group (10%g1%h) (Fig. 1a), 30% higher than the lowest (7.5%g1%h) group (ANOVA p=0.13). Incorporating hydrogels into chips increased cell metabolic activity and mineralisation compared to uncoated chips (Fig. 1b). Hydrogel thickness effect on cellular metabolic activity (Alamar Blue) indicated a thickness of 1 mm (100 µL hydrogel/well) had the highest levels of Alamar Blue reduction (Fig. 1b) at Day 21 (ANOVA P<.001). Similar results were observed for ViaFluor fluorescence. Alkaline phosphatase absorption was highest for 1mm thick samples, ~25% more than 0.5mm samples(p=0.13).

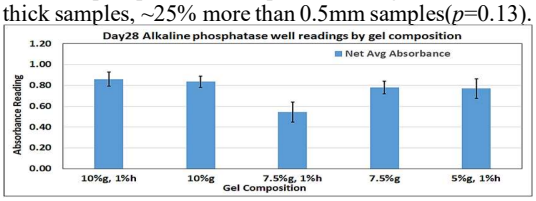

Fig. 1a: Alkaline phosphatase absorption for various GelMA (g) hydrogel compositions ±1% hyaluronic acid (h).

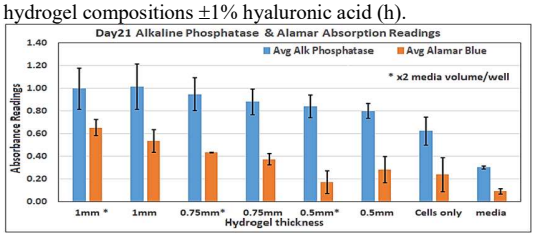

Fig. 1b: Comparative cell activity demonstrated using Alamar Blue reduction and alkaline phosphatase absorption for different thicknesses of 10%g1%h hydrogel at Day 21.

DISCUSSION AND CONCLUSIONS

Hydrogel incorporation into the microfluidic-based chip led to more favourable cell culture conditions. Chips with 1 mm of hydrogel comprising 10%GelMa with 1% hyaluronic acid showed the best metabolic activity and mineralisation. The optimised hydrogel composition and thickness led to a two-fold increase in cell and proliferation activity (Fig 1b). Alkaline phosphatase absorption (calcium inference) showed a ~30% difference between best and worst cases (Fig 1a, b), and a generally consistent trend between hydrogels tested. The next studies will involve an *in vitro* assessment of cellular response to varying specific parameters (i.e., flow rate and centrifugal loading) within the microfluidic-based chip.

REFERENCES

1. Lopa L. *(et al.),* Stem Cells Int., 2018:1-14, 2018.
2.Vereshchagina E. *(et al.),* Biomicrofluidics 7.3:034101

ACKNOWLEDGEMENTS

Funded by SFI CRT-AI under grant number 18/CRT/6223.

PHYSICOCHEMICAL PROPERTIES OF MACROMOLECULAR CROWDING AGENTS AFFECT THE EXTRACELLULAR MATRIX DEPOSITION IN EUKARYOTIC CELL CULTURES

Chaniotaki, L., Zeugolis, D.
Regenerative, Modular & Developmental Engineering Laboratory (REMODEL), Conway Institute of Biomolecular & Biomedical Research and School of Mechanical & Materials Engineering, University College of Dublin (UCD), Dublin, Ireland
email: lefki.chanotaki@ucdconnect.ie

INTRODUCTION

Macromolecular crowding (MMC) is a biophysical phenomenon, based on the exclude volume effect principle, that characterises crowded solutions [1]. MMC reduces diffusion and increases the kinetics of biochemical reactions and biological processes by several orders of magnitude [2]. In eukaryotic cell culture, MMC has been shown to enhance and accelerate extracellular matrix (ECM) deposition in a MMC agent dependent manner [3] Herein, we correlate the physicochemical properties of the most widely used MMC agents (carrageenan, CR [4], and Ficoll® cocktail, FC [5]) to the rate of ECM deposition in skin fibroblast cultures.

MATERIALS AND METHODS

Skin fibroblasts and bone marrow mesenchymal stromal cells were cultured with CR and FC for 4, 6 and 8 days. Physiological cell function was assessed via cell morphology, viability, proliferation and metabolic activity. ECM deposition was assessed via electrophoresis and immunofluorescence. Hydrodynamic radius, polydispersity, molecular weight and shape were evaluated through dynamic light scattering (Litesizer™ 500, Anton Paar, Germany), mass photometry, size-exclusion chromatography combined with multi-angle direct light scattering and analytical ultracentrifugation. Zeta potential was evaluated though electrophoretic light scattering (Litesizer™ 500, Anton Paar, Germany).

RESULTS

Neither CR nor FC affected basic cell function. CR significantly increased collagen type I deposition, whilst FC significantly increased collagen type III deposition. CR induced a globular ECM deposition, whilst FC induced a bidirectional ECM deposition. Electrophoretic light scattering analysis made apparent that CR had negative charge, whilst FC was found to be neutral. Dynamic light scattering was not able to accurate measure the dispersity of highly polydispersed samples, such as CR. Mass photometry, size-exclusion chromatography combined with multi-angle direct light scattering and analytical ultracentrifugation are in progress.

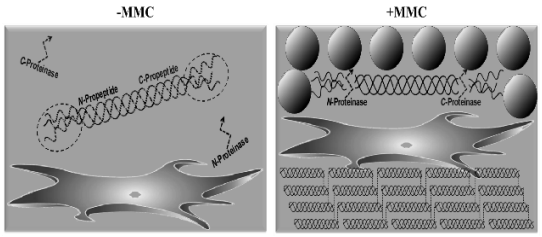

Figure 1 MMC agents prohibit the diffusion of C and N proteinases from C and N propeptides, resulting in the quicker transformation of procollagen to collagen and higher ECM deposition [6].

DISCUSSION

It is already known that MMC agents enhance and accelerated ECM deposition [7]. This work indicates that MMC agents' physicochemical properties and the ECM deposition have a direct link. More specifically, it indicates that negatively charged and highly polydisperse MMC agents induce the highest ECM deposition due to more effective volume exclusion effect.

REFERENCES

[1] Badowski (et al.), Molecular Crowding – (in Cell Culture), Springer International Publishing, 2020.
[2] Chen (et al.), Adv Drug Deliv Rev 63(4-5):277-90, 2011.
[3] Tsiapalis (et al.), Biomaterials 275:120943, 2021.
[4] De Pieri (et al.), Int J Biol Macromol 164:434-436, 2020.
[5] Gaspar (et al.), Acta Biomat 88:197-210, 2019.
[6] Raghunath (et al.), Trends Biochem Sci 46:805-811, 2021
[7] Kumar (et al.), Sci Rep 5:8729, 2015

DESIGN OF BIOMIMETIC EXTRACELLULAR MATRIX-BASED BIOINKS FOR BIOPRINTING OF AN INTERVERTEBRAL DISC MODEL

Kersten, MV.[1,2], Thomas, J.[1,2], Haffner, T. [1,2] and Buckley, CT.[1,2,3]
[1] Trinity Centre for Biomedical Engineering, Trinity College Dublin, Ireland
[2] AMBER Centre, Royal College of Surgeons in Ireland & Trinity College Dublin
[3] Tissue Engineering Research Group, Department of Anatomy and Regenerative Medicine, Royal College of Surgeons in Ireland
email: kerstenm@tcd.ie

INTRODUCTION

Lower back pain is a global epidemiologic and socioeconomic problem with an 80% prevalence [1]. Injury and/or degeneration can cause tears or fissures in the lamellar annulus fibrosus (AF) tissue, which allows protrusion of the central gelatinous nucleus pulposus (NP) tissue resulting in pain and reduced disc height. Despite intensive research into the intervertebral disc (IVD), the pathology remains to be fully understood. Advances in 3D- and bioprinting facilitated biofabrication of IVD models [2,3], which though had clearly defined NP and AF regions, lacked the complex 3D structure inherent to the extracellular matrix (ECM) and were unable to replicate the native mechanical strength or the dynamic changes that signify degeneration, and are therefore unsuited as an *in vitro* platform to study IVD pathology or evaluate novel therapies. This work aims to design and characterise biomimetic ECM-based bioinks of NP, inner (i)AF, and outer (o)AF, which can be used to bioprint a controlled and reproducible 3D disc model.

MATERIALS AND METHODS

Caudal bovine discs were obtained from a local butcher and characterised to determine baseline target properties. Native disc dimensions, tissue compressive and tensile strength and ECM biochemical composition were analysed. ECM was isolated (0.2M NaOH, cryomilling, 2U/ml Benzonase nuclease, 18kU/ml pepsin, salt precipitation) and methacrylated to form ECM-MA. Simultaneously, elastin and chondroitin sulphate (CS; a glycosaminoglycan and major disc ECM component) were also methacrylated, and the three components were mixed in native concentrations to create biomimetic bioinks. Bioink were characterised and 3D-printed using a custom HYREL 3D-printer.

RESULTS

Native disc measurements informed the dimensions of a 3D model, while mechanical testing showed a compressive and tensile modulus of 0.947±0.137 and 0.725±0.305 MPa respectively for NP that increased to 1.064±0.155 and 10.393±1.786 MPa for iAF, and 1.401±0.163 and 30.636±14.644 MPa for oAF. Biochemical analysis revealed the major ECM components and their relative concentrations, which were used to create the following bioink compositions:

Table 1: Bioink compositions of ECM, CS and Elastin for NP, iAF and oAF

Bioink (w/v)	**NP**	**iAF**	**oAF**
Solvent	1000 µl	1000 µl	1000 µl
ECM	7%	14%	36%
CS	17%	13%	6%
Elastin	4%	6%	10%

Bioinks were successfully printed using a 23G nozzle and a custom HYREL 3D-printer. Preliminary cell work in mid-ECM concentrations showed good viability and no adverse effects upon application of shear.

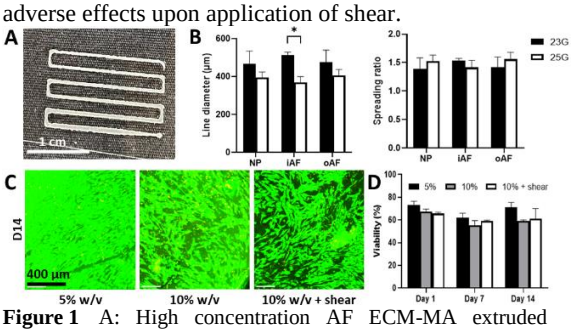

Figure 1 A: High concentration AF ECM-MA extruded through 23G nozzle. B: Line diameter (µm) and spreading ratio (%). C: Viability of 5%, 10%, and 10% shear. 400 µm scalebar. D: Semi-quantitative cell viability.

DISCUSSION

Biomimetic bioinks were designed and fabricated from ECM. Rheological parameters were characterised and the bioinks could be printed with high shape fidelity. AF cell viability after encapsulation remained stable under shear application. Moreover, shear stress accelerated the cells' adoption of an elongated fibroblastic morphology, highlighting the beneficial impact of a biomimetic 3D environment combined with transient mechanical stress. This work represents the first step in the development of biologically relevant IVD models as a controlled and reproducible platform for ex vivo studies of pathological progression and the development of novel treatments.

ACKNOWLEDGEMENTS

This work was supported by the European Research Council (ERC-2019-CoG-864104: INTEGRATE).

REFERENCES

[1] Dieleman *et al*. JAMA, 316(24): 2627-2646, 2016
[2] Zhu *et al*. Mater Sci Eng C Biol Appl, 128: 112310, 2021 [3] Sun *et al*. Bioact Mater, 6(1): 179-190, 2020.

GRANULAR HYDROGEL VISCOELASTICITY PROMOTES PLURIPOTENT STEM CELL MORPHOGENESIS AND ORGANOID FORMATION

Kennedy, O.[1,2], **Ventura, L.**[1,2], **Daly, A.**[1,2]
[1] Biomedical Engineering, University of Galway, Galway, Ireland
[2] CÚRAM, SFI Research Centre for Medical Devices University of Galway, Galway, Ireland
email: (o.kennedy6@universityofgalway.ie)

INTRODUCTION

During organogenesis, pluripotent stem cells self-organise and differentiate into multicellular tissues and organs. The viscoelasticity of the extracellular matrix plays a critical role in modulating the morphogenesis of pluripotent stem cells (PSCs), with previous work demonstrating that viscoelastic hydrogels can regulate stem cell spreading, migration and proliferation[1,2]. However, the impact of viscoelasticity on key aspects of organogenesis, like volumetric tissue growth and cell fate specification, remains poorly understood. This study aimed to investigate how ECM viscoelasticity affects PSC morphogenesis, growth, and differentiation. To achieve this, we engineered granular hydrogels by fragmenting norbornene-modified hyaluronic acid (Nor-HA) hydrogels. We hypothesized that these granular gels, with inherent viscoelasticity, would promote greater PSC morphogenesis and volumetric growth compared to non-granular bulk hydrogels, which exhibit predominantly elastic behaviour (Fig. 1A).

MATERIALS AND METHODS

Hyaluronic acid was modified with 5-norbornene-2-methylamine groups following a protocol outlined by Truong et al. in which the carboxylic acid groups were targeted and replaced by norbornene groups[3]. To fabricate bulk hydrogels, LAP was used as a photoinitiator, dithiol crosslinker was added at a 1 mM concentration and photocrosslinking was caried out using 405 nm light. To produce granular gels, fragmentation of the bulk material was carried out using a homogeniser at 15,000 rpm for 3 minutes. PSCs were encapsulated in the hydrogels as single cell suspensions. For granular gel encapsulation, 1-part single cell suspension was mixed with 2-parts granular hydrogel and 5% v/v Matrigel. To carry out bulk encapsulations the cell suspension was mixed with hydrogel precursor solution at the same ratio, Matrigel was added, and the gels were photocrosslinked for 2 minutes.

RESULTS

Nor-HA bulk hydrogels displayed stiff, elastic properties, with a compressive modulus of 2.85 kPa and only 10% stress relaxation after 10 minutes (Fig 1B). However, granular Nor-HA had a reduced compressive modulus of 1.2 kPa and a stress relaxation half-time of just 1.25 s (Fig. 1B). Fragmentation of bulk hydrogels results in a material with viscoelastic properties.

PSCs encapsulated in granular Nor-HA formed clusters within 24 hours and began to proliferate. Overtime the cell clusters organised to form structures, reminiscent of embryoid bodies (EBs) (Fig. 1C). As these EBs continued to grow, they began to morph together and produce larger structures, with the surface area increasing by more than 30 times (Day0 mean = 1319 ± 167 μm^2, Day7 mean = 44,529 ± 19,317 μm^2) (Fig. 1D). Immunostaining results indicate that pluripotency was maintained up to 7 days, with EBs staining positively for OCT 4 and SSEA4 (Fig. 1E).

While cells encapsulated in bulk gels did form EBs, their growth was limited (Day 0 mean = 505 ± 13.7 μm^2, Day 7 mean = 2796 ± 532 μm^2) (Fig. 1C, D). The EBs did not morph together and they remained circular in morphology.

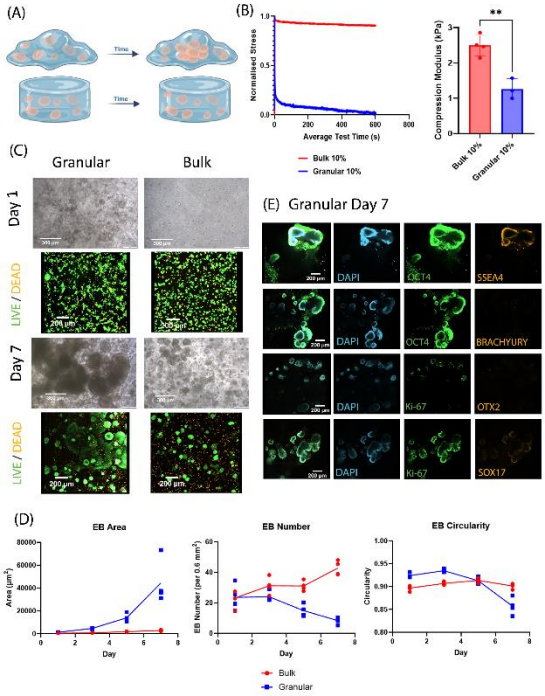

Figure 1 (A) Schematic of cells encapsulated in granular vs. bulk material (B) Stress relaxation and compression modulus of materials (C) 7-day PSC encapsulation in granular and bulk materials (D) PSC growth quantification (E) Pluripotency immunostaining in granular material after 7 days in culture

DISCUSSION

Compared with traditional bulk hydrogels, the viscoelastic nature of granular hydrogels, demonstrated by the short relaxation half-time, allows for reduced resistance to mechanical strain. This promotes increased cell proliferation, migration and changes in morphology, while also appearing to maintain pluripotency.

REFERENCES

1. D. Indana *(at al.)*, Adv. Mater. 2021, 33, 2101966.
2. Simunovic M *(et al.), Nat* Cell Biol. 2019 Jul;21(7):900-910.
3. Truong NF (*et al*.), Acta Biomater. 2019 Aug;94:160-172.

MULTISCALE PROTEOMIC ASSESSMENT OF BIOPROSTHETIC STRUCTURAL VALVE DEGENERATION AND NATIVE CALCIFIC AORTIC VALVE DISEASE

Cahalane, R.[1,2], Clift, C.[1], Blaser, M.[1], Turner, M.[1], Kasai, T.[1], Campedelli, A.[1], Billaud, M.[3], Muehlschlegel, J.[4], Hendrickx, A.[5], van den Bosch, M.[5], Rega, F.[5], Aikawa, M.[1,3], McNamara, L.[2,6], Meuris, B.[5], Singh, S.[1,3], Aikawa, E.[1,3]

[1]Center for Interdisciplinary Cardiovascular Sciences, Cardiovascular Division, Department of Medicine, Brigham and Women's Hospital, Harvard Medical School, MA, USA. [2]Mechanobiology and Medical Device Research group, Biomedical Engineering, College of Science and Engineering, University of Galway, Ireland. [3]Center for Excellence in Vascular Biology, Cardiovascular Division, Department of Medicine, Brigham and Women's Hospital, Harvard Medical School, MA, USA. [4]Department of Anesthesiology and Critical Care Medicine, Johns Hopkins University School of Medicine, MD, USA. [5]Department of Cardiovascular Sciences, KU Leuven, Belgium. [6]CÚRAM, SFI Research Centre for Medical Devices, Galway, Ireland.

email: rachel.cahalane@universityofgalway.ie

INTRODUCTION

Heart valve disease is predicted to be the next cardiac epidemic.[1] Currently, the leading treatment option is implantation of bioprosthetic (BP) valve, which is comprised of glutaraldehyde-fixed bovine pericardium mounted onto a stent or frame.[2] However, for one-third of BP patients the implant degenerates by 8 years,[3] and certain cohorts, including younger adults, are at risk of accelerated degeneration.[4] The risk factors and presentation of BP valve degeneration and native calcific aortic valve (AV) stenosis are similar. In AV disease, an accumulation of extracellular vesicles (EVs) and lipids, thrombosis, fibrosis, and calcification occur.[5] However, the processes governing BP degeneration are insufficiently explored. Here we conduct 1) gross pathological, histopathological, and ultrastructural assessments of explanted degenerated BP valves and 2) multiscale proteomic comparative analyses of BP degeneration versus AV disease.

MATERIALS AND METHODS

Explanted bovine pericardial BP leaflets (n=48) and native human AV valves (n=19) were acquired from AV replacement and BP revision surgeries. Tissues were macroscopically segmented by diseased state (BP: non-degenerated, thrombotic, neotissue, and calcified and AV: non-diseased, fibrotic, and calcified), validated by histopathology. Segment-specific mass-spectrometry-based proteomics was performed (Fig.1A(i)). Laser capture microdissection enabled spatially resolved proteomics for distinct calcified BP regions: bioprosthetic pericardium, internal haemorrhage, surface thrombus, and neotissue (Fig.1B(i)). Transmission electron microscopy (TEM) was performed to identify BP leaflet EVs (Fig.1C(i)), which were then extracted by enzymatic digestion, (ultra)centrifugation, density gradient separation, and then underwent proteomic analysis (Fig.1C(ii)).

RESULTS

AV and BP proteomes show moderate overlap (58%) and both principal component analyses cluster based on diseased segment. Correlations of segment proteome-wide abundances revealed the highest intra- and inter-tissue similarity between macroscopically non-degenerated and calcified BP valves (r_p=0.87), and BP neotissue and calcified AV (r_p=0.69) (Fig.1A(ii)), indicating novel calcified BP subtypes. Histopathology confirmed four distinct regions of BP degeneration, each capable of calcifying: BP pericardium, internal haemorrhage, surface thrombosis, and neotissue (Fig.1B(ii)). Proteins involved in the calcific remodelling of each distinct region are largely unique, suggesting different mechanisms (Fig.1B(iii)). For the first time, EVs were identified within degenerated BP tissue compared with non-implanted controls. A comparison of tissue EV proteomes from AV and BP valves revealed conserved proteins linked to wound healing and included metalloproteinases (MMP9/12/14/23B, TIMP1/3), while coagulation (GO:0072378) and immune (GO:0002697) processes were uniquely enriched for BP EVs (Fig.1C(iii)).

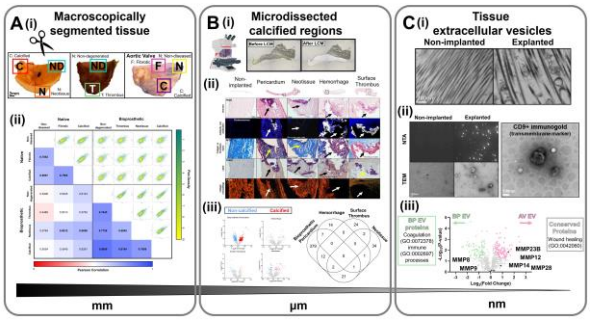

Figure 1: Multiscale proteomic assessment of bioprosthetic (BP) valve degeneration and native aortic valve (AV) disease. (A) (i) Macroscopically segmented valve tissue (BP: ND; non-degenerated, T; thrombus, N; neotissue, C; calcification. AV: N; non-diseased, F; fibrotic, C; calcified). (ii) Correlations of segment proteome-wide abundances. (B) (i) Laser capture microdissection. (ii) Calcification within different BP regions. (iii) Differential abundance analysis of calcific process within each calcified BP region with Venn diagram of overlapping proteins. (C) (i) TEM of BP tissue ultrastructure vs control. (ii) Tissue EV isolation and characterisation by NTA, TEM. (iii) Differential abundance analysis of BP vs AV EVs protein cargos.

DISCUSSION

A proteomic pipeline was developed for cross-species cardiovascular tissue, marking the first comparative study of degenerated BP and diseased AV valves. These results provide insights into degeneration mechanisms which can inform future treatment of xenogenic matrix for commercial bioprosthetic tissue production.

REFERENCES

1. d'Arcy (*et al.*), **Heart**, 97(2):91-93 (2011). **2.** Persson (*et al.*), **JAMA Network Open**, 5:e220962 (2022). **3.** Salaun (*et al.*), **Circulation**, 138:971–985 (2018). **4.** Saleeb (*et al.*), **Circulation**, 130:51-60 (2014), **5.** Kraler (*et al.*), **European Heart Journal** 43:683-697 (2021)

ACKNOWLEDGEMENTS

This project was funded by the EU's Horizon 2020 Marie Sklodowska-Curie grant agreement No. 101023041.

EVALUATION OF THE INFLUENCE OF PEEK POLYMER PROCESSING CONDITIONS ON THE PROPERTIES OF 3D PRINTED PARTS

Carey,S. Dowling, D.[1]
[1] I-Form Centre, School of Mechanical and Materials Engineering, University College Dublin
email:sadhbh.carey@ucd.ie

INTRODUCTION

This work focuses on optimising the 3D printing processing conditions for PEEK (polyethertherketone), which is widely used for medical device implants including cranial implants (Figure 1) and spinal cage devices.[1] PEEK exhibits superior thermal properties, chemical resistance, mechanical and biocompatibility.[2] The 3D printing of PEEK can be inherently difficult mainly due to its high temperature sensitivity and the semi crystalline nature of the material.[3] To address these difficulties, multiple printing parameters such as print and bed temperature, grade of PEEK, and print speed, need to be considered. This study investigated PEEK printing using the Fused Filament Fabrication technique. The printing studies were carried out using a pre-production scale reactor called the miniFactory Ultra 2 [4]. This system incorporates a heated build chamber with an integrated drying and annealing system, in addition to smart features such as remote monitoring and control. By utilising this monitoring technology, the printing parameters can be precisely controlled and their effects on PEEK printed parts monitored, with the aim of optimising the process to produce printed parts exhibiting both a high level of interlayer adhesion along with good geometric part print accuracies.

MATERIALS AND METHODS

The PEEK filament was first dried at 100ºC using an integrated heated chamber within the printer, to remove any moisture. The miniFactory system is fitted with a range of sensors for continuous monitoring of print parameters including nozzle, bed and chamber temperature, flow rate, feeding rate and fan cooling rate. Furthermore, these settings can be monitored and adjusted in real-time on a laptop. A smart alarm system is triggered if a deviation in the set parameters is detected outside of customised tolerance values. During printing process data is monitored so that the effect of printing parameters layer by layer can be evaluated. The study investigated the effects of altering multiple parameters such as the grade of PEEK, nozzle diameter, nozzle temperature, print speed, chamber temper and more were reviewed on the porosity, dimensions, warping and the internal structure of printed parts.

RESULTS

The research to date has focused on the influence of printing parameters such as the print nozzle temperature, preheat and cooldown cycle, nozzle diameter, grade of PEEK and bed material (aluminium and glass print beds). Investigations have included studies on the effect these parameters on morphology, namely warping of the part and printing of 'turbulators', which are small complex geometries integrated into printed PEEK pharmaceutical reactor components, which facilitate the mixing of chemical precursors.

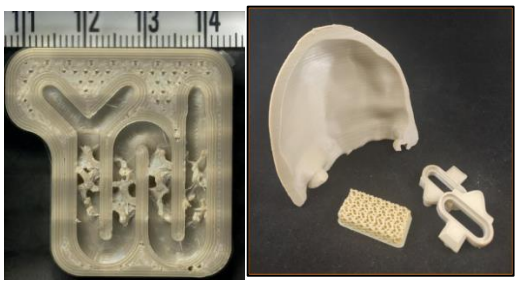

Figure 1 PEEK pharmaceutical reactor which incorporate mixers printed at 440ºC. This reactor design is used to help evaluate the geometric accuracy of the prints. The image on the right is photograph of a 3D printed cranial implant device demonstrator.

The research results to-date have demonstrated that a major factor influencing distortion is Z level calibration. The use of a heated aluminium bed exhibited superior performance to a glass bed, for print adhesion. Print head temperatures have been investigated in the range 425 to 450ºC, along with the use of both a 0.4 and 0.3 mm print nozzle. It was concluded that printing at 440ºC resulted in the highest quality part with respect to geometry and quality. The use of a 0.3 mm nozzle exhibited better print geometries on more complex parts, compared with those obtained with a 0.4 mm nozzle. The 0.3 mm nozzle is however more prone to clogging. Further research will investigate how print speed and filament flow rate influence the properties of the printed parts. In the case of the pharma reactor parts, these will be tested under high pressure processing conditions (up to 100 Bar).

References

[1] M. R. Senra *et al*, 'Poly (Ether-Ether-Ketone) for Biomedical Applications: From Enhancing Bioactivity to Reinforced-Bioactive Composites—An Overview', *Polymers*, vol. 15, no. 2, Art. no. 2, Jan. 2023.
[2] X. Ling *et al*, 'Polyether Ether Ketone (PEEK) Properties and Its Application Status', *IOP Conference Series: Earth and Environmental Science*, vol. 453, p. 012080, Apr. 2020
[3] 'Research on the Fused Deposition Modeling of Polyether Ether Ketone'. [Online]. Available: https://www.mdpi.com/2073-4360/13/14/2344
[4] 'Ultra 2 high-performance 3D printer', miniFactory. [Online]. Available: https://minifactory.fi/industrial-3d-printer/ultra-2/

POLYELECTROLYTE MULTILAYERS FOR BIO-SCAFFOLD APPLICATIONS- A FIRST LAYER INVESTIGATION

New, SG., McFerran, A., Acheson, JG, Chang, MW, Hamilton, JWJ. and Lemoine, P
Ulster University, Belfast
email: New-S1@ulster.ac.uk

INTRODUCTION

Bone tissue scaffolds coated with 'layer-by-layer' (LBL) assembly are an alternative treatment method for critical size bone defects. This process allows for control of coating thickness and stiffness, cell adhesion and optimised drug uptake and release [1,2]. Growth regimes can be linear or exponential depending on the strength of electrostatic (ES) interactions between the layers. Here, for the first time, we use solution-based and surface-based analytical techniques to investigate the relative contributions of hydro-phobic/philic interactions and ES interactions in the layer binding and in the cohesion of the multilayer system.

MATERIALS AND METHODS

All systems studied used the polyanion polyacrylic acid (PAA) and polycations polyethylenimine (PEI), poly(diallydimethylammonium chloride) (PDDA). In this investigation, the coatings were deposited onto doped-Si substrates. The 1 wt.% aqueous solutions were analysed by dynamics light scattering (DLS), electrophoretic spectroscopy (EPS) and optical tensiometry (OT). The dispersive and polar components of the surface tension was determined using the Owens-Wendt equation [3] using glass, doped Si and PDMS as surfaces with known surface energies. The surfaces were investigated by AFM microscopy in bimodal mode to map out the Young modulus of the coatings. In addition scanning Kelvin probe microscopy (SKPM) was also used to map out the surface charge distribution on the coatings.

RESULTS AND DISCUSSION

The zeta potentials measured by EPS for of the PEI, PAA and PDDA solutions were, respectively, +5.10 ±0.17 mV, -3.25 ±1.05 mV and +45.17 ±4.93 mV and were strongly influenced by the respective pH of the polyelectrolyte solutions, as expected. OT showed similar contact angles for the PEI and PAA solutions on doped silicon (θ_{PEI}=66 ±4°, θ_{PAA}=66 ±5°), suggesting similar affinity towards the surface for the three solutions. Figure 1a shows the dispersive and polar surface tension components when determined from contact angle on doped-Si and PDMS surfaces. It indicates very small dispersive components for the PEI and PAA solutions and hydrophilic affinities between the two solutions, confirming the contact angle measurements done for these two solutions.

PEI first layers were deposited with various dwell times and withdrawing speeds. For all conditions, the layer is mostly continuous with roughness values < 1 nm (fig.1b) and the first layer thickness is constant over the full sample length (8.5±0.7 nm) and does not vary appreciably with withdrawing speed (fig.2a).

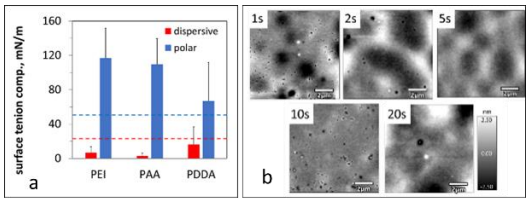

Figure 1 *a/ Surface tension components of the polyelectrolyte solutions. The dashed lines represent the DI water values. b/ AFM scans of PEI first layers, roughness values were similar for all dwell times; R_q=0.93±0.33 nm.*

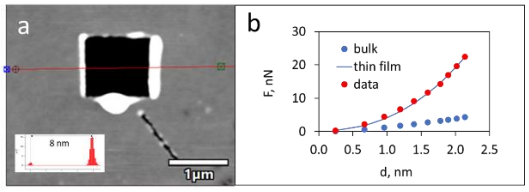

Figure 2 *AFM measurements on PEI first layer: a/ CAFM scratch image and b/ Thin film modelling of AFM force curve.*

Mechanical data on these first layers were also acquired using both traditional AFM force curves and biomodal AMFM imaging. High resolution FESEM imaging of the AFM tips permitted to use a Hertzian thin film model to take into account the substrate effect for these ultra low depth measurements (fig.2b). In addition the use of doped Si substrates permits more quantitative SKPM data to estimate surface charge density on these vey thin films. Overall, the study contributes to our understanding of the structure-property relationships of first layers and helps establish better strategies for developing multilayer coatings for bio-implant applications.

REFERENCES

1/McFerran *et al.*, Bioengineering 9: 585, 2022.
2/Acheson *et al.*, Surface & Coatings Technology 458: 129335, 2023.
3/Zhang, Col. Surf.A 676: 13223, 2023

CONTROLLED SYNTHESIS OF PLGA NANOPARTICLES IN MICROFLUIDIC CHIPS BY ANALYSING IMPACT OF MIXING PARAMETERS ON NANOPARTICLE PROPERTIES

Saeed, Muhammad Mubashar.[1], Dunne, Nicholas.[1], Carthy, Eadaoin.[1], Kinahan, David.[1]

[1] Dublin City University, Ireland
email: (David.kinahan@dcu.ie)

INTRODUCTION

Nanoparticles (NPs) have gained pivotal importance due to their very wide range of applications in modern biomedical research, particularly in drug delivery and diagnostics. This is because of NPs nanoscale properties that enhance therapeutic outcomes [1].
Poly(lactic-co-glycolic acid) (PLGA) nanoparticles have very special biodegradability and biocompatibility properties which make them highly suitable for sustained drug release and controlled delivery systems[2].
However, traditional methods for synthesizing PLGA NPs, such as emulsification, solvent evaporation, and nanoprecipitation, often lack precise control over NPs physical properties like size, polydispersity index (PDI), and surface charge. Having a better control over these properties can help in better in-vivo performance. Microfluidic synthesis provides a promising alternative to conventional approaches. It enables an enhanced control over particle characteristics by precisely manipulating mixing conditions within microchannels.

MATERIALS AND METHODS

In this study, investigation has been performed about the impact of varying mixing parameters in a microfluidic chip on the properties of PLGA NPs. Utilizing a 3 inlet hydrodynamic flow-focusing (HFF) setup, we introduce 15mg/ml solution of PLGA in acetonitrile through the central channel and 0.3% polyvinyl alcohol (PVA) solution in deionized (DI) water in side channels that provides the sheath flow (fig 1a). Initial flow visualization experiments with 5% solution of potassium thiocyanide (KSCN) and 5% solution of iron (III) chloride ($FeCl_3$) were conducted to evaluate mixing dynamics based on visible color change upon mixing, with mixing time analysed across various flow rates and flow rate ratios (fig 1b). Following flow visualization and python based image analysis to measure the complete mixing, we have synthesized PLGA NPs at these optimized conditions and assessed their properties using dynamic light scattering (DLS) and electron microscopy (SEM/TEM).

RESULTS

25 different flow conditions have been tested and analysed in this study for five different flow rate ratios. It has been found that different flow combinations gives the same mixing time. For example mixing time at 50ul/min : 5ul/min (sheath flow : central flow) has been found same as at 20ul/min : 1ul/min. PLGA NPs synthesized at these different flow conditions with similar mixing time also demonstrated the same properties.

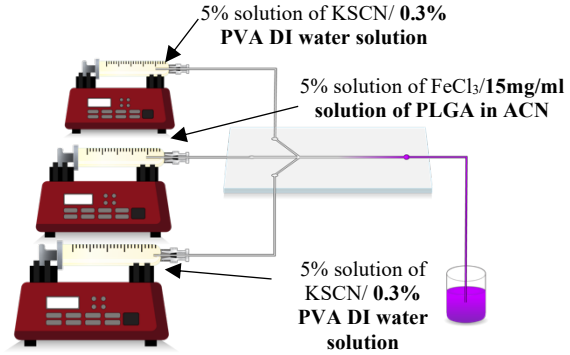

(a)

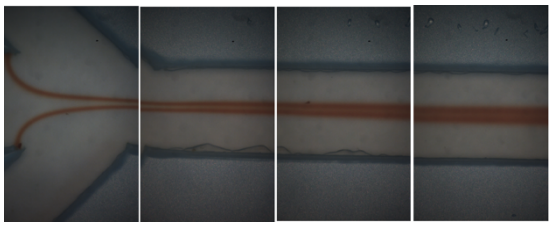

(b)

Figure 1 a) Microfluidic setup for mixing analysis/ **NPs synthesis** in the microchannel b) Sequential Imaging at 1mm Intervals along the microchannel.

DISCUSSION

Our results demonstrate that precise control over PLGA NPs properties can be achieved by tuning the flow rates and flow rate ratios in the microfluidic system. This study highlights the potential of microfluidic platforms for fine-tuning NP synthesis, paving the way for more controlled and scalable NPs production.

REFERENCES

1. Wilczewska, Agnieszka Z., et al. "Nanoparticles as drug delivery systems." *Pharmacological reports* 64.5 (2012): 1020-1037.
2. Narmani, Asghar, et al. "Biomedical applications of PLGA nanoparticles in nanomedicine: advances in drug delivery systems and cancer therapy." *Expert Opinion on Drug Delivery* 20.7 (2023): 937-954.

3D *IN VITRO* MODEL OF LUNG CANCER TO STUDY THE PRE METASTATIC NICHE IN LUNG CANCER

Almeida, V.[1, 2], O'Leary, C.[1, 2], Curtin, CM.[2, 3, 4]

[1]School of Pharmacy and Biomolecular Sciences, Royal College of Surgeons in Ireland, Dublin, Ireland. [2]Tissue Engineering Research Group, Dept. of Anatomy and Regenerative Medicine, Royal College of Surgeons in Ireland, Dublin, Ireland. [3]Trinity Centre for Biomedical Engineering (TCBE), Trinity College Dublin (TCD), Dublin, Ireland. [4]Advanced Materials and Bioengineering Research Centre (AMBER), RCSI and TCD, Dublin, Ireland.

INTRODUCTION

Lung cancer metastasis is the major cause of cancer-related death in the world (1). Alterations in the extracellular matrix are known to play a role in pre-metastatic niche formation (2). Unfortunately, current 2D models fail to accurately model the tumour microenvironment (3). This highlights the need for the development of a representative *in vitro* 3D model, in which to study pre-metastatic niche (PMN) formation and identify new treatment targets. This project aims to develop a 3D gelatin methacryloyl (GelMA) hydrogel co-culture model of lung cancer cells and cancer associated fibroblasts (CAFs), both highly expressed in lung tumours, in which to investigate the role of tumour microenvironment stiffness in PMN formation in lung cancer.

MATERIALS AND METHODS

GelMA hydrogel formulations with varying stiffness were fabricated using different concentrations of Lithium phenyl-2, 4, 6-trimethylbenzoylphosphinate (LAP) (non-cancerous (~5kPa), precancerous (~15kPa) and cancerous (~30kPa)) for 3D *in vitro* applications. Hydrogel properties were characterised using 1H NMR, degradation testing, rheology, permeability assays, pore analysis, and mechanical testing. A549 lung cancer and WI38 lung fibroblast cell lines were seeded at a density of 50,000 cells/well on GelMA hydrogels in monoculture and as co-cultures at a ratio of 1:2 (16,000 and 34,000 cells/well, respectively) for up to 7 days. Cell viability and proliferation were assessed with Live/Dead, AlamarBlue, dsDNA assays and immunofluorescence staining. Additionally, a cytokine array was performed to examine the impact of GelMA stiffness on cytokine expression when culturing A549 and WI38 cells in monoculture versus co-culture.

RESULTS

Alterations in the LAP concentration increased the stiffness of hydrogels in a concentration-dependent manner to mimic non-cancerous, pre-cancerous, and cancerous lung tissue properties, with values ranging from 5-30 kPa, thus covering the stiffness spectrum of non-cancerous (~5kPa), pre-cancerous (~15kPa), and cancerous (~30kPa) lung tissue. Stiffer hydrogels supported higher metabolic activity and faster proliferation of A549 and WI38 cells, indicating a correlation between hydrogel stiffness and cell behaviour. Increased stiffness, as observed in pre-cancerous group, led to heightened expression of cytokines, such as ENA-78, MCP-1, angiogenin, and IL-8 in A549 cells, while WI38 cells cultured on stiffer hydrogels significantly increased expression of IL-6, MCP-1, angiogenin, GRO, GRO-Alpha and IL-8 suggesting that ECM stiffness impacts the cytokine profile within the tumour microenvironment.

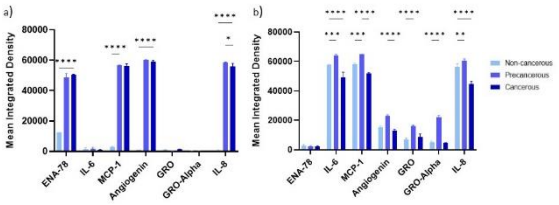

Figure 1 GelMA stiffness alters cytokine expression.. The increase in hydrogel stiffness significantly increased expression of ENA-78, MCP-1, angiogenin, and IL-8 in A549 cells in monoculture, while WI38 cells cultured on stiffer hydrogels significantly increased expression of IL-6, MCP-1, angiogenin, GRO, GRO-Alpha and IL-8. *P < 0.05, P** <0.01, P**** <0.0001, N=3 Hydrogels.

DISCUSSION

Gelatin-based hydrogels composed of varying ECM stiffness have been developed. Altering the mechanical stiffness of the gelatin-based hydrogels within a range that represents cancerous lung tissue is achievable. Each hydrogel supported lung cancer and fibroblast cell viability and proliferation.

The stiffness of hydrogels influenced the cytokine expression profiles of A549 and WI38 cells in monoculture, leading to increased production of cytokines that promote tumor growth, enhance angiogenesis, and facilitate immune evasion. This highlights the impact of extracellular matrix (ECM) composition on cancer progression, this finding will be further investigated in future studies. The gelatin-based hydrogels have the potential to mimic the ECM of lung tissue and have the capacity to be used as 3D models for lung cancer research.

REFERENCES

1. Siegel et al., Cancer Statistics, 2019
2. Steeg et. al., Nat Rev Cancer, 2016
3. O'Leary et.al, Elservier, 2019

MODULATION OF OSTEOCLASTOGENESIS BY MESENCHYMAL STROMAL CELL-DERIVED APOPTOTIC BODIES: A RANKL DEPENDENT ROLE IN MONOCYTE DIFFERENTIATION

Shen, Yeyu [1], Buckley, Fiona [1], Brennan, Meadhbh Á. [1, 2, 3]
[1] Regenerative Medicine Institute (REMEDI), School of Medicine, University of Galway.
[2] Biomedical Engineering, School of Engineering, University of Galway.
[3] Curam, School of Engineering, University of Galway
Email: meadhbh.brennan@universityofgalway.ie

INTRODUCTION

Human mesenchymal stromal cells (MSCs) die by apoptosis when transplanted with biomaterials in preclinical and clinical studies and initiate a bone regeneration cascade[1]. As a pivotal role in fracture healing, osteoclasts initiate bone healing by clearing necrotic tissue, promoting new bone formation, and facilitating bone remodelling[2], while excessively active osteoclasts can also impact the bone quality following fracture healing[3]. Interestingly, osteoclast presence has been shown to be a prerequisite for bone healing facilitated by transplanted MSCs[4]. The aim of this study was to investigate if apoptotic bodies derived from MSCs (MSC-ABs) impact bone regeneration by regulating monocyte-to-osteoclast differentiation.

MATERIALS AND METHODS

Apoptosis was induced in human bone marrow-derived MSCs by ultraviolet (UV) irradiation in EV-free media and verified by flow cytometry of apoptotic MSCs, scanning electron microscopy, and caspase 3 quantification. MSCs-ABs were isolated from conditioned media via differential centrifugation and characterized by total protein and RNA content, morphology, and surface marker expression by flow cytometry. MSC-ABs were treated onto human peripheral blood-derived CD14+ monocytes in an in vitro osteoclast differentiation protocol.

RESULTS

Results suggested that the MSCs-ABs have a pro-osteoclastic effect, assessed by tartrate-resistant acid phosphatase (TRAP, predominantly found in osteoclasts) staining (Figure 1.A&B) and also by measuring the phosphatase concentration assay in the culture supernatant (Figure 1.C). Conversely, MSCs-ABs had an inhibitory effect on osteoclast formation in the presence of the receptor activator of nuclear factor kappa-B ligand (RANK-L). Additionally, the enzyme-linked immunosorbent assay revealed that AB-treated cells secreted significantly higher levels of IL-6 and IL-10 (Data not shown), which are known to have a dual effect on osteoclastic differentiation.

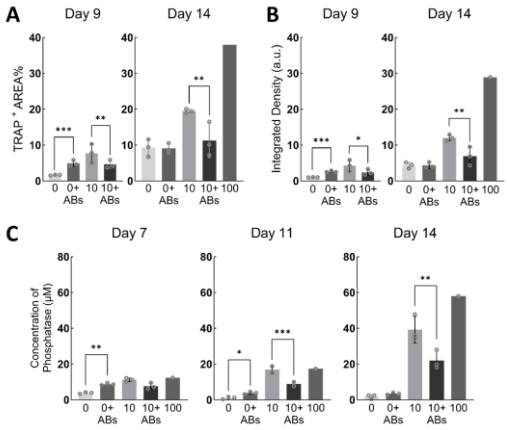

Figure 1 Human peripheral blood-derived CD14+ monocyte-to-osteoclast *in vitro* differentiation experiments. A. The area of $TRAP^+$ staining analyzed by ImageJ. B. The integrated density of $TRAP^+$ analyzed by ImageJ. C. The secreting phosphatase in the monocyte/osteoclast culture supernatant. "0, 10, or 100" = the concentration of treated RANK-L (ng/mL), "ABs" = Apoptotic Bodies. Statistical analysis was performed using Graphpad Prism software, the significance of differences between groups was assessed by one-way ANOVA. "*" = $P < 0.05$, "**" = $P < 0.01$, "***" = $P < 0.001$, a p-value less than 0.05 was considered statistically significant.

DISCUSSION

To understand these findings, we are currently sequencing the RNA of the MSC-ABs, then polymerase chain reaction and western blotting could be used for verifying underlying mechanisms. This study may contribute to clarifying the currently ambiguous mechanisms by which MSC-ABs regulate osteoclast differentiation and promote bone regeneration, which may provide a promising therapeutic bone regeneration strategy.

REFERENCES

1. Galleu et al., Sci. Transl. Med. 9, eaam7828 (2017);
2. Humbert et al., Front. Immunol., Volume 10 (2019);
3. Takehito et al., Histochemistry and Cell Biology 149:325–341 (2018);
4. Humbert et al., Acta Biomaterialia, 176: 417–431 (2024).

THE ENGINEERING OF OSTEOCHONDRAL GRAFTS BY SPATIALLY PATTERNING GROWTH FACTORS INTO BATHS OF RADIALLY CONFINED MICROTISSUES

Giordano, T.[1], Kronemberger, GS.[1] Kelly, DJ.[1]
[1] Trinity College Dublin, Department of Mechanical and Manufacturing Engineering, Dublin, Ireland
email: giordant@tcd.ie

INTRODUCTION

Diseases stemming from damage of articular cartilage (AC) in joints, such as osteoarthritis, are causes of significant socioeconomic burden and impairment of patient's quality of life[1]. As global life expectancy rises, the number of people affected by this disease is projected to increase[2]. Due in part to its avascular nature, AC has a limited regenerative capacity. Thus, early detection of AC and osteochondral defects and their subsequent treatment are urgently needed. Such treatments include allogeneic osteochondral grafts and autografts, however these are subjected to numerous drawbacks including limits in supply, transmission of diseases or donor site morbidity[3]. To tackle this challenge, tissue engineering (TE) approaches—encompassing the use of cells, scaffolds, and biochemical cues—aim to engineer functional cartilage and osteochondral grafts to overcome these limitations.

In recent years there has been increased interested in the use of cellular spheroids, microtissues or organoids as biological building blocks for bottom-up tissue engineering strategies. This method harnesses the ability of stem or progenitor cells to form spherical aggregates involving high cell-cell interactions. This has been shown as being similar to stem cell condensation during cartilage morphogenesis[4]. As a result, constructs made by the fusion and self-organization of so-called cartilage microtissues (µTs) can have a structure and biomechanical properties similar to AC[5]. This can be facilitated by using physical boundaries, such as radially confining wells, to effectively shape AC-like structures[6].

There are a number of challenges associated with the use of such µTs for tissue engineering applications. They are inherently cell-dense, hence nutrient transport can be limited to central regions of the graft, necessitating the use of printed channels or engineered vasculature networks to maintain cell viability[7]. Spatial regulation of cellular differentiation, which is integral to the engineering of interfaces such as the osteochondral unit, is also challenging.

The overall goal of this study is to engineer osteochondral grafts by spatially pattering a homogenous population of mesenchymal stem/stromal cell (MSC) derived µTs with regulatory factors to promote either a stable hyaline cartilage phenotype or an endochondral bone forming phenotype. To this end 3D bioprinting will be used to spatially pattern a bath consisting of µTs and microgels (µGs) with regulatory factors.

MATERIALS AND METHODS

Alginate µGs will be synthesized using methods such as electro spraying, grinding, or water-in oil emulsions. The resulting size distribution and morphology will be assessed using confocal microscopy.

Bone marrow caprine MSCs derived µTs will be fabricated using an in-house medium-high throughput system and be cultured for up to 2 days in chondrogenic induced medium[8]. Both µGs and µTs will be mixed and placed into radially confining agarose wells. Such constructs will be cultured 6 weeks in chondrogenic induced medium to promote tissue formation. The influence of µT:µG volume ratio, µG morphology, size and degradation will be explored. Constructs will then be harvested and their structure, composition and mechanical properties will be assessed. Histological staining, immunochemistry and biochemical assays will be used to identify the presence of collagen types I and II, Glycosaminoglycan and DNA content, respectively. Mechanical properties will be assessed with unconfined compression and biaxial tests.

In the final phase of the project, 3D bioprinting will be used to spatially pattern factors promoting a stable cartilage phenotype into one side of the construct, and factors promoting endochondral bone formation into the opposite side of the construct.

CONCLUSION

By optimizing the biofabrication process, this work aims to address critical challenges in nutrient diffusion and structural stability, potentially leading to more effective and scalable solutions for cartilage repair.

REFERENCES

[1] Briggs *(et al.), Bulletin of the WHO* vol. 96,5 (2018)
[2] Hay *(et al.), Lancet* vol. 390,10100 (2017)
[3] Andrade *(et al.), J EXP ORTOP* **3**, 31 (2016)
[4] Ofek *(et al.), PLoS ONE* 3(7) (2008)
[5] Hu *(et al.), Tissue Eng.* 12, 969–979 (2006)
[6] Burdis *(et al.) Adv. healthcare mat.* vol. 13,3 (2024)
[7] Skylar-Scott *(et al.), Sci. Adv.* **5** (2019)
[8] Nulty *(et al.), Frontiers in bioeng. & biotech.* vol. 9 661989. (2021)

MACROMOLECULAR CROWDING AND HUMAN PLATELET LYSATE REGULATE *IN VITRO* COLLAGEN DEPOSITION FOR THE DEVELOPMENT OF TENDON TISSUE SUBSTIITUTES

Rossoni, A.[1], Zeugolis, DI.[1]

[1] Regenerative, Modular & Developmental Engineering Laboratory (REMODEL), Charles Institute of Dermatology, Conway Institute of Biomolecular & Biomedical Research and School of Mechanical & Materials Engineering, University College Dublin (UCD), Dublin, Ireland

email: andrea.rossoni@ucdconnect.ie

INTRODUCTION

Tendon injuries constitute a significant portion of musculoskeletal diseases, posing a heavy burden on healthcare and reducing patients' quality of life. Current treatments fall short of fully restoring tendon function, and with the aging population, these issues are expected to rise. Tissue-engineered therapies using autologous tendon cells offer a promising solution for tendon healing; however, they are not commercially available due to the long culture time required to obtain sufficient tendon extracellular matrix (ECM) for implantation and due to the rapid loss of phenotype of human tenocytes (hTCs) during in vitro culture. To tackle this limitation, a promising solution resides in macromolecular crowding (MMC), a simple and cost-effective tool that dramatically increases the deposition rate of novel ECM by the cells through the excluded volume effect principle. This work explores how different MMC agents affects the deposition of tendon ECM by human tendon cells (hTCs). In addition, this work tackles the challenge of substituting xenogeneic cell culture media supplements such as foetal bovine serum (FBS) with an allogeneic substitute like human platelet lysate (hPL) for hTCs culture to eliminate the ethical concerns and regulatory limitations linked to the use of FBS for the development of ATMPs.

MATERIALS AND METHODS

First, a panel of MMC agents was screened to assess their ability to increase the deposition of collagen type I (COL I) by hTCs in vitro using SDS-PAGE and immunocytochemistry (ICC). Then, the MMC agents that induced maximum COL I deposition were to culture hTCs isolated and expanded using typical cell culture media supplemented with FBS or with hPL. COL I deposition was assessed using SDS-PAGE and ICC, whereas cell proliferation, metabolic activity and viability were assessed, namely, by nuclei counting, AlamarBlue® assay and LIVE/DEAD™ assay.

RESULTS

The MMC agents screening showed that two different types of carrageenan (CR), namely κλ CR and λ CR, induced the highest COL I deposition compared to the other MMC agents (up to 70 times higher compared to the non-crowded control by SDS-PAGE densitometry). Moreover, κλ CR increased COL I deposition in hTCs cultured either with FBS or hPL (up to 50 times higher compared to non-crowded control for both groups) (Figure 1). Notably, hPL dramatically increased cell proliferation (up to 5 times compared to FBS) and metabolic activity (1.7 times higher compared to FBS).

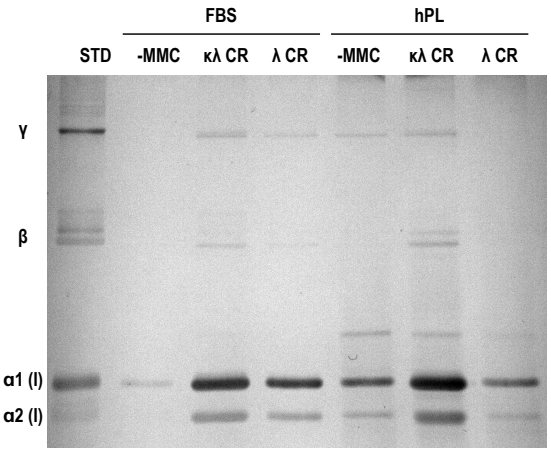

Figure 1 SDS-PAGE of COL I deposited by hTCs cultured either with FBS or hPL using different MMC agents.

DISCUSSION

This work demonstrates the efficacy of MMC combined with allogeneic media supplements to enhance the deposition of tendon ECM in vitro from hTCs. In particular, hTCs supplemented with hPL induce the highest COL I deposition amount when treated with κλ CR. In addition, hTCs cultured with hPL dramatically promotes cells metabolic activity and proliferation compared to FBS, thus making hPL a promising allogeneic cell culture supplement capable of decreasing cell culture times and, at the same time, eliminating the use of xenogeneic media supplements for the development of ATMPs for tendon repair and regeneration.

REFERENCES

Rampin A *et al.*, Eur J Cell Biol. 103(3):151445, 2024.

Tsiapalis D *et al.*, Biomater Biosyst. 30;1:100009, 2021.

3D HUMAN SPHEROIDS MODELS OF ADIPOSE TISSUE FOR IMPROVING WOUND HEALING

Sander, E., Ankrum, J.
[1] Roy J. Carver Department of Biomedical Engineering, University of Iowa, Iowa City, Iowa
email: edward-sander@uiowa.edu

INTRODUCTION

Adipose tissues are composed of a continuum of adipocyte lineage cells, including adipocyte-derived stem cells (ADSCs), preadipocytes, and adipocytes, each of which play important roles in regulating extracellular matrix (ECM) remodelling either directly or through interactions with fibroblasts[1]. These interactions are important to understand in the contexts of wound healing. Using our spheroid model systems, we have found that human adipocyte spheroids secrete factors that convert fibroblasts to myofibroblasts independent of TGF-β1[2,3] and that the secretion profile of adipocytes and pre-adipocytes differs considerably[4], as does the composition of ECM proteins they produce[5]. More recently, we have begun exploring the temporal changes in ECM production that occur in these spheroid systems as they mature and how these matrix profiles are altered by the communication that occurs in co-cultures.

MATERIALS AND METHODS

Immortalized human dermal fibroblasts (HDFs), preadipocytes (NPADs), and adipocytes (ADs) were formed into homotypic 3D spheroids. Medium from these spheroids were analysed for secreted factors and ECM proteins via an adipokine panel and mass spectrometry. Heterotypic 3D spheroids consisting of different ratios of HDFs, NPADs, and ADs were further characterized via time-lapse imaging and proteomics to assess changes in morphology, cell distribution, and ECM content.

RESULTS

Major differences in the secretion profile and ECM content were found among the spheroids. ADs produced significantly higher levels of adiponectin, adipsin, RBP4, and IFN-γ than NPADs ($p<0.0001$) (Fig. 1A). NPADs secreted higher levels of IL-8 and IL-6 than ADs, though not significantly different. Analysis of the matrisome produced by homotypic spheroids revealed significant differences in the composition of the ECM, including the amounts and distributions of collagens (Fig 1B). Eight collagens were identified via label free quantification (LFQ), with the most prevalent collagens being either type I or type VI collagen (Fig. 1B). Comparisons between homotypic HDF and NPAD spheroids with heterotypic 50:50 HDF:NPAD spheroids revealed that interactions between NPADs and HDFs impacted spheroid (Fig.1C) and lipid droplet size (Fig.1D).

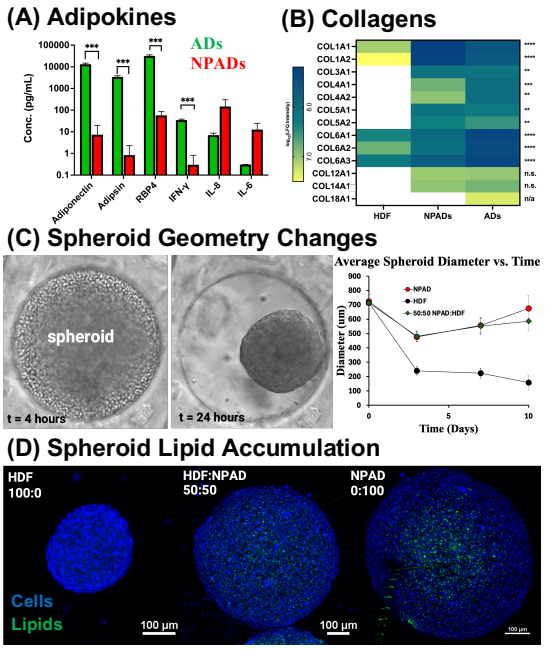

Figure 1 Characterization of spheroid properties.

DISCUSSION

Cell spheroids mimic aspects of native tissue function and facilitate manipulation, visualization, and quantification of cell-cell and cell-matrix interactions that coincide with remodelling events, such as those that occur during wound healing. Current efforts are now focused on quantifying how differences in ECM composition relate to mechanical properties. Such data will help us develop adipose-tissue based therapeutic strategies to improve healing.

REFERENCES

[1] Schmidt *et al.*, Development, 140:1517, 2013.
[2] El-Hattab *et al.*, Sci. Reports, 10:10286, 2020.
[3] El-Hattab et al. R. Soc. Interface, 20:20230004, 2023.
[4] Liszewksi et al. Adipocyte, 13: 2347215, 2024.
[5] Sander *et al.*, Cell. Mol. Bioeng., 10:10286, 2024.

ACKNOWLEDGEMENTS
National Institutes of Health, NIGMS R01GM145626, NIEHS P42 ES013661

A 4D BIOPRINTING PLATFORM TO ENGINEER ANISOTROPIC MUSCULOSKELETAL TISSUES BY SPATIALLY PATTERNING MICROTISSUES INTO TEMPORALLY ADAPTING SUPPORT BATHS

Spagnuolo, F.D[1], Kronemberger G.[1], Kelly D.J[1]
[1]Department of Mechanical, Manufacturing and Biomedical Engineering, Trinity College Dublin
email: spagnuof@tcd.ie

INTRODUCTION

The function of musculoskeletal tissues is tightly linked to the specialized architecture of their extracellular matrix (ECM) (1). Damage to such tissues (e.g. cartilage, meniscus, ligament) often leads to the development of osteoarthritis. Traditional tissue engineering (TE) strategies to treat damaged musculoskeletal tissues typically involve seeding cells into 3D scaffolds, but limitations with such approaches have spurred increased interest in scaffold-free TE strategies, which leverage the capacity of stem or progenitor cells to self-organise in response to external stimuli. Mesenchymal stem/stromal cells (MSCs) can be used to generate microtissues (µTs), which can potentially be used as scaffold-free biological building blocks for the fabrication of functional grafts. Recognising that stem cells not only respond to gradients in growth factors (2), but also external factors like substrate stiffness (3), the goal of this study was to provide precise physical boundaries to MSC-derived µTs to engineer constructs with user-defined shapes, structures, and functions. Specifically, we sought to guide bioprinted µTs to self-organize and differentiate within a temporally adapting support bath, thereby enabling the creation of anisotropic musculoskeletal tissues with highly aligned collagen fibers.

MATERIALS AND METHODS

The µTs (2,000 cells/ µTs) were encapsulated into a 1% gelatin bioink and bioprinted at a density of 45,000 µTs /mL into different concentrations of a methacrylate xanthan gum (XG-MA) support bath, using a pneumatic printhead. 3 weeks post printing and culture in media supplemented with transforming growth factor beta 3, tissue differentiation was assessed by histology, immunohistochemistry, polarised light microscopy, SEM imaging and RT-qPCR.

RESULTS

The density of 45,000 µT/mL of bioink enabled the bioprinting of continuous filaments of living tissue. By varying the concentration of XG-MA in the support bath, it was possible to temporally modulate the printed filament diameter, with smaller diameters observed for larger XG-MA concentrations. As expected, bath stiffness also increased with XG-MA concentration, from 20 kPa for 0.25% XG-MA to 70 kPa for 2% XG-MA. We then bioprinted µTs into XG-MA baths of varying concentrations (0.25%, 0.5%, 1%, 2%) and cultured them for 3 weeks. Increasing the bath stiffness led to increased collagen I (Col I) deposition, decreased collagen II (Col II) deposition, elevated alpha-smooth muscle actin (α-SMA) and greater collagen fiber alignment in the print direction (Figure 1). Increasing bath stiffness resulted in a decrease in the expression of chondrogenic markers (COL2, COMP, CHAD) and an increase in the expression of fibrocartilage/tendon-specific markers (COL1, ACTA2, TNC). Building on these findings, we developed support baths for specific tissues (e.g., 1% XG-MA bath for meniscus tissue) and demonstrated the utility of the platform by bioprinting structurally organized articular cartilage, meniscus, and ligament tissues.

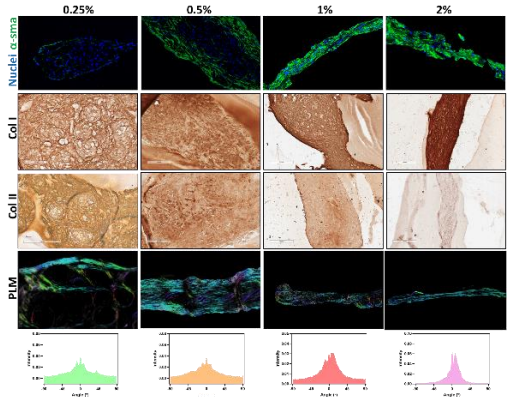

Figure 1. The stiffness of the bath influences the long-term tissue development and alignment of the collagen fiber of bioprinted microtissues.

DISCUSSION

In this study we used extrusion bioprinting to spatially deposit large numbers of immature µTs into support baths with distinct rheological and mechanical properties. The physical properties of the support bath not only modulated print fidelity, but also directed the differentiation of bioprinted µTs towards distinct tissue phenotypes and enabled the engineering of structurally anisotropic musculoskeletal tissues. Greater collagen fiber alignment (parallel to the print direction) was observed with higher bath stiffness, making stiffer baths ideal for producing anisotropic tissues with highly aligned collagen fibers. We also demonstrated that it is possible to scale up the fabrication of highly aligned musculoskeletal tissues while preserving the specific phenotype required for each engineered tissue.

REFERENCES

(1) Cunniffe *et al*, Biomaterials: 188, 63-73, 2019.
(2) Norotte *et al*., Nature Biomedical Engineering: 1, 939-956, 2017.
(3) Park *et al*, Biomaterials: 32 (16), 3921-3930.

ELUCIDATING THE IMPACT OF MACROMOLECULAR CROWDING AGENT CHEMISTRY ON MESENCHYMAL STROMAL CELL RESPONSE

Giuffredi, G.[1], **Zevgolis, D.**[1,2]
[1] REMODEL, Conway Institute and School of Mechanical & Materials Engineering, University College Dublin (UCD), Dublin, Ireland
[2] Science Foundation Ireland (SFI) Centre for Research in Medical Devices (CÚRAM), Biomedical Sciences Building, National University of Ireland Galway (NUI Galway), Galway, Ireland
email: dimitrios.zevgolis@ucd.ie

INTRODUCTION

Tissue engineered medicines require prolonged *ex vivo* cultures to develop implantable micro-tissues. This is due to the diluted conditions of traditional eukaryotic cell culture, where the enzymatic conversion of procollagen into collagen occurs slowly [1, 2]. Macromolecular crowding (MMC), a biophysical process rooted in the excluded-volume effect, reduces molecular diffusion and increases protein interaction and enzymatic processes [3, 4], resulting in increased and accelerated extracellular matrix (ECM) deposition during *in vitro* cultures [5, 6]. Despite its extensive use in eukaryotic cell culture, the optimal MMC agents for enhanced ECM deposition in hBM-MSC is still elusive. Further, it is still unclear how different MMC agents affect hBM-MSC lineage commitment and fate.

MATERIALS AND METHODS

hBM-MSCs from three donors were cultured without and with different MMC agents (carrageenan (CR), a sulphated polysaccharide, Ficoll™ (FC), a non-sulphated polysaccharide and polyacrylic acid (PAA), a synthetic macromolecule). Analyses at different timepoints (5, 8 and 11 days) included assessment of cell morphology, viability, proliferation and metabolic activity; collagen type I deposition via SDS-PAGE; immunofluorescence for collagen types I, III, IV and V. Cell fate was assessed via tri-lineage analysis, mass spectrometry and RNA-seq.

RESULTS

Basic cellular function analyses indicated the safety of all MMC agents in hBM-MSC cultures. SDS-PAGE revealed that CR induced the highest collagen type I deposition. Immunofluorescence analysis showed that in comparison to the no MMC group, CR significantly increased collagen types I, IV and V deposition, FC significantly increased collagen type IV deposition and PAA significantly increased collagen type V deposition. Mass spectrometry revealed that all MMC agents affected translation pathways; CR influenced cell-matrix adhesion; FC influenced ECM remodelling and immune system and PAA influenced ECM regulation. RNA-seq analysis showed that all MMC groups affected, among others, ECM regulation, organisation and remodelling pathways. Tri-lineage differentiation analysis is currently in progress.

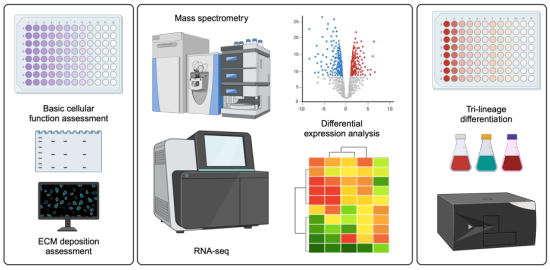

Figure 1 Study graphical abstract

DISCUSSION

This work clearly illustrates a MMC agent dependent cell response and argues that the chemistry of the MMC agent should be considered in the developmental cycle of an advanced therapy medicinal product that is manufactured under MMC conditions.

REFERENCES

[1] B. Goldberg, C.J. Sherr, Secretion and extracellular processing of procollagen by cultured human fibroblasts, Proc Natl Acad Sci U S A 70(2) 361-365 (1973).
[2] H.F. Limeback, J. Sodek, Procollagen synthesis and processing in periodontal ligament in vivo and in vitro. A comparative study using slab-gel fluorography, Eur J Biochem 100(2) 541-550 (1979).
[3] R.J. Ellis, Macromolecular crowding: Obvious but underappreciated, Trends Biochem Sci 26(10) 597-604 (2001).
[4] A.P. Minton, Influence of macromolecular crowding upon the stability and state of association of proteins: Predictions and observations, J Pharm Sci 94(8) 1668-1675 (2005).
[5] P. Kumar, *et al*., Macromolecularly crowded in vitro microenvironments accelerate the production of extracellular matrix-rich supramolecular assemblies, Sci Rep 5 (2015) 8729.
[6] A. Satyam, *et al*., Macromolecular crowding meets tissue engineering by self-assembly: A paradigm shift in regenerative medicine, Adv Mater 26(19) 3024-3034 2014).

EFFECT OF MECHANICAL STIMULATION ON OSTEOGENIC CAPABILITY OF PRE-OSTEOBLASTS ON A BIOMIMETIC BONE SUBSTITUTES FOR REPAIR

Jaiswal, S.[1], Redmond, J.[1], Agarwal, S.[1], Tzagiollari, A.[2], Insley, G.[3] Levingstone, T.J.[1], Dunne, N.[1]
[1] School of Mechanical and Manufacturing Engineering, Dublin City University, Dublin, Ireland.
[2]Biomimetic Innovations Ltd (affiliate of PBC Biomed), Limerick, Clare, Ireland. [3]PBC Biomed, Accelerating Medical Innovation, Limerick, Clare, Ireland
email: nicholas.dunne@dcu.ie

INTRODUCTION

The human musculoskeletal system supports the body, permits movement, and shields important organs while undergoing repeated compression and tension-loading cycles in daily activities [1]. Thus, it is crucial to examine biophysical aspects when assessing *in vitro* cell behaviour of bone substitute materials underdevelopment. Mechanical cues are known to tailor the osteoblast cells' potential towards osteogenic differentiation via mechanotransduction mechanisms [2]. A novel bone adhesive (i.e., OsStic), combining phosphoserine-modified alpha-tricalcium phosphate (α-TCP), has been developed as a promising option that supports bone healing by binding damaged bone together following bone fracture [3]. This study investigates the effect of mechanotransduction on the proliferation and differentiation of preosteoblast MC3T3-E1 cells seeded on OsStic. In addition, the OsStic material was compared with α-TCP and commercially available Hydroset™ under static and dynamic conditions.

MATERIALS AND METHODS

Disc-shaped samples (Ø12 mm and 2 mm thickness) of OsStic, α-TCP and Hydroset™ were prepared using a silicon mould. The previously optimised composition of phosphoserine, α-TCP and $CaSiO_3$ was used for the OsStic samples [3]. All samples were preconditioned in Ringer's solution and α-MEM medium for 72 and 48 hours, respectively. After preconditioning, the samples were seeded with preosteoblast MC3T3-E1 cells at a seeding density of $5x10^4$ cells/cm^2. In static culture condition, cell seeded samples were incubated at 37°C in CO_2, while, in case of dynamic culture, mechanical stimulation was applied using the MechanoCulture TX compression bioreactor (CellScale, Canada) at a constant strain of 3% and frequency of either 0.5, 1, or 1.5 Hz. Samples were subjected to cyclic uniaxial compression for 40 mins/day for up to 21 days, and the proliferation and biomineralisation response was compared to samples exposed to static culture conditions. Cell proliferation was assessed using the colourimetric alamarBlue™ assay. Alizarin red staining determined the biomineralisation potential. Cell morphology on the sample surface was observed using SEM at various frequencies after 7 days of static and dynamic culture.

RESULTS

Sustained cell proliferation on the surface of the OsStic was observed for up to 28 days (Figure 1(a)) when subjected to either the static or dynamic culture condition regimen. The application of mechanical stimulus did not negatively affect cell proliferation in any sample groups. Further, the cell proliferation rate was observed to be comparatively higher at the frequency of 1 Hz. SEM analysis demonstrated the successful attachment and proliferation of cells onto the OsStic material, with the formation of a complete confluent cell sheet observed by Day 7, irrespective of the culture conditions (Figure 1(b-c)). However, better adherence of the cell layer was observed on the substrate surface when subjected to mechanical stimulation. A higher level of biomineralisation was observed on the OsStic substrate compared to α-TCP and the proprietary bone substitute material (HydroSet™), irrespective of the application of mechanical stimulation (at 1 Hz) during cell culturing (Figure 1(d-e)).

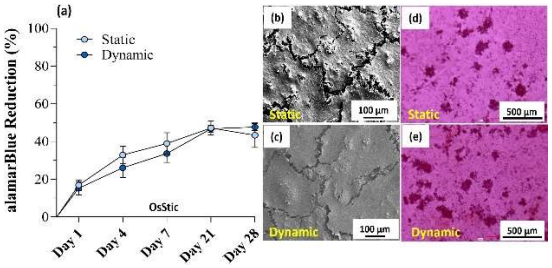

Figure 1 (a) Cell proliferation activity (at 0.5 Hz), (b-c) SEM morphological analysis of OsStic surfaces after 7 days of cell culture (at 0.5 Hz) (d-e) Alizarin red staining on OsStic surface for static and dynamic conditions (1 Hz) at Day 7.

DISCUSSION

The alamarBlue reduction study demonstrated a sustained cell proliferation on OsStic, α-TCP and Hydroset™ materials in both static and dynamic conditions. Application of various loading frequencies did not affect the cell proliferation negatively in any group of samples. Moreover, the rate of cell proliferation was increased with the loading frequency of 1 Hz. A fully confluent cell layer was observed for both static and dynamic conditions after 7 days, highlighting the biocompatibility of the OsStic material. An increasing trend of biomineralisation, which is crucial for bone repair, on OsStic surfaces was observed after 21 days of mechanical stimulation. Initial results highlight the promising use of a mechanical stimulation device in understanding the complex role mechanotransduction has on cell differentiation and osteogenic capability in bone repair and regeneration.

REFERENCES

[1] Zhang *et al.*, Adv. Mater 34, 2110267, 2022, [2] Aragona *et al.* Cell, 154, 1047, 2013 [3] Tzagiollari *et al.*, Acta Biomater, 174, 447-462, 2024

MACROMOLECULAR CROWDING INCREASES EXTRACELLULAR MATRIX DEPOSITION BY MODULATING *IN VITRO* COLLAGEN BIOPROCESSING

Trujillo Cubillo, L., Zeugolis, D.
Regenerative, Modular & Developmental Engineering Laboratory (REMODEL), Charles Institute of Dermatology, Conway Institute of Biomolecular & Biomedical Research and School of Mechanical & Materials Engineering, University College Dublin (UCD), Dublin, Ireland
email: laura.trujillocubillo@ucdconnect.ie

INTRODUCTION

Macromolecular crowding (MMC) is a biophysical phenomenon that decreases molecular diffusion and increases protein-protein binding and enzymatic activities, among others (**Figure 1**) [1]. By incorporating MMC into the development of tissue engineered medicines, we recapitulate *in vitro* the *in vivo* crowded microenvironments [2], where biological processes occur rapidly. MMC has been shown to increase extracellular matrix (ECM) deposition [3-4] and carrageenan (CR) has been shown to outperform all other MMC agents, with respect to highest ECM deposition in the shortest period of time [5], allowing cells to engineer their own matrix. Nonetheless, the effect of different CR subtypes, and the impact of MMC on collagen bioprocessing and turnover mechanisms remained to be studied in detail.

MATERIALS AND METHODS

Human dermal fibroblasts (hDFs) were seeded at a concentration of 25000 cells/cm^2, and six different CR molecules in 10 different concentrations were screened to identify the optimal MMC agent in terms of collagen deposition via SDS-PAGE and immunocytochemistry (ICC) with no impact on cell morphology, viability assessed by LIVE/DEAD ™ or metabolic activity assessed by alamarBlue® after 4, 6 and 8 days of culture. The impact of the optimal MMC agent on collagen bioprocessing was assessed with ELISA for procollagen C-proteinase (PCP) and procollagen I C-propeptide (PICP) on cell sheets and culture media. The extent of collagen crosslinking by lysyl oxidase (LOX) and transglutaminase (TG) activity was evaluated with a colorimetric assay and ICC respectively. ECM turnover was evaluated using an antibody array for matrix metalloproteinases (MMPs). Further effect of MMC on cell-cell and cell-ECM interaction was determined by immunostaining for integrin beta and connexin 43.

RESULTS

Supplementation with 50 µg/ml λ-CR showed the highest collagen I deposition, with a 4.8 fold increase with respect to -MMC at day 8, while collagen III, associated with fibrotic tissues, cell morphology, viability and metabolism were comparable with -MMC. Supplementation with CR significantly increased levels of PICP in cell sheets and cell culture media while PCP levels on the cell culture media were significantly higher for -MMC, showing that MMC increases ECM deposition by promoting collagen processing *in vitro*. LOX and TG activities were significantly higher in cell sheets cultured under MMC, accounting for the crosslinking and maturation of collagen fibrils. MMPs quantification showed increased ECM under MMC. Finally, MMC led to increased expression of integrin beta accounting for increased cell-ECM interaction.

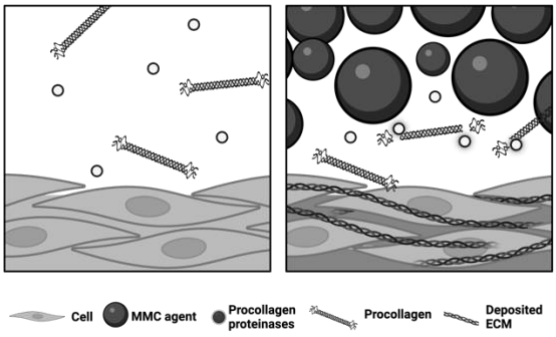

Figure 1 MMC promotes the interaction of procollagen and proteinases upon secretion, favoring PICP cleavage by PCP and resulting in an accelerated deposition of collagen fibers.

DISCUSSION

It has been suggested that MMC increases collagen deposition by decreasing the diffusion rates of procollagen and proteinases, impacting their enzymatic reaction rates [6]. We showed that cells cultured under MMC resulted in an increased collagen I deposition and presence of PICP while presenting lower PCP indicating a more efficient collagen bioprocessing under MMC. Additionally, collagen deposited under MMC conditions showed higher extent of crosslinking compared to -MMC. This further demonstrates the mechanisms behind MMC and its potential to efficiently recreate biological processes *in vitro*, resulting in more biologically relevant environments.

REFERENCES

[1]Djalali-Cuevas (*et al.*), Mater Today Bio 25:100977, 2024.
[2]Tsiapalis (*et al.*), Biomaterials 275:120943, 2021.
[3]Garnica-Galvez (*et al.*), Acta Biomat 15:111, 2023.
[4]Shierly (*et al.*), Front Bioeng Biotechnol 11:1091157, 2023.
[5]Du (*et al.*), Int J Biol Macromol 251:126353, 2023.
[6]Kumar (*et al.*), Sci Rep 5(1):8729, 2015.

EMBEDDED BIOPRINTING OF PLURIPOTENT STEM CELLS IN GRANULAR SUPPORT HYDROGELS

Ventura i Blanco, L.[1,2], Daly, A.[1,2]
[1] Biomedical Engineering, University of Galway, Galway, Ireland
[2] CÚRAM, SFI Research Centre for Medical Devices University of Galway, Galway, Ireland
email: l.ventura1@universityofgalway.ie

INTRODUCTION

Organ bioprinting holds great promise for regenerative medicine, with pluripotent stem cells (PSCs) serving as ideal building blocks due to their capacity to differentiate into any cell type. However, creating bioinks that maintain PSC viability and promote their proliferation after printing remains a significant hurdle. For example, traditional PSC culture matrices like matrigel, while optimised for promoting cell growth, lack the viscosity and shear-thinning properties required for extrusion bioprinting. Embedded bioprinting, where the bioink is extruded into a shear-thinning and self-healing granular support bath, is one strategy to overcome this. Due to the modularity of granular hydrogels, they can be used to spatiotemporally control the release of growth factors and morphogens in a 3D space. Such properties hold great potential for 4D bioprinting applications[1]. The objective of this work was to develop granular support hydrogels for embedded bioprinting of Matrigel bioinks containing PSCs. We aimed to explore how the embedded printing process could influence print quality and PSC viability.

MATERIALS AND METHODS

To generate the granular support hydrogels for embedded bioprinting, we modified the carboxylic acid group of the hyaluronic acid (HA) with norbornene groups (Nor) from 5-norbornene-2methylamine to synthesize NorHA[2] and NMR was used to verify this. 2wt% NorHA gels were fabricated using LAP, 0.1mM DTT, and photocrosslinked with LED 405 nm light for 5min at 5W/cm^2 (Fig 1A). These gels were mechanically fragmented to generate granular hydrogels (Fig 1A). The rheological test performed was amplitude sweep with 1Hz frequency and shear strain from 0.1% to 250%. The bioink consists of Matrigel and E8 media in a ratio of 1:4. BioFrame, a custom build printer, was used for embedded bioprinting keeping the ink at 4°C with the Puredyne cool head system and using the Puredyne extrusion pump with a 25G blunt needle (Fig 1D i).

RESULTS

NMR was used to determine the modification percentage of HA with Norbornene groups which was 45 ± 5% (Fig 1B). The fabrication of NorHA microgels was achieved and they were jammed together to form granular hydrogels (Fig 1B). The storage (G') and loss (G'') modulus of these gels increased when fragmenting the gels at high speed (20000rpm) (Fig 1C).
We successfully printed rectangles of 10x5x3 mm (15 layers) using the NorHA granular hydrogels as support bath (Fig 1D). The ink did not diffuse through the support bath and maintained the printed structure, demonstrating that NorHA granular hydrogels can be used as a support bath. Matrigel bioinks sustain PSCs viability and pluripotency in 4 days culture. Better results were obtained when using bioinks with low concentration of Matrigel (data not shown).

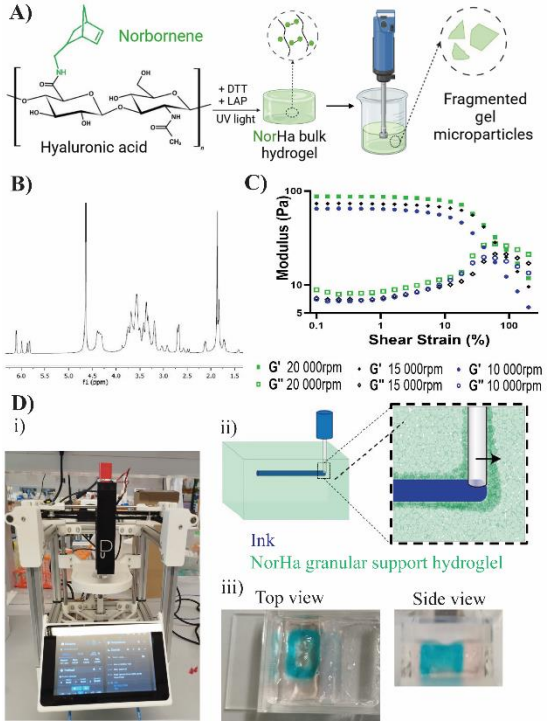

Figure 1 (A) NorHA granular hydrogels manufacturing process, (B) NMR spectra, (C) Storage (G') and Loss (G'') Modulus of different fragmentation speeds, (D) Embedded bioprinting with NorHA support bath, i) BioFrame, ii) printing schematic, iii) Printed 10x5x3 mm rectangle.

DISCUSSION

NorHA granular support hydrogels can be used for embedded bioprinting of Matrigel bioinks, which sustain PSCs viability and pluripotency.
We are currently working on the optimisation of the bioprinting parameters. Future work will explore how bioprinting in the granular support material can be used to create 4D morphogen gradients to direct PSC differentiation and morphogenesis.

REFERENCES

1. Daly, A. C, *Adv. Healthcare Materials*, 2023.
2. Truong, N. F, (et al.), *Acta Biomateriala* 94: 160–172, 2019

HARNESSING MICRO-X-RAY FLUORESCENCE SPECTROSCOPY AS A TOOL TO ASSESS EXTRACELLULAR VESICLE-INDUCED BIOMINERALISATION

Brunet, M.Y. [1,2*], **McGuinness, A.**[1], **Man, K.**[3], **Jones, M.**[4], **Cox. S.C.**[1]
[1]School of Chemical Engineering, University of Birmingham, Birmingham, UK
[2]Trinity Centre for Biomedical Engineering, Trinity College Dublin, Dublin, Ireland.
[3]Department of Oral and Maxillofacial Surgery & Special Dental Care, University Medical Center Utrecht, Utrecht, The Netherlands.
[4]School of Pharmacy, Institute of Clinical Sciences, University of Birmingham, Birmingham, UK
**email: brunetmy@tcd.ie*

INTRODUCTION

Extracellular vesicles (EVs) derived from bone cells have been increasingly investigated as novel acellular strategy for bone repair [1]. In particular, osteoblast-derived EVs have been shown to play various roles in the process of biomineralisation [2]. With the emergence of nanotherapeutics, there is a growing demand for innovative methodologies evaluating their pro-osteogenic potency which commonly lies in the assessment of cell-mediated mineral deposition. Herein, we detail a novel methodology to assess the osteogenic potential of an EV-therapy using µ-X-ray fluorescence spectroscopy (µ-XRF) which has been tailored to biological workflow requirements.

MATERIALS AND METHODS

Osteoblast-derived EVs were obtained from the conditioned media of 14-day mineralising cultures (MO-EVs) by differential ultracentrifugation followed by their comprehensive characterisation including size, concentration (TEM, NTA) and protein content analysis as well as the detection of EV markers via single-particle interferometric reflectance imaging sensor (SP-IRIS). The osteogenic potency of MO-EVs was then evaluated on osteoblasts by ALP activity, alizarin red and picrosirius red staining. µ-XRF was first employed to quantify the relative levels of calcium and phosphorous as markers of minerals allowing a spot size <20 µm to detect each element and generating 2D elemental maps of the mineralised cultures. Post-acquisition analysis were then performed to generates new hypermaps displaying the percentage of area covered by minerals as well as the relative composition of the mineral phases in terms of calcium and phosphorous elements.

RESULTS

MO-EVs were successfully isolated presenting with a vesicular morphology and an average size of 213 ± 3 nm (Fig. 1A,B). SP-IRIS analysis confirmed the presence of CD9, CD63 and CD81 at the surface of MO-EVs. Standard biomineralisation study confirmed that MO-EVs induced a significant increase in calcium deposition, collagen production and ALP activity after 14 days in osteogenic cultures ($p<0.05$). Importantly, the in-depth downstream analysis of the elemental maps obtained by µ-XRF revealed that MO-EVs were modulating mineralisation in a time- and concentration-dependent manner as MO-EV concentration from 5 µg/mL significantly increased mineral coverage and the levels of calcium/phosphate ($p<0.001$) (Fig. 1C,D,E). Finally, an XRF-standard curve for a range of known Ca/P compounds was successfully generated to identify the degree of maturity of formed minerals (data not shown).

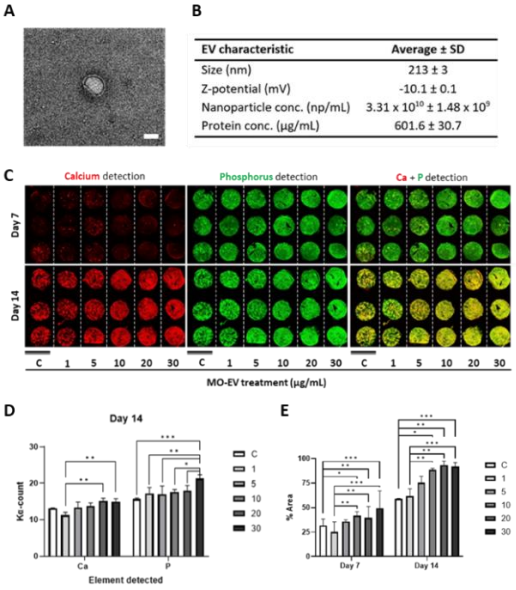

Figure 1 (**A**) TEM observation (scale bar – 100 nm). (**B**) Summary of MO-EV characteristics. (**C**) µ-XRF elemental maps obtain after MO-EV dose response on osteoblasts (scale bar = 10 mm). (**D**) Calcium and phosphorous quantification from elemental maps at day 14. (**E**) Quantification of mineralised area between day 7 and day 14 by image analysis. Data expressed as average ± SD. *$p \leq 0.05$, **$p \leq 0.01$, and ***$p \leq 0.001$.

DISCUSSION

These results demonstrated the potential of µ-XRF to obtain a more in-depth and high-throughput characterisation of mineralised matrices *in vitro* compared to histochemical methods such as alizarin red staining. By examining elemental levels, mineral coverage and chemical phases in a single process, this µ-XRF methodology offered a new platform to shed the light on the effects of osteoblast-derived extracellular vesicles on early biomineralisation.

REFERENCE

[1] Xu (et al.), *Adv Therap*, 7, 2024.
[2] Fang (et al.), *Bone Res*, 12, 2024.

Development of mRNA vaccines for breast cancer immunotherapy using 3D scaffolds

Zhao, N.[1], Dixon, J.E.[4],Chen, H.[5], Curtin, C.M.[1, 2, 3]

[1]Tissue Engineering Research Group (TERG), Royal College of Surgeons in Ireland (RCSI), Dublin, Ireland. [2]Trinity Centre for Biomedical Engineering (TCBE), Trinity College Dublin, Ireland. [3]Advanced Materials and Bioengineering Research Centre (AMBER), RCSI and TCD, Dublin, Ireland. [4] Division of Regenerative Medicine & Cellular Therapies (RMCT), School of Pharmacy, University of Nottingham, UK [5]Laboratory of Nanomedicine and Molecular Imaging, Soochow University, Suzhou, China.

email: (nazhao23@rcsi.com)

INTRODUCTION

mRNA cancer vaccines show promise in immunotherapy by inducing innate and adaptive immunity, but delivery challenges persist due to instability and poor cellular uptake [1]. Nanoparticle systems like lipid nanoparticles (e.g., MessengerMax) and cell penetrating peptides (e.g., glycosaminoglycan enhanced transduction (GET) peptides) address these issues, enhancing stability and delivery. Modified GET peptides improve endosomal escape [2]. A further method to control the distribution and enhance the protection of nanoparticles is to incorporate them into scaffolds. After surgery, these scaffolds may be applied to fill the tumour site for example, releasing medication to prevent cancer metastasis [3].

This study proposes two types of mRNA-activated scaffolds; a p53 mRNA scaffold that can be implanted after breast tumour removal, allowing residual tumour cells to produce p53 protein, which can inhibit further progression, and a MUC1 mRNA scaffold, placed near lymph nodes post-surgery, that can promote immune cell migration to transcribe antigen protein, activating the immune system to target remaining cancer cells.

MATERIALS AND METHODS

In order to determine the optimal delivery vector for mRNA, EGFP and firefly luciferase mRNA nanoparticles (MessengerMax and mGET) were added to DC2.4 mouse dendritic cell line and MDA-MB-231 breast cancer cells in 12-well plates. MessengerMax was incubated for 6 hours at 37°C, and mGET for 24 hours at 37°C, followed by medium replacement. Transfection efficiency was evaluated using fluorescence microscopy and the Luciferase Assay System. Additionally, collagen-hyaluronic acid scaffolds were prepared according to lab protocols [4], and mRNA nanoparticles and different cells were seeded onto them to evaluate mRNA transfection efficiency in a 3D platform. Statistical analysis was conducted by t-test, one-way ANOVA followed by Tukey's test (****p<0.0001).

RESULTS

MessengerMax-mRNA nanoparticles (v/w 1.5 and 3) achieved the highest transfection efficiency, with v/w 3 outperforming v/w 1.5 in DC2.4 and MDA-MB-231 cells. Among mGET groups, N/P 9 showed slightly better efficiency in DC2.4, and N/P 15 in MDA-MB-231, though differences were minor. In scaffold-based studies, unlike 2D results, MessengerMax-mRNA nanoparticles showed significantly higher reporter protein expression, while mGET with varying N/P ratios performed poorly.

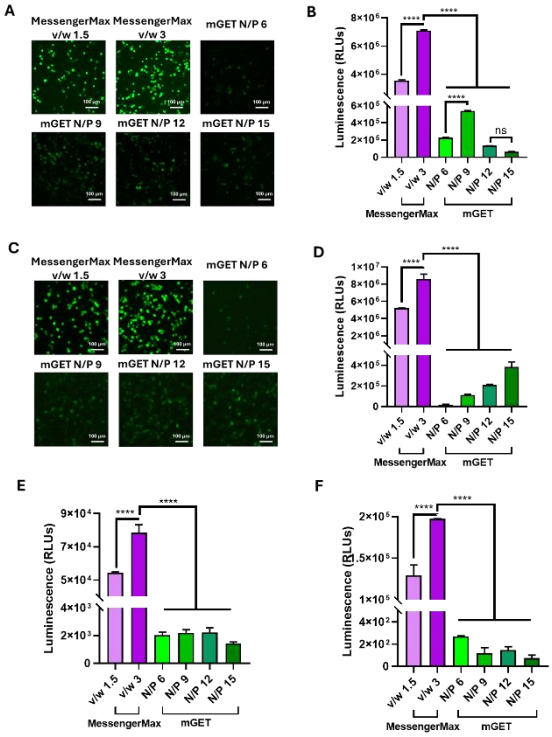

Figure 1. (A, C) EGFP mRNA transfection in DC2.4 and MDA-MB-231 cells. (B, D) Firefly luciferase mRNA quantification of transfection efficiency. Luciferase expression in scaffolds with DC2.4 (E) and MDA-MB-231 cells (F) was analyzed after 24 hours and v/w 3 demonstrated the best performance *in vitro*.

DISCUSSION

MessengerMax demonstrated the highest mRNA delivery efficiency in DC2.4 and MDA-MB-231 cells, with consistent results observed in collagen-hyaluronic acid scaffolds, highlighting its superior performance. Current results suggest that the MessengerMax v/w 3 group is the optimal choice for subsequent animal studies.

REFERENCES

[1] Xiang Li *(et al.)*, Theranostics. Jan 14(2): 738-760, 2024. [2] Rachanel N Power *(et al.)*, Int J Mol Sci. Jan 23(3): 1460, 2022. [3] Yue Zhang *(et al.)*, Adv Mater. Dec 33(48): e2106768, 2021. [4] Amos Matsiko *(et al.)*, J Mech Behav Biomed Mater. Jul 11: 41-52, 2012.

DNA and mRNA vaccines for neuroblastoma: design, development, and therapeutic testing

King, E[1-2], Saha, C[4], Saleem, R[1-2], Cottone, F[1-2], McCathy, H[4], Piskareva, O[1-3]

[1] Cancer Bioengineering Group & Tissue Engineering Research Group (TERG), Department of Anatomy and Regenerative Medicine, RCSI University of Medicine and Health Sciences, Dublin, Ireland.

[2] School of Pharmacy and Biomolecular Sciences, RCSI University of Medicine and Health Sciences, Dublin, Ireland.

[3] Advanced Materials and Bioengineering Research Centre (AMBER), RCSI University of Medicine and Health Sciences and Trinity College Dublin, Dublin, Ireland

[4] School of Pharmacy, Material and Advanced Technologies for Healthcare, Queen's University Belfast, Belfast, NI

e-*mail: olgapiskareva@rcsi.ie*

INTRODUCTION

Glypican-2 (GPC2), a membrane-expressed proteoglycan, is an emerging immunotherapeutic target with evolving significance in rare cancers. Various groups have shown promising results in targeting GPC2 via CAR-T cells and antibody-drug conjugates to reduce neuroblastoma tumour burden, with no significant associated toxicities, however the development of new immunotherapeutic modalities is desperately needed (Fig 1A) [1].

From a technological perspective, CAR-T is costly and time-consuming, requires access to human material, while the mRNA vaccine offers an 'off-the-shelf' product.

MATERIALS AND METHODS

pGPC2 and mGPC2 candidates were complexed with RALA, an amphipathic peptide that spontaneously condenses and protects nucleic acids, facilitating intracellular cargo delivery, to form positively charged particles less than 100nm in size [2]. To compare the immunogenicity of the vaccine candidates, C57/BL6 mice were immunised in a 6-week prime-boost regimen via intradermal (ID) or intravenous (IV) injection. The cellular immune response was assessed via ELISpot and intracellular T cell cytokine staining (ICS) to identify changes in the expression of interferon-gamma (IFNγ), and interleukin-2 (IL-2).

RESULTS

Physiochemical characterisation and *in vitro* transfection confirmed vaccine functionality with significant (8-fold) membrane-bound over-expression of GPC2 observed in a dendritic cell line ($p \leq 0.05$) Fig 1B-C.

ELISpot data shows mice vaccinated with mGPC2/RALA have 100-fold IFN-γ (107.1 ± 18.65; $p<0.0001$) and IL-2 (100.6 ± 22.61; $p<0.001$) expression compared to naive, a robust response comparable to vaccine industry standards. ICS data highlights mGPC2/RALA-induced TNFα and CD62L expression in both CD4+ and CD8+ T cells (Fig 1D). Interestingly, IV injection favours TNFα release from CD4+ T cells and ID injection favours the same from CD8+ T cells.

In the next step, immunisation with mGPC2/RALA delayed time until tumour development by at least 50 days and continue to slowdown the tumour growth.

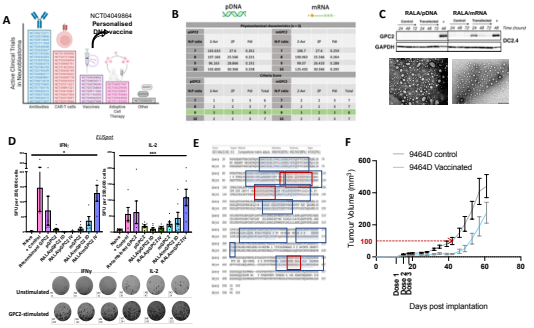

Figure 1 Current immunotherapy clinical trials in neuroblastoma (A); Scoring matrix to evaluate the most effective formulation for RALA/mRNA/pDNA (B) and their uptake and GPC2 expression in DC2.4 cells over 4 days (C); Human and mouse GPC2 has 83% homology. Red rectangles ->regions with MHCI affinity, blue rectangles -> regions with MCHII affinity(E); Tumour growth delay study (F)

DISCUSSION

mGPC2/RALA overperformed pGPC2/RALA, stimulating a potent, antigen-specific cellular immune response in vivo. The studies showed injection route-dependent cytokine expression trends. Importantly, mGPC2/RALA demonstrated its functionality and therapeutic vaccine action in the murine model of neuroblastoma.

REFERENCES

[1] King E, *et al.* The triad in current neuroblastoma challenges: Targeting antigens, enhancing effective cytotoxicity and accurate 3D in vitro modelling Transl Oncol. 2024

[2] Wilson JJ, *et al.* Synthesis and characterisation of a nucleotide based pro-drug formulated with a peptide into a nano-chemotherapy for colorectal cancer. J Control Release. 2024.

NOBOCAP: UNLOCKING MDR/IVDR REGULATIONS FOR INNOVATORS IN EUROPE

[1] Gavin, G., [2] Walsh C., [1] Brougham, C.
[1] School of Mechanical Engineering, Technological University Dublin
[2] Enterprise Academy, Technological University Dublin
email: graham.gavin@tudublin.ie

INTRODUCTION

The implementation of the Medical Device Regulations and In Vitro Device Regulations has proved challenging for both SMEs and Notified Bodies (NBs). The overall aim of these regulations is to have high standards of quality and safety for medical devices and to have a more robust and modernised framework [1]. Some of the identified consequences, however, for the EU marketplace [2][3] are:

- Legacy devices no longer being available due to device certificate expiring and/or manufacturers no longer pursuing recertification for that device.
- New medical device time to market and cost being increased due to additional technical and/or clinical data requirements etc.
- MedTech Startups (and established manufacturers) focussing efforts on the other markets, primarily the US.

In addition to these challenges, there are:

- new, emerging and advanced technologies that place further demands on Notified Bodies and their assessment of complex devices and systems.

NOBOCAP PROJECT

The NoBoCap project (nobocap.eu) is aimed at addressing some of the challenges encountered by both SMEs and Notified Bodies across the EU. It is a multi-organizational consortium including universities, a Notified Body, and Bio-health and Innovation Hubs and Clusters. The NoBoCap project has several work packages focussed on:

- Design and delivery of funded short-term courses.
- Creating a dedicated NB job board.
- Design and delivery of funded university accredited modules.
- Design and development of e-tools to support manufacturers.
- Develop a community platform to act as a voice for start-ups and SMEs

Immediately relevant to the present audience is the development of courses and training opportunities that may benefit SMEs, startups and university spinouts in understanding how the regulations apply to their technology. In designing content, the aim was:

- To support learners in technical documentation preparation in MDR and IVDR.
- To increase learners' awareness of the role of NBs and to consider careers in this space.

PROJECT OUTPUTS TO DATE

University Accredited Modules: Three CPD Modules have been developed by knowledge experts Notified Body SGS and accredited at NQF Level 9 (EQF Level 7) in TU Dublin, Ireland and TG Mures, Romania. These modules are delivered by the Notified Body experts and practitioners in the space:

- Module 1: Implementing Regulatory Requirements for Medical Devices.
- Module 2: Generating Data for Technical Documentation (MDR)
- Module 3: Generating Data for Technical Documentation (IVDR)

To date, over 215 learners from across the EU have registered onto the CPD programmes in TU Dublin. These will continue to be available throughout 2025 in one of the host universities. A follow up surveys will provide further evidence of programme benefits.

Specialised Short Courses: Two specialised courses have been developed to support individuals in SMEs:

- Training for C-level Management - MDR/IVDR Implementation and Resource Allocation
- AI-supported Medical Devices

E Tool: An interactive tool to:

- guide manufacturers in classifying their device
- assist in identifying the applicable codes
- identify Notified Bodies that have competency in the applicable codes.

CONCLUSION

The NoBoCap project is providing funded learning opportunities and tools to support SMEs and learners in navigating the MDR and IVDR landscape.

REFERENCES

[1] Melvin *(et al.)*, Effort Open Rev. 4(6): 351-356, 2019.
[2] Kearney *(et al.)*, Ther Innov Reguk Sci. 57(4): 783-796, 2023
[3] Verboven (*et al.),* NoBoCap Summit, Brussels,2024

DECLARATION

Co-Funded by the European Union. Views and opinions expressed are however those of the author(s) only and do not necessarily reflect those of the European Union or the European Health and Digital Executive Agency (HADEA). Neither the European Union nor the granting authority can be held responsible for them.

A NOVEL EX VIVO PORCINE MODEL OF LOCALIZED OEDEMA FOR STUDYING SUB-EPIDERMAL MOISTURE

Brunetti G.[1, 3], **Patton D.**[2], **Moore Z.**[2], **Palomeque-Chavez J. C.**[1, 3], **Boyle C. J.**[1, 3], **O'Brien F. J.**[1, 3]
[1] Tissue Engineering Research Group, Dept. of Anatomy & Regenerative Medicine, Royal College of Surgeons in Ireland (RCSI), 123 St Stephen's Green, Dublin 2, Ireland
[2] Skin Wounds and Trauma Research Centre, School of Nursing and Midwifery, Royal College of Surgeons in Ireland (RCSI), 123 St Stephen's Green, Dublin 2, Ireland
[3] Advanced Materials and Bioengineering Research (AMBER) Centre, Royal College of Surgeons in Ireland (RCSI) & Trinity College Dublin (TCD), Ireland
email: giuliobrunetti@rcsi.com

INTRODUCTION

The current gold standard for pressure injury detection relies on Visual Skin Assessment (VSA)[1], which requires visible tissue damage to have already occurred. Furthermore, this approach is particularly challenging for individuals with darker skin tones, where VSA's reliability is significantly reduced[2]. Sub-epidermal moisture (SEM) measurement has been proposed as a method for detecting localised oedema (an early pressure injury indicator) before damage is visible[3]. Lab studies have helped to determine the sensitivity of SEM scanners to moisture using physical tissue phantoms[4]. However, these simplified models cannot capture the distinct structure and composition of human soft tissue.
Thus, the aim of this study is to describe and validate a novel *ex vivo* porcine model of localised oedema. We use the model to evaluate and quantify the sensitivity of a commercial SEM scanner to detect changes in sub-epidermal moisture.

MATERIALS AND METHODS

The adult porcine calcaneus was selected as a bony prominence due to its anatomical similarities to the human heel. SEM was controlled using intradermal injection of phosphate-buffered saline (PBS) via a precision syringe pump. Oedema was inspected using colourimetry (visual inspection). A commercial SEM scanner was used to quantify SEM at the injection site (localised oedema formation site) and a control site near the bony prominence. Tests were performed on ten specimens, with ten repetitions within each specimen of four raw SEM measurements. Raw SEM, SEM **Δ** (variation of SEM in a minimum of three readings; used to indicate damage clinically) and fluid delivered were recorded.

RESULTS

Moisture was found to remain within 2 cm of the injection site successfully indicating localised oedema. Raw SEM readings increased at the intervention site as moisture content increased, with SEM statistically significantly greater after 1 ml injection than baseline (Figure 1 B, $p<0.05$). Raw SEM values continued to increase as fluid content increased, although the rate of increase reduced, suggesting saturation of the detector at higher moisture volumes. SEM **Δ** increased as sub-epidermal moisture increased, with the clinically relevant score of 0.6 breached after 1 ml injection ($p<0.05$).

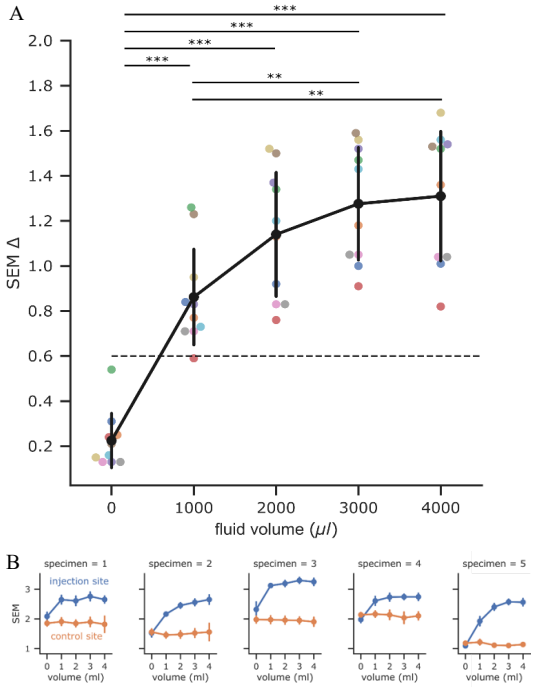

Figure 1. Raw SEM (A) and SEM Δ (B) measurements show positive response to increased localised moisture content. Four consecutive injections of 1 ml at the flow rate of 500 µl/min of PBS were performed.

DISCUSSION

A SEM scanner successfully detected non-visible variations in SEM content in a complex model such as *ex vivo* porcine soft tissue. An injection of 1 ml of fluid was sufficient for the scanner to indicate early damage. A novel *ex vivo* clinical model was successfully established for this purpose, providing a valuable tool for further research. Further study is needed to refine spatial control and characterisation of localised SEM in this newly developed *ex vivo* model.

REFERENCES

1. O'Brien *et al.,* J Tissue Viability. 2018;27(4):232-7.
2. Bates-Jensen *et al.,* J Wound Ostomy Continence Nurs. 2009;36(3):277-84
3. Clendenin *et al*., J Tissue Viability. 2015;24(1):17-23.
4. Peko and Gefen, Int Wound J. 2019;16(4):979-88.

ACKNOWLEDGEMENTS

This project was funded by Bruin Biometrics Ltd, whose SEM scanner was used in this study.

FINITE ELEMENT MODELLING OF STENT EXPANSION IN THE SUPERIOR VENA CAVA

Khaydukova, I.V. [1], Kenny, G. [2], Hulk, V. [2], O'Cearbhaill, E.D. [1]
[1]UCD Centre for Biomedical Engineering, School of Mechanical and Materials Engineering, University College Dublin, Ireland
[2]Croívalve, Dublin, Ireland
email: irina.khaydukova@ucd.ie

INTRODUCTION

Currently, there is no safe and effective treatment for all patients with Tricuspid Regurgitation (TR). Both replacement and repair options have proven ineffective at managing the severe TR cases. The CroíValve DUO™ Tricuspid Coaptation Valve System is a new device that seeks to address these limitations by combining aspects of repair and replacement. This system includes a stent positioned in the superior vena cava (SVC) and a valve situated within the native patient valve. The present study examines the process of stent expansion within the SVC using the finite element method.

MATERIALS AND METHODS

Measuring the material properties of the SVC in animals presents challenges, as the SVC is short, located near the head, and thus unavailable from abattoir sources. Due to its visual similarity to the SVC, greater length (~10 cm), and ease of procurement, the pig inferior vena cava (IVC) was selected for the current study.

The material properties of the IVC were evaluated using a biaxial ElectroForce Planar Biaxial TestBench. The HOG constitutive model was applied to the tissue. Each sample was subjected to equibiaxial testing up to a 0.4 stretch, with the resulting stress-strain relationship approximated in Spyder software.

Finite element modeling of the stent was conducted in Abaqus. Shape-setting involved expanding the stent from an as-cut profile to the final configuration introduced into the patient, using Dynamic Implicit analysis. The stent was modeled as a shell structure with 0.06 mm S4R elements, and only half of the stent was simulated. Nitinol was selected as the stent material. Following modeling, the stent geometry was exported without residual strains or stresses for crimping analysis. The crimping and expansion tools were represented as rigid surfaces, and stent expansion in the vein was performed in Abaqus Explicit analysis, with a 1-second step duration to allow for equilibration

RESULTS AND DISCUSSION

Sample equibiaxial porcine IVC stress-strain curves are compared with relevant literature data in Fig. 1. We could not determine which vena cava was measured in the study by Silver et al. [1]; however, since the pig SVC is challenging to obtain, it is likely that their results also reflect the properties of the porcine IVC. Differences were observed in the circumferential properties of the IVC compared to Silver et al. [1], but there was substantial variability across individual animals. Notably, one result aligned well with the curve from Mattson et al. [2]. In contrast, the longitudinal results showed minimal inter-individual variation, with overlapping data across samples.

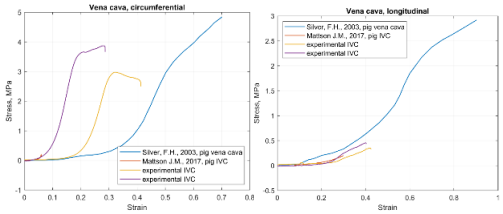

Figure 1 Comparison of experimental equibiaxial porcine IVC stress-strain data to available relevant literature.

The experimental results were approximated using the HOG model. The coefficients are presented in Table 1.

Table 1. HOG model coefficients.

C_{10}	D	k_1	k_2	κ	Θ_1	Θ_2
0.260 6865	1e-6	1.466 1292	19.54 3191	0.296 8647	0.174 5297	0.680 8163

Vessel after stent expansion is presented in Fig. 2. The half of the stent is conical to accommodate the varying diameter of patients SVC. This modelling approach can be used as a basis to understand the interaction of self-expanding stents, like this component of the CroíValve DUO™ system, and the vessels of the vena cava.

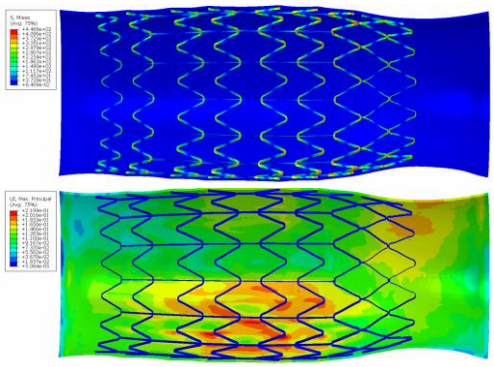

Figure 2 The vessel after the stent expansion.

REFERENCES

[1] Silver *(et al.)*, Materials & Design 198:1–12, 2021.
[2] Mattson *(et al.)*, Materials & Design 198:1–12, 2021.

BIOACTIVE COATINGS FOR ENHANCED CORROSION RESISTANCE AND BIOFUNCTIONALISATION OF MAGNESIUM MEDICAL IMPLANTS FOR SKELETAL REPAIR

Hashemi, T. [1*], **Persson, C.**[2], **D'Elia, F.**[2], **Levingstone, T.J.**[1], **Dunne, N.**[1]
[1.]Centre for Medical Engineering Research, School of Mechanical and Manufacturing Engineering, DCU.
[2.]Department of Materials Science and Engineering, Uppsala University, Sweden
**Email: tina.hashemi2@mail.dcu.ie*

INTRODUCTION

Biodegradable magnesium (Mg) implants are increasingly used clinically, but their full adoption is limited due to concerns about their corrosion behaviour [1]. Surface modification through the application of bioactive coatings has been proposed as an efficient and cost-effective route to reducing the corrosion, and hence the degradation rate, of Mg-based medical implants [2]. This investigation focuses on untangling the corrosion mechanisms associated with 3D-printed WE43 magnesium alloy for orthopaedic applications, with a focus on tailoring corrosion to facilitate effective bone remodelling. This study aims to develop a novel composite coating with enhanced adhesion, improved corrosion resistance, and superior bioactivity by incorporating phosphoserine (PS) into bioactive calcium phosphate (CaP) coatings, specifically dicalcium phosphate dihydrate (DCPD) and octacalcium phosphate (OCP), using varying molar ratios.

MATERIALS AND METHODS

The substrate material used was WE43 magnesium alloy (10 mm × 10 mm × 3 mm), supplied by NMD GmbH (Hemseen, Germany). A process for the synthesis of powder OCP and DCPD was developed based on previous work through the preparation of sodium dihydrogen phosphate anhydrous and calcium acetate monohydrate solutions at 68ºC with a pH values of 4 and 5, respectively [3]. After the reaction was completed, PS was added to the DCPD and OCP solution at different molar ratios of 1:1, 1:2, and 2:1, at 37 °C for 5 minutes to obtain the composite product. A wet chemistry approach was applied to deposit the DCPD, OCP, DCPD-PS and OCP-PS coating onto the substrate of the Mg specimen. For chemical characterisation, XRD, FTIR, and XPS were utilised to determine the phase composition, chemical structure, and chemical bonding, respectively. The surface wettability was evaluated using contact angle measurements, while the morphological features of the CaP-PS coating were analysed using SEM. The corrosion behaviour was evaluated using an electrochemical test, gravimetric analysis, and hydrogen evolution. Biological studies assessed the biocompatibility (ISO 10993:Parts 5-6) properties.

RESULTS

Based on the coating adhesion and electrochemical studies, the optimised molar ratio was determined to be 1:1 for DCPD/PS and 1:2 for OCP/PS. The addition of PS significantly (p-value <0.001) enhanced the coating adhesion strength, increasing it from 8.3 ± 0.24 N for OCP-WE43 to 10.33 ± 0.6 N for OCP-PS-WE43, and from 2.56 ± 0.3 N for DCPD-WE43 to 5 ± 0.41 N for DCPD-PS-WE43. Furthermore, the addition of PS intensified the XRD peaks of OCP, indicating improved crystallinity and a more ordered crystalline structure. In contrast, the XRD pattern of DCPD-PS-WE43 exhibited broader and less intense peaks compared to DCPD-WE43, confirming the formation of a less crystalline CaP phase. Electrochemical tests revealed that the addition of PS led to a two-fold improvement in corrosion rate for DCPD-PS-WE43 and three-fold for OCP-PS-WE43 compared to their CaP-WE43 counterparts. Additionally, weight loss measurements after 14 days in Hank's solution showed that OCP-PS-WE43 had the lowest weight loss (0.035 g/cm³) compared to the uncoated WE43 specimen (0.22 g/cm³) (Figure 1). The MC3T3-E1 cells exposed to extracts from all groups demonstrated a mean viability of ≥100% after 72 hours, which is significantly higher than the 70% viability requirements according to the ISO standard. In terms of the cell morphology assessment, visual assessment showed an increase in cell population by Day 7 across coated specimens, with densely populated cell aggregates particularly prominent in the OCP-PS-WE43 group.

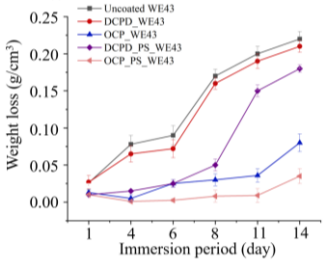

Figure 1 Cumulative weight loss of uncoated and coated Mg specimens in Hank's solution at 37 ± 1 ◦C and pH 7.4 ± 0.1.

DISCUSSION

This study demonstrated the successful deposition of composite CaP-PS coatings onto WE43 Mg alloy, providing an effective strategy for controlling the corrosion behaviour of Mg specimens. The application of PS as an adjuvant was investigated to enhance the bonding between the CaP-based coating and the Mg substrate, as well as to decelerate the corrosion rate of the Mg. Electrochemical tests and weight loss measurements showed a five-fold reduction in the corrosion rate of OCP-PS-WE43 compared to uncoated WE43 Mg alloy. The incorporation of CaP and PS combined their benefits, improving adhesion and promoting cell attachment through the porous OCP structure. Overall, this approach effectively enhanced the corrosion resistance of Mg-based orthopaedic implants, potentially making them more suitable for clinical applications.

REFERENCES

1. Krischak G (*et al.*), Arch Orthop Trauma Surg. 104–13, 2004; 2. Li K, Wang (et al) J Biomater App. 375-384, 2013; 3. Hashemi T (et al) J surface and coating technology, 2024.

Early Stage Researcher (PhD Year 1)		Post-Doctoral Researcher/Senior Researcher/PI	X
Entry for the Engineers Ireland Biomedical Research Medal		Corresponding author has completed PhD and would like to review BinI abstract submissions	

Please place an X in any appropriate categories

ENHANCING CIRCULATORY LOOP SIMULATION OF RIGHT HEART HYDRODYNAMICS

Belikov, N.V.[1], Albadawi, M. [1], Kenny, G. [2], Abaei, A.R. [2], O'Rourke, M.J. [1]
[1]UCD Centre for Biomedical Engineering, School of Mechanical and Materials Engineering, University College Dublin, Ireland
[2]Croívalve, Dublin, Ireland
email: nikita.belikov@ucd.ie

INTRODUCTION

Tricuspid valve regurgitation and its complications significantly impact the quality of life. Transcatheter methods for tricuspid valve repair and replacement are currently the most promising surgical solutions to address this issue. To analyse the hydrodynamic parameters of these devices, it is essential to evaluate their performance in a controlled and representative environment. Circulatory loops that simulate in vivo valve conditions are used for this purpose.

Enhancing these loops, approximating the valve's operating conditions to real-life scenarios, and improving the qualitative and quantitative assessment of the hydrodynamic profile near and within the valve are critical practical challenges. This study describes methods for improving a previously developed circulatory loop to analyse the hydrodynamic parameters of devices for treating tricuspid regurgitation.

MATERIALS AND METHODS

To enhance the simulation capabilities of right-heart hydrodynamics, several modifications and improvements were developed and implemented in the legacy loop system (Fig 1). The compliance chambers were made adjustable to allow simulation of various conditions. This functionality was implemented using a movable piston, with the distance between the piston and the liquid surface controlled by a screw mechanism. To minimize the effect of fluid oscillations on measurement results, the compliance chamber diameter was increased from 80 to 150 mm. This effectively dampens internal wave reflections, reducing secondary flow disturbances caused by pulse waves bouncing off chamber walls.

Two versions of the compliance chamber were developed for testing and evaluating devices designed to replace or assist the tricuspid valve. The chamber, submerged in a glycerol tank, allows Particle Image Velocimetry (PIV) measurements of flows passing through the valve. Pressure ports are located at the inlet and outlet, and a flow meter is positioned at the inlet. A securing mechanism enables fixation of transcatheter systems with anchor-type deployment in heart vessels. The modular design allows fluid flow to enter either from the chamber's end or side. Unused chamber ends can facilitate visual inspection of valve function, including high-speed camera observations. Devices can be tested in silicone cylinders that block external flow or in realistic valve models made from biological or synthetic materials.

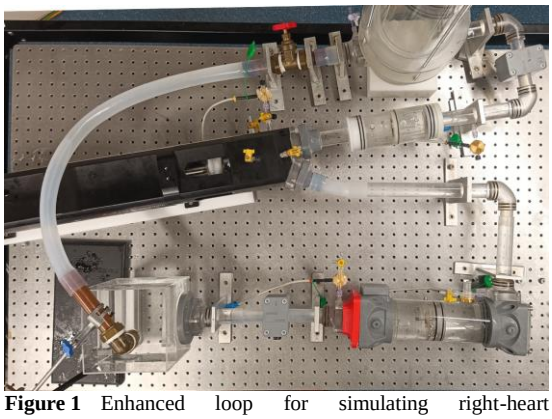

Figure 1 Enhanced loop for simulating right-heart hydrodynamics.

The first chamber version was produced using FDM 3D printing, but difficulties in removing supports, low strength, and surface quality led to a second version. This version utilized SLA printing, with reinforced structural elements requiring strength and eliminating the need for post-processing.

Simulating right-heart function requires creating low-pressure conditions, and reducing pressure losses along the flow path is crucial. Analysis showed that internal connectors within the tube lumen cause a 3-5 mmHg pressure drop. Therefore, all connectors were replaced with external fittings that wrap around the tubes.

RESULTS AND DISCUSSION

Several improvements were proposed to enhance the circulatory loop's capability to simulate right-heart hydrodynamics.:

- Maximizing compliance chamber diameter reduces flow noise.
- Adjustable chamber volume increases flexibility in simulating different conditions.
- Chambers with transparent end windows allow both flow parameter assessment and visual valve function inspection.

The proposed changes will not only allow for more accurate modeling of the working conditions of devices for replacing and assisting the tricuspid valve, but also enable a wide range of variations.

HIGH PERFORMANCE OPEN SOURCE TOPOLOGY OPTIMISATION SOFTWARE FOR BIOMEDICAL DEVICES

Rao C.P., [1,2], **Moerman K. M.**[1,2]

School of Engineering, Mechanical Engineering, University of Galway, Ireland
Lero, the SFI Research Centre for Software, Limerick, Ireland
email: kevin.moerman@universityofgalway.ie

INTRODUCTION

The emergence of additive manufacturing has opened new pathways for design optimisation in biomedical devices. One of the primary numerical methods utilised for design optimisation, in terms of structural mechanics, is topology optimisation, wherein the material layout is redistributed to ensure the overall stiffness of the structure is maximised while keeping the overall volume fraction constant. Topology optimisation has been implemented for biomedical devices such as hip implants, orthopaedics, and orthodontic applications [1]. For the development of biomedical devices, having software dedicated to building an optimal design is invaluable. This study aims to develop open source topology optimisation software that can be used for biomedical research applications, building upon an existing framework. Sigmund O [2], presented an introductory resource for topology optimisation, which includes a finite element solver for a 2D case (for the linear elastic case), optimality criteria as the optimiser, incorporates a mesh-independency filter, and is extendable to different boundary conditions. However, it does not address non-linear cases or multiple constraints. Furthermore, most educational resources in this domain utilise MATLAB, a proprietary software. Liu *et al.* [3], presented a 3D case for topology optimisation, which, similar to the 2D case is limited by simplified boundary conditions, assumptions of linear elasticity, normalised applied loads, and hard-coded element stiffness matrices, restricting their applicability to larger or more complex systems involving non-linear mechanics [2, 3]. The present work seeks to overcome these limitations by creating a generalised framework that serves as both an accessible introduction for early-stage researchers and a scalable solution for the non-linear conditions observed in biomedical applications.

METHODS

The novel topology optimisation framework is implemented in Julia. Julia is a high level open source programming language that offers high performance, making it ideally suited to the demands of an optimisation framework [4]. This work focuses on the implementing of the Solid Isotropic Material with Penalisation (SIMP) topology optimisation method, which features a power law approach, and an objective function for compliance minimisation, as shown in equation 1:

$$\begin{aligned} &\min_{x} : c(\mathbf{x}) = \mathbf{U}^\top \mathbf{K}\mathbf{U} = \textstyle\sum_{e=1}^{N} (x_e)^p \mathbf{u}_e^\top \mathbf{K}_e \mathbf{u}_e \\ \text{Subject to} \quad &: \tfrac{V(\mathbf{x})}{V_0} = f \\ &: \mathbf{K}\mathbf{U} = \mathbf{F} \\ &: 0 < x_{min} \leq x_e \leq 1 \end{aligned} \tag{1}$$

Where, $\mathbf{U}$ and $\mathbf{F}$ are the global displacements and force vectors, respectively, $\mathbf{K}$ is the global stiffness matrix. $\mathbf{u}_e$ and $\mathbf{K}_e$ are the element displacement vectors and stiffness matrix respectively. $\mathbf{x}$ is the vector of design variables, x_{min} is the minimum relative density (non zero to avoid singularities), N is the number of elements used to discretize the design domain, p is the penalization power ($p = 3$). $V(\mathbf{x})$ and V_0 is the material volume and the design domain value respectively, and f is the volume fraction. The optimisation problem is solved using an optimality criteria (OC), keeping the volume fraction as a constraint. This basic SIMP method is implemented in Julia, and verified in 2D for the half-beam (Fig. 1A), and in 3D for both the beam (Fig. 1B) and a wheel resembling structure (Fig. 1C). Additionally, high performance visualisation was here added using the Julia package COMODO.

RESULTS

The SIMP-based topology optimisation method was successfully implemented in Julia and was verified with the existing MATLAB implementations. Fig 1 shows results for the 2D (A) and 3D (B, C) benchmarks. The initial 3D implementation showed a 10% speed enhancement over MATLAB (for a 30x10x2 grid), but further significant speed enhancements are expected as the code is optimised. In terms of visualisation the Julia implementation is vastly superior, since high resolution 3D rendering is easily enabled.

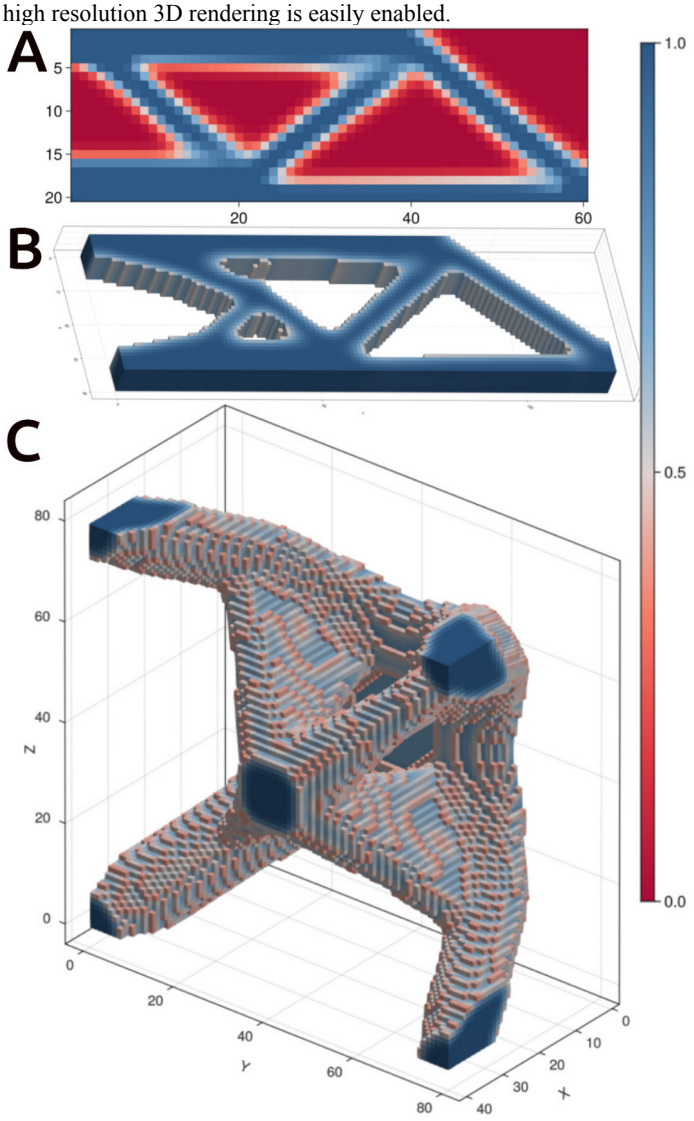

Figure 1 2D/3D results of MBB case in Julia (A and B), C different boundary conditions for wheel geometry.

CONCLUSION

A novel, high performance, and open source implementation of topology optimisation is here presented. Future work will focus on extending the current framework to be more generalised. Through further optimisation and generalisation of the finite element implementation, the software will be able to handle larger structures, more complex geometries, flexible definition of boundary conditions. Furthermore the software will be extended to handle multi-objective optimisation (e.g. featuring both compliance and local material stress). Through these extensions the work will become both a valuable education resource, as well as a high-performance and scalable solution for biomedical device design researchers.

REFERENCES

1. Ibhadode, O. (et al.), Virtual and Physical Prototyping 18:e2181192, 2023.
2. Sigmund, O., Structural and Multidisciplinary Optimization 21:120–127, 2001.
3. Liu, K., and Tovar, A., Structural and Multidisciplinary Optimization 50:1175–1196, 2014.
4. Coleman,C (et al.), Computational economics 58:1263-88, 2021.

NUMERICAL AND EXPERIMENTAL INVESTIGATION OF THE DYNAMIC BEHAVIOR OF VIBRATING NITI GUIDEWIRE

Rafiei Anamagh M., Ullah M. and Gavin G.
School of Mechanical Engineering, Technological University Dublin
email: graham.gavin@tudublin.ie

INTRODUCTION

Minimally invasive interventions often utilise slender wires to access and navigate to target sites. These guidewires act as rails, facilitating access for other therapies. In endovascular procedures, the guidewires facilitate angioplasty balloons, stenting and other dilation procedures. Due to their small profile and flexibility, endovascular guidewires have limited ability to transfer forces to their tip and as a result cannot penetrate hard calcified blockages, commonly referred to as chronic total occlusions (CTOs) [1-2]. One method proposed to overcome this limitation is the application of vibrations to the wire. The vibrations are transmitted along the length of the wire to the distal tip, where the micro reciprocating action can ablate or disrupt calcified material [3]. To better understand how NiTi can transmit these vibrations, a straight NiTi wire of guidewire dimension, is simulated and analysed numerically, with the displacement at the wire's distal tip obtained and compared to experimental results.

MATERIALS AND METHODS

The finite element method is applied using ABAQUS software, where the wire is modelled with beam elements. An experimental rig (Figure 1) was developed to measure the displacement at the distal tip of the wire. The excitation amplitude and frequency are comparable with those reported in the literature. The wire is stabilized within a fluid filled catheter at 37 deg. Celsius.

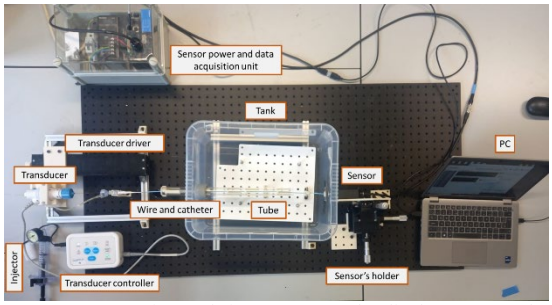

Figure 1 Experimental rig to measure the displacement at the distal tip of the wire.

A laser displacement sensor (Keyence) was used to capture displacement at the wire distal tip. To model the wire accurately, an experimental analysis was conducted to determine the damping ratio of the system. The damping ratio, along with the elastic properties of the NiTi wire, was then incorporated into the numerical model.

RESULTS

The numerical method was validated by comparing its results with experimental data. The experimental study examines the effect of wire length on the displacement amplitude at the distal tip. The wire lengths tested range from 78 cm to 104 cm. Figures 2 shows the comparison of the peak-to-peak displacement result for the numerical and the experimental results.

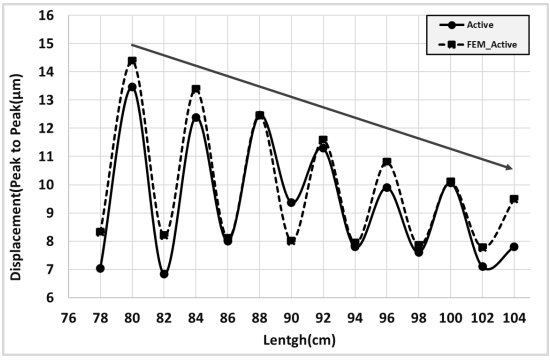

Figure 2 Comparison of experimental and numerical displacement at the distal tip of the wire.

DISCUSSION

The results lead to the following conclusions:
(I) The developed numerical method can accurately predict the displacement at the tip of the wire, with a maximum error of 10%.
(II) As the length of the wire increases, the overall displacement decreases due to losses.
(III) The oscillatory behaviour suggests that, at a specific wire length, the wire's natural frequency aligns with the excitation frequency, resulting in maximum displacement.
In summary, an FE method was developed that effectively predicts the dynamic behaviour of NiTi wire, allowing for accurate analysis in various situations.

REFERENCES

[1] Hiramoto *(et al.)*, Nat Rev Cardiol 15:332–50, 2018.
[2] Sakes *(et al.)*, Cardio. Eng Technol 15:103-117, 2016.
[3] Gavin, Exp. and Num. Invest. of Therap. Ultrasound Angioplasty, PhD, DCU, 2005.

ACKNOWLEDGEMENT

This work is funded under a DTIF award managed by the Department of Enterprise, Trade and Employment and administered by Enterprise Ireland.

COMODO: OPEN SOURCE SOFTWARE FOR COMPUTATIONAL (BIO)MECHANICS AND DESIGN

Moerman K.M.[1,2]
School of Engineering, Mechanical Engineering, University of Galway, Ireland
Lero, the SFI Research Centre for Software, Limerick, Ireland
email: kevin.moerman@universityofgalway.ie

INTRODUCTION

This work presents a novel open source library called Comodo [1], written in the high performance language Julia. The story of Comodo starts with GIBBON [2], a MATLAB library for computational biomechanics developed by the author. Although GIBBON itself is open source, and offers an extensive range of functionality, it ultimately relies on the proprietary runtime MATLAB. As MATLAB is not open source, its scientific functionality cannot be fully built upon, optimised, or verified by individual researchers. Furthermore, being an interpreted language, MATLAB's performance does not scale well for high performance applications. In the context of biomedical engineering such applications may include medical device design optimisation, in-silico clinical trials, and clinical software deployment. To address this gap we here introduce Comodo, which loosely stands for COmputational MOdelling for Design Optimisation.

METHOD IMPLEMENTATION

Although its scope is similar to GIBBON, focussing on geometry processing tools, surface meshing, solid meshing, and coupling with finite element analysis (FEA), Comodo offers a more advanced and modern implementation and can scale for high performance applications. Comodo is implemented in the language Julia, which is a high-level general purpose programming language combining an easy Python/MATLAB-like syntax with the performance expected from a compiled language like Fortran or C.

Figure 1 shows visualisations from Comodo example codes. Fig.1A-B are examples of CAD-like processes to create surface geometry from curves. For instance extrusion (Fig.1A), revolution, lofting, sweeping (Fig.1B), and filleting. For each the mesh type, e.g. triangles or quadrilateral elements, can be freely chosen. Fig.1A shows an example of "up to surface" extrusion with a smooth, node shared, Bezier spline transition region.

Once surface models are imported or designed within Comodo, a range of surface processing techniques can be used on them. Fig.1C-G shows surface curvature analysis, which is useful when defining constrained smoothing for instance to increase/decrease smoothing for regions of a given curvature. Fig.1D shows how an imported surface could be segmented into separate surface features based on local curvature.

In Fig.1E shows an example of shrinkage avoiding surface smoothing. The top shows a noisy mesh and the bottom the smoothed result. Fig.1F shows an example of geodesic distance marching. This is useful for evenly spaced geodesic point sampling. Fig.1G shows the implementation of high quality geodesic surface remeshing (based on [3]). Besides these surface processing methods Comodo also features functionality for solid meshes. This includes tetrahedral meshing (through incorporation of TetGen [4]), as well as structured hexahedral meshing based on mesh thickening. Fig.1H shows how a swept triangulated surface mesh was thickened to produce a layer of pentahedral elements. Next, Comodo supports coupling with FEA. For instance one may use FEBio [5] through the developed wrapper FEBio.jl (Fig.1I). Finally, Comodo uses efficient GPU accelerated visualisation based on the Julia library Makie. An example is Fig.1J where all BodyParts3D surfaces (1.3Gb of STLs!) could be easily visualised (and rotated and interacted with) on a standard laptop.

CONCLUSION

This work presents Comodo, a novel open source and high performance Julia library for computational (bio)mechanics and computational design. By combining advanced geometry processing techniques with finite element meshing and analysis techniques, this library offers a "open stop shop" for computational biomechanics and researchers. Current work is focussed on extending Comodo with lattice structure design, and levelset and topology optimisation methods.

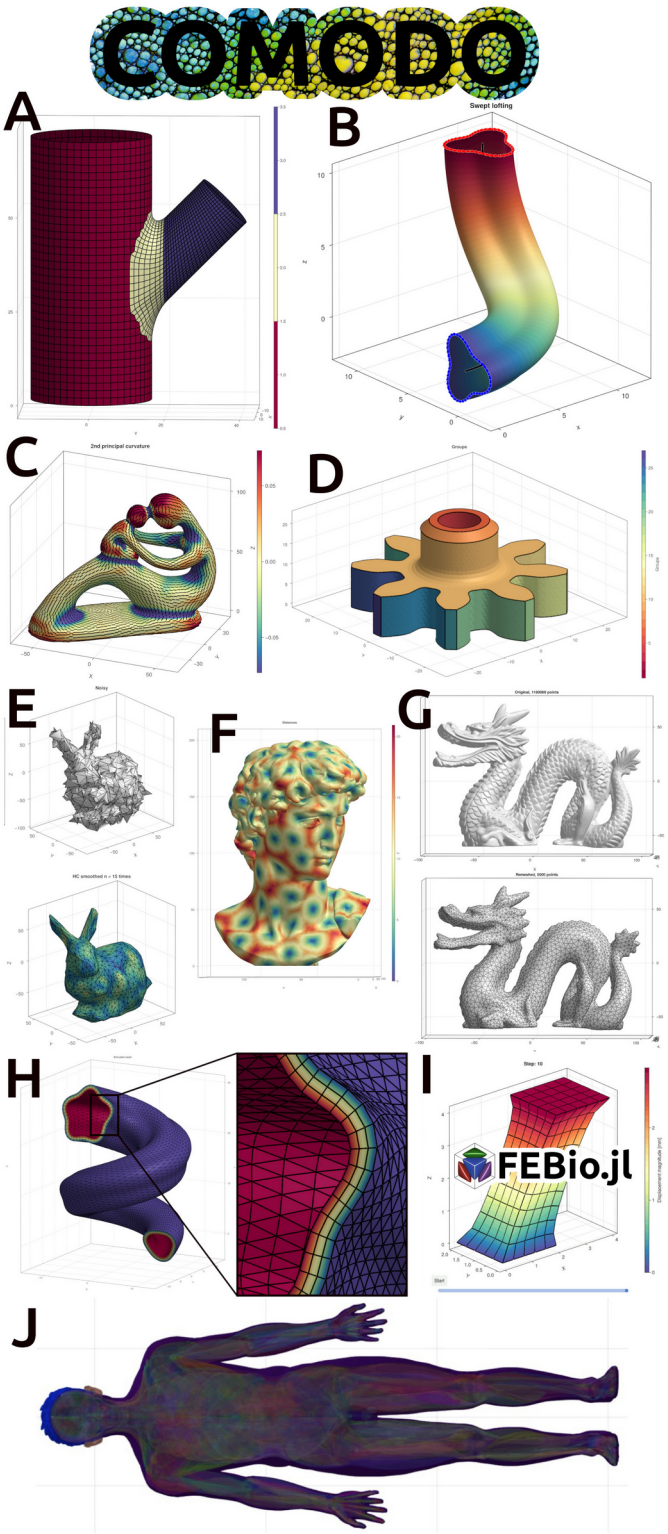

Figure 1 Overview Comodo.jl functionality

REFERENCES

1. Moerman K.M, https://github.com/COMODO-research/Comodo.jl.
2. Moerman K.M, J. of Open Source Software, vol. 3, no. 22, p. 506, Feb. 2018, doi: 10.21105/joss.00506.
3. Lévy B. et al. Proc. 21st Int. Meshing Roundtable, 2013, doi: 10.1007/978-3-642-33573-0_21.
4. Si H. et al. *ACM Trans. on Math. Software*, vol. 41, no. 2, pp. 1–36, Feb. 2015, doi: 10.1145/2629697.
5. Maas S. et al. J. of Biomech. Eng., vol. 134, no. 1, pp. 011005–011005, 2012, doi: 10.1115/1.4005694.

TOWARDS STANDARDISED SIZING STRATEGIES FOR TRANSCATHETER AORTIC VALVE IMPLANTATION IN THE BICUSPID AORTIC VALVE: A PATIENT-SPECIFIC COMPUTATIONAL STUDY

Boxwell, S.[1], Armfield D.[2], Cardiff P.[2], Hickey, W.[3], Cook, S.[3], Kelly, P.[3], McNamara, L.[1]
[1]Mechanobiology and Medical Device Research Group (MMDRG), Department of Biomedical Engineering, College of Science and Engineering, University of Galway, Galway, Ireland
[2]School of Mechanical and Materials Engineering, University College Dublin, Dublin, Ireland
[3]Structural Heart, Boston Scientific Corporation, Galway, Ireland
email: s.boxwell1@universityofgalway.ie

INTRODUCTION

The bicuspid aortic valve (BAV) is a common congenital disease, whereby the aortic valve presents with two, rather than three functional cusps. Recent studies report that up to 50% of younger patients undergoing aortic valve replacement present with BAV morphology, whereby transcatheter aortic valve implantation (TAVI) is increasingly utilised [1]. However, TAVI in the BAV is challenging, due to the presence of asymmetrical, heavily calcified cusps, commissural fusions and concomitant aortopathy [2]. Appropriate device sizing is necessary to ensure prosthesis-anatomy interaction and prevent paravalvular leakage (PVL) [3]. Although rates of PVL following TAVI in the BAV have reduced over recent years [3], balloon post-dilatation to resolve incomplete apposition is frequently required [2]. This may be due to the lack of standardized sizing for BAV patients, and although BAV-specific sizing approaches have been proposed, these methods are not yet widely understood [2-4].

Patient-specific computational modelling, including finite element (FE) and computational fluid dynamics (CFD) approaches, have been applied to optimise TAVI device sizing and positioning in the BAV cohort [5,6]. However, such approaches have not been applied to compare various sizing strategies, nor examine the impact of balloon post-dilatation on the occurrence of PVL.

The objective of this study is to develop, verify and validate a computational framework for simulating TAVI in the BAV utilising clinical and in vitro data. Using this validated approach, we investigate the impact of balloon valvuloplasty and sizing on the occurrence of PVL following TAVI in the BAV.

METHODS

A retrospective type-1 BAV patient-specific model with severe aortic stenosis was reconstructed from pre-TAVI computed tomography (CT) scans using MIMICs (Materialise). Next, we created FE and CFD models of the self-expanding ACURATE Prime TAVI device (Boston Scientific) using Abaqus/Explicit (v2023, Dassault Systèmes) and OpenFOAM-v2312, respectively. The computational framework simulated the complete TAVI procedure including (1) crimping, (2) deployment, (3) the cardiac cycle (Fig. 1(a)) and (4) systolic flow.

For validation of these models, we conducted hydrodynamic device (n = 3) testing in a pulse duplicator, where the device was deployed within a 3D printed model of the BAV patient-specific anatomy (Fig. 1(b)). We also validated using post-TAVI clinical (CT and transesophageal echocardiogram (TEE)) data. Following validation, we investigated how post-TAVI balloon valvuloplasty may impact the occurrence of PVL using a FE model of a non-compliant balloon, which was inflated to 22 mm at a recommended pressure of 3 atm.

RESULTS

Validation against In Vitro Testing: FE models predict similar geometric orifice area (1.68 cm^2 vs. 1.75 ± 0.075 cm^2) and stent deflection (P1: 1.71 mm vs. 1.73 ± 0.26 mm, P2: 1.13 mm vs. 1.10 ± 0.08 mm, P3: 0.86 mm vs. 1.12 ± 0.05 mm) to in vitro testing conducted in a 3D printed patient-specific annulus (Fig. 1(c)).

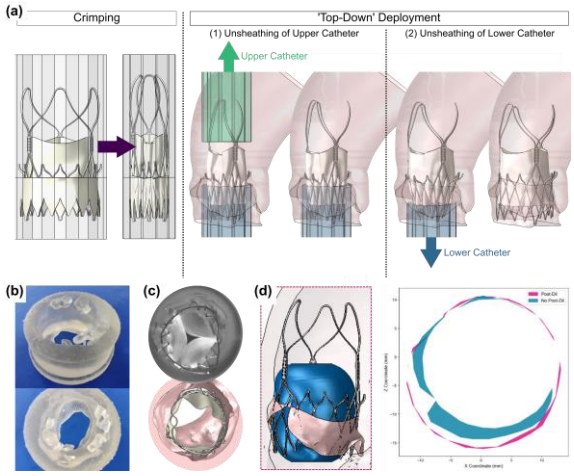

Figure 1: *(a) Simulation of TAVI in BAV. (b) 3D Printed Patient-Specific Annulus for In Vitro Testing. (c) Device Dynamics during Cardiac Cycle for In Vitro (top) and FE Model (bottom). (d) Impact of Balloon Valvuloplasty on Paravalvular Gap Area.*

Validation against Clinical Data: To compare deployment, we calculate the eccentricity index of the stent. At the inflow and outflow plane, our FE model predicts a more circular deployment, when compared to the post-TAVI CT (11.2% vs 26.1%, 7.3% vs 30.4% respectively). The predicted paravalvular gap area, located between the native anatomy and TAVI device, is 62 mm^2.

Impact of Balloon Valvuloplasty: Our model predicts that post-TAVI balloon valvuloplasty using a non-complaint balloon operated at an inflation pressure of 3 atm reduces the total area of paravalvular gap to 14 mm^2 (Fig. 1(d)), when compared to 62 mm^2.

DISCUSSION

Here, we developed a novel framework for predicting the performance of TAVI in a patient-specific BAV model and validated against clinical and in vitro data. Ongoing work aims to include calcifications, which may significantly impact device deployment predictions. Although the paravalvular gap area is assumed to be proportional to the risk of PVL, further work aims to validate these predictions using CFD. We are also assessing the use of various tailored BAV-specific sizing strategies [2-4]. Further work also aims to integrate deep learning-based methods within the current framework for anatomical analysis and reconstruction from CT to assess the impact of TAVI device sizing in a large BAV cohort [7]. In this patient-specific study, we showed that post-TAVI balloon valvuloplasty reduced paravalvular gap, which may reduce PVL following TAVI in the BAV.

REFERENCES: [1] Roberts et al., Circulation, 2005. [2] Xiong et al., Nat Rev Cardiol, 2023. [3] Tchetche et al., Circ-Cardiovasc Inte, 2019. [4] Petronio et al., J Cardiovasc Comput, 2020. [5] McGee at al., Biomech Model Mechan, 2019. [6] Lavon et al., Med Biol Eng Comput, 2019. [7] Rouhollahi et al., Comput Med Imag Grap, 2023.

ACKNOWLEDGEMENTS: Funded by the IRC Government of Ireland Postgraduate Scholarship (GOIPG/2022/2032).

SWELLING BEHAVIOR AND CHARACTERIZATION OF PH-RESPONSIVE HYDROGELS FOR BIOMEDICAL APPLICATIONS

Peterson, I.[1], Heavey, P.[1], Higginbotham, C.[1]
[1] Technological University of the Shannon, Midlands
email: (A00261208@student.tus.ie)

INTRODUCTION

pH-responsive hydrogels hold immense potential for targeted drug delivery, particularly in treating or managing a variety of diseases, where precise drug release is essential. This study focuses on developing novel hydrogels combining PEGDMA, Eudragit S100, and NVCL, designed to exhibit dual pH and temperature sensitivity.

MATERIALS AND METHODS

Hydrogels were synthesized using UV photopolymerization with the biocompatible photoinitiator Irgacure® 2959, offering a safer, eco-friendly alternative to traditional chemical cross-linking. Formulations were divided into three sets: the HE series (HE1–HE3) with PEGDMA (550 or 750 MW), Eudragit S100, and photoinitiator; the HN series (HN1–HN5) with PEGDMA (550 or 750 MW), PNVCL, and photoinitiator; and the HNE series (HNE1–HNE5) with PEGDMA (550 or 750 MW), PNVCL, Eudragit S100, and photoinitiator. Control formulations used PEGDMA (550 or 750 MW) and photoinitiator. Eudragit® S100 dissolves at pH 6-7, enhancing drug bioavailability and controlled release, while thermosensitive Poly(N-vinylcaprolactam) (PNVCL) transitions at ~33°C, offering biocompatibility for drug delivery. Formulations were characterized for gel fraction and swelling behaviour to assess the impact of polymer composition on responsiveness. Further evaluations included ATR-FTIR for chemical structure analysis, DSC for thermal properties (e.g., glass transition temperature, Tg), contact angle measurements for surface wettability, and compression tests for mechanical strength.

RESULTS

At pH 7.4, all samples exhibited higher gel fraction and swelling, reflecting enhanced stability and hydrophilicity in neutral conditions. Control samples showed the highest gel fraction, while swelling was more pronounced in the HE, HN, and HNE series. At pH 1.2, gel fractions decreased, particularly in HNE 750, indicating reduced network integrity. Swelling was lower in acidic conditions but remained significant in the HNE series, highlighting its hydrophilic properties. Higher molecular weights (750) resulted in increased swelling but slightly reduced gel fractions compared to 550. ATR-FTIR confirmed chemical composition and crosslinking.

Figure 1 Comparison of hydrogel formulations (Control, HE1, HE2, HE3) with molecular weight 550.

DISCUSSION

This study demonstrates the suitability of UV-cured, stimuli-responsive hydrogels as a potential for controlled drug delivery. The observed pH-dependent behaviour, with higher gel fraction and swelling at pH 7.4, indicates stability in neutral environments like the intestine, while reduced integrity at pH 1.2 supports site-specific release potential. ATR-FTIR confirmed successful crosslinking and chemical composition. Future contact angle measurements will evaluate hydrophilic properties critical for drug absorption, and compression testing will validate mechanical integrity. Overall, these findings highlight the potential of these hydrogels to improve drug delivery systems, enabling precise targeting and minimizing side effects in controlled release therapies.

REFERENCES

Barron (et al.), European Polymer Journal 75:25–35, 2016.
Burke (et al.), Journal of the Mechanical Behavior of Biomedical Materials 99:1–10, 2019a.
Burke (et al.), Polymers 11:1339, 2019b.
Coimbra (et al.), The Journal of Supercritical Fluids 45:272–281, 2008.
Devine (et al.), Polymer 44:7851–7860, 2003.
dos Santos (et al.), *Pharmaceutics* 13:1424, 2021.
Fallon (et al.), *Gels* 5:41, 2019.
Gaballa (et al.), J Polym Sci B Polym Phys 51:1555–1564, 2013.
Gonzalez-Urias (et al.), *International Journal of Molecular Sciences* 23:4722, 2022.
Halligan (et al.), Gels 9:439, 2023a.
Halligan (et al.), Polymers 15:1595, 2023b.
Killion (et al.), Journal of the Mechanical Behavior of Biomedical Materials 4:1219–1227, 2011.
Killion (et al.), Materials Science and Engineering: C 33:4203–4212, 2013.
Tie (et al.), Gels 9:248, 2023.
Yang (et al.), Polymers 14:4377, 2022.